Structure–Activity Relationship Studies on Isoform Selective Sphingosine Kinase Inhibitors

Molly Day Congdon

Dissertation submitted to the faculty of the Virginia Polytechnic Institute and State University in partial fulfillment of the requirements for the degree of

Doctor of Philosophy
In
Chemistry

Webster L. Santos, chair
Felicia A. Etzkorn
Richard D. Gandour
David G. I. Kingston

July 18th 2016
Blacksburg, Virginia

Key words: sphingosine, sphingosine kinase, sphingosine-1-phosphate, structure-activity relationship, molecular docking

Structure–Activity Relationship Studies on Isoform Selective Sphingosine Kinase Inhibitors

Molly Day Congdon

ABSTRACT

A variety of diseases including Alzheimer's disease, asthma, cancer, fibrosis, multiple sclerosis, and sickle cell disease have been associated with elevated levels of sphingosine-1-phosphate (S1P). S1P, a pleiotropic lipid mediator involved in a broad range of cellular processes, is synthesized solely by the phosphorylation of sphingosine (Sph) and is catalyzed by the two isoforms of sphingosine kinase (SphK1 and SphK2). Therefore, SphKs are a potential therapeutic target; however, the physiological role of SphK2 is still emerging. In order to determine the role of SphK2 *in vivo*, more potent and selective small molecule inhibitors of SphK2, as well as dual inhibitors are necessary. Herein, explorations and advancements on the second generation SphK2 selective inhibitor **SLR080811** are disclosed.

Investigations into the lipophilic tail region of the hSphK2 inhibitor **SLR080811** are detailed. This investigation highlights the dependency of SphK2 selectivity and potency on overall compound length. More importantly, this study identified the internal aryl ring of **SLR080811** as a key pharmacophore of the scaffold.

To further probe the significance of the aromatic region, the phenyl ring was replaced by a 2,6-naphthyl ether skeleton. Investigations into the tail region of this scaffold are described in detail. Key discoveries from this structure–activity relationship study include **SLC5111312**

(hSphK2 K_i = 0.90 μM, dual hSphK inhibitor), **SLC5091592** (hSphK2 K_i = 1.02 μM, > 20-fold hSphK2 selective) and **SLC5121591** (hSphK2 K_i = 0.61 μM, >16-fold hSphK2 selective). Molecular modeling studies with hSphK2 indicate that the extended aromatic group is able to participate in π–π stacking interactions with Phe548. *In silico* docking studies indicate that a guanidine hydrogen bond to Asp211 is key for SphK2 selectivity, and incorporation of a 3'-hydroxyl group on the pyrrolidine ring increases hydrogen bonding to Asp308, thereby increasing SphK1 potency and reducing selectivity. Additionally, biological studies employing **SLC5111312** have helped to further elucidate the role of SphK2, suggesting that SphK2 has a catalytic role in the regulation of blood S1P levels.

The shape of the hSphK2 binding pocket was probed by introducing an indole moiety in place of the naphthyl ring and varying its substitution pattern. One key discovery from this study is **SLC5101465** (hSphK2 K_i = 0.09 μM, > 111 fold SphK2 selective), which has a 1,5-indole substitution pattern with an *N*-nonyl "tail". Molecular docking simulations highlight the importance of rotatable bonds and a relatively linear orientation between the "head group" and "tail group" to maintain essential hydrogen bond interactions to Asp residues with the guanidine moiety while minimizing steric interactions in the middle of the binding pocket.

Expanding upon the 1,5-indole scaffold of **SLC5101465**, a series of aryl tail derivatives are examined. This study confirms the necessity of electron withdrawing groups located at the end of the inhibitor scaffold to optimize binding in the tail region of the SphK2 binding pocket.

Acknowledgements

First, I would like to thank my advisor, Dr. Webster Santos, for the opportunity of working in his laboratory for the past 6 years and on a project that I love. Through countless iterations of "how's life?" and "where's my compound?", he has always expressed interest in my work and pushed me to become a better, independent chemist. Through seemingly insurmountable deadlines, I have learned to push myself beyond what I believed was physically possible and attain the unattainable. He has taught me the phrase "work–life-balance", a concept that I did not know when I first joined his group. Although, I still struggle with this concept today, it is a goal I will always try to achieve. I would especially like to thank him for all the opportunities he has given me over the years including the opportunities to instruct the organic laboratory course during the summer and to intern at SphynKx Therapeutics. Both of these experiences were indispensable for guiding me towards my future path as a chemist. It is impossible to put into words all that I have learned from having him as my advisor.

I would also like to thank my committee members: Dr. Felicia Etzkorn, Dr. Richard Gandour and Dr. David Kingston, for their guidance during my tenure at Virginia Tech. My heartfelt gratitude goes to Dr. Kingston for the kind, critical feedback given me over the years. I am very appreciative to Dr. Gandour for paying attention to the details in both my writing and presentations. Thanks to his scrutiny, I am a better chemist and presenter. Additionally, I would especially like to thank Dr. Etzkorn for her support and encouragement. I hope that one day I can be as good a role model for women, who choose the field of chemistry, in the future.

To my group members and friends, I would like to express my extreme appreciation. You have played a vital role in my graduate career at Virginia Tech. I would like to thank Jessica

Wynn, Hanlie (Wessels) Schoonover, and Amanda Nelson who have been with me from day one. You have supported me through the good, the bad and the 13 hour teaching and class extravaganzas. I would also like to thank all of the members of my subgroup over the years: Dr. Neeraj Patwardhan, Dr. Mithun Raje, Dr. Srinath Pashikanti, Beth Childress, Hao Li, Christopher Sibley, Emily Morris and Ken Knott, as well as, our collaborators Dr. Kevin Lynch and Dr. Yugesh Kharel at the University of Virginia and Dr. David Bevan, Dr. Anne Brown and Dr. Stephanie Lewis at Virginia Tech. I have learned so much from our discussions about the Sphingosine Kinase project. To the rest of our group, Cheryl Peck, Russell Snead, Ashley Peralta, Eric Medici, Dr. Xi Gao, and Dr. Yumin Dai, thank you for educating me about your projects and your indispensable support and feedback during group meetings. I would also like to thank Karen Iannaccone for her assistance with scheduling and departmental paperwork over the years. I would especially like to thank Hanlie (Wessels) Schoonover and Beth Childress for all of the long walks and coffee runs when things in lab were not going well and for their assistance with editing my thesis. It has been a pleasure working with all of you. I will miss all of you and hope that we can keep in touch.

Furthermore, I would like to express my extreme gratitude to my parents, Marjorie and Benjamin Congdon, for their infinite support during this stage of my life. They always encouraged me to do my best and never give up when the going got tough. I would especially like to thank them for making sure that I ate and was safe in lab during the wee hours of the morning when I was pushing to meet a deadline and had barely slept for over a month. A girl could never wish or hope for better parents.

Finally, I would like to express my dearest thanks to Guinness for being there for me 24/7. You always helped calm me down when I was frustrated after a bad day and were there to celebrate all the milestones. You are a wicked awesome kitty.

Dedication

To my Mom and Dad.

Table of Contents

List of Figures

List of Schemes

List of Tables

List of Abbreviations

A549: human lung carcinoma cell line

Aβ25-35: beta-amyloid peptide fragment 23-35

ABC transporters: ATP-binding-cassette transporters

AD: Alzheimer's Disease

ADP: Adenosine Diphosphate

ADT: androgen deprivation therapy

AKT: protein kinase B

Alb: albumin

AMD: age-related macular degeneration

ApoM: apolipoprotein M

Ar: androgen receptor

ATF4: activating transcription factor 4

ATP: Adenosine Triphosphate

BACE1: Beta-secretase 1

BAK: B-cell lymphoma 2 antagonist-killer

Bax: Bcl2-like protein 4

Bcl-2: B-cell lymphoma 2

Bcl-x_L: B-cell lymphoma- extra large

bFGF: basic fibroblast growth factor

BVDV: Bovine viral diarrhea virus

C1P: ceramide-1-phosphate

CCL2: chemokine (C-C motif) ligand 2

CCR7: counteracting chemokine receptor 7

CD8: cluster or differentiation 8 cells

Cer: Ceramide

CERK: ceramide kinase

CHIKV: chikungunya virus

CKCL1: chemokine (C-X-C motif) ligand 1

CLCL13: chemokine (C-X-C motif) ligand 13

cLogD: calculated distribution coefficient

cLogP: calculated partition coefficient

COX-2: cyclooxygenase-2

CNV: choroidal neovasuclarization

$cPLA_2$: cytosolic phospholipase A_2

CTD: C-terminal domain

CTGF: connective tissue growth factor

Cyt c: Cytochrome c

DEG: dihydroceramide desaturase

DENV: Dengue virus

Des1: dihydroceramide desaturase-1

EC: endothelial cell

EC_{50}: half maximal effective concentration

ECM: extracellular matrix

ED_{50}: median effective dose

ELISA: enzyme-linked immunosorbent assay

eNOS: endothelial nitric oxide synthase

ER: endoplasmic reticulum

ERK1: extracellular signal-regulated kinase 1

ERK2: extracellular signal-regulated kinase 2

eS1P: extracellular S1P

Fab: fragment antigen binding fragment

FAK: focal adhesion kinase

FcεRI: high affinity IgE receptor

$G_{12/13}$: heterotrimeric G protein subunit that regulate cell processes via guanine nucleotide exchange factors

Gαs: heterotrimeric G protein subunit that activates adenylyl cyclase

G_i: heterotrimeric G protein subunit that inhibits adenylyl cyclase

G_q: heterotrimeric G protein subunit that activates phospholipase C

GTP: Guanosine Triphosphate

HCMV: Human cytomegalovirus

HDAC: histone deacetylase

HDL: high-density lipoproteins

HeLa: human cervical cell line

IC_{50}: half maximal inhibitory concentration

ICAM1: intracellular adhesion molecule-1

IFNα: interferon α

IFNγ: interferon γ

IgE: immunoglobulin E

IL-1β: interleukin 1β

IL-2: interleukin 2

IL-4: interleukin 4

IL-5: interleukin 5

IL-6: interleukin 6

IL-8: interleukin 8

IL-10: interleukin 10

IL-12: interleukin 12

IL-13: interleukin 13

IL-17: interleukin 17

iS1P: intracellular S1P

JAK2: Janus kinase 2

JNK: Jun *N*-terminal kinase

K_i: inhibition constant

KSHV: Kaposi's Sarcoma-associated Herpesvirus

LARG: Leukemia-associated Rho guanine nucleotide exchange factor

LN229: human brain glioblastoma cells

LPA: lysophosphatidic acid

LPS: lipopolysaccharide

mAb: monoclonal antibody

MCP1: monocyte chemoattractant protein 1

MDA MB-231: human breast adenocarcinoma cell line

MDA MB-468: human mammary gland/breast cancer cell line

MEF: mouse embryonic fibroblasts

MEK: mitrogen-activated protein kinase kinase

MCF-7: Michigan Cancer Foundation-7 cells

MS: Multiple sclerosis

MV: Measles virus

NES: nuclear export signals

NGF: nerve growth factor

NFκB : nuclear factor κB

NK: natural killer cells

NLS: nuclear localization signal

NS2-3: nonstructural protein 2-3

NS3: nonstructural protein 3

NTD: *N*-terminal domain

p90RSK: p90 ribosomal s6 kinase

PCV: polypoidal choroidal vasculopathy

PDGF: platelet-derived growth factor

PGE_2: prostaglandin E_2

PHB2: prohibitin 2

PI3K: phosphatidylinositol 3-kinase

PKB: protein kinase B

PKC: protein kinase C

PKCα: protein kinase C α

PKCβ: protein kinase C β

PKD: protein kinase D

PP1: protein phosphatase 1

PP2A: protein phosphatase 2A

PS: phosphatidylserine

PTEN: phosphate and tensin homologue

RCC: remal cell carcinoma

RKT: receptor tyrosine kinases

Rock: Rho-associated protein kinase

RRMS: Relapsing Remitting Multiple Sclerosis

S1P: Sphingosine-1-phosphate

$S1P_1$: S1P receptor 1

$S1P_2$: S1P receptor 2

$S1P_3$: S1P receptor 3

$S1P_4$: S1P receptor 4

$S1P_5$: S1P receptor 5

SAR: Structure–Activity Relationship

Saos2: human osteosarcoma cell line

SC: conserved domain

SCD: Sickle cell disease

SKOV3: human ovary adenocarcinoma cell line

SM: Sphingomyelin

SMase: Sphingomyelinase

Sph: Sphingosine

SphKc: Sphingosine Kinase catalytic domain

SphK1: Sphingosine Kinase 1

SphK2: Sphingosine Kinase 2

Spns2: spinster homolog 2 transporter

STAT3: signal transducer and activator of transcription 3

STAT4: signal transducer and activator of transcription 4

TGF-β: transforming growth factor β

Th2: helper T cells type 2

TLC: Thin Layer Chromatography

TM: transmembrane region

TNFα: Tumor Necrosis Factor α

TPA: tissue plasminogen activator

TRAF2: TNF receptor-associated factor 2

TRF1: transferrin receptor 1

TYK2: tyrosine kinase 2

U937: human histiocytic lymphoma leukemia cell line

VCAM1: vascular cell adhesion molecule-1

VEGF: vascular endothelial growth factor

WM266-4: human malignant melanoma cell line

WT: wild type

Chapter 1 The Role of Sphingosine Kinase/Sphingosine-1-Phosphate Signaling in Disease and Current Therapeutic Strategies

1.1. Introduction

Sphingosine kinase (SphK) is an important metabolic enzyme that catalyzes the conversion of sphingosine (Sph) into sphingosine-1-phosphate (S1P). S1P has been shown to possess an important role in regulating cell survival, while its upstream precursor, ceramide (Cer), is a key regulator of apoptosis. A delicate balance exists among these lipids, and has been designated as the ceramide-sphingosine-S1P rheostat. The roles of this rheostat, SphKs, S1P, and downstream receptors of S1P are complex in cancer, as cellular proliferation and apoptosis are determined by S1P levels. Proliferative effects of S1P can be prevented with the use of SphK inhibitors or S1P receptor agonists and antagonists. Currently, there exists a wide structural variety of S1P receptor agonists and antagonists, as well as SphK inhibitors that vary in SphK selectivity and potency. This review will be centered on the roles of the rheostat, isoforms of SphK, S1P, and S1P receptors in various diseased states, as well as current therapeutic methods for targeting the rheostat. Current efforts in developing monoclonal antibodies, receptor agonists and antagonists, and SphK inhibitors will be presented.

1.2. Sphingolipid Metabolism in the cell

Sphingolipids, molecules containing a sphingosine backbone, are synthesized *de novo* from L-serine and acetyl coenzyme A. This condensation occurs at the cytosolic leaflet of the endoplasmic reticulum (ER), where enzymes necessary for Cer synthesis can be found.[1]

Cer is involved in a multitude of metabolic pathways including the stress-activated protein kinase cascade, mitogen-activated protein kinase cascade,[2] and the ceramide-

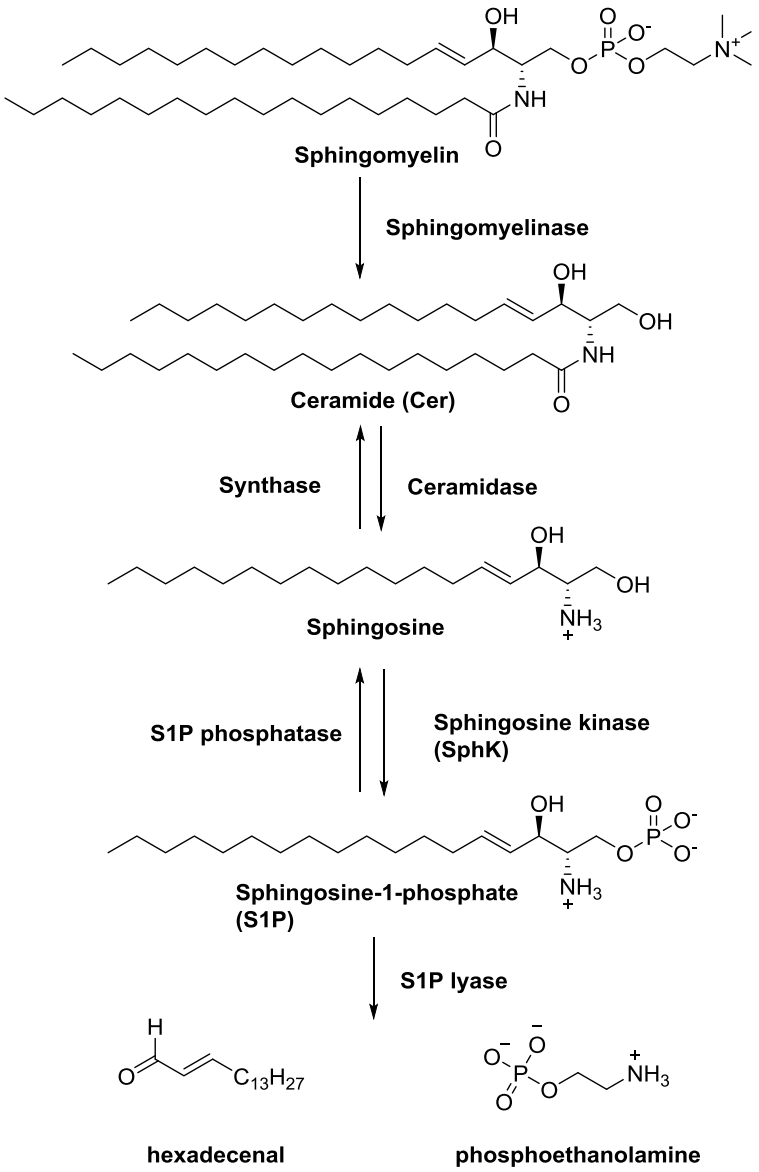

Figure 1.1. Ceramide-Sphingosine-Sphingosine-1-Phosphate Synthesis

sphingosine-S1P rheostat[3] shown in Figure 1.1. It is either synthesized *de novo* or via the hydrolysis of sphingomyelin (SM) by sphingomyelinase (SMase) on the luminal side of the Golgi apparatus.[1] Cer is further hydrolyzed by ceramidase to yield sphingosine (Sph). This process can be reversed by the enzyme ceramide synthase. Sph is then phosphorylated by SphK, which utilizes adenosine triphosphate (ATP) as the phosphate source[4] to generate S1P. S1P can be converted back into Sph by S1P phosphatase or degraded by sphingosine lyase to produce

hexadecenal and phosphoethanolamine.[2, 5] This degradation is the only way in which the sphingosine backbone can be abolished *in vivo*.[5] Intracellularly, S1P has been shown to regulate a multitude of targets including histone deacetylase 1 and 2 (HDAC1 and 2),[6] prohibitin 2,[7] p21 activated kinase 1,[8] and E3 ubiquitin ligase TNF receptor associated factor 2 (TRAF2).[9] It has also been implicated in the release of cytochrome-*c* (cyt c) from mitochondria.[10] S1P can also be employed in a multitude of other cellular processes such as regulation of cell motility, cytoskeletal rearrangement, vascular maturation,[11] angiogenesis,[12] lymphocyte trafficking,[1] transient calcium mobilization, mitogenesis and prevention of apoptosis.[13]

Cer levels can be affected by a number of stimuli and cellular stresses including chemotherapeutic agents and increased amounts of tumor necrosis factor α (TNFα).[14, 15] Since several targets of Cer, such as ceramide activated protein kinase C ζ,[16] protease prICE,[17] cathepsin D and serine/threonine protein phosphatases (PP1 and PP2A),[18] facilitate its apoptotic function, increased levels of Cer promote apoptosis. In contrast, S1P acts as a second messenger for cellular proliferation[3, 19] and increased S1P levels have been shown to induce mitosis.[15] Increased levels of S1P can be obtained through stimulation of SphK by ATP, and a variety of growth factors, including platelet-derived growth factor (PDGF), nerve growth factor (NGF), and vascular endothelial growth factor (VEGF).[2, 14, 20] PDGF is known to induce translocation of SphK1 towards the edge of cells.[1] The opposing downstream actions of Cer and S1P result in a complex, dynamic equilibrium in the ceramide-sphingosine-S1P rheostat, which determines the fate of the cell.

1.3. Isoforms of Sphingosine Kinase

There are two isoforms of SphK (SphK1 and SphK2) that vary in their cellular localization, expression levels, and genetic makeup. Chromosomes $17_q25.2$ and $19_q13.2$ contain the genes for SphK1 and SphK2 respectively.[19] SphK1a is comprised of 384 amino acids, approximately 43 kDa, while SphK2a is comprised of 618 amino acids, approximately 66 kDa.[19, 21, 22] Although the large differences in size result in only 45% sequence similarity between SphK1 and 2, most of the SphK1 sequence aligns with portions of SphK2 which results in an 80% similarity between the enzymes. Both sequences of human SphK1 and SphK2 possess five conserved domains (SC1–5) and catalytic domains (SPHKc) which contain a retained ATP binding sequence in SC2 (Figure 1.2).[4, 19] The additional amino acid residues in SphK2 are predominantly located in the longer *N*-terminus, a proline-rich region towards the middle of the structure and in four transmembrane regions (TM1–4).[2, 5, 23] These additions to SphK2 may assist in preventing secretion of SphK2 or retention in the nuclear membrane.[2]

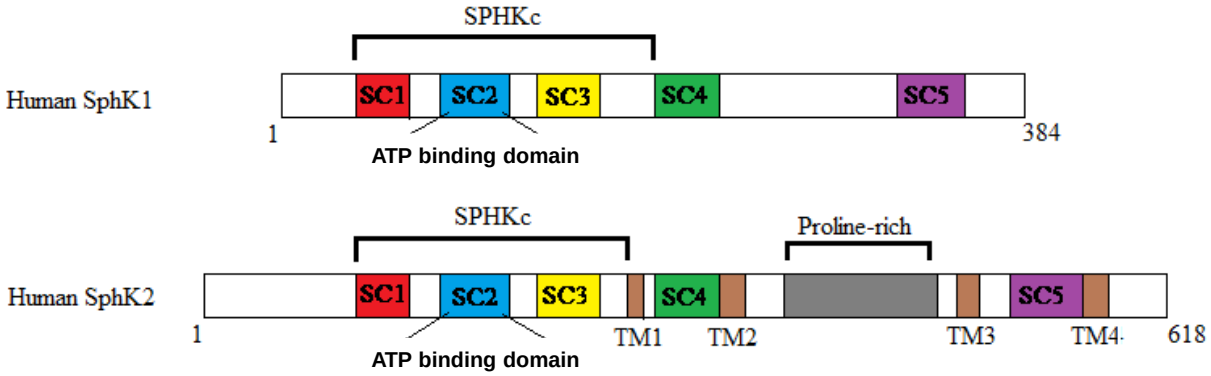

Figure 1.2. Sphingosine Kinase 1 and 2 Protein Sequence

Although the isoforms have high sequence similarity, biological studies indicate that differences exist in the substrate binding pockets.[21, 24-30] To date only the SphK1 crystal structure has been solved,[31, 32] and as a result, a direct comparison between the binding pockets cannot be

made. SphK1 is more selective than SphK2, which can phosphorylate a wide range of synthetic and biological lipids. D -*erythro*-Sphingosine and D-*erythro*-dihydrosphingosine are substrates for both isoforms.[11, 21] Additional substrates of SphK2 include D,L-*threo*-dihydrosphingosine, phytosphingosine, and FTY720 (*vide infra*).[21, 22, 33, 34]

Despite the differences in the protein sequences of SphK1 and SphK2, both are intracellular enzymes that lack a membrane anchor.[5] As a result, SphK1 and SphK2 are cytosolic enzymes.[35] Both isoforms can be activated by a variety of cytokines, growth factors, extracellular signal-related protein kinases 1 and 2 (ERK1 and 2), and agonists.[21, 36-38] Activation via phosphorylation by ERK1 and 2 has been shown to increase SphK1 activity 14-fold, while phosphorylation by ERK1 only doubles SphK2 activity.[37, 39] SphK1 and 2 also display catalytic activity that is independent of post-translational modification.[21, 40] It is believed that the role of this basal level of SphK activity is to maintain cellular concentrations of upstream metabolites Sph and Cer.[41] Further evidence of the importance of SphK is the functional redundancy between the isoforms. SphK1$^{-/-}$ or SphK2$^{-/-}$ null mice do not display a noticeable phenotype;[42, 43] however, the double knockout is embryonically lethal as a result of vascular and neurological defects.[42] Deletion of SphK2 reduces plasma S1P concentrations by only 25% indicating that the majority of S1P is produced by SphK1.[44] Even though both isoforms are ubiquitously expressed in all tissues, SphK1 is found in higher concentrations in leukocytes, lung and spleen, while SphK2 is mainly localized in bone marrow, brain, heart, kidney, and liver cells.[2, 22, 44, 45]

1.3.1. Sphingosine Kinase 1

SphK1 is the more studied isoform and has been shown to be a proliferative enzyme in numerous studies.[23, 46, 47] In 2013, the first crystal structure of SphK1 (residues 9–364) was published by Wang, Z., *et al*.[31] This study found that SphK1 can be divided into 2 domains, an

N-terminal domain (NTD) and a *C*-terminal domain (CTD), which are comprised of a total of 9 α helices, 17 β strands and a 3_{10}-helix.[31] The NTD encompasses amino acid residues 9–150 and 357–364 and contains SC1–3. The CTD includes amino acid residues 151–356 and SC4–5. Co-crystallization of SphK1 with Sph found that the lipid binding pocket is located deep in the CTD. The ATP nucleotide binding site is located in a small crevice between the NTD and CTD. Together the ATP and lipid binding pocket of the SphK1 create a catalytic site which incorporates SC1–5.[31]

Analysis of cellular fractions has shown that SphK1 is predominantly found in cytosolic fractions with a very small amount found in membrane fractions. Phosphorylation of SphK1 on Ser225, catalyzed by ERK1 and ERK2, results in translocation from the cytosol to the plasma membrane.[3, 5] Translocation occurs via binding to calcium and integrin binding protein-1.[36, 37, 48] Stimulation of the M3 muscarinic receptor by carbachol can also cause translocation of SphK1.[5] The mechanisms of translocation are still unknown.[3, 5] Additional phosphorylation-independent mechanisms have also been reported to induce SphK1 translocation.[49, 50] Once localized at the plasma membrane, SphK1 catalyzes the phosphorylation of membrane-associated Sph. The S1P formed can interact with intracellular targets and easily be released to the extracellular matrix where it can bind to S1P receptors (discussed in sections 1.4 and 1.5) to promote a wide range of effects including: cell survival, proliferation, angiogenesis, migration and inflammation.[1, 14, 51-56]

1.3.2. Sphingosine Kinase 2

SphK2 exists in multiple isoforms designated SphK2a, SphK2b, and SphK2c.[21] SphK2a is the most characterized, shortest isoform and is typically referenced in literature as SphK2.[22] SphK2a activation by ERK1 and 2 is believed to be the result of phosphorylation of Ser351 and Thr578.[39] SphK2b is a larger isoform which contains an additional 36 amino acid residues in the

N-terminus.[57] It is believed that SphK2b is formed from a different start codon. Furthermore, SphK2b is expected to be the most important isoform physiologically since it has been found to be the primary isoform in a variety of human cells and tissues.[57] It has been proposed that phosphorylation of Ser387 and Thr619 on SphK2b are involved in SphK2b activation by ERK1 and 2.[39] The mRNA for a third isoform, SphK2c, has been found. SphK2c is the largest isoform and contains both an extended *N*-terminus and *C*-terminus.[21] Unfortunately, a crystal structure for SphK2 has not been obtained.

SphK2 possesses a conflicting role to SphK1. While SphK1 is proliferative, overexpression of SphK2 was shown to cause apoptosis and cell cycle arrest.[23, 57, 58] The role of SphK2 is highly dependent upon its localization (Figure 1.3). SphK2, which was principally thought to be located in the nucleus or near the ER,[3] undergoes translocation as the result of a nuclear export signal, which prompts phosphorylation by protein kinase D (PKD).[3, 5] Confocal immunofluorescence microscopy has confirmed the localization of both SphK1 and 2, and shown that SphK2 is found in the cytoplasm, but not in the plasma membrane.[2]

Unlike SphK1, SphK2 contains nuclear localization signals (NLS) in the *N*-terminus and nuclear export signals (NES) in the proline rich region.[58] Nuclear localized SphK2 produces S1P and dihydro-S1P which inhibit HDAC1/2 activity.[6] HDAC1/2 inhibition causes an increase in histone acetylation on a variety of promoters, and increased transcription of p21 (a cyclin-dependent kinase inhibitor) and c-fos (a transcriptional regulator) which leads to inhibition of DNA synthesis.[6, 58] Nuclear export of SphK2 to the cytoplasm is controlled by PKD-mediated phosphorylation of Ser419 or Ser421 in the NES.[59]

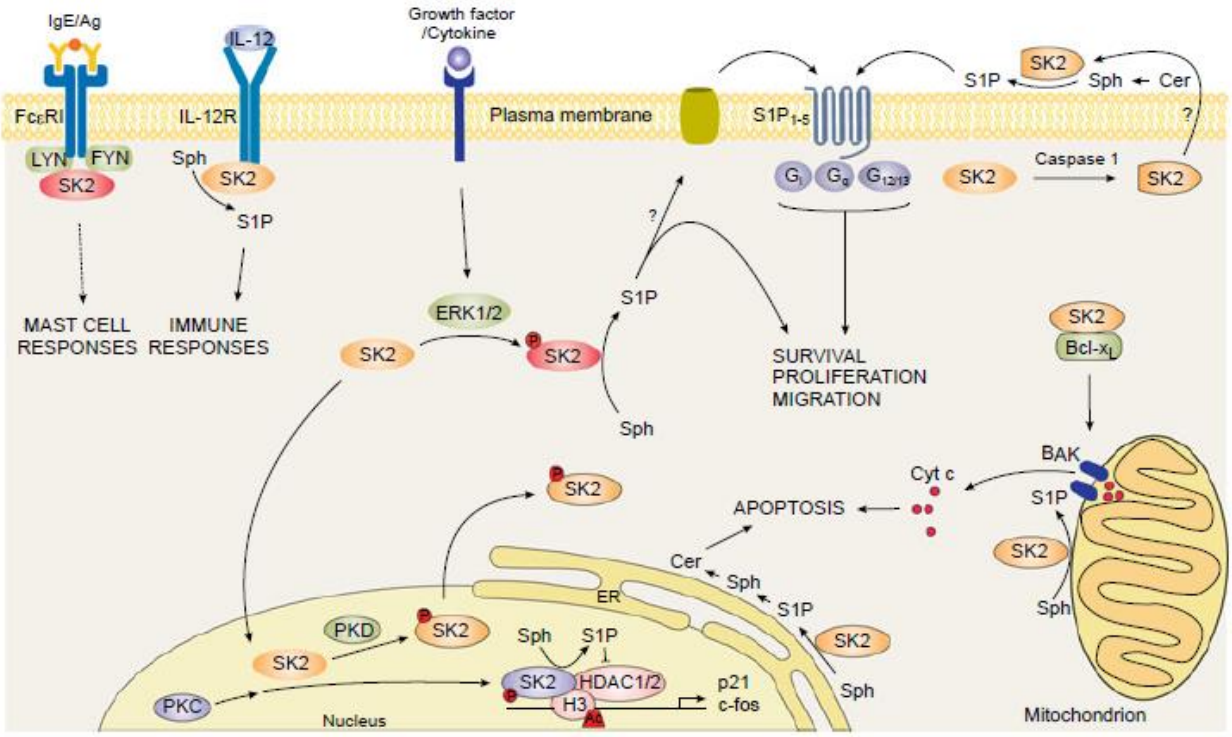

Figure 1.3. Signaling and Regulation of Sphingosine Kinase 2. Figure reprinted with permission from reference 21. Copyright (2013) Wiley

Once exported from the nucleus, SphK2 has been reported to be localized near organelles. A BH3-binding domain was identified in the *N*-terminus of SphK2.[60] This domain enables SphK2 to interact with B-cell lymphoma-extra-large (Bcl-x_L), a pro-survival member of the B-cell lymphoma 2 (Bcl-2) family. This complex can activate mitochondria localized B-cell lymphoma 2 antagonist-killer (BAK), leading to an increase in the permeability of the mitochondrial membrane and release of apoptotic cytochrome c.[10 7] Mitochondria localized S1P can also bind to PHB2, which is localized on the inner mitochondrial membrane and is involved in regulating mitochondria function.[7] PHB2 interacts with complex IV of cytochrome-*c* oxidase, the last enzyme in the respiratory electron transport chain. Reduction of S1P-PHB2 interaction or decreased SphK2 levels have been shown to lead to mitochondria respiratory dysfunction via cytochrome-*c* oxidase.[7] SphK2 has also been shown to be localized near the ER under stress

conditions.[23] Here, SphK2 can catalyze the production of S1P that is funneled into ER-localized S1P phosphatase and ceramide synthase, resulting in an increase in pro-apoptotic Cer.[23]

SphK2 can be a proliferative enzyme when it is localized near the plasma membrane.[61] In apoptotic cells, SphK2 can be cleaved at the *N*-terminus by caspase-1 which allows SphK2 to be exported from the cell. The proliferative effects observed are the result of S1P export, proposed phosphorylation of extracellular Sph to S1P and S1P receptor signaling.[61]

SphK2 located near the plasma membrane can also be involved in receptor-mediated signaling. Two examples are shown in Figure 1.3. Interleukin 12 (IL-12) is a key cytokine that promotes differentiation of helper T-cells and is involved in a multitude of cell-mediated immune responses.[62] IL-12 can activate Janus kinase 2 (JAK2), tyrosine kinase 2 (TYK2), signal transducer and activators of transcription 3 and 4 (STAT3 and STAT4), as well as, activating signaling pathways such as phosphatidylinositol 3-kinase (PI3K)/protein kinase B (PKB/AKT) and mitogen-activated protein kinase 6/p38.[62, 63] The proline rich region of SphK2 interacts with the IL-12Rβ1 region of IL-12.[63] This binding of SphK2 to IL-12Rβ1 induces production of interferon γ (IFNγ) and suggests that SphK2 has a role in regulating IL-12 signaling.[63] SphK2 can also be activated by FcεRI, a high-affinity immunoglobulin E (IgE) receptor of immunoglobulin in mast cells.[64] Non-receptor tyrosine kinases Fyn and Lyn were also found to activate and translocate SphK2 to the plasma membrane.[64] SphK2 is the primary producer of extracellular S1P in mast cells, increases Ca^{2+} levels, and activates of variety of downstream pathways such as protein kinase C α and β (PKCα and β), and nuclear factor κB (NFκB), which lead to increased cytokine production and degranulation.[65]

1.4. Inside-out Signaling of Sphingosine-1-Phosphate

S1P is present in both plasma of mammalian cells and blood serum; however, the concentrations of S1P are different. It has been shown that S1P concentration in plasma ranges from 0.1–0.4 μM, and from 0.4–1.1 μM in serum.[66, 67] The presence of this large S1P gradient indicates that S1P, synthesized inside the cell through the phosphorylation of Sph by SphKs, is being exported out of the cell (Figure 1.4).

Intramembrane transport of S1P from the cytosol to the extracellular plasma can be achieved through the use of ATP-binding-cassette transporters (ABC transporters) or a spinster homolog 2 transporter (Spns2).[1, 35, 66, 68-71] The ABC transporter responsible for exporting S1P out of the cell varies upon cell type. ABCA1, ABCC1 and ABCG2 have been reported to export S1P in astrocytes, mast cells, and breast cancer cells, respectively.[69] ABCC1 has also been shown to be upregulated by dexamethasone where it shuttles cytosolic S1P out of the cell to sphingosine-1-phosphate receptor 3 ($S1P_3$).[72] ABC transporters have a crucial role in S1P release from astrocytes and emission from platelets.[1] Spns2 is involved in the export of S1P and the regulation of lymph S1P levels, and can influence lymphocyte trafficking.[68, 69] Spns2 is required to transport S1P to plasma.[68]

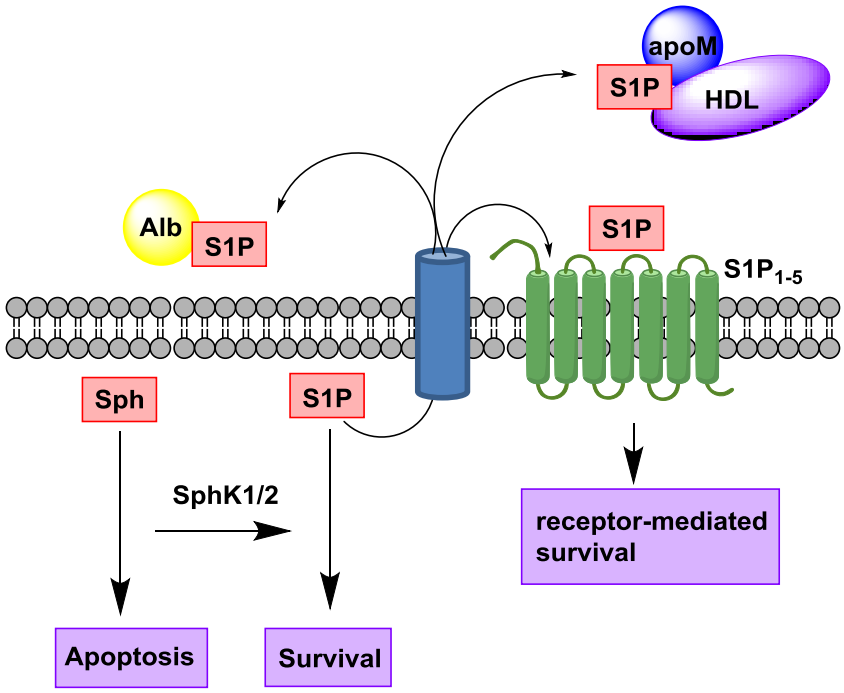

Figure 1.4. Inside-out Signaling of Sphingosine-1-Phosphate

Upon export out of the cell, S1P binds to either albumin (Alb) or apoliproptein M (apoM). In plasma, approximately 65% of S1P is bound to M while the remaining 35% is bound to Alb.[73] The S1P–apoM complex can also bind to high-density lipoproteins (HDL). This larger complex accounts for approximately 5% of HDL particles.[73] Extracellular S1P participates in a plethora of biological pathways. Some of these pathways involve the binding of S1P to five different sphingosine-1-phosphate receptors ($S1P_{1-5}$);[74] however, the mechanism in which HDL-complexed S1P interacts with $S1P_{1-5}$ is still unknown.[51]

1.5. Sphingosine-1-Phosphate Receptors

The S1P receptors are a subfamily of G-protein coupled receptors that are located in the cell membrane and involved in a variety of cellular signaling responses (Figure 1.5). These receptors couple to various guanine nucleotide binding proteins (heterotrimeric G-proteins) excluding Gαs.[11, 14] $S1P_{1,3,4,5}$ couple to G_i. $S1P_1$ activation also fuels Rac-coupled pathways such as cortical actin formation.[20] $S1P_2$ couples to all G proteins and stimulates Rho-coupled pathways such as stress fiber formation. It also inhibits activation of Rac protein.[20] $S1P_3$ couples to G_q and $G_{12/13}$ while $S1P_4$ couples to G_i, and G_{12}; however, this coupling is not the result of S1P-$S1P_4$ binding.[20] Binding of S1P to any of the S1P receptors initiates receptor dependent biological pathways, causing a variety of downstream effects. Activation of $S1P_{1,5}$ increases cellular proliferation, while activation of $S1P_{1,3}$ increases cellular migration.[20] In contrast, $S1P_2$ activation through Rho inhibits migration.

$S1P_1$ is ubiquitously expressed in cells including immune cells, neural cells, endothelial cells (EC), and smooth muscles cells.[1, 12] S1P produced by the translocation of SphK1 stimulates $S1P_1$ causing a directional movement in the cell.[1] Activation of $S1P_1$ promotes downstream enhancement of growth factor production and emission, phosphorylation of receptor tyrosine kinases (RTKs), and cross-talk among intracellular receptors. $S1P_1$ can also be involved in the binding of receptors to proteins and the formation of receptor/receptor complexes.[1] Genetic removal of $S1P_1$ is embryonically lethal indicating that the receptor has a key role in endothelial barrier function, vascular maturation, immune cell trafficking, angiogenesis, and neurogenesis.[14, 42, 51] Targeted deletion of $S1P_1$ from EC leads to the development of renal ischemia/reperfusion injury in the liver and kidneys.[51] $S1P_1$ is able to regulate migration by counteracting chemokine receptor (CCR7) retention signals. $S1P_1$ may play a role in the activation and differentiation of T-

and B- immune cells.[75] $S1P_1$ reduction of T-cell localized $S1P_1$ has been shown to reduce the ability of T-cells to coordinate to T-helper 17 and lessen disease pathology. On the other hand, $S1P_1$, when it has been deactivated via receptor internalization, increases the ability of T-cells to coordinate to T-helper 17 and escalate disease pathology and immune cell trafficking.[75] Studies with $S1P_{1,3}$ antagonists **FTY720** and **BAF312** (*vide infra*) suggest that $S1P_1$ regulates bradycardia.[76]

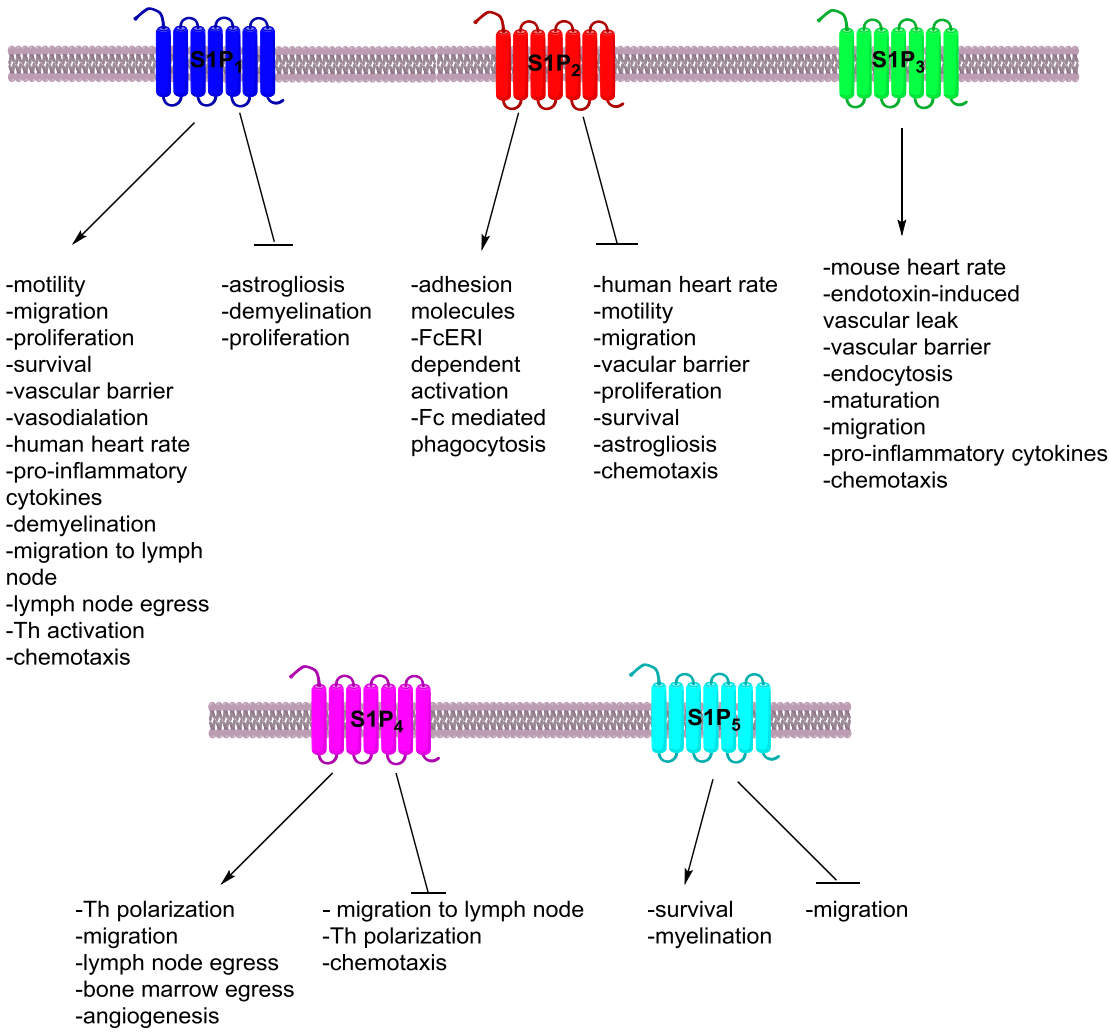

Figure 1.5. Sphingosine-1-Phosphate Receptor Signaling

$S1P_2$ has widespread expression and it is vital in the auditory and vestibular systems.[12] Genetic deletion of $S1P_2$ produces an increase in neocortical pyramidal neurons,[14] causing the inner ear to develop abnormally. As a result, $S1P_2$ deficiency produces deafness.[11] $S1P_2$ null mice have also been found to be seizure prone, developing random, sometimes lethal seizures.[14] S1P stimulation of $S1P_2$ results in cellular motility that opposes that produced by $S1P_1$.[1] $S1P_2$ has also been shown to trigger pro-inflammatory properties through initiation of TNFα which eventually activates NFκB and increases vascular cell adhesion molecule-1 (VCAM1) and intracellular adhesion molecule-1 (ICAM1). Other studies have indicated that $S1P_2$ is an important regulator of vascular permeability and activation, and a suppressor of angiogenic sprouting via activation of RhoC by leukemia-associated Rho guanine nucleotide exchange factor (LARG) .[51] These results also indicate a possible antagonistic relationship between $S1P_1$ and $S1P_2$ in EC during injury.

$S1P_3$ is largely expressed in the heart, intestine, kidney, lung, and spleen.[1, 12] This receptor is involved in pulmonary functions with opposing properties of $S1P_1$ on pulmonary endothelial and epithelial barriers.[1] Unlike the other receptors, $S1P_3$ deficiency does not produce any obvious phenotype.[1] Dual genetic deletion of $S1P_2$ and $S1P_3$, and triple deletion of $S1P_{1-3}$, are both embryonically lethal.[14] $S1P_{1-3}$ deletion produces immense hemorrhaging. On the other hand, survivors of $S1P_{2,3}$ deletion do not possess any observable phenotype, but are more susceptible to injury via ischemia, inadequate blood circulation to a specific location resulting from a blood vessel blockage, and reperfusion, the restoration of blood flow to deprived organs or tissues.[14] Studies with $S1P_{1,3}$ antagonists **FTY720** and **BAF312** (*vide infra*) suggest that $S1P_3$ regulates hypertension.[76] It has been determined that S1P binding to $S1P_3$ causes dexamethasone-induced cytoprotection of human fibroblasts.[72] Furthermore, $S1P_3$ has been implicated in the

proliferative effects of **FTY720-P**, activation of Bcl-2 phosphorylation, and mitochondrial membrane charge stabilization.[77]

$S1P_4$, with the most restricted expression of all of the S1P receptors,[1] is found on leukocytes, lymphocytic and hematopoietic cells in the immune system, and airway smooth muscle cells.[12, 78] $S1P_4$ suppresses T-cell proliferation, but does not induce T-cell migration.[79] $S1P_4$ has been implicated in cytokine secretion. Generation of cytokines interleukins 2 and 4 (IL-2 and IL-4), and IFN-γ are substantially suppressed by S1P-$S1P_4$ activation; however, interleukin 10 (IL-10) expression is enhanced in $S1P_4$-only T-cells.[79] The overall suppression of T-cell activation is the net result of reduction of IL-4 an IL-2 (T-cell activators) and enhancement of IL-10 (T-cell suppressor). $S1P_4$ appears to play a small role in the trafficking of cluster of differentiation 8 (CD8) effector T-cells to lymph nodes. [78] Cytokine secretion and migration of dendritic cells were significantly altered by $S1P_4$ deficiency which exhibited decreased polarization and differentiation of T-helper 17 in helper T-cells. $S1P_4^{-/-}$ mice displayed decreased pathology in a model of sodium-induced colitis.[78]

$S1P_5$ is expressed in the central nervous system, particularly in the oligodendrocytes of the white matter tracts,[14] and the myelinating cells of the brain.[1] Despite this location, genetic deletion of $S1P_5$ does not produce any obvious phenotype such as reduced myelination.[14] As a result, the exact role of this receptor is still elusive. Expression of $S1P_5$ in natural killer (NK) cells was found to be mandatory to move NK cells to inflamed organs.[1, 51] $S1P_5$ is also highly expressed in human brain capillary endothelial cells. $S1P_5$ plays a major role in blood brain barrier function. Reduction of $S1P_5$ concentration via genetic silencing or antagonism of $S1P_5$ led to reduced brain barrier integrity and increased transmigration of monocytes.[80] Conversely, activation of $S1P_5$ via an $S1P_5$ agonist led to increased barrier function and reduced permeability,

as well as reduced transmigration of monocytes. Increased cell-cell junction proteins were also observed and suggest that $S1P_5$ agonism reduces inflammation of brain endothelium. The study also suggested that $S1P_5$ is involved in $S1P_{1,3}$ expression since $S1P_5$-deficient brain EC also exhibited a substantial reduction of $S1P_{1,3}$. [80]

1.6. Sphingosine Kinase and Sphingosine-1-Phosphate in Disease and Disorder

Over expression of SphK1 and/or SphK2 and S1P has been implicated in a multitude of diseases. A selection of these disorders and diseases will be summarized in the following sections.

1.6.1. Inflammation

Numerous studies have shown that sphingolipid signaling is involved in inflammatory responses via several different mechanisms (Figure 1.6).[81, 82] TNFα is a pro-inflammatory cytokine that can activate SMase to increase Cer production.[83, 84] Cer has been found to upregulate nuclear factor –κB (NF-κB), a pro-inflammatory transcription factor that transcribes genes for pro-inflammatory cytokines, chemokines and enzymes including interleukins 1β, 6, and 8 (IL-1β, IL-6, IL-8), monocyte chemoattractant protein 1 (MCP1), and cyclooxygenase-2 (COX-2).[85] Activation of cytosolic phospholipase A_2 ($cPLA_2$) by Cer and ceramide-1-phosphate (C1P) can also activate COX-2.[84] [82]Upregulation of COX-2 increased formation of pro-inflammatory prostaglandin E_2 (PGE_2).[85] Other studies found that COX-2 activation induced by TNFα was dependent upon production of S1P and S1P receptor signaling.[82, 86]

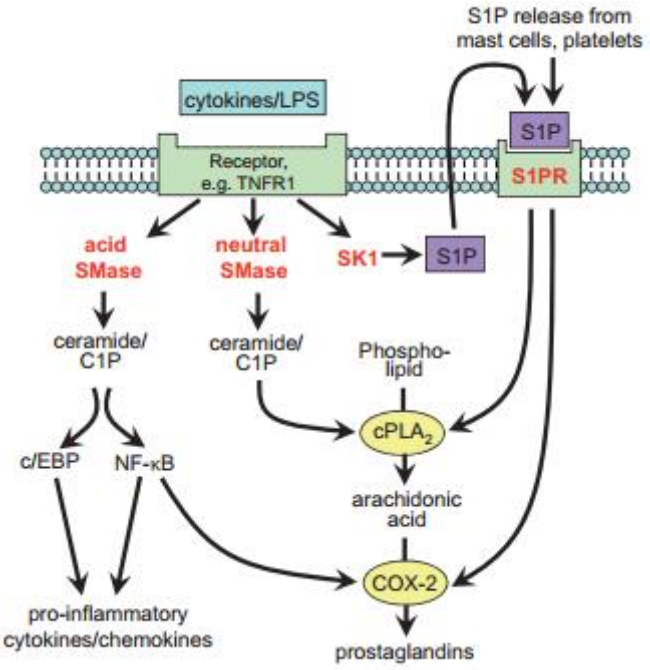

Figure 1.6. Intracellular Inflammatory Pathways Involving Sphingolipids.

Reprinted with permission from reference 81. Copyright (2009), Elsevier.

S1P is also an important metabolite involved in inflammation, but its role is dependent on the cellular environment and localization.[81, 82] Although increased activation of SphK elevates intracellular S1P levels, S1P predominantly influences inflammatory responses through S1P receptors.[82] In mast cells, SphK2 is primarily responsible for S1P formation.[64, 65] Mast cell localized $S1P_1$ is involved in cellular migration while $S1P_2$ signaling promoted degranulation.[87, 88] In other cell types, activation of $S1P_2$ increases COX-2-mediated inflammatory responses.[81, 89] SphK1 is to be involved in TNFα and COX-2 inflammatory signaling and not in lipopolysaccharide (LPS) inflammatory signaling.[90] In addition, S1P through $S1P_3$ activates cPLA2 to produce arachidonic acid.[91] $S1P_2$ was also found to upregulate COX2-mediated inflammation in corneal endothelial cells.[92]

1.6.2. Vascular Integrity

Vascular integrity is vitally important to maintain cardiovascular homeostasis, maintaining blood flow, and regulating leukocyte movement into and out of the blood stream. S1P is also a key modulator of vascular EC barrier integrity (Figure 1.7).[20, 93] A large gradient in S1P concentration exists between tissue and plasma. Interruption to this gradient causes a disruption in EC monolayer integrity and leads to vascular leakage and oedema. Plasma concentrations of S1P range from 200–400 nM.[94] In plasma, S1P is complexed with apoM and HDL or bound to Alb.[73, 93] S1P can bind to EC $S1P_1$ and induce Rac-dependent cytoskeletal rearrangements. Increasing the adherens junctions and contacts between cells and the matrix

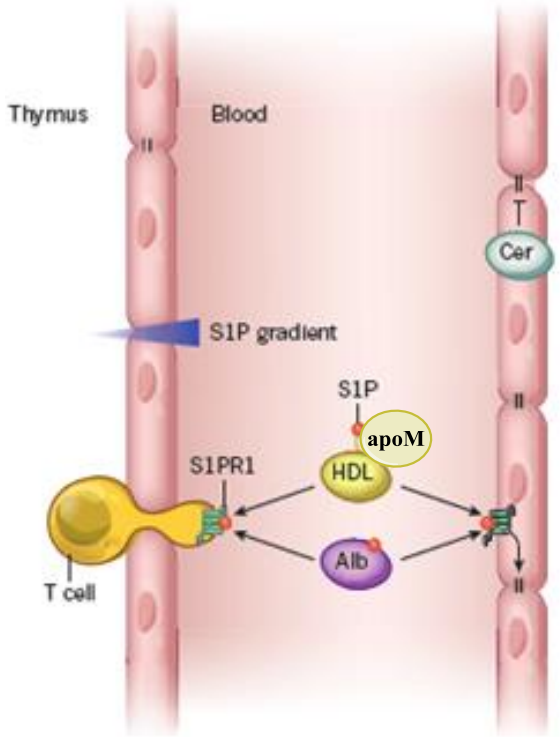

Figure 1.7. S1P and S1P1 Control Lymphocyte Trafficking and Vascular Integrity. Reprinted with permission from reference 93. Copyright (2014) Nature Publishing Group.

strengthens the integrity of the EC barrier. Decreasing the S1P gradient between tissue and plasma or increasing Cer concentration, inhibits the formation of adherens junctions, weakening the EC barrier integrity and possibly leading to barrier leakage.[20, 95] Cer initiates EC death through activation of multiple pathways including caspases, PP1, and PP2A. Additionally, endothelial nitric oxide synthase (eNOS), which is activated by the formation of Cer micro-pockets, also decreases barrier integrity.[93] During periods of inflammation, pro-inflammatory cytokines and permeating immune cells weaken the vascular barrier.

1.6.3. Asthma

Asthma is a chronic inflammatory disorder that affects over 300 million people. Its symptoms include recurring episodes of breathlessness, coughing, and wheezing.[96] The origins of asthma can be divided into two general categories: allergic and non-allergic, which are identified by the presence or absence of IgE antibodies to the allergen. During an asthma attack, the airway is permeated with helper T-cells (Th2). The Th2 cells flood the area with cytokines, such as IL-4, interleukins 5, and 13 (IL-5 and IL-13), which activate various inflammation pathways, stimulate macrophages, mast cells, and IgE production by B-cells.[96] Interactions among the inflammatory cells, cytokines, antibodies and airway cells lead to hyper sensitivity of the airway and remodeling of the airway walls.

In mast cells FcεRI activates the SphK signaling pathway by inducing SphK1 activity and Ca^{2+} mobilization.[96, 97] Activation of FcεRI also leads to SphK1-dependent mast cell degranulation.[97] S1P receptors are involved in mast cell asthma responses. $S1P_1$ and $S1P_2$ have non-redundant roles in mast cell signaling.[88, 98] $S1P_1$ is vital for cytoskeletal rearrangement and migration,[88] while upregulation of $S1P_2$ by FcεRI induces mast cell degranulation and inhibits migration.[98]

Asthma mouse models show that SphK1 is overexpressed near bronchial epithelial walls and in inflamed areas.[99] SphK inhibition or SphK knockout reduces the inflammatory response and levels of inflammatory cytokines such as IL-4, IL-5, IL-13, interleukin 17 (IL-17) and IFN-γ in bronchoalveolar lavage fluid.[99-101] A reduction in mucus production and airway hyper-responsiveness was also observed.[99-101] Increased levels of S1P have been found in bronchoalveolar lavage fluid of allergic asthma patients.[102] Further studies determined that elevated expression of SphK1 and SphK2, as well as, $S1P_2$ and $S1P_3$ induced airway hyper-responsiveness in bronchi.[103, 104] S1P increased the formation of stress fibers and contraction of airway smooth muscle cells.[105] Exogenous administration of S1P caused contraction of bronchi and increased resistance throughout the airway system.[106]

1.6.4. Cancer

French *et al*. compared the expression level of SphK in tumor and adjacent normal tissue in a wide variety of cancer types including cancers of the breast, colon, kidney, lung, ovary, rectum, stomach, and uterus.[107] In each type of cancer, SphK was found to be upregulated with expression levels approximately 190–300% greater than in normal tissue.[107] Upregulation of SphK results in increased levels of intracellular S1P. *In vivo* assays of cells transfected with human SphK cDNA have displayed a wide range of SphK expression from 12–800 fold, with only a 4–8 fold increase in intracellular S1P levels.[108] Despite the increase in S1P, there was no noticeable increase in extracellular S1P levels, indicating that overexpression of SphK does not directly correlate to increased extracellular S1P levels.[47, 108] Proliferation of cells possessing increased S1P concentrations was observed through enhanced cell growth for up to 7 days, anchorage-independent growth, increase in colony size and a 20–50 fold increase in number of colonies.[108] Proliferation of the cells continued after saturation density had been obtained

suggesting that contact inhibition no longer restricted cellular growth.[108] Cells with increased S1P concentrations have been shown to produce tumors in mice.[108]

SphK1 has been associated with key pathways involved in cancer such as Ras-dependent formation of fibrosarcoma.[108] A common cancer mutation, K-RasG12V, was found to increase SphK1 activity and promote translocation of SphK1 through Raf, mitrogen activated protein kinase kinase (MEK), and ERK signaling to the plasma membrane from the cytosol.[49] Once located at the plasma membrane, SphK1 can generate S1P and activate $S1P_2$. S1P–$S1P_2$ binding can leading to increased expression of transferrin receptor 1 (TFR1).[109] SphK1-mediated cell proliferation, survival and fibroblast transformation are reduced by TFR1 inhibition.[3] Systemic SphK1 generated S1P, not tumor-derived S1P, increases metastasis.[110] Transforming growth factor β (TGF-β), elevated SphK1, S1P and $S1P_2$ activation have been correlated with increased metastasis and cell viability.[111, 112] SphK1–S1P–$S1P_1$ signaling is associated with pro-inflammatory NFκB and cytokine IL-6 production and activation of transcription factor STAT3. In this pathway, which has been associated with chronic inflammation and colon cancer, S1P acts as the driving force in a signaling amplification.[113, 114] $S1P_3$, SphK1 generated S1P, and ERK1/2 are associated with a signaling amplification loop that promotes progression of ER-positive Michigan Cancer Foundation-7 (MCF-7) breast cancer.[115] In MCF-7 cells, S1P activation of $S1P_3$ was also found to increase translocation of SphK1 to the plasma membrane.[115]

Other studies have linked SphK1 activation to tumor neovascularization via *paracrine* angiogenesis and lymphangiogenesis, as well as cell migration of breast and glioma cancer cells.[116] Reduced S1P levels via reduction of SphK1 reduced tumor incidence, multiplicity, and volume, while increasing cell apoptosis in head and neck squamous cell carcinoma.[117] SphK1

and S1P have also been correlated with chemotherapeutic resistance. In prostate cancer cells, S1P was found to induce resistance to chemotherapy and radiotherapy.[111]

SphK1 and SphK2 display non-overlapping, non-redundant functions in tumor cells. A study of SphK1 and SphK2 siRNA in various cancer cell lines determined that SphK1 and SphK2 stimulate different effects on a variety of signaling proteins including p21, p53, ERK1/2, focal adhesion kinase (FAK), and VCAM1.[118] Reduction of SphK2 was found to have a greater proliferative effect on the cancer cells than SphK1 reduction. Inhibition of SphK2 is associated with apoptosis, as well as reduced cell growth and cell cycle progression in prostate cancer.[118] Additional studies have linked SphK2 and the regulatory Myc pathway. In B-cell acute lymphoblastic leukemia, SphK2 regulates Myc expression through an S1P-dependent HDAC1/2 inhibitory mechanism.[119] SphK2 reduction has also been related to reduced Myc levels and slower disease progression.[119, 120] In a study of MCF-7 breast cancer, SphK2 reduction was shown to reduce cell growth, and an increase in anti-tumor phenotype.[121] Tumors also displayed elevated expression of pro-inflammatory indicators such as TNFα, and IL-12 and reduced expression of anti-inflammatory indicators such as IL-10.[121]

1.6.5. Relapsing Remitting Multiple Sclerosis

Multiple sclerosis (MS) is a chronic inflammatory autoimmune disorder of the central nervous system. MS is a neurodegenerative disease that impairs physical and cognitive functions, as well as causing other symptoms including pain, fatigue, and depression.[122-124] MS is believed to be caused by autoimmune lymphocytes and T-cells that are translocated to the blood and are able to cross the blood-brain barrier. Once in the central nervous system, the lymphocytes cause inflammation and neurodegeneration via axonal damage, demyelination, and gliosis.[125, 126] During the course of the disease, recurring inflammatory attacks prevent repair mechanisms from

repairing all of the damage. This leads to incomplete recovery and a buildup of cellular damage and is known as relapsing remitting multiple sclerosis (RRMS).[123]

Numerous studies have implicated S1P signaling in MS. The white matter of MS patients contains elevated Sph and depressed SM and S1P levels;[127, 128] however, S1P levels are elevated in cerebrospinal fluid.[129] The increased extracellular S1P levels can increase S1P receptor pro-inflammatory responses. Other studies found increased expression of $S1P_1$and $S1P_3$ in astrocytes from MS lesions,[130] and that under inflammatory conditions, SphK1 and $S1P_3$ are upregulated in astrocytes.[131] $S1P_5$ expression has also been found to be reduced in demyelinated MS lesions.[132]

The S1P signaling pathway has attracted attention as a therapeutic target due to the dysregulation observed in MS. Application of MS drug Fingolimod (FTY720, Figure 1.12) promotes remyelination through $S1P_5$ signaling pathways.[133] Additional studies employing selective S1P receptor agonists show that chemokine (C-X-C motif) ligand 1 (CKCL1) cytokine release is regulated by S1P–$S1P_3$ signaling in astrocytes and not $S1P_1$.[54, 131] $S1P_1$ has been associated with lymphocyte egress from lymph nodes via chemokine receptor 7. Fingolimod acts as an antagonist for $S1P_1$ and prevents chemokine receptor 7-positive lymphocyte egress.[12, 123, 134] Fingolimod has also been shown to enhance pulmonary endothelial barrier function independent of $S1P_1$.[135]

1.6.6. Fibrosis

In general, fibrosis is defined as an imbalance in the formation and degradation of extracellular matrix (ECM) components which leads to tissue scarring and damage to organ structure, which can lead to organ failure.[136] This imbalance can be initiated by acute injury to tissue as a result of chemical, inflammatory, physical, or viral stimulators.[137] Typically, acute

injury initiates normal repair processes and regeneration of tissues; however, persistent or chronic irritation or injury can inhibit the repair processes leading to fibrosis.[137] Fibrosis can affect a wide range of tissues including heart, kidney, liver, lung, retinal pigmented epithelial cells, and skin.[136-139]

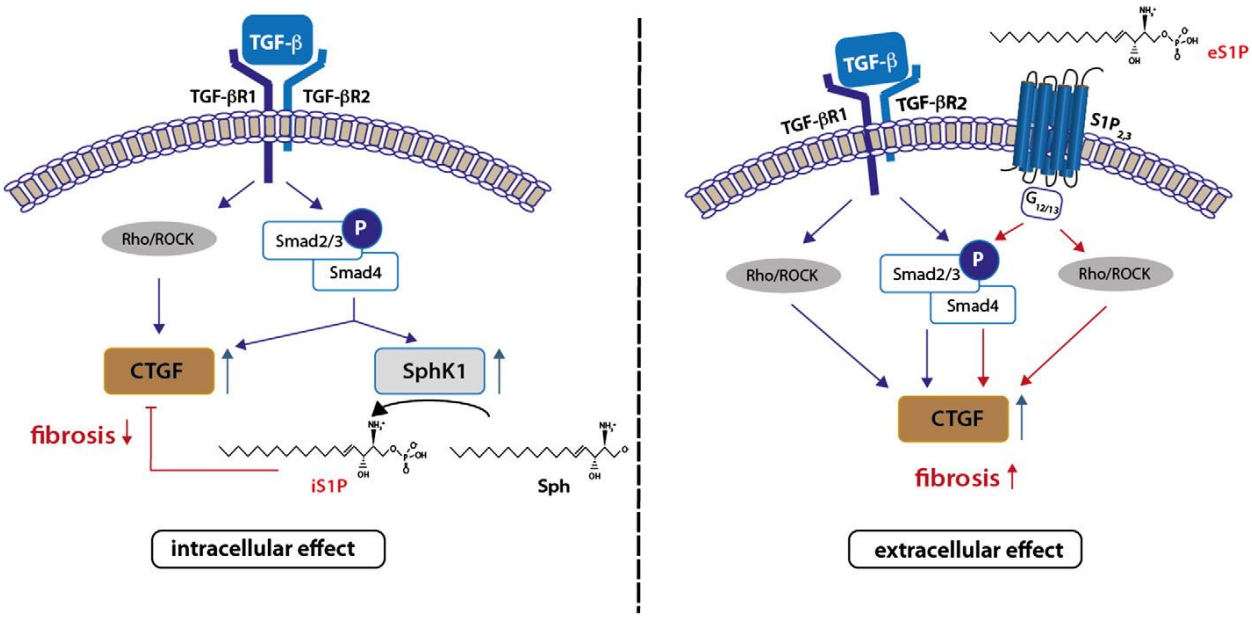

Figure 1.8. The Janus-faced Effects of Intracellular and Extracellular S1P on the Expression of Pro-fibrotic Connective Tissue Growth Factor. Reprinted with permission from reference 137. Copyright (2013), Elsevier.

S1P has been described as a Janus-faced mediator of fibrosis since it is involved in pro-fibrotic and anti-fibrotic pathways depending upon its localization (Figure 1.8).[137, 138] In fibrotic conditions, stimulation of TGF-β activates the Rho/Rock and Smad2/3 pathways, which in turn activates connective tissue growth factor (CTGF). This leads to an increase in ECM production. Intracellular S1P (iS1P) is an anti-fibrotic metabolite since it inhibits CTGF reducing ECM production.[137-139] Once exported outside the cell, extracellular S1P (eS1P) is a pro-fibrotic

metabolite. Binding of eS1P to $S1P_{2-3}$ activates the downstream Rho/Rock and Smad 2/3 pathways, leading to upregulation of CTGF and an increase in fibrosis.[137] $S1P_1$ has an important role in pulmonary fibrosis as a result of its role in maintaining endothelial barrier integrity. While acute stimulation of $S1P_1$ has been shown to improve barrier integrity and decrease fibrosis, chronic stimulation via $S1P_1$-selective agonist **AUY945** (Figure 1.12), was found to increase lung injury and fibrosis.[34, 140]

1.6.7. Alzheimer's Disease

Neurodegenerative conditions such as brain ischemia, hypoxia and inflammation, as well as Alzheimer's disease (AD) have been associated with perturbed lipid levels.[141, 142] AD is a severe, progressive form of dementia. The exact cause and mechanism of AD is unknown; it is more common in the older population. One key pathological indicator of AD is the formation of beta-amyloid plaques in extracellular space.[143] Recent studies have found that SphK2 is overexpressed in the brain of AD patients.[21, 144] Inhibition of SphK2 diminished beta-secretase 1 (BACE1) activity, a rate limiting enzyme in amyloid-peptide production.[144] This study suggests that S1P formed by SphK2 regulates BACE1 activity and increases the production of beta-amyloid plaques. SphK1 can produce the same effect; however, SphK2 has a greater effect on reducing BACE1. Other studies found that beta-amyloid peptide fragment 23–35 (Aβ25–35) reduced expression of pro-apoptotic Bcl2-like protein 4 (Bax) and increased expression of proliferative Bcl2 proteins. Toxicity associated with Aβ25–35 is caused by the inhibition of SphK1 and increased apoptotic-Cer levels.[145, 146]

1.6.8. Sickle Cell Disease

Sickle cell disease (SCD) is an inherited red blood cell disorder. It is estimated that SCD affects approximately 100,000 Americans and millions of people worldwide.[147] SCD is

predominately found in the middle-east, Caribbean, Central America, Africa and Mediterranean.[147] While normal red blood cells are round, red blood cells from a person suffering from sickle cell disease are "sickled" or crescent shaped. This alteration to the cellular shape reduces the amount of oxygen the cells can transport and hinders the ability of the sickled cells to flow through blood vessels, where they can form a clog, impeding blood flow. These clogs can cause pain, acute chest syndrome and stroke.[147]

In 2014, a study was published that identified increased levels of S1P and SphK1 expression in red blood cells and plasma from both SCD patients and an SCD mouse model. In a SCD mouse model, a SphK1 selective inhibitor (**PF-543**, Figure 1.16) reduced red blood cell S1P levels. Surprisingly, there was also a substantial decrease (approximately 75%) in the amount of sickled cells.[148] The mechanism by which S1P signaling promotes the signaling of red blood cells has not yet been elucidated.

1.6.9. Diabetes

Diabetes is a complex disease in which pancreatic β-cells fail to produce insulin.[149] In type 1 diabetes, the immune system attacks the β-cells, leading to a reduction of insulin levels. Type 1 diabetes patients develop the disease early in life and require daily doses of insulin. Conversely, type 2 diabetes, which accounts for approximately 90% of diabetes cases, is characterized by hyperinsulinemia or an over production of insulin.[149] This eventually leads to β-cell failure. Patients with type 2 diabetes are noninsulin dependent; however, insulin treatments may be required to manage glycemic levels. Type 2 diabetes is frequently diagnosed later in life and associated with other health risk factors and complications such as cardiovascular disease, kidney failure, obesity, neuropathy and retinopathy.[149]

SphK1 and 2 play a complex role in diabetes. A relatively recent study found that mice genetically lacking SphK1 (SphK1$^{-/-}$) and fed a high fat diet experienced an approximately 3-fold reduction of insulin when compared to wild type (WT) mice. The SphK1$^{-/-}$ mice also had a 50% decrease in the mass of β-cells while WT mice had an 140% increase in β-cells mass.[150] These results suggest that a loss of SphK1 predisposes diet-induced obese mice to the onset of diabetes. Mice overexpressing SphK1 and fed a high fat diet exhibited reduced Cer levels and improved insulin sensitivity.[151] In addition to being a pro-apoptotic metabolite, Cer induces insulin resistance.[151]

Another study investigating the role of SphK2 found that high fat diet fed mice overexpressing SphK2 displayed improved hepatic insulin signaling which improved glucose tolerance and insulin sensitivity.[152] This study also found that ER stress activators such as tunicamycin and lipopolysaccharides caused transcriptional activation of SphK2 via activating transcription factor 4 (ATF4). Upregulation of SphK2 increased S1P levels, and increased fatty acid oxidation in the liver by up-regulating fatty acid oxidizing genes.[152]

1.6.10. Infectious Diseases

As discussed previously, SphK and S1P have been implicated in a variety of disorders and diseases (Figure 1.9). More recently, studies have shown that the Sph–S1P signaling pathway is dysregulated by a variety of infectious agents.[153] Since S1P metabolism exists as a tipping point between cell survival and apoptosis and is implicated in a variety of downstream signaling pathways, alteration of S1P metabolism by either deactivation of SphKs or altering S1P production can have a substantial impact on the survival of the pathogen.

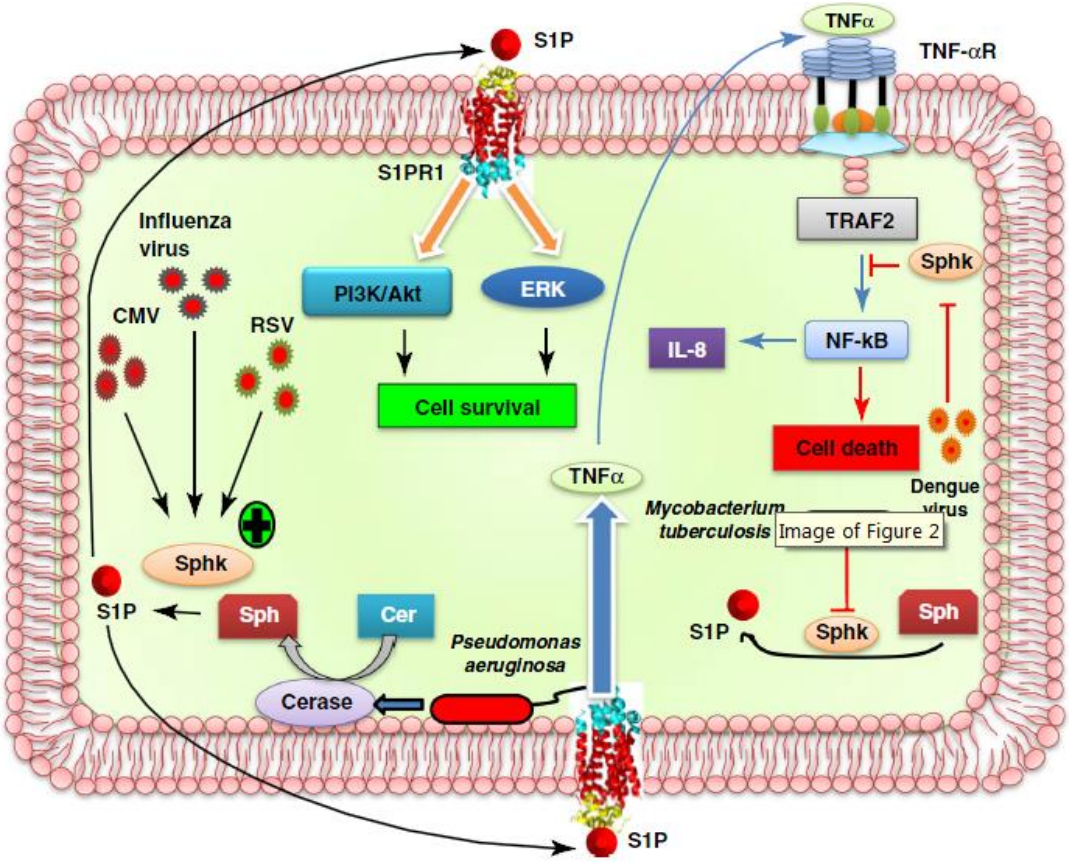

Figure 1.9. Methods in which Infectious Pathogens Manipulate Sphingolipid Signaling. Reprinted with permission from reference 153. Copyright (2016), Elsevier**.**

1.6.10.1. Viral Infections

Every year, viral infections cause serious illness, hospitalization, death and substantial medical costs. Multiple studies have reported that the S1P signaling pathway becomes dysregulated during viral infection (Figure 1.9).[153] Dengue virus (DENV) is a mosquito borne pathogen that causes dengue fever.[154] Bovine viral diarrhea virus (BVDV) is known to cause a variety of disorders in cattle.[155] Both DENV and BVDV are from the virus family *Flaviviridae* and have been found to inhibit the catalytic activity of SphK1.[156, 157] DENV inhibition of SphK1 has been associated with the 3′-untranslated region of DENV-2 RNA.[154] It is believed that the reduction of SphK1 activity is the result of DENV-2 binding to eukaryotic elongation factor 1A

out-competing the binding of SphK1.[154] SphK1 inhibition has been reported to increase cell death of infected cells.[154] This effect is believed to be the result of altered TNF-α signaling.[156] BVDV inhibits SphK1 activity by directly binding nonstructural proteins 3 and 2–3 (NS3 and NS2–3) to SphK1.[155, 157] SphK1 inhibition by BVDV resulted in elevated viral RNA expression.[157] The role of SphK and S1P signaling pathways in other Flaviruses including Zika, West Nile, Tick-borne encephalitis, and yellow fever, have yet to be determined and may be new potential therapeutic targets to treat infection.

In contrast, infections caused by the influenza virus, measles virus (MV), and human cytomegalovirus (HCMV) have been shown to possess an increase in SphK1 activation and protein levels.[158-161] Studies employing SphK1 inhibitors have determined that the SphK1 activation has a direct impact on viral growth and gene expression.[161] SphK inhibition reduced activation of NFκB activation by MV. It is believed that intracellular S1P is a vital signaling molecule for MV replication.[160] Respiratory syncytial virus increased S1P production via activation of SphK, and ceramidase.[162] S1P in turn activates the AKT-ERK pathway which increases viral replication and cell survival.[162]

SphK inhibition during influenza infection was found to reduce synthesis of viral RNAs and proteins, as well as virus-induced NFκB activation.[158] SphK also alters ERK, AKT, and p90 ribosomal s6 kinase (p90RSK) phosphorylation.[158, 163] SphK activation is correlated to the activation of Ran-binding protein 3, a cofactor of chromosome region maintenance 1, and is involved in nuclear export of the viral ribonucleoprotein complex.[158] These results suggest that SphK is a pro-viral regulatory factor.[163] $S1P_1$ signaling is also altered with influenza infection.[164] Influenza infection results in a cytokine storm including: IFN-α, IL-6, TNFα, IFNγ.[164, 165] Downregulation of $S1P_1$-mediated cytokine and chemokine production was shown to increase

survival of infected mice while maintaining neutralizing antibody and cytotoxic T-cell responses.[165-167]

While many viruses have been associated with SphK1, some viruses have been shown to dysregulate SphK2 activity. Chikungunya virus (CHIKV) is a mosquito-borne alpha-virus within the Togavirus family.[168] Inhibition of SphK with dual inhibitor **SKI-II** (Figure 1.14) reduced CHIKV infection by 20% at 10 μM while SphK2 selective inhibitor **ABC294640** (Figure 1.14) reduced CHIKV infection by 60% at 10 μM.[168] The SphK2 selectivity for CHIKV was recapitulated in knockout studies of SphK1 and 2 gene expression. The study also showed that CHIKV RNA and nonstructural proteins co-localize with SphK2 during infection, suggesting that SphK2 may have a role in viral replication and propagation.[168] SphK2 has also been associated with Kaposi's Sarcoma-associated Herpesvirus (KSHV).[169] Selective inhibition of SphK2 was found to induce apoptosis in KSHV infected cells via reduced viral gene expression and to be an important regulator in viral latency.[169]

1.6.10.2. Bacterial Infections

The predominant focus of S1P signaling related to bacterial infections has focused on intracellular bacteria such as *Mycobacterium tuberculosis* and *smegmatis*, *Clostridium perfingens, Pseudomonas aeruginosa*, *Yersinia pestis* and *Borrelia burgdorferi* (Figure 1.9).[153, 170, 171] In a study of *M. tuberculosis,* the causative agent of tuberculosis, and *M. smegmatis,* a fast growing, non-pathogenic mycobacterium, S1P possessed antimicrobial activity for both species. This activity leads to the intracellular killing of the bacteria and is facilitated by phospholipase D.[171] Infection with *M. tuberculosis* reduced S1P levels in patients compared to uninfected controls.[172] Treatment with S1P via intravenous injection reduced bacterial growth by 3-fold 5 days after infection.[171, 172] Upstream metabolite Sph had no noticeable effect on bacteria

growth.[171] Additional studies of *M. tuberculosis* found that infection inhibited macrophage maturation, by inhibiting SphK1 and reducing cytosolic Ca^{2+} levels.[173, 174] In *M. smegmatis* infected macrophages, SphK1 induced inflammatory responses including ERK1/2 activation and TNFα production.[174, 175]

Another bacterium that has been associated with the S1P signaling pathway is *Yersinia pestis. Y.pestis* is a gram-negative bacteria that causes the bubonic plague.[176] Infection is characterized by swollen lymph nodes or buboes. Treatment of *Y. pestis* infected mice with **FTY720** (S1P receptor agonist, Figure 1.12) and **SEW2871** ($S1P_1$-selective agonist, Figure 1.12) reduced *Y. pestis* infection significantly. Reduction of $S1P_1$ also limited progression of *Y. pestis* from primary to secondary lymph nodes after peripheral infection and limited disease progression from the bubonic state to the systemic (pneumonic and septicemic) disease states.[176] Treatment with S1P receptor agonists led to approximately 80% survival rate 13 days after treatment, while vehicle controls displayed 0% survival after 9 days.[176]

Clostridium perfingens is a gram-positive bacteria and a common cause of food poisoning and gas gangrene.[177] *C. perfigens* produces α-toxin that exhibits phospholipase C and SMase activities and has been known to cause necrosis, and hemolysis. In a study investigating toxin-induced hemolysis, it was determined that α-toxin stimulated hemolysis was concurrent with reduced levels of SM and increased levels of Cer and S1P.[177] Treatment with SphK inhibitors reduced S1P levels and decreased hemolysis, suggesting that hemolysis is associated with sphingolipid metabolism and S1P receptors.[177]

Ceramidase isolated from *Pseudomonas aeruginosa* was found to increase production of pro-inflammatory cytokines TNFα and IL-8 via S1P receptor signaling.[178] Elevated S1P

synthesis was also reported in human keratinocytes and is associated with increased Cer production as a result of *P. aeruginosa* ceramidase.[178]

Borrelia burgdorferi, the causative agent of Lyme Disease and Lyme Neuroborreliosis, has also been shown to elevate levels of pro-inflammatory cytokines such as IL-6,8, TNFα, chemokine (C-X-C motif) ligand 13 (CXCL13), and chemokine (C-C motif) ligand 2 (CCL2).[179-182] *B. burgdorferi* infection in Lyme Neuroborreliosis patients resulted in elevated blood S1P levels and a two-fold increase in cerebrospinal fluid.[170] More studies are needed to determine if the elevated S1P levels are due to dysregulation of SphK or S1P signaling pathways, or a byproduct of upregulation of pro-inflammation pathways.

1.6.10.3. Fungal Infections

There are very few reports of the effects of fungal infections on S1P signaling. One report of SphK1$^{-/-}$ mice with *Cryptococcus neoformans* infection found an increase in fungal load with decreased S1P levels.[183] In contrast, *C. neoformans* infected wild-type mice possessed lower fungal loads and increased survival rates.[183] Furthermore, granuloma formation is dependent upon SphK1 and S1P.[184] Extracellular S1P increased phagocytosis of anti-body labeled *C. neoformans*, but does not affect fungal growth.[185] $S1P_2$ signaling was shown to regulate phagocytic Fcγ receptors.[185] Administration of extracellular S1P restored antifungal activity in *C. neoformans* infected SphK1$^{-/-}$ mice. This observation associates the SphK1–S1P pathway with host defense against fungal infection.[184] Increased Cer levels have been associated with the formation of neutrophil extracellular traps which bind to and assist in the clearance of pathogens. While the mechanism for this observation is still unknown, it suggests that the SphK1–S1P pathway assists in host-defense mechanisms against *C. neoformans* infection and could assist in

pathogen clearance.[184, 186] Further studies are required to determine if S1P signaling can be a valuable therapeutic target to intracellular fungal infections.

1.6.10.4. Protozoan Infections

Protozoans are single-cell eukaryotic organisms that frequently avoid detection by the immune system by suppressing and altering the membrane lipid content of the host cell.[153, 187] Protozoan parasites selectively incorporate host lipids since they possess incomplete lipid metabolic machinery.[187] As a result, lipid metabolism pathways of the host organism may be a potential therapeutic target to fight infection. Infection with *Trypanosoma cruzi,* a parasite that can cause American trypanosomiasis or Chagas disease, suggests that infection causes a decrease in SphK activity and an increase in S1P lyase.[188, 189] Infection also resulted in an increase of pro-inflammatory cytokines IL-17 and TNFα.[189] Downregulation of $S1P_1$ signaling with $S1P_1$ selective antagonist **FTY720** (Figure 1.12) reduced the protective immunity of the host to *T. cruzi* infection.[190]

Decreased S1P levels were found in serum isolated from children with cerebral malaria.[191, 192] This decrease in S1P levels could lead to the dysregulation of inflammatory responses and vascular endothelium observed in cerebral malaria. S1P $lyase^{-/-}$ mice infected with *Plasmodium berghei,* a murine model for cerebral malaria, also displayed improved survival compared to WT mice.[191, 192] Application of $S1P_1$ antagonist **FTY720** (Figure 1.12), in conjunction with malarial drug Artesunate, was also able to increase survival to infection.[192] It is unclear if the decrease in S1P is the result of SphK inhibition or S1P lyase activation; however, these results suggest that the S1P signaling pathway may be a new therapeutic target in the treatment of malaria.

1.7. Therapeutic Pathways Affecting Sphingosine-1-Phosphate

Due to the complexity of S1P metabolism, there are multiple avenues that can be explored as potential therapies. There are two ways to stop the proliferative effects that result from the production of S1P in the cell and the downstream actions caused by its interactions with S1P receptors (Figure 1.10). The first way is to alter the level of S1P *in vivo* through the use of SphK inhibitors, which prevent the phosphorylation of Sph to S1P. The second method is to block the binding of S1P to the S1P receptors, thereby preventing any downstream effects. This can be done through the use of S1P receptor agonists that can internalize and degrade the receptor to prevent binding or by the use of an antagonist. These compounds may work on one or more S1P receptors as an agonist, antagonist, or a combination of both.[14] The compounds may also display agonistic effects on some receptors while displaying antagonistic effects on others.

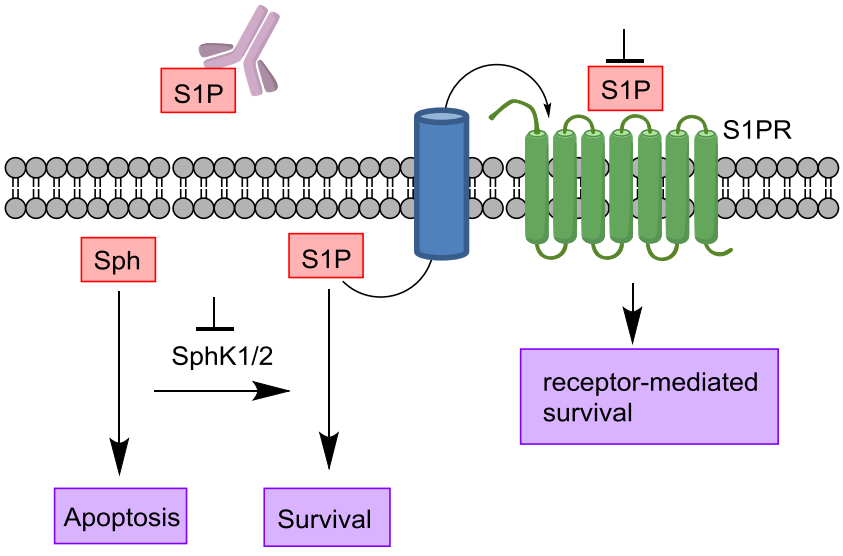

Figure 1.10. Methods of Targeting the S1P Signaling Pathway

1.7.1. Monoclonal Antibodies

Monoclonal antibodies (mAb) are monospecific in that they are produced by identical immune cells and possess a monovalent affinity for a specific substrate. Use of monoclonal antibodies provides a direct approach to alter extracellular S1P levels while avoiding some limitations presented with S1P receptor agonists and antagonists and SphK inhibitors. Two mAbs have been created for S1P, **LT1002**/Sphingomab™ and **LT1009**/Sonepcizumab™.[193, 194] Sphingomab™ is a murine derived S1P-mAb that has been shown to reduce tumor growth in multiple cell lines including MDA MB-231 and MDA MB-468 breast cancer, SKOV3 ovarian cancer, as well as a subcutaneous zenograft model with lung adenocarcinoma A549 cells.[195] The reduction in tumor growth is attributed to Sphingomab™ blocked EC migration and capillary formation, as well as Sphingomab™ inhibition of VEGF and basic fibroblast growth factor (bFGF) initiated blood vessel formation. Sphingomab™ reduced S1P-induced proliferation and caused up to a 4-fold reduction of proangiogenic cytokines levels.[195]

Following the promising results of Sphingomab™, a human derived version, Sonepcizumab™, was produced.[193] Since humanized antibodies are less likely to stimulate an immune response, they are a more attractive therapy. A competition enzyme-linked immunosorbent assay (ELISA) with a screen of structurally similar lipids showed that lysophosphatidic acid (LPA), phosphatidylserine (PS), Cer, Sph, dihydrosphingosine, dihydrosphingosine-1-phosphate, and others, Sonepcizumab™ and Sphingomab™ have been have high affinity and specificity for S1P.[193] In a phase I clinical trial in patients with advanced solid tumors, Sonepcizumab™ was found to have a half-life of 4 days and cause no serious adverse effects.[196] The mAb was well tolerated at high dosing levels (100 mg/kg) in cynomolgus monkeys.[196] Sonepcizumab™ was also found to block the release of proangiogenic and

prometastic cytokines, specifically IL-8.[193, 195] When a dose of Sonepcizumab™ was administered 1 day prior and 6 days after laser photocoagulation treatment, choroidal neovascularization (CNV) lesion volume was reduced by 98% 14 days after injury.[193]

The binding mode of Sonepcizumab™ to S1P was examined in a crystal structure of a fragment antigen binding (Fab) fragment and S1P (Figure 1.11).[197] This crystal structure revealed a unique binding mode in which S1P complexes to Sonepcizumab™ in a series of complementary electrostatic interactions. One oxygen atom from the S1P phosphate forms electrostatic interactions with two bridging Ca^{2+} atoms. These Ca^{2+} atoms also form trivalent interactions with the Fab.[197] The C2-amino group of S1P participates in hydrogen bonding interactions GluL-50 on an amino acid side chain of the Fab, suggesting that this interaction is vital for S1P specificity.[197] Additional van der Waals interactions occur between the aliphatic chain of S1P and multiple hydrophobic residues on the Fab. The affinity was determined to be 1.1 nM for the Fab.[194, 197] High binding affinities of 0.03-0.06 nM were found for full-length mAbs.[193, 194]

Sonepcizumab™ has been studied in preclinical trials for diabetic retinopathy, eye disorders including CNV of age-related macular degeneration (AMD), heart failure, inflammation, and multiple sclerosis.[196] A phase I trial for the treatment of advanced solid tumors (NCT00661414) was completed in December 2011 and found that Sonepcizumab™ was well tolerated at doses of up to 24 mg/kg.[198] No dose-limiting toxicities or drug-related severe adverse events were reported; however, reactions at infusion site, anemia and vomiting were reported in 3/9 patients who received the 24 mg/kg dose.[198] A second phase I trial to treat persistent pigment epithelia detachment (PED) in patients with AMD or polypoidal choroidal vasculopathy (PCV) (NCT01334255) was terminated by Lpath and Pfizer.[196] A phase 2 study of

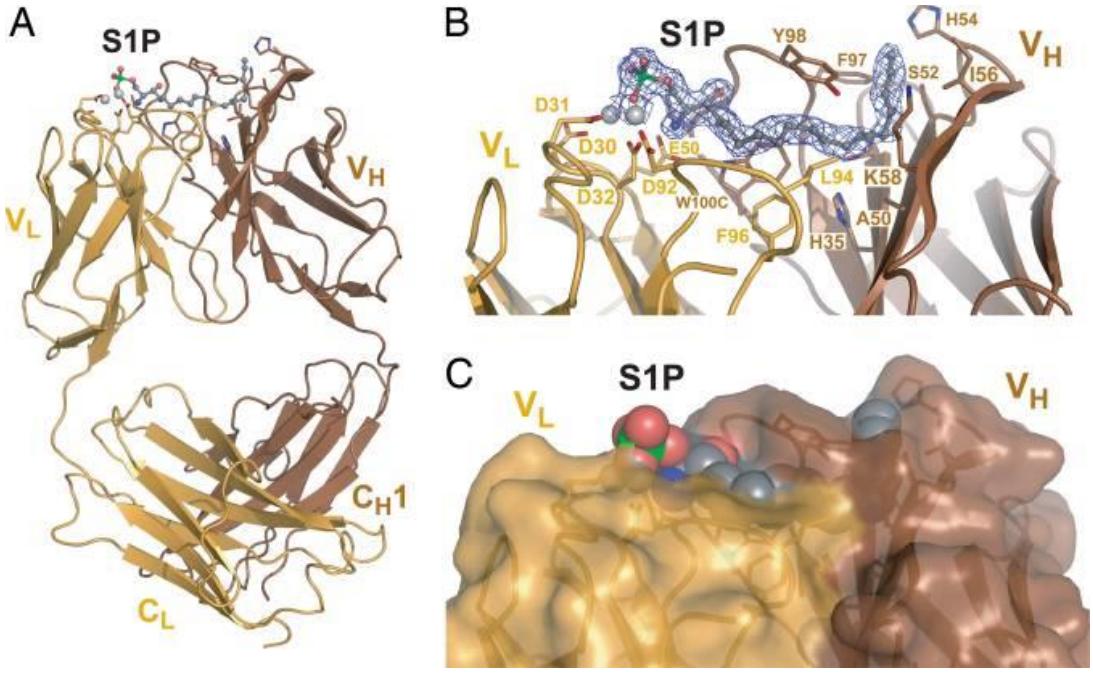

Figure 1.11. Complex of S1P with mAb Fab. X-ray crystal structure of the LT1009 Fab: S1P complex. (*A*) A ribbon diagram representation of the antibody Fab fragment. The light chain is colored gold and the heavy chain is brown. S1P is depicted as a ball-and-stick model and the 2 Ca^{2+} ions are represented as light gray spheres. (*B*) Close-up view of the S1P binding site. (*C*) A semitransparent surface representation of the Fab reveals the extent to which S1P is buried upon binding to LT1009. Reprinted with permission from reference 197. Copyright (2009) from the Proceedings of the National Academy of Sciences of the USA.

Sonepcizumab™ to treat unresectable and refractory renal cell carcinoma (RCC) (NCT01762033) was terminated in September of 2015. RCC patients did not exhibit the primary outcome measure of statistically significant progression-free survival within 8 weeks.[196] A phase I safety study of Sonepcizumab™ as treatment for neovascular AMD (NCT00767949) was completed in 2010. This study found no adverse effects in patients at doses of up to 1.8 mg/eye,

which were delivered via interavitreal injection.[199] In September 2015, a phase IIa nexus trial in patients with wet AMD was concluded (NCT01414153). Unfortunately, patients did not display any statistically significant improvement in visual acuity after 120 days of treatment with Sonepcizumab™ as either a monotherapy or as an adjunctive therapy with Ranibizumab or Bevacizumab (VEGF inhibitors).[196]

1.7.2. S1P-Receptor Agonists and Antagonists

A second method to reduce the proliferative effects of S1P signaling is through the use of S1P receptor agonists (Figure 1.12) and antagonists (Figure 1.13). These compounds interrupt ligand-binding by internalizing or degrading the receptor.

1.7.2.1. S1P Receptor Agonists

One agonist (Figure 1.12), known as **AUY954,** is an analog of Fingolimod (**FTY720**), which will be discussed in depth later. **AUY954** is a low nanomolar, selective $S1P_1$ agonist (half maximal effective concentration, $EC_{50} \approx 1.2$ nM) with a median effective dose (ED_{50}) of 0.7 mg/kg.[200, 201] Binding assays indicate that **AUY954** displays an over 280-fold greater selectivity for $S1P_1$ than any of the other receptors, however, it has shown some activity at $S1P_5$ at high concentrations ($EC_{50} \approx 340$ nM).[51, 201] **AUY954** has good oral bioavailability in Lewis rats (33%) and cynomologus monkeys (74%) and short half-lives (5.0 and 11.6 hours, respectively).[201]

Another agonist that is also selective for $S1P_1$ is **SEW2871** which has an $EC_{50} \approx 14$ nM.[201] Unfortunately, the agonist has a short half-life.[202] **SEW2871** has been shown to activate AKT, ERK1/2, and Rac signals. It has also been shown to cause internalization and recycling of $S1P_1$.[203] Modeling studies of $S1P_1$ suggest that **SEW2871** binds to the same key receptor residues as the phosphate headgroup of S1P.[203]

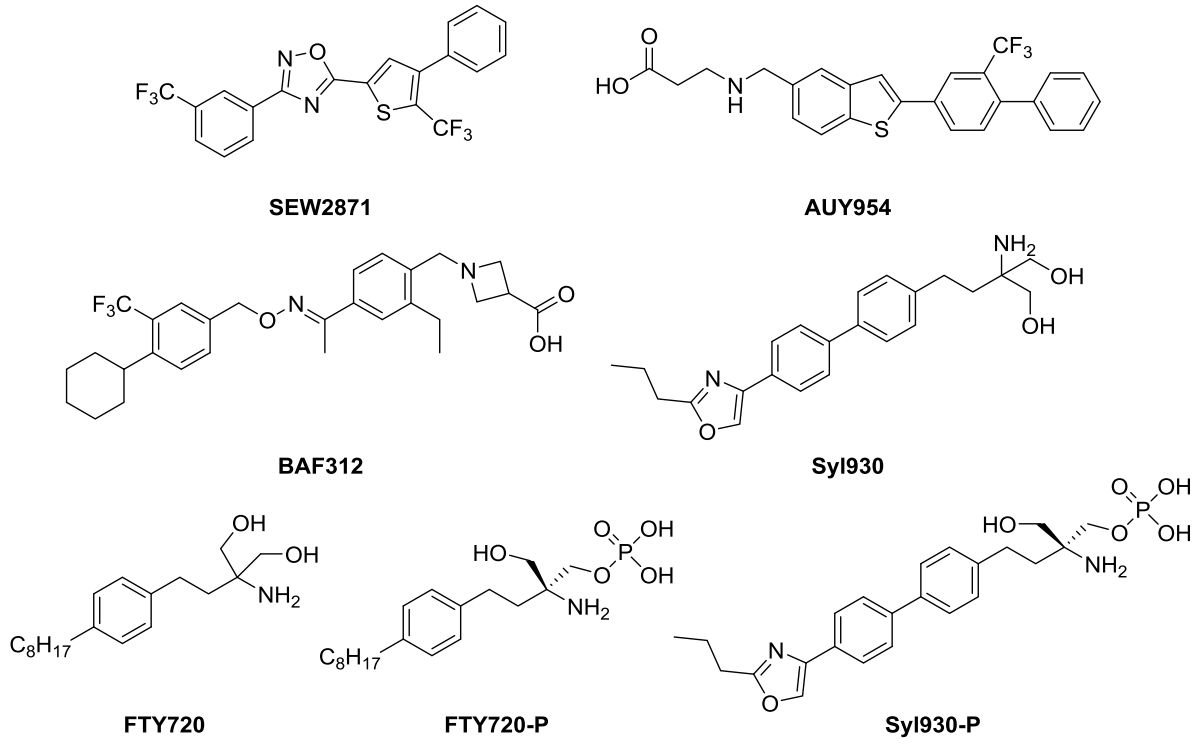

Figure 1.12. Select Sphingosine-1-Phosphate Receptor Agonists

After many years of study, Fingolimod (**FTY720**), under the trade name of Gilenya®, was approved by the Federal Drug Administration for use in the United States on September 22, 2010.[204] The immunosuppressant lead natural product, ISP-1, was isolated by Fuijita and colleagues from the fungus *Isaria sinclairii.*[205] A structural evaluation indicated that this compound is identical to myriocin, which was previously identified in 1972.[204]

FTY720 naturally displays very weak affinity for S1P receptors demonstrating no instant agonist or antagonistic effects on ligand-receptor binding or signaling. However, it was shown to inhibit S1P-mediated [Ca^{2+}] signaling at low nM concentrations.[206] *In vivo* assays and SphK null mice have shown that **FTY720**, a prodrug, is phosphorylated by SphK2 to produce **FTY720-P**, a structural analog of S1P (Figure 1.12).[33, 44, 207] Binding of **FTY720** to SphK1 can also transpire; however, phosphorylation does not occur.[208] Upon phosphorylation, an

equilibrium of 3:1 (phosphate: alcohol) is obtained in the blood.[209] This suggests that cycling of **FTY720**/**FTY720-P** exists *in vivo* much like the cycling of Sph/S1P.[13] **FTY720-P** can be hydrolyzed *in vivo* by S1P phosphatase, reproducing **FTY720**.[13, 207] Phosphorylation of **FTY720** can produce either the R or S enantiomer of **FTY720-P**; however, the S enantiomer is the predominant biologically active structure as binding of **(*R*)-FTY720-P** is weaker by over 100-fold.[210, 211] Unlike its precursor, **FTY720-P** has been shown to possess over a 1000-fold increase in affinity for all S1P receptors excluding $S1P_2$.[209] **FTY720-P** is a highly potent agonist for $S1P_{1,3,5}$, as well as, a modest agonist for $S1P_4$.[13] **FTY720-P** has an EC_{50} of 23 and 65 nM for $S1P_1$ and $S1P_3$ respectively.[212] Binding studies have shown a 20-fold increase in affinity compared to S1P. **FTY720-P** has a half maximal inhibitory concentration (IC_{50}) value of 5.9 nM for $S1P_4$, while the IC_{50} value of S1P is 95 nM.[209]

While S1P acts as an agonist and causes recycled internalization (movement of receptor into the cell upon binding to S1P, followed by the return of the receptor to the membrane) of the S1P receptors, binding of **FTY720-P** blocks the recycling pathway resulting in degradation of the receptor.[206, 213] At nanomolar concentrations, **FTY720** is able to achieve $S1P_{1,2,5}$ internalization. Receptor recovery is dependent upon the initial concentration of **FTY720** and is only obtained after a few days or weeks once the compound has been completely removed.[206] Through $S1P_1$ inhibition, **FTY720-P** is able to induce lymphopenia, a low level of white blood cell lymphocytes in the blood.[206] Unlike S1P**, FTY720** does not inhibit chemotaxis caused by binding to $S1P_3$[206], but does block $S1P_1$ chemotaxis in T-lymphocytes.[67]

FTY720 has also been evaluated as a potential anticancer drug against three types of breast cancer and two types of colorectal cancer. At a concentration of 10 μM, **FTY720** was shown to cause down-regulation of SphK1.[208] Treatment also increased caspase-3 activation and

reduced ERK1/2 phosphorylation resulting in apoptosis.[208] **FTY720** is still undergoing clinical trials to assess its safety and oral efficacy in a variety of diseases including but not limited to: children with Rett Syndrome (NCT02061137), acute stroke (NTC02002390), schizophrenia (NCT01779700), neurodegeneration in RRMS patients (NCT02575365), as a combination therapy with antidepressants in RRMS patients suffering from depression (NCT01436643) and in conjunction with radiation and Temozolomide in patients with high grade glioma (NCT02490930).

Due to the kinase selectivity and therapeutic potential of **FTY720**, many derivatives have been synthesized in the past decade. A small study of 2,2-disubstituted 2-aminoethanols by Kiuchi *et al.* found that both hydroxyl groups of **FTY720** are not always required to produce an active compound.[211] An inverse relationship was discovered between the size of the group replacing the hydroxyl and the activity displayed by the compounds.[211] Kiuchi *et al*. also found that substituting the benzylic carbon with an oxygen also decreased activity levels.[211]

BAF312 is an $S1P_{1,4,5}$ receptor agonist that was discovered by Novartis. **BAF312** has EC_{50} values of 0.39 nM, 750 nM, and 0.98 nM for $S1P_1$, $S1P_4$ and $S1P_5$, respectively and a half-life of 30 hours.[214] Screening of **BAF312** against a large panel of ion channel transporters, receptors and kinases revealed no significant activity at 1 μM indicating that off-target effects should be minimal.[215] **BAF312** also reduced $S1P_1$ expression by 91% after cells were incubated with 1 μM of **BAF312** for 1 hour. Three hours later, $S1P_1$ expression was still reduced by 87% indicating that **BAF312** causes long lasting receptor internalization.[214] *In vivo*, **BAF312** decreased circulating monocytes in WT mice.[51, 215] **BAF312** causes a dose-dependent reduction in heart rate; however, maximum heart rate reduction occurred approximately 2 hours after dosing.[214] **BAF312** does not significantly affect blood pressure at doses of up to 30.0 mg/kg/d.[76]

Unfortunately, **BAF312** was found to elicit acute bradycardia, suggesting that $S1P_1$ receptors mediate bradycardia.

More recently, $S1P_{1,3}$ agonist **Syl903** was disclosed. The phosphorylated form of **Syl903** (**Syl930-P**) is the active form. Additionally, **Syl903-P** a has good pharmacokinetic profile with an EC_{50} of 22 nM and 1230 nM for $S1P_1$ and $S1P_3$, respectively, as well as a half-life of 11.5 hours.[212] Similar to **FTY720-P**, **Syl903-P** acts as a functional antagonist by reducing $S1P_1$ expression through receptor internalization. *In vivo,* **Syl903** decreased the concentration of peripheral blood lymphocytes in a dose dependent manner. A 10 mg/kg oral dose of **Syl903** did not significantly reduce heart rate in rats, while a comparable dose of **FTY720** reduced heart rate by approximately 25%.[212] This data indicates that **Syl903** does not cause Bradycardia like **FTY720** and may be a potential new treatment for MS.

1.7.2.2. S1P Receptor Antagonists

Antagonists can also be employed to block ligand binding to S1P receptors (Figure 1.13). **W146** is a highly selective $S1P_1$ receptor antagonist (K_i = 77 nM).[216] No significant activity was observed with $S1P_{2\text{-}5}$ at higher concentrations (10 μM) of **W146**. **W146** has a half-life of 73 minutes in rats.[217] Further *in vivo* studies determined that **W146** inhibits S1P1 agonist-induced lymphocyte sequestration, increased vascular leakage and induced pulmonary edema.[216 217]

JTE-013 was originally reported as an $S1P_2$ selective antagonist ($IC_{50} \approx 17$ nM),[218] however, other studies have suggested that **JTE-013** is active at $S1P_4$ and other off-target, non-S1P receptor sites. [219-221] **JTE-013** exhibited activity at $S1P_{1,3}$ at concentrations > 10 μM.[218] **JTE-013** was found to block $S1P_2$ signaling via Rho-associated protein kinase (ROCK) and activation of phosphatase and tensin homologue (PTEN).[89]

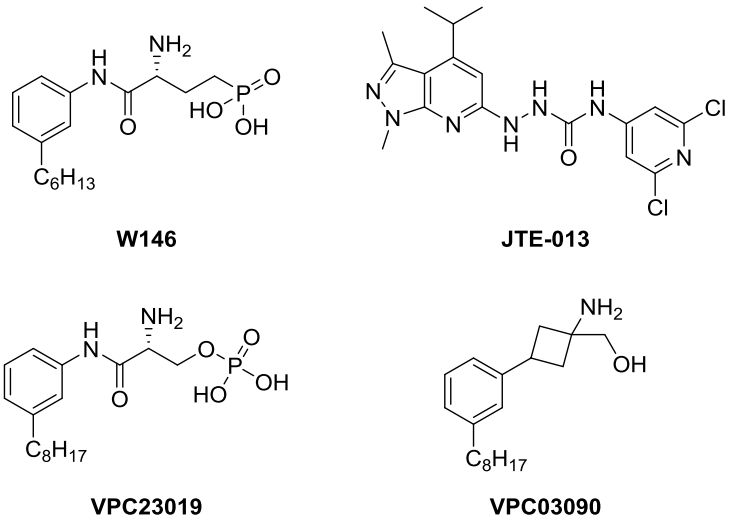

Figure 1.13. Select Sphingosine-1-Phosphate Receptor Antagonists

VPC23019 is an aryl amide analog of **W146**. It is a competitive antagonist of $S1P_{1,3}$ (pK_i = 7.86 nM and 5.93 nM, respectively).[222] **VPC23019** inhibits cellular migration induced by S1P *in vivo*.[1] **VPC23019** has no significant agonist or antagonistic effects on $S1P_2$; however, it is an $S1P_{4,5}$ agonist (pEC_{50} 6.58 nM and 7.07 nM, respectively).[222] Unfortunately, **VPC23019** has poor stability and a low *in vivo* efficacy limit.[51, 219]

VPC03090, an **FTY720** analog, was synthesized by Kennedy *et al*. after completing structure–activity relationship studies and pharmacokinetic property studies of **FTY720**.[223] Unlike **FTY720**, **VPC03090** contains a cyclobutyl, instead of an ethyl linker. This substitution removed the necessary *in vivo* recycling of **FTY720** to produce the more active (*S*)-configuration of the phosphorylated amino carbon, while maintaining a relatively similar distance between the tail and head groups. Previous studies of potential antagonists have also shown that alteration of the linker structure from an alkyl chain to a cyclopentyl moiety increased the lifetime of the compounds.[223] The octyl chain in **VPC03090** was also moved from the para to the meta position which increased the activity of the molecule.

A pharmacokinetic study of **VPC03090** and its phosphorylated form (**VPC03090-P**) found that **VPC03090** is phosphorylated by SphK2 and that **VPC03090-P** acts as an $S1P_1$ and $S1P_3$ competitive antagonist.[223] Guanosine triphosphate [γ^{35}-S] (GTP[γ^{35}-S]) binding studies showed that **VPC03090-P** is a competitive antagonist for human $S1P_1$, $S1P_3$ and mouse $S1P_1$ with K_i values of 24 nM, 51 nM, and 14 nM respectively.[223] In addition, **VPC03090-P** was shown to be an agonist of $S1P_4$ and a partial agonist of $S1P_5$, while displaying no activity for $S1P_2$. **VPC03090-P** has the greatest receptor affinity for $S1P_5$, with decreasing affinity for $S1P_4$, $S1P_1$ and $S1P_3$ respectively. Plasma analysis, completed after a 10 mg/kg oral dosing in wild type C57BL/6 mice, showed that **VPC03090** is rapidly phosphorylated, and **VPC03090-P** is long lasting with a half-life of 30 hours. Not only was **VPC03090-P** detectable in plasma after 30 minutes in roughly a 1:1 ratio (**VPC03090**: **VPC03090-P**), this ratio was present in the plasma for 6 days following the initial dose.[223]

While **VPC03090** was found to be lethal at doses larger than 30 mg/kg, treatment with **VPC03090** or **VPC03090-P** did not weaken the vascular integrity of mouse lung endothelium. **VPC03090** was also tested for anti-tumor efficacy against mouse models of Lewis lung carcinoma and 4T1 mammary carcinoma. After two weeks, the tumor size had not been significantly inhibited in the Lewis lung cancer model. On the other hand, the mammary cancer model displayed approximately 3-fold tumor reduction.[223]

1.7.3. Sphingosine Kinase Inhibitors

As more and more studies implicate S1P and SphK in a multitude of diseased states, interest in SphK as a therapeutic target has grown.[24, 29, 55, 56, 138, 146, 148, 149, 224, 225] Inhibiting SphK directly is the most efficient way to affect S1P levels and downstream metabolic processes. Unlike previous methods discussed, SphK inhibitors must also be cell permeable and

metabolically stable. The discovery of potent (picomolar-nanomolar) dual and highly selective (> 100-fold) SphK inhibitors that are metabolically stable would provide important biological tools to assist in elucidating the role(s) of SphK beyond phosphorylation of Sph to S1P. A crystal structure for either isoform did not exist until the disclosure of the SphK1 crystal structure in 2013.[226] As a result, it was challenging to completely and accurately design a molecule to fit in the binding pocket of either kinase, until recently.[227] The publication of the SphK1 crystal structure[31] has facilitated homology modeling of SphK and structure-based inhibitor design projects.[26] Over the years, SphK inhibitors with wide structural variety have been synthesized. These compounds display low to moderate potency and varying degrees of selectivity. A selection of these compounds will be discussed in the following sections.

1.7.3.1. First Generation Sphingosine Kinase Inhibitors

First generation SphK inhibitors can be divided into two subgroups, simple lipophilic analogs of Sph and non-lipophilic inhibitors (Figure 1.14). These first inhibitors had low SphK potency and poor isoform selectivity. The closest Sph analog is D,L-*threo*-dihydrosphingosine (**DHS**, safingol) in which the double bond of Sph was reduced. **DHS** is a reported competitive SphK1 inhibitor (K_i of ~3–6 μM for SphK1), but a substrate for SphK2 which can enter the sphingolipid metabolic pathway.[22] As a result, **DHS** exhibits many off-target effects, including inhibition of PKCα.[228]

One of the more widely utilized first generation SphK inhibitors is *N*,*N*-dimethylsphingosine (**DMS**). It is a dimethylated analog of Sph, only differing by the inclusion of two methyl groups on the amine. **DMS** is an inhibitor of both isoforms of SphK; however, it is a more potent inhibitor for both purified and recombinant SphK1 (K_i ~5–8 μM)[40, 45] than for SphK2 ($K_i \approx 12$ μM).[22] Studies have also shown that while **DMS** is an inhibitor of both SphK1

and 2, it is a competitive inhibitor for SphK1, and a noncompetitive inhibitor of SphK2.[22] **DMS** displays similar properties to **DHS** and inhibits PKC, ceramide kinase activity,[229] and sphingosine dependent kinase activity.[230] Treatment with **DMS** has been proven to decrease S1P formation by approximately 60% in a variety of cells, thereby causing an increase in the Cer/S1P ratio and reducing the proliferative effects caused by high S1P concentrations.[15, 229]

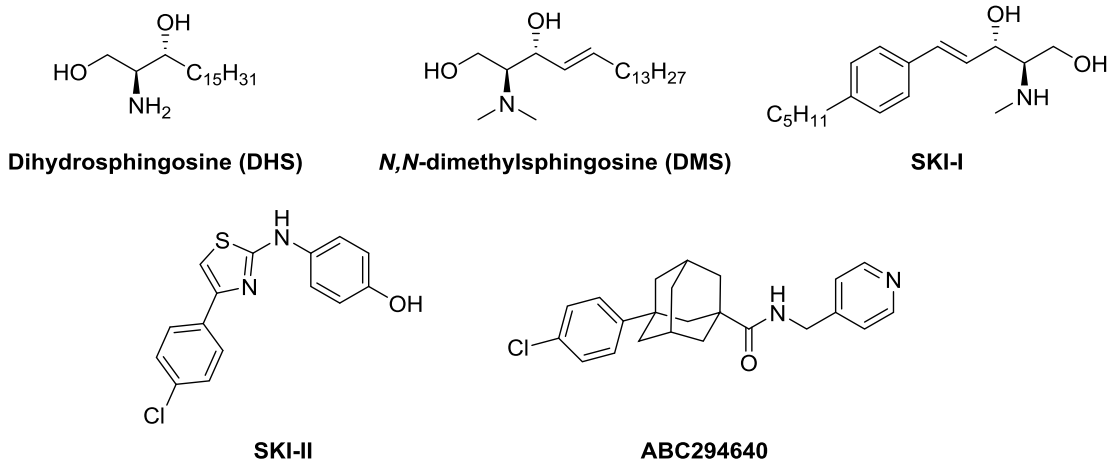

Figure 1.14. First Generation Sphingosine Kinase Inhibitors

SK1-I is another analog of Sph and **DMS,** which displays increased water solubility due to the decreased length of the lipophilic alkyl chain and phenyl moiety. **SK1-I** is selective for SphK1 ($K_i \approx 10$ μM) and has no activity for SphK2.[227] Furthermore, it displayed minimal effects when studied against a panel of kinases at a concentration of 5 μM.[227] **SK1-I** is not phosphorylated by either SphK 1 or 2. **SKI-I** also displays dose dependent growth inhibition. Through SphK1 inhibition, **SK1-I** is able to reduce the level of S1P, thereby preventing proliferation and increasing apoptotic Sph and Cer concentrations.[227] Growth in a variety of leukemia, as well as multiple glioblastoma cell lines was decreased after treatment with **SKI-I** (10 μM).[46, 227] Similar to **DHS** and **DMS**, **SK1-I** was found to be cytotoxic to leukemia cells,

specifically Jurkat-T and glioblastoma cells.[46, 227] Treatment of LN229 cells with **SKI-I** exhibited a 4-fold reduction in tumor weight and decreased vascularization.[46, 227] The molecular structure of **SKI-I** resembles **FTY720** (*vide supra*), but it possesses a shorter alkyl chain, contains a methylamine and the hydroxyl groups are located on different carbons.

A nonselective, Sph-competitive SphK inhibitor is **SKI-II** which has a SphK1 K_i value of 16 μM and SphK2 K_i value of 7.9 μM and a half-life of 15.3 hours.[31, 231, 232] Dosing with **SKI-II** has also been shown to reduce S1P levels and cause an increase in pro-apoptotic dihydroceramides (dhCers).[233, 234] **SKI-II** has been shown to inhibit SphK1 expression by initiating lysosomal degradation.[235] **SKI-II** was shown to initiate proteasomal degradation.[236] By downregulating protein expression **SKI-II** is also able to reduce agonist-enhanced SphK1 activity, specifically TGF-β and tissue plasminogen activator (TPA)-activated signaling.[235] Treatment with **SKI-II** in a mouse model of ulcerative colitis was found to reduce levels of multiple inflammatory cytokines including: TNFα, IL-1β, IFN-γ, and IL-6.[234] A crystal structure of **SKI-II** bound in SphK1 indicates that the 4-chlorophenyl moiety occupies the hydrophobic ("tail") region of the Sph binding pocket (Figure 1.15).[31] The crystal structure also indicates the presence of hydrogen bonding between the amine adjacent to the thaizole ring and Tyr196 and between the phenol hydroxyl group and Asp178.[31]

Recently, studies investigating the anticancer properties of **SKI-II** were released, which identified dihydroceramide desaturase-1 (Des1) as an additional target of **SKI-II**.[233, 237] **SKI-II** is a noncompetitive inhibitor of Des1 (K_i = 0.3 μM).[233] Through an SAR investigation, it was determined that inhibition of Des1 is predominately responsible for the antiproliferative effects of **SKI-II**.[237]

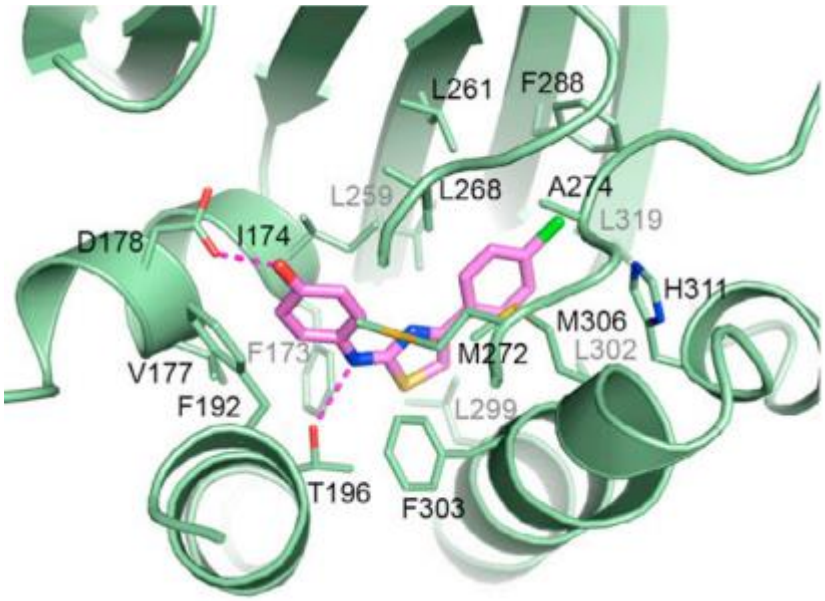

Figure 1.15. SKI-II Bound in hSphK1 Isoform 3. Reprinted with permission from reference 31. Copyright (2013) Elsevier

Another first generation SphK inhibitor is **ABC294640**. This compound is a selective SphK2 competitive inhibitor possessing a K_i value of 9.8 μM.[238] The drug is orally available with a half-life of 4.5 hours in plasma.[238] Inhibition and antitumor activity by **ABC294640** is dose dependent. Tissue cultures from a wide range of tumor cells have shown that **ABC294640** is able to reduce cellular migration and proliferation.[238] **ABC294640** was able to reduce proliferation in a variety of disease models including: Crohn's disease,[239] lupus,[240] osteoarthritus,[241] and ulceratve colitis.[234] **ABC294640** was used in a phase I clinical trial to treat patients with advanced solid tumors (NCT01488513). While this trial was completed in July 2015, the results have not been published. Participants are currently being recruited for another phase I clinical trial to evaluate the efficacy of **ABC294640** in patients with refractory/relapsed diffuse large B-cell lymphoma (NCT02229981).

Dosing with **ABC294640** was found to substantially decrease tumor growth in androgen deprivation therapy (ADT)-sensitive prostate cancer cells.[242] **ABC294640** was found to inhibit the androgen receptor (Ar) and c-Myc (Myc) pathways, which are key signaling pathways in prostate cancer disease progression in both early-stage and advanced prostate cancer models.[242] The downregulation of these pathways are the result of decreased gene expression and increased proteasome degradation.[242, 243] A greater than 3-fold increase in dihydroceramide was observed upon treatment with **ABC294640**, even in SphK2-deficient cells. This suggests that **ABC294640** may inhibit dihydroceramide desaturase (DEG).[243] **ABC294640** has also been associated with downregulation of several additional signaling proteins including: AKT, ERK, FAK, p21, p53 and STAT3.[244]

1.7.3.2. Second Generation Sphingosine Kinase Inhibitors

As interest in targeting SphK has grown, the pharmaceutical industry began to develop SphK programs. As a result, second generation SphK inhibitors contain a wider range of structural diversity and improved "drug-like" properties (Figure 1.16).

Expansion upon the **SK1-II** scaffold, led to the development analog **Amgen 82**, a potent dual SphK inhibitor (SphK1 IC_{50} = 20 nM, SphK2 IC_{50} = 100 nM).[28] **Amgen 82** incorporates a hydroxylated piperidine "head group", which mimics the interactions of the aminopropanediol of Sph. The 2-hydroxyl forms a water-assisted hydrogen-bonding network with Ser168, Gly342 and Ala339 while the 4-hydroxyl hydrogen bonds to Asp81 (Figure 1.17).[28] The thiazole rings in **Amgen 82** and **SKI-II** both occupy a similar position in the binding pocket. **Amgen 82** has moderate pharmacokinetic parameters and is reasonably bioavailable (32% at 5 mg/kg).[28] *In vivo* analysis verified that S1P levels decreased upon dosing with **Amgen 82** as expected; however, there was no noticeable effect on cell viability across 11 different cell lines including HeLa,

LN229, WM266-4, and Saos2 cells.[245] Treatment of a mouse tumor xenograph model with **Amgen 82** did not show any noteworthy effect on tumor volume.[28] These studies suggest that apoptosis and proliferation observed in cancer cells are not the sole result of decreased S1P levels.

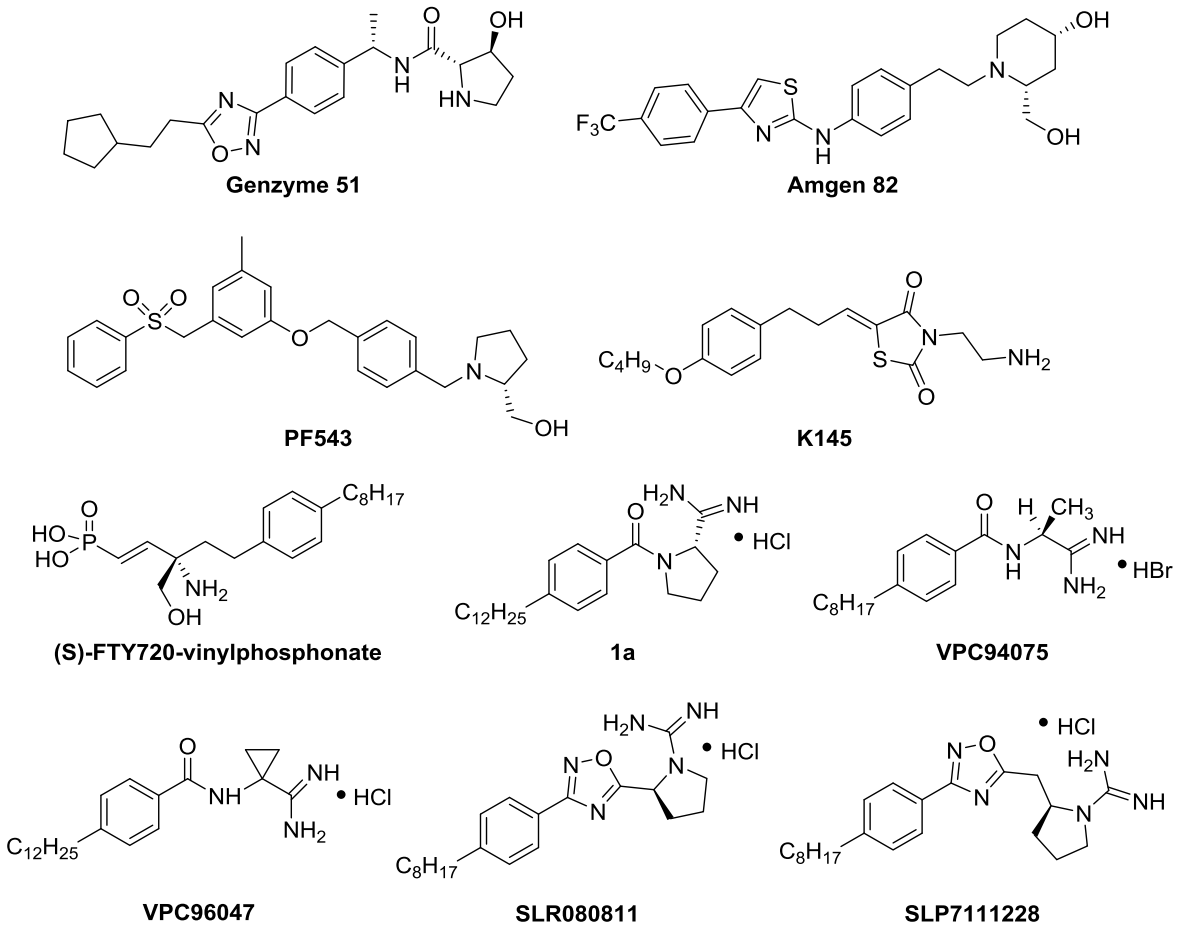

Figure 1.16. Second Generation Sphingosine Kinase Inhibitors

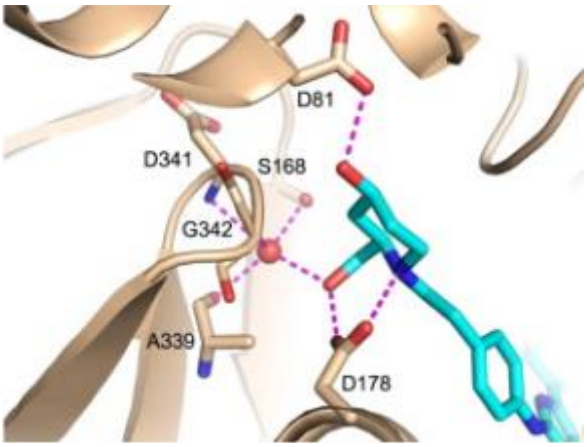

Figure 1.17. Amgen 82 Bound in hSphK1. Reprinted with permission from references 28. Copyright (2013) Elsevier.

A program to develop SphK inhibitors was also created at Pfizer. **PF-543** a potent (K_i = 3.6 nM), 132-fold SphK1 selective inhibitor first disclosed in 2012, was discovered by combining hit fragments from two separate screening projects.[246] **PF-543** is a competitive inhibitor with Sph. Screening of **PF-543** at 10 μM, against a panel of 48 protein and lipid kinases further verified the specificity of the compound. Similar to **Amgen 82**, **PF-543** incorporates a hydroxymethylpyrrolidine "head group", a cyclic isostere of the aminopropanediol head group of Sph. The crystal structure of SphK1 and **PF-543** (Figure 1.18) indicates that hydrogen bonds are formed between the "head group" nitrogen and hydroxyl to Asp264, which is known to be involved in the recognition of Sph while the terminal phenyl ring sits inside a hydrophobic pocket.[32] Overall, **PF-543** takes on a bent conformation, which has been seen with Sph and **SKI-II** bound in the SphK1 crystal structure.[31] Interestingly, treatment of head and neck carcinoma cells with **PF-543** caused a 10-fold reduction of S1P levels with no change in cell viability. **PF-543** also decreased cellular SphK1 expression; however, the effect was reversed with proteasomal inhibitor MG132. This observation suggests that **PF-543** induces proteasomal

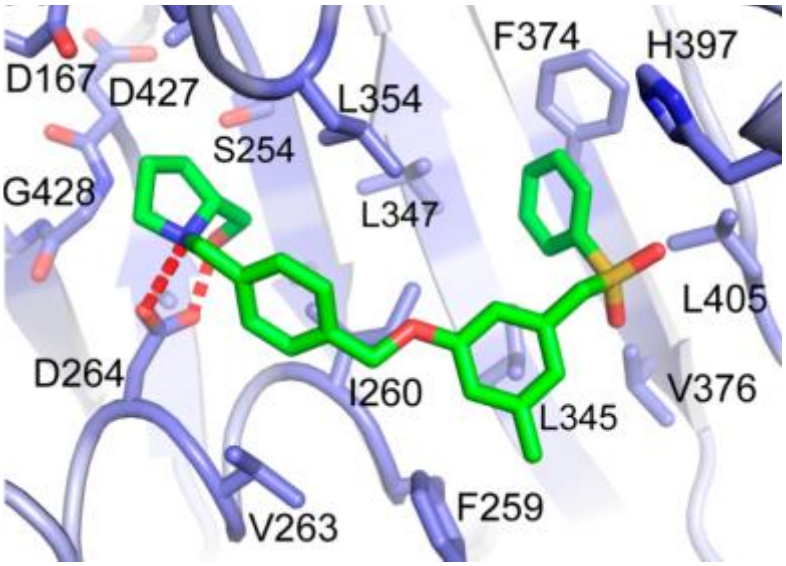

Figure 1.18. PF543 Bound to hSphK1 Isoform 2. Subtract 72 to get the equivalent residues in isoform 1 or 86 to get the equivalent residues in isoform 3 (as used in the previous structure of SphK1). Reprinted with permission from reference 32. Copyright (2014) ACS.

degradation of SphK1 upon binding.[247] **PF-543** has also been used in the study of sickle cell disease where SphK1 is over expressed. *In vivo* and *in vitro* studies indicate that **PF-543** reduces the sickling of red blood cells.[148] Unfortunately, **PF-543** had to be administered via an osmotic minipump, indicating that the compound possesses a poor pharmacokinetic profile. Nevertheless, as the most potent SphK1 inhibitor to date, **PF-543** is a vital tool for probing the S1P signaling pathway.

SphK inhibitors designed at Genzyme were disclosed in 2009 and 2010.[30, 248] Among these compounds, **Genzyme 51** has received the most attention. **Genzyme 51** is a potent (IC_{50} = 58 nM) SphK1 selective compound that did not display any significant inhibition of SphK2 at concentrations up to 10 μM.[30] Biological evaluation to determine the pharmacokinetic profile of

Genzyme 51 showed that the compound has a half-life of 7.6 hours in rat plasma and is 18% orally bioavailable.[30]

Further investigations into Sph analogs led to the discovery of **K145** by Liu *et al*.[249] **K145** is a SphK2 selective, Sph competitive inhibitor (K_i = 6.4 μM) that does not substantially inhibit SphK1 at concentrations up to 10 μM. Since **K145** is competitive with Sph, **K145** was screened for activity against ceramide kinase (CERK) and a panel of 11 other protein kinases, which verified the selectivity of **K145** at a concentration of up to 10 μM.[249] U937 cells exhibited a small decrease in S1P concentration upon treatment with **K145**. Additional *in vitro* studies showed a dose dependent, apoptotic effect on U937 cells treated with **K145**. *In vivo* mouse studies showed significant suppression of tumor growth when **K145** was administered orally or intraperitoneally. These results indicated that **K145** is an orally bioavailable, nontoxic, tumor suppressor.[249]

Upon the discovery of SphK2 specific substrate **FTY720**, multiple investigations into developing FTY720 analogs as potential SphK inhibitors were initiated. One analog of **FTY720-P**, **(S)-FTY720 vinylphosphonate**, has been shown to inhibit SphK1.[208] Like **FTY720-P**, the S-enantiomer is a more potent inhibitor of SphK1 than (*R*)-FTY720 **vinylphosphonate**.[208] While **(*S*)-FTY720 vinylphosphonate** has been shown to inhibit SphK1 by more than 80%, **(*R*)-FTY720 vinylphosphonate** only inhibits SphK1 by approximately 40%.[208] **(*S*)-FTY720 vinyl phosphonate** has also been found to surmount chemotherapeutic resistance in prostate cancer cells, possibly through the reduction of SphK1 levels.[208]

Another **FTY720** analog scaffold was developed in the MacDonald laboratory.[250-252] This scaffold incorporates a positively charged amidine "head group" which helps overcome the

lipophilic nature of the compounds caused by the long chains, and increases water solubility. Molecular docking studies of this scaffold in a SphK1 model suggest that the amidine is a bidentate chelator that binds directly to the γ-phosphate of ATP.[253] These compounds also contain an amide linker between the internal phenyl and cyclic headgroup. A potent 24-fold SphK1 selective inhibitor, **1a** (SphK1 K_i = 100 nM, SphK2 K_i = 1.5 μM) was disclosed.[253] Unfortunately, **1a** has a very short half-life (< 10 min.) and rapidly cleared *in vivo*.[252] Other inhibitors in this series of amidines include **VPC94075** and **VPC96047**.[250, 251] **VPC94075** possesses a K_i value of 83 μM for SphK1, and 33 μM for SphK2. A single 20 mg/kg dose of **VPC94075** has also been shown to reduce S1P levels for over eight hours.[250] **VPC96047,** the most potent SphK inhibitor in the series, possesses a K_i value of 0.2 μM for SphK1 and 0.3 μM for SphK2.[251]

Additional **FTY720** analog studies were launched in the Santos Laboratory and led to the discovery of **SLR080811**.[254] Similar to **1a**, **VPC94075** and **VPC96047**, **SLR080811** contains a charged guanidine polar "head group" instead of an amidine group and a 1,2,4-oxadiazole ring in place of the amide linker.[254] **SLR080811** is an 11-fold hSphK2 selective inhibitor (hSphK1 K_i = 16 μM and hSphK2 K_i = 1.4 μM).[26] In addition to switching the isoform selectivity, incorporation of the guanidine and oxadiazole moieties resulted in a compound with an improved metabolic half-life of approximately 5 hours.[255] Further biological evaluation of **SLR080811** has suggested that SphK2 has a secondary role beyond the ATP-dependent phosphorylation of Sph.[255, 256] Dosing of the U937 leukemia cell line with **SLR080811** resulted in lowered S1P levels. This observation was confirmed by monitoring the phosphorylation of exogenously added **FTY720**. Since application of **SLR080811** resulted in decreased levels of **FTY720-P**, it was concluded that the decrease in S1P was the result of SphK2 inhibition. *In vivo* mice studies of

SLR080811 indicated that SphK2 inhibition causes a rapid increase in blood S1P levels.[255, 256] This observation was not observed in similar studies with **1a, SLP7111228** (SphK1 selective), **ABC294640** (SphK2 selective) or **Amgen 82** (SphK1/2 dual inhibitors).[28, 240, 252, 254] The mechanism in which SphK2 inhibition increases blood S1P levels is still unknown and under investigation.

SLP7111228 is an **SLR080811** derivative that incorporates a methylene spacer between the pyrolidine and 1,2,4-oxadiazole rings.[254] **SLP7111228**, is a highly potent (hSphK1 K_i = 48 nM and SphK2 K_i = > 10 μM), greater than 200-fold SphK1 selective inhibitor with a half-life of 4 hours. Treatment of U937 cells with **SLP7111228** has shown a dose-dependent decrease in S1P levels. This dependency has also been described in blood S1P levels with *in vivo* rat models.[254]

1.7.3.3. Third Generation Sphingosine Kinase Inhibitors

Third generation SphK inhibitors are currently being developed and have only recently begun to appear in the literature (Figure 1.19). **MP-A08** is an ATP competitive SphK inhibitor that was discovered through *in silico* docking of small molecule libraries to a structural homology model of the ATP-binding site of SphK.[257] Unlike previously reported compounds, **MP-A08** is a modestly potent, 3-fold selective SphK2 inhibitor (SphK1 K_i = 27 μM, SphK2 K_i = 3.9 μM).[257] Dosing with **MP-A08** *in vivo*, resulted in a significant increase of pro-apoptotic Sph and Cer levels, a dose-dependent activation loss in multiple S1P activated pro-survival and proliferative pathways (AKT and ERK1/2), and activation of apoptotic associated pathways (p38 and Jun *N*-terminal kinase, JNK).[257] Double knockout and WT mouse embryonic fibroblasts (MEF) were also treated with **MP-A08**. WT-MEFs displayed a dose-dependent increase in apoptosis, while double knockout-MEFs were unaffected. These results indicate that the

apoptotic effects observed upon treatment with **MP-A08** are the result of SphK inhibition and reduced S1P levels.

Binding of **MP-A08** to SphK1 does not induce proteasomal degradation, which has been observed with Sph competitive inhibitors **SKI-II** and **PF-543**.[208, 236, 247, 257, 258] **MP-A08** was able to reduce neoplastic growth in a variety of solid cancer lines including: A549 lung adenocarcinoma cells, MCF-7 and MDA-MB-231 breast adenocarcinoma cells, BJ7-human foreskin fibroblasts and Jurkat cells. A549 human lung adenocarcinoma xenographs in mice showed a reduction in tumor volume of approximately 50%. The tumors showed significantly reduced S1P levels and vasculature (a reduction of CD31 blood vessels), suggesting that **MP-A08** induces apoptosis and blocks angiogenesis.[257]

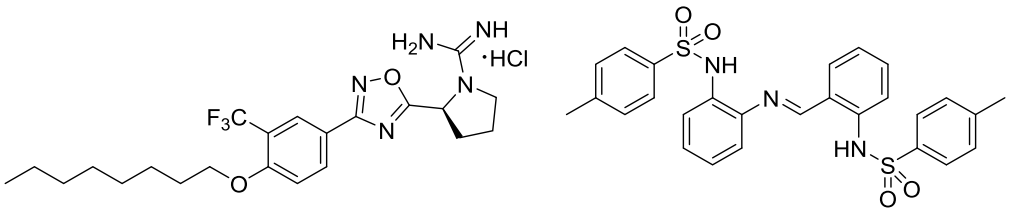

Figure 1.19. Third Generation Sphingosine Kinase Inhibitors

One third generation SphK inhibitor developed on the **SLR080811** scaffold is known as **SLM6031434** (Figure 1.19). This compound incorporates a *meta*-trifluoromethyl group on the internal phenyl ring and an ether linkage between the phenyl ring and the lipophilic alkyl chain.[259] **SLM6031434** (hSphK2 K_i 370 nm) is 23-fold selective for hSphK2.[259] Dosing with **SLM6031434** *in vitro* produces a decrease in S1P levels, while mice exhibit an increase in blood S1P concentration *in vitro*.[256] These results are in agreement with studies of less potent hSphK2

inhibitor **SLR080811**.[252] Additional third generation inhibitors are disclosed in Chapters 2–5 of this dissertation.

1.8. Conclusions

S1P is a pleiotropic lipid mediator, which is involved in a broad range of cellular processes including inflammation, migration, and proliferation. S1P is solely formed through the phosphorylation of Sph by the two isoforms of SphK (SphK1 and SphK2). As a result, SphKs are potential therapeutic targets for various diseases such as cancer, fibrosis, Alzheimer's, MS, and sickle cell disease. While the potency and selectivity of available SphK inhibitors has improved substantially, there is still a great deal of improvement to be made. In the following chapters, recent advances into third generation SphK2 inhibitors will be discussed in detail. These compounds display nanomolar to low micromolar potency and up to 111-fold SphK2. Selective inhibitors will help decipher the complex role of SphK2 in physiological and pathological states.

1.9. Dissertation Overview

Chapter 1 introduced the biological pathways associated with SphK and S1P. Physical and biological differences between SphK isoforms SphK1 and SphK2 were analyzed. The role of SphK and S1P in various diseases including cancer, fibrosis, Alzheimer's and sickle cell disease were examined. The three major methods of affecting the Cer-Sph-S1P rheostat were discussed. Finally, efforts in developing monoclonal antibodies, receptor agonists and antagonists, and a selection of current SphK inhibitors were presented.

In Chapter 2, an investigation into the "tail region" of SphK selective inhibitor **SLR080811** is presented. The synthesis and biological screening of these compounds is discussed. This SAR identifies key structural features that are essential for SphK potency and selectivity. Although a variety of structural motifs presented do not display SphK potency or selectivity, the rational for these observations is proposed. The dependency of SphK2 potency and selectivity on alkyl tail length is examined and suggests that the lipophilic binding cavity in SphK2 is substantially larger in SphK1.

Chapter 3 discloses an SAR of naphthalene-containing SphK inhibitors. Key discoveries from this SAR include **SLC5091592**, a 1.0 μM, 20-fold hSphK2 inhibitor, and **SLC5111312** a 0.90 μM dual hSphK1/2 inhibitor that contains a 3′OH on the pyrrolidine ring. Molecular modeling with an hSphK2 homology model is examined. This model proposes that hydrogen bonding to Asp211 is crucial for hSphK2 selectivity, and suggests that compounds incorporating a 3′OH on the pyrolidine ring partake in increased hydrogen bonding interactions between Asp308 and the 3′OH. This model suggests that intermolecular interaction is the source of the increased SphK1 potency observed with these compounds. Chapter 3 also employs **SLC5111312** to assist in elucidating the role of SphK2. These studies suggest that SphK2 possess a secondary role in the clearance of S1P from blood.

Chapter 4 probes the conformation of the hSphK2 binding pocket. The synthesis of a series of *N*-alkyl indoles with varying substitution of the "linker and head groups" at the C3–C6 positions of the indole ring is presented. Biological screening for activity in hSpHK1 and hSphK2, as well as, the K_i values for select compounds are discussed. Molecular modeling of the various indole scaffolds in an hSphK2 homology model suggests that hydrogen bonding to Asp residues near the ATP binding site and minimal steric interactions with Val304 and Phe548 are

key to potency and selectivity differences between the indole scaffolds. Surprisingly, the modeling studies propose a unique binding mode for the 1,3-scaffold that does not incorporate the Asp-hydrogen bonding. Additional investigations into this binding mode are presented. This investigation discloses the discovery of **SLC5101465**, a 90 nM, greater than 111-fold SphK2 selective inhibitor.

Chapter 5 expands upon the work of Chapter 4 and investigates the incorporation of non-alkyl groups on the 1,5-indole scaffold. The synthesis and biological screening for hSphK1 and hSphK2 activity is discussed. In general, these compounds are inactive in hSphK1 and frequently inhibit hSphK2 by over 40% at 1 μM inhibitor concentration in the broken cell assay. Molecular modeling of various tail groups, suggest that interactions in the bottom of the binding pocket are key for potency. This investigation also discloses the discovery of **SLC5031698**, a 280 nM, greater than 18-fold SphK2 selective inhibitor.

In Chapter 6, potential future directions for the Sphingosine Kinase project are discussed.

Finally, Chapter 7 contains the general chemical methodology, instrumentation, experimental details and characterization for all products in Chapters 2–5, as well as the general procedures for all of the biological assays. The methodology for creating the hSphK2 homology model and docking inhibitors is presented.

1.10. References

1. Takabe, K.; Paugh, S. W.; Milstien, S.; Spiegel, S., "Inside-Out" Signaling of Sphingosine-1-Phosphate: Therapeutic Targets. *Pharmacol. Rev.* **2008,** *60* (2), 181–195.
2. Huwiler, A.; Pfeilschifter, J., Altering the Sphingosine-1-Phosphate/Ceramide Balance: A Promising Approach for Tumor Therapy. *Curr. Pharm. Des.* **2006,** *12* (35), 4625–4635.
3. Pyne, N. J.; Pyne, S., Sphingosine-1-Phosphate and Cancer. *Nat. Rev. Cancer* **2010,** *10* (7), 489–503.
4. Spiegel, S.; Milstien, S., Sphingosine 1-Phosphate, a Key Cell Signaling Molecule. *J. Biol. Chem.* **2002,** *277* (29), 25851–25854.
5. Wattenberg., B. W., Role of Sphingosine Kinase Localization in Sphingolipid Signaling. *World J. Biol. Chem.* **2010,** *1* (12), 362–368.
6. Hait, N. C.; Allegood, J.; Maceyka, M.; Strub, G. M.; Harikumar, K. B.; Singh, S. K.; Luo, C.; Marmorstein, R.; Kordula, T.; Milstien, S.; Spiegel, S., Regulation of Histone Acetylation in the Nucleus by Sphingosine-1-Phosphate. *Science* **2009,** *325* (5945), 1254–1257.
7. Strub, G. M.; Paillard, M.; Liang, J.; Gomez, L.; Allegood, J. C.; Hait, N. C.; Maceyka, M.; Price, M. M.; Chen, Q.; Simpson, D. C.; Kordula, T.; Milstien, S.; Lesnefsky, E. J.; Spiegel, S., Sphingosine-1-Phosphate Produced by Sphingosine Kinase 2 in Mitochondria Interacts with Prohibitin 2 to Regulate Complex IV Assembly and Respiration. *FASEB J.* **2011,** *25* (2), 600–612.
8. Maceyka, M.; Alvarez, S. E.; Milstien, S.; Spiegel, S., Filamin A Links Sphingosine Kinase 1 and Sphingosine-1-Phosphate Receptor 1 at Lamellipodia To Orchestrate Cell Migration. *Mol. Cell. Bio.* **2008,** *28* (18), 5687–5697.

9. Alvarez, S. E.; Harikumar, K. B.; Hait, N. C.; Allegood, J.; Strub, G. M.; Kim, E. Y.; Maceyka, M.; Jiang, H.; Luo, C.; Kordula, T.; Milstien, S.; Spiegel, S., Sphingosine-1-Phosphate is a Missing Cofactor for the E3 Ubiquitin Ligase TRAF2. *Nature* **2010,** *465* (7301), 1084–1088.

10. Chipuk, J. E.; McStay, G. P.; Bharti, A.; Kuwana, T.; Clarke, C. J.; Siskind, L. J.; Obeid, L. M.; Green, D. R., Sphingolipid Metabolism Cooperates with BAK and BAX to Promote the Mitochondrial Pathway of Apoptosis. *Cell* **2012,** *148* (5), 988–1000.

11. Lynch, K. R.; Macdonald, T. L., Sphingosine-1-Phosphate Chemical Biology. *Biochim. Biophys. Acta.* **2008,** *1781* (9), 508–512.

12. Brinkmann, V.; Billich, A.; Baumruker, T.; Heining, P.; Schmouder, R.; Francis, G.; Aradhye, S.; Burtin, P., Fingolimod (FTY720): Discovery and Development of an Oral Drug to Treat Multiple Sclerosis. *Nat. Rev. Drug Discov.* **2010,** *9* (11), 883–897.

13. Brinkmann, V.; Davis, M. D.; Heise, C. E.; Albert, R.; Cottens, S.; Hof, R.; Bruns, C.; Prieschl, E.; Baumruker, T.; Hiestand, P.; Foster, C. A.; Zollinger, M.; Lynch, K. R., The Immune Modulator FTY720 Targets Sphingosine 1-Phosphate Receptors. *J. Biol. Chem.* **2002,** *277* (24), 21453–21457.

14. Brinkmann, V., Sphingosine-1-Phosphate Receptors in Health and Disease: Mechanistic Insights from Gene Deletion Studies and Reverse Pharmacology. *J. Pharmacol. Ther.* **2007,** *115* (1), 84–105.

15. Cuvillier, O.; Pirianov, G.; Kleuser, B.; Vanek, P. G.; Coso, O. A.; Gutkind, J. S.; Spiegel, S., Suppression of Ceramide-Mediated Programmed Cell Death by Sphingosine-1-Phosphate. *Nature* **1996,** *381* (6585), 800–803.

16. Lozano, J.; Berra, E.; Municio, M. M.; Diaz-Meco, M. T.; Dominguez, I.; Sanz, L.; Moscat, J., Protein Kinase C Isoform Is Critical for kB-dependent Promoter Activation by Sphingomyelinase. *J. Biol. Chem.* **1994,** *269* (30), 19200–19202.

17. Smyth, M.; Perry, D. K.; Zhang, J.; Poirier, G. G.; Hannun, Y. A.; Obeid, L. M., prICE: a Downstream Target for Ceramide-Induced Apoptosis and for the Inhibitory Action of Bcl-2. . *Biochem. J.* **1996,** *316* (1), 25–28.

18. Pettus, B. J.; Chalfant, C. E.; Hannun, Y. A., Ceramide in Apoptosis: An Overview and Current Perspectives. *Biochim. Biophys. Acta.* **2002,** *1585* (2-3), 114–125.

19. Wadgaonkar, R.; Patel, V.; Grinkina, N.; Romano, C.; Liu, J.; Zhao, Y.; Sammani, S.; Garcia, J. G. N.; Natarajan, V., Differential Regulation of Sphingosine Kinases 1 and 2 in Lung Injury. *Am. J. Physiol. Lung Cell. Mol. Physiol.* **2009,** *296* (4), L603–L613.

20. Lee, M.-J.; Thangada, S.; Claffey, K. P.; Ancellin, N.; Liu, C. H.; Kluk, M.; Volpi, M.; Sha'afi, R. I.; Hla, T., Vascular Endothelial Cell Adherens Junction Assembly and Morphogenesis Induced by Sphingosine-1-Phosphate. *Cell* **1999,** *99* (3), 301–312.

21. Neubauer, H. A.; Pitson, S. M., Roles, Regulation and Inhibitors of Sphingosine Kinase 2. *FEBS J.* **2013,** *280* (21), 5317–5336.

22. Liu, H.; Sugiura, M.; Nava, V. E.; Edsall, L. C.; Kono, K.; Poulton, S.; Milstien, S.; Kohama, T.; Spiegel, S., Molecular Cloning and Functional Characterization of a Novel Mammalian Sphingosine Kinase Type 2 Isoform. *J. Biol. Chem.* **2000,** *275* (26), 19513–19520.

23. Maceyka, M.; Sankala, H.; Hait, N. C.; Le Stunff, H.; Liu, H.; Toman, R.; Collier, C.; Zhang, M.; Satin, L. S.; Merrill, A. H., Jr.; Milstien, S.; Spiegel, S., SphK1 and SphK2,

Sphingosine Kinase Isoenzymes with Opposing Functions in Sphingolipid Metabolism. *J. Biol. Chem.* **2005,** *280* (44), 37118–37129.

24. Orr Gandy, K. A.; Obeid, L. M., Targeting the Sphingosine Kinase/Sphingosine-1-Phosphate Pathway in Disease: Review of Sphingosine Kinase Inhibitors. *Biochim. Biophys. Acta. Mol. Cell Biol.Lipids* **2013,** *1831* (1), 157–166.

25. Congdon, M. D.; Childress, E. S.; Patwardhan, N. N.; Gumkowski, J.; Morris, E. A.; Kharel, Y.; Lynch, K. R.; Santos, W. L., Structure–Activity Relationship Studies of the Lipophilic Tail Region of Sphingosine Kinase 2 Inhibitors. *Bioorg. Med. Chem. Lett.* **2015**, *25*, 4956–4960.

26. Congdon, M. D.; Kharel, Y.; Brown, A. M.; Lewis, S. N.; Bevan, D. R.; Lynch, K. R.; Santos, W. L., Structure–Activity Relationship Studies and Molecular Modeling of Naphthalene-Based Sphingosine Kinase 2 Inhibitors. *ACS Med. Chem. Lett.* **2016**, *7*, 229–234.

27. Patwardhan, N. N.; Morris, E. A.; Raje, M. R.; Gao, M.; Kharel, Y.; Tomsig, J. L.; Lynch, K. R.; Santos, W. L., Structure-Activity Relationship Studies and In Vivo Activity of Guanidine-based Sphingosine Kinase Inhibitors: Discovery of SphK 1 and 2 Selective Inhibitors. *J. Med. Chem.* **2015,** *58* (4), 1879–1899.

28. Gustin, D. J.; Li, Y.; Brown, M. L.; Min, X.; Schmitt, M. J.; Wanska, M.; Wang, X.; Connors, R.; Johnstone, S.; Cardozo, M.; Cheng, A. C.; Jeffries, S.; Franks, B.; Li, S.; Shen, S.; Wong, M.; Wesche, H.; Xu, G.; Carlson, T. J.; Plant, M.; Morgenstern, K.; Rex, K.; Schmitt, J.; Coxon, A.; Walker, N.; Kayser, F.; Wang, Z., Structure Guided Design of a Series of Sphingosine Kinase (SphK) Inhibitors. *Bioorg. Med. Chem. Lett.* **2013,** *23* (16), 4608–4616.

29. Santos, W. L.; Lynch, K. R., Drugging Sphingosine Kinases. *ACS Chem. Biol.* **2015,** *10* (1), 225–233.

30. Xiang, Y.; Hirth, B.; Kane Jr, J. L.; Liao, J.; Noson, K. D.; Yee, C.; Asmussen, G.; Fitzgerald, M.; Klaus, C.; Booker, M., Discovery of Novel Sphingosine Kinase-1 Inhibitors. Part 2. *Bioorg. Med. Chem. Lett.* **2010,** *20* (15), 4550–4554.

31. Wang, Z.; Min, X.; Xiao, S.-H.; Johnstone, S.; Romanow, W.; Meininger, D.; Xu, H.; Liu, J.; Dai, J.; An, S.; Thibault, S.; Walker, N., Molecular Basis of Sphingosine Kinase 1 Substrate Recognition and Catalysis. *Structure* **2013,** *21* (5), 798–809.

32. Wang, J.; Knapp, S.; Pyne, N. J.; Pyne, S.; Elkins, J. M., Crystal Structure of Sphingosine Kinase 1 with PF-543. *ACS Med. Chem. Lett.* **2014,** *5* (12), 1329–1333.

33. Paugh, S. W.; Payne, S. G.; Barbour, S. E.; Milstien, S.; Spiegel, S., The Immunosuppressant FTY720 is Phosphorylated by Sphingosine Kinase Type 2. *FEBS Lett.* **2003,** *554* (1–2), 189–193.

34. Sanchez, T.; Estrada-Hernandez, T.; Paik, J. H.; Wu, M. T.; Venkataraman, K.; Brinkmann, V.; Claffey, K.; Hla, T., Phosphorylation and Action of the Immunomodulator FTY720 Inhibits Vascular Endothelial Cell Growth Factor-Induced Vascular Permeability. *J. Biol. Chem.* **2003,** *278* (47), 47281–42790.

35. Spiegel, S.; Milstein, S., Sphingosine-1-Phosphate: Signaling Inside and Out. *FEBS Lett.* **2000,** *476* (1-2), 55–57.

36. Pitson, S. M.; Xia, P.; Leclercq, T. M.; Moretti, P. A. B.; Zebol, J. R.; Lynn, H. E.; Wattenberg, B. W.; Vadas, M. A., Phosphorylation-Dependent Ttranslocation of Sphingosine Kinase to the Plasma Membrane Drives its Oncogenic Signalling. *J. Exp. Med.* **2005,** *201* (1), 49–54.

37. Pitson, S. M.; Moretti, P. A. B.; Zebol, J. R.; Lynn, H. E.; Xia, P.; Vadas, M. A.; Wattenberg, B. W., Activation of Sphingosine Kinase 1 by ERK1/2-Mediated Phosphorylation. *EMBO J.* **2003,** *22* (20), 5491–5500.

38. Hait, N. C.; Sarkar, S.; Le Stunff, H.; Mikami, A.; Maceyka, M.; Milstien, S.; Spiegel, S., Role of Sphingosine Kinase 2 in Cell Migration toward Epidermal Growth Factor. *J. Biol. Chem.* **2005,** *280* (33), 29462–29469.

39. Hait, N. C.; Bellamy, A.; Milstien, S.; Kordula, T.; Spiegel, S., Sphingosine Kinase Type 2 Activation by ERK-mediated Phosphorylation. *J. Biol. Chem.* **2007,** *282* (16), 12058–12065.

40. Pitson, S.; M. D'andrea, A. J; Vandeleur, L.; Moretti, P. A; Xia, P.; Gamble, J. R; Vadas, M. A; Wattenberg, B. W, Human Sphingosine Kinase: Purification, Molecular Cloning and Characterization of the Native and Recombinant Enzymes. . *Biochem. J.* **2000** *350* (2), 429–441.

41. Chan, H.; Pitson, S. M., Post-Translational Regulation of Sphingosine Kinases. *Biochim. Biophys. Acta. Mol. Cell Biol. Lipids* **2013,** *1831* (1), 147–156.

42. Mizugishi, K.; Yamashita, T.; Olivera, A.; Miller, G. F.; Spiegel, S.; Proia, R. L., Essential Role for Sphingosine Kinases in Neural and Vascular Development. *Mol. Cell. Biol.* **2005,** *25* (24), 11113–11121.

43. Zemann, B.; Urtz, N.; Reuschel, R.; Mechtcheriakova, D.; Bornancin, F.; Badegruber, R.; Baumruker, T.; Billich, A., Normal Neutrophil Functions in Sphingosine Kinase Type 1 and 2 Knockout Mice. *Immunol. Letters.* **2007,** *109* (1), 56–63.

44. Kharel, Y.; Lee, S.; Snyder, A. H.; Sheasley-O'Neill, S. L.; Morris, M. A.; Setiady, Y.; Zhu, R.; Zigler, M. A.; Burcin, T. L.; Ley, K.; Tung, K. S. K.; Engelhard, V. H.;

Macdonald, T. L.; Pearson-White, S.; Lynch, K. R., Sphingosine Kinase 2 Is Required for Modulation of Lymphocyte Traffic by FTY720. *J. Biol. Chem.* **2005,** *280* (44), 36865–36872.

45. Melendez, A. J.; Carlos-Dias, E.; Gosink, M.; Allen, J. M.; Takacs, L., Human Sphingosine Kinase: Molecular Cloning, Functional Characterization and Tissue Distribution. *Gene* **2000,** *251* (1), 19–26.

46. Kapitonov, D.; Allegood, J. C.; Mitchell, C.; Hait, N. C.; Almenara, J. A.; Adams, J. K.; Zipkin, R. E.; Dent, P.; Kordula, T.; Milstien, S.; Spiegel, S., Targeting Sphingosine Kinase 1 Inhibits AKT Signaling, Induces Apoptosis, and Suppresses Growth of Human Glioblastoma Cells and Xenografts. *Cancer Res.* **2009,** *69* (17), 6915–6923.

47. Olivera, A.; Kohama, T.; Edsall, L.; Nava, V.; Cuvillier, O.; Poulton, S.; Spiegel, S., Sphingosine Kinase Expression Increases Intracellular Sphingosine-1-Phosphate and Promotes Cell Growth and Survival. *J. Cell Biol.* **1999,** *147* (3), 545–558.

48. Jarman, K. E.; Moretti, P. A. B.; Zebol, J. R.; Pitson, S. M., Translocation of Sphingosine Kinase 1 to the Plasma Membrane Is Mediated by Calcium- and Integrin-binding Protein 1. *J. Biol. Chem.* **2010,** *285* (1), 483–492.

49. Gault, C. R.; Eblen, S. T.; Neumann, C. A.; Hannun, Y. A.; Obeid, L. M., Oncogenic K-Ras Regulates Bioactive Sphingolipids in a Sphingosine Kinase 1-dependent Manner. *J. Biol. Chem.* **2012,** *287* (38), 31794–31803.

50. ter Braak, M.; Danneberg, K.; Lichte, K.; Liphardt, K.; Ktistakis, N. T.; Pitson, S. M.; Hla, T.; Jakobs, K. H.; Meyer zu Heringdorf, D., Gαq-Mediated Plasma Membrane Translocation of Sphingosine Kinase-1 and Cross-Activation of S1P Receptors. *Biochim. Biophys. Acta. Mol. Cell Biol. Lipids* **2009,** *1791* (5), 357–370.

51. Blaho, V. A.; Hla, T., An Update on the Biology of Sphingosine-1-Phosphate Receptors. *J. Lipid Res.* **2014,** *55* (8), 1596–1608.

52. Karliner, J. S., Sphingosine Kinase and Sphingosine-1-Phosphate in the Heart: A Decade of Progress. *Biochim. Biophys. Acta. Mol. Cell Bio. Lipids* **2013,** *1831* (1), 203–212.

53. Allende, M. L.; Proia, R. L., Sphingosine-1-phosphate receptors and the development of the vascular system. *Biochim. Biophys. Acta.* **2002,** *1582,* (1–3), 222–227.

54. Subei, A. M.; Cohen, J. A., Sphingosine-1-Phosphate Receptor Modulators in Multiple Sclerosis. *CNS Drugs* **2015,** *29* (7), 565–575.

55. Pyne, N. J.; McNaughton, M.; Boomkamp, S.; MacRitchie, N.; Evangelisti, C.; Martelli, A. M.; Jiang, H.-R.; Ubhi, S.; Pyne, S., Role of Sphingosine-1-Phosphate Receptors, Sphingosine Kinases and Sphingosine in Cancer and inflammation. *Adv. Biol. Regul.* **2016,** *60*, 151–159.

56. Huwiler, A.; Pfeilschifter, J., New Players on the Center Stage: Sphingosine-1-Phosphate and Its Receptors as Drug Targets. *Biochem. Pharmacol.* **2008,** *75* (10), 1893–1900.

57. Okada, T.; Ding, G.; Sonoda, H.; Kajimoto, T.; Haga, Y.; Khosrowbeygi, A.; Gao, S.; Miwa, N.; Jahangeer, S.; Nakamura, S.-i., Involvement of *N*-terminal-extended Form of Sphingosine Kinase 2 in Serum-dependent Regulation of Cell Proliferation and Apoptosis. *J. Biol. Chem.* **2005,** *280* (43), 36318–36325.

58. Igarashi, N.; Okada, T.; Hayashi, S.; Fujita, T.; Jahangeer, S.; Nakamura, S., Sphingosine Kinase 2 Is a Nuclear Protein and Inhibits DNA Synthesis. *J. Biol. Chem.* **2003,** *278* (47), 46832–46839.

59. Ding, G.; Sonoda, H.; Yu, H.; Kajimoto, T.; Goparaju, S. K.; Jahangeer, S.; Okada, T.; Nakamura, S., Protein Kinase D-mediated Phosphorylation and Nuclear Export of Sphingosine Kinase 2. *J. Biol. Chem.* **2007,** *282* (37), 27493–27502.

60. Liu, H.; Toman, R. E.; Goparaju, S. K.; Maceyka, M.; Nava, V. E.; Sankala, H.; Payne, S. G.; Bektas, M.; Ishii, I.; Chun, J.; Milstien, S.; Spiegel, S., Sphingosine Kinase Type 2 Is a Putative BH3-only Protein That Induces Apoptosis. *J. Biol. Chem.* **2003,** *278* (41), 40330–40336.

61. Weigert, A.; Cremer, S.; Schmidt, M. V.; von Knethen, A.; Angioni, C.; Geisslinger, G.; Brüne, B., Cleavage of Sphingosine Kinase 2 by Caspase-1 Provokes its Release from Apoptotic Cells. *Blood* **2010,** *115* (17), 3531–3540.

62. Watford, W. T.; Hissong, B. D.; Bream, J. H.; Kanno, Y.; Muul, L.; O'Shea, J. J., Signaling by IL-12 and IL-23 and the Immunoregulatory Roles of STAT4. *Immunol. Rev.* **2004,** *202* (1), 139–156.

63. Yoshimoto, T.; Furuhata, M.; Kamiya, S.; Hisada, M.; Miyaji, H.; Magami, Y.; Yamamoto, K.; Fujiwara, H.; Mizuguchi, J., Positive Modulation of IL-12 Signaling by Sphingosine Kinase 2 Associating with the IL-12 Receptor β1 Cytoplasmic Region. *J. Immunol.* **2003,** *171* (3), 1352–1359.

64. Olivera, A.; Urtz, N.; Mizugishi, K.; Yamashita, Y.; Gilfillan, A. M.; Furumoto, Y.; Gu, H.; Proia, R. L.; Baumruker, T.; Rivera, J., IgE-dependent Activation of Sphingosine Kinases 1 and 2 and Secretion of Sphingosine 1-Phosphate Requires Fyn Kinase and Contributes to Mast Cell Responses. *J. Biol. Chem.* **2006,** *281* (5), 2515–2525.

65. Olivera, A.; Mizugishi, K.; Tikhonova, A.; Ciaccia, L.; Odom, S.; Proia, R. L.; Rivera, J., The Sphingosine Kinase–Sphingosine-1-Phosphate Axis is a Determinant of Mast Cell Function and Anaphylaxis. *Immunity* **2007,** *26* (3), 287–97.

66. Venkataraman, K.; Thangada, S.; Michaud, J.; Oo, M. Lin.; Ai, Y.; Lee, Y.; Wu, M.; Parikh, N. S.; Khan, F.; Proia, R. L.; Hla, Ti., Extracellular Export of Sphingosine Kinase-1a Contributes to the Vascular S1P Gradient. *Biochem J.* **2006,** *397* (3), 461–471.

67. Matloubian, M.; Lo, C. G.; Cinamon, G.; Lesneski, M. J.; Xu, Y.; Brinkmann, V.; Allende, M. L.; Proia, R. L.; Cyster, J. G., Lymphocyte Egress from Thymus and Peripheral Lymphoid Organs is Dependent on S1P Receptor 1. *Nature* **2004,** *427* (6972), 355–360.

68. Mendoza, A.; Bréart, B.; Ramos-Perez, W. D.; Pitt, L. A.; Gobert, M.; Sunkara, M.; Lafaille, J. J.; Morris, A. J.; Schwab, S. R., The Transporter Spns2 is Required for Secretion of Lymph but not Plasma Sphingosine-1-Phosphate. *Cell Rep.* **2012,** *2* (5), 1104–1110.

69. Nagahashi, M.; Kim, E. Y.; Yamada, A.; Ramachandran, S.; Allegood, J. C.; Hait, N. C.; Maceyka, M.; Milstien, S.; Takabe, K.; Spiegel, S., Spns2, a Transporter of Phosphorylated Sphingoid Bases, Regulates Their Blood and Lymph Levels, and the Lymphatic Network. *FASEB J.* **2013,** *27* (3), 1001–1011.

70. Hisano, Y.; Kobayashi, N.; Kawahara, A.; Yamaguchi, A.; Nishi, T., The Sphingosine 1-Phosphate Transporter, SPNS2, Functions as a Transporter of the Phosphorylated Form of the Immunomodulating Agent FTY720. *J. Biol. Chem.* **2011,** *286* (3), 1758–1766.

71. Donoviel, M. S.; Hait, N. C.; Ramachandran, S.; Maceyka, M.; Takabe, K.; Milstien, S.; Oravecz, T.; Spiegel, S., Spinster 2, a Sphingosine-1-Phosphate Transporter, Plays a

Critical Role in Inflammatory and Autoimmune Diseases. *FASEB J.* **2015,** *29* (12), 5018–5028.

72. Nieuwenhuis, B.; Lüth, A.; Chun, J.; Huwiler, A.; Pfeilschifter, J.; Schäfer-Korting, M.; Kleuser, B., Involvement of the ABC-transporter ABCC1 and the Sphingosine-1-Phosphate Receptor Subtype S1P3 in the Cytoprotection of Human Fibroblasts by the Glucocorticoid Dexamethasone. *J. Mol. Med.* **2009,** *87* (6), 645–657.

73. Christoffersen, C.; Obinata, H.; Kumaraswamy, S. B.; Galvani, S.; Ahnström, J.; Sevvana, M.; Egerer-Sieber, C.; Muller, Y. A.; Hla, T.; Nielsen, L. B.; Dahlbäck, B. In Endothelium-Protective Sphingosine-1-Phosphate Provided by HDL-Associated Apolipoprotein *M*, *Proc. Natl. Acad. Sci. U.S.A.* **2011**; *108* (23), 9613–9618.

74. Chun, J.; Goetzl, E. J.; Hla, T.; Igarashi, Y.; Lynch, K. R.; Moolenaar, W.; Pyne, S.; Tigyi, G., Lysophospholipid Receptor Nomenclature. *Pharmacol. Rev.* **2002,** *54* (2), 265–269.

75. Garris, C. S.; Wu, L.; Acharya, S.; Arac, A.; Blaho, V. A.; Huang, Y.; Moon, B. S.; Axtell, R. C.; Ho, P. P.; Steinberg, G. K.; Lewis, D. B.; Sobel, R. A.; Han, D. K.; Steinman, L.; Snyder, M. P.; Hla, T.; Han, M. H., Defective Sphingosine-1-Phosphate Receptor 1 (S1P1) Phosphorylation Exacerbates TH17-Mediated Autoimmune Neuroinflammation. *Nat. Immunol.* **2013,** *14* (11), 1166–1172.

76. Fryer, R. M.; Muthukumarana, A.; Harrison, P. C.; Nodop Mazurek, S.; Chen, R. R.; Harrington, K. E.; Dinallo, R. M.; Horan, J. C.; Patnaude, L.; Modis, L. K.; Reinhart, G. A., The Clinically-tested S1P Receptor Agonists, FTY720 and BAF312, Demonstrate Subtype-Specific Bradycardia (S1P(1)) and Hypertension (S1P(3)) in Rat. *PLoS ONE* **2012,** *7* (12), e52985.

77. Potteck, H.; Nieuwenhuis, B.; Lüth, A.; van der Giet, M.; Kleuser, B., Phosphorylation of the Immunomodulator FTY720 Inhibits Programmed Cell Death of Fibroblasts Via the S1P3 Receptor Subtype and Bcl-2 Activation. *Cell Physiol. Biochem.* **2010,** *26* (1), 67–78.

78. Schulze, T.; Golfier, S.; Tabeling, C.; Räbel, K.; Gräler, M. H.; Witzenrath, M.; Lipp, M., Sphingosine-1-Phospate Receptor 4 (S1P4) deficiency Profoundly Affects Dendritic Cell Function and TH17-cell Differentiation in a Murine Model. *FASEB J.* **2011,** *25* (11), 4024–4036.

79. Wang, W.; Graeler, M. H.; Goetzl, E. J., Type 4 Sphingosine-1-Phosphate G Protein-Coupled Receptor (S1P4) Transduces S1P Effects on T-cell Proliferation and Cytokine Secretion Without Signaling Migration. *FASEB J.* **2005,** *19* (12), 1731–1733.

80. van Doorn, R.; Lopes Pinheiro, M. A.; Kooij, G.; Lakeman, K.; van het Hof, B.; van der Pol, S. M.; Geerts, D.; van Horssen, J.; van der Valk, P.; van der Kam, E.; Ronken, E.; Reijerkerk, A.; de Vries, H. E., Sphingosine-1-Phosphate Receptor 5 Mediates the Immune Quiescence of the Human Brain Endothelial Barrier. *J. Neuroinflammation* **2012,** *9* (1), 1–15.

81. Nixon, G. F., Sphingolipids in Inflammation: Pathological Implications and Potential Therapeutic Targets. *Br. J. Pharmacol.* **2009,** *158* (4), 982–993.

82. Chalfant, C. E.; Spiegel, S., Sphingosine-1-Phosphate and Ceramide-1-Phosphate: Expanding Roles in Cell Signaling. *J. Cell Sci.* **2005,** *118* (20), 4605–4612.

83. Schütze, S.; Potthoff, K.; Machleidt, T.; Berkovic, D.; Wiegmann, K.; Krönke, M., TNF Activates NF-kappa B by Phosphatidylcholine-Specific Phospholipase C-Induced "Acidic" Sphingomyelin Breakdown. *Cell* **1992,** *71* (5), 765–776.

84. Wiegmann, K.; Schütze, S.; Machleidt, T.; Witte, D.; Krönke, M., Functional Dichotomy of Neutral and Acidic Sphingomyelinases in Tumor Necrosis Factor Signaling. *Cell* **1994,** *78* (6), 1005–1015.

85. Xiao, C.; Ghosh, S., NF-κB, an Evolutionarily Conserved Mediator of Immune and Inflammatory Responses. *Adv. Exp. Med. Biol.* **2005***, 560,* 41–45.

86. Zeidan, Y. H.; Pettus, B. J.; Elojeimy, S.; Taha, T.; Obeid, L. M.; Kawamori, T.; Norris, J. S.; Hannun, Y. A., Acid Ceramidase but Not Acid Sphingomyelinase Is Required for Tumor Necrosis Factor-α-induced PGE2 Production. *J. Biol. Chem.* **2006,** *281* (34), 24695–24703.

87. Olivera, A., Unraveling the Complexities of Sphingosine-1-Phosphate Function: The Mast Cell Model. *Prostaglandins Other Lipid Mediat.* **2008,** *86* (1–4), 1–11.

88. Jolly, P. S.; Bektas, M.; Olivera, A.; Gonzalez-Espinosa, C.; Proia, R. L.; Rivera, J.; Milstien, S.; Spiegel, S., Transactivation of Sphingosine-1–Phosphate Receptors by FcεRI Triggering Is Required for Normal Mast Cell Degranulation and Chemotaxis. *J. Exp. Med.* **2004,** *199* (7), 959–970.

89. Sanchez, T.; Skoura, A.; Wu, M. T.; Casserly, B.; Harrington, E. O.; Hla, T., Induction of Vascular Permeability by the Sphingosine-1-Phosphate Receptor–2 (S1P2R) and its Downstream Effectors ROCK and PTEN. *Arterioscler. Thromb. Vasc. Biol.* **2007,** *27* (6), 1312–1318.

90. Hammad, S. M.; Crellin, H. G.; Wu, B.; Melton, J.; Anelli, V.; Obeid, L. M., Dual and Distinct Roles for Sphingosine Kinase 1 and Sphingosine-1-Phosphate in the Response to Inflammatatory Stimulin Raw Macrophages. *Prostaglandins Other Lipid Mediat.* **2008,** *85* (3-4), 107–114.

91. Chen, L.-Y.; Woszczek, G.; Nagineni, S.; Logun, C.; Shelhamer, J. H., Cytosolic Phospholipase A(2)α Activation Induced by S1P is Mediated by the S1P3 Receptor in Lung Epithelial Cells. *Am. J. Physiol. Lung Cell. Mol. Physiol.* **2008,** *295* (2), L326–L335.

92. Skoura, A.; Sanchez, T.; Claffey, K.; Mandala, S. M.; Proia, R. L.; Hla, T., Essential Role of Sphingosine-1-Phosphate Receptor 2 in Pathological Angiogenesis of the Mouse Retina. *J. Clin. Invest.* **2007,** *117* (9), 2506–2516.

93. Maceyka, M.; Spiegel, S., Sphingolipid Metabolites in Inflammatory Disease. *Nature* **2014,** *510* (7503), 58–67.

94. Dimasi, D. P.; Pitson, S. M.; Bonder, C. S., Examining the Role of Sphingosine Kinase-2 in the Regulation of Endothelial Cell Barrier Integrity. *Microcirculation* **2016,** *23* (3), 248–265.

95. Natarajan, V.; Dudek, S. M.; Jacobson, J. R.; Moreno-Vinasco, L.; Huang, L. S.; Abassi, T.; Mathew, B.; Zhao, Y.; Wang, L.; Bittman, R.; Weichselbaum, R.; Berdyshev, E.; Garcia, J. G. N., Sphingosine-1–Phosphate, FTY720, and Sphingosine-1–Phosphate Receptors in the Pathobiology of Acute Lung Injury. *Am. J. Resp. Cell Mol.* **2013,** *49* (1), 6–17.

96. Lai, W.-Q.; Wong, W. S. F.; Leung, Bernard, P., Sphingosine Kinase and Sphingosine-1-Phosphate in Asthma. *Bioscience Rep.* **2011,** *31* (2), 145–150.

97. Melendez, A. J.; Khaw, A. K., Dichotomy of Ca2+ Signals Triggered by Different Phospholipid Pathways in Antigen Stimulation of Human Mast Cells. *J. Biol. Chem.* **2002,** *277* (19), 17255–17262.

98. Yokoo, E.; Yatomi, Y.; Takafuta, T.; Osada, M.; Okamoto, Y.; Ozaki, Y., Sphingosine-1-Phosphate Inhibits Migration of RBL-2H3 Cells via S1P2: Cross-Talk between Platelets and Mast Cells. *J. Biochem.* **2004,** *135* (6), 673–681.

99. Nishiuma, T.; Nishimura, Y.; Okada, T.; Kuramoto, E.; Kotani, Y.; Jahangeer, S.; Nakamura, S., Inhalation of Sphingosine Kinase Inhibitor Attenuates Airway Inflammation in Asthmatic Mouse Model. *Am. J. Physiol. Lung Cell. Mol. Physiol.* **2008,** *294* (6), L1085–L1093.

100. Lai, W.-Q.; Goh, H. H.; Bao, Z.; Wong, W. S. F.; Melendez, A. J.; Leung, B. P., The Role of Sphingosine Kinase in a Murine Model of Allergic Asthma. *J. Immunol.* **2008,** *180* (6), 4323–4329.

101. Roviezzo, F.; D'Agostino, B.; Brancaleone, V.; De Gruttola, L.; Bucci, M.; De Dominicis, G.; Orlotti, D.; D'Aiuto, E.; De Palma, R.; Rossi, F.; Sorrentino, R.; Cirino, G., Systemic Administration of Sphingosine-1-Phosphate Increases Bronchial Hyperresponsiveness in the Mouse. *Am. J. Resp. Cell Mol.* **2010,** *42* (5), 572–577.

102. Ammit, A. J.; Hastie, A. T.; Edsall, L. C.; Hoffman, R. K.; Amrani, Y.; Krymskaya, V. P.; Kane, S. A.; Peters, S. P.; Penn, R. B.; Spiegel, S.; Panettieri, J., Reynold A., Sphingosine-1-Phosphate Modulates Human Airway Smooth Muscle Cell Functions that Promote Inflammation and Airway Remodeling in Asthma. *FASEB J.* **2001**, *15* (7), 1212–1214.

103. Trifilieff, A.; Fozard, J. R., Sphingosine-1-Phosphate-Induced Airway Hyper-Reactivity in Rodents Is Mediated by the Sphingosine-1-Phosphate Type 3 Receptor. *J. Pharmacol. Exp. Ther.* **2012,** *342* (2), 399–406.

104. Roviezzo, F.; Di Lorenzo, A.; Bucci, M.; Brancaleone, V.; Vellecco, V.; De Nardo, M.; Orlotti, D.; De Palma, R.; Rossi, F.; D'Agostino, B.; Cirino, G., Sphingosine-1-Phosphate/Sphingosine Kinase Pathway Is Involved in Mouse Airway Hyperresponsiveness. *Am. J. Resp. Cell Mol.* **2007,** *36* (6), 757–762.

105. Rosenfeldt, H. M.; Amrani, Y.; Watterson, K. R.; Murthy, K. S.; Panettieri, R. A.; Spiegel, S., Sphingosine-1-Phosphate Stimulates Contraction of Human Airway Smooth Muscle Cells. *FASEB J.* **2003,** *17* (13), 1789–1799.

106. Kume, H.; Takeda, N.; Oguma, T.; Ito, S.; Kondo, M.; Ito, Y.; Shimokata, K., Sphingosine-1-Phosphate Causes Airway Hyper-Reactivity by Rho-Mediated Myosin Phosphatase Inactivation. *J. Pharmacol. Exp. Ther.* **2007,** *320* (2), 766–773.

107. French, K. J.; Schrecengost, R. S.; Lee, B. D.; Zhuang, Y.; Smith, S. N.; Eberly, J. L.; Yun, J. K.; Smith, C. D., Discovery and Evaluation of Inhibitors of Human Sphingosine Kinase. *Cancer Res.* **2003,** *63* (18), 5962–5969.

108. Xia, P.; Gamble, J. R.; Wang, L.; Pitson, S. M.; Moretti, P. A. B.; Wattenberg, B. W.; D'Andrea, R. J.; Vadas, M. A., An Oncogenic Role of Sphingosine Kinase. *Curr. Biol.* **2000,** *10* (23), 1527–1530.

109. Pham, D. H.; Powell, J. A.; Gliddon, B. L.; Moretti, P. A. B.; Tsykin, A.; Van der Hoek, M.; Kenyon, R.; Goodall, G. J.; Pitson, S. M., Enhanced Expression of Transferrin Receptor 1 Contributes to Oncogenic Signalling by Sphingosine Kinase 1. *Oncogene* **2014,** *33* (48), 5559–5568.

110. Ponnusamy, S.; Selvam, S. P.; Mehrotra, S.; Kawamori, T.; Snider, A. J.; Obeid, L. M.; Shao, Y.; Sabbadini, R.; Ogretmen, B., Communication Between Host Organism and

Cancer Cells is Transduced by Systemic Sphingosine Kinase 1/Sphingosine-1-Phosphate Signalling to Regulate Tumour Metastasis. *EMBO Moll. Med.* **2012,** *4* (8), 761–775.

111. Brizuela, L.; Martin, C.; Jeannot, P.; Ader, I.; Gstalder, C.; Andrieu, G.; Bocquet, M.; Laffosse, J.-M.; Gomez-Brouchet, A.; Malavaud, B.; Sabbadini, R. A.; Cuvillier, O., Osteoblast-Derived Sphingosine-1-Phosphate to Induce Proliferation and Confer Resistance to Therapeutics to Bone Metastasis-derived Prostate Cancer Cells. *Mol. Oncol.* **2014,** *8* (7), 1181–1195.

112. Stayrook, K. R.; Mack, J. K.; Cerabona, D.; Edwards, D. F.; Bui, H. H.; Niewolna, M.; Fournier, P. G. J.; Mohammad, K. S.; Waning, D. L.; Guise, T. A., TGFβ-Mediated Induction of SphK1 as a Potential Determinant in Human MDA-MB-231 Breast Cancer Cell Bone Metastasis. *BoneKEy Rep.* **2015,** *4*, (719), 1–13.

113. Pyne, N. J.; Pyne, S., Sphingosine-1-Phosphate Is a Missing Link between Chronic Inflammation and Colon Cancer. *Cancer Cell.* **2013,** *23* (1), 5–7.

114. Liang, J.; Nagahashi, M.; Kim, E. Y.; Harikumar, K. B.; Yamada, A.; Huang, W.-C.; Hait, N. C.; Allegood, J. C.; Price, M. M.; Avni, D.; Takabe, K.; Kordula, T.; Milstien, S.; Spiegel, S., Sphingosine-1-Phosphate Links Persistent STAT3 Activation, Chronic Intestinal Inflammation, and Development of Colitis-Associated Cancer. *Cancer Cell.* **2013,** *23* (1), 107–120.

115. Long, J. S.; Edwards, J.; Watson, C.; Tovey, S.; Mair, K. M.; Schiff, R.; Natarajan, V.; Pyne, N. J.; Pyne, S., Sphingosine Kinase 1 Induces Tolerance to Human Epidermal Growth Factor Receptor 2 and Prevents Formation of a Migratory Phenotype in Response to Sphingosine 1-Phosphate in Estrogen Receptor-Positive Breast Cancer Cells. *Mol. Cell. Bio.* **2010,** *30* (15), 3827–3841.

116. Anelli, V.; Gault, C. R.; Snider, A. J.; Obeid, L. M., Role of Sphingosine Kinase-1 in Paracrine/Transcellular Angiogenesis and Lymphangiogenesis *in vitro*. *FASEB J.* **2010,** *24* (8), 2727–2738.

117. Shirai, K.; Kaneshiro, T.; Wada, M.; Furuya, H.; Bielawski, J.; Hannun, Y. A.; Obeid, L. M.; Ogretmen, B.; Kawamori, T., A Role of Sphingosine Kinase 1 in Head and Neck Carcinogenesis. *Cancer Prev. Res.* **2011,** *4* (3), 454–462.

118. Gao, P.; Smith, C. D., Ablation of Sphingosine Kinase-2 Inhibits Tumor Cell Proliferation and Migration. *Mol. Cancer Res.* **2011,** *9* (11), 1509–1519.

119. Wallington-Beddoe, C. T.; Powell, J. A.; Tong, D.; Pitson, S. M.; Bradstock, K. F.; Bendall, L. J., Sphingosine Kinase 2 Promotes Acute Lymphoblastic Leukemia by Enhancing MYC Expression. *Cancer Res.* **2014,** *74* (10), 2803–2815.

120. Evangelisti, C.; Evangelisti, C.; Teti, G.; Chiarini, F.; Falconi, M.; Melchionda, F.; Pession, A.; Bertaina, A.; Locatelli, F.; McCubrey, J. A.; Beak, D. J.; Bittman, R.; Pyne, S.; Pyne, N. J.; Martelli, A. M., Assessment of the Effect of Sphingosine Kinase Inhibitors on Apoptosis, Unfolded Protein Response and Autophagy of T-cell Acute Lymphoblastic Leukemia Cells; Indications for Novel Therapeutics. *Oncotarget* **2014,** *5* (17), 7886–7901.

121. Weigert, A.; Schiffmann, S.; Sekar, D.; Ley, S.; Menrad, H.; Werno, C.; Grosch, S.; Geisslinger, G.; Brüne, B., Sphingosine Kinase 2 Deficient Tumor Xenografts Show Impaired Growth and Fail to Polarize Macrophages Towards an Anti-Inflammatory Phenotype. *Int. J. Cancer* **2009,** *125* (9), 2114–2121.

122. Gasperini, C.; Ruggieri, S.; Mancinelli, C. R.; Pozzilli, C., Advances in the Treatment of Relapsing–Remitting Multiple Sclerosis—Critical Appraisal of Fingolimod. *Ther. Clin. Risk Manag.* **2013,** *9*, 73–85.

123. Chun, J.; Hartung, H.-P., Mechanism of Action of Oral Fingolimod (FTY720) in Multiple Sclerosis. *Clin. Neuropharmacol.* **2010,** *33* (2), 91–101.

124. Hunter, S. F.; Bowen, J. D.; Reder, A. T., The Direct Effects of Fingolimod in the Central Nervous System: Implications for Relapsing Multiple Sclerosis. *CNS Drugs* **2016,** *30* (2), 135–147.

125. Compston, A.; Coles, A., Multiple Sclerosis. *Lancet* **2008,** *372* (9648), 1502–1517.

126. Kutzelnigg, A.; Lassmann, H., Chapter 2 - Pathology of Multiple Sclerosis and Related Inflammatory Demyelinating Diseases. In *Handbook of Clinical Neurology*, Douglas, S. G., Ed. Elsevier: 2014; Vol. Volume 122, pp 15–58.

127. Qin, J.; Berdyshev, E.; Goya, J.; Natarajan, V.; Dawson, G., Neurons and Oligodendrocytes Recycle Sphingosine 1-Phosphate to Ceramide: Signigicances for Apoptosis and Multiple Sclerosis. *J. Biol. Chem.* **2010,** *285* (19), 14134–14143.

128. Wheeler, D.; Bandaru, V. V. R.; Calabresi, P. A.; Nath, A.; Haughey, N. J., A Defect of Sphingolipid Metabolism Modifies the Properties of Normal Appearing White Matter in Multiple Sclerosis. *Brain* **2008,** *131* (11), 3092–3102.

129. Kułakowska, A.; Żendzian-Piotrowska, M.; Baranowski, M.; Konończuk, T.; Drozdowski, W.; Górski, J.; Bucki, R., Intrathecal Increase of Sphingosine-1-Phosphate at Early Stage Multiple Sclerosis. *Neurosci. Lett.* **2010,** *477* (3), 149–152.

130. Van Doorn, R.; van Horssen, J.; Verzijl, D.; Witte, M.; Ronken, E.; Van het Hof, B.; Lakeman, K.; Dijkstra, C. D.; van der Valk, P.; Reijerkerk, A., Sphingosine-1-phosphate

Receptor 1 and 3 are Upregulated in Multiple Sclerosis Lesions. *Glia* **2010,** *58* (12), 1465–1476.

131. Fischer, I.; Alliod, C.; Martinier, N.; Newcombe, J.; Brana, C.; Pouly, S., Sphingosine Kinase 1 and Sphingosine-1-Phosphate Receptor 3 Are Functionally Upregulated on Astrocytes Under Pro-Inflammatory Conditions. *PLoS ONE* **2011,** *6* (8), e23905.

132. Brana, C.; Frossard, M. J.; Pescini Gobert, R.; Martinier, N.; Boschert, U.; Seabrook, T. J., Immunohistochemical Detection of Sphingosine-1-Phosphate Receptor 1 and 5 in Human Multiple Sclerosis Lesions. *Neuropathol. Appl. Neurobiol.* **2014,** *40* (5), 564–578.

133. Miron, V. E.; Ludwin, S. K.; Darlington, P. J.; Jarjour, A. A.; Soliven, B.; Kennedy, T. E.; Antel, J. P., Fingolimod (FTY720) Enhances Remyelination Following Demyelination of Organotypic Cerebellar Slices. *Am. J. Pathol.* **2010,** *176* (6), 2682–2694.

134. Groves, A.; Kihara, Y.; Chun, J., Fingolimod: Direct CNS Effects of Sphingosine-1-Phosphate (S1P) Receptor Modulation and Implications in Multiple Sclerosis Therapy. *J. Neurol. Sci.* **2013,** *328* (1–2), 9–18.

135. Dudek, S. M.; Camp, S. M.; Chiang, E. T.; Singleton, P. A.; Usatyuk, P. V.; Zhao, Y.; Natarajan, V.; Garcia, J. G., Pulmonary Endothelial Cell Barrier Enhancement by FTY720 Does Not Require the S1P1 Receptor. *Cell. Signal.* **2007,** *19* (8), 1754–1764.

136. Wynn, T. A., Common and Unique Mechanisms Regulate Fibrosis in Various Fibroproliferative Diseases. *J. Clin. Invest.* **2007,** *117* (3), 524–529.

137. Schwalm, S.; Pfeilschifter, J.; Huwiler, A., Sphingosine-1-Phosphate: A Janus-faced Mediator of Fibrotic Diseases. *Biochim. Biophys. Acta. Mol. Cell Biol. Lipids* **2013,** *1831* (1), 239–250.

138. Takuwa, Y.; Ikeda, H.; Okamoto, Y.; Takuwa, N.; Yoshioka, K., Sphingosine-1-Phosphate as a Mediator Involved in Development of Fibrotic Diseases. *Biochim. Biophys. Acta. Mol. Cell Biol. Lipids* **2013,** *1831* (1), 185–192.

139. Pyne, N. J.; Dubois, G.; Pyne, S., Role of Sphingosine-1-Phosphate and Lysophosphatidic Acid in Fibrosis. *Biochim. Biophys. Acta. Mol. Cell Biol. Lipids* **2013,** *1831* (1), 228–238.

140. Shea, B. S.; Brooks, S. F.; Fontaine, B. A.; Chun, J.; Luster, A. D.; Tager, A. M., Prolonged Exposure to Sphingosine-1-Phosphate Receptor-1 Agonists Exacerbates Vascular Leak, Fibrosis, and Mortality after Lung Injury. *Am. J. Resp. Cell Mol.* **2010,** *43* (6), 662–673.

141. Haughey, N. J.; Bandaru, V. V. R.; Bai, M.; Mattson, M. P., Roles for Dysfunctional Sphingolipid Metabolism in Alzheimer's Disease Neuropathogenesis. *Biochim. Biophys. Acta.* **2010,** *1801* (8), 878–886.

142. Gassowska, M.; Cieslik, M.; Wilkaniec, A.; Strosznajder, J. B., Sphingosine Kinases/Sphingosine-1-Phosphate and Death Signalling in APP-Transfected Cells. *Neurochem. Research.* **2014,** *39* (4), 645–652.

143. Kosicek, M.; Hecimovic, S., Phospholipids and Alzheimer's Disease: Alterations, Mechanisms and Potential Biomarkers. *Int. J. Mol. Sci.* **2013,** *14* (1), 1310–1322.

144. Takasugi, N.; Sasaki, T.; Suzuki, K.; Osawa, S.; Isshiki, H.; Hori, Y.; Shimada, N.; Higo, T.; Yokoshima, S.; Fukuyama, T.; Lee, V. M.; Trojanowski, J. Q.; Tomita, T.; Iwatsubo,

T., BACE1 Activity is Modulated by Cell-Associated Sphingosine-1-Phosphate. *J. Neurosci.* **2011,** *31* (18), 6850–6857.

145. Cieślik, M.; Czapski, G. A.; Strosznajder, J. B., The Molecular Mechanism of Amyloid β42 Peptide Toxicity: The Role of Sphingosine Kinase-1 and Mitochondrial Sirtuins. *PLoS ONE* **2015,** *10* (9), e0137193.

146. Pyne, S.; Adams, D. R.; Pyne, N. J., Sphingosine-1-Phosphate and Sphingosine Kinases in Health and Disease: Recent advances. *Prog. Lipid. Res.* **2016,** *62*, 93–106.

147. Centers for Disease Control and Prevention, Sickle Cell Disease, **2016**, http://www.cdc.gov/ncbddd/sicklecell/index.html, (accessed May 01, 2016).

148. Zhang, Y.; Berka, V.; Song, A.; Sun, K.; Wang, W.; Zhang, W.; Ning, C.; Li, C.; Zhang, Q.; Bogdanov, M.; Alexander, D. C.; Milburn, M. V.; Ahmed, M. H.; Lin, H.; Idowu, M.; Zhang, J.; Kato, G. J.; Abdulmalik, O. Y.; Zhang, W.; Dowhan, W.; Kellems, R. E.; Zhang, P.; Jin, J.; Safo, M.; Tsai, A. L.; Juneja, H. S.; Xia, Y., Elevated Sphingosine-1-Phosphate Promotes Sickling and Sickle Cell Disease Progression. *J. Clin. Invest.* **2014,** *124* (6), 2750–61.

149. Haass, N. K.; Nassif, N.; McGowan, E. M., Switching the Sphingolipid Rheostat in the Treatment of Diabetes and Cancer Comorbidity from a Problem to an Advantage. *BioMed Res. Int.* **2015,** *2015* (165105), 1–9.

150. Qi, Y.; Chen, J.; Lay, A.; Don, A.; Vadas, M.; Xia, P., Loss of Sphingosine Kinase 1 Predisposes to the Onset of Diabetes Via Promoting Pancreatic β-Cell Death in Diet-Induced Obese Mice. *FASEB J.* **2013,** *27* (10), 4294–4304.

151. Bruce, C. R.; Risis, S.; Babb, J. R.; Yang, C.; Kowalski, G. M.; Selathurai, A.; Lee-Young, R. S.; Weir, J. M.; Yoshioka, K.; Takuwa, Y.; Meikle, P. J.; Pitson, S. M.;

Febbraio, M. A., Overexpression of Sphingosine Kinase 1 Prevents Ceramide Accumulation and Ameliorates Muscle Insulin Resistance in High-Fat Diet–Fed Mice. *Diabetes* **2012,** *61* (12), 3148–3155.

152. Lee, S. Y.; Hong, I. K.; Kim, B. R.; Shim, S. M.; Sung Lee, J.; Lee, H. Y.; Soo Choi, C.; Kim, B. K.; Park, T. S., Activation of Sphingosine Kinase 2 by Endoplasmic Reticulum Stress Ameliorates Hepatic Steatosis and Insulin Resistance in Mice. *Hepatology* **2015,** *62* (1), 135–146.

153. Arish, M.; Husein, A.; Kashif, M.; Saleem, M.; Akhter, Y.; Rub, A., Sphingosine-1-Phosphate Signaling: Unraveling its Role as a Drug Target Against Infectious Diseases. *Drug Discov. Today* **2016,** *21* (1), 133–142.

154. Carr, J. M.; Kua, T.; Clarke, J. N.; Calvert, J. K.; Zebol, J. R.; Beard, M. R.; Pitson, S. M., Reduced Sphingosine Kinase 1 Activity in Dengue Virus Type-2 Infected Cells Can be Mediated by the 3′-Untranslated Region of Dengue Virus Type-2 RNA. *J. Gen. Virol.* **2013,** *94* (11), 2437–2448.

155. Zhang, G.; Flick-Smith, H.; McCauley, J. W., Differences in Membrane Association and Sub-cellular Distribution Between NS2–3 and NS3 of Bovine Viral Diarrhoea Virus. *Virus Res.* **2003,** *97* (2), 89–102.

156. Wati, S.; Rawlinson, S. M.; Ivanov, R. A.; Dorstyn, L.; Beard, M. R.; Jans, D. A.; Pitson, S. M.; Burrell, C. J.; Li, P.; Carr, J. M., Tumour Necrosis Factor Alpha (TNF-α) Stimulation of Cells with Established Dengue Virus Type 2 Infection Induces Cell Death that is Accompanied by a Reduced Ability of TNF-α to Activate Nuclear Factor κB and Reduced Sphingosine Kinase-1 Activity. *J. Gen. Virol.* **2011,** *92* (4), 807–818.

157. Yamane, D.; Zahoor, M. A.; Mohamed, Y. M.; Azab, W.; Kato, K.; Tohya, Y.; Akashi, H., Inhibition of Sphingosine Kinase by Bovine Viral Diarrhea Virus NS3 Is Crucial for Efficient Viral Replication and Cytopathogenesis. *J. Biol. Chem.* **2009,** *284* (20), 13648–13659.

158. Seo, Y.-J.; Pritzl, C. J.; Vijayan, M.; Bomb, K.; McClain, M. E.; Alexander, S.; Hahm, B., Sphingosine Kinase 1 Serves as a Pro-Viral Factor by Regulating Viral RNA Synthesis and Nuclear Export of Viral Ribonucleoprotein Complex upon Influenza Virus Infection. *PLoS ONE* **2013,** *8* (8), e75005.

159. Carr, J. M.; Mahalingam, S.; Bonder, C. S.; Pitson, S. M., Sphingosine kinase 1 in Viral Infections. *Rev. Med. Virol.* **2013,** *23* (2), 73–84.

160. Vijayan, M.; Seo, Y. J.; Pritzl, C. J.; Squires, S. A.; Alexander, S.; Hahm, B., Sphingosine Kinase 1 Regulates Measles Virus Replication. *Virology* **2014,** *450–451*, 55–63.

161. Machesky, N. J.; Zhang, G.; Raghavan, B.; Zimmerman, P.; Kelly, S. L.; Merrill, A. H.; Waldman, W. J.; Van Brocklyn, J. R.; Trgovcich, J., Human Cytomegalovirus Regulates Bioactive Sphingolipids. *J. Biol. Chem.* **2008,** *283* (38), 26148–26160.

162. Monick, M. M.; Cameron, K.; Powers, L. S.; Butler, N. S.; McCoy, D.; Mallampalli, R. K.; Hunninghake, G. W., Sphingosine Kinase Mediates Activation of Extracellular Signal–Related Kinase and Akt by Respiratory Syncytial Virus. *Am. J. Resp. Cell Mol.* **2004,** *30* (6), 844–852.

163. Vijayan, M.; Hahm, B., Influenza Viral Manipulation of Sphingolipid Metabolism and Signaling to Modulate Host Defense System. *Scientifica* **2014,** *2014* (793815), 1–9.

164. Teijaro, J. R.; Walsh, K. B.; Cahalan, S. M.; Fremgen, D. M.; Roberts, E.; Scott, F.; Martinborough, E.; Peach, R.; Oldstone, M. B. A.; Rosen, H., Endothelial Cells are Central Orchestrators of Cytokine Amplification During Influenza Virus Infection. *Cell* **2011,** *146* (6), 980–991.

165. Walsh, K. B.; Teijaro, J. R.; Wilker, P. R.; Jatzek, A.; Fremgen, D. M.; Das, S. C.; Watanabe, T.; Hatta, M.; Shinya, K.; Suresh, M.; Kawaoka, Y.; Rosen, H.; Oldstone, M. B. A. Suppression of Cytokine Storm with a Sphingosine Analog Provides Protection Against Pathogenic Influenza Virus, *Proc. Natl. Acad. Sci. U.S.A.* **2011**, *108* (29), 12018–12023.

166. Marsolais, D.; Hahm, B.; Edelmann, K. H.; Walsh, K. B.; Guerrero, M.; Hatta, Y.; Kawaoka, Y.; Roberts, E.; Oldstone, M. B. A.; Rosen, H., Local Not Systemic Modulation of Dendritic Cell S1P Receptors in Lung Blunts Virus-Specific Immune Responses to Influenza. *Mol. Pharmacol.* **2008,** *74* (3), 896–903.

167. Marsolais, D.; Hahm, B.; Walsh, K. B.; Edelmann, K. H.; McGavern, D.; Hatta, Y.; Kawaoka, Y.; Rosen, H.; Oldstone, M. B. A., A Critical Role for the Sphingosine Analog AAL-R in Dampening the Cytokine Response During Influenza Virus Infection, *Proc. Natl. Acad. Sci. U.S.A.* **2009**; *106* (5), 1560–1565.

168. Reid, S. P.; Tritsch, S. R.; Kota, K.; Chiang, C.-Y.; Dong, L.; Kenny, T.; Brueggemann, E. E.; Ward, M. D.; Cazares, L. H.; Bavari, S., Sphingosine Kinase 2 is a Chikungunya Virus Host Factor Co-localized with the Viral Replication Complex. *Emerg. Microbes Infect.* **2015,** *4* (10), e61.

169. Dai, L.; Plaisance-Bonstaff, K.; Voelkel-Johnson, C.; Smith, C. D.; Ogretmen, B.; Qin, Z.; Parsons, C., Sphingosine Kinase-2 Maintains Viral Latency and Survival for KSHV-Infected Endothelial Cells. *PLoS ONE* **2014,** *9* (7), e102314.

170. Kułakowska, A.; Byfield, F. J.; Żendzian-Piotrowska, M.; Zajkowska, J. M.; Drozdowski, W.; Mroczko, B.; Janmey, P. A.; Bucki, R., Increased Levels of Sphingosine-1-Phosphate in Cerebrospinal Fluid of Patients Diagnosed with Tick-Borne Encephalitis. *J. Neuroinflamm.* **2014,** *11* (193), 1–9.

171. Garg, S. K.; Volpe, E.; Palmieri, G.; Mattei, M.; Galati, D.; Martino, A.; Piccioni, M. S.; Valente, E.; Bonanno, E.; De Vito, P.; Baldini, P. M.; Spagnoli, L. G.; Colizzi, V.; Fraziano, M., Sphingosine-1-Phosphate Induces Antimicrobial Activity Both In Vitro and In Vivo. *J. Infect. Dis.* **2004,** *189* (11), 2129–2138.

172. Garg, S. K.; Santucci, M. B.; Panitti, M.; Pucillo, L.; Bocchino, M.; Okajima, F.; Bisen, P. S.; Saltini, C.; Fraziano, M., Does Sphingosine-1-Phosphate Play a Protective Role in the Course of Pulmonary Tuberculosis? *Clin. Immunol.* **2006,** *121* (3), 260–264.

173. Malik, Z. A.; Thompson, C. R.; Hashimi, S.; Porter, B.; Iyer, S. S.; Kusner, D. J., Cutting Edge: Mycobacterium Tuberculosis Blocks Ca2+ Signaling and Phagosome Maturation in Human Macrophages Via Specific Inhibition of Sphingosine Kinase. *J. Immunol.* **2003,** *170* (6), 2811–2815.

174. Yadav, M.; Clark, L.; Schorey, J. S., Macrophage's Proinflammatory Response to a Mycobacterial Infection Is Dependent on Sphingosine Kinase-Mediated Activation of Phosphatidylinositol Phospholipase C, Protein Kinase C, ERK1/2, and Phosphatidylinositol 3-Kinase. *J. Immunol.* **2006,** *176* (9), 5494–5503.

175. Prakash, H.; Lüth, A.; Grinkina, N.; Holzer, D.; Wadgaonkar, R.; Gonzalez, A. P.; Anes, E.; Kleuser, B., Sphingosine Kinase-1 (SphK-1) Regulates *Mycobacterium smegmatis* Infection in Macrophages. *PLoS ONE* **2010,** *5* (5), e10657.

176. St. John, A. L.; Ang, W. X. G.; Huang, M.-N.; Kunder, C. A.; Chan, E. W.; Gunn, M. D.; Abraham, S. N., S1P-Dependent Trafficking of Intracellular *Yersinia pestis* Through Lymph Nodes Establishes Buboes and Systemic Infection. *Immunity* **2014,** *41* (3), 440–450.

177. Ochi, S.; Oda, M.; Matsuda, H.; Ikari, S.; Sakurai, J., *Clostridium perfringens* α-Toxin Activates the Sphingomyelin Metabolism System in Sheep Erythrocytes. *J. Biol. Chem.* **2004,** *279* (13), 12181–12189.

178. Oizumi, A.; Nakayama, H.; Okino, N.; Iwahara, C.; Kina, K.; Matsumoto, R.; Ogawa, H.; Takamori, K.; Ito, M.; Suga, Y.; Iwabuchi, K., Pseudomonas-Derived Ceramidase Induces Production of Inflammatory Mediators from Human Keratinocytes via Sphingosine-1-Phosphate. *PLoS ONE* **2014,** *9* (2), e89402.

179. Ramesh, G.; Didier, P. J.; England, J. D.; Santana-Gould, L.; Doyle-Meyers, L. A.; Martin, D. S.; Jacobs, M. B.; Philipp, M. T., Inflammation in the Pathogenesis of Lyme Neuroborreliosis. *Am. J. Pathol.* **2015,** *185* (5), 1344–1360.

180. Cook, M. J., Lyme Borreliosis: a Review of Data on Transmission Time After Tick Attachment. *Int. J. Gen. Med.* **2015,** *8*, 1–8.

181. Ramesh, G.; Borda, J. T.; Dufour, J.; Kaushal, D.; Ramamoorthy, R.; Lackner, A. A.; Philipp, M. T., Interaction of the Lyme Disease Spirochete *Borrelia burgdorferi* with Brain Parenchyma Elicits Inflammatory Mediators from Glial Cells as Well as Glial and Neuronal Apoptosis. *Am. J. Pathol.* **2008,** *173* (5), 1415–1427.

182. Ramesh, G.; Santana-Gould, L.; Inglis, F. M.; England, J. D.; Philipp, M. T., The Lyme Disease Spirochete *Borrelia burgdorferi* Induces Inflammation and Apoptosis in Cells from Dorsal Root Ganglia. *J. Neuroinflammation* **2013,** *10* (88), 1–14.

183. McQuiston, T.; Luberto, C.; Del Poeta, M., Role of Host Sphingosine Kinase 1 in the Lung Response Against Cryptococcosis. *Infect. Immuno.* **2010,** *78* (5), 2342–2352.

184. Farnoud, A. M.; Bryan, A. M.; Kechichian, T.; Luberto, C.; Del Poeta, M., The Granuloma Response Controlling Cryptococcosis in Mice Depends on the Sphingosine Kinase 1–Sphingosine-1-Phosphate Pathway. *Infect. Immun.* **2015,** *83* (7), 2705–2713.

185. McQuiston, T.; Luberto, C.; Del Poeta, M., Role of Sphingosine-1-Phosphate (S1P) and S1P receptor 2 in the Phagocytosis of *Cryptococcus neoformans* by Alveolar macrophages. *Microbiology* **2011,** *157* (Pt 5), 1416–1427.

186. Bryan, A. M.; Del Poeta, M.; Luberto, C., Sphingolipids as Regulators of the Phagocytic Response to Fungal Infections. *Mediators Inflamm.* **2015,** *2015* (640540), 1–12.

187. Rub, A.; Arish, M.; Husain, S. A.; Ahmed, N.; Akhter, Y., Host-Lipidome as a Potential Target of Protozoan Parasites. *Microbes Infect.* **2013,** *15* (10–11), 649–660.

188. Centers for Disease Control and Prevention, Parasites - American Trypanosomiasis (also known as Chagas Disease). http://www.cdc.gov/parasites/chagas/ (accessed May 01, 2016).

189. Lepletier, A.; de Almeida, L.; Santos, L.; da Silva Sampaio, L.; Paredes, B.; González, F. B.; Freire-de-Lima, C. G.; Beloscar, J.; Bottasso, O.; Einicker-Lamas, M.; Pérez, A. R.; Savino, W.; Morrot, A., Early Double-Negative Thymocyte Export in *Trypanosoma cruzi* Infection Is Restricted by Sphingosine Receptors and Associated with Human Chagas Disease. *PLoS Negl. Trop. Dis.* **2014,** *8* (10), e3203.

190. Dominguez, M. R.; Ersching, J.; Lemos, R.; Machado, A. V.; Bruna-Romero, O.; Rodrigues, M. M.; de Vasconcelos, J. R. C., Re-circulation of Lymphocytes Mediated by Sphingosine-1-Phosphate Receptor-1 Contributes to Resistance Against Experimental Infection with the Protozoan Parasite *Trypanosoma cruzi*. *Vaccine* **2012,** *30* (18), 2882–2891.

191. Centers for Disease Control and Prevention, Malaria, **2016**. http://www.cdc.gov/malaria/index.html, (accessed May 01, 2016).

192. Finney, C. A. M.; Hawkes, C. A.; Kain, D. C.; Dhabangi, A.; Musoke, C.; Cserti-Gazdewich, C.; Oravecz, T.; Liles, W. C.; Kain, K. C., S1P Is Associated with Protection in Human and Experimental Cerebral Malaria. *Mol. Med.* **2011,** *17* (7–8), 717–725.

193. O'Brien, N.; Jones, S. T.; Williams, D. G.; Cunningham, H. B.; Moreno, K.; Visentin, B.; Gentile, A.; Vekich, J.; Shestowsky, W.; Hiraiwa, M.; Matteo, R.; Cavalli, A.; Grotjahn, D.; Grant, M.; Hansen, G.; Campbell, M.-A.; Sabbadini, R., Production and Characterization of Monoclonal Anti-Sphingosine-1-Phosphate Antibodies. *J. Lipid Res.* **2009,** *50* (11), 2245–2257.

194. Sabbadini, R. A., Sphingosine-1-Phosphate Antibodies as Potential Agents in the Treatment of Cancer and Age-Related Macular Degeneration. *Br. J. Pharmacol.* **2011,** *162* (6), 1225–1238.

195. Visentin, B.; Vekich, J. A.; Sibbald, B. J.; Cavalli, A. L.; Moreno, K. M.; Matteo, R. G.; Garland, W. A.; Lu, Y.; Yu, S.; Hall, H. S.; Kundra, V.; Mills, G. B.; Sabbadini, R. A., Validation of an Anti-Sphingosine-1-Phosphate Antibody as a Potential Therapeutic in Reducing Growth, Invasion, and Angiogenesis in Multiple Tumor Lineages. *Cancer Cell.* **2006,** *9* (3), 225–38.

196. Adis Insight, Sonepcizumab, **2016**, http://adisinsight.springer.com/drugs/800024045 (accessed March 28th, 2016).

197. Wojciak, J. M.; Zhu, N.; Schuerenberg, K. T.; Moreno, K.; Shestowsky, W. S.; Hiraiwa, M.; Sabbadini, R.; Huxford, T. The crystal structure of sphingosine-1-phosphate in complex with a Fab fragment reveals metal bridging of an antibody and its antigen, *Proc. Natl. Acad. Sci. U.S.A.* **2009**; *106* (42) 7717-17722.

198. Trials, A., A multi-center, open-label, single-Arm, phase 1, dose escalation study of ASONEP (sonepcizumab/LT1009) administered as a single agent weekly to subjects with refractory advanced solid tumors. May 21 2008 ed.; Springer International Publisher AG: 2008.

199. Trials, A., A Phase 1, Dose-Escalating, Multi-Center, Study of iSONEP (Sonepcizumab [LT1009]) Administered as an Intravitreal Injection to Subjects With Choroidal Neovascularization Secondary to Age-Related Macular Degeneration. Springer International Publishing AG: 2013.

200. Zhang, Z. Y.; Zhang, Z.; Zug, C.; Nuesslein-Hildesheim, B.; Leppert, D.; Schluesener, H. J., AUY954, a Selective S1P1 Modulator, Prevents Experimental Autoimmune Neuritis. *J. Neuroimmunology* **2009,** *216* (1–2), 59–65.

201. Pan, S.; Mi, Y.; Pally, C.; Beerli, C.; Chen, A.; Guerini, D.; Hinterding, K.; Nuesslein-Hildesheim, B.; Tuntland, T.; Lefebvre, S.; Liu, Y.; Gao, W.; Chu, A.; Brinkmann, V.; Bruns, C.; Streiff, M.; Cannet, C.; Cooke, N.; Gray, N., A Monoselective Sphingosine-1-Phosphate Receptor-1 Agonist Prevents Allograft Rejection in a Stringent Rat Heart Transplantation Model. *Chem. Biol.* **2006,** *13* (11), 1227–1234.

202. Bigaud, M.; Guerini, D.; Billich, A.; Bassilana, F.; Brinkmann, V., Second Generation S1P Pathway Modulators: Research Strategies and Clinical Developments. *Biochim. Biophys. Acta.* **2014,** *1841* (5), 745–58.

203. Jo, E.; Sanna, M. G.; Gonzalez-Cabrera, P. J.; Thangada, S.; Tigyi, G.; Osborne, D. A.; Hla, T.; Parrill, A. L.; Rosen, H., S1P1-Selective *In Vivo*-Active Agonists from High-Throughput Screening: Off-the-Shelf Chemical Probes of Receptor Interactions, Signaling, and Fate. *Chem. Biol.* **2005,** *12* (6), 703–715.

204. Strader, C. R.; Pearce, C. J.; Oberlies, N. H., Fingolimod (FTY720): A Recently Approved Multiple Sclerosis Drug Based on a Fungal Secondary Metabolite. *J. Nat. Prod.* **2011,** *74* (4), 900–907.

205. Adachi, K.; Kohara, T.; Nakao, N.; Arita, M.; Chiba, K.; Mishina, T.; Sasaki, S.; Fujita, T., Design, Synthesis, and Structure–Activity Relationships of 2- Substituted-2-amino-1,3-propanediols: Discovery of a Novel Immunosuppressant, FTY720. *Bioorg. Med. Chem. Lett* **1995,** *5* (8), 853–865.

206. Gräler, M. H.; Goetzl, E. J., The immunosuppressant FTY720 Down-Regulates sSphingosine-1-Phosphate G-Protein-Coupled Receptors. *FASEB J.* **2004,** *18* (3), 551–553.

207. Zemann, B.; Kinzel, B.; Müller, M.; Reuschel, R.; Mechtcheriakova, D.; Urtz, N.; Bornancin, F.; Baumruker, T.; Billich, A., Sphingosine Kinase Type 2 is Essential for Lymphopenia Induced by the Immunomodulatory Drug FTY720. *Blood* **2006,** *107* (4), 1454–1458.

208. Tonelli, F.; Lim, K. G.; Loveridge, C.; Long, J.; Pitson, S. M.; Tigyi, G.; Bittman, R.; Pyne, S.; Pyne, N. J., FTY720 and (S)-FTY720 Vinylphosphonate Inhibit Sphingosine

Kinase 1 and Promote its Proteasomal Degradation in Human Pulmonary Artery Smooth Muscle, Breast Cancer and Androgen-Independent Prostate Cancer Cells. *Cell. Signal.* **2010,** *22* (10), 1536–1542.

209. Mandala, S.; Hajdu, R.; Bergstrom, J.; Quackenbush, E.; Xie, J.; Milligan, J.; Thornton, R.; Shei, G.-J.; Card, D.; Keohane, C.; Rosenbach, M.; Hale, J.; Lynch, C. L.; Rupprecht, K.; Parsons, W.; Rosen, H., Alteration of Lymphocyte Trafficking by Sphingosine-1-Phosphate Receptor Agonists. *Science* **2002,** *296* (5566), 346–349.

210. Kenji, C., FTY720, a New Class of Immunomodulator, Inhibits Lymphocyte Egress from Secondary Lymphoid Tissues and Thymus by Agonistic Activity at Sphingosine-1-Phosphate Receptors. *Pharmacol. Ther.* **2005,** *108* (3), 308–319.

211. Kiuchi, M.; Adachi, K.; Kohara, T.; Teshima, K.; Masubuchi, Y.; Mishina, T.; Fujita, T., Synthesis and Biological Evaluation of 2,2-Disubstituted 2-Aminoethanols: Analogues of FTY720. *Bioorg. Med. Chem. Lett.* **1998,** *8* (1), 101–106.

212. Jin, J.; Hu, J.; Zhou, W.; Wang, X.; Xiao, Q.; Xue, N.; Yin, D.; Chen, X., Development of a Selective S1P1 Receptor Agonist, Syl930, as a Potential Therapeutic Agent for Autoimmune Encephalitis. *Biochem. Pharmacol.* **2014,** *90* (1), 50–61.

213. Adachi, K.; Chiba, K., FTY720 Story. Its Discovery and the Following Accelerated Development of Sphingosine 1-Phosphate Receptor Agonists as Immunomodulators Based on Reverse Pharmacology. *Perspect. Med. Chem.* **2007,** *2007* (1), 11–23.

214. Gergely, P.; Nuesslein-Hildesheim, B.; Guerini, D.; Brinkmann, V.; Traebert, M.; Bruns, C.; Pan, S.; Gray, N. S.; Hinterding, K.; Cooke, N. G.; Groenewegen, A.; Vitaliti, A.; Sing, T.; Luttringer, O.; Yang, J.; Gardin, A.; Wang, N.; Crumb Jr, W. J.; Saltzman, M.; Rosenberg, M.; Wallström, E., The Selective Sphingosine-1-Phosphate Receptor

Modulator BAF312 Redirects Lymphocyte Distribution and has Species-Specific Effects on Heart Rate. *Br. J. Pharmacol.* **2012,** *167* (5), 1035–1047.

215. Pan, S.; Gray, N. S.; Gao, W.; Mi, Y.; Fan, Y.; Wang, X.; Tuntland, T.; Che, J.; Lefebvre, S.; Chen, Y.; Chu, A.; Hinterding, K.; Gardin, A.; End, P.; Heining, P.; Bruns, C.; Cooke, N. G.; Nuesslein-Hildesheim, B., Discovery of BAF312 (Siponimod), a Potent and Selective S1P Receptor Modulator. *ACS Med. Chem. Lett.* **2013,** *4* (3), 333–337.

216. Sanna, M. G.; Wang, S. K.; Gonzalez-Cabrera, P. J.; Don, A.; Marsolais, D.; Matheu, M. P.; Wei, S. H.; Parker, I.; Jo, E.; Cheng, W. C.; Cahalan, M. D.; Wong, C. H.; Rosen, H., Enhancement of Capillary Leakage and Restoration of Lymphocyte Egress by a Chiral S1P1 Antagonist *in Vivo*. *Nat. Chem. Biol.* **2006,** *2* (8), 434–441.

217. Oo, M. L.; Chang, S. H.; Thangada, S.; Wu, M. T.; Rezaul, K.; Blaho, V.; Hwang, S. I.; Han, D. K.; Hla, T., Engagement of S1P1-Degradative Mechanisms Leads to Vascular Leak in Mice. *J. Clin. Invest.* **2011,** *121* (6), 2290–2300.

218. Osada, M.; Yatomi, Y.; Ohmori, T.; Ikeda, H.; Ozaki, Y., Enhancement of Sphingosine-1-Phosphate-Induced Migration of Vascular Endothelial Cells and Smooth Muscle Cells by an EDG-5 Antagonist. *Biochem. Bioph. Res. Co.* **2002,** *299* (3), 483–487.

219. Salomone, S.; Waeber, C., Selectivity and Specificity of Sphingosine-1-Phosphate Receptor Ligands: Caveats and Critical Thinking in Characterizing Receptor-Mediated Effects. *Front. Pharmacol.* **2011,** *2* (9), 1–8.

220. Salomone, S.; Potts, E. M.; Tyndall, S.; Ip, P. C.; Chun, J.; Brinkmann, V.; Waeber, C., Analysis of Sphingosine-1-Phosphate Receptors Involved in Constriction of Isolated Cerebral Arteries with Receptor Null Mice and Pharmacological Tools. *Br. J. Pharmacol.* **2008,** *153* (1), 140–147.

221. Pyne, N. J.; Pyne, S., Selectivity and Specificity of Sphingosine 1-Phosphate Receptor Ligands: 'Off-Target' or Complex Pharmacology? *Front. Pharmacol.* **2011,** *2* (5), 1–5.

222. Davis, M. D.; Clemens, J. J.; Macdonald, T. L.; Lynch, K. R., Sphingosine 1-Phosphate Analogs as Receptor Antagonists. *J. Biol. Chem.* **2005,** *280* (11), 9833–9841.

223. Kennedy, P. C.; Zhu, R.; Huang, T.; Tomsig, J. L.; Mathews, T. P.; David, M.; Peyruchaud, O.; Macdonald, T. L.; Lynch, K. R., Characterization of a Sphingosine-1-Phosphate Receptor Antagonist Prodrug. *J. Pharmacol. Exp. Ther.* **2011,** *338* (3), 879–889.

224. Cohen, J. A.; Barkhof, F.; Comi, G.; Hartung, H. P.; Khatri, B. O.; Montalban, X.; Pelletier, J.; Capra, R.; Gallo, P.; Izquierdo, G.; Tiel-Wilck, K.; de Vera, A.; Jin, J.; Stites, T.; Wu, S.; Aradhye, S.; Kappos, L., Oral Fingolimod or Intramuscular Interferon for Relapsing Multiple Sclerosis. *N. Engl. J. Med.* **2010,** *362* (5), 402–415.

225. Schwalm, S.; Pfeilschifter, J.; Huwiler, A., Targeting the Sphingosine Kinase/Sphingosine 1-Phosphate Pathway to Treat Chronic Inflammatory Kidney Diseases. *Basic Clin. Pharmacol. Toxicol.* **2014,** *114* (1), 44–49.

226. Wang, Z.; Min, X.; Xiao, S. H.; Johnstone, S.; Romanow, W.; Meininger, D.; Xu, H.; Liu, J.; Dai, J.; An, S.; Thibault, S.; Walker, N., Molecular Basis of Sphingosine Kinase 1 Substrate Recognition and Catalysis. *Structure* **2013,** *21* (5), 798–809.

227. Paugh, S. W.; Paugh, B. S.; Rahmani, M.; Kapitonov, D.; Almenara, J. A.; Kordula, T.; Milstien, S.; Adams, J. K.; Zipkin, R. E.; Grant, S.; Spiegel, S., A Selective Sphingosine Kinase 1 Inhibitor Integrates Multiple Molecular Therapeutic Targets in Human Leukemia. *Blood* **2008,** *112* (4), 1382–1391.

228. J. Coward, G. A., E. Musi, J.P. Truman, A. Haimovitz-Friedman, J.C. Allegood, E. Wang, A.H. Merrill Jr., G.K. Schwartz, Safingol (*L*-threo-sphinganine) Induces Autophagy in Solid Tumor Cells Through Inhibition of PKC and the PI3-Kinase Pathway. *Autophgy* **2009,** *5* (2), 184–193.

229. Edsall, L. C.; Van Brocklyn, J. R.; Cuvillier, O.; Kleuser, B.; Spiegel, S., N,N-Dimethylsphingosine Is a Potent Competitive Inhibitor of Sphingosine Kinase but Not of Protein Kinase C: Modulation of Cellular Levels of Sphingosine 1-Phosphate and Ceramide. *Biochemistry* **1998,** *37* (37), 12892–12898.

230. Megidish, T.; Takio, K.; Titani, K.; Iwabuchi, K.; Hamaguchi, A.; Igarashi, Y.; Hakomori, S., Endogenous Substrates of Sphingosine-Dependent Kinases (SDKs) Are Chaperone Proteins: Heat Shock Proteins, Glucose-Regulated Proteins, Protein Disulfide Isomerase, and Calreticulin. *Biochemistry* **1999,** *38* (11), 3369–3378.

231. French, K. J.; Upson, J. J.; Keller, S. N.; Zhuang, Y.; Yun, J. K.; Smith, C. D., Antitumor Activity of Sphingosine Kinase Inhibitors. *J. Pharmacol. Exp. Ther.* **2006,** *318* (2), 596–603.

232. Lim, K. G.; Tonelli, F.; Li, Z.; Lu, X.; Bittman, R.; Pyne, S.; Pyne, N. J., FTY720 Analogues as Sphingosine Kinase 1 Inhibitors: Enzyme Inhibition Kinetics, Allosterism, Proteasomal Degradation, and Actin Rearrangement in MCF-7 Breast Cancer Cells. *J. Biol. Chem.* **2011,** *286* (21), 18633–18640.

233. Cingolani, F.; Casasampere, M.; Sanllehí, P.; Casas, J.; Bujons, J.; Fabrias, G., Inhibition of dihydroceramide desaturase activity by the sphingosine kinase inhibitor SKI II. *J. Lipid Res.* **2014,** *55* (8), 1711–1720.

234. Maines, L. W.; Fitzpatrick, L. R.; French, K. J.; Zhuang, Y.; Xia, Z.; Keller, S. N.; Upson, J. J.; Smith, C. D., Suppression of Ulcerative Colitis in Mice by Orally-Available Inhibitors of Sphingosine Kinase. *Digest. Dis. Sci.* **2008,** *53* (4), 997–1012.

235. Ren, S.; Xin, C.; Pfeilschifter, J.; Huwiler, A., A Novel Mode of Action of the Putative Sphingosine Kinase Inhibitor 2-(p-hydroxyanilino)-4-(p-chlorophenyl) Thiazole (SKI II): Induction of Lysosomal Sphingosine Kinase 1 Degradation. *Cell. Physiol. Biochem.* **2010,** *26* (1), 97–104.

236. Loveridge, C.; Tonelli, F.; Leclercq, T.; Lim, K. G.; Long, J. S.; Berdyshev, E.; Tate, R. J.; Natarajan, V.; Pitson, S. M.; Pyne, N. J.; Pyne, S., The Sphingosine Kinase 1 Inhibitor 2-(p-Hydroxyanilino)-4-(p-chlorophenyl)thiazole Induces Proteasomal Degradation of Sphingosine Kinase 1 in Mammalian Cells. *J. Biol. Chem.* **2010,** *285* (50), 38841–38852.

237. Aurelio, L.; Scullino, C. V.; Pitman, M. R.; Sexton, A.; Oliver, V.; Davies, L.; Rebello, R. J.; Furic, L.; Creek, D. J.; Pitson, S. M.; Flynn, B. L., From Sphingosine Kinase to Dihydroceramide Desaturase: A Structure–Activity Relationship (SAR) Study of the Enzyme Inhibitory and Anticancer Activity of 4-((4-(4-Chlorophenyl)thiazol-2-yl)amino)phenol (SKI-II). *J. Med. Chem.* **2016,** *59* (3), 965–984.

238. French, K. J.; Zhuang, Y.; Maines, L. W.; Gao, P.; Wang, W.; Beljanski, V.; Upson, J. J.; Green, C. L.; Keller, S. N.; Smith, C. D., Pharmacology and Antitumor Activity of ABC294640, a Selective Inhibitor of Sphingosine Kinase-2. *J. Pharmacol. Exp. Ther.* **2010**. *333* (1), 129–139.

239. Maines, L. W.; Fitzpatrick, L. R.; Green, C. L.; Zhuang, Y.; Smith, C. D., Efficacy of a Novel Sphingosine Kinase Inhibitor in Experimental Crohn's Disease. *Inflammopharmacology* **2010,** *18* (2), 73–85.

240. Snider, A. J.; Ruiz, P.; Obeid, L. M.; Oates, J. C., Inhibition of Sphingosine Kinase-2 in a Murine Model of Lupus Nephritis. *PLoS ONE* **2013,** *8* (1), e53521.

241. Fitzpatrick, L. R.; Green, C.; Maines, L. W.; Smith, C. D., Experimental Osteoarthritis in Rats Is Attenuated by ABC294640, a Selective Inhibitor of Sphingosine Kinase-2. *Pharmacology* **2011,** *87* (3–4), 135–143.

242. Schrecengost, R. S.; Keller, S. N.; Schiewer, M. J.; Knudsen, K. E.; Smith, C. D., Downregulation of Critical Oncogenes by the Selective SK2 Inhibitor ABC294640 Hinders Prostate Cancer Progression. *Mol. Cancer Res.* **2015,** *13* (12), 1591–1601.

243. Venant, H.; Rahmaniyan, M.; Jones, E. E.; Lu, P.; Lilly, M. B.; Garrett-Mayer, E.; Drake, R. R.; Kraveka, J. M.; Smith, C. D.; Voelkel-Johnson, C., The Sphingosine Kinase 2 Inhibitor ABC294640 Reduces the Growth of Prostate Cancer Cells and Results in Accumulation of Dihydroceramides *In Vitro* and *In Vivo*. *Mol. Cancer Ther.* **2015,** *14* (12), 2744–2752.

244. Gao, P.; Peterson, Y. K.; Smith, R. A.; Smith, C. D., Characterization of Isoenzyme-Selective Inhibitors of Human Sphingosine Kinases. *PLoS ONE* **2012,** *7* (9), e44543.

245. Rex, K.; Jeffries, S.; Brown, M. L.; Carlson, T.; Coxon, A.; Fajardo, F.; Frank, B.; Gustin, D.; Kamb, A.; Kassner, P. D.; Li, S.; Li, Y.; Morgenstern, K.; Plant, M.; Quon, K.; Ruefli-Brasse, A.; Schmidt, J.; Swearingen, E.; Walker, N.; Wang, Z.; Watson, J. E.; Wickramasinghe, D.; Wong, M.; Xu, G.; Wesche, H., Sphingosine Kinase Activity is Not Required for Tumor Cell Viability. *PloS ONE* **2013,** *8* (7), e68328.

246. Schnute, M. E.; McReynolds, M. D.; Kasten, T.; Yates, M.; Jerome, G.; Rains, J. W.; Hall, T.; Chrencik, J.; Kraus, M.; Cronin, C. N.; Saabye, M.; Highkin, M. K.; Broadus, R.; Ogawa, S.; Cukyne, K.; Zawadzke, L. E.; Peterkin, V.; Iyanar, K.; Scholten, J. A.;

Wendling, J.; Fujiwara, H.; Nemirovskiy, O.; Wittwer, A. J.; Nagiec, M. M., Modulation of Cellular S1P Levels with a Novel, Potent and Specific Inhibitor of Sphingosine Kinase-1. *Biochem. J.* **2012,** *444* (1), 79–88.

247. Byun, H.-S.; Pyne, S.; MacRitchie, N.; Pyne, N. J.; Bittman, R., Novel Sphingosine-Containing Analogues Selectively Inhibit Sphingosine Kinase (SK) Isozymes, Induce SK1 proteasomal degradation and reduce DNA synthesis in human pulmonary arterial Smooth Muscle Cells. *Med. Chem. Commun.* **2013,** *4* (10), 1394–1399.

248. Xiang, Y.; Asmussen, G.; Booker, M.; Hirth, B.; Kane Jr, J. L.; Liao, J.; Noson, K. D.; Yee, C., Discovery of Novel Sphingosine Kinase 1 Inhibitors. *Bioorg. Med. Chem. Lett.* **2009,** *19* (21), 6119–6121.

249. Liu, K.; Guo, T. L.; Hait, N. C.; Allegood, J.; Parikh, H. I.; Xu, W.; Kellogg, G. E.; Grant, S.; Spiegel, S.; Zhang, S., Biological Characterization of 3-(2-Amino-ethyl)-5-[3-(4-butoxyl-phenyl)-propylidene]-thiazolidine-2,4-dione (K145) as a Selective Sphingosine Kinase-2 Inhibitor and Anticancer Agent. *PLoS ONE* **2013,** *8* (2), e56471.

250. Lynch, K. R.; MacDonald, T. L.; Kharel, Y.; Mathews, T. P.; Wamhoff, B. R. Preparation of Amidine Analogs as Inhibitors of Sphingosine Kinase. WO2009146112A1, 2009.

251. Lynch, K. R.; MacDonald, T. L.; Mathews, T. P.; Kennedy, A.; Kharel, Y. Imidamide Sphingosine Kinase Inhibitors. WO2011020116A1, 2011.

252. Kharel, Y.; Mathews, T. P.; Gellett, A. M.; Tomsig, J. L.; Kennedy, P. C.; Moyer, M. L.; Macdonald, T. L.; Lynch, K. R., Sphingosine Kinase Type 1 Inhibition Reveals Rapid Turnover of Circulating Sphingosine-1-Phosphate. *Biochem. J.* **2011,** *440* (3), 345–353.

253. Kennedy, A. J.; Mathews, T. P.; Kharel, Y.; Field, S. D.; Moyer, M. L.; East, J. E.; Houck, J. D.; Lynch, K. R.; Macdonald, T. L., Development of Amidine-Based Sphingosine Kinase 1 Nanomolar Inhibitors and Reduction of Sphingosine 1-Phosphate in Human Leukemia Cells. *J. Med. Chem.* **2011,** *54* (10), 3524–3548.

254. Patwardhan, N. N.; Morris, E. A.; Kharel, Y.; Raje, M. R.; Gao, M.; Tomsig, J. L.; Lynch, K. R.; Santos, W. L., Structure−Activity Relationship Studies and *in Vivo* Activity of Guanidine-Based Sphingosine Kinase Inhibitors: Discovery of SphK1- and SphK2-Selective Inhibitors. *J. Med. Chem.* **2015,** *58* (4), 1879–1899.

255. Kharel, Y.; Raje, M.; Gao, M.; Gellett, A. M.; Tomsig, J. L.; Lynch, K. R.; Santos, W. L., Sphingosine Kinase Type 2 Inhibition Elevates Circulating Sphingosine-1-Phosphate. *Biochem J.* **2012,** *447* (1), 149–157.

256. Kharel, Y.; Morris, E. A.; Congdon, M. D.; Thorpe, S. B.; Tomsig, J. L.; Santos, W. L.; Lynch, K. R., Sphingosine Kinase 2 Inhibition and Blood Sphingosine-1-phosphate Levels. *J. Pharmacol. Exp. Ther.* **2015**. *355*,23–31 .

257. Pitman, M. R.; Powell, J. A.; Coolen, C.; Moretti, P. A. B.; Zebol, J. R.; Pham, D. H.; Finnie, J. W.; Don, A. S.; Ebert, L. M.; Bonder, C. S.; Gliddon, B. L.; Pitson, S. M., A Selective ATP-Competitive Sphingosine Kinase Inhibitor Demonstrates Anti-Cancer Properties. *Oncotarget* **2015,** *6* (9), 7065–7083.

258. Tonelli, F.; Alossaimi, M.; Natarajan, V.; Gorshkova, I.; Berdyshev, E.; Bittman, R.; Watson, D.; Pyne, S.; Pyne, N., The Roles of Sphingosine Kinase 1 and 2 in Regulating the Metabolome and Survival of Prostate Cancer Cells. *Biomolecules* **2013,** *3* (2), 316–333.

259. Morris, E. A. Structure–Activity Relationship Studies and Biological Evaluation of Selective Sphingosine Kinase Inhibitors. Virginia Polytechnic Institute and State University, 2015.

Chapter 2 Structure–Activity Relationship Studies of the Lipophilic Tail Region of Sphingosine Kinase 2 Inhibitors

2.1 Contributions

The work described in this chapter was conducted in collaboration with Elizabeth Childress, Dr. Neeraj Patwardhan, James Gumkowski, Emily Morris and Dr. Yugesh Kharel. The author is solely responsible for the synthesis of final compounds **2.6e, 2.32, 2.40a–c** and the corresponding intermediate structures. Elizabeth Childress is responsible for final compounds **2.12d,e, 2.17a–d** and the corresponding intermediate structures. Dr. Neeraj Patwardhan is responsible for final compounds **2.6f, 2.11c,f,g, 2.25** and the corresponding intermediate structures. James Gumkowski is responsible for final compounds **2.6d,g,h** and the corresponding intermediate structures. Emily Morris is responsible for final compound **2.6a** and the corresponding intermediate structures. All biological assays were conducted by Dr. Yugesh Kharel at the University of Virginia. The final manuscript was prepared by Dr. Webster Santos and the author. This work has been published in Bioorganic Medicinal Chemistry Letters and is available online. [Reprinted from Bioorganic Medicinal Chemistry Letters, 25, Congdon, M.D.; Childress, E.S.; Patwardhan, N.N.; Gumkowski, J.; Morris, E.A.; Kharel, Y.; Lynch, K.R. and Santos, W.L., Structure-activity relationship studies of the lipophilic tail region of sphingosine kinase 2 inhibitors, 4956-4960, Copyright (2015), DOI:10.1016/j.bmcl.2015.03.041, with permission from Elsevier.]

2.2 Abstract

Sphingosine-1-phosphate (S1P) is a ubiquitous, endogenous small molecule that is synthesized by two isoforms of sphingosine kinase (SphK1 and 2). Intervention of the S1P signaling pathway has attracted significant attention because alteration of S1P levels is linked to several disease states including cancer, fibrosis, and sickle cell disease. While intense investigations have focused on developing SphK1 inhibitors, only a limited number of SphK2-selective agents have been reported. Herein, we report our investigations on the structure–activity relationship studies of the lipophilic tail region of **SLR080811**, a SphK2-selective inhibitor. Our studies demonstrate that the internal phenyl ring is a key structural feature that is essential in the **SLR080811** scaffold. Further, we show the dependence of SphK2 activity and selectivity on alkyl tail length, suggesting a larger lipid binding pocket in SphK2 compared to SphK1.

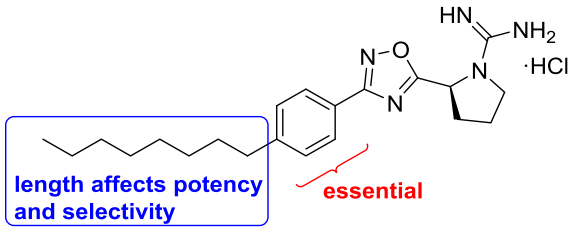

2.3 Introduction

Sphingosine 1-phosphate (S1P) is both an intermediate in the catabolism of sphingolipids and an extracellular signaling molecule. The synthesis of S1P *in vivo* is controlled by two isoforms of sphingosine kinase (SphK1 and SphK2), which phosphorylate sphingosine (Sph) to S1P. S1P is involved in a variety of important intracellular and extracellular functions through a complex network of signaling pathways including G-protein coupled receptors $S1P_{1-5}$. S1P signaling has been associated with a variety of diseases including cancer, fibrosis, multiple sclerosis, and sickle cell disease.[1-4] As a result of its key role in Sph and S1P metabolism, regulation of SphKs has attracted an increasing amount of attention as a therapeutic target. The ability to control SphK function would also aid in the understanding of their *in vivo* function as well as their effects in the sphingolipid signaling pathway.

Many differences exist between SphK1 and SphK2 including size, cellular localization, and intracellular roles.[5, 6] While double knockout studies in mice suggests that SphKs are the sole source of S1P, some functional redundancy exists as SphK1 or SphK2 null mice are viable and fertile. Although development of SphK1 inhibitors has been a focus of intense studies,[7] inhibitors of SphK2 are emerging (Figure 2.1). For example, **ABC294640** (K_i = 10 μM) was the first inhibitor with SphK2 activity that has been deployed in a variety of disease models including lupus nephritis, diabetic nephropathy, Crohn's disease, ulcerative colitis, and osteoarthritis.[6, 8] However, it was recently reported to inhibit estrogen receptors in breast cancer cells by acting as a partial agonist similar to tamoxifen.[9] Another inhibitor, thiazolidine-2,4-dione **K145** (K_i = 6.4 μM), which is an analog of sphingosine, was recently reported as a selective SphK2 inhibitor.[10] **K145** was shown to inhibit leukemia cell growth *in vitro* as well as in a xenograph mouse model.

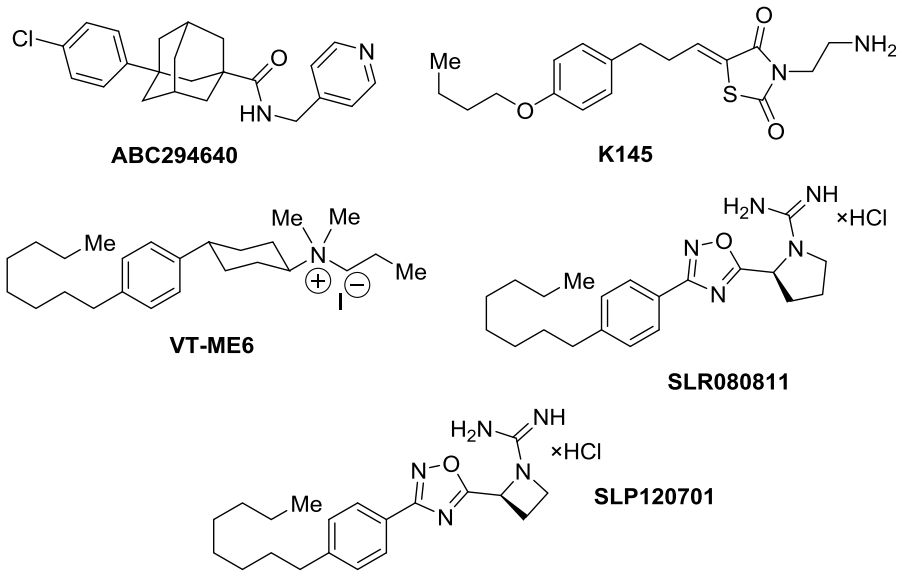

Figure 2.1. Select Structures of Sphingosine Kinase Inhibitors

Due to our interest in understanding the *in vivo* function of SphK2 and the lack of highly potent and selective inhibitors,[11] we focused our studies on developing unique scaffolds to achieve our goals. Our first generation inhibitor, **VT-ME6**, contained a quaternary ammonium group as a warhead and established that a positively charged moiety is necessary for engaging key amino acid residues in the enzyme binding pocket.[12, 13] This compound is moderately potent (K_i = 8 μM) and displays three-fold selectivity for SphK2 over SphK1. Subsequent improvement resulted in a scaffold that featured a 1,2,4-oxadiazole linker and guanidine as warhead: **SLR080811** possesses K_i values of 13.3 μM and 1.3 μM for SphK1 and SphK2 respectively.[14] A significant finding from these studies was that pharmacological inhibition of SphK2 resulted in elevated S1P levels in mice. Further structure–activity relationship studies on the guanidine core revealed that an azetidine-containing derivative **SLP1201701** improved the half-life from 4 to 8 hrs in mice.[15] In this report, we detail our investigations on the tail region of the scaffold (Figure 2.2). Our studies demonstrate that the internal phenyl ring is essential to maintain inhibitory

activity for SphK2 and that the alkyl tail length has a significant effect on the potency and selectivity towards SphK2.

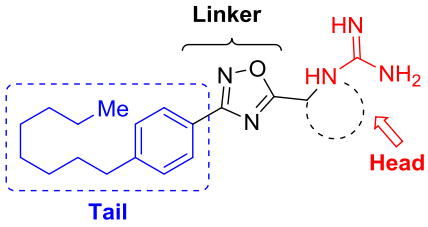

Figure 2.2. Pharmacophore of Guanidine-Based Inhibitors

2.4 Synthesis of SLR080811 and SLP120701 Tail Region Derivatives

The synthesis of **SLR080811** derivatives with varying alkyl length as well as heterocycles attached to the phenyl ring is shown in Schemes 2.1 and 2.2. In Scheme 2.1, 4-iodobenzonitrile was cross-coupled to a series of alkynes or hydroboration intermediates under standard Sonogashira or Suzuki–Miyaura conditions. Subsequent reaction with hydroxylamine afforded amidoximes **2.2a**–**e**, which were cyclized to 1,2,4-oxadiazoles **2.3a**–**f** in the presence of HCTU and Boc-L-proline. Deprotection with HCl and reduction of alkynyl groups with tosylhydrazine at reflux yielded amines **2.4a–h**. To install the guanidine moiety, the amines were treated with DIEA and *N*,*N*′-di-Boc-1*H*-pyrazole-1-carboxamidine for several days at room temperature and deprotected with HCl to produce the desired derivatives **2.6a,d,f–h.** A similar synthetic strategy was employed to access the remaining phenyl/alkyl derivatives (**2.12c** and **2.12f**,**g**); however, heterocycles **2.12d**,**e** were obtained via Buchwald–Hartwig coupling conditions as shown in Scheme 2.2. Similarly, Scheme 2.3 illustrates the synthesis of various amidopiperazine tail surrogates **2.17a**–**d** using Buchwald–Hartwig and amide coupling reactions.

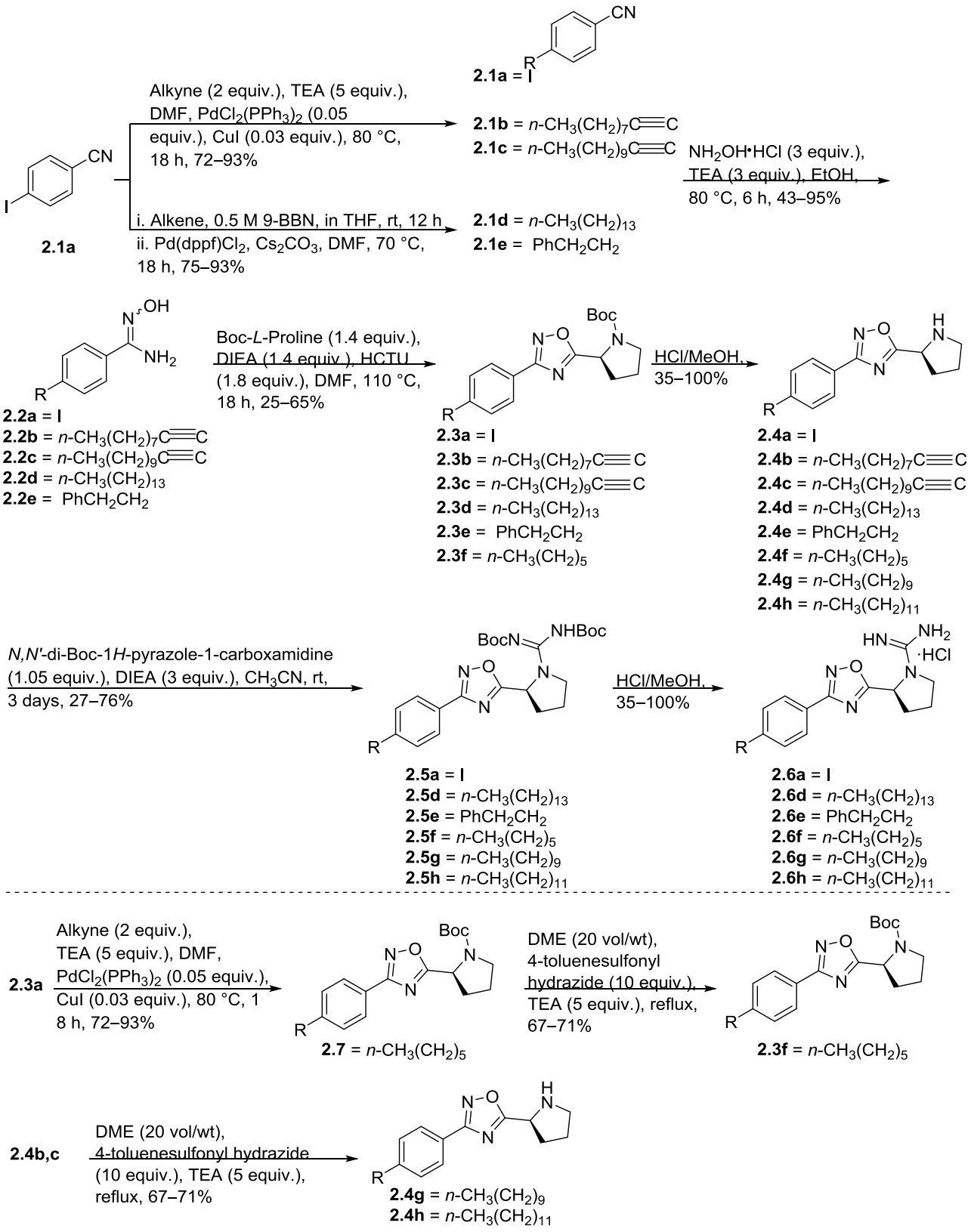

Scheme 2.1. Synthesis of SLR080811 Alkyl Derivatives

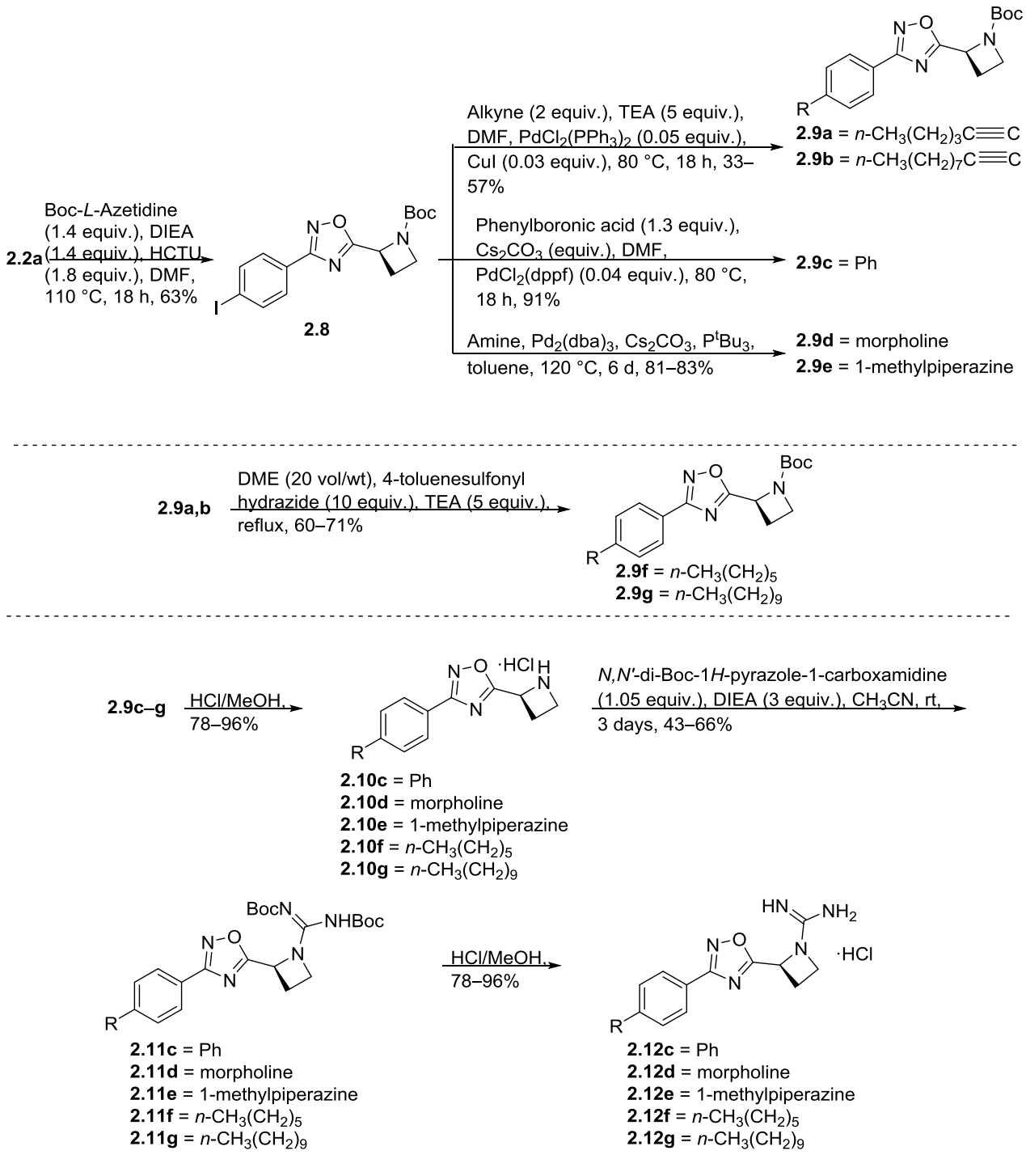

Scheme 2.2. Synthesis of SLP120701 Derivatives

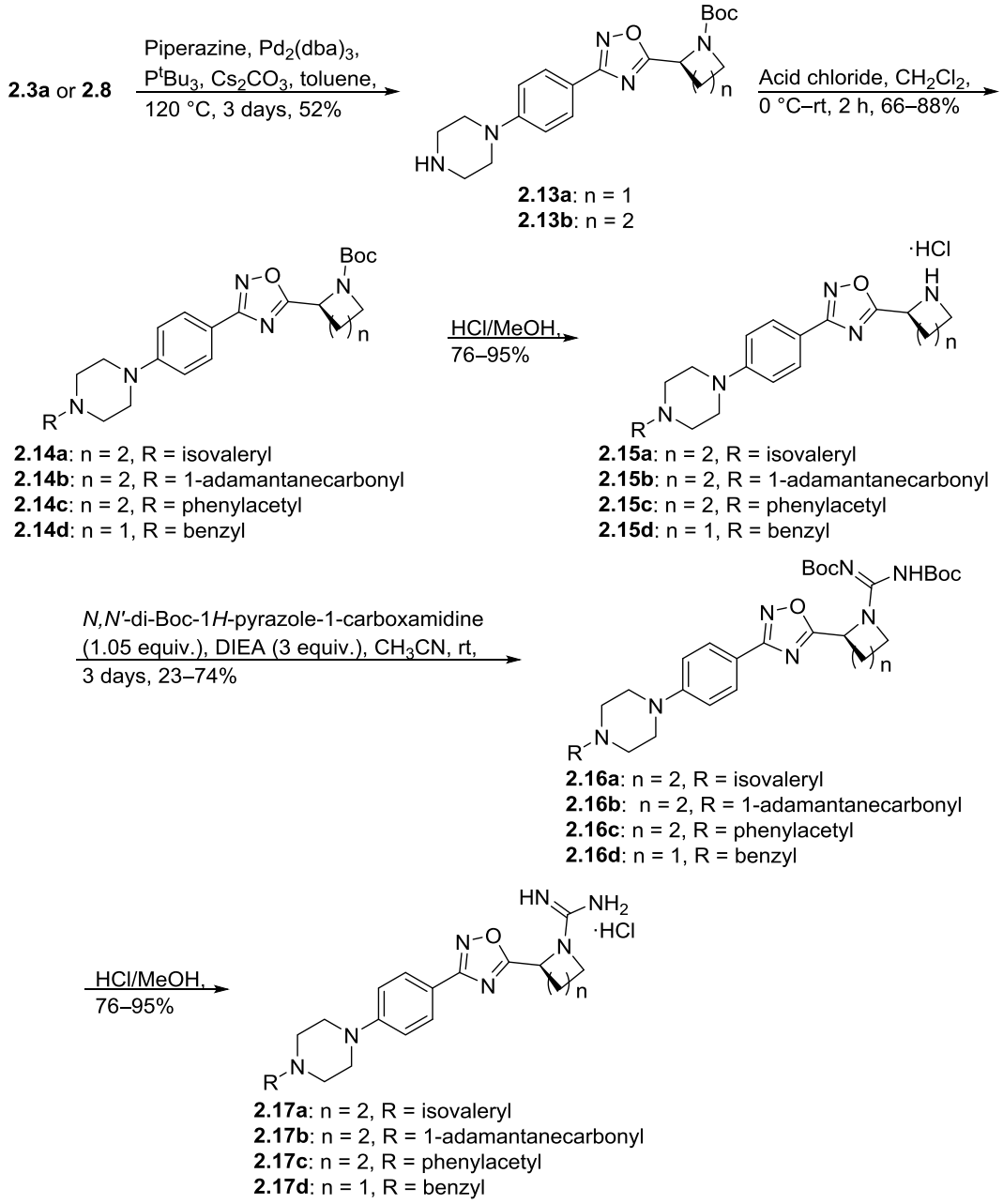

Scheme 2.3. Synthesis of SLR080811 Aminopiperazine Derivatives

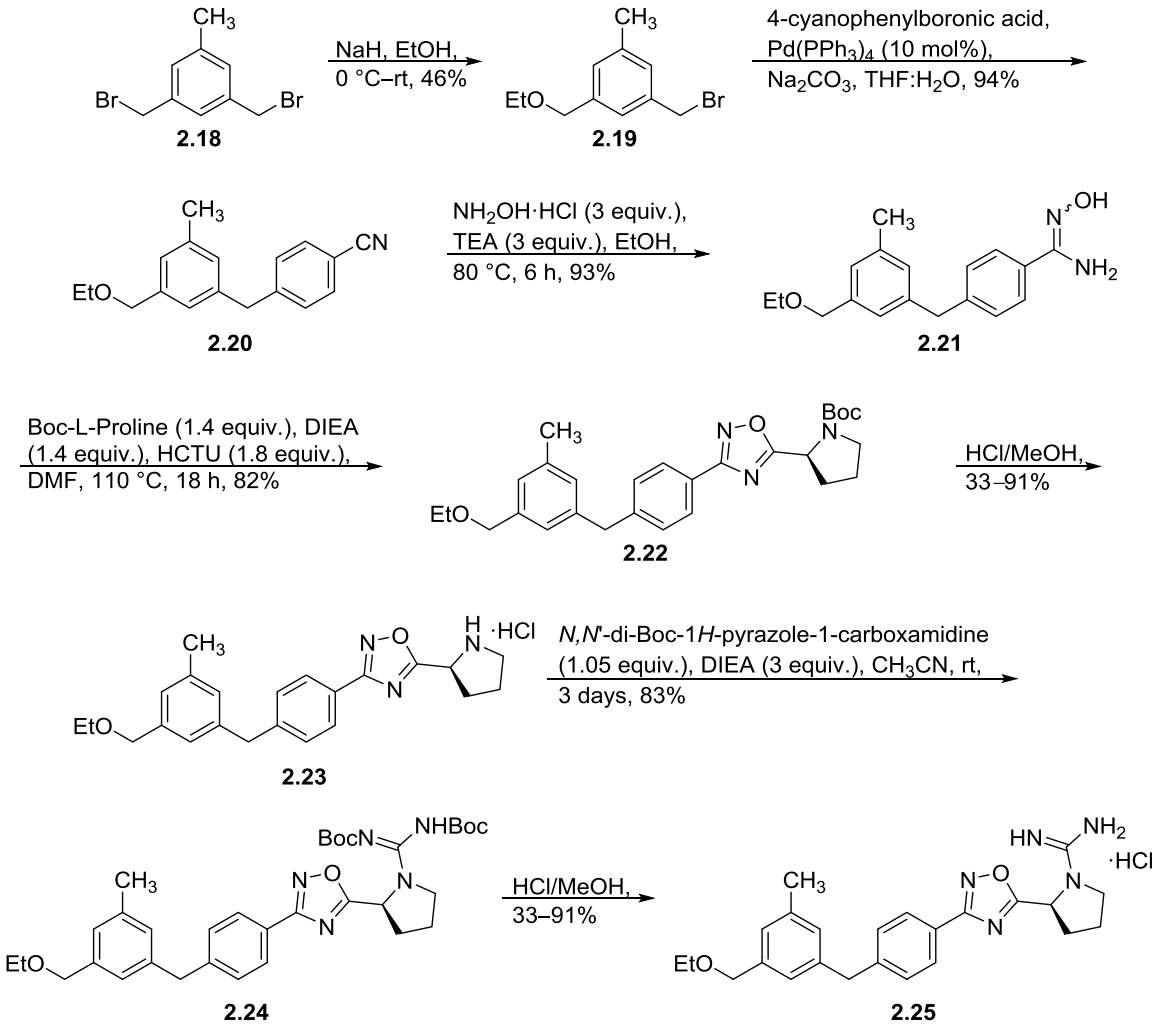

Scheme 2.4. Synthesis of Compound 2.25

Compounds **2.25** and **2.32** were synthesized as shown in Schemes 2.4 and 2.5. 4-(3-ethoxymethyl)-5-methylbenzyl)benzonitrile **2.20** was formed in two steps via mono-substitution of 1,3-bis(bromomethyl)-5-methylbenzene **2.18** and subsequent palladium-catalyzed cross coupling reaction with 4-cyanophenylboronic acid to afford **2.20**. Alternatively, benzonitrile **2.27** was achieved using sodium benzenesulfonate and **2.26**. Standard oxadiazole formation, guanidinylation, and deprotection afforded **2.25** and **2.32**. Finally, a series of alkyl tails directly linked to the oxadiazole ring were synthesized (Scheme 2.6). Treatment of alkylbromides with

potassium cyanide gave alkylnitriles **2.34a–c**, which were converted into amidoximes **2.35a–c**. Transformation into oxadiazoles **2.36a–c** was effected either by HCTU mediated cyclization at 110 °C or by two-step coupling/TBAF-catalyzed cyclization, which eventually led to **2.36a–c**. Standard guanidylation and deprotection afforded **2.40a–c**.

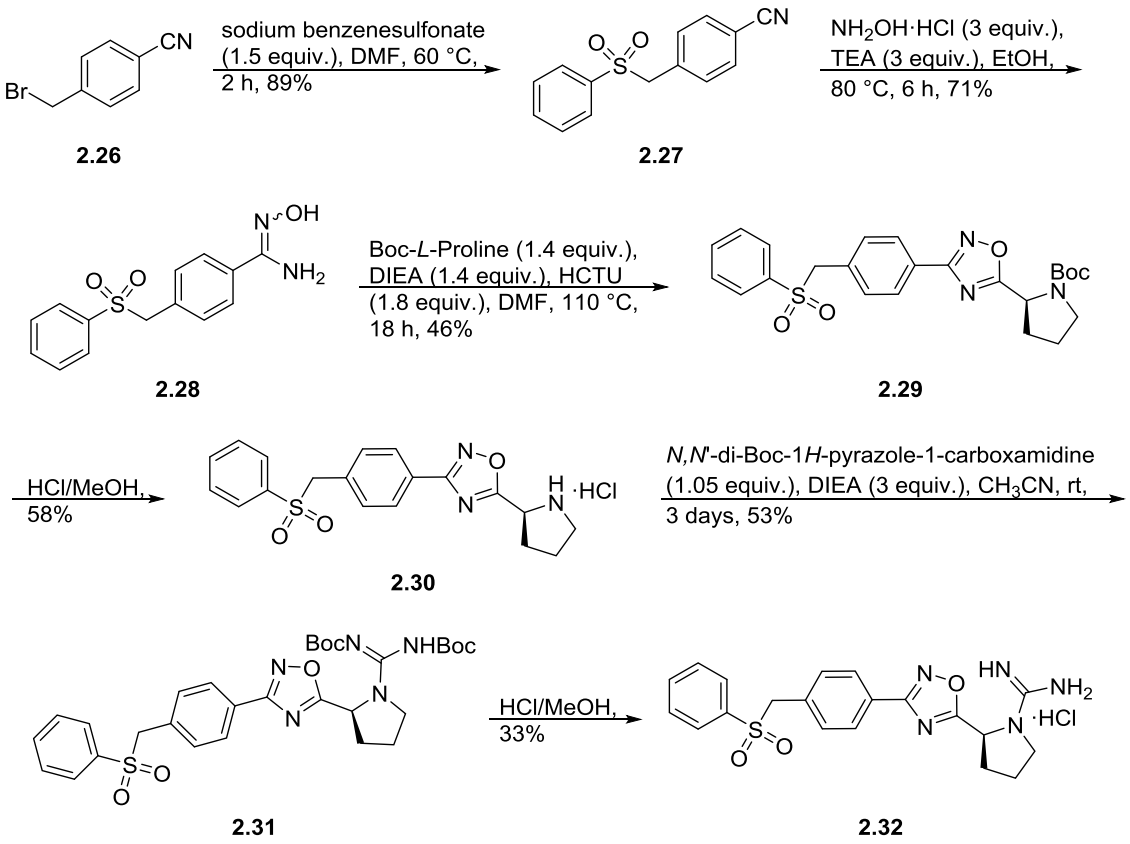

Scheme 2.5. Synthesis of Compound 2.32

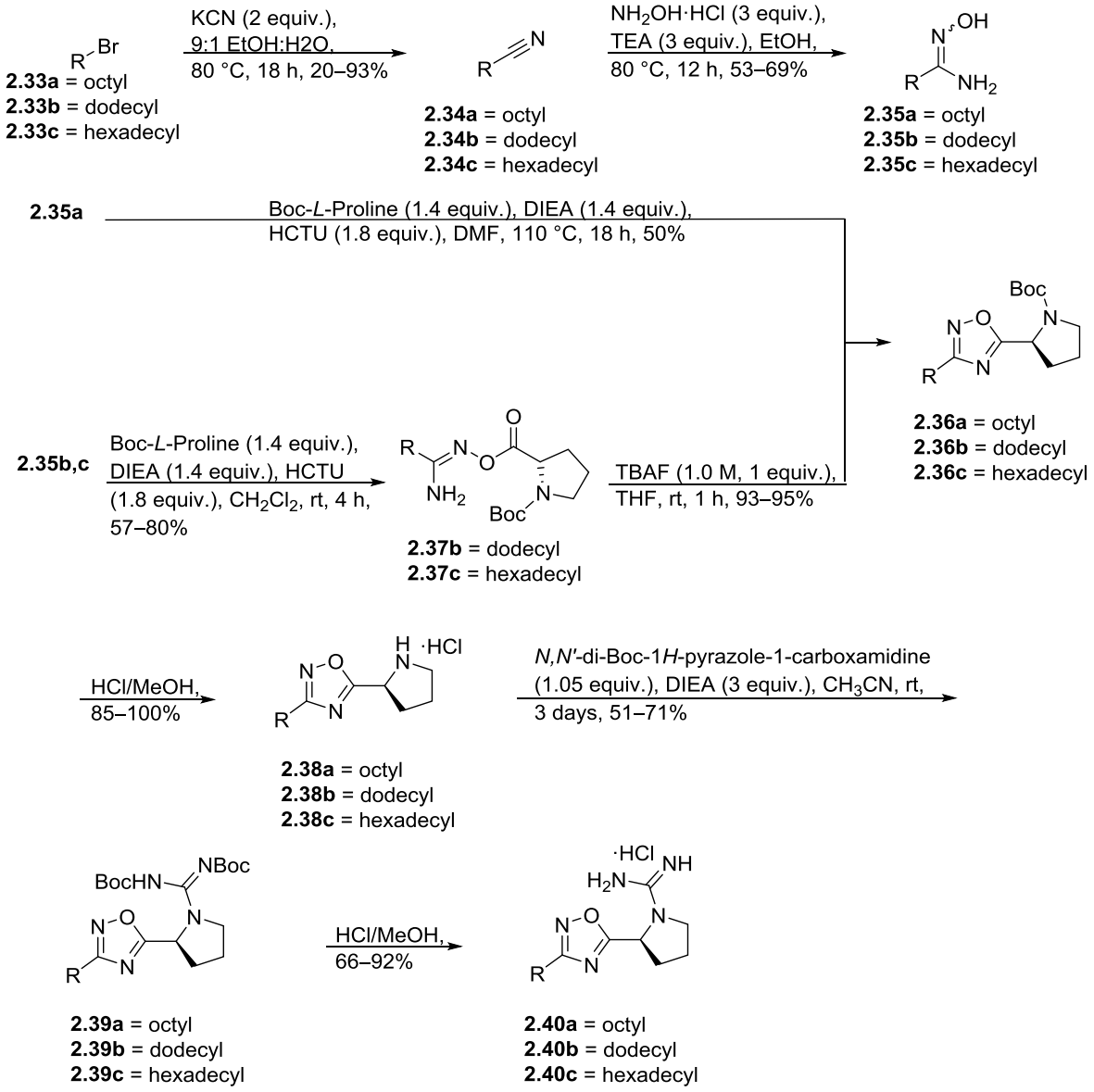

Scheme 2.6. Synthesis of SLR080811 Derivatives 2.40a–c

2.5 Biological Screening of Compounds

With the library of putative inhibitors synthesized, the inhibitory effects of the compounds were determined for human SphK1 (hSphK1) and mouse SphK2 (mSphK2) using a previously published protocol (Table 2.1).[15] Briefly, Sph and cell lysate containing recombinant

SphK1 or SphK2 were incubated with or without inhibitor in the presence of γ-[^{32}P]ATP. After 20 minutes, the reaction mixtures were extracted, separated using thin layer chromatography, and quantified using liquid scintillation counting. The kinase inhibition was determined as the amount of ^{32}P-S1P produced as a function of inhibitor concentration. Compounds were screened at 10 μM inhibitor concentrations.

As shown in Table 2.1, replacement of the octyl chain of **SLR080811** with iodide, phenyl or phenethyl groups did not improve inhibitory activity (entries 1–3). Decreasing or increasing the lipophilic alkyl tail length from hexyl to tetradecyl in two-carbon increments resulted in compounds with similar inhibitory activity as **SLR080811** (entries 4–10), although the hexyl chain was slightly less active. In cases where the kinase activity was similar to **SLR080811** at 10 μM, rescreening at a more stringent inhibitor concentration (1 μM) was performed. The results indicated that none of these analogs had improved activity compared to **SLR080811**. We also note that the pyrrolidine and azetidine rings have been shown to have similar potency, but with the advantage of improved *in vivo* half-life for the azetidine derivatives.[15] Interestingly, as the alkyl tail increased to a decyl group, SphK2 selectivity decreased as SphK1 inhibition increased. However, as the chain length increased further to a dodecyl and tetradecyl, inhibition of SphK1 decreased while maintaining SphK2 activity. These results suggest that the lipid binding pocket in SphK2 is much larger than that of SphK1 and is consistent with the prediction based on a crystal structure of SphK1 bound to SphK1 inhibitor **PF-543**.[16] We next investigated the effect of the phenyl substituent next to the 1,2,4-oxadiazole ring. Removal of this ring while maintaining the overall length of the molecule resulted not only in diminished SphK2 selectivity but also inhibitory activity (entries 11-13). Our data indicate that the phenyl ring is necessary for selectivity and potency using this scaffold.

To further determine features of the lipid binding pocket, morpholine and a series of heterocyclic rings were synthesized (entries 14–19). In particular, a piperazine ring is attractive because of increased conformational rigidity as well as an anchor point to which various groups can be appended. Morpholine, *N*-methyl and *N*-benzyl piperazine were inactive. As these substituents are positively charged, and there is a strong likelihood that the lipid binding pocket is lined with hydrophobic groups, neutral amide versions with increasing steric bulk were tested. Isovaleryl, phenacetyl, and adamantylcarbonyl groups were also inactive. Finally, trisubstituted aryl **2.25** as well as sulfonate **2.32** bearing groups, featured in SphK1 inhibitor **PF-543**, were tested and also found to be poor inhibitors (entries 20–21).[17]

Table 2.1. Inhibitory Effects of SLR080811 Derivatives on hSphK1 and mSphK2[a]

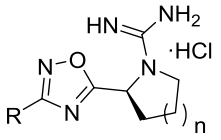

entry	R	n	% kinase activity[b]	
			SphK1	SphK2
1 (**2.6a**)	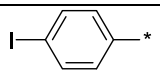	1	100 ± 2	63 ± 1
2 (**2.12c**)	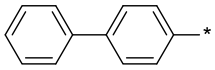	0	101 ± 1	91 ± 1
3 (**2.6e**)	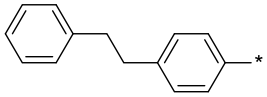	1	78 ± 1	70 ± 7
4 (**2.6f**)	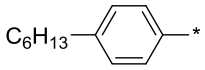	1	103 ± 2	35 ± 3 (76 ± 6)
5 (**2.12f**)	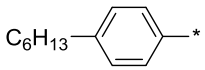	0	94 ± 2	45 ± 2 (86 ± 6)
6 (**SLR080811**)	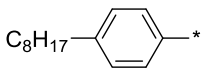	1	60 ± 1	9 ± 4 (44 ± 4)
7 (**2.6g**)	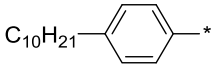	1	18 ± 9 (64 ± 4)	9 ± 7 (46 ± 5)
8 (**2.12g**)	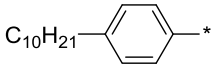	0	11 ± 4	12 ± 2
9 (**2.6h**)	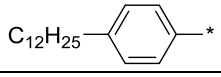	1	37 ± 2 (82 ± 3)	15 ± 1 (56 ± 1)

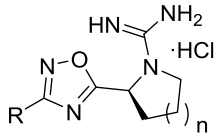

entry		R	n	% kinase activity [b] SphK1	% kinase activity [b] SphK2
10	(**2.6d**)	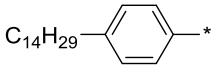	1	75 ± 1 (88 ± 3)	16 ± 10 (52 ± 4)
11	(**2.40a**)	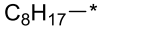	1	96 ± 1	88 ± 1
12	(**2.40b**)	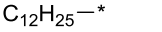	1	60 ± 1	57 ± 1
13	(**2.40c**)	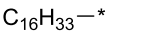	1	37 ± 5	52 ± 2
14	(**2.12d**)	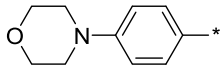	0	90 ± 4	94 ± 2
15	(**2.12e**)	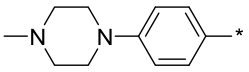	0	97 ± 2	90 ± 3
16	(**2.17d**)	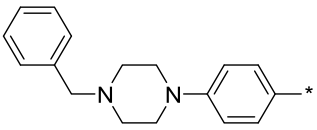	1	89 ± 2	89 ± 3
17	(**2.17a**)	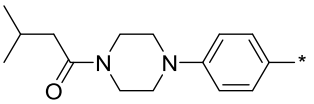	1	79 ± 2	90 ± 2
18	(**2.17c**)	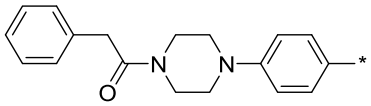	1	90 ± 2	86 ± 2
19	(**2.17b**)	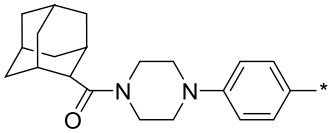	1	81 ± 28	87 ± 3
20	(**2.25**)	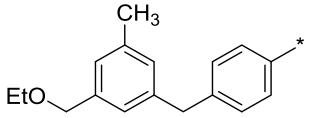	1	96 ± 1	46 ± 9 (99 ± 3)
21	(**2.32**)	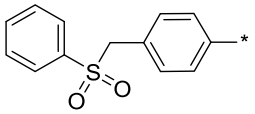	1	99 ± 1	88 ± 2

[a]Values represent percent activity of human SphK1 or mouse SphK2 with 10 and 5 μM Sph, respectively, in the presence of 10 μM inhibitor. Each value is an average of two experiments. Lower SphK activity level indicates better inhibition. [b]Values in parenthesis indicate compounds assayed at 1 μM.

2.6 Conclusions

In summary, a focused library of SphK2-selective inhibitor **SLR080811** derivatives that interrogated the lipophilic tail region of the pharmacophore were synthesized. Our studies demonstrate the dependence of SphK2 inhibitory activity on alkyl chain length; the optimal length includes octyl and decyl substituents, which suggests an ideal 'head-to-tail' (positive charge to terminal methyl group) length of approximately 18–21 atoms. Furthermore, our studies provide evidence for the much larger lipophilic binding cavity in SphK2 over SphK1. In the **SLR080811** scaffold, the internal phenyl ring appears to be essential for activity and is likely interacting with residues in the kinase binding pocket. These predictions could be confirmed by a SphK2 crystal structure, which is currently unavailable.

2.7 Acknowledgements

This work was achieved with financial support from the NIH (Grants R01 GM104366 and R01 GM067958).

2.8 References

1. Bigaud, M.; Guerini, D.; Billich, A.; Bassilana, F.; Brinkmann, V., Second Generation S1P Pathway Modulators: Research Strategies and Clinical Developments. *Biochim. Biophys. Acta.* **2014,** *1841* (5), 745–758.
2. Takuwa, N.; Du, W.; Kaneko, E.; Okamoto, Y.; Yoshioka, K.; Takuwa, Y., Tumor-Suppressive Sphingosine-1-Phosphate Receptor-2 Counteracting Tumor-Promoting Sphingosine-1-Phosphate Receptor-1 and Sphingosine Kinase 1. *Am. J. Cancer Res.* **2011,** *1*, 460–481.
3. Kunkel G. T; Maceyka M; Milstien S; Spiegel, S., Targeting the Sphingosine-1-Phosphate Axis in Cancer, Inflammation and Beyond. *Nat. Rev. Drug Discov.* **2013,** *12* (9), 688–702.
4. Zhang, Y.; Berka, V.; Song, A.; Sun, K.; Wang, W.; Zhang, W.; Ning, C.; Li, C.; Zhang, Q.; Bogdanov, M.; Alexander, D. C.; Milburn, M. V.; Ahmed, M. H.; Lin, H.; Idowu, M.; Zhang, J.; Kato, G. J.; Abdulmalik, O. Y.; Zhang, W.; Dowhan, W.; Kellems, R. E.; Zhang, P.; Jin, J.; Safo, M.; Tsai, A. L.; Juneja, H. S.; Xia, Y., Elevated Sphingosine-1-Phosphate Promotes Sickling and Sickle Cell Disease Progression. *J. Clin. Invest.* **2014,** *124* (6), 2750–2761.
5. Maceyka, M.; Sankala, H.; Hait, N. C.; Le Stunff, H.; Liu, H.; Toman, R.; Collier, C.; Zhang, M.; Satin, L. S.; Merrill, A. H., Jr.; Milstien, S.; Spiegel, S., SphK1 and SphK2, Sphingosine Kinase Isoenzymes with Opposing Functions in Sphingolipid Metabolism. *J. Biol. Chem.* **2005,** *280* (44), 37118–37129.
6. Neubauer, H. A.; Pitson, S. M., Roles, Regulation and Inhibitors of Sphingosine Kinase 2. *FEBS J.* **2013,** *280* (21), 5317–5336.

7. Plano, D.; Amin, S.; Sharma, A. K., Importance of Sphingosine Kinase (SphK) as a Target in Developing Cancer Therapeutics and Recent Developments in the Synthesis of Novel SphK Inhibitors. *J. Med. Chem.* **2014,** *57* (13), 5509–5524.

8. French, K. J.; Zhuang, Y.; Maines, L. W.; Gao, P.; Wang, W.; Beljanski, V.; Upson, J. J.; Green, C. L.; Keller, S. N.; Smith, C. D., Pharmacology and Antitumor Activity of ABC294640, a Selective Inhibitor of Sphingosine Kinase-2. *J. Pharmacol. Exp. Ther.* **2010,** *333*, 129–139.

9. Antoon, J. W.; White, M. D.; Meacham, W. D.; Slaughter, E. M.; Muir, S. E.; Elliott, S.; Rhodes, L. V.; Ashe, H. B.; Wiese, T. E.; Smith, C. D.; Burow, M. E.; Beckman, B. S., Antiestrogenic effects of the novel sphingosine kinase-2 inhibitor ABC294640. *Endocrinology* **2010,** *151* (11), 5124–5135.

10. Liu, K.; Guo, T. L.; Hait, N. C.; Allegood, J.; Parikh, H. I.; Xu, W.; Kellogg, G. E.; Grant, S.; Spiegel, S.; Zhang, S., Biological Characterization of 3-(2-amino-ethyl)-5-[3-(4-butoxyl-phenyl)-propylidene]-thiazolidine-2,4-dione (K145) as a Selective Sphingosine Kinase-2 Inhibitor and Anticancer Agent. *PLoS ONE* **2013,** *8* (2), e56471.

11. Santos, W. L.; Lynch, K. R., Drugging Sphingosine Kinase. *ACS Chem. Biol*. **2015**, 10 (1), 225–233.

12. Raje, M. R.; Knott, K.; Kharel, Y.; Bissel, P.; Lynch, K. R.; Santos, W. L., Design, Synthesis and Biological Activity of Sphingosine Kinase 2 Selective Inhibitors. *Bioorg. Med. Chem. Lett.* **2012,** *20* (1), 183–194.

13. Knott, K.; Kharel, Y.; Raje, M. R.; Lynch, K. R.; Santos, W. L., Effect of Alkyl Chain Length on Sphingosine Kinase 2 Selectivity. *Bioorg. Med. Chem. Lett.* **2012,** *22* (22), 6817–6820.

14. Kharel, Y.; Raje, M.; Gao, M.; Gellett, A. M.; Tomsig, J. L.; Lynch, K. R.; Santos, W. L., Sphingosine Kinase Type 2 Inhibition Elevates Circulating Sphingosine 1-Phosphate *Biochem. J.* **2012,** *447*, 149–157.

15. Patwardhan, N. N.; Morris, E. A.; Kharel, Y.; Raje, M. R.; Gao, M.; Tomsig, J. L.; Lynch, K. R.; Santos, W. L., Structure−Activity Relationship Studies and in Vivo Activity of Guanidine-Based Sphingosine Kinase Inhibitors: Discovery of SphK1 and 2 Selective Inhibitors. *J. Med. Chem.* **2015,** *58* (4), 1879–1899.

16. Wang, J.; Knapp, S.; Pyne, N. J.; Pyne, S.; Elkins, J. M., Crystal Structure of Sphingosine Kinase 1 with PF-543. *ACS Med. Chem. Lett.* **2014,** *5* (12), 1329–1333.

17. Schnute, M. E.; McReynolds, M. D.; Kasten, T.; Yates, M.; Jerome, G.; Rains, J. W.; Hall, T.; Chrencik, J.; Kraus, M.; Cronin, C. N.; Saabye, M.; Highkin, M. K.; Broadus, R.; Ogawa, S.; Cukyne, K.; Zawadzke, L. E.; Peterkin, V.; Iyanar, K.; Scholten, J. A.; Wendling, J.; Fujiwara, H.; Nemirovskiy, O.; Wittwer, A. J.; Nagiec, M. M., Modulation of Cellular S1P Levels with a Novel, Potent and Specific Inhibitor of Sphingosine Kinase-1. *Biochem. J.* **2012,** *444* (1), 79–88.

Chapter 3 Structure–Activity Relationship Studies and Molecular Modeling of Naphthalene-Based Sphingosine Kinase 2 Inhibitors

3.1 Contributions

The work described in this chapter was conducted in collaboration with Dr. Yugesh Kharel, Dr. Anne M. Brown and Dr. Stephanie N. Lewis. The author is solely responsible for the synthesis of the final compounds and the corresponding intermediate structures. All biological assays were conducted by Dr. Yugesh Kharel at the University of Virginia. All molecular modeling was conducted by Dr. David R. Bevan lab by Dr. Anne M. Brown and Dr. Stephanie N. Lewis in the Biochemistry Department at Virginia Tech. The final manuscript was prepared by Dr. Webster L. Santos and the author. This work has been published in ACS Medicinal Chemistry Letters and is available online. "Reprinted with permission from ACS Medicinal Chemistry Letters, {Congdon, M. D.; Kharel, Y.; Brown, A. M.; Lewis, S. N.; Bevan, D. R.; Lynch, K. R.; Santos, W. L., Structure-Activity Relationship Studies and Molecular Modeling of Naphthalene-Based Sphingosine Kinase 2 Inhibitors, ACS Med. Chem. Lett., **2016**, *7* (3), 229–234}. Copyright (2016) American Chemical Society."

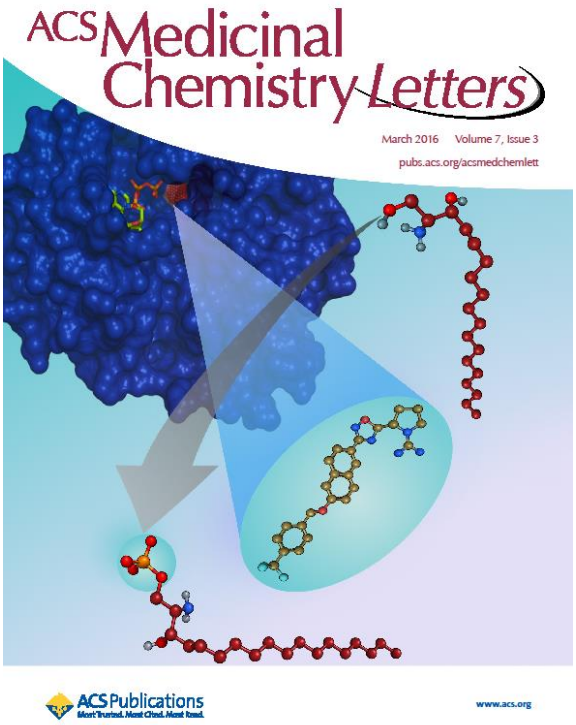

3.2 Abstract

The two isoforms of sphingosine kinase (SphK1 and SphK2) are the only enzymes that phosphorylate sphingosine to sphingosine-1-phosphate (S1P), which is a pleiotropic lipid mediator involved in a broad range of cellular processes including migration, proliferation, and inflammation. SphKs are targets for various diseases such as cancer, fibrosis, Alzheimer's and sickle cell disease. Herein, we disclose the structure-activity profile of naphthalene-containing SphK inhibitors and molecular modeling studies that reveal a key molecular switch that controls SphK selectivity.

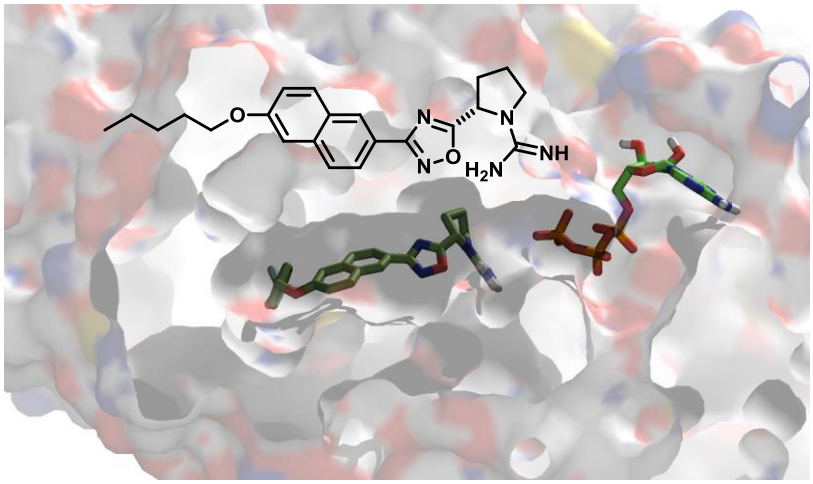

3.3 Introduction

Sphingolipids not only play a central role in eukaryotic membrane structural integrity but also in cell signaling pathways. Catabolism of sphingolipids generates ceramide (Cer), sphingosine (Sph), and sphingosine-1-phosphate (S1P), the concentrations of which are controlled by their respective enzymes. Studies have shown that these cellular metabolites can regulate the growth and survival balance of the cell.[1, 2] Ceramide and sphingosine are pro-apoptotic while S1P promotes cell proliferation. S1P acts as a ligand to five G-protein coupled receptors ($S1P_{1-5}$), which leads to diverse physiological and pathophysiological processes. The druggability of the S1P pathway was validated with the approval of Fingolimod [Gilenya®, FTY720 (Figure 1.12)] by the FDA for relapsing-remitting multiple sclerosis.[3, 4]

Sphingosine kinases (SphK) catalyze the phosphorylation of sphingosine to S1P. The S1P generated functions in a paracrine and autocrine fashion and regulates a complex signaling network to elicit a specific response such as migration and proliferation. SphKs exist in two isoforms, SphK1 and SphK2, which are localized in different compartments of the cell.[5] A variety of diseases such as cancer, Alzheimer's disease, fibrosis, multiple sclerosis, and sickle cell disease are implicated with S1P signaling pathways.[6-10] Therefore, controlling *in vivo* levels of S1P as a therapeutic modality is an attractive approach for these diseases. For example, S1P neutralizing antibodies such as Sonepcizumab are currently undergoing clinical trials for age-related macular degeneration (NCT01414153) and advanced solid tumors (NCT00661414).[11] SphK inhibitors are a complementary therapeutic strategy.[12] Drug discovery campaigns have been deployed to develop isoform-selective SphK inhibitors. Examples of current SphK inhibitors are shown in Figure 3.1. In particular, SphK1 has been a major focus by both academia and the pharmaceutical industry as an oncology target.[13] For example, an SphK1 selective

inhibitor, **PF543** (K_i = 3.5 nM, > 100 fold selective), decreased in vivo S1P levels that correlated with reduced sickling of red blood cells in a mouse model of sickle cell disease. [9] A dual inhibitor, Amgen **82**, had no statistical effect in reducing tumor volume in a xenograft mouse model.[14] Comparatively, there are a limited number of SphK2 specific inhibitors reported, and these have K_i values in the 1–10 micromolar range. **ABC294640**[15, 16] was the first selective SphK2 inhibitor (K_i = 9.8 μM) disclosed and is currently in phase I clinical trials for pancreatic

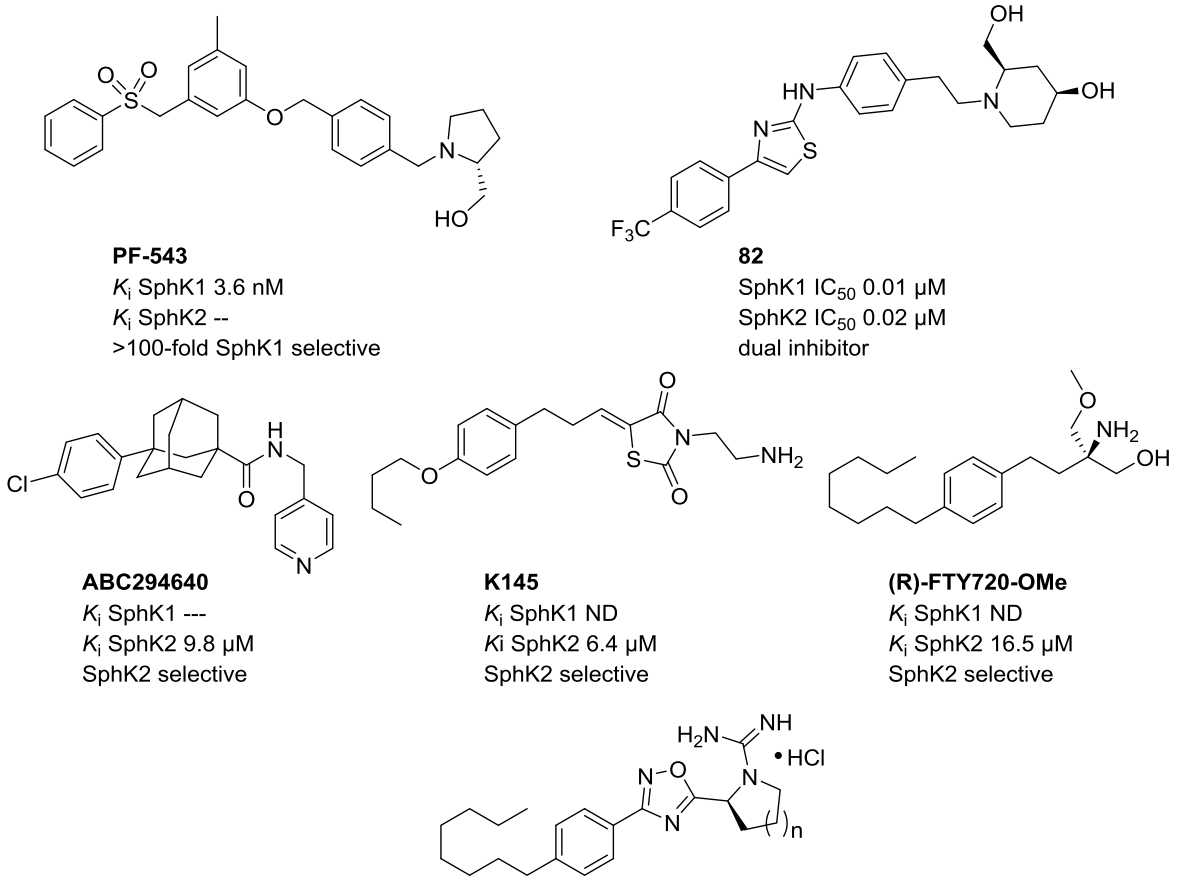

Figure 3.1. Select Structures of Sphingosine Kinase Inhibitors

cancer and solid tumors (NCT01488513), and refractory/relapsed diffuse large B-cell lymphoma (NCT02229981). Recent studies suggest that **ABC294640** has a tamoxifen-like activity.[17]

As a result of our interest in understanding the *in vivo* function of SphK2, our investigations focus on identifying improved inhibitors of SphK2. We previously established the requirement for a positively charged moiety that is proposed to interact with key amino acid Asp residues in the enzyme binding pocket.[18, 19] Further structure–activity studies resulted in the discovery of **SLR080811**, which featured a 1,2,4-oxadiazole linker and a cationic guanidine head group.[20] **SLR080811** was the first SphK2 inhibitor to demonstrate an increase in blood S1P levels on dosing in mice.[21] Although this finding was surprising, it is in agreement with genetic studies with SphK2 null mice wherein S1P levels increased 2–3 fold over wild-type (WT).[22-24] Subsequent studies of the tail region of **SLR080811** demonstrated the necessity for the internal phenyl ring and a dependence of SphK2 inhibitory activity with alkyl chain length.[19, 25] In this report, we detail our investigations on the tail region of a scaffold that features a naphthalene ring. Molecular modeling efforts revealed key hydrophobic and hydrogen bonding interactions within the sphingosine binding pocket. In addition, structure–activity relationship (SAR) studies indicated that removal of a hydroxyl group on the pyrrolidine ring of the inhibitor acts as a molecular switch to induce selective SphK2 inhibition.

3.4 Design and Synthesis of Naphthalene-Based Derivatives of SLR080811

Our previous studies reported in chapter 2 have indicated the importance of the internal phenyl ring in the **SLR080811** scaffold. Compounds **2.40a–c** displayed substantial decreases in potency and selectivity for mSphK2 compared to **SLR080811**. Despite the lack of potency, these compounds still displayed the general trend between alkyl chain length and mSphK2 inhibition.

From this data we concluded that the internal phenyl ring had a significant role in binding to the enzyme and hypothesized that by increasing the aromatic motif hSphK2 potency could be improved. To test this hypothesis, a naphthyl moiety was substituted for the internal phenyl of **SLR080811**. This alteration would allow us to slightly increase the aromatic area at this position without adding rotatable bonds present in a biphenyl moiety or substantially increasing steric bulk.

Numerous compounds possessing the naphthalene motif are commercially available which allows for the incorporation of the naphthyl moiety to be achieved via numerous synthetic routes. To assist in solubility and decrease lipophilicity, it was decided that an ether linkage would be employed to connect the remainder of the "tail" group to the structure. This linkage could be obtained by using a hydroxyl moiety as the synthetic handle which would allow the remaining portion of the "tail" motif to be added via Williamson ether synthesis or a substitution reaction. Through the use of primary alkyl halides, vast structural diversity could easily be obtained due to the large number of commercially available reagents and help to further elucidate an SAR around the "tail" region. Based on our previous knowledge concerning the installation of the 1,2,4-oxdiazole moiety into our compounds, it was decided that a hydroxyl-naphthonitrile would be utilized as starting material. Specifically, 6-hydroxy-2-naphthonitrile (**3.1**) was chosen to mimic the para substitution of the **SLR080811** phenyl ring which has been shown to be more potent than the meta substituted analogs (data not published).

3.4.1 Synthesis of Initial Naphthalene Derivatives

To initially examine whether the naphthalene moiety would be an advantageous substitution to the **SLR080811** scaffold, initial compounds were synthesized in a linear fashion, as shown in Scheme 3.1, using previously published conditions. First, the tail portion was

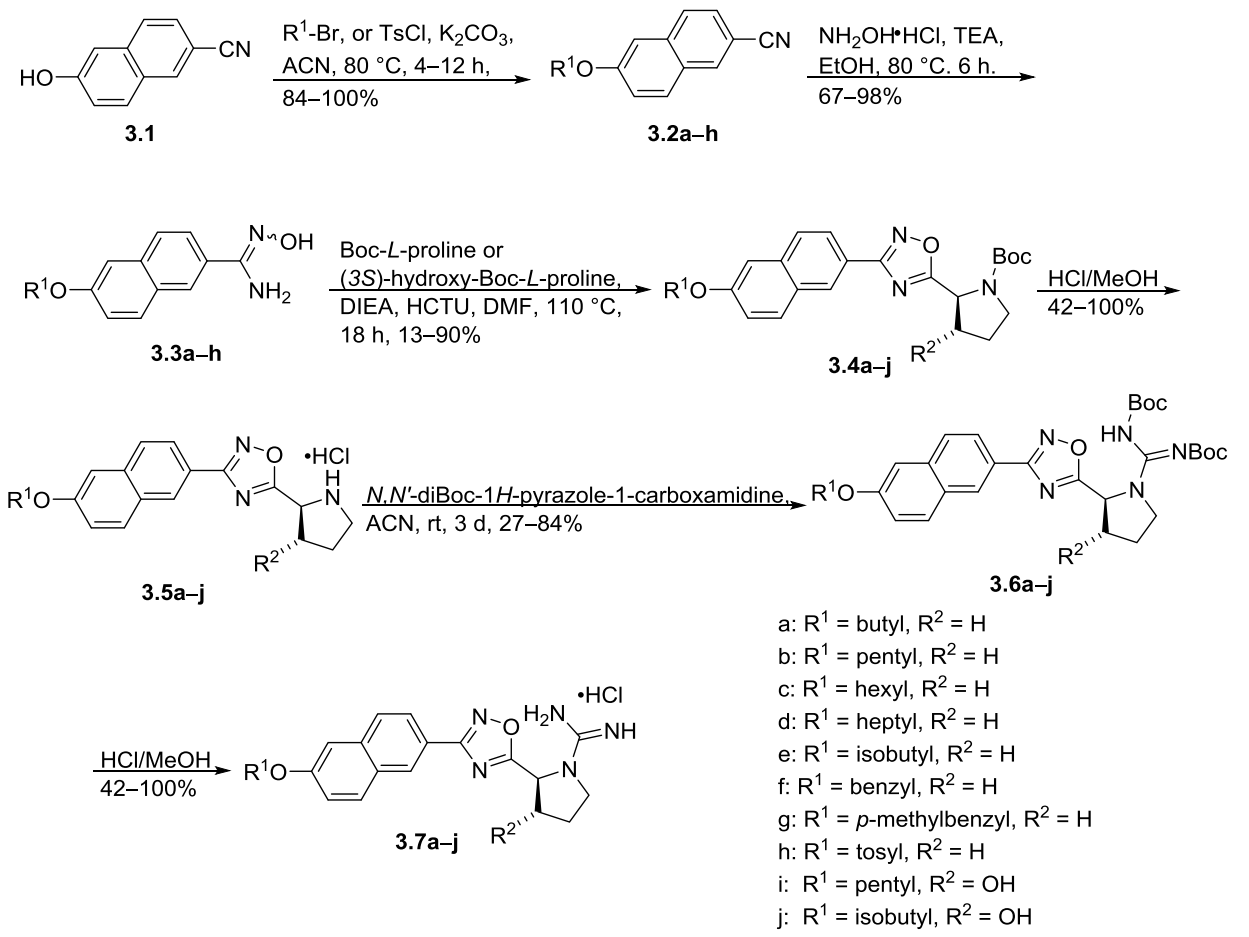

Scheme 3.1. Preliminary Approach to Naphthalene Derivatives

installed when 6-hydroxy-2-naphthonitrile **3.1** was coupled to a series of primary alkyl bromides or tosylchloride using standard Williamson ether synthesis conditions to afford naphthylethers **3.2a–h**. Subsequent reaction with hydroxylamine hydrochloride and triethylamine yielded amidoximes **3.3a**–**h**. Treatment of **3.3a**–**h** with Boc-*L*-proline or (3*S*)-hydroxy-Boc-*L*-Proline and HCTU produced 1,2,4-oxadiazoles **3.4a**–**j**. The Boc group was removed in acidic methanol to give pyrrolidines **3.5a**–**j**, which were subsequently reacted with DIEA and *N,N*′-di-Boc-1H-pyrazole-1-carboxamidine for several days at room temperature to generate intermediates **3.6a**–**j**. It should be noted that the guanidylation reaction was most efficient following these conditions

as heating resulted in decomposition. Removal of the Boc groups with HCl produced the desired guanidine derivatives **3.7a–j**.

3.4.2 Synthesis of Naphthalene-Based Derivatives via a Common Intermediate Pathway

Since the naphthalene moiety appeared to be a beneficial addition, a common intermediate pathway was employed for high-throughput to rapidly access a more diverse set of analogs, (Scheme 3.2). Naphthol **3.11** was identified as a key diversifying element since it allowed for diversification at the latest possible stage of synthesis. As a result, the overall number of reactions and columns required to complete the SAR were minimized.

In general, the reactions used were identical to those employed in Scheme 1. The main difference was the utilization of a Biotage microwave reactor, which drastically decreased the time required for select reactions. N'-6-Dihydroxy-2-naphthimidamide (**3.8**) was formed quickly and in decent yield from the unprotected naphthol using the microwave. Cyclization and dehydration of **3.8** to produce the Boc-protected-1,2,4-oxadiazole (**3.9**) was completed using a standard benchtop procedure, since a faster microwave procedure with equivalent or higher yield was not known. Boc-deprotection was achieved using 4N HCl in dioxane to yield HCl salt **3.10** as a white solid. Finally, the di-Boc-guanidine common intermediate (**3.11**) was formed in good yield using standard guanylation reagents and microwave conditions. Use of the microwave and higher reaction molarity resulted in increased product yield and substantially decreased reaction time. This reaction, which normally takes a minimum of 3 days with stirring under nitrogen at room temperature, was accomplished in only 30 minutes at 85 °C in the Biotage microwave.

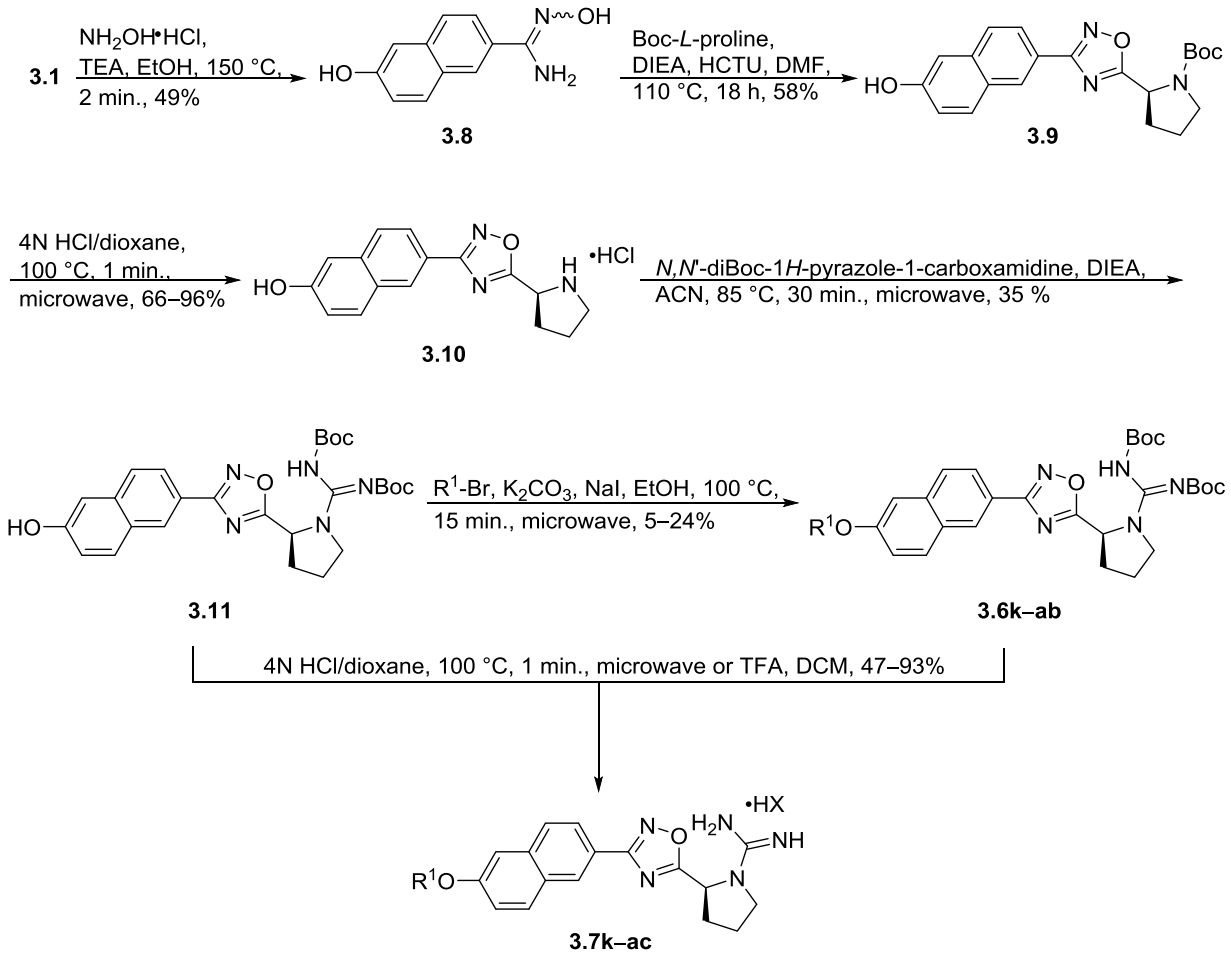

Scheme 3.2. Common Intermediate Synthetic Pathway to Naphthalene Derivatives

Williamson ether synthesis was used to diversify the structures from the common intermediate (**3.11**) to produce the di-Boc-protected compounds (**3.6k–ab**). A variety of conditions were attempted (Table 3.1); however, only low yields were obtained. This is in part due to the instability of the common intermediate **3.11** and product at high temperatures for long periods of time. In general, reactions were first attempted using **3.9.** Once conditions were discovered that gave the desired product, in any yield, the reaction was repeated using di-Boc-guanidine **3.11** as the limiting reagent. The progress of all reactions was monitored by TLC. Standard conditions (entry 1) produced the desired product (**3.12**) in 4% yield; however, the addition of sodium iodide, an additive frequently used to promote a halide exchange, did not

increase the formation of **3.12** (entry 2). Unfortunately, when intermediate **3.11** was subjected to these conditions, the desired product (**3.6m**) was not produced (entry 3). Additional solvents including acetone, DMF and ethanol were screened. No product was detected, when acetone was used (entries 4–6). Furthermore, increasing the reaction duration from 10 minutes to overnight did not affect the yield (entries 4 and 5). When DMF was employed, formation of **3.12** was not detected after heating to 110 °C for 30 minutes (entry 7); however, when the temperature was increased to 150 °C, **3.12** was produced in 4% yield (entry 8). Potassium carbonate was exchanged for cesium carbonate due to increased solubility in DMF (entries 9 and 10). These reactions, which employed **3.11**, did not use sodium iodide and were run at lower temperatures, did not produce product. When ethanol was used as the solvent, heating at 80 °C did not result in the formation of **3.12** and **3.6m** after 10 minutes (entries 11 and 14, respectively). Raising the temperature to 100 °C led to formation of **3.12** and **3.6m** (entries 12, 15). Further elevation of the reaction temperature was found to inhibit product formation (entry 13). Extending the duration of the reaction from 5 minutes to 15 minutes produced no noticeable change in yield (entry 16). It should be noted that in some cases, longer reaction times (greater than 15 minutes) produced increased amounts of side products and did not seem to increase the product yield [based on thin layer chromatography (TLC) observations]. Moreover reactions left running overnight resulted in the complete degradation of **3.11** and formation of multiple side products. The same was not observed when the starting material was **3.9** indicating that some of the difficulty of the reaction was the result of the stability of the starting material. TLC analysis indicated that **3.9** was still present in the reaction mixture and that fewer side products had formed. When the reaction was heated for a total of 15 minutes, comparable yields to entry 15 was obtained with minimal side product formation based on TLC. The utilized conditions are shown in entry 16.

Table 3.1. Optimization of Williamson Ether Synthesis with Common Intermediates

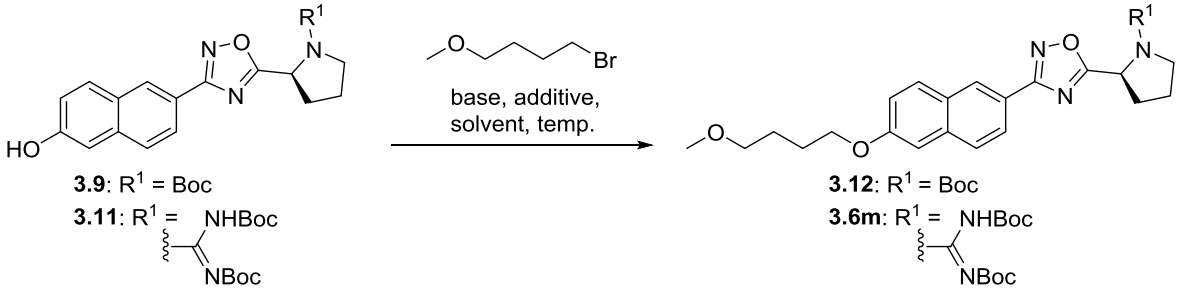

Entry	Limiting Reagent	Solvent	Base	Temp (°C)	Time	Additive	% Yield
1	**3.9**	ACN	K_2CO_3	80	overnight	--	4
2	**3.9**	ACN	K_2CO_3	80	overnight	NaI	4
3	**3.11**	ACN	K_2CO_3	80	overnight	NaI	0
4	**3.9**	Acetone	K_2CO_3	55	10 min	NaI	0
5	**3.9**	Acetone	K_2CO_3	55	overnight	NaI	0
6	**3.9**	Acetone	K_2CO_3	80	10 min	NaI	0
7	**3.9**	DMF	K_2CO_3	110	30 min	NaI	0
8	**3.9**	DMF	K_2CO_3	150	30 min	NaI	4
9	**3.11**	DMF	Cs_2CO_3	80	5 min	--	0
10	**3.11**	DMF	Cs_2CO_3	85	30 min	--	0
11	**3.9**	EtOH	K_2CO_3	80	10 min	NaI	0
12	**3.9**	EtOH	K_2CO_3	100	10 min	NaI	4
13	**3.9**	EtOH	K_2CO_3	150	10 min	NaI	0
14	**3.11**	EtOH	K_2CO_3	80	5 min	NaI	0
15	**3.11**	EtOH	K_2CO_3	100	5 min	NaI	17
16	**3.11**	EtOH	K_2CO_3	100	15 min	NaI	14

Once **3.6k–ab** and **3.11** were obtained, a final Boc-deprotection with either 4N HCl in dioxane or TFA in DCM achieved the desired compounds **3.7k–ac**. It should be noted that **3.7k–ac** were resynthesized to obtain complete characterization. Due to increased compound stability, better reactivity and ease of separation, **3.9** was used as the common intermediate when the compounds were resynthesized.

3.5 Biological Evaluation

3.5.1 Initial Screening for Sphingosine Kinase Inhibition

With necessary compounds at hand, the inhibitory effects on human SphK1 and SphK2 were determined using a previously established protocol.[26] In this assay, cell lysate containing recombinant human SphK1 or SphK2, sphingosine and [γ-^{32}P]ATP with or without inhibitor were incubated for 20 minutes. After extraction, the resulting mixture was separated by thin layer chromatography and quantified by scintillation counting. SphK activity was determined by the amount of [γ-^{32}P]-S1P as a function of inhibitor concentration. Compounds were screened at 1 μM inhibitor concentrations.

The results of the inhibition assay are shown in Table 3.2 with **SLR080811** as the standard. As expected, removal of the lipophilic tail completely abolished inhibitory activity (entry 1). Incremental increases of an aliphatic chain from a short butyl to a longer heptyl group demonstrated a length dependence on inhibition (entries 2–5). In this series, optimal alkyl chain length is achieved with a pentyl group (**3.7b**), where the distance between the charged guanidine group and the omega carbon is approximately 19 atoms away. Compound **3.7b** (entry 3) is slightly more potent than lead compound **SLR080811**. The cyclopentyl derivative **3.7k** had

Table 3.2. Inhibitory Effects of Compounds with hSphK1 and hSphK2

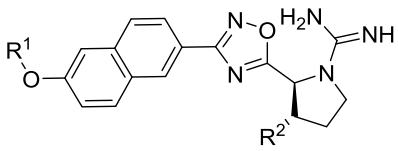

entry		R^1	R^2	% kinase activity	
				hSphK1	hSphK2
SLR080811		– [b]	–	88 ± 1	61 ± 6
1	**3.7ac**	H	H	114 ± 5	106 ± 6
2	**3.7a**	C_4H_9—*	H	88 ± 4	69 ± 3
3	**3.7b**	C_5H_{11}—*	H	90 ± 7	51 ± 1
4	**3.7c**	C_6H_{13}—*	H	98 ± 1	64 ± 4
5	**3.7d**	C_7H_{15}—*	H	90 ± 1	83 ± 1
6	**3.7e**	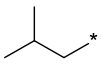	H	76 ± 5	74 ± 3
7	**3.7k**	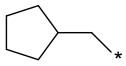	H	103 ± 1	57 ± 8
8	**3.7l**	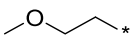	H	87 ± 4	118 ± 6
9	**3.7m**	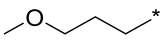	H	112 ± 10	109 ± 3
10	**3.7f**	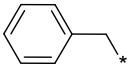	H	82 ± 10	97 ± 3
11	**3.7g**	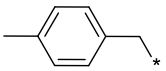	H	96 ± 2	94 ± 9
12	**3.7h**	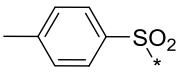	H	92 ± 5	89 ± 3
13	**3.7n**	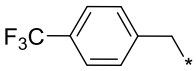	H	113 ± 3	42 ± 5
14	**3.7o**	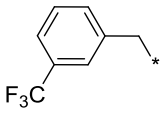	H	91 ± 2	81 ± 1
15	**3.7p**	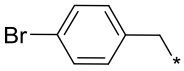	H	85 ± 1	35 ± 3
16	**3.7q**	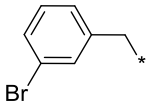	H	103 ± 2	49 ± 4
17	**3.7r**	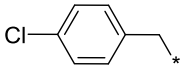	H	96 ± 1	56 ± 6

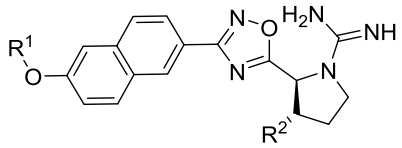

entry		R^1	R^2	% kinase activity	
				hSphK1	hSphK2
18	**3.7s**	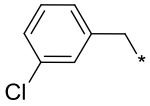	H	96 ± 1	46 ± 6
19	**3.7t**	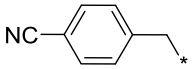	H	92 ± 1	43 ± 1
20	**3.7u**	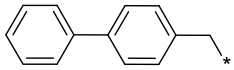	H	101 ± 1	51 ± 1
21	**3.7v**	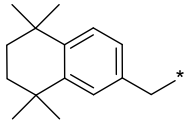	H	104 ± 5	104 ± 14
22	**3.7w**	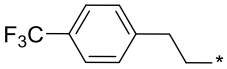	H	95 ± 3	30 ± 1
23	**3.7x**	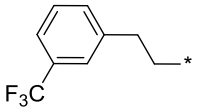	H	90 ± 3	34 ± 6
24	**3.7y**	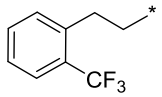	H	98 ± 8	47 ± 3
25	**3.7z**	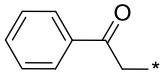	H	103 ± 1	103 ± 4
26	**3.7aa**	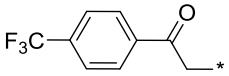	H	91 ± 1	65 ± 1
27	**3.7ab**	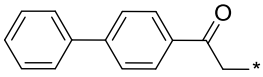	H	83 ± 3	77 ± 2
28	**3.7i**	C_5H_{11}—*	OH	40 ± 2	46 ± 12
29	**3.7j**	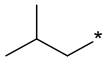	OH	42 ± 6	53 ± 4

[a] Values are percent activity of hSphK1 or hSphK2 with 10 and 5 μM Sph, respectively, in the presence of 1 μM inhibitor. Each value is an average of three experiments. Lower SphK activity level indicates better inhibition. [b] See Fig. 1 for structure. The K_m of SphK1 and SphK2 is 10 μM and 5 μM, respectively.

similar activity, indicating that some steric bulk is allowed towards the end terminus of the binding pocket, while a branched alkane (**3.7e**) or introduction of an ether linkage at the omega carbon did not improve kinase inhibition (entries 6–9). Substitution with a benzyl (**3.7f**), *para*-methylbenzyl (**3.7g**) or a tosyl (**3.7h**) group resulted in minimal inhibition (entries 10–12). However, substitution of a 4-trifluoromethylbenzyl group (**3.7n**) resulted in significant inhibition of SphK2 without any inhibition of SphK1 at 1 μM inhibitor concentration. As this CF_3 group can impart SphK2 selectivity, the corresponding meta version (**3.7o**) was generated, but it was less potent; however, a series of halogens (Br and Cl) in the meta and para positions, as well as a small 4-cyano (**3.7t**) or phenyl (**3.7u**) group, were equally potent (entries 15–20). A larger, hydrophobic 1,1,4,4-tetramethyltetralin (**3.7v**) was found to be inactive. To determine the optimal chain length for **3.7n**, homologated versions bearing the CF_3 around the benzene ring (**3.7w**–**x**) were tested and found to have slightly better activity. The ketone counterparts were found to induce minimal amounts of inhibition in SphK1 and SphK2 (entries 25–27). Finally, we installed a hydroxyl moiety on the pyrrolidine ring of one of the most potent and selective inhibitors in the series (**3.7b**) and a less potent, dual inhibitor (**3.7e**) to mimic one of the hydroxyl groups of sphingosine-1-phosphate to afford **3.7i** and **3.7j**, respectively. These compounds were found to be potent inhibitors of both SphK1 and SphK2 (entries 28–29).

3.5.2 Determination of K_i and Clog P Values

To further characterize the activity of the inhibitors with SphK1 and SphK2, we selected inhibitors that reduced hSphK2 activity below 50% for further studies. As shown in Table 3.3, when a *trans*-hydroxyl group was installed on the pentyl (**SLC5111312**, **3.7i)** and isobutyl (**SLC5121314**, **3.7j**) derivatives, equipotent inhibition of SphK1 and 2 was observed, suggesting that these are dual inhibitors.[27] Interestingly, both of these compounds have the lowest cLogP

and cLogD values in this set, which suggests that the 3′OH also improves the solubility of the compounds. We predict that this hydroxyl group mimics the interaction of one of the hydroxyl groups of sphingosine, leading to dual SphK1 and SphK2 inhibition (*vide infra*).

As expected, the *des*-hydroxy naphthyl analogs restored SphK2 selectivity. **SLC5081308** (**3.7b**) bearing a pentyl ether has K_i values of 7.2 and 0.98 μM with hSphK1 and 2, respectively, affording 7-fold selectivity towards SphK2. The hexyl derivative **SLC5011416** (**3.7c**) is slightly less potent and selective. In contrast, the *para*-trifluoromethylbenzyl ether derivative **SLC5091592** (**3.7n**) has a K_i value of 1.0 μM, and over 20-fold selectivity towards hSphK2. When comparing the *para* and *meta*-bromobenzyl ether derivatives (**SLC5111585** (**3.7p**) and **SLC5111586** (**3.7q**) respectively) the para version was more potent and selective (hSphK2 K_i = 0.75 μM, > 13-fold selective) for hSphK2 than its meta counterpart (hSphK2 K_i = 1.0 μM, > 10-fold selective). The 4-cyanobenzyl ether derivative **SLC5111587** (**3.7t**) has a K_i value of 0.91 μM, indicating that it is slightly more potent than **SLC5091592** (**3.7n**); however, **3.7t** displays a 9-fold decrease in hSphK2 selectivity compared to **SLC5091592** (**3.7n**). Although the *para*-chlorobenzyl ether derivative (**3.7r**) did not meet the criteria for further study, it should be noted that the *meta*-chlorobenzyl ether version **SLC5111577** (**3.7s**) (hSphK2 K_i = 1.2 μM, > 8.3-fold selective) was still less potent and selective than the para-substituted derivatives. This further supports the general trend that a para-substituted isomer is more potent than a meta-substituted isomer. When comparing the homologated versions bearing the CF_3 around the benzene ring (**3.7w-x**) the ortho-substituted derivative **SLC5111589** (**3.7y**) was found to be equipotent to **SLC5091592** (**3.7n**), but only half as selective for hSphK2. As one would expect, the para-substituted derivative **SLC5121591** (**3.7w**) was more potent and selective than the meta analog **SLC5121590** (**7x**). **SLC5121591** (**3.7w**) has a K_i value of 0.61 μM and is over 16-fold selective.

Table 3.3. Inhibition Constants of Select Inhibitors

compound	K_i (μM)[a]		hSphK2 selectivity	cLogP	cLogD (7.4)
	hSphK1	hSphK2			
SLR080811	16 ± 2.9	1.4 ± 0.2	11	5.2	2.66
SLC5111312 (3.7i)	0.73 ± 0.2	0.90 ± 0.2	0.8	3.0	0.60
SLC5121314 (3.7j)	0.93 ± 0.1	0.98 ± 0.3	0.9	2.3	0.14
SLC5081308 (3.7b)	7.2 ± 0.9	0.98 ± 0.2	7.3	4.2	1.70
SLC5011416 (3.7c)	>10	3.8 ± 0.8	> 2.6	4.7	2.12
SLC5091592 (3.7n)	>20	1.02 ± 0.2	> 20	4.7	2.63
SLC5111585 (3.7p)	>10	0.75 0.1	>13	4.7	2.52
SLC5111586 (3.7q)	>10	1.0 ± 0.2	>10	4.7	2.52
SLC5111577 (3.7s)	>10	1.2 ± 0.2	>8.3	4.5	2.31
SLC5111587 (3.7t)	>10	0.91 ± 0.11	>11	3.3	1.60
SLC5121591 (3.7w)	>10	0.61 ± 0.06	>16	5.0	2.90
SLC5121590 (3.7x)	>10	0.77 ± 0.09	>13	5.0	2.90
SLC5111589 (3.7y)	>10	1.02 ±0.09	>9.8	5.0	2.90

[a] Inhibitory constants for recombinant enzymes were obtained by kinetic analysis of S1P production using variable concentrations of sphingosine and a fixed concentration of ATP in the presence or absence of compounds as described previously.[21] Selectivity for each compound was determined by dividing the K_m SphK2 by the K_m of SphK1.

for hSphK2, while **SLC5121590** (**3.7x**) has a K_i value of 0.77 μM and is over 13-fold selective for hSphK2. Interestingly, **SLC5121591** (**3.7w**) is 40% more potent for hSphK2 than **SLC5091592** (**3.7n**), suggesting that the additional length and bond rotation gained from the extra methylene is beneficial for fitting in the binding pocket; however, **SLC5121591** (**3.7w**) is 4-fold less selective for hSphK2 than **SLC5091592** (**3.7n**).

In terms of pharmacokinetic parameters, the new inhibitors in Table 3.3 are less lipophilic (cLogP = 2.3–5.0) than the lead compound **SLR080811** (cLogP = 5.2) or the native substrate, sphingosine (cLogP = 5.96). We then compared the activity of these inhibitors against known

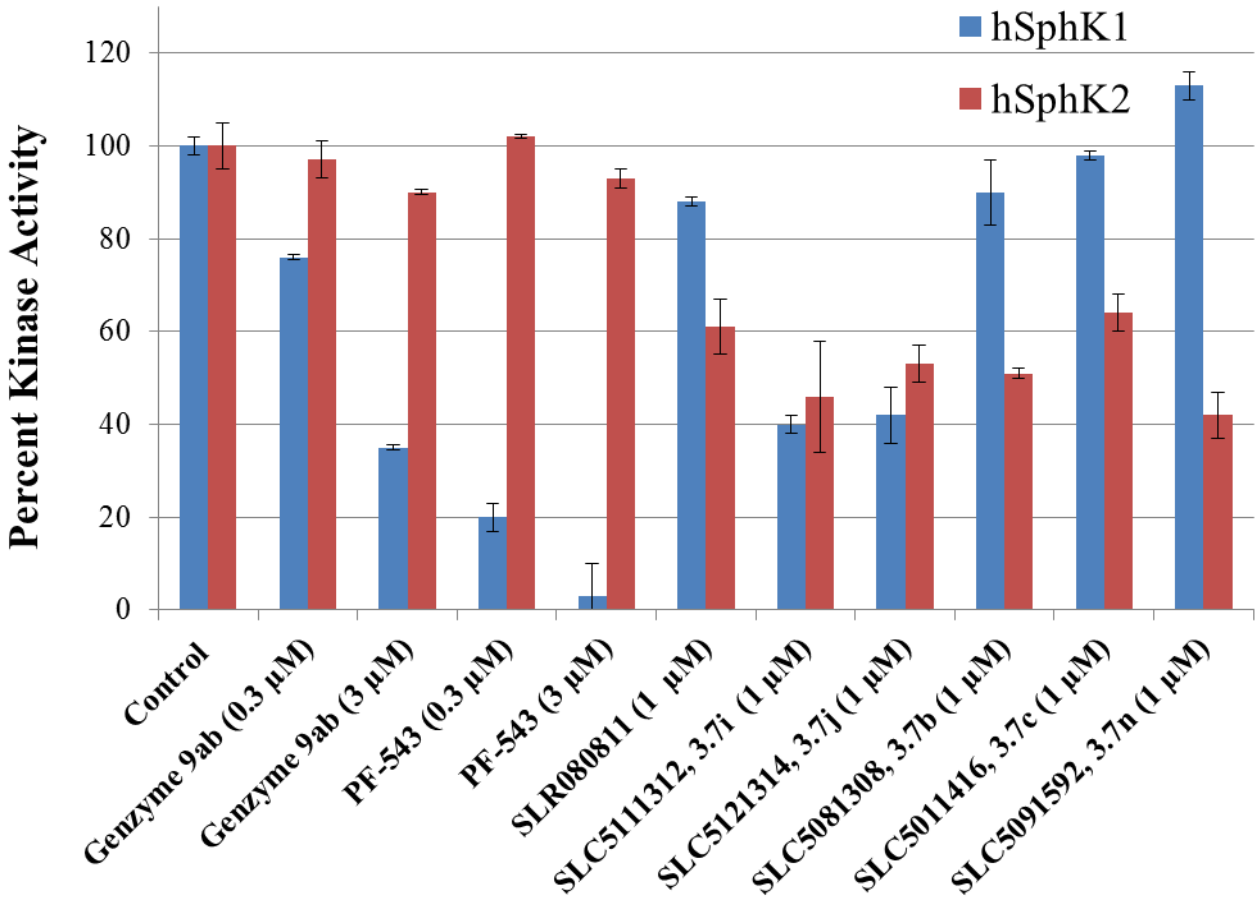

Figure 3.2. Sphingosine Kinase Activity of Select Inhibitors

SphK inhibitors. As shown in Figure 3.2, Genzyme **9ab** and **PF-543** are potent hSphK1 inhibitors whereas **SLC5091592** (**3.7n**) is clearly a SphK2 selective inhibitor. Both of the 3′-hydroxyl derivatives, **SLC5111312** (**3.7i**) and **SLC5121314** (**3.7j**), display almost equipotent inhibition of hSphK 1 and 2, indicating their functionality as dual inhibitors.

3.6 Molecular Modeling

To understand the binding mode of these compounds, a homology model of hSphK2 was generated based on the published crystal structure of hSphK1 in a complex with adenosine diphosphate (ADP) and magnesium (PDB ID: 3VZB).[28] We modified ADP to ATP by adding a phosphate group to the ADP of the crystal structure and energy minimized the resulting structure. Following the equilibration and validation of our hSphK2 homology model with ATP and Mg^{2+} bound, **SLC5091592** (**3.7n**, hSphK1 K_i > 20 μM, hSphK2 K_i = 1.02 μM), **SLC5081308** (**3.7b**, hSphK1 K_i = 7.2 μM, hSphK2 K_i = 0.98 μM), and **SLC5111312** (**3.7i**, hSphK1 K_i = 0.73 μM, hSphK2 K_i = 0.90 μM) were docked into the substrate-binding cavity. Our research has previously shown that these analogs are competitive with sphingosine and not with ATP.[21] As illustrated in Figure 3.3A, **SLC5091592** (**3.7n**) adopts a 'J-shape' conformation similar to the lipid portion of the sphingosine/SphK1 and PF-543/SphK1 crystal structures.[29] For **SLC5091592** (**3.7n**), two hydrogen bonds are formed: guanidine to Asp211 and nitrogen (position 4) of the oxadiazole ring to Asp308. The cationic guanidine group is situated in an area surrounded by anionic residues (Asp) and the phosphate of ATP. In **SLC5081308** (**3.7b**), a hydrogen bond is formed between Asp308 and the guanidine nitrogen of the pyrrolidine ring, indicating a slight change in position as caused by alteration of the tail region in the inhibitors (Figure 3.3A and B) and can relate to potency. In **SLC5091592** (**3.7n**), a favorable π-stacking interaction between the

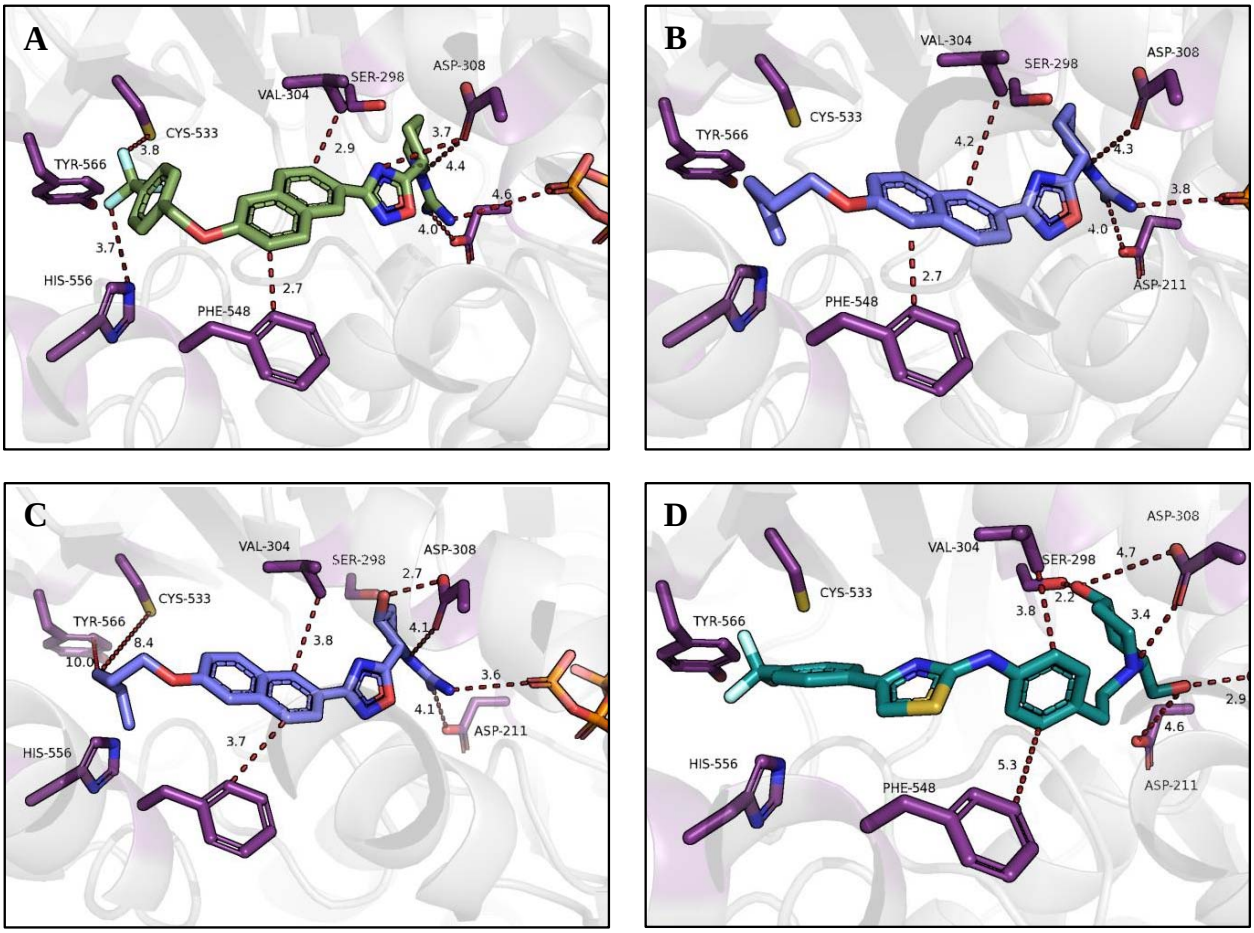

Figure 3.3. Docking of Inhibitors into SphK2. (A) **SLC5091592** (**3.7n**, hSphK1 K_i > 20 μM, hSphK2 K_i = 1.02 μM), (B) **SLC5081308** (**3.7b**, hSphK1 K_i = 7.2 μM, hSphK2 K_i = 0.98 μM), (C) **SLC5111312** (**3.7i**, hSphK1 K_i = 0.73 μM, hSphK2 K_i = 0.90 μM), and (D) **Amgen 82** (hSphK1 IC_{50} = 0.01 μM, hSphK2 IC_{50} = 0.02 μM) docked into a homology model of hSphK2. Key active site residues are labeled and shown as purple sticks, while ATP is shown as green sticks (colored by element). Hydrogen bonds are indicated with red dashes. Magnesium is not shown for clarity.

naphthalene ring and Phe548 is observed, in addition to the benzyltrifluoromethyl 'tail' being positioned in a hydrophobic pocket that is capped by residues Cys533, Tyr566, and His556. Cys533 in hSphK2 corresponds to Phe288 in hSphK1 and is one of four residue differences in the hSphK1 and hSphK2 binding cavity. Finally, the conformationally restricted pyrrolidine hydroxyl group present in **SLC5111312** (**3.7i**) forms a hydrogen bond with Asp308 of SphK2 (Figure 3.3C), which is missing in **SLC5081308** (**3.7b**) (Figure 3.3B), allowing it to function as a dual SphK1/SphK2 inhibitor by moving the inhibitor up in the pocket and away from Asp211. Asp178 of SphK1 similarly forms this hydrogen bond with **SLC5111312** (**3.7i**) (Figure 3.4). Interestingly, in the co-crystal structure of sphingosine with SphK1, an analogous interaction between the internal hydroxyl group and Asp178 exists.[28] This interaction, in conjunction with our results, indicates that the hydroxyl on **SLC5111312** (**3.7i**) stabilizes interactions of the inhibitor in the top of the binding cavity near residues Asp308 and Ser298. These interactions weaken or remove electrostatic and polar interactions with Asp211 and impart dual SphK activity.

To further validate our studies, we docked another dual inhibitor, **Amgen 82**, and found that a hydrogen bond exists between the piperidine hydroxyl group and Ser298 while the hydrogen bond to Asp308 or Asp211 is abolished (Figure 3.3D). The hydrogen bond with Ser298 moves **Amgen 82** up into the binding pocket and away from Asp 211. The hydrogen bond between the **Amgen 82** piperidine hydroxyl group and Ser298 acts similarly to the hydrogen bond between Asp308 and **SLC5111312** (**3.7i**) in regards to overall ligand positioning in the binding cavity. As a result, dual Sphk activity is observed for both **Amgen 82** and **SLC5111312** (**3.7i**).

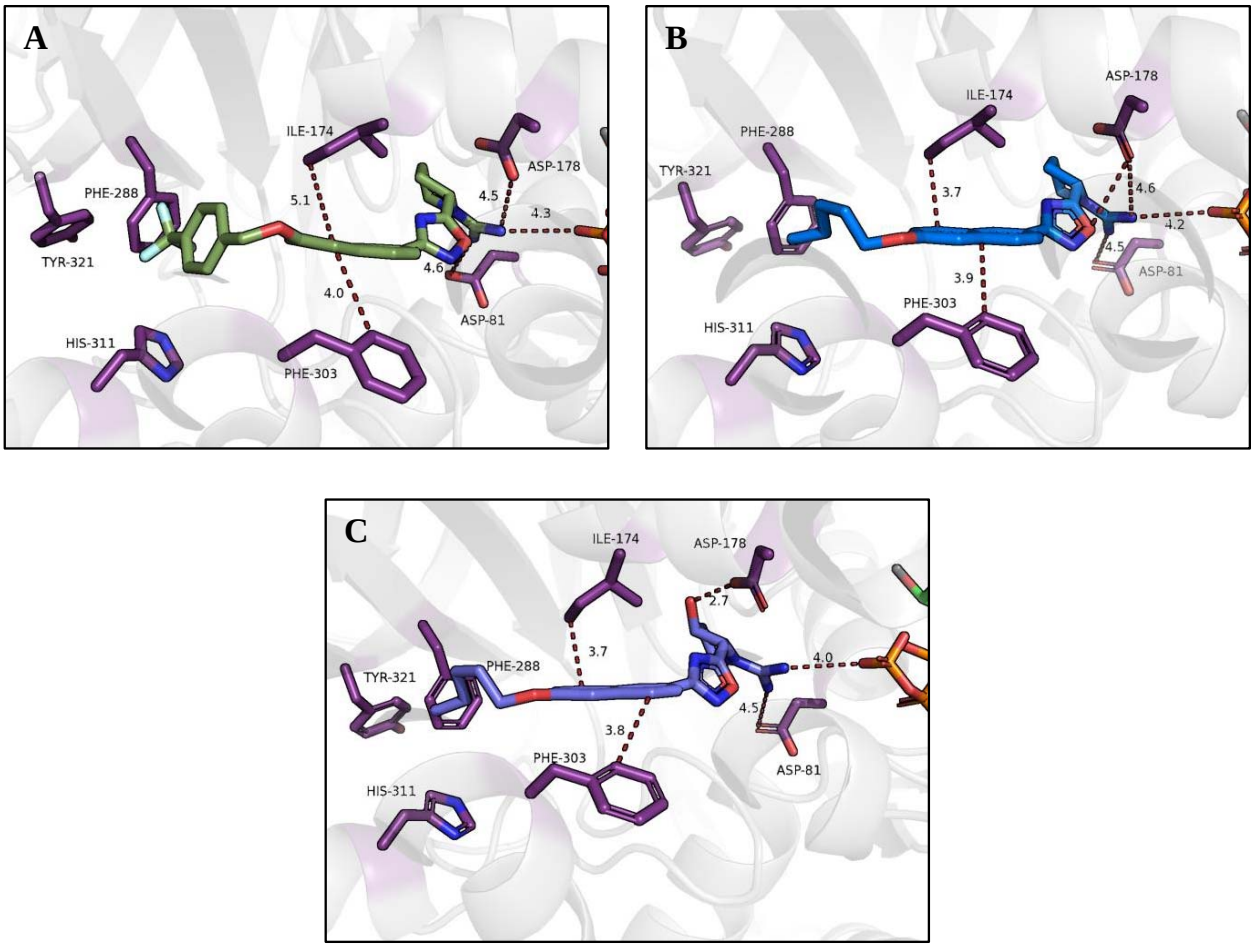

Figure 3.4. Select Inhibitors Docked in hSphK1. (A) **SLC5091592** (**3.7n**, hSphK1 K_i > 20 μM, hSphK2 K_i = 1.02 μM), (B) **SLC5081308** (**3.7b**, hSphK1 K_i = 7.2 μM, hSphK2 K_i = 0.98 μM), and (C) **SLC5111312** (**3.7i**, hSphK1 K_i = 0.73 μM, hSphK2 K_i = 0.90 μM). Key active site residues are labeled and shown as purple sticks, while ATP is shown as green sticks (colored by element). Hydrogen bonds are indicated with red dashes. Magnesium is not shown for clarity.

3.7 Elucidating the Role of SphK and S1P

As previously reported, mice treated with **SLR080811**, the lead structure to the naphthalene SAR reported herein, displayed a rapid increase of blood S1P levels. This result was surprising, as **SLR080811** was shown to reduce S1P levels in histiocytic lymphoma (U937) cells.[21] Furthermore, it contradicted *in vivo* studies using SphK1 selective (**1a, 82**), and SphK2 selective (**ABC294640**) inhibitors in which S1P levels decreased.[26, 30, 31] To further assist in elucidating the role and mechanism of SphK and S1P, **SLC511312** (**3.7i**) was used in a series of biological studies with a SphK2 selective inhibitor (**SLM6031434**, discussed in Chapter 1) and its less potent enantiomer **SLM6081442** as a control.

3.7.1 Effect of Species on Potency and Selectivity

Initial investigations began by determining the potency of the compounds in recombinant mice and rat SphK1 and SphK2, as both potency and selectivity has been shown to be species-dependent for a variety of chemical scaffolds.[9, 14, 20, 32] As seen in Table 3.3, **SLR080811** has almost identical K_i values for hSphK1 and mSphK1. A similar observation can be made for SphK2, as **SLR080811** possesses comparable potency across all three species suggesting that it is not a species dependent inhibitor. A comparable trend is observed with SphK2 inhibitor **SLM6031434**, although it displays improved SphK2 potency. As expected, **SLM6081442** was substantially less potent. Interestingly **SLC5111312** (**3.7i**) was found to be a 20-fold SphK2-selective inhibitor in mice. This selectivity arises from a substantial difference in hSphK1 and mSphK1 potency as it retains similar potency between hSphK2 and mSphK2. As a result, **SLC5111312** (**3.7i**) is a unique tool which can be employed as either a SphK2-selective (mouse) or dual (human and rat) inhibitor.

Table 3.4. Potency of SphK Inhibitors Assessed in vitro with Recombinant Human, Mouse and Rat SphK1 and SphK2

Inhibitor	hSphk1	hSphK2	mSphK1	mSphK2	rSphK1	rSphK2
SLR080811	16	1.4	15	1.3	N.D.	1.4
SLC5111312 (**3.7i**)	0.73	0.90	20	1	0.8	1.1
SLM6031434	19	0.4	>20	0.4	22	0.5
SLM6081442	N.D.	N.D.	>20	19	N.D.	N.D.

Inhibitor constants for recombinant enzymes were obtained by kinetic analysis of S1P production using a variable concentration of sphingosine and a fixed concentration of ATP in the presence and absence of inhibitors as described previously.[21] Values corresponding to K_i values are expressed in micromolar units (μM). (Table reproduced with permission from reference 27. Copyright (2015), American Society for Pharmacology and Experimental Therapeutics).

3.7.2 Characterization of Inhibitors in Cultured Cells

U937 cells, which display strong SphK1 and SphK2 activities, were employed to determine whether the inhibitors were active on whole cells. The U937 cells were incubated with the inhibitors for 2 hours before being harvested and lysed. The amounts of S1P, Sph, and inhibitors were then quantified (Figure 3.5A–C, respectively). A concentration-dependent decrease in S1P levels can be seen with increased concentration of inhibitors (Figure 3.5A); while simultaneously, a concentration-dependent increase in Sph is observed (Figure 3.5B). As anticipated, **SLC5111312** (**3.7i**, dual inhibitor) had the most prominent effect on S1P and Sph levels. **SLM6031434** (SphK2 selective) reduced S1P levels, but to a lesser extent while

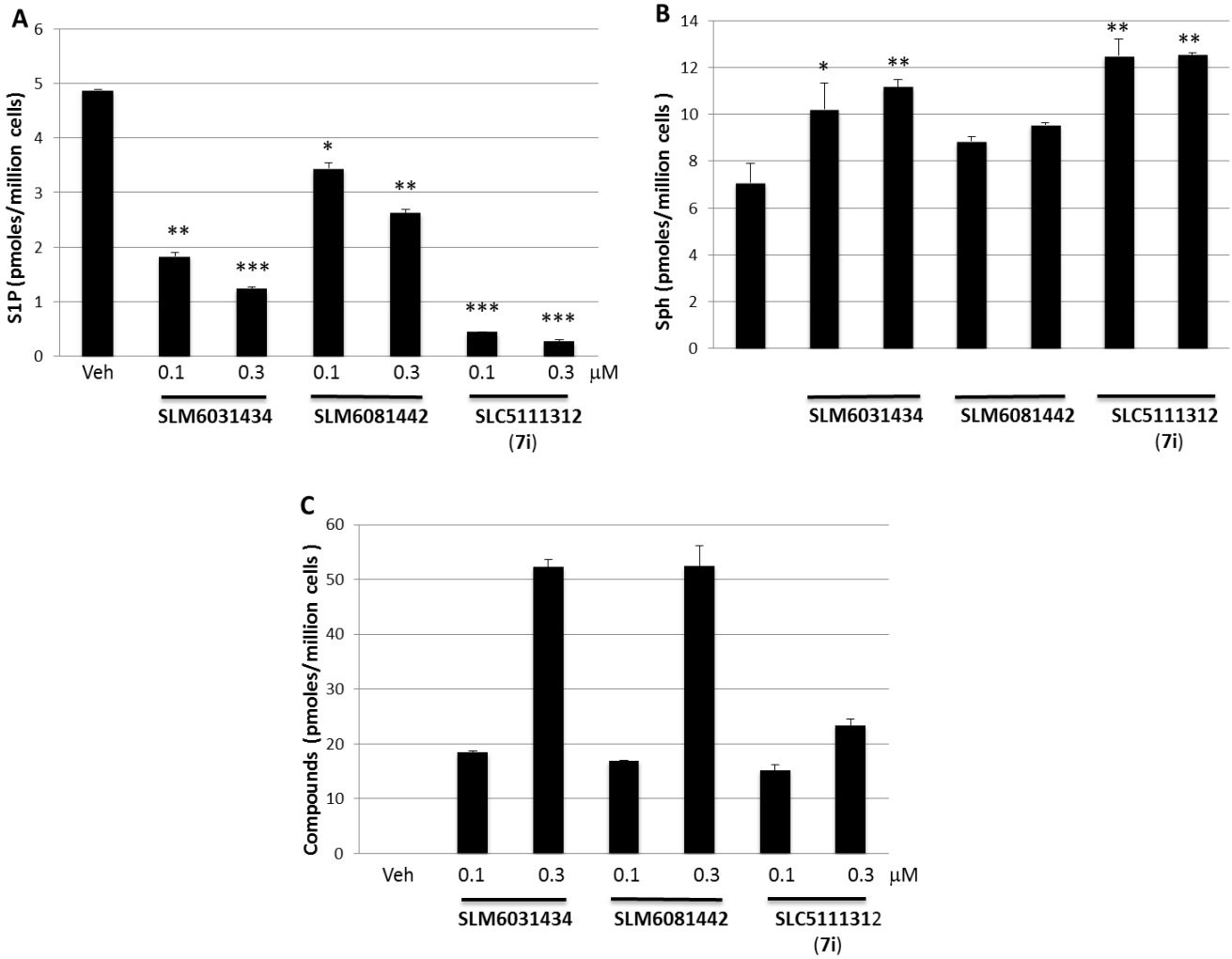

Figure 3.5. Effect of SphK2 Inhibitors on Sphingolipid Levels in Cultured U937 Cells. Cells were treated for 2 hours with two different concentrations of inhibitors and then harvested and lysed, and the amounts of sphingolipids were measured by LC/MS. The amount of sphingolipids and inhibitors in the cells are expressed in pmoles per million cells: (A) S1P; (B) sphingosine; (C) inhibitors. Data correspond to the mean ± S.D. of three independent experiments. The level of significance is indicated for each experiment (*P < 0.05; **P < 0.01; and ***P < 0.001) using one-way analysis of variance with the Bonferroni multiple comparison test compared with control. (Figure was reproduced with permission from reference 27. Copyright (2015), American Society for Pharmacology and Experimental Therapeutics).

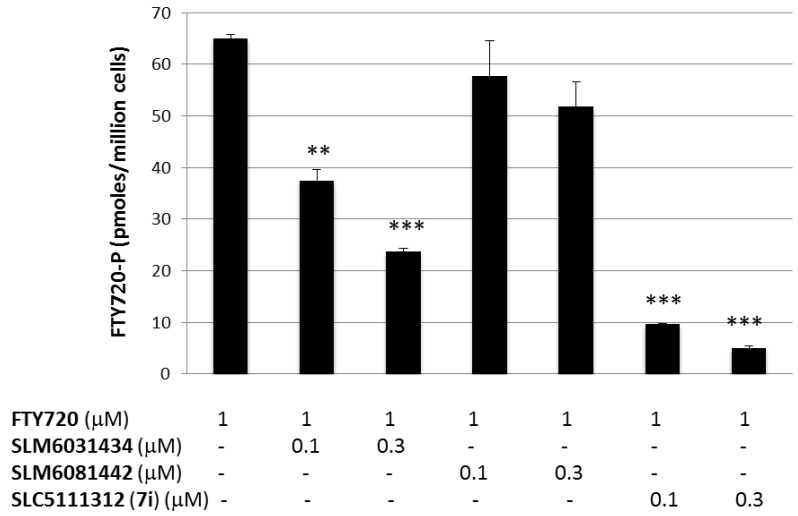

Figure 3.6. Blockade of FTY720 Phosphorylation by SphK2 Inhibitors in Cultured U937 Cells. U937 cells were exposed to 1 M of FTY720 and different concentrations of **SLM6031434**, **SLM6081442** and **SLC5111312** (**3.7i**) as indicated for 2 hours. Cells were harvested by centrifugation and processed for LC/MS. Accumulation of FTY720-P was measured by LC/MS. Data correspond to the mean ± S.D. of three independent experiments. The level of significance is indicated for each experiment (*P < 0.05; **P < 0.01; and ***P < 0.001) using one-way analysis of variance with the Bonferroni multiple comparison test compared with control. (Figure was reproduced with permission from reference 27. Copyright (2015), American Society for Pharmacology and Experimental Therapeutics).

SLM6081442 displayed minimal inhibition. Additionally, an increase in cell-associated inhibitor concentration was observed as the inhibitor concentration was increased (Figure 3.5C).

To verify that the inhibitors were active at SphK2, the experiment was conducted in the presence of 1 μM FTY720, a SphK2-selective substrate. Following incubation, the amount of phosphorylated FTY720 (FTY720-P) in the cell extracts was quantified (Figure 3.6). As expected, both **SLM6031434** (SphK2 selective) and **SLC5111312** (**3.7i**, dual inhibitor) reduced the amount of FTY720-P produced.

3.7.3 Characterization of SphK Inhibitors in Mice

As previously shown with **SLR080811**, blood S1P levels rapidly change upon treatment with a SphK inhibitor, and as a result, are a useful pharmacodynamic marker.[21] To further evaluate the selectivity of the inhibitors, SphK1 and SphK2 null mice (SphK1-/- and SphK2-/-), which lack the corresponding functional SphK alleles, were treated with the inhibitors. Upon treatment with **SLM6031434** (SphK2 selective) or **SLC5111312** (**3.7i**, SphK2 selective) a decrease in the blood S1P levels of the SphK1-/- mice was detected (Figure 3.7A). When the SphK2-/- mice were treated with the inhibitors, no substantial change in blood S1P levels was detected (Figure 3.7B). This data supports the work previously published on lead SphK2 inhibitor **SLR080811.**[21]

Interestingly, the results were very different when WT mice were treated with **SLM6031434** and **SLC5111312** (**3.7i**) (Figure 3.8A–C). As shown in Figure 3.8A, blood S1P levels were noticeably increased within 2 hours of treatment with the inhibitors and continued to rise after 6 hours despite decreasing inhibitor concentration (Figure 3.8B). S1P levels were still noticeably elevated 24 hours after dosing. For comparison, WT mice treated with **SLM6081442**

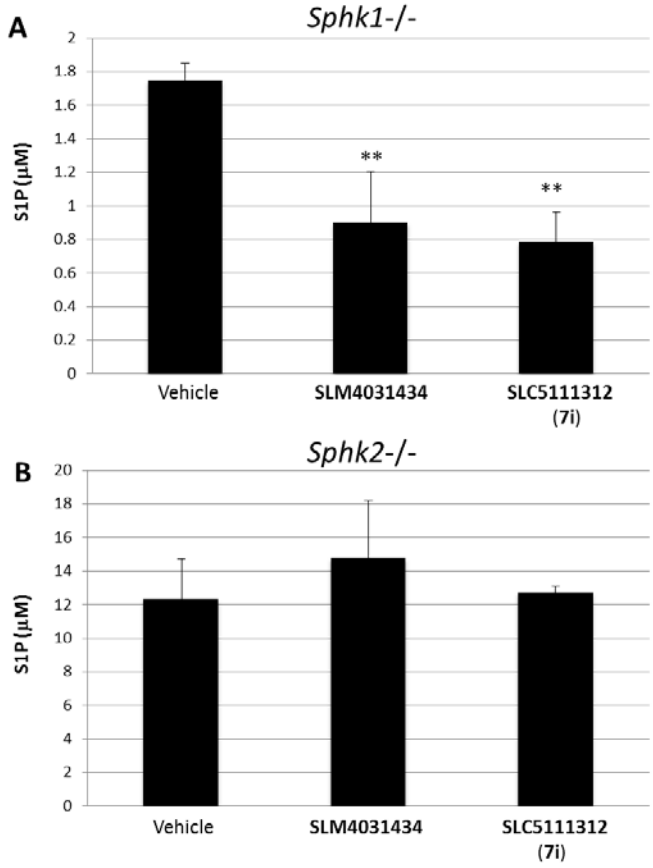

Figure 3.7. Blood S1P Levels in SphK1-/- (A) and SphK2-/- (B) Mice Treated with Inhibitors. Cohorts of male mice (congenic on a C57BL/6j background) of the specified genotypes were injected intravenously with 5 mg/kg **SLM6131434** or 10 mg/kg **SLC5111312** (**3.7i**). Blood was drawn after 2 hours and analyzed for S1P levels by LC/MS. The level of significance is indicated for each experiment (**P < 0.01) using one-way analysis of variance with the Bonferroni multiple comparison test. (Figure was reproduced with permission from reference 27. Copyright (2015), American Society for Pharmacology and Experimental Therapeutics).

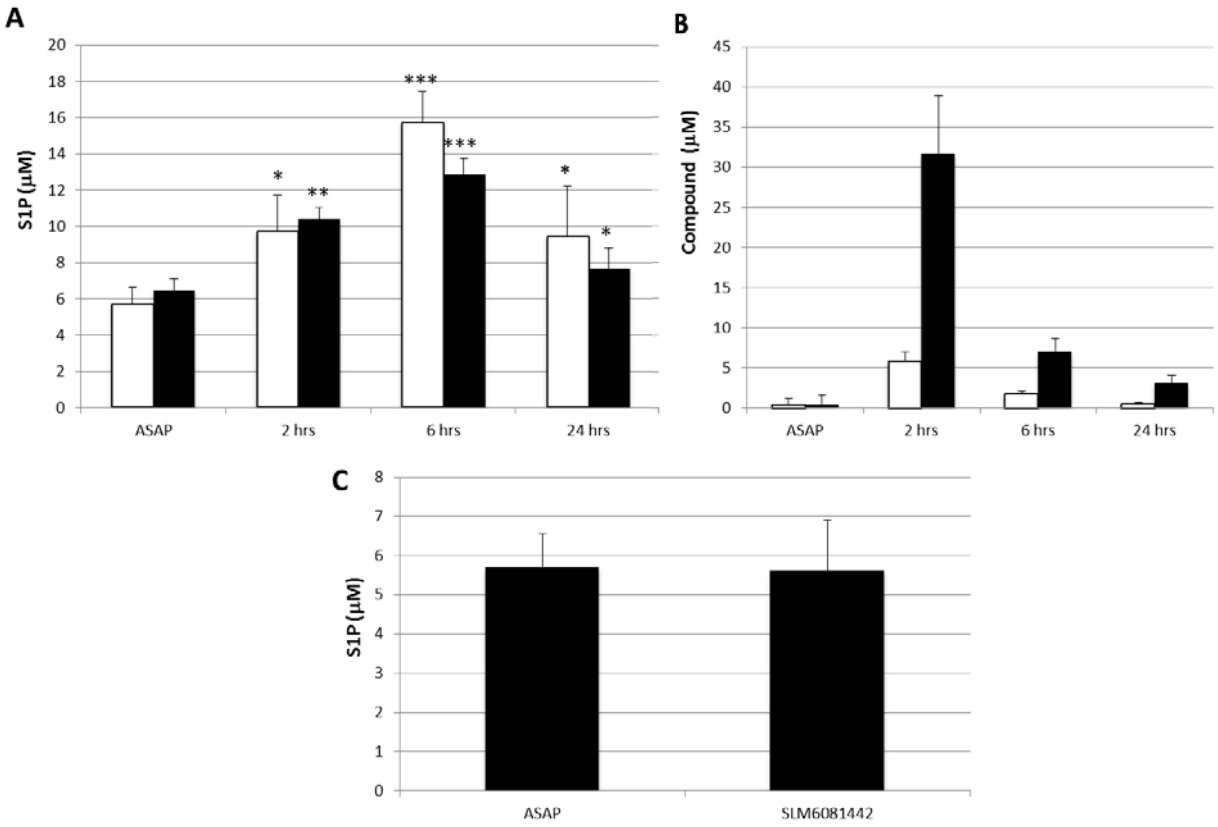

Figure 3.8. Blood S1P Levels in Wild-type Mice Injected with SphK Inhibitors. C57BL/6j male mice (N = 3-4 per group) were injected (i.p.) with 5 mg/kg of **SLM6031434**, 10 mg/kg of **SLM6081442** or **SLC5111312** (**3.7i)**. After the indicated periods, blood was drawn and S1P and inhibitors were extracted and measured by LC/MS. Levels of S1P (A) and inhibitors (B) in mice treated with **SLM6031443** (open bars) and **SLC5111312** (**3.7i**, filled bars) are shown. (C) S1P levels in mice treated with (10 mg/kg i.p.) **SLM6081442** for 6 hours. Data correspond to the mean ± S.D. of three independent experiments. The level of significance is indicated for each experiment (*P < 0.05; **P < 0.01; and ***P < 0.001) using one-way analysis of variance with the Bonferroni multiple comparison test compared with control. (Figure was reproduced with permission from reference 27. Copyright (2015), American Society for Pharmacology and Experimental Therapeutics).

displayed no noticeable change in blood S1P levels (Figure 3.8C). This result was expected as **SLM6081442** is a substantially less potent SphK2 inhibitor. Overall, the results with WT mice further validate studies with **SLR080811**.[21] Furthermore, the data suggest that the increase in blood S1P levels is the result of SphK2 inhibition instead of an undetermined off-target effect. One possible explanation is that inhibition of SphK2 causes an increase in S1P produced by SphK1. A second possibility is that SphK2 has a secondary role in S1P clearance from blood, which is obstructed upon SphK2 inhibition.

3.7.4 Determining the Tipping Point between the Raising and Lowering Blood S1P Levels

Utilization of a dual SphK inhibitor could help further validate that inhibition of SphK2 results in elevation of blood S1P. As stated previously, treatment with SphK2 selective inhibitor **SLR080811** results in elevated blood S1P levels.[21] However, additional studies with SphK1 inhibitor **1a** have shown that treatment with an SphK1 inhibitor results in reduced blood S1P levels.[33] These studies suggest that there is a tipping point in which SphK inhibition switches between elevated and reduced blood S1P levels.

Due to a loss of mSphK1 potency with the studied inhibitors, the dual inhibitor study was conducted in rats (Figure 3.9). The general trend of changing blood S1P levels as a result of application of an SphK inhibitor have been shown in both species. Rats treated with **SLR080811** (10-fold SphK2 selective) showed the expected elevation of S1P levels (Figure 3.9A), while additional studies have shown that rats treated with S**LP7111228**, a SphK1 selective inhibitor, exhibited a reduction in blood S1P levels.[20] As seen in Figure 3.9B, rats dosed with **SLC5111312** (**3.7i**, dual inhibitor in rats) showed lowered blood S1P levels by approximately

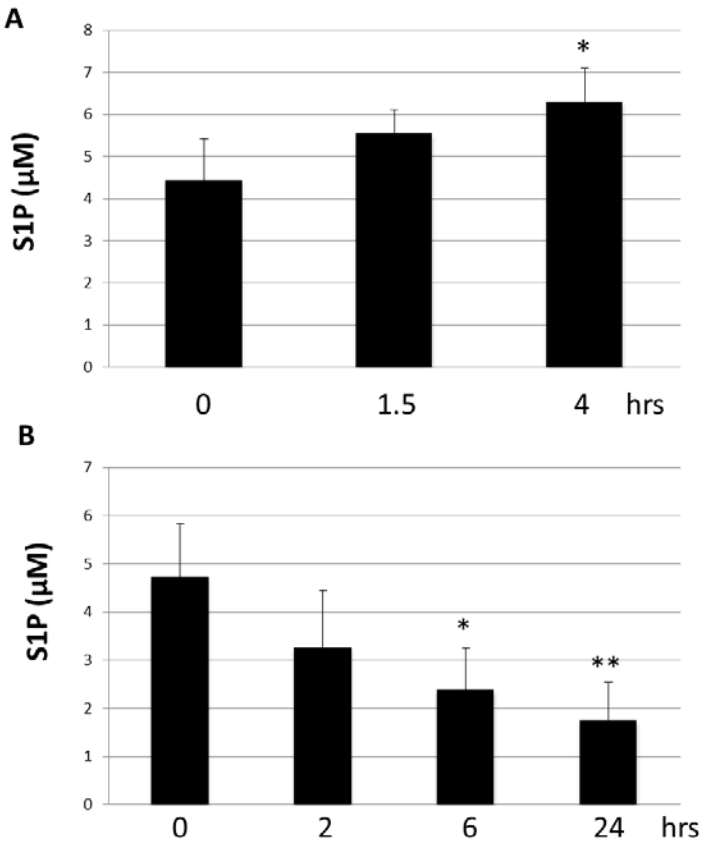

Figure 3.9. Blood S1P Levels in Rats Treated with SphK Inhibitors. Sprague-Dawley male rats (8-10 weeks; n = 4) were injected with 10 mg/kg of **SLR080811** (A) or **SLC5111312** (**3.7i**, B) for the indicated period. Blood was drawn, and S1P was extracted and measured by LC/MS. Data correspond to the mean ± S.D. of three independent experiments. The level of significance is indicated for each experiment (*P < 0.05; **P < 0.01; and ***P < 0.001) using one-way analysis of variance with the Bonferroni multiple comparison test compared with control. (Figure was reproduced with permission from reference 27. Copyright (2015), American Society for Pharmacology and Experimental Therapeutics).

60% after 24 hours. This data suggests that the tipping point between increasing and decreasing blood S1P levels lies somewhere between dual and 10-fold selective inhibition of SphK2.

3.8 Conclusions

In conclusion, we described the structure-activity relationship profile of naphthalene-based SphK2 inhibitors. A key discovery of our studies is **SLC5091592** (**3.7n**), a potent analog that incorporates a 4-trifluomethylbenzyl 'tail' and displays increased selectivity (> 20 fold) towards SphK2 when compared to **SLR080811**. Molecular docking studies suggest that the inhibitors possess a binding mode similar to sphingosine in the ligand binding pocket and emphasize the role of the tail region of the pocket on SphK selectivity. Our investigation identifies the importance of two other crucial interactions that impart SphK2 selectivity: a guanidine hydrogen bond to Asp211 and the removal of a pyrrolidine hydroxyl group that abolishes a hydrogen bond to Asp308. This work provides an avenue towards improved sphingosine kinase inhibitors.

Furthermore, biological studies employing **SLC5111312** (**3.7i**) have helped to further elucidate the role of SphK2 in S1P clearance from blood. These studies have shown that changes in blood S1P concentrations occur rapidly after dosing with a SphK2 inhibitor. Our investigations indicate that the tipping point between increasing and decreasing blood S1P levels exists between dual and 10-fold selective inhibition of SphK2. Finally, the data suggests that SphK2 has a critical role in the regulation of blood S1P levels.

3.9 Acknowledgements

The work was supported by NIH Grants R01 GM104366, R01 GM067958, and R43 GM106495.

3.10 Notes

The authors declare the following competing financial interest(s): Webster L. Santos and Kevin R. Lynch are among the co-founders of SphynKx Therapeutics LLC, which was created to commercialize S1P-related discoveries, including SphK inhibitors, discovered and characterized in their laboratories. Final products **3.7k-ac** were initially synthesized by Molly D. Congdon during an internship at SphynKx from January 2014 to May 2014. The compounds described in this manuscript are included in a patent application licensed to SphynKx.

3.11 References

1. Spiegel, S.; Milstein, S., Sphingosine-1-Phosphate: Signaling Inside and Out. *FEBS Lett.* **2000,** *476* (1-2), 55–57.
2. Spiegel, S.; Milstien, S., Sphingosine-1-Phosphate, a Key Cell Signaling Molecule. *J. Biol. Chem.* **2002,** *277* (29), 25851–25854.
3. Cohen, J. A.; Barkhof, F.; Comi, G.; Hartung, H. P.; Khatri, B. O.; Montalban, X.; Pelletier, J.; Capra, R.; Gallo, P.; Izquierdo, G.; Tiel-Wilck, K.; de Vera, A.; Jin, J.; Stites, T.; Wu, S.; Aradhye, S.; Kappos, L., Oral Fingolimod or Intramuscular Interferon for Relapsing Multiple Sclerosis. *N. Engl. J. Med.* **2010,** *362* (5), 402–415.
4. Kappos, L.; Radue, E. W.; O'Connor, P.; Polman, C.; Hohlfeld, R.; Calabresi, P.; Selmaj, K.; Agoropoulou, C.; Leyk, M.; Zhang-Auberson, L.; Burtin, P., A Placebo-Controlled Trial of Oral Fingolimod in Relapsing Multiple Sclerosis. *N. Engl. J. Med.* **2010,** *362* (5), 387–401.
5. Neubauer, H. A.; Pitson, S. M., Roles, Regulation and Inhibitors of Sphingosine Kinase 2. *FEBS J.* **2013,** *280* (21), 5317–5336.
6. Bigaud, M.; Guerini, D.; Billich, A.; Bassilana, F.; Brinkmann, V., Second Generation S1P Pathway Modulators: Research Strategies and Clinical developments. *Biochim. Biophys. Acta.* **2014,** *1841* (5), 745–758.
7. Takuwa, N.; Du, W.; Kaneko, E.; Okamoto, Y.; Yoshioka, K.; Takuwa, Y., Tumor-Suppressive Sphingosine-1-Phosphate Receptor-2 Counteracting Tumor-Promoting Sphingosine-1-Phosphate Receptor-1 and Sphingosine Kinase 1. *Am. J. Cancer Res.* **2011,** *1*, 460–481.

8. Kunkel G., T; Maceyka M; Milstien S; Spiegel, S., Targeting the Sphingosine-1-Phosphate Axis in Cancer, Inflammation and Beyond. *Nat. Rev. Drug Discov.* **2013,** *12* (9), 688–702.

9. Zhang, Y.; Berka, V.; Song, A.; Sun, K.; Wang, W.; Zhang, W.; Ning, C.; Li, C.; Zhang, Q.; Bogdanov, M.; Alexander, D. C.; Milburn, M. V.; Ahmed, M. H.; Lin, H.; Idowu, M.; Zhang, J.; Kato, G. J.; Abdulmalik, O. Y.; Zhang, W.; Dowhan, W.; Kellems, R. E.; Zhang, P.; Jin, J.; Safo, M.; Tsai, A. L.; Juneja, H. S.; Xia, Y., Elevated Sphingosine-1-Phosphate Promotes Sickling and Sickle Cell Disease Progression. *J. Clin. Investi.* **2014,** *124* (6), 2750–2761.

10. Takasugi, N.; Sasaki, T.; Suzuki, K.; Osawa, S.; Isshiki, H.; Hori, Y.; Shimada, N.; Higo, T.; Yokoshima, S.; Fukuyama, T.; Lee, V. M.; Trojanowski, J. Q.; Tomita, T.; Iwatsubo, T., BACE1 Activity is Modulated by Cell-Associated Sphingosine-1-Phosphate. *J. Neurosci.* **2011,** *31* (18), 6850–6857.

11. Visentin, B.; Vekich, J. A.; Sibbald, B. J.; Cavalli, A. L.; Moreno, K. M.; Matteo, R. G.; Garland, W. A.; Lu, Y.; Yu, S.; Hall, H. S.; Kundra, V.; Mills, G. B.; Sabbadini, R. A., Validation of an Anti-Sphingosine-1-Phosphate Antibody as a Potential Therapeutic in Reducing Growth, Invasion, and Angiogenesis in Multiple Tumor Lineages. *Cancer Cell.* **2006,** *9* (3), 225–238.

12. Santos, W. L.; Lynch, K. R., Drugging Sphingosine Kinases. *ACS Chem. Biol.* **2015,** *10* (1), 225–233.

13. Plano, D.; Amin, S.; Sharma, A. K., Importance of Sphingosine Kinase (SphK) as a Target in Developing Cancer Therapeutics and Recent Developments in the Synthesis of Novel SphK Inhibitors. *J. Med. Chem.* **2014,** *57* (13), 5509–5524.

14. Rex, K.; Jeffries, S.; Brown, M. L.; Carlson, T.; Coxon, A.; Fajardo, F.; Frank, B.; Gustin, D.; Kamb, A.; Kassner, P. D.; Li, S.; Li, Y.; Morgenstern, K.; Plant, M.; Quon, K.; Ruefli-Brasse, A.; Schmidt, J.; Swearingen, E.; Walker, N.; Wang, Z.; Watson, J. E.; Wickramasinghe, D.; Wong, M.; Xu, G.; Wesche, H., Sphingosine Kinase Activity is Not Required for Tumor Cell Viability. *PLoS ONE* **2013,** *8* (7), e68328.

15. French, K. J.; Zhuang, Y.; Maines, L. W.; Gao, P.; Wang, W.; Beljanski, V.; Upson, J. J.; Green, C. L.; Keller, S. N.; Smith, C. D., Pharmacology and Antitumor Activity of ABC294640, a Selective Inhibitor of Sphingosine Kinase-2. *J. Pharmacol. Exp. Ther.* **2010,** *333*, 129139.

16. Beljanski, V.; Knaak, C.; Smith, C. D., A Novel Sphingosine Kinase Inhibitor Induces Autophagy in Tumor Cells. *J. Pharmacol. Exp. Ther.* **2010,** *333* (2), 454–464.

17. Antoon, J. W.; White, M. D.; Meacham, W. D.; Slaughter, E. M.; Muir, S. E.; Elliott, S.; Rhodes, L. V.; Ashe, H. B.; Wiese, T. E.; Smith, C. D.; Burow, M. E.; Beckman, B. S., Antiestrogenic Effects of the Novel Sphingosine Kinase-2 Inhibitor ABC294640. *Endocrinology* **2010,** *151* (11), 5124–5135.

18. Raje, M. R.; Knott, K.; Kharel, Y.; Bissel, P.; Lynch, K. R.; Santos, W. L., Design, Synthesis and Biological Activity of Sphingosine Kinase 2 Selective Inhibitors. *Bioorg. Med. Chem.* **2012,** *20* (1), 183–194.

19. Knott, K.; Kharel, Y.; Raje, M. R.; Lynch, K. R.; Santos, W. L., Effect of Alkyl Chain Length on Sphingosine Kinase 2 Selectivity. *Bioorg. Med. Chem. Lett.* **2012,** *22* (22), 6817–6820.

20. Patwardhan, N. N.; Morris, E. A.; Kharel, Y.; Raje, M. R.; Gao, M.; Tomsig, J. L.; Lynch, K. R.; Santos, W. L., Structure−Activity Relationship Studies and *in Vivo* Activity of

Guanidine-Based Sphingosine Kinase Inhibitors: Discovery of SphK1- and SphK2-Selective Inhibitors. *J. Med. Chem.* **2015,** *58* (4), 1879–1899.

21. Kharel, Y.; Raje, M.; Gao, M.; Gellett, A., M.; Tomsig, J., L.; Lynch, K., R.; Santos, W., L., Sphingosine Kinase Type 2 Inhibition Elevates Circulating Sphingosine-1-Phosphate. *Biochem. J.* **2012,** *447* (1), 149–157.

22. Zemann, B.; Kinzel, B.; Muller, M.; Reuschel, R.; Mechtcheriakova, D.; Urtz, N.; Bornancin, F.; Baumruker, T.; Billich, A., Sphingosine Kinase Type 2 is Essential for Lymphopenia Induced by the Immunomodulatory Drug FTY720. *Blood* **2006,** *107* (4), 1454–1458.

23. Olivera, A.; Mizugishi, K.; Tikhonova, A.; Ciaccia, L.; Odom, S.; Proia, R. L.; Rivera, J., The sphingosine Kinase-Sphingosine-1-Phosphate Axis is a Determinant of Mast Cell Function and Anaphylaxis. *Immunity* **2007,** *26* (3), 287–297.

24. Sensken, S. C.; Bode, C.; Nagarajan, M.; Peest, U.; Pabst, O.; Graler, M. H., Redistribution of Sphingosine-1-Phosphate by Sphingosine Kinase 2 Contributes to Lymphopenia. *J. Immunol.* **2010,** *184* (8), 4133–4142.

25. Congdon, M. D.; Childress, E. S.; Patwardhan, N. N.; Gumkowski, J.; Morris, E. A.; Kharel, Y.; Lynch, K. R.; Santos, W. L., Structure–Activity Relationship Studies of the Lipophilic Tail Region of Sphingosine Kinase 2 Inhibitors. *Bioorg. Med. Chem. Lett.* **2015,** *25* (21), 4956–4960.

26. Kharel, Y.; Mathews, T. P.; Kennedy, A. J.; Houck, J. D.; Macdonald, T. L.; Lynch, K. R., A Rapid Assay for Assessment of Sphingosine Kinase Inhibitors and Substrates. *Anal. Biochem.* **2011,** *411* (2), 230–235.

27. Kharel, Y.; Morris, E. A.; Congdon, M. D.; Thorpe, S. B.; Tomsig, J. L.; Santos, W. L.; Lynch, K. R., Sphingosine Kinase 2 Inhibition and Blood Sphingosine 1-Phosphate Levels. *J. Pharmacol. Exp. Ther.* **2015,** *355* (1), 23–31.

28. Wang, Z.; Min, X.; Xiao, S.-H.; Johnstone, S.; Romanow, W.; Meininger, D.; Xu, H.; Liu, J.; Dai, J.; An, S.; Thibault, S.; Walker, N., Molecular Basis of Sphingosine Kinase 1 Substrate Recognition and Catalysis. *Structure* **2013,** *21* (5), 798–809.

29. Wang, J.; Knapp, S.; Pyne, N. J.; Pyne, S.; Elkins, J. M., Crystal Structure of Sphingosine Kinase 1 with PF-543. *ACS Med. Chem. Lett.* **2014,** *5* (12), 1329–1333.

30. Snider, A. J.; Ruiz, P.; Obeid, L. M.; Oates, J. C., Inhibition of Sphingosine Kinase-2 in a Murine Model of Lupus Nephritis. *PLoS ONE* **2013,** *8* (1), e53521.

31. Gustin, D. J.; Li, Y.; Brown, M. L.; Min, X.; Schmitt, M. J.; Wanska, M.; Wang, X.; Connors, R.; Johnstone, S.; Cardozo, M.; Cheng, A. C.; Jeffries, S.; Franks, B.; Li, S.; Shen, S.; Wong, M.; Wesche, H.; Xu, G.; Carlson, T. J.; Plant, M.; Morgenstern, K.; Rex, K.; Schmitt, J.; Coxon, A.; Walker, N.; Kayser, F.; Wang, Z., Structure Guided Design of a Series of Sphingosine Kinase (SphK) Inhibitors. *Bioorg. Med. Chem. Lett.* **2013,** *23* (16), 4608–4616.

32. Schnute, M. E.; McReynolds, M. D.; Kasten, T.; Yates, M.; Jerome, G.; Rains, J. W.; Hall, T.; Chrencik, J.; Kraus, M.; Cronin, C. N.; Saabye, M.; Highkin, M. K.; Broadus, R.; Ogawa, S.; Cukyne, K.; Zawadzke, L. E.; Peterkin, V.; Iyanar, K.; Scholten, J. A.; Wendling, J.; Fujiwara, H.; Nemirovskiy, O.; Wittwer, A. J.; Nagiec, M. M., Modulation of Cellular S1P Levels with a Novel, Potent and Specific Inhibitor of Sphingosine Kinase-1. *Biochem. J.* **2012,** *444* (1), 79–88.

33. Kharel, Y.; Mathews, T. P.; Gellett, A. M.; Tomsig, J. L.; Kennedy, P. C.; Moyer, M. L.; Macdonald, T. L.; Lynch, K. R., Sphingosine Kinase Type 1 Inhibition Reveals Rapid Turnover of Circulating Sphingosine-1-Phosphate. *Biochem. J.* **2011,** *440* (3), 345–353.

Chapter 4 Probing the Conformation of the Sphingosine Kinase 2 Binding Pocket: Structure–Activity Relationship Studies and Molecular Modeling of Indole Based Sphingosine Kinase 2 Inhibitors

4.1. Contributions

The work described in this chapter was conducted in collaboration with Dr. Yugesh Kharel, and Dr. Anne M. Brown. The author is solely responsible for the synthesis of the final compounds and the corresponding intermediate structures. All biological assays were conducted by Dr. Yugesh Kharel at the University of Virginia. All molecular modeling was conducted by Dr. Anne M. Brown in the Biochemistry Department at Virginia Tech. The final manuscript is currently being prepared by the author.

4.2. Abstract

Increased expression of sphingosine kinases (SphK) and elevated levels of sphingosine-1-phosphate (S1P) have been implicated with a variety of diseases including: cancer, fibrosis, Alzheimer's disease, asthma, and sickle cell disease. Of the two isoforms, the role of SphK2 in the S1P signaling pathway has not been fully elucidated. SphK2 has been shown to be an apoptotic enzyme when localized in the nucleus, endoplasmic reticulum, and mitochondria; however, it is a proliferative enzyme when located in the cytosol. Consequently, SphK2 has attracted attention as a potential therapeutic target and the need for more potent SphK2-selective inhibitors has grown. Previously, our group reported an Sphk2 selective inhibitor, **SLC5081308**, which displays approximately 7-fold selectivity for hSphK2 over hSphK1 and an SphK2 K_i value of 0.98 μM. Herein, we report the design, synthesis and biological evaluation of **SCL5081308** derivatives that contain varying substitution patterns around an indole ring. These compounds display excellent inhibitory activity, good SphK2 selectivity, and low micromolar K_i values for hSphK2. This structure–activity-relationship profile around the bicyclic aromatic tail examines the effects of substitution and helps elucidate the shape of the SphK2 binding pocket.

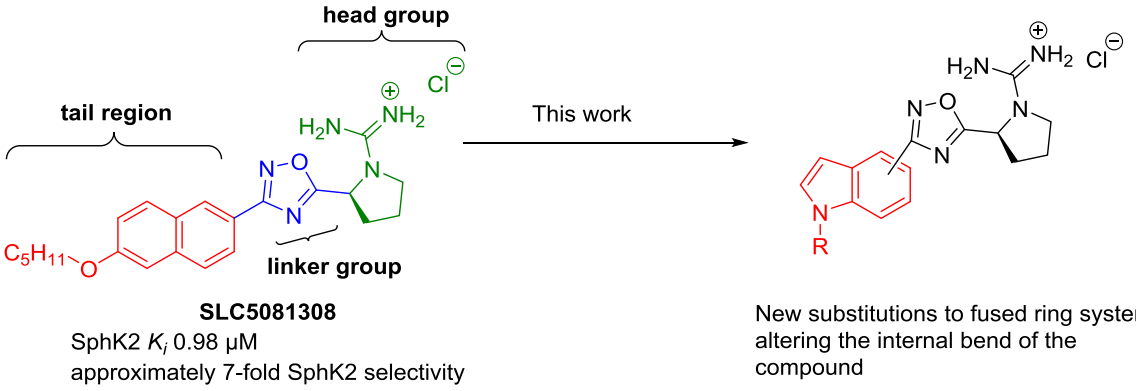

4.3. Introduction

Sphingolipids play an important role as structural components of eukaryotic membranes and cellular signaling metabolites. Ceramide, sphingosine and sphingosine-1-phosphate (S1P) are key cellular metabolites formed from the metabolic degradation of sphingolipids. The concentrations of these metabolites are controlled by their respective enzymes and can regulate cellular growth and survival.[1, 2] Ceramide and sphingosine have been shown to be pro-apoptotic metabolites while S1P promotes cellular proliferation. Once transported outside of the cell, S1P can act as a ligand to five G-protein coupled receptors ($S1P_{1-5}$) and initiate diverse physiological processes. In 2010, Fingolimod was approved by the FDA for treatment of relapsing and remitting multiple sclerosis. Fingolimod, also known as **FTY720**, acts as an S1P G-protein receptor antagonist and verified the druggability of the S1P pathway as a therapeutic target.[3, 4]

The phosphorylation of sphingosine to produce S1P is catalyzed by sphingosine kinases which exist in two isoforms, SphK1 and SphK2. While both isoforms perform the same metabolic function and catalyze the phosphorylation of Sph to S1P, they differ in size and cellular localization.[5] The smaller isoform, SphK1, is primarily found in the cytosol where the generated S1P can initiate numerous cell survival pathways. As a result, SphK1 is a proliferative enzyme. The larger isoform, SphK2, contains 5 transmembrane domains and is primarily localized in the nucleus. Additionally, SphK2 contains a BH3 binding domain which allows the enzyme to bind to the BCL_{XL} in the mitochondria. This binding eventually leads to the release of pro-apoptotic cytochrome c and allows SphK2 to be classified as a proliferative or pro-apoptotic enzyme depending upon its cellular localization.[5] SphK1 and SphK2 have been implicated in a variety of diseases including Alzheimer's disease, cancer, fibrosis, multiple sclerosis and sickle cell disease due to elevated over expression and elevated levels of S1P.[6-10]

As a result of the role of SphKs in the cell and the importance of this metabolic pathway in a variety of disease states, research has focused on the development of dual and specific SphK inhibitors. While SphK1 has been the major focus of academia and the pharmaceutical industry, the functional role of SphK2 is still under investigation[11-13] Consequently, a wide array of compounds have been identified as either SphK1 selective or dual inhibitors (Figure 4.1). A bioassay of SphK1 inhibitor **PF543** (K_i = 3.5 nM, >100 fold selective) has shown that SphK1 inhibition results in decreased *in vivo* S1P levels and has been employed in the study of sickle cell disease to reduce the sickling of red blood cells.[10] Amgen **82,** a reported dual inhibitor, was unsuccessful at altering tumor volume in xenograph models.[14] Only a limited number of compounds, with high micromolar K_i values, have been reported as SphK2 specific inhibitors (Figure 4.1). The first SphK2 selective inhibitor was **ABC294640** (K_i = 9.8 μM). **ABC294640** has also been reported to inhibit estrogen receptors of breast cancer cells in a partial agonistic manner similar to tamoxifen.[15-17] An inhibitor, **K145** (K_i = 6.4 μM), has been shown to be SphK2 selective and to reduce leukemia cell growth *in vivo*.[18] **SLR080811** (K_i = 1.4 μM) was the first SphK2 selective inhibitor to reveal an increase in blood S1P levels with SphK2 inhibition in mice.[19]

One reason for the vast diversification of structural motifs present in existing SphK inhibitors was the lack of a crystal structure for the target enzymes. In 2013, a structure of SphK1 with ADP and sphingosine bound was crystalized by Wang et al. and studies have since focused on the lipid-binding pocket of the enzyme.[20] Further crystallization efforts produced the crystal structure of SphK1 with **PF543** bound in the lipid-binding domain.[21] All of these bound ligands and previously reported inhibitors supported the necessity for hydrogen bonding with

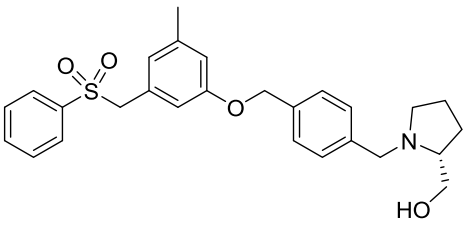

PF-543
K_i SphK1 3.6 nM
K_i SphK2 --
>100-fold SphK1 selective

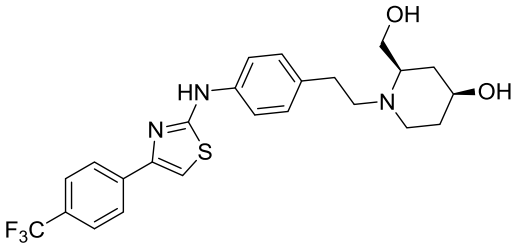

82
SphK1 IC_{50} 0.01 μM
SphK2 IC_{50} 0.02 μM
dual inhibitor

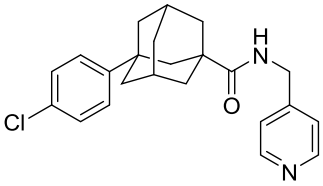

ABC294640
K_i SphK1 ---
K_i SphK2 9.8 μM
SphK2 selective

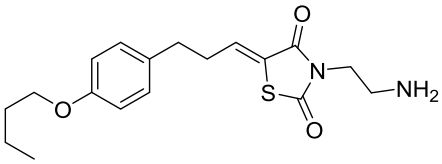

K145
K_i SphK1 ND
K_i SphK2 6.4 μM
SphK2 selective

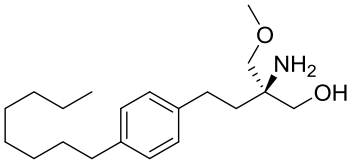

(R)-FTY720-OMe
K_i SphK1 ND
K_i SphK2 16.5 μM
SphK2 selective

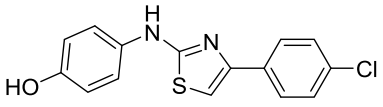

SKI-II
K_i hSphK1 16 μM
K_i hSphK2 7.9 μM
2-fold hSphK2 selective

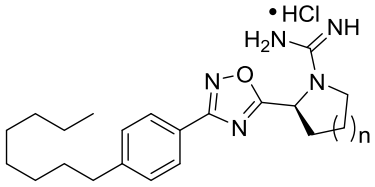

SLR080811
n = 1
K_i hSphK1 16 μM
K_i hSphK2 1.4 μM
11-fold hSphK2 selective

SLP120701
n = 0
K_i hSphK1 16 μM
K_i mSphK2 1 μM
> 10-fold SphK2 selective

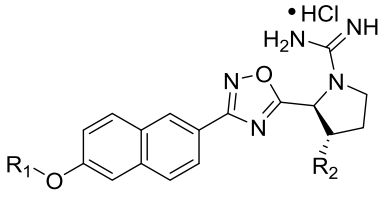

SLC5081308
R_1 = C_5H_{11}
R_2 = H
K_i hSphK1 0.98 μM
K_i hSphK2 7.2 μM
7-fold hSphK2 selective

SLC5091592
R_1 = *p*-(CF_3)benzyl
R_2 = H
K_i hSphK1 >20 μM
K_i hSphK2 1.02 μM
> 20-fold hSphK2 selective

SLC5111312
R_1 = C_5H_{11}
R_2 = OH
K_i hSphK1 0.73 μM
K_i hSphK2 0.90 μM
dual inhibitor

Figure 4.1. Select Structures of Sphingosine Kinase Inhibitors

Asp residues near the ATP binding domain of the inhibitor. Furthermore, all of the crystal structures indicated the presence of a bent or "J-shaped" lipophilic binding pocket for SphK1.[20-22] Presently, the SphK2 crystal structure has yet to be obtained.

To further the understanding of the *in vivo* function of SphK2, our group focuses on the development of potent and selective SphK2 inhibitors. Towards this goal, we have identified key structural requirements and interactions that must occur in the binding pocket. **SLR080811,** which contains a positively charged guanidine moiety or head group, can participate in hydrogen bonding with both Asp211 and 308.[23] Initial investigation into the tail region of **SLR080811** established a dependence of SphK2 inhibition and selectivity on alkyl tail length and the necessity of an internal phenyl ring.[24] Further probing of the internal phenyl ring led to the development of **SLC5081308** (K_i = 0.98 μM) and **SLC5091592** (K_i = 1.02 μM), second generation derivatives of the **SLR080811** scaffold, which are 7-fold and >20-fold selective for SphK2 respectively.[25] The increase in selectivity of **SLC5091592** is due to increased π-stacking interactions between the naphthyl moiety and Phe548 and van der Waals interactions with Cys533, Tyr566 and His556 in the tail region of the binding pocket of SphK2.[25]

Another exciting discovery was **SLC5111312** (K_i = 0.90 μM), which isSphK2 selective in mice, but acts as a dual inhibitor in humans due to increased hydrogen bonding with Asp308 and a 3′ hydroxyl on the proline head group.[13, 25] This SAR incorporated a 2,6-naphthyl ring in place of the phenyl ring and an ether linkage to the remaining portion of the tail. Upon discovering that the increased planarity and aromaticity of our lead molecule **SLC5081308** was tolerated, it was decided to probe the size and shape of the SphK2 binding pocket by altering the substitution around a fused ring moiety in the tail region. In this report, we describe our investigation in the tail region of a scaffold, varying the substitution of the linker and head

groups around an indole ring. Molecular modeling studies highlight the effects of the different substitution patterns on key hydrophobic and hydrogen bonding interactions in the binding cavity, and help elucidate the size and shape of the sphingosine binding pocket in SphK2.

4.4. Synthesis of N-alkyl Indole Derivatives

Due to the limited commercially available substitution patterns around a naphthalene ring, it was decided that the naphthalene moiety would be exchanged for an indole ring. Not only did this substitution provide us with a moiety which possesses better biological properties than the naphthalene, it provided us with a relatively simple synthetic pathway which contained a common intermediate for each substitution pattern and did not require protection of the indoyl nitrogen (Scheme 4.1–5). Therefore, the desired cyanoindoles (**4.1**, **4.8**, **4.15** and **4.22**) were purchased from either: AK Scientific, Combi-Blocks, or Oakwood Chemicals. Previously published methods were utilized to convert the nitriles to the corresponding amidoximes (**4.2**, **4.9**, **4.16**, **4.23**, and **4.30**) and to install the Boc-*L*-pyrrolindine or Boc-*L*-β-homopyrrolidine moiety while forming the 1,2,4-oxadiazole linker (**4.3**, **4.10**, **4.17**, **4.24** and **4.31**). Compounds **4.3**, **4.10**, **4.17**, and **4.24** were utilized as common intermediates for each substitution scaffold. Installation of the alkyl tails (**4.4a–f**, **4.11a–d**, **4.18a–e**, **4.25a–d,** and **4.29**) was achieved via deprotonation of the indoyl nitrogen with sodium hydride followed by a substitution reaction with the corresponding alkyl bromide. Boc-deprotections were achieved by bubbling HCl gas in methanol and carried forward without purification to produce the di-Boc-guanidine intermediates (**4.6a–f**, **4.13a–d**, **4.20a–e**, **4.27a–d,** and **4.33**). The di-Boc-guanidine moiety was installed using previously reported reagents in a microwave at a slightly elevated temperature (50 °C). This procedural alteration reduced the reaction time from 3 days to 2 hours. A second Boc-

deprotection yielded the final products (**4.7a–f**, **4.14a–d**, **4.21a–e**, **4.28a–d,** and **4.34**) as HCl salts. Since only one homologated compound (**4.34**) was synthesized, the alkyl chain was added first to reduce compound polarity and allow for easier purification (Scheme 4.5).

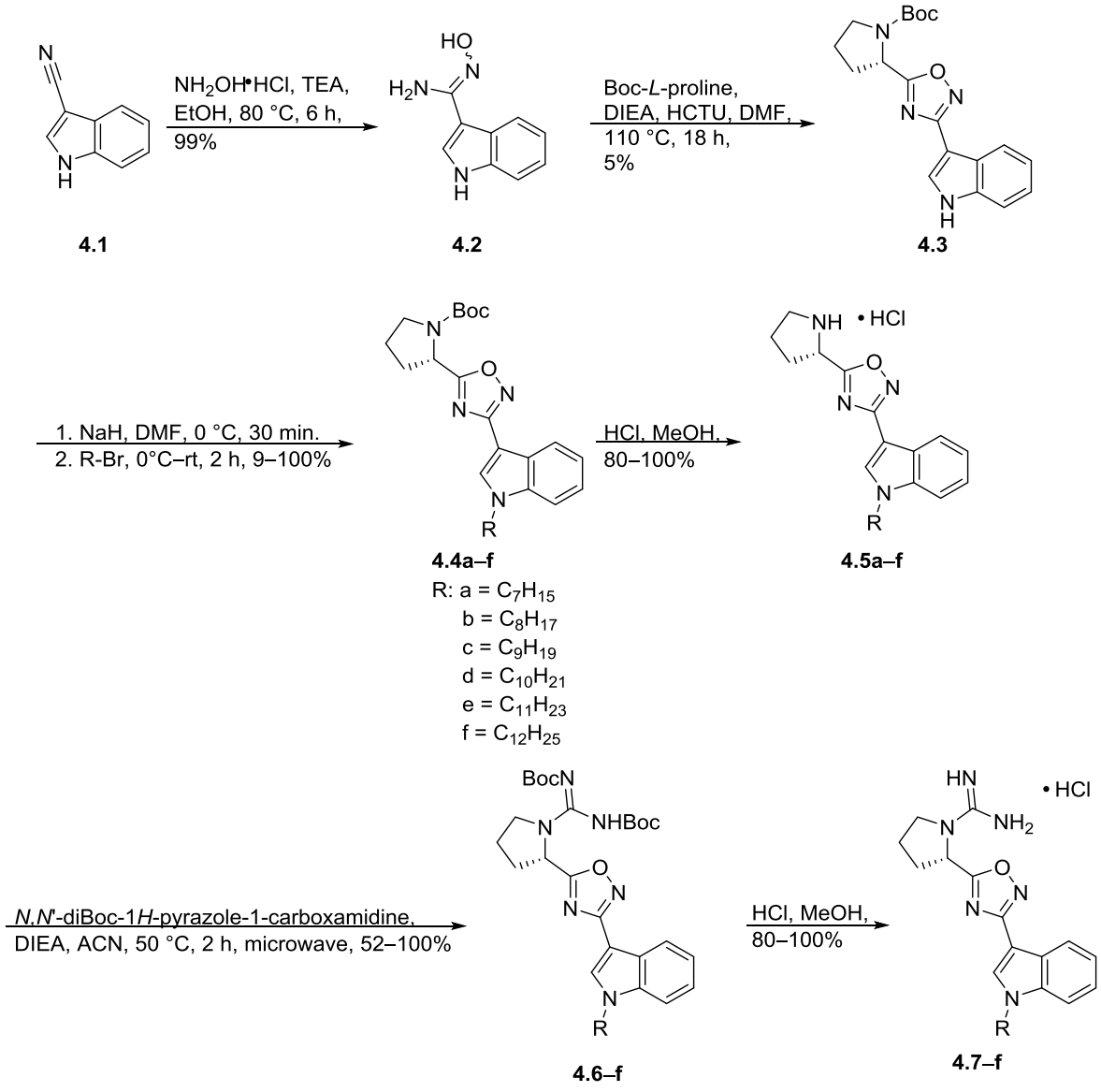

Scheme 4.1. Synthesis of *N*-alkyl-3-Indole Derivatives

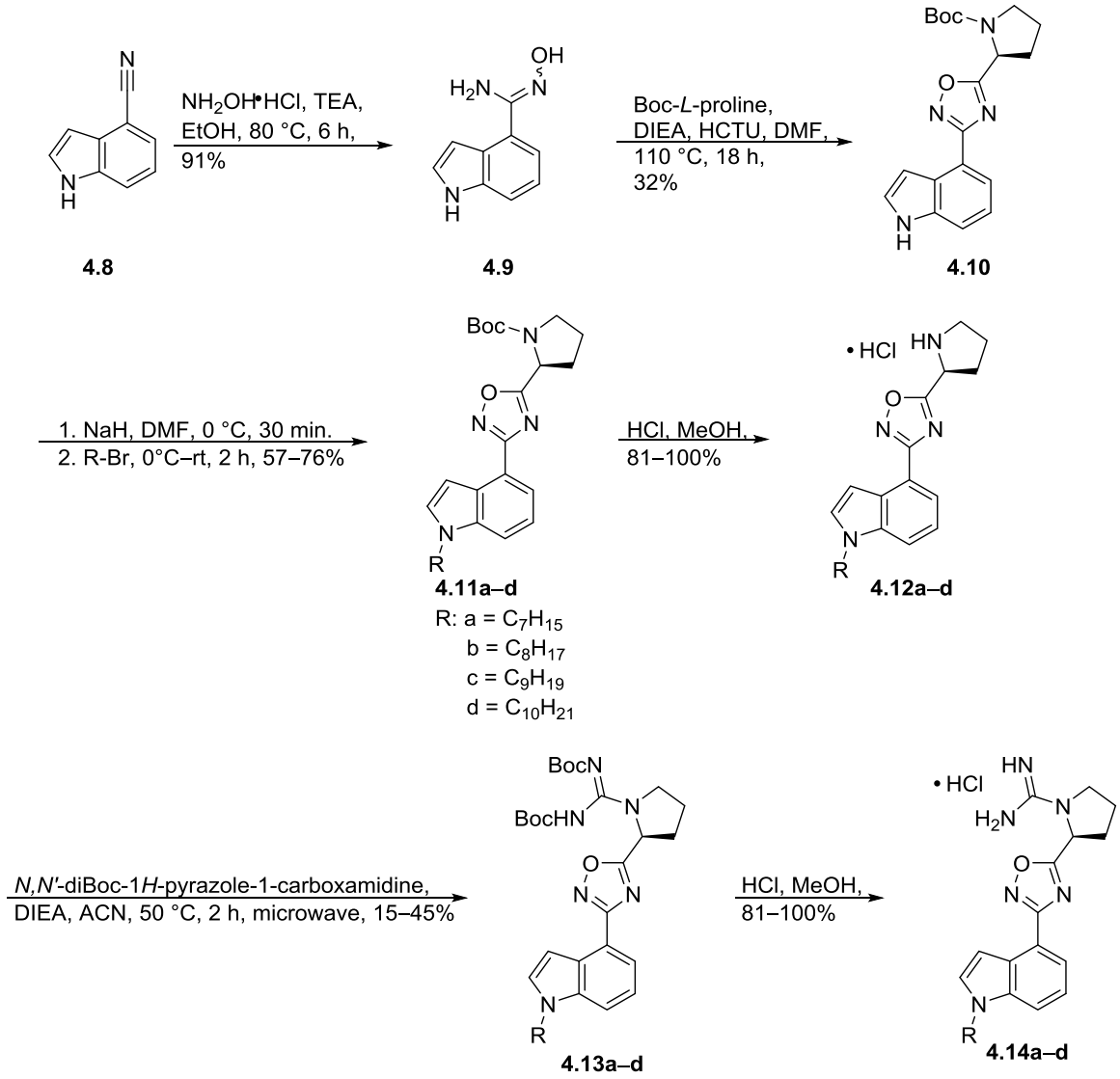

Scheme 4.2. Synthesis of *N*-alkyl-4-Indole Derivatives

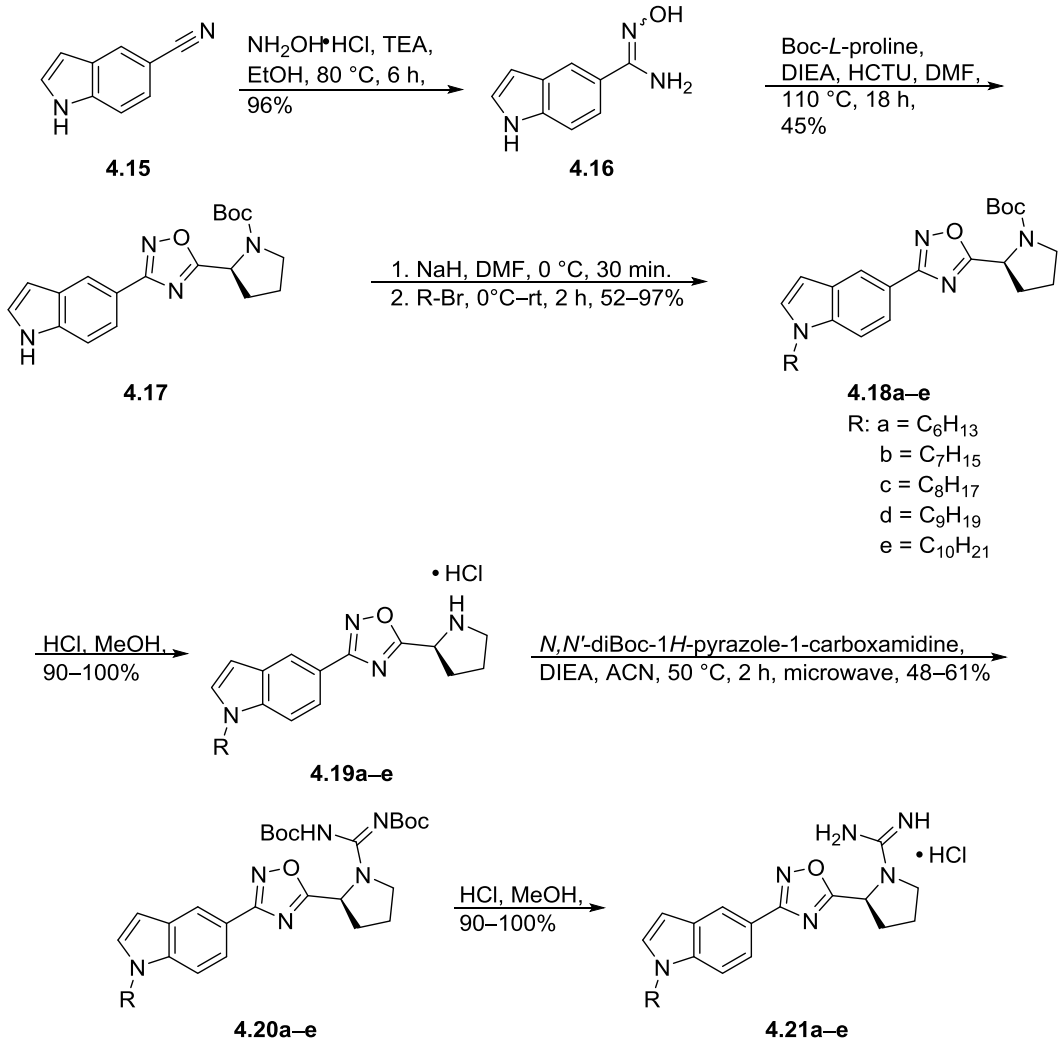

Scheme 4.3. Synthesis of *N*-alkyl-4-Indole Derivatives

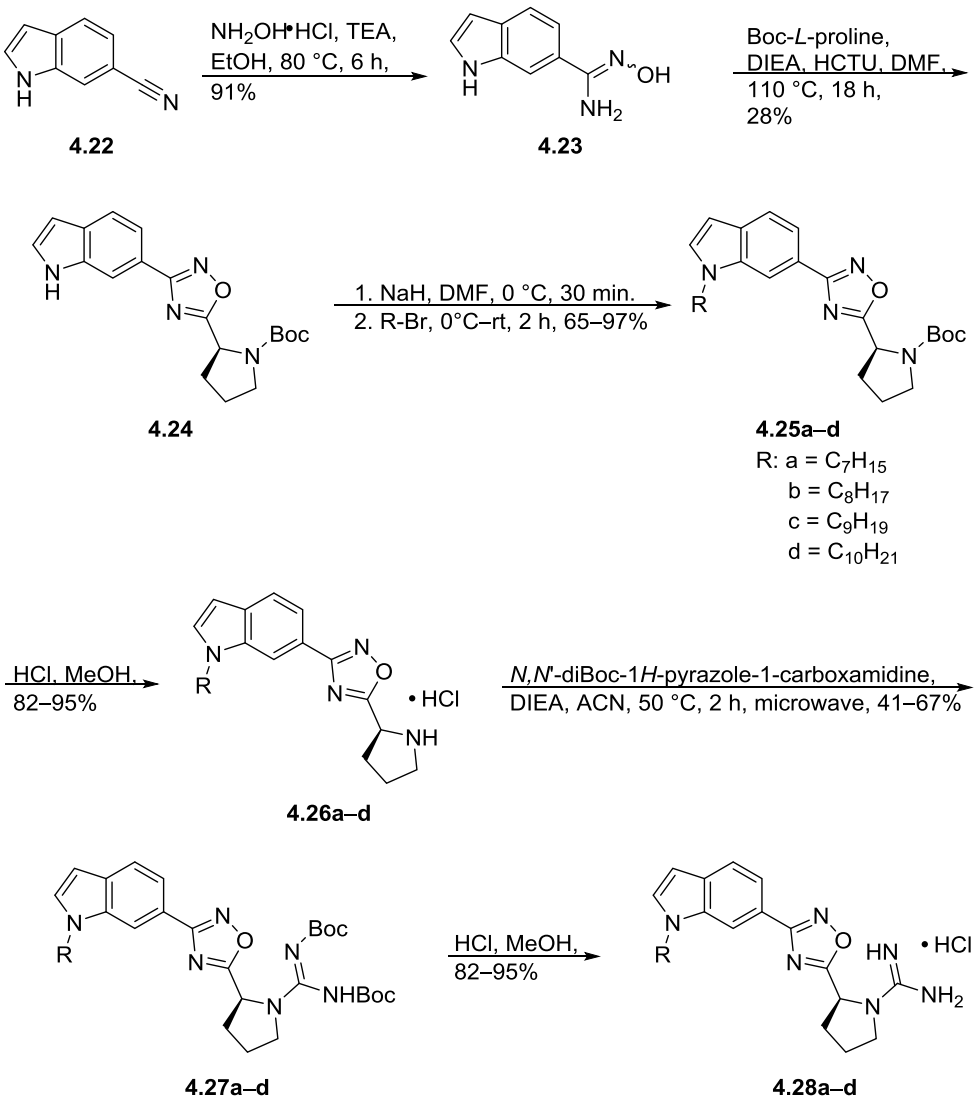

Scheme 4.4. Synthesis of *N*-alkyl-6-Indole Derivatives

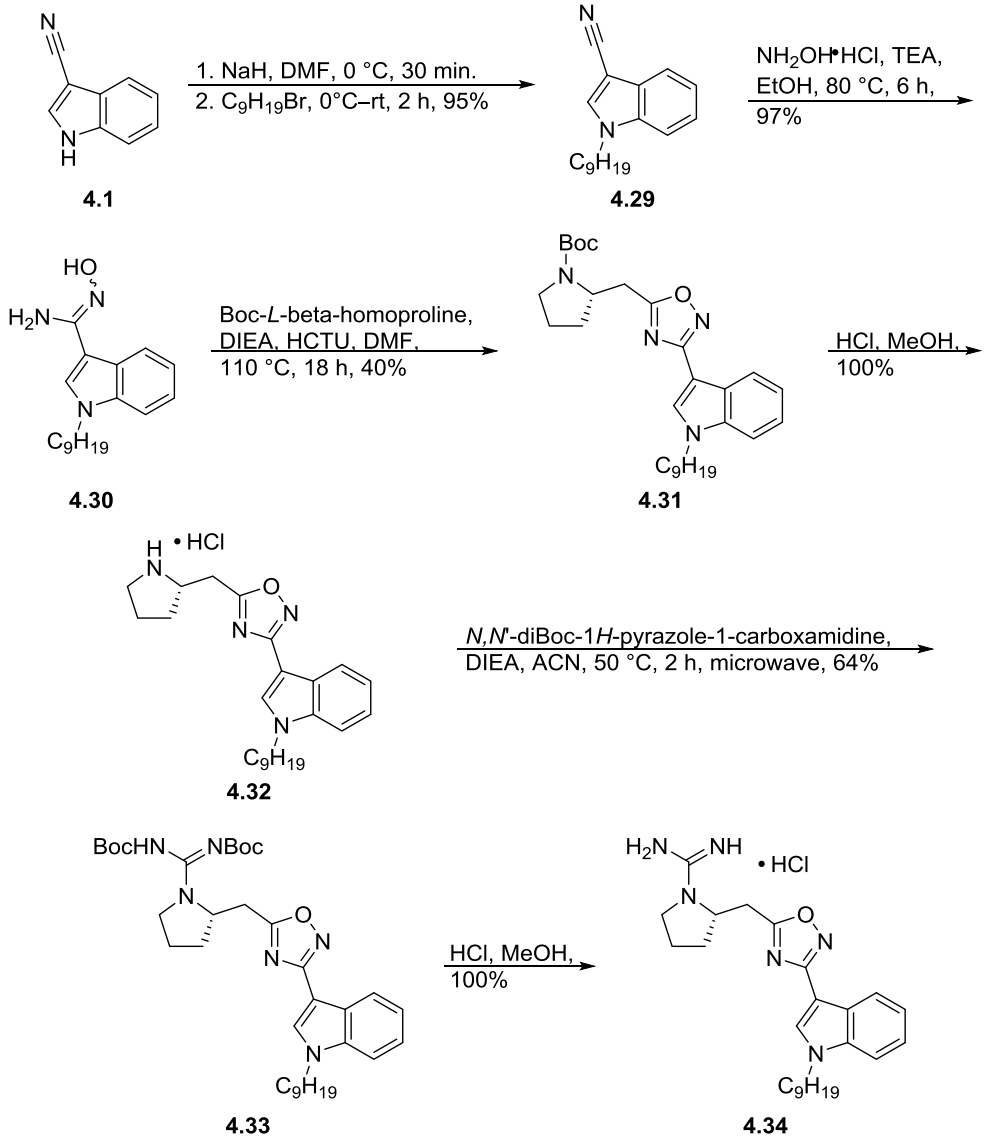

4.1 **4.29** **4.30** **4.31** **4.32** **4.33** **4.34**

Scheme 4.5. Synthesis of Compound 4.34

4.5. Biological Evaluation

4.5.1. Initial Screening of *N*-alkyl Indole Derivatives

Once the final compounds were obtained, the inhibitory effects on human SphK1 and SphK2 were determined using a previously established protocol.[26] In summary, cell lysate containing either recombinant hSphK1 or hSphK2, sphingosine, and [γ-^{32}P]ATP was incubated

for 20 minutes with or without inhibitor. Afterwards the reaction mixture was extracted, separated by thin layer chromatography and quantified by scintillation counting. The level of hSphK activity was determined by the amount of [γ-^{32}P]-S1P produced as a function of inhibitor concentration. Compounds were screened at 1 μM inhibitor concentrations in hSphK1 and 0.3 μM concentrations with hSphK2.

The results of the inhibition assay are shown in Table 4.1. Heptyl through decyl alkyl tail lengths were tested for each of the four substitution patterns studied. These lengths resulted in final compounds that ranged from approximately 18–22 atoms in length from the charged guanidine to the omega carbon. Our previous investigations into the tail region of **SLR080811**, **SLC5081308** and earlier lead compounds concluded that the ideal compound length is in this range.[24, 25, 27] Additional compounds possessing either an undecyl or docecyl tail were synthesized on the 1,3-indole scaffold to account for the shorter distance through the indole ring while maintaining the correct compound length in the study. With all scaffolds, kinase activity decreased as the overall length of the compound increases until an optimum length is obtained. Both the decyl and dodecyl tails (**4.7d** and **4.7f**) of the 1,3-scaffold (entries 5 and 7) inhibited hSphK2 by over 50%, however, **4.7d** possessed greater selectivity between the isoforms as it barely impacted hSphK1 activity. The decyl tail also presented the best potency and selectivity for the 1,4- and 1,6-scaffolds (**4.14d** and **4.28d**, entries 11 and 20). Continuing this trend, the decyl tail also exhibited excellent potency and selectivity for hSphK2 with the 1,5-scaffold (**4.21e**, entry 16); however, on this scaffold the nonyl tail (**4.21d**, entry 15) decreased hSphK2 activity by an additional 6% while not altering hSphK1 activity. The best compound from each scaffold was 21 atoms long with the exception of the 1,3-scaffold where the best compound was 20 atoms long. When comparing the best compound from each scaffold it is clearly evident that

Table 4.1. SphK1 and SphK2 Activity Upon Exposure to *N*-Alkyl Indole Derivatives

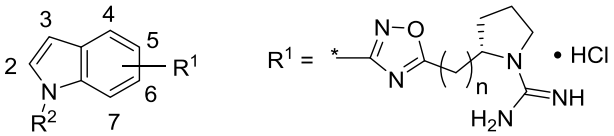

Entry	Compound	R^1 Position	R^2	n	% SphK Activity [a]	
					SphK1 (1 μM)	SphK2 (0.3 μM)
1	**SLC5081308**[b]	---	---	---	90 ± 7	95 ± 5
2	**SLC5101462** (**4.7a**)	3	Heptyl	0	110 ± 4	96 ± 5
3	**SLC5101461** (**4.7b**)	3	Octyl	0	93 ± 2	73 ± 3
4	**SLC5101460** (**4.7c**)	3	Nonyl	0	88 ± 1	59 ± 7
5	**SLC5101463** (**4.7d**)	3	Decyl	0	96 ± 6	47 ± 1
6	**SLC5121469** (**4.7e**)	3	Undecyl	0	107 ± 4	79 ± 12
7	**SLC5121467** (**4.7f**)	3	Dodecyl	0	76 ± 3	46 ± 7
8	**SLC5071449** (**4.14a**)	4	Heptyl	0	105 ± 6	89 ± 4
9	**SLC5071450** (**4.14b**)	4	Octyl	0	98 ± 7	84 ± 2
10	**SLC5091459** (**4.14c**)	4	Nonyl	0	90 ± 1	68 ± 4
11	**SLC5071451** (**4.14d**)	4	Decyl	0	87 ± 2	64 ± 3
12	**SLC5051505**(**4.21a**)	5	Hexyl	0	106 ± 1	72 ± 10
13	**SLC5051506** (**4.21b**)	5	Heptyl	0	96 ± 2	93 ± 7
14	**SLC5051507** (**4.21c**)	5	Octyl	0	101 ± 5	87 ± 9
15	**SLC5101465** (**4.21d**)	5	Nonyl	0	103 ± 1	25 ± 3
16	**SLC5101464** (**4.21e**)	5	Decyl	0	99 ± 6	31 ± 1
17	**SLC5081454** (**4.28a**)	6	Heptyl	0	98 ± 6	103 ± 1
18	**SLC5081455** (**4.28b**)	6	Octyl	0	94 ± 1	93 ± 6
19	**SLC5081457** (**4.28c**)	6	Nonyl	0	107 ± 2	79 ± 5

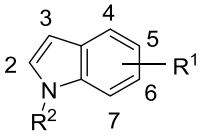

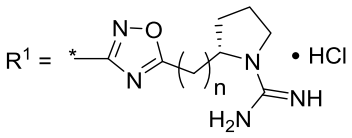

Entry	Compound	R^1 Position	R^2	n	% SphK Activity [a]	
					SphK1 (1 μM)	SphK2 (0.3 μM)
20	**SLC5081458** (**4.28d**)	6	Decyl	0	98 ± 2	68 ± 2
21	**SLC5101572** (**4.34**)	3	Nonyl	1	98 ± 1	98 ± 3

[a] Values are percent activity of hSphK1 or hSphK2 with 10 and 5 μM Sph, respectively, in the presence of inhibitor. Each value is an average of three experiments. Lower SphK activity level indicates better inhibition. [b]See Fig. 1 for structure. The K_m of SphK1 and SphK2 is 10 μM and 5 μM, respectively.

the 1,5-scaffold is ideal in terms of potency and selectivity. Both the **4.21d** and **4.21e** reduced hSphK2 activity by 70% or more while having no effect on hSphK1 activity levels. At best, the 1,3-scaffold (**4.7d**) was able to reduce the hSphK2 levels by 53% and only alter hSphK1 levels by 4%. Although this compound is potent and selective, the 1,5-scaffold was able to reduce hSphK2 activity by an additional 20%. The 1,4- and 1,6-scaffolds were only able to reduce hSphK2 activity by a maximum of 36% and 32% respectively with the alkyl tails in this study.

4.5.2. Determination of K_i and cLogP Values

To further characterize the activity of inhibitors with hSphK1 and hSphK2, we selected a threshold level of approximately 50% enzyme activity. As shown in Table 4.2, the 1,3-substituted indoles **SLC5011463** (**4.7d**) and **SLC5121467** (**4.7f**) possess K_i values of > 10 μM

Table 4.2. Inhibition Constants of Select Inhibitors

compound	K_i (μM)[a]		SphK2 selectivity	cLogP
	hSphK1	hSphK2		
SLC5081308	7.2 ± 0.9	0.98 ± 0.2	4	4.2
SLC5091592	>20	1.02 ± 0.2	> 10	4.7
SLC5101463 (**4.7d**)	>10	0.30 ± 0.05	> 33	6.2
SLC5121467 (**4.7f**)	8 ± 1.7	0.29 ± 0.08	28	7.3
SLC5101465 (**4.21d**)	>10	0.09 ± 0.01	> 111	5.7
SLC5101464 (**4.21e**)	>10	0.12 ± 0.03	> 83	6.2

[a] Inhibitory constants for recombinant enzymes were obtained by kinetic analysis of S1P production using variable concentration of sphingosine and a fixed concentration of ATP in the presence or absence of compounds as described previously.[19] Selectivity for each compound was determined by dividing the K_m SphK2 by the K_m of SphK1.

and 8 μM for hSphK1 and K_i values of 0.30 μM and 0.29 μM for hSphK2. Both of these compounds display a 3-fold increase in hSphK2 selectivity and potency over **SLC5081308**. The 1,5-substituted indoles **SLC5101465** (**4.21d**) and **SLC5101464** (**4.21e**) both possess K_i values of >10 μM for hSphK1 and K_i values of 0.09 μM and 0.12 μM for hSphK2 respectively. These compounds are substantially more potent than the naphthalene leads, and they display drastically improved selectivity for hSphK2 of > 111-fold and > 83-fold for hSphK2, respectively. In terms of pharmacokinetic parameters, the new inhibitors in Table 4.2 have higher cLogP values than **SLC5081308** (cLogP = 4.2) and **SLC5091592** (cLogP = 4.7). Overall the 1,3-scaffold has a higher cLogP than the 1,5-scaffold when comparing compounds with identical chain lengths.

Additionally, of the most potent compounds shown in Table 4.2, the shorter tail lengths provide slightly greater selectivity than their analogs with an additional methylene.

4.6. Molecular Modeling

4.6.1. Comparison of Indole Substitution Patterns

To further our understanding of the potential binding interactions exhibited by these compounds and elucidate essential interactions in the hSphK2 binding pocket, select compounds were docked in our previously reported homology model of hSphK2.[25] This homology model was generated based on the published crystal structure of hSphK1 complexed with ADP and magnesium (PDB ID: 3VZB). For the purpose of our experiments, ADP was converted to ATP in the ATP binding site by adding a phosphate group and energy minimizing the resulting structure. The most potent and selective structure **SLC5101465** (**4.21d**) as well as the corresponding compounds possessing the nonyl tail of the other scaffolds (**4.7c, 4.14c**, and **4.28c**), were subsequently docked into the substrate-binding cavity of hSphK2. As shown in Figure 4.2, each scaffold uniquely occupies the binding cavity in a different orientation, which affects the positioning of the guanidine head group and 1,2,4-oxadiazole ring, as well as the resulting essential electrostatic interactions and hydrogen bonding with Asp211 and Asp308. Scaffolds branching off the benzene moiety of the indole group appear to situate the indole group in a way that is more horizontal or linear, that is to say both the benzene ring and five-membered nitrogen-containing ring are in-line with the acyl tail, in the binding cavity. This positioning of the indole group allows for key hydrophobic interactions with Phe548 and Val304. Scaffolds branching off the five-membered nitrogen-containing ring place the benzene group out of line with the acyl tail, which pushes the compound into the back of the active site towards Phe557.

The positioning of **SLC5101460** (**4.7c**) towards the tail of the active site is due to positioning of the scaffold; the benzene ring of the indole group must be forced further into the bottom of the pocket in order to avoid steric clashes with Phe548. This change in position in the active site causes hydrogen bonding interactions with Asp308 and Asp211 to be lost, giving rise to the slight increase in hSphk2 activity and highlights the influence of key interactions of the tail region in the active site with Cys533, His556, and Tyr566. The potency observed with the 1,3-indole scaffold is presumably due to positioning in the bottom of the active site, whereas the loss in SphK2 specificity is due to loss of interactions with Asp308 and Asp211.

The other scaffolds allow for more favorable hydrophobic interactions and positioning between Phe548 and Val304, leading to more central positioning in the binding cavity and the ability to interact with either/or Asp211 and Asp308. The variance in 1,4-indole-, 1,5-indole-, and 1,6-indole-scaffold positions is due to the changes in rotatable bonds associated with the head group of the inhibitors. The 1,4-scaffold (Figure 4.2B) positions the inhibitor to have hydrophobic interactions with both Val304 and Phe548, in addition to electrostatic and hydrogen bonding with Asp308 and ATP. In comparison, the 1,5-scaffold has hydrogen bonding with both Asp308 and Asp211 and maintains hydrophobic interactions with Val304 and Phe548, while the 1,6-scaffold (Figure 4.2D) maintains interactions with both Asp211 and Asp308 near the ATP binding site. In both of these scaffolds, the linearity of the position in the active site affords the potential for π-stacking interactions.

By comparing the 1,5-scaffold, the 1,3-scaffold, and previously observed interactions,[25] it is apparent that interaction with both Asp308 and Asp211 is critical for inhibitor selectively over hSphK1. The linearity of the naphthalene containing compounds and the 1,4-indole-, 1,5-indole-, and 1,6-indole-scaffolds affords stronger electrostatic interactions with Asp211 and correlates to

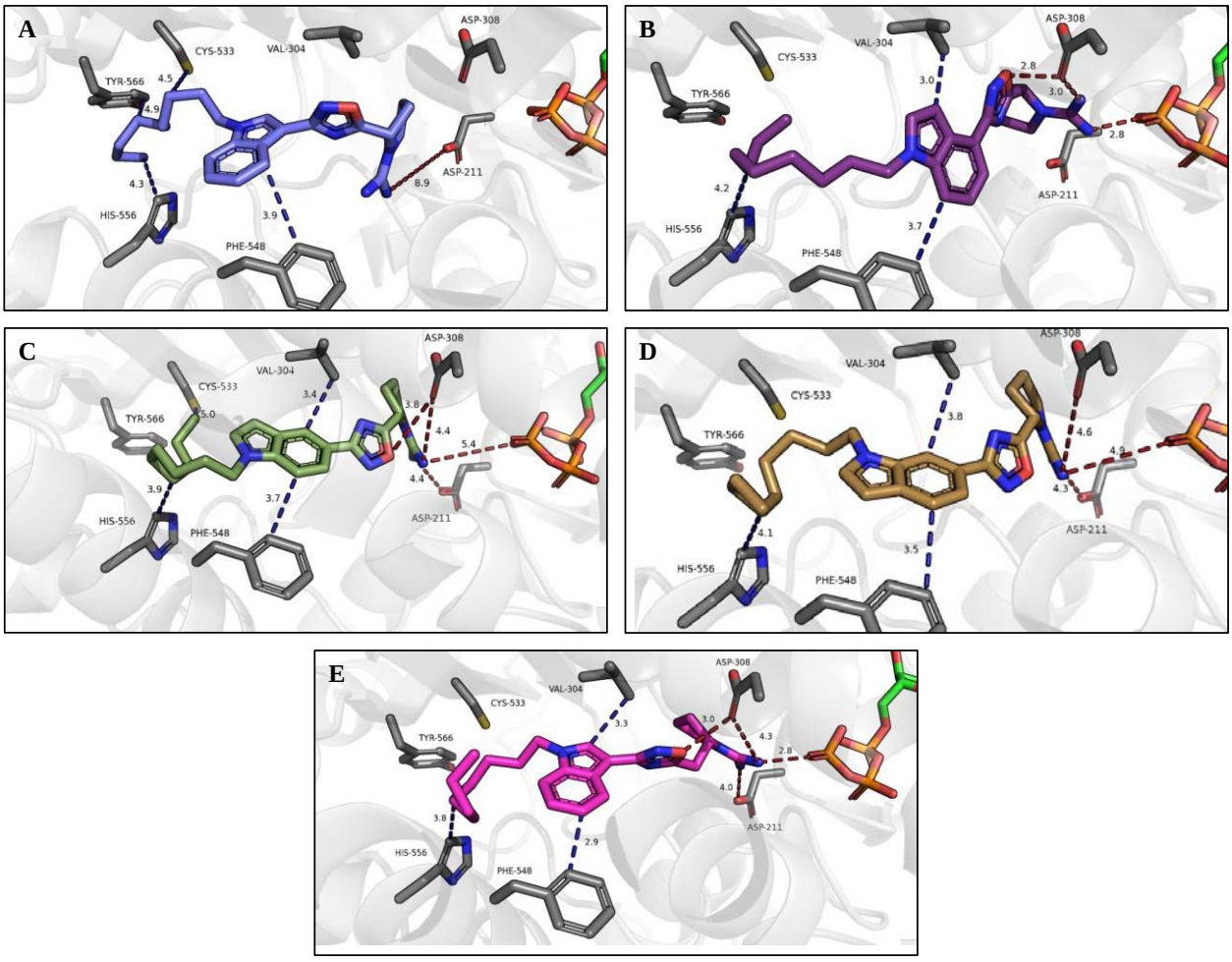

Figure 4.2. Docking of Inhibitors in the hSphK2 Homology Model. A) **SLC5101460** (**4.7c**-blue, hSphK2 activity 59% with 0.3 µM of compound), B) **SLC5091459** (**4.14c**-purple, hSphK2 activity 68% with 0.3 µM of compound), C) **SLC5101465** (**4.21**-green, hSphK2 activity 25% with 0.3 µM of compound), D) **SLC5081457** (**4.28c**-gold, hSphK2 activity 79% with 0.3 µM of compound), and E) SLC5101572 (4.34-pink, hSphK2 activity 98% with 0.3 µM of compound). hSphK2 is shown as a light grey cartoon with key amino acids being shown as sticks and labeled. ATP is shown as green sticks and colored by element. Magnesium is not shown for clarity. Blue dashed lines indicate hydrophobic interactions and red dashed lines indicate hydrogen bonds.

inhibitor specificity. The 1,5-indole- and 1,6-indole-scaffolds (Figure 4.2C and D) further provide evidence for a more linear position of the inhibitor in the binding cavity and strong electrostatic interactions with both Asp211 and Asp308 in order to enhance specificity towards hSphK2. **SLC5101465** (**4.21d**) is predicted to be the most potent and selective inhibitor given the maintenance of the hydrophobic interaction with Val308 Phe548, His556, and Cys533, in addition to strong electrostatic interactions and hydrogen bonding with both Asp211 and Asp308. **SLC5101457** (**4.28c**) is less potent than **SLC5101465** (**4.21d**) since the hydrogen bonding and electrostatic interactions with Asp211 and Asp308 are weakened due to greater bond distances (4.0 Å vs 3.8 Å and 4.3 Å vs. 3.8 Å, respectively). The hydrophobic interaction with SphK2 specific Cys533 is also diminished. In SphK1 this residue is Phe. **SLC5101459** (**4.14c**) is more potent than **SLC5101457** (**4.28c**) given the distance interaction with Asp308 (3.0 Å vs. 4.0 Å); however, specificity begins to diminish in **SLC5101459** (**4.14c**) due to lack of interaction with Asp211. Therefore, we propose that the space between Val304 and Phe548 can be a limiting factor on functional groups linked to the 1,2,4-oxadiazole ring and influence interaction strength with Asp211 and Asp308. Steric clashes with Phe548 caused the inhibitor to position itself in towards the tail of the active site with **SLC5101460** (**4.7c**). Longer acyl chains on 1,3-scaffolds were more effective than shorter chains due to the acyl chains having hydrophobic interactions at the tail of the active site which cause inhibition. These results further highlight the influence of the tail region residues. The shorter acyl chains lost these interactions, which corresponds with a loss in inhibition activity.

4.6.2. Increasing Hydrogen Bonding to Aspartic Acid with the 1,3-Indole Scaffold

To further understand the unique binding mode of the 1,3-indole scaffold, **SLC5101572** (**4.34**) was also docked in the homology model. Based on previous work, incorporation of the

homopyrrolidine head group increased compound potency for hSphK1;[23] however, in this work, it was hypothesized that the addition of the methylene would move the inhibitor up and into the front of the active site, while also maintaining interactions with Cys533, His556, and Tyr566. Surprisingly, this compound was inactive in both isoforms (Table 4.1, entry 21). Based on the docking results, it appears that the lack of rotatable bonds in the indole region of **SLC5101572** (**4.34**) causes steric clashes with Phe548 and removes tail region interactions (Figure 4.2E). This change in position in the binding cavity of **SLC5101572** (**4.34**) was caused by the adjustment to the positioning of the guanidine moiety, which was being driven towards Asp308 as a result of the extra methylene. In addition to positively influencing interactions with key Asp residues, the extra methylene pulled the indole group away from essential tail interactions. More importantly, the alterations to the indole positioning created unfavorable steric interactions with Val304 and Phe548. Additional methylene groups may be required in this region to extend the length of the compound so that the key Asp and tail interactions can be obtained while minimizing steric hindrance with Val304 and Phe548.

4.6.3. Determining the Internal Angle of Select Indole Derivatives

The 1,4-indole, 1,5-indole and 1,6-indole scaffolds provide information that emphasize the importance of rotation along the 1,2,4-oxadiazole ring in order to achieve interaction with both Asp211 and Asp308, and therefore afford SphK2 specificity and potency. In order to assess the relative rotation of the indole and 1,2,4-oxadiazole ring to one another, an angle measurement between the three linker atoms of the indole group, the 1,2,4-oxadiazole ring, and the guanidine head group was performed. Table 4.3 details an example of the three atoms (1,2,3) selected for angle measurement and the resulting angle. As previously described, the most selective compound, **SLC5101465** (**4.21d**), sits linearly between Val304 and Phe548. This is

Table 4.3. Investigations of the Internal Angle of Select Indole Derivatives Relative to the 1,2,4-oxadiazole Group

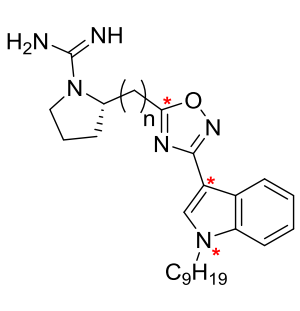

4.7c and **4.34**
1,3-substitution

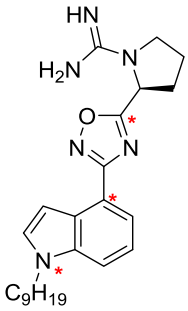

4.14c
1,4-substitution

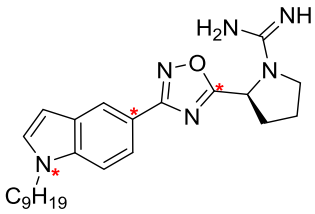

4.21d
1,5-substitution

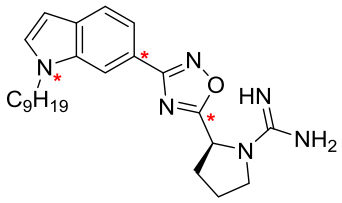

4.28c
1,6-substitution

Compound	Indole Substitution	n	Angle (°)[b]
SLC5091592[a]	---	---	170°
SLC5101457 (**4.28c**)	1,6 (T,H)	---	136°
SLC5101459 (**4.14c**)	1,4 (T,H)	---	147°
SLC5101572 (**4.34**)	1,3 (T,H)	1	153°
SLC5101460 (**4.7c**)	1,3 (T,H)	0	156°
SLC5101465 (**4.21d**)	1,5 (T,H)	---	168°

[a] See Figure 4.1 for structure. [b] Angle shown in red on each substitution pattern.

demonstrated with a 168° angle between the designated linker atoms. This aligns well with the angle measurement (170°) of SphK2 inhibitor **SLC5091592**, the most selective SphK2 inhibitor on the **SLC5081308** naphthalene scaffold.[25] This details the ideal position of the fused, bicyclic, aromatic moiety related to the 1,2,4-oxadiazole ring in order to achieve interactions with Asp211 and Asp308 while maintaining positioning between Val304 and Phe548. Other compounds that exhibited decreased potency and/or selectivity possessed smaller angles between the indole

moiety and 1,2,4-oxadiazole ring (Table 4.3) which either reduced interactions with essential residues or resulted in steric clashes with Phe548.

4.7. Conclusions

In conclusion, we described the structure–activity relationship profile of indole-based sphingosine kinase 2 inhibitors in which the substitution pattern around the indole moiety is varied. Our studies indicate that the 1,5-indole-scaffold affords the most potent analog (**SLC5101465**, **4.21d**) with increased selectivity (> 111-fold) towards SphK2 when compared to **SLC5081308**. Homology molecular docking studies indicate that these indole derivatives maintain a binding mode similar to sphingosine in the ligand binding pocket. The molecular docking studies emphasize the importance of rotatable bonds of the various substitution patterns and emphasize the significance of the tail region of the pocket on SphK selectivity. A key discovery in our investigation is the ability of the 1,3-scaffold to occupy the deepest region of the binding pocket, where it is able to gain hSphK2 potency while losing selectivity as a result of the inability to hydrogen bond to Asp211 and Asp308. In addition, this work brings focus on ligand positioning and exploration of Val304 and Phe548, while beginning to assess the influence of exploitable residues in the tail region of the SphK2 active site. Finally, this work provides a pathway to more potent and selective hSphK2 inhibitors.

4.8. Acknowledgements

This work was supported by NIH Grants R01 GM104366 and R01 GM067958.

4.9. Notes

The authors declare the following competing financial interest(s): W.L.S. and K.R.L. are among the co-founders of SphynKx Therapeutics LLC, which was created to commercialize S1P-related discoveries, including SphK inhibitors, discovered and characterized in their laboratories. The compounds described in this manuscript are included in a patent application licensed to SphynKx.

4.10. References

1. Spiegel, S.; Milstein, S., Sphingosine-1-Phosphate: Signaling Inside and Out. *FEBS Lett.* **2000,** *476* (1-2), 55–57.
2. Spiegel, S.; Milstien, S., Sphingosine-1-Phosphate, a Key Cell Signaling Molecule. *J. Biol. Chem.* **2002,** *277* (29), 25851–25854.
3. Kappos, L.; Radue, E. W.; O'Connor, P.; Polman, C.; Hohlfeld, R.; Calabresi, P.; Selmaj, K.; Agoropoulou, C.; Leyk, M.; Zhang-Auberson, L.; Burtin, P., A Placebo-Controlled Trial of Oral Fingolimod in Relapsing Multiple Sclerosis. *N. Engl. J. Med.* **2010,** *362* (5), 387–401.
4. Cohen, J. A.; Barkhof, F.; Comi, G.; Hartung, H. P.; Khatri, B. O.; Montalban, X.; Pelletier, J.; Capra, R.; Gallo, P.; Izquierdo, G.; Tiel-Wilck, K.; de Vera, A.; Jin, J.; Stites, T.; Wu, S.; Aradhye, S.; Kappos, L., Oral Fingolimod or intramuscular Interferon for Relapsing Multiple Sclerosis. *N. Engl. J. Med.* **2010,** *362* (5), 402–415.
5. Neubauer, H. A.; Pitson, S. M., Roles, Regulation and Inhibitors of Sphingosine Kinase 2. *FEBS J.* **2013,** *280* (21), 5317–5336.
6. Bigaud, M.; Guerini, D.; Billich, A.; Bassilana, F.; Brinkmann, V., Second Generation S1P Pathway Modulators: Research Strategies and Clinical Developments. *Biochim. Biophys. Acta.* **2014,** *1841* (5), 745–758.
7. Takuwa, N.; Du, W.; Kaneko, E.; Okamoto, Y.; Yoshioka, K.; Takuwa, Y., Tumor-Suppressive Sphingosine-1-Phosphate Receptor-2 Counteracting Tumor-Promoting Sphingosine-1-Phosphate Receptor-1 and Sphingosine Kinase 1. *Am. J. Cancer Res.* **2011,** *1*, 460–481.

8. Kunkel G. T; Maceyka M; Milstien S; S., S., Targeting the Sphingosine-1-Phosphate Axis in Cancer, Inflammation and Beyond. *Nat. Rev. Drug Discov.* **2013,** *12* (9), 688–702.

9. Takasugi, N.; Sasaki, T.; Suzuki, K.; Osawa, S.; Isshiki, H.; Hori, Y.; Shimada, N.; Higo, T.; Yokoshima, S.; Fukuyama, T.; Lee, V. M.; Trojanowski, J. Q.; Tomita, T.; Iwatsubo, T., BACE1 Activity is Modulated by Cell-Associated Sphingosine-1-Phosphate. *J. Neurosci.* **2011,** *31* (18), 6850–6857.

10. Zhang, Y.; Berka, V.; Song, A.; Sun, K.; Wang, W.; Zhang, W.; Ning, C.; Li, C.; Zhang, Q.; Bogdanov, M.; Alexander, D. C.; Milburn, M. V.; Ahmed, M. H.; Lin, H.; Idowu, M.; Zhang, J.; Kato, G. J.; Abdulmalik, O. Y.; Zhang, W.; Dowhan, W.; Kellems, R. E.; Zhang, P.; Jin, J.; Safo, M.; Tsai, A. L.; Juneja, H. S.; Xia, Y., Elevated Sphingosine-1-Phosphate Promotes Sickling and Sickle Cell Disease Progression. *J. Clin. Invest.* **2014,** *124* (6), 2750–2761.

11. Plano, D.; Amin, S.; Sharma, A. K., Importance of Sphingosine Kinase (SphK) as a Target in Developing Cancer Therapeutics and Recent Developments in the Synthesis of Novel SphK Inhibitors. *J. Med. Chem.* **2014,** *57* (13), 5509–5524.

12. Santos, W. L.; Lynch, K. R., Drugging Sphingosine Kinases. *ACS Chem. Biol.* **2015,** *10* (1), 225–233.

13. Kharel, Y.; Morris, E. A.; Congdon, M. D.; Thorpe, S. B.; Tomsig, J. L.; Santos, W. L.; Lynch, K. R., Sphingosine Kinase 2 Inhibition and Blood Sphingosine 1-phosphate Levels. *J. Pharmacol. Exp. Ther.* **2015,** *355*, 23–31.

14. Rex, K.; Jeffries, S.; Brown, M. L.; Carlson, T.; Coxon, A.; Fajardo, F.; Frank, B.; Gustin, D.; Kamb, A.; Kassner, P. D.; Li, S.; Li, Y.; Morgenstern, K.; Plant, M.; Quon,

K.; Ruefli-Brasse, A.; Schmidt, J.; Swearingen, E.; Walker, N.; Wang, Z.; Watson, J. E.; Wickramasinghe, D.; Wong, M.; Xu, G.; Wesche, H., Sphingosine Kinase Activity is Not Required for Tumor Cell Viability. *PLoS ONE* **2013,** *8* (7), e68328.

15. Beljanski, V.; Knaak, C.; Smith, C. D., A Novel Sphingosine Kinase Inhibitor Induces Autophagy in Tumor Cells. *J. Pharmacol. Exp. Ther.* **2010,** *333* (2), 454–464.

16. French, K. J.; Zhuang, Y.; Maines, L. W.; Gao, P.; Wang, W.; Beljanski, V.; Upson, J. J.; Green, C. L.; Keller, S. N.; Smith, C. D., Pharmacology and Antitumor Activity of ABC294640, a Selective Inhibitor of Sphingosine Kinase-2. *J. Pharmacol. Exp. Ther.* **2010,** *333*, 129–139.

17. Antoon, J. W.; White, M. D.; Meacham, W. D.; Slaughter, E. M.; Muir, S. E.; Elliott, S.; Rhodes, L. V.; Ashe, H. B.; Wiese, T. E.; Smith, C. D.; Burow, M. E.; Beckman, B. S., Antiestrogenic Effects of the Novel Sphingosine Kinase-2 Inhibitor ABC294640. *Endocrinology* **2010,** *151* (11), 5124–5135.

18. Liu, K.; Guo, T. L.; Hait, N. C.; Allegood, J.; Parikh, H. I.; Xu, W.; Kellogg, G. E.; Grant, S.; Spiegel, S.; Zhang, S., Biological Characterization of 3-(2-amino-ethyl)-5-[3-(4-butoxyl-phenyl)-propylidene]-thiazolidine-2,4-dione (K145) as a Selective Sphingosine Kinase-2 Inhibitor and Anticancer Agent. *PLoS ONE* **2013,** *8* (2), e56471.

19. Kharel, Y.; Raje, M.; Gao, M.; Gellett, A. M.; Tomsig, J. L.; Lynch, K. R.; Santos, W. L., Sphingosine Kinase type 2 Inhibition Elevates Circulating Sphingosine-1-Phosphate. *Biochem. J.* **2012,** *447* (1), 149–157.

20. Wang, Z.; Min, X.; Xiao, S.-H.; Johnstone, S.; Romanow, W.; Meininger, D.; Xu, H.; Liu, J.; Dai, J.; An, S.; Thibault, S.; Walker, N., Molecular Basis of Sphingosine Kinase 1 Substrate Recognition and Catalysis. *Structure* **2013,** *21* (5), 798–809.

21. Wang, J.; Knapp, S.; Pyne, N. J.; Pyne, S.; Elkins, J. M., Crystal Structure of Sphingosine Kinase 1 with PF-543. *ACS Med. Chem. Lett.* **2014,** *5* (12), 1329–1333.

22. Gustin, D. J.; Li, Y.; Brown, M. L.; Min, X.; Schmitt, M. J.; Wanska, M.; Wang, X.; Connors, R.; Johnstone, S.; Cardozo, M.; Cheng, A. C.; Jeffries, S.; Franks, B.; Li, S.; Shen, S.; Wong, M.; Wesche, H.; Xu, G.; Carlson, T. J.; Plant, M.; Morgenstern, K.; Rex, K.; Schmitt, J.; Coxon, A.; Walker, N.; Kayser, F.; Wang, Z., Structure Guided Design of a Series of Sphingosine Kinase (SphK) Inhibitors. *Bioorg. Med. Chem. Lett.* **2013,** *23* (16), 4608–4616.

23. Patwardhan, N. N.; Morris, E. A.; Kharel, Y.; Raje, M. R.; Gao, M.; Tomsig, J. L.; Lynch, K. R.; Santos, W. L., Structure−Activity Relationship Studies and *in Vivo* Activity of Guanidine-Based Sphingosine Kinase Inhibitors: Discovery of SphK1- and SphK2-Selective Inhibitors. *J. Med. Chem.* **2015,** *58* (4), 1879–1899.

24. Congdon, M. D.; Childress, E. S.; Patwardhan, N. N.; Gumkowski, J.; Morris, E. A.; Kharel, Y.; Lynch, K. R.; Santos, W. L., Structure–Activity Relationship Studies of the Lipophilic Tail Region of Sphingosine Kinase 2 Inhibitors. *Bioorg. Med. Chem. Lett.* **2015,** *25* (21), 4956–4960.

25. Congdon, M. D.; Kharel, Y.; Brown, A. M.; Lewis, S. N.; Bevan, D. R.; Lynch, K. R.; Santos, W. L., Structure–Activity Relationship Studies and Molecular Modeling of Naphthalene-Based Sphingosine Kinase 2 Inhibitors. *ACS Med. Chem. Lett.* **2016,** *7* (3), 229–234.

26. Kharel, Y.; Mathews, T. P.; Kennedy, A. J.; Houck, J. D.; Macdonald, T. L.; Lynch, K. R., A Rapid Assay for Assessment of Sphingosine Kinase Inhibitors and Substrates. *Anal. Biochem.* **2011,** *411* (2), 230–235.

27. Knott, K.; Kharel, Y.; Raje, M. R.; Lynch, K. R.; Santos, W. L., Effect of Alkyl Chain Length on Sphingosine Kinase 2 Selectivity. *Bioorg. Med. Chem. Lett.* **2012,** *22* (22), 6817–6820.

Chapter 5 Structure–Activity Relationship Studies of the Lipophilic Tail Region of Indole Derived Sphingosine Kinase 2 Inhibitors

5.1. Contributions

The work described in this chapter was conducted in collaboration with Dr. Yugesh Kharel, and Dr. Anne M. Brown. The author is solely responsible for the synthesis of all final compounds and the corresponding intermediate structures. All biological assays were conducted by Dr. Yugesh Kharel at the University of Virginia. All molecular modeling was conducted by Dr. Anne M. Brown in the Biochemistry Department at Virginia Tech. The final manuscript is currently being prepared by the author.

5.2. Abstract

A variety of diseases, including: Alzheimer's disease, sickle cell disease, asthma, cancer, and fibrosis, have been associated with elevated levels of sphingosine-1-phosphate (S1P). S1P is synthesized by the transfer of a phosphoryl group, catalyzed by the two isoforms of sphingosine kinase (SphK1 and SphK2). While SphK1 is the more studied isoform, the functional role of SphK2 is still emerging. Therefore, potent, selective small molecule inhibitors of SphK2 are necessary to aid in determining its physiological role in vivo. Previously, our group reported a Sphk2 selective inhibitor, **SLC5101465**, which displays approximately 111-fold selectivity for hSphK2 over hSphK1 and an hSphK2 K_i value of 0.09 μM. Herein, we report the design, synthesis, and biological evaluation of **SLC5101465** tail region derivatives. These compounds display good inhibition activity, excellent SphK2 selectivity. Our study highlights key electrostatic and steric interactions in the binding pocket.

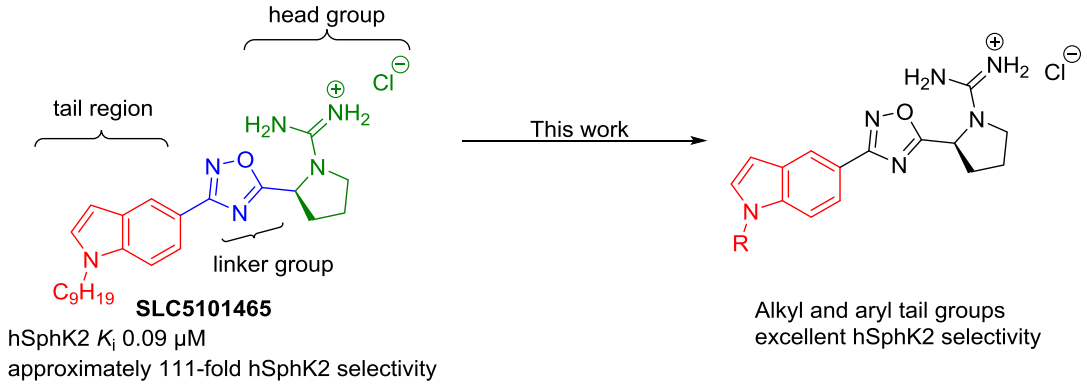

5.3. Introduction

Ceramide (Cer), sphingosine (Sph), and sphingosine-1-phosphate (S1P) are cellular signaling molecules formed from the catabolism of sphingolipids and have been shown to control cell growth and survival.[1-3] Studies have shown that Cer and Sph are pro-apoptotic metabolites. S1P causes cellular proliferation through intramolecular pathways and as a ligand to G-protein coupled receptors ($S1P_{1-5}$), which signal diverse physiological and pathophysiological processes[3-5]. The concentrations of these metabolites are regulated by their respective enzymes. Unfortunately, a plethora of diseases including: Alzheimer's disease, cancer, fibrosis, multiple sclerosis, and sickle cell disease have been correlated to the S1P signaling pathway and to over expression of S1P.[4, 6-11] As a result, the S1P pathway has attracted attention as a potential therapeutic target.[12] The druggability of this pathway was verified when Fingolimod (Gilenya®, **FTY720**), an $S1P_1$ receptor antagonist, was approved by the FDA in 2010 for the treatment of relapsing-remitting multiple sclerosis.[13-16]

A second route for targeting the S1P pathway and controlling *in vivo* levels of S1P is through the use of sphingosine kinase (SphK) inhibitors. S1P is formed solely by the ATP-dependent phosphorylation of Sph by SphK, which exists as two isoforms (SphK1 and SphK2).[17, 18] While these isoforms perform the same catalytic role, they differ in size and cellular localization. Furthermore, studies have proposed that SphK2 may have a secondary catalytic role beyond the phosphorylation of Sph.[19]

Many drug discovery ventures have targeted the development of SphK selective inhibitors; however, they have predominantly focused on SphK1.[20] As a result, there is a limited selection of SphK2 selective inhibitors. Examples of current SphK inhibitors are shown in Figure

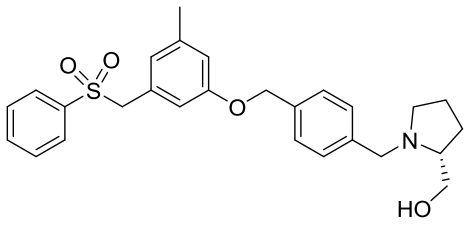

PF-543
K_i SphK1 3.6 nM
K_i SphK2 --
>100-fold SphK1 selective

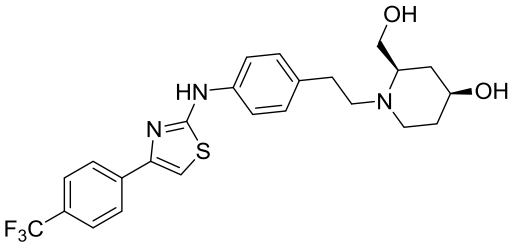

Amgen 82
SphK1 IC_{50} 0.01 μM
SphK2 IC_{50} 0.02 μM
dual inhibitor

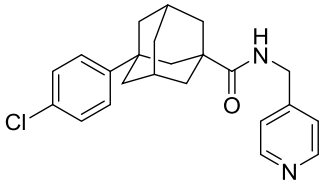

ABC294640
K_i SphK1 ---
K_i SphK2 9.8 μM
SphK2 selective

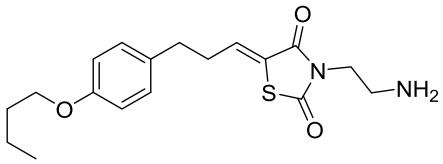

K145
K_i SphK1 ND
K_i SphK2 6.4 μM
SphK2 selective

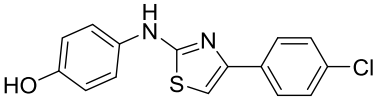

SKI-II
K_i hSphK1 16 μM
K_i hSphK2 7.9 μM
2-fold hSphK2 selective

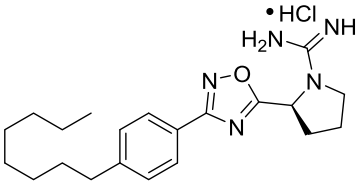

SLR080811
K_i hSphK1 16 μM
K_i hSphK2 1.4 μM
11-fold hSphK2 selective

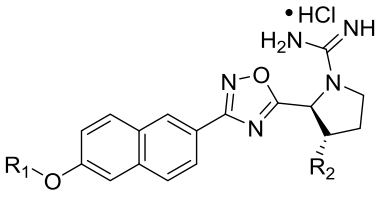

SLC5091592
R_1 = p-(CF_3)benzyl
R_2 = H
K_i hSphK1 >20 μM
K_i hSphK2 1.02 μM
> 20-fold hSphK2 selective

SLC5081308
R_1 = C_5H_{11}
R_2 = H
K_i hSphK1 0.98 μM
K_i hSphK2 7.2 μM
7-fold hSphK2 selective

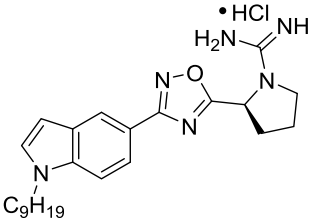

SLC5101465
K_i hSphK1 >10 μM
K_i hSphK2 0.09 μM
> 111-fold hSphK2 selective

SLC5111312
R_1 = C_5H_{11}
R_2 = OH
K_i hSphK1 0.73 μM
K_i hSphK2 0.90 μM
dual hSphK1/2 inhibitor

Figure 5.1. Selection of Current Sphingosine Kinase Inhibitors

5.1. In a mouse model of sickle cell disease was treated with the most potent SphK1 inhibitor to date (**PF-543**, K_i 3.5 nM, >100-fold SphK1 selective) decreased *in vivo* levels of S1P, which corresponded with decreased sickling of the red blood cells.[7] **SKI-II** (K_i = 17 μM), a nonselective inhibitor, has been shown to inhibit proliferation across a variety of cancer lines;[21] however, some of the **SKI-II** activity is due to off target effects with a proteasome that initiates degradation of SphK2.[22] Application of dual inhibitor Amgen **82**, the most potent dual inhibitor to date, was shown to reduce S1P levels as expected. When therapeutic concentrations of Amgen **82** were applied in a xenograft mouse model, no noticeable effect on cell viability was observed.[23] **ABC294640,** an analog of **SKI-II**, has a K_i value of 10 μM, and it has been shown to reduce proliferation in multiple cancer cell lines *in vitro*. **ABC294640** is currently undergoing phase I clinical trials for pancreatic cancer, unspecified solid tumors (NCT01488513) and refractory/relapsed diffuse large B-cell lymphoma (NCT02229981); however, data from the trials is yet to be released. [24, 25] To assist further understanding of the role of SphK2, rat and mouse models have been treated with second generation SphK inhibitors, **SLR080811** (SphK2 inhibitor) and **SLC5111312 (**dual inhibitor). These studies suggest that SphK2 may have a secondary role in the catalytic clearance of S1P from blood.[19, 26]

Our group strives to understand the role of SphK2 both *in vivo* and in diseased states. To that end, we focus on developing potent, selective SphK inhibitors and have identified essential structural requirements and interactions that must occur in the SphK2 binding pocket. Our first generation SphK2 inhibitor **SLR080811**, identified the need for structural components that can participate in hydrogen bonding.[27] In **SLR080811**, this structural component is a positively charged guanidine moiety. Further investigations of the **SLR080811** scaffold established a correlation between alkyl tail length and SphK2 potency and selectivity, as well as, the necessity

for an internal phenyl ring.[28] Additional investigations into the internal phenyl ring led to the discovery of a 2,6-naphthyl ether scaffold. Several inhibitors emerged from this structure-activity relationship (SAR): **SLC5081308** (K_i = 098 μM, 7-fold hSphK2 selective), **SLC5091592** (K_i = 1.02 μM, > 20-fold hSphK2 selective), **SLC121591** (K_i 0.61 μM, >16-fold hSphK2 selective) and **SLC5111312** (K_i = 0.90μM, dual h/rSphK1/2 inhibitor, 20-fold mSphK2 selective).[19, 29]

Molecular modeling studies revealed that increased π-stacking interactions between the naphthyl moiety and Phe548, and van der Waals interactions with Cys533, Tyr566 and His556 in the tail region of the binding pocket, were responsible for the increased SphK2 selectivity.[29] This study showed that the guanidine moiety participates in hydrogen bonding with Asp211 and Asp308. Moreover, it was found that increased bonding to Asp211 increases SphK selectivity. Likewise, increased SphK1 inhibition is observed with increased binding to Asp308, as seen with the 3′-hydroxyl on the pyrrolidine ring in **SLC5111312**.[29] Since crystal structures suggested a "J-shaped" bend in the SphK1 binding pocket, our next generation of compounds was designed to probe the internal bend within the binding pocket of SphK2.[30, 31] With the insight gained from the naphthalene series, we designed the SAR around an indole ring and varied the substitution pattern. The results of this study are discussed in detail in chapter 4; however, one key discovery was **SLC5101465** (K_i = 0.09 μM, 111-fold hSphK2 selective), which contained a 1,5-substituted indole moiety. Since aryl tail groups displayed equivalent or increased inhibition of SphK2 on the naphthalene scaffold, it was hypothesized that these groups may further enhance the potency of the 1,5-indole scaffold. Herein, we expand upon the 1,5-indole scaffold discussed in chapter 4 and describe our exploration of tail region derivatives of **SLC5101465**.

5.4. Synthesis of SLC5101465 Tail Derivatives

Since the most potent and selective indole scaffold was the 1,5-substituted scaffold, a series of non-aliphatic tail derivatives was created on the 1,5-indole scaffold. As shown in Scheme 5.1, the overall synthesis occurred in the same manner as the alkyl tail derivatives in chapter 4. Various alkyl halides were installed on common intermediate **4.3c** using NaH. The resulting intermediates **5.1a–k** were isolated in good yield. Boc-deprotection was achieved by bubbling HCl gas through methanol. The resulting pyrrolidines (**5.2a–k**) were subsequently reacted with DIEA and *N,N'*-di-Boc-1*H*-pyrazole-1-carboxamidine to generate intermediates **5.3a–k**. A final Boc-deprotection produced the final guanidine derivatives **5.4a–k**.

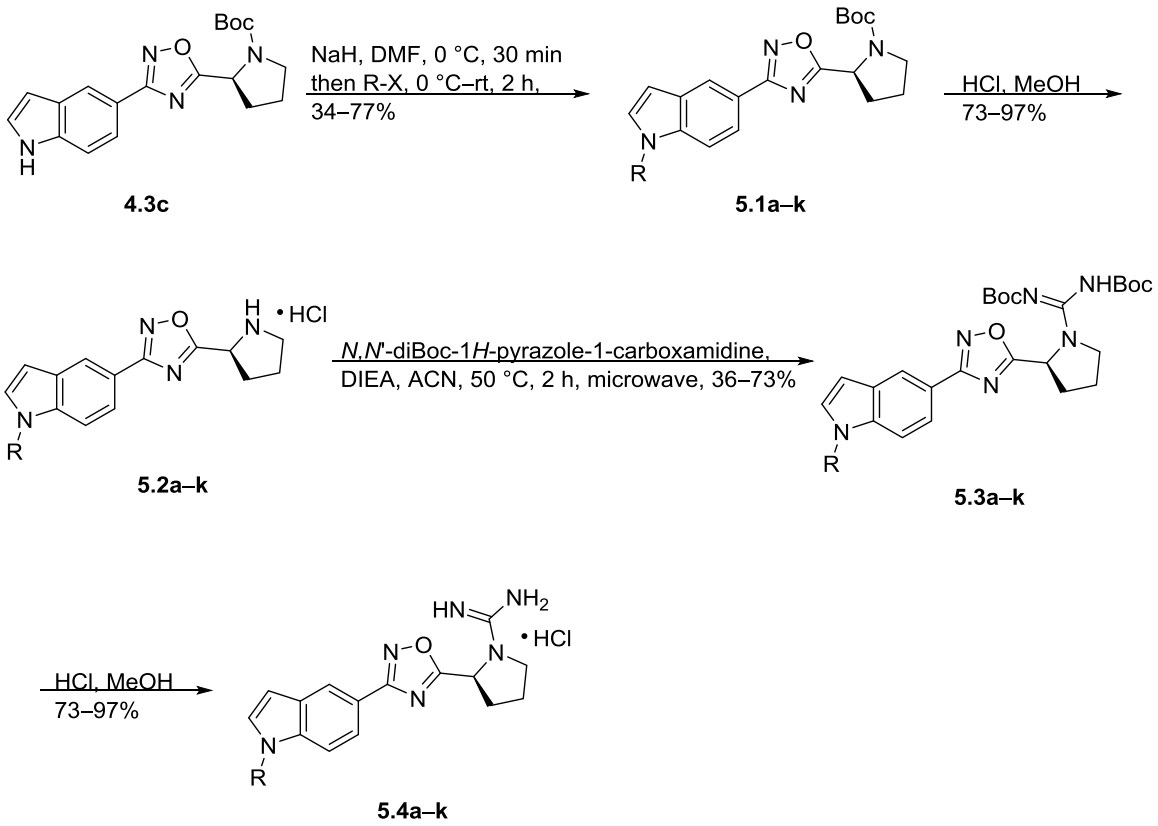

Scheme 5.1. Synthesis of SLC5101465 Tail Derivatives

5.5. Biological Evaluation

5.5.1. Initial Screening of SLC5101465 Tail Derivatives

Once the desired set of compounds had been synthesized, the inhibitory effects of the compounds were determined for human SphK1 and SphK2 (hSphK1and hSphK2) using a previously published protocol (Table 5.1).[32] In short, a cell lysate comprised of Sph, either recombinant hSphK1 or hSphK2, Sph and [γ-^{32}P]ATP were incubated for 20 minutes with or without inhibitor. After incubation, the mixtures were extracted and separated using thin layer chromatography. Liquid scintillation counting was employed to determine the amount of [γ-^{32}P-S1P] produced. Kinase inhibition was analyzed as the amount of [γ-^{32}P-S1P] produced as a function of inhibitor concentration. In this study, compounds were screened at 1 μM inhibitor concentrations. The results of this kinase inhibition screening are shown in Table 5.1.

Table 5.1. Inhibitory Effects of SLC5101465 Derivatives with hSphK1 and hSphK2[a]

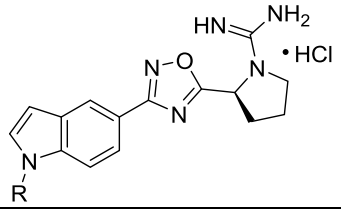

Entry	Compound	R	% SphK Activity[b]	
			hSphK1 (1 μM)	hSphK2 (1 μM)
1	**SLC5101465**	C_9H_{19}—*	103 ± 1	20 ± 1 (25 ± 3)
2	**5.4a**	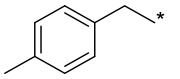	107 ± 3	71 ± 1 (90 ± 1)
3	**5.4b**	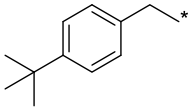	97 ± 3	66 ± 1 (85 ± 1)
4	**5.4c**	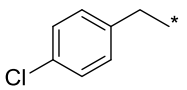	102 ± 1	62 ± 3 (80 ± 6)

		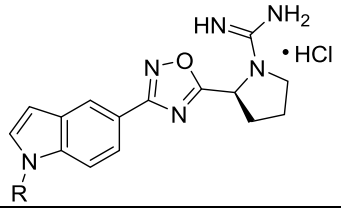		
5	**5.4d**	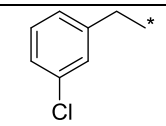	93 ± 3	51 ± 1 (70 ± 2)
6	**5.4e**	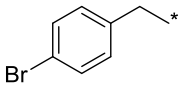	104 ± 2	50 ± 7 (65 ± 5)
7	**5.4f**	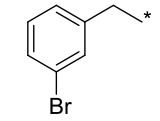	103 ± 2	62 ± 1 (80 ± 1)
8	**5.4g**	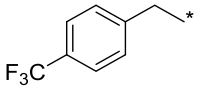	102 ± 1	63 ± 4 (85 ± 1)
9	**5.4h**	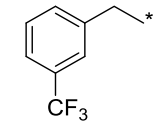	100 ± 3	57 ± 1 (75 ± 1)
10	**5.4i**	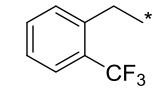	102 ± 5	62 ± 1 (81 ± 1)
11	**5.4j**	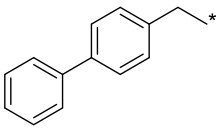	100 ± 2	36 ± 2 (51 ± 1)
12	**5.4k**	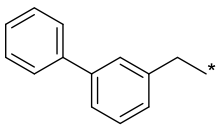	110 ± 5	41 ± 4 (55 ± 2)

[a]Values represent percent activity of human SphK1 or SphK2, with 10 and 5 μM Sph respectively, in the presence of 1 μM inhibitor. Each value is an average of two experiments. Lower SphK activity level indicates better inhibition. [b]Values in parenthesis indicate compounds assayed at 0.3 μM.

As shown in Table 5.1, a variety of substituted aryl moieties were employed as tail groups slightly reducing the lipophilicity of the compounds. The inhibitory activity of lead indole **SLC5101465** (**4.7s**, entry 1) is given for comparison. Interestingly, all of the compounds screened were inactive against hSphK1. This suggests that the selectivity of this scaffold arises

from π-stacking interactions of the 1,5-indole moiety and hydrogen bonding interactions between the guanidine moiety with Asp211 and Asp308 (as discussed in Chapter 4). Furthermore, these results emphasize the importance that interactions between the "tail group" and the amino acid residues in the bottom of the active site have on potency.

When the nonyl chain of **SLC5101465** was replaced with electron donating derivatives such as a *p*-methylbenzyl (**5.4a**) or a *p-tert*-butylbenzyl (**5.4b**) hSphK2 inhibition was decreased (entries 2–3). A series of electron withdrawing groups (chloro, bromo, and trifluoromethyl) were studied on the benzyl ring (entries 4–10). In general, these derivatives were able to reduce hSphK2 activity by 40–50%. Unlike previous studies, there is no observable trend between benzyl substitution (ortho, meta or para) and increased hSphK2 potency.[29] These derivatives are approximately 10% less potent than the 2,6-naphthyl analogs discussed in Chapter 3. It is possible that there are increased steric interactions between the aryl tail group and the binding pocket due to the gradual internal bend of the 1,5-indole scaffold compared to the linear naphthalene scaffold. The overall compound length of these derivatives is slightly shorter than the naphthalene analogs, suggesting the compounds are not large enough to establish the hydrophobic interactions with Cyc533, His556 and Tyr566 which have been previously reported.[29] When biphenyls were utilized, a substantial increase in hSphK2 potency was observed (entries 11-12). A 4-substituted biphenyl (**5.4j**) reduced hSphK2 activity by an additional 6% compared to the corresponding 3-substituted biphenyl (**5.4k**). The slight increase in hSphK2 activity between isomers could be caused by steric interactions in the binding pocket. These results support previous studies that indicate that the lipid binding pocket of SphK2 is larger than SphK1 and overall compound length plays a vital role in SphK2 potency.[28-30, 33]

Determination of K_i and cLogP Values

5.5.2. Determination of K_i and cLogP Values

Further characterization was conducted for compounds reducing enzyme activity by approximately 50% when tested at 0.3 μM. As shown in Table 5.2, two biphenyl derivatives **SLC5031698** (**5.4j**) and **SLC5031699** (**5.4k**) possess K_i values of > 5 μM for hSphK1 and K_i values of 0.0.28 μM and 0.30 μM for hSphK2. Both of these compounds display reduced hSphK2 selectivity and potency over **SLC5101465**. **SLC5031698** (**5.4j**) is over 18-fold hSphK2 selective, while **SLC5031699** (**5.4k**) is over 16-fold hSphK2 selective. It should be noted that the K_i values for hSphK1 have not been studied concentrations > 5 μM. As a result, it is assumed that the selectivity of these compounds is greater than those reported. In terms of pharmacokinetic parameters, the new inhibitors in Table 5.2 have lower cLogP values than **SLC5101465** (cLogP = 5.6).

Table 5.2. Inhibition Constants for Select Inhibitors

compound	K_i (μM)[a]		SphK2 selectivity	cLogP
	hSphK1	hSphK2		
SLC5101465	> 10	0.09 ± 0.01	> 111	5.6
SLC5031698 (5.4j)	> 5	0.28 ± 0.10	> 18	4.8
SLC5031699 (5.4k)	> 5	0.32 ± 0.15	> 16	4.8

[a] Inhibitory constants for recombinant enzymes were obtained by kinetic analysis of S1P production using variable concentration of sphingosine and a fixed concentration of ATP in the presence or absence of compounds as described previously.[34] Selectivity for each compound was determined by dividing the K_m SphK2 by the K_m of SphK1.

5.6. Molecular Modeling

To expand upon our knowledge of the binding interactions of exhibited by these indole derivatives, select compounds were docked in our previously reported homology model of hSphK2 which was generated from the published hSphK1 complexed with ADP and magnesium (PDB ID: 3VZB).[29] The most potent and hSphK2 selective structure (**5.4j**) was docked in the hSphK2 binding cavity, as well as, **5.4g** which incorporates the *p*-trifluoromethylbenzyl moiety found in the > 20-fold hSphK2 selective inhibitor **SLC5091592** (Chapter 3). As shown in Figure 5.2, the guanidine head group and indole ring of **5.4g** and **5.4j** occupy similar positions within the binding pocket. The structures maintain key electrostatic interactions and hydrogen bonding

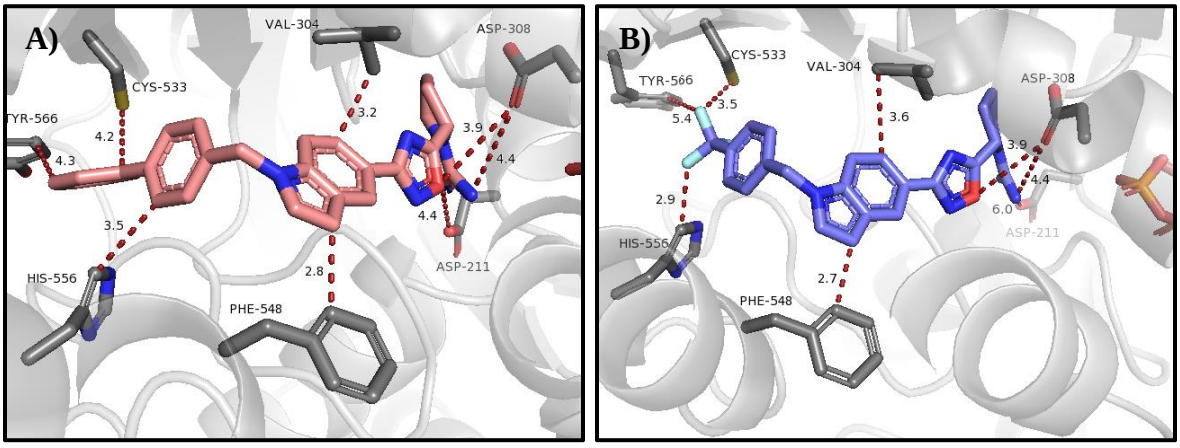

Figure 5.2. Docking of Inhibitors in the hSphK2 Homology Model. A) **SLC5031698** (**5.4j**-pink, hSphK2 K_i = 0.28 μM), B) **SLC5031602** (**5.4g**-blue, hSphK2 activity = 85% with 0.3 μM compound). hSphK2 is shown as a light grey cartoon with key amino acid residues labeled and shown as grey sticks. ATP is shown as green sticks (colored by element). Electrostatic interactions are indicated with red dashes. Magnesium is not shown for clarity.

with Asp211 and Asp308 and hydrophobic interactions with Val304 and Phe548 as previously reported with naphthalene-based inhibitor **SLC5101592** and 1,5-substituted indole inhibitor **SLC5101465**. Upon closer inspection, the difference in potency of **5.4g** and **5.4j** is due to slight differences in Asp binding and the binding of the different "tail groups" in the structures. **5.4j** participates in stronger binding to Asp211 and weak electrostatic interactions with Cys533, His556, and Tyr566, which cap the hydrophobic region of the binding pocket. The stronger binding to Asp211 may be the result of the longer biphenyl moiety causing the structure to sit slightly higher in the binding pocket. Conversely, **5.4g** exhibits comparable binding to Asp308 as **5.4j** and negligible binding to Asp211. Furthermore, the *p*-trifluoromethylbenzyl tail moiety of **5.4g** is able to participate in stronger electrostatic interactions with Cys533 and His556 than **5.4j**. Due to the decreased length the tail group of **5.4g** is further away from Tyr566, resulting in minimal electrostatic interactions. This data recapitulates the importance of binding to Asp211 and Asp308 for potency. Moreover, the data suggests that stronger binding in the hydrophobic pocket of hSphK2 may compensate for a slight loss of binding to the Asp residues.

5.7. Conclusions

In summary, a focused library of SphK2-selective inhibitor **SLC5101465** derivatives was synthesized. These compounds expand upon the 1,5-indole scaffold previously disclosed in chapter 4 by interrogating the lipophilic tail region of the pharmacophore. This study reiterates the preference for electron withdrawing groups to achieve optimal binding in the tail region of the binding pocket. Furthermore, our studies provide further support for a much larger lipophilic binding cavity in SphK2 over SphK1 since the benzyl substitution pattern displayed negligible effects on potency.

5.8. Acknowledgements

This work was achieved with financial support from the NIH (Grants R01 GM104366 and R01 GM067958).

5.9. Notes

The authors declare the following competing financial interest(s): W.L.S. and K.R.L. are among the co-founders of SphynKx Therapeutics LLC, which was created to commercialize S1P-related discoveries, including SphK inhibitors, discovered and characterized in their laboratories. The 17 compounds described in this manuscript are included in a patent application licensed to SphynKx.

5.10. References

1. Spiegel, S.; Milstein, S., Sphingosine-1-Phosphate: Signaling Inside and Out. *FEBS Lett.* **2000,** *476* (1–2), 55–57.
2. Spiegel, S.; Milstien, S., Sphingosine 1-Phosphate, a Key Cell Signaling Molecule. *J. Biol. Chem.* **2002,** *277* (29), 25851–25854.
3. Takabe, K.; Paugh, S. W.; Milstien, S.; Spiegel, S., "Inside-Out" Signaling of Sphingosine-1-Phosphate: Therapeutic Targets. *Pharmacol. Rev.* **2008,** *60* (2), 181–195.
4. Bigaud, M.; Guerini, D.; Billich, A.; Bassilana, F.; Brinkmann, V., Second Generation S1P Pathway Modulators: Research Strategies and Clinical Developments. *Biochim. Biophys. Acta.* **2014,** *1841* (5), 745–758.
5. Edmonds, Y.; Milstien, S.; Spiegel, S., Development of Small-Molecule Inhibitors of Sphingosine-1-Phosphate Signaling. *Pharmacol. Ther.* **2011,** *132* (3), 352–360.
6. Kunkel GT; Maceyka M; Milstien S; Spiegel., S., Targeting the Sphingosine-1-Phosphate Axis in Cancer, Inflammation and Beyond. *Nat. Rev. Drug Discov.* **2013,** *12* (9), 688–702.
7. Zhang, Y.; Berka, V.; Song, A.; Sun, K.; Wang, W.; Zhang, W.; Ning, C.; Li, C.; Zhang, Q.; Bogdanov, M.; Alexander, D. C.; Milburn, M. V.; Ahmed, M. H.; Lin, H.; Idowu, M.; Zhang, J.; Kato, G. J.; Abdulmalik, O. Y.; Zhang, W.; Dowhan, W.; Kellems, R. E.; Zhang, P.; Jin, J.; Safo, M.; Tsai, A. L.; Juneja, H. S.; Xia, Y., Elevated Sphingosine-1-Phosphate Promotes Sickling and Sickle Cell Disease Progression. *J. Clin. Invest.* **2014,** *124* (6), 2750–2761.
8. Takasugi, N.; Sasaki, T.; Suzuki, K.; Osawa, S.; Isshiki, H.; Hori, Y.; Shimada, N.; Higo, T.; Yokoshima, S.; Fukuyama, T.; Lee, V. M.; Trojanowski, J. Q.; Tomita, T.; Iwatsubo,

T., BACE1 Activity is Modulated by Cell-Associated Sphingosine-1-Phosphate. *J. Neurosci.* **2011,** *31* (18), 6850–6857.

9. Nagahashi, M.; Takabe, K.; Terracina, K. P.; Soma, D.; Hirose, Y.; Kobayashi, T.; Matsuda, Y.; Wakai, T., Sphingosine-1-Phosphate Transporters as Targets for Cancer Therapy. *BioMed Res. Int.* **2014,** *2014*, 651727.

10. Takuwa, N.; Du, W.; Kaneko, E.; Okamoto, Y.; Yoshioka, K.; Takuwa, Y., Tumor-Suppressive Sphingosine-1-Phosphate Receptor-2 Counteracting Tumor-Promoting Sphingosine-1-Phosphate Receptor-1 and Sphingosine Kinase 1. *Am. J. Cancer Res.* **2011,** *1*, 460–481.

11. Schwalm, S.; Pfeilschifter, J.; Huwiler, A., Sphingosine-1-phosphate: A Janus-Faced Mediator of Fibrotic Diseases. *Biochim. Biophys. Acta. Mol. Cell Biol. Lipids* **2013,** *1831* (1), 239–250.

12. Orr Gandy, K. A.; Obeid, L. M., Targeting the Sphingosine Kinase/Sphingosine-1-Phosphate Pathway in Disease: Review of Sphingosine Kinase Inhibitors. *Biochim. Biophys. Acta. Mol. Cell Biol. Lipids* **2013,** *1831* (1), 157–166.

13. Kappos, L.; Radue, E. W.; O'Connor, P.; Polman, C.; Hohlfeld, R.; Calabresi, P.; Selmaj, K.; Agoropoulou, C.; Leyk, M.; Zhang-Auberson, L.; Burtin, P., A Placebo-Controlled Trial of Oral Fingolimod in Relapsing Multiple Sclerosis. *N. Engl. J. Med.* **2010,** *362* (5), 387–401.

14. Cohen, J. A.; Barkhof, F.; Comi, G.; Hartung, H. P.; Khatri, B. O.; Montalban, X.; Pelletier, J.; Capra, R.; Gallo, P.; Izquierdo, G.; Tiel-Wilck, K.; de Vera, A.; Jin, J.; Stites, T.; Wu, S.; Aradhye, S.; Kappos, L., Oral Fingolimod or Intramuscular Interferon for Relapsing Multiple Sclerosis. *N. Engl. J. Med.* **2010,** *362* (5), 402–415.

15. Kihara, A.; Igarashi, Y., Production and Release of Sphingosine 1-Phosphate and the Phosphorylated Form of the Immunomodulator FTY720. *Biochim. Biophys. Acta. Mol. Cell Biol. Lipids* **2008,** *1781* (9), 496–502.

16. Schwalm, S.; Pfeilschifter, J.; Huwiler, A., Targeting the Sphingosine Kinase/Sphingosine-1-Phosphate Pathway to Treat Chronic Inflammatory Kidney Diseases. *Basic Clin. Pharmacol. Toxicol.* **2014,** *114* (1), 44–49.

17. Neubauer, H. A.; Pitson, S. M., Roles, Regulation and Inhibitors of Sphingosine Kinase 2. *FEBS J.* **2013,** *280* (21), 5317–5336.

18. Chan, H.; Pitson, S. M., Post-translational Regulation of Sphingosine Kinases. *Biochim. Biophys. Acta. Mol. Cell Biol. Lipids* **2013,** *1831* (1), 147–156.

19. Kharel, Y.; Morris, E. A.; Congdon, M. D.; Thorpe, S. B.; Tomsig, J. L.; Santos, W. L.; Lynch, K. R., Sphingosine Kinase 2 Inhibition and Blood Sphingosine 1-Phosphate Levels. *J. Pharmacol. Exp. Ther.* **2015,** *355*, 23–31.

20. Plano, D.; Amin, S.; Sharma, A. K., Importance of Sphingosine Kinase (SphK) as a Target in Developing Cancer Therapeutics and Recent Developments in the Synthesis of Novel SphK Inhibitors. *J. Med. Chem.* **2014,** *57* (13), 5509–5524.

21. French, K. J.; Upson, J. J.; Keller, S. N.; Zhuang, Y.; Yun, J. K.; Smith, C. D., Antitumor Activity of Sphingosine Kinase Inhibitors. *J. Pharmacol. Exp. Ther.* **2006,** *318* (2), 596–603.

22. Loveridge, C.; Tonelli, F.; Leclercq, T.; Lim, K. G.; Long, J. S.; Berdyshev, E.; Tate, R. J.; Natarajan, V.; Pitson, S. M.; Pyne, N. J.; Pyne, S., The Sphingosine Kinase 1 Inhibitor 2-(*p*-Hydroxyanilino)-4-(*p*-chlorophenyl)thiazole Induces Proteasomal Degradation of Sphingosine Kinase 1 in Mammalian Cells. *J. Biol. Chem.* **2010,** *285* (50), 38841–38852.

23. Rex, K.; Jeffries, S.; Brown, M. L.; Carlson, T.; Coxon, A.; Fajardo, F.; Frank, B.; Gustin, D.; Kamb, A.; Kassner, P. D.; Li, S.; Li, Y.; Morgenstern, K.; Plant, M.; Quon, K.; Ruefli-Brasse, A.; Schmidt, J.; Swearingen, E.; Walker, N.; Wang, Z.; Watson, J. E.; Wickramasinghe, D.; Wong, M.; Xu, G.; Wesche, H., Sphingosine Kinase Activity is Not Required for Tumor Cell Viability. *PLoS ONE* **2013,** *8* (7), e68328.

24. French, K. J.; Zhuang, Y.; Maines, L. W.; Gao, P.; Wang, W.; Beljanski, V.; Upson, J. J.; Green, C. L.; Keller, S. N.; Smith, C. D., Pharmacology and Antitumor Activity of ABC294640, a Selective Inhibitor of Sphingosine Kinase-2. *J. Pharmacol. Exp. Ther.* **2010,** *333*, 129–139.

25. Beljanski, V.; Knaak, C.; Smith, C. D., A Novel Sphingosine Kinase Inhibitor Induces Autophagy in Tumor Cells. *J. Pharmacol. Exp. Ther.* **2010,** *333* (2), 454–464.

26. Kharel, Y.; Mathews, Thomas, P.; Gellett, A., M.; Tomsig, J., L.; Kennedy,P., C.; Moyer, M., L.; Macdonald, T., L.; Lynch, K., R., Sphingosine Kinase Type 1 Inhibition Reveals Rapid Turnover of Circulating Sphingosine-1-Phosphate. *Biochem. J.* **2011,** *440* (3), 345–353.

27. Patwardhan, N. N.; Morris, E. A.; Kharel, Y.; Raje, M. R.; Gao, M.; Tomsig, J. L.; Lynch, K. R.; Santos, W. L., Structure−Activity Relationship Studies and *in Vivo* Activity of Guanidine-Based Sphingosine Kinase Inhibitors: Discovery of SphK1- and SphK2-Selective Inhibitors. *J. Med. Chem.* **2015,** *58* (4), 1879–1899.

28. Congdon, M. D.; Childress, E. S.; Patwardhan, N. N.; Gumkowski, J.; Morris, E. A.; Kharel, Y.; Lynch, K. R.; Santos, W. L., Structure–Activity Relationship Studies of the Lipophilic Tail Region of Sphingosine Kinase 2 Inhibitors. *Bioorg. Med. Chem. Lett.* **2015,** *25* (21), 4956–4960.

29. Congdon, M. D.; Kharel, Y.; Brown, A. M.; Lewis, S. N.; Bevan, D. R.; Lynch, K. R.; Santos, W. L., Structure–Activity Relationship Studies and Molecular Modeling of Naphthalene-Based Sphingosine Kinase 2 Inhibitors. *ACS Med. Chem. Lett.* **2016,** *7* (3), 229–234.

30. Wang, J.; Knapp, S.; Pyne, N. J.; Pyne, S.; Elkins, J. M., Crystal Structure of Sphingosine Kinase 1 with PF-543. *ACS Med. Chem. Lett.* **2014,** *5* (12), 1329–1333.

31. Wang, Z.; Min, X.; Xiao, S. H.; Johnstone, S.; Romanow, W.; Meininger, D.; Xu, H.; Liu, J.; Dai, J.; An, S.; Thibault, S.; Walker, N., Molecular Basis of Sphingosine Kinase 1 Substrate Recognition and Catalysis. *Structure* **2013,** *21* (5), 798–809.

32. Kharel, Y.; Mathews, T. P.; Kennedy, A. J.; Houck, J. D.; Macdonald, T. L.; Lynch, K. R., A Rapid Assay for Assessment of Sphingosine Kinase Inhibitors and Substrates. *Anal. Biochem.* **2011,** *411* (2), 230–235.

33. Knott, K.; Kharel, Y.; Raje, M. R.; Lynch, K. R.; Santos, W. L., Effect of Alkyl Chain Length on Sphingosine Kinase 2 Selectivity. *Bioorg. Med. Chem. Lett.* **2012,** *22* (22), 6817–6820.

34. Kharel, Y.; Raje, M.; Gao, M.; Gellett, A. M.; Tomsig, J. L.; Lynch, K. R.; Santos, W. L., Sphingosine Kinase Type 2 Inhibition Elevates Circulating Sphingosine-1-Phosphate. *Biochem. J.* **2012,** *447* (1), 149–157.

Chapter 6 Future Directions Towards the Development of Sphingosine Kinase Inhibitors

6.1. Introduction

As detailed in Chapter 1, a wide variety of diseases including: cancer, fibrosis, multiple sclerosis, Alzheimer's disease and sickle cell disease have been associated with dysregulation of sphingosine-1-phosphate (S1P) signaling pathways.[1-10] S1P is formed solely by the ATP-dependent phosphorylation of Sph by sphingosine kinases (SphK), which exists as two isoforms (SphK1 and SphK2).[11, 12] Although SphK1 and SphK2 perform the same catalytic role, they differ in size and cellular localization. Furthermore, SphK2 is involved in both proliferative and apoptotic pathways, as well as, a proposed secondary catalytic role associated with clearance of S1P from blood.[11, 13] Many drug discovery programs have concentrated on targeting the S1P pathway through the development of monoclonal antibodies, S1P receptor agonists and antagonists, and selective SphK inhibitors.[14-19]

The Santos group aims to further the understanding of the role of SphK2 both *in vivo* and in diseased states. As a result, the group focuses on developing potent, selective SphK inhibitors. Examples of current SphK inhibitors are shown in Figure 6.1. Over the years, essential structural requirements and interactions in the SphK2 binding pocket have been identified. Through investigations into a 2,6-naphthyl ether scaffold, several inhibitors including: **SLC5081308** , **SLC5091592**, **SLC5121591,** and **SLC5111312** were discovered (Chapter 3).[13, 17] Further investigations into indole derivatives with varied substitution patterns led to the key discovery of 1,5-substituted indole **SLC5101465** (Chapter 4). Molecular modeling studies with our hSphK2 homology model highlighted the importance of π-stacking interactions between the naphthyl moiety and Phe548, as well as, van der Waals interactions with Cys533, Tyr566 and His556, which cap the binding pocket, for the increased SphK2 selectivity.[17] The modeling also identified key hydrogen bonding interactions between the guanidine moiety and Asp211 and

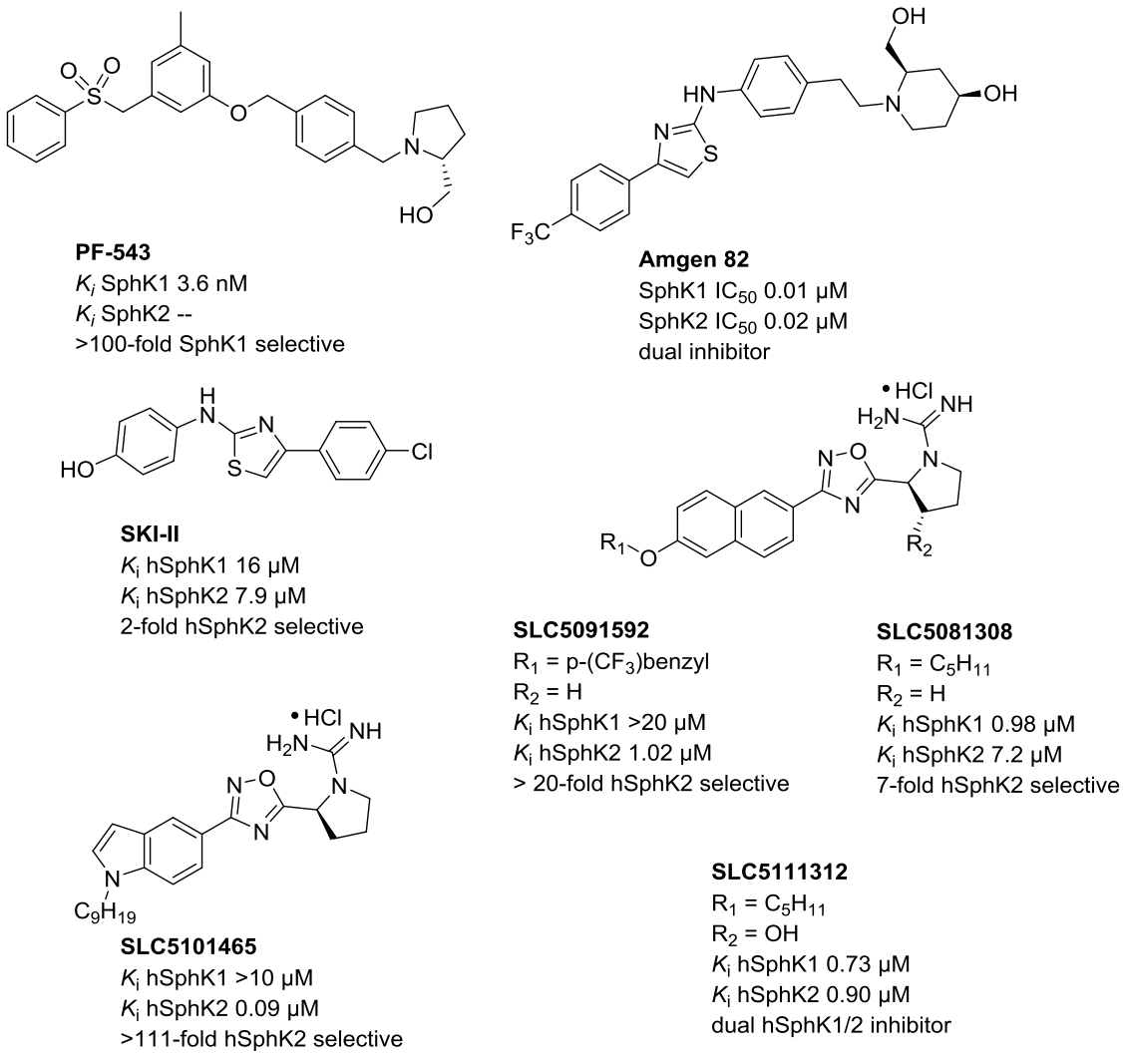

Figure 6.1. Select Sphingosine Kinase Inhibitors

Asp308. Specifically, it was found that increased bonding to Asp211 increases SphK2 selectivity, while increased binding to Asp308 led to elevated SphK1 inhibition.[17] Initial expansion upon the tail region of the 1,5-substitued indole scaffold (Chapter 5) highlighted the SphK2 selectivity of this scaffold and the importance of maintaining binding to Asp211 and Asp308, as well as, Cys533, His556 and Tyr566. Despite all of our advancements in the field of SphK inhibitors, improvements in potency (picomolar) and selectivity (> 200-fold) can still be

made. The following sections briefly discuss potential future directions for the indole scaffold and a new approach to utilizing molecular modeling.

6.2. 1,3-Substituted Indole Homologation

Chapter 4 focused on studying the effects of varying the substitution pattern around an indole ring on SphK potency and selectivity. One key discovery from this study was the unique binding mode of the 1,3-scaffold (Figure 4.2A). Molecular modeling of **SLC5101460** (Figure 6.2) indicated that the 1,3-scaffold is able to occupy the deepest region of the binding pocket to minimize steric interactions with Phe548, but is unable to participate in any type of electrostatic interactions with Asp211 and Asp 308. Extending the alkyl tail of docked **SLC5101460** by one methylene yielded **SLC5101463** which was able to reduce hSphK2 activity by an additional 10% with minimal inhibition of hSphK1 (Table 4.1). The increase in potency is attributed to better binding in the hydrophobic cavity of the hSphK2 binding pocket. It was hypothesized that homologation of **SLC5101460** would extend the guanidine moiety towards Asp211 and Asp308 and allow the moiety to participate in hydrogen bonding. As a result, **SLC5101572** was synthesized, and unfortunately, found to be inactive against hSphK1 and hSphK2 (Table 4.1).

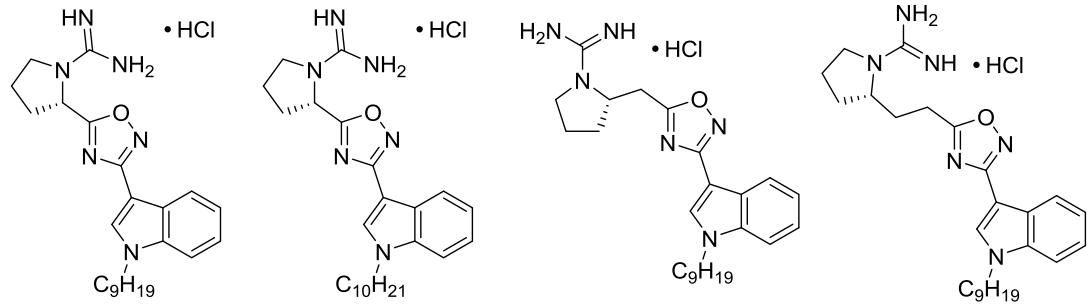

SLC5101460
hSphK1 activity 88%
with 1 μM compound
hSphK2 activity 59%
with 0.3 μM compound

SLC5101463
hSphK1 K_i > 10 μM
hSphK2 K_i 300 nM

SLC5101572
hSphK1 activity 98%
with 1 μM compound
hSphK2 activity 98%
with 0.3 μM compound

6.1
proposed structure

Figure 6.2. 1,3-Substituted Indole Inhibitors and Proposed Homologated Structure

Molecular docking of **SLC5101572** (Figure 4.2E) revealed steric interactions between the indole ring and Phe548 and the loss of electrostatic interactions with Cys533 and Tyr566. As a result of these observations, it is hypothesized that further homologation of **SLC5101572** via synthesis of **6.1** (Figure 6.2) would provide the extra length required to extend the guanidine moiety to within hydrogen bonding distance of Asp211 and Asp308, while simultaneously allowing the *N*-alkyl indole ring to sit deeper in the binding pocket to avoid steric interactions with Phe548.

6.3. Additional Indole Substitution Scaffolds

Another discovery from the SAR disclosed in Chapter 4 was the importance of a linear orientation between the indole tail substitution, 1,2,4,-oxadiazole linker, and guanidine head group (Table 4.3). The most potent and selective 1,5-substituted indole scaffold and the 2,6-naphthylene scaffold possess similar internal angles (168 ° and 170 °, respectively). As shown in Figure 6.3, a variety of indole scaffolds remain to be examined. First, tri-substituted 1,3,5-indole and 1,3,6-indole scaffolds can be tested. To maintain the overall internal bend of the structure between the head and tail groups, the larger tail moieties would occupy position R_1 on both scaffolds. A variety of small substituents, including but not limited to: methyl, ethyl, trifluoromethyl, and halides could potentially occupy the R_2 positions. Based on the molecular modeling of the indole scaffolds (Figure 4.2) and **SLM6031434** (data not shown) the R_2 groups must remain relatively small to minimize the potential for steric interactions with Val304 and Phe548.

Additional di-substituted indole scaffolds also remain to be investigated. As shown in Figure 6.3, these scaffolds include the 2,5-substituted indole, 2,6-substituted indole and 3,6-substituted indole scaffolds. The 3,6-substituted scaffold should maintain a relatively similar

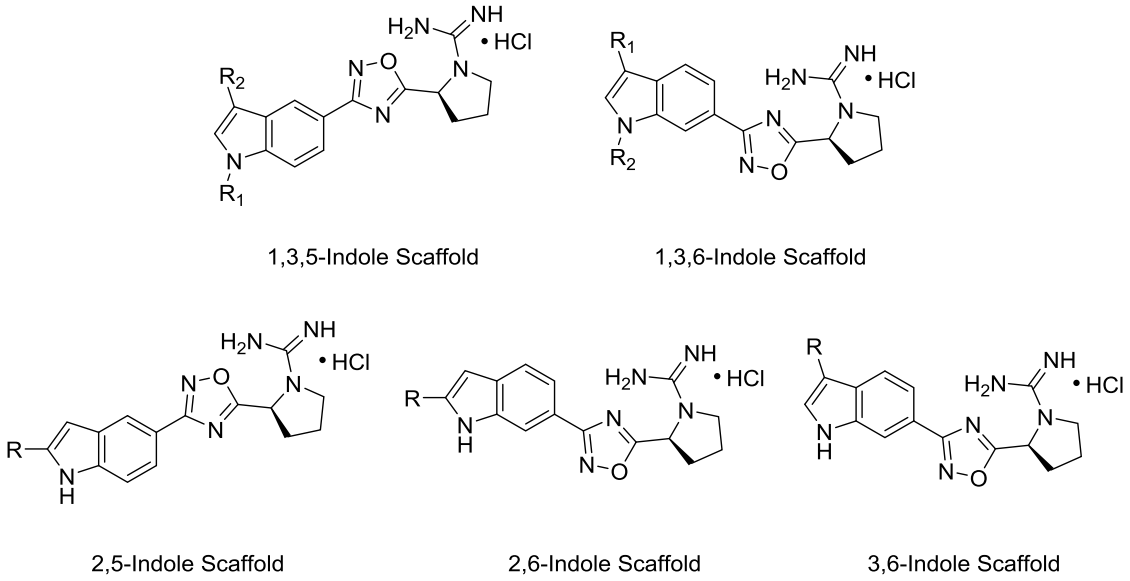

Figure 6.3. Additional Indole Substitution Scaffolds

internal angle to the 1,5-substituted indole scaffold reported in Chapter 4; however, the angle of the 2,5-substituted and 2,6-substituted scaffolds will be slightly decreased. These scaffolds will help narrow the optimal internal angle range in the scaffold and binding pocket. Furthermore, indole nitrogen of these two proposed scaffolds is unsubstituted. This alteration enables the nitrogen to potentially participate in hydrogen bonding interactions such as those reported with amino-thiazole inhibitor **SKI-II** in hSphK1.[20] Furthermore, this modification may take advantage of structural differences in between the binding pockets of hSphK1 and hSphK2 and provide unique insights into imparting SphK1 or SphK2 selectivity within the compounds. Overall, these proposed scaffolds would allow for further probing of important interactions in the internal region of the hSphK2 binding pocket. The knowledge gained from these compounds will aid in the development of novel hSphK1 and hSphK2 selective and dual inhibitors.

6.4. Further Indole Tails Modifications

In addition to examining new substitutions around the indole moiety, new "tail groups" can be examined. Previous studies from our group have highlighted the importance of the tail

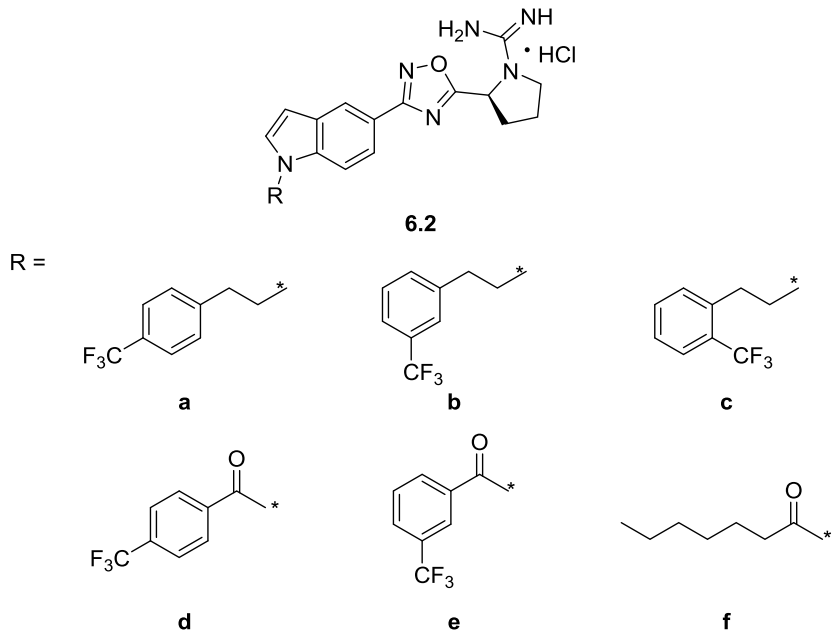

Figure 6.4. Further Tail Modifications to the SLC5101465 Scaffold

region to compound potency.[17, 21, 22] Figure 6.4 shows the remaining modifications to be incorporated in the tail region SAR of **SLC5101465** discussed in Chapter 5. These compounds are in the process of being remade for characterization purposes and rescreening. The modifications of **6.2a–c** provide further extension of the tail region by one methylene unit. This extension should provide improved electrostatic binding between the tail region of the compounds and terminal amino acid residues Cys533, His556 and Tyr566 of the hydrophobic binding pocket of SphK2. Furthermore, altering the substitution of the trifluoromethyl group will provide a greater chance for optimal binding in the binding pocket. Additionally, **6.2a–f** will allow for additional interrogation of steric and electronic interactions in the binding pocket.

Additional proposed tail modifications are shown in Figure 6.5. These modifications would extend the aromatic region of the compound further into the tail region. Various di-substituted indole scaffolds are shown in Figure 6.5 for visual aid. Proposed tail modifications include isomers of oxadiazole and amino thiazole rings, as well as, mono and di-substituted

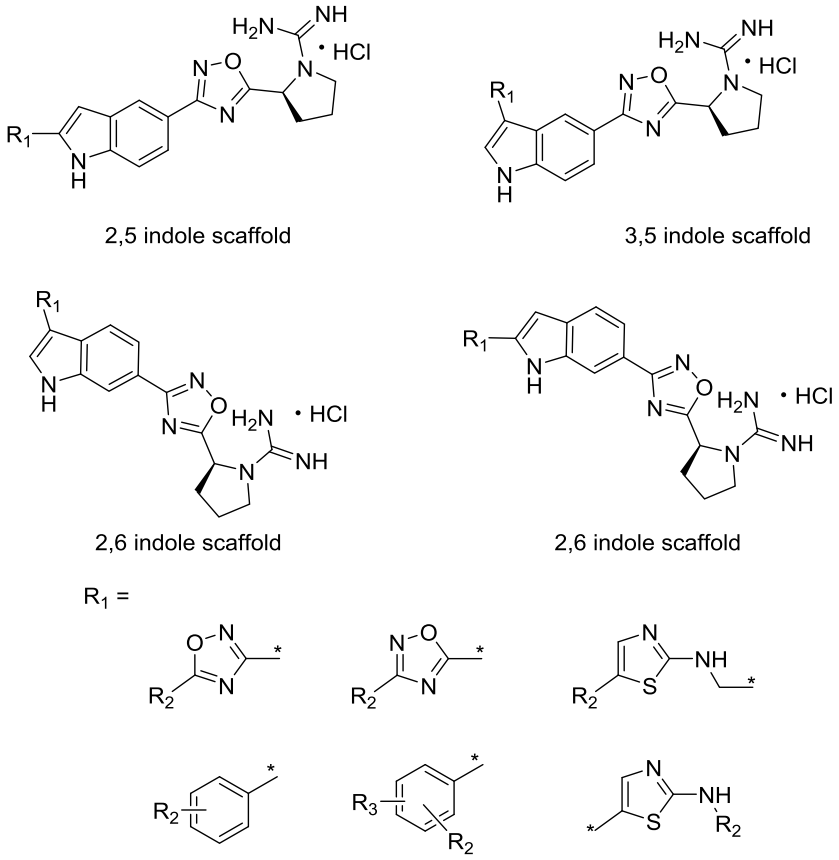

Figure 6.5. Further Tail Modifications to the Indole Scaffolds

phenyl rings. The R_2 groups shown in the proposed modifications can include but is not limited to: alkyl, alkenyl, alkynyl, alkoxy, halogens or halogenated alkanyl substituents depending upon the specific structure. Incorporation of these proposed modifications could lead to stronger electrostatic interactions with Cyc533, His556, Tyr566 and other residues in the binding pocket. Moreover, the incorporation of secondary amines and the unsubstituted indole nitrogen, which can act as hydrogen bond donors, could lead to increase hydrogen bonding in the binding pocket.

6.5. Incorporation of a "New" 2-hydroxymethylpyrrolidine Head Group

Over the years our research group has made substantial advancements in the development of SphK2 selective inhibitors and many of these are discussed in this dissertation; however, there

remains a need to develop potent, slightly SphK1 selective inhibitors. These inhibitors would be valuable tools for determining the tipping point of elevating or lowering blood S1P levels *in vivo*. To this end the group has begun to employ a "new" 2-hydroxymethylpyrrolidine head group on our scaffold. This head group has been previously employed in SphK1 selective **PF543** and a series of compounds published from the Bittman lab.[23, 24]

Last year, I proposed incorporating this 2-hydroxymethylpyrrolidine head group on the indole and naphthalene scaffolds to allow for easy comparison between this new moiety and the guanidine head group previously employed in our research group (Figure 6.6). Initial investigations incorporated alkyl tail groups; however, the compounds did not display any potency or selectivity for hSphK1 or hSphK2 (data not shown). Since the new scaffolds do not incorporate the 1,2,4-oxadiazole ring or an alternate moiety to maintain consistent overall compound length, it is hypothesized that the decreased potency and selectivity is the result of reduced π-stacking interactions with Phe548 and increased steric interactions binding pockets. Molecular modeling and further SAR studies are need to verify this hypothesis. To further verify this hypothesis, it is proposed that the "new" head group be incorporated on a 2,5-substituted indole scaffold where the tail group is located at the 2-position (Figure 6.6). This substitution pattern would increase the linearity of the structure and reduce any potential steric interaction caused by the *N*-substituted (1,5-substituted) indole scaffold. Moreover, the unsubstituted indole nitrogen on the proposed 2,5-substituted indole scaffold could potentially participate in electrostatic interactions or hydrogen bonding.

Although this 2-hydroxymethylpyrrolidine has been incorporated in SphK1 selective inhibitors, our group has shown that interactions in the tail region of the binding pocket can drastically alter selectivity and/or potency. As a result, the R group shown on these new scaffolds

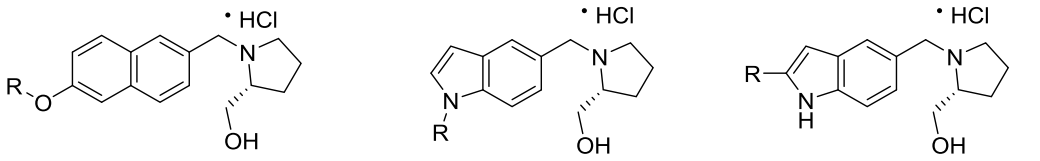

2,6-Naphthalene scaffold with 2-hydroxymethylpyrrolidine head group

1,5-indole scaffold with 2-hydroxymethylpyrrolidine head group

2,5-indole scaffold with 2-hydroxymethylpyrrolidine head group

Figure 6.6. Proposed Naphthalene and Indole Scaffolds with a 2-hydroxymethyl-pyrrolidine Head Group

can include but is not limited to: alkyl, alkenyl, alkynyl, alkoxy, halogens, halogenated alkanyl, mono, di or triphenyl substituents depending upon the specific structure. Initial investigations into the tail regions of these scaffolds should incorporate tail moieties previously identified by our group to provide potent or selective inhibitors such as trifluoromethylbenzyl derivatives, as well as any required modifications to account for the altered overall compound length due to the loss of the oxadiazole linker.

6.6. Molecular Modeling

The crystal structure of SphK1 was finally obtained and published in 2013.[20] This development signaled beginning of a new era of SphK inhibitor development. Proposed structures can now be docked in a molecular model of SphK1 to assessed and ranked on their ability to be potent and selective inhibitors. The disclosure of the SphK1 crystal structure also allowed for the development SphK2 homology models which can be utilized in a similar manner. To maximize future inhibitor development in the Santos lab, a ranking system, based on key interactions in the binding pocket, needs to be developed for both the SphK1 and SphK2 models currently used by our collaborators, and verified by docking previously reported SphK inhibitors. Common trends in the location of electron-donating, electron-withdrawing, aromatic, hydrogen-bond donating, hydrogen-bond accepting, and sterically bulky groups can also be identified. Once this system has been developed, any proposed structures or scaffolds can be quickly

screened for potency and selectivity. This new approach to inhibitor design would save time and money typically spent on SAR development, since only promising compounds would be synthesized.

6.7 Conclusions

In conclusion, a variety of novel substituted indole scaffolds are proposed. Compound **6.1** may lead to the development of a more potent hSphK2 selective inhibitor. Conversely, the new proposed indole scaffolds have the potential to participate in new modes of binding which will further illuminate key interactions in the binding pockets of hSphK1 and hSphK2. By increasing our understanding of the crucial differences between the binding pockets of hSphK1 and hSphK2 that impart isoform selectivity, we will be able to rationally design better inhibitors. Additionally, these modifications may lead to the development of more potent dual and selective SphK inhibitors, enhancing the tools available for use in biological studies. Through the development of better inhibitors, we can further elucidate the roles and importance of SphK1 and SphK2 in various diseases, as well as, the role of SphK2 during homeostasis and its hypothesized involvement in S1P clearance from blood.

6.7. References

1. Kunkel G. T; Maceyka M; Milstien S; Spiegel, S., Targeting the Sphingosine-1-Phosphate Axis in Cancer, Inflammation and Beyond. *Nat. Rev. Drug Discov.* **2013,** *12* (9), 688–702.
2. Zhang, Y.; Berka, V.; Song, A.; Sun, K.; Wang, W.; Zhang, W.; Ning, C.; Li, C.; Zhang, Q.; Bogdanov, M.; Alexander, D. C.; Milburn, M. V.; Ahmed, M. H.; Lin, H.; Idowu, M.; Zhang, J.; Kato, G. J.; Abdulmalik, O. Y.; Zhang, W.; Dowhan, W.; Kellems, R. E.; Zhang, P.; Jin, J.; Safo, M.; Tsai, A. L.; Juneja, H. S.; Xia, Y., Elevated Sphingosine-1-Phosphate Promotes Sickling and Sickle Cell Disease Progression. *J. Clin. Invest.* **2014,** *124* (6), 2750–2761.
3. Takasugi, N.; Sasaki, T.; Suzuki, K.; Osawa, S.; Isshiki, H.; Hori, Y.; Shimada, N.; Higo, T.; Yokoshima, S.; Fukuyama, T.; Lee, V. M.; Trojanowski, J. Q.; Tomita, T.; Iwatsubo, T., BACE1 Activity is Modulated by Cell-Associated Sphingosine-1-Phosphate. *J. Neurosci.* **2011,** *31* (18), 6850–6857.
4. Nagahashi, M.; Takabe, K.; Terracina, K. P.; Soma, D.; Hirose, Y.; Kobayashi, T.; Matsuda, Y.; Wakai, T., Sphingosine-1-Phosphate Transporters as Targets for Cancer Therapy. *BioMed Res. Int.* **2014**, 651727.
5. Takuwa, N.; Du, W.; Kaneko, E.; Okamoto, Y.; Yoshioka, K.; Takuwa, Y., Tumor-Suppressive Sphingosine-1-Phosphate Receptor-2 Counteracting Tumor-Promoting Sphingosine-1-Phosphate Receptor-1 and Sphingosine Kinase 1. *Am. J. Cancer Res.* **2011,** *1*, 460–481.

6. Bigaud, M.; Guerini, D.; Billich, A.; Bassilana, F.; Brinkmann, V., Second Generation S1P Pathway Modulators: Research Strategies and Clinical Developments. *Biochim. Biophys. Acta.* **2014,** *1841* (5), 745–758.

7. Schwalm, S.; Pfeilschifter, J.; Huwiler, A., Sphingosine-1-phosphate: A Janus-faced mediator of fibrotic diseases. *Biochim. Biophys. Acta. Mol. Cell Biol. Lipids* **2013,** *1831* (1), 239–250.

8. Haughey, N. J.; Bandaru, V. V. R.; Bai, M.; Mattson, M. P., Roles for Dysfunctional Sphingolipid Metabolism in Alzheimer's Disease Neuropathogenesis. *Biochim. Biophys. Acta.* **2010,** *1801* (8), 878–886.

9. Kosicek, M.; Hecimovic, S., Phospholipids and Alzheimer's Disease: Alterations, Mechanisms and Potential Biomarkers. *Int. J. Mol. Sci.* **2013,** *14* (1), 1310–1322.

10. Walter, S.; Faßbender, K., Spingolipids in Multiple Sclerosis. *Cell. Physiol. Biochem.* **2010,** *26* (1), 49–56.

11. Neubauer, H. A.; Pitson, S. M., Roles, Regulation and Inhibitors of Sphingosine Kinase 2. *FEBS J.* **2013,** *280* (21), 5317–5336.

12. Chan, H.; Pitson, S. M., Post-Translational Regulation of Sphingosine Kinases. *Biochim. Biophys. Acta. Mol. Cell Biol. Lipids* **2013,** *1831* (1), 147–156.

13. Kharel, Y.; Morris, E. A.; Congdon, M. D.; Thorpe, S. B.; Tomsig, J. L.; Santos, W. L.; Lynch, K. R., Sphingosine Kinase 2 Inhibition and Blood Sphingosine 1-phosphate Levels. *J. Pharmacol. Exp. Ther.* **2015,** *355*, 23–31.

14. Plano, D.; Amin, S.; Sharma, A. K., Importance of Sphingosine Kinase (SphK) as a Target in Developing Cancer Therapeutics and Recent Developments in the Synthesis of Novel SphK Inhibitors. *J. Med. Chem.* **2014,** *57* (13), 5509–5524.

15. Santos, W. L.; Lynch, K. R., Drugging Sphingosine Kinases. *ACS Chem. Biol.* **2015,** *10* (1), 225–233.

16. Patwardhan, N. N.; Morris, E. A.; Kharel, Y.; Raje, M. R.; Gao, M.; Tomsig, J. L.; Lynch, K. R.; Santos, W. L., Structure−Activity Relationship Studies and *in Vivo* Activity of Guanidine-Based Sphingosine Kinase Inhibitors: Discovery of SphK1- and SphK2-Selective Inhibitors. *J. Med. Chem.* **2015,** *58* (4), 1879–1899.

17. Congdon, M. D.; Kharel, Y.; Brown, A. M.; Lewis, S. N.; Bevan, D. R.; Lynch, K. R.; Santos, W. L., Structure–Activity Relationship Studies and Molecular Modeling of Naphthalene-Based Sphingosine Kinase 2 Inhibitors. *ACS Med. Chem. Lett.* **2016,** *7* (3), 229–234.

18. Orr Gandy, K. A.; Obeid, L. M., Targeting the Sphingosine Kinase/Sphingosine-1-Phosphate Pathway in Disease: Review of Sphingosine Kinase Inhibitors. *Biochim. Biophys. Acta. Mol. Cell Biol. Lipids* **2013,** *1831* (1), 157–166.

19. Sanllehí, P.; Abad, J.-L.; Casas, J.; Delgado, A., Inhibitors of Sphingosine-1-Phosphate Metabolism (Sphingosine Kinases and Sphingosine-1-Phosphate Lyase). *Chem. Phys. Lipids* **2016,** *197*, 69–81.

20. Wang, Z.; Min, X.; Xiao, S.-H.; Johnstone, S.; Romanow, W.; Meininger, D.; Xu, H.; Liu, J.; Dai, J.; An, S.; Thibault, S.; Walker, N., Molecular Basis of Sphingosine Kinase 1 Substrate Recognition and Catalysis. *Structure* **2013,** *21* (5), 798–809.

21. Knott, K.; Kharel, Y.; Raje, M. R.; Lynch, K. R.; Santos, W. L., Effect of Alkyl Chain Length on Sphingosine Kinase 2 Selectivity. *Bioorg. Med. Chem. Lett.* **2012,** *22* (22), 6817–6820.

22. Congdon, M. D.; Childress, E. S.; Patwardhan, N. N.; Gumkowski, J.; Morris, E. A.; Kharel, Y.; Lynch, K. R.; Santos, W. L., Structure–Activity Relationship Studies of the Lipophilic Tail Region of Sphingosine Kinase 2 Inhibitors. *Bioorg. Med. Chem. Lett.* **2015,** *25* (21), 4956–4960.

23. Wang, J.; Knapp, S.; Pyne, N. J.; Pyne, S.; Elkins, J. M., Crystal Structure of Sphingosine Kinase 1 with PF-543. *ACS Med. Chem. Lett.* **2014,** *5* (12), 1329–1333.

24. Baek, D. J.; MacRitchie, N.; Anthony, N. G.; Mackay, S. P.; Pyne, S.; Pyne, N. J.; Bittman, R., Structure–Activity Relationships and Molecular Modeling of Sphingosine Kinase Inhibitors. *J. Med. Chem.* **2013,** *56* (22), 9310–9327.

Chapter 7 Experimental and Characterization for Chapters 2–5

7.1 Chemistry

7.1.1 Materials

All reagents were purchased from commercial sources and used without further purification. Solvents were purchased from commercial sources and dried with 4.0 Å molecular sieves. Reactions conducted in the microwave were completed in a Biotage Initiator+. Flash chromatography was performed on silica gel (Zeoprep 60 ECO, 43- 60 μM) using either a Combiflash Rf or Biotage Isolera purification system and TLC on silica gel 200μM, F254.

7.1.2 Instrumentation

^{1}H NMR spectra were obtained with either a Bruker Avance-II 500 MHz, Agilent 400-MR 400 MHz, or an Agilent U4-DD2-400 MHz spectrometer. Chemical shifts are reported in ppm with the solvent resonance as the internal standard ($CDCl_3$: 7.26 ppm, CD_3OD:3.31 ppm). Data are reported as follows: chemical shift, multiplicity (s = singlet, d = doublet, t = triplet, q = quartet, p = pent-let, m = multiplet), coupling constants (Hz), and integration. ^{13}C NMR spectra were obtained on either a Bruker Avance-II 500 MHz (125 MHz), Agilent 400-MR (101 MHz), or an Agilent U4-DD2-400 MHz (101 MHz) spectrometer. Chemical shifts are reported in ppm with the solvent resonance as the internal standard ($CDCl_3$: 77.16 ppm, CD_3OD: 49.00 ppm). ^{19}F NMR spectra were obtained on either an Agilent 400-MR (376 MHz) or an Agilent U4-DD2-400 (376 MHz) spectrometer. High resolution mass spectra (HRMS) were performed on an Agilent LC-ESI-TOF or a Shimadzu Qp-5000MS attached to a GC17A gas chromatography instrument. Low resolution mass spectra and HPLC traces were obtained with a Thermo Electron TSQ triple quadrupole mass spectrometer equipped with and ESI source. Chiral purity analysis was performed on a Waters Acquity UPC2 system.

7.1.3 Calculations of clogP and cLogD values

The cLogP values for key compounds were determined using ChemDraw Professional 15.0 with the protonated species of the final products.

The cLogD for key compounds was calculated using MarvinSketch 15.9.14 software and the consensus logP method. Electrolyte concentrations were set at 0.1. Due to the potential resonance in the guanidine moiety, tautomerization/ resonance was taken into consideration in the calculations.

7.1.4 Methodology for Determining Chiral HPLC Spectra for Compounds 3.7i and 3.7j

Chiral purity of compounds **3.7i** and **3.7j** was determined using Ultra High Performance Supercritical fluid chromatography (UHPSFC). Previously published diastereomers **BD22** and **SLM120702** were used as standards to optimize separation. Experiments were performed using a Waters Acquity UPC2 system (Milford, MA, USA) equipped with a high pressure mixing binary solvent delivery manager, a fixed loop design autosampler, an active back pressure regulator, column compartment with active heating and column switching control, photodiode array (PDA) and evaporative light scattering (ELS) detectors. The experiment was carried out using an ACQUITY UPC² TrefoilT CEL1, 2.5µm column at a temperature of 25°C. The mobile phase consisted of compressed CO_2 as mobile phase A and 99.75% methanol with 0.25% isopropyl alcohol as mobile phase B. The mobile phase flow rate was maintained at 1–2 mL/min with a gradient of 5% B to 95% B over 12 minutes and held at 5% B for 2 minutes to equilibrate the column to the initial condition. The backpressure was maintained isobarically by the active backpressure regulator (ACQUITY CCM) at a pressure of 1500 psi. The injection volume was varied 1–2 µL for PDA and ELSD. The photodiode array detection was monitored at a

wavelength range 190–400 nm with reference of 400–500 nm. The Waters ACQUITY ELSD detector was operated with nebulizer cooling, drift tube: 50 °C, gas pressure: 40 psi and gain 10, make up flow (isopropyl alcohol) was added at 0.2 mL/min before ELSD.

7.1.5 Deuterium Exchange on the *N*-alkyl Indole Scaffold

Verification of hydrogen-deuterium exchange of the proton at the C3 position of the final indole salts (**4.14a–d, 4.21a–e, 4.28a–d** and **5.4a–k**) in a deuterated polar protic solvent under acidic conditions was completed with a time study. Immediately following sample preparation of **5.4c** in CD_3OD, a ^{1}H-NMR was taken. Additional spectra obtained taken every 15 minutes for the following 5 hours, after which point spectra were obtained every 30 minutes for the following 15 hours. For comparative purposes, the signal at δ 5.44, which includes the chiral proton and the methylene protons, was used as an internal standard with the integration set to 3 protons. As shown in Table 7.1, during the course of this time study, the intensity of the C3 proton signal was reduced by 50% indicating that the deuterium exchange occurs. Based on observations with the rate at which the deuterium exchange occurs is dependent upon the concentration of acid present in the sample. Samples that were not meticulously washed with diethyl ether multiple times, displayed faster rates of deuterium exchange compared to samples that were only washed the standard two–three times. For a direct visualization of deuterium exchange, a plot of the indole C3 peak integration is shown in Figure 7.1 and select spectra are overlaid in Figure 7.2. The results of this study indicate that the C3 proton of the 1,4-substituted, 1,5-substituted and 1,6-substituted indole scaffolds can undergo a deuterium-hydrogen exchange when exposed to a deuterated polar protic solvent and under highly acidic conditions for an extended period of time.

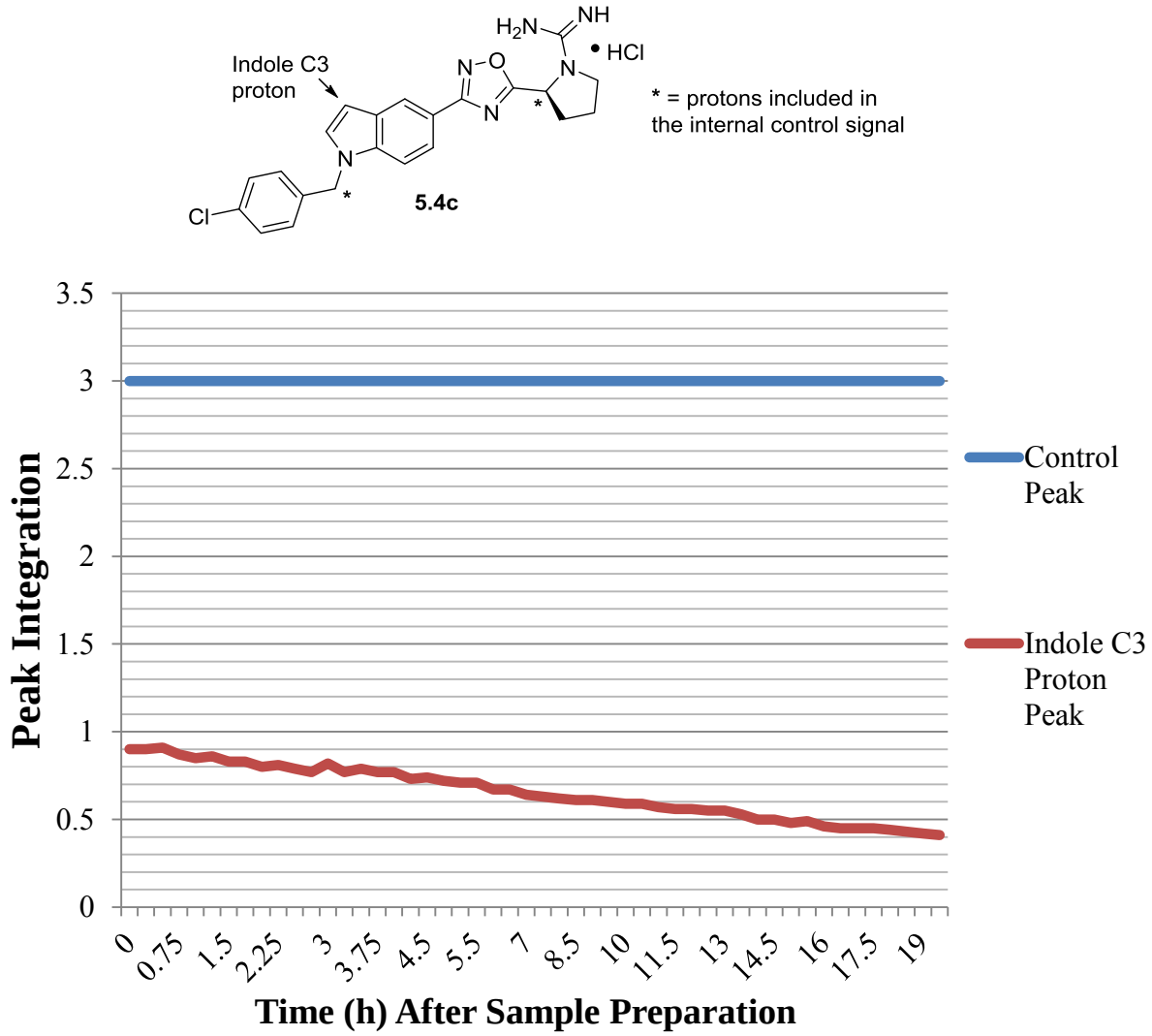

Figure 7.1. Plot of the Deuterium–Hydrogen Exchange of Indole C3 Proton

Table 7.1. Results from the Deuterium–Hydrogen Exchange Time Study

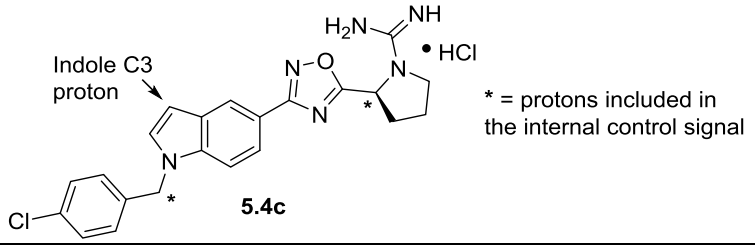

5.4c

entry	Time (hours) after sample preparation	Integration of Control Peak (δ 5.44)	Integration of C3 proton (δ 6.64)
1	0	3.00	0.90
2	0.25	3.00	0.90
3	0.5	3.00	0.91
4	0.75	3.00	0.87
5	1	3.00	0.85
6	1.25	3.00	0.86
7	1.5	3.00	0.83
8	1.75	3.00	0.83
9	2	3.00	0.80
10	2.25	3.00	0.81
11	2.5	3.00	0.79
12	2.75	3.00	0.77
13	3	3.00	0.82
14	3.25	3.00	0.77
15	3.5	3.00	0.79
16	3.75	3.00	0.77
17	4	3.00	0.77
18	4.25	3.00	0.73
19	4.5	3.00	0.74
20	4.75	3.00	0.72
21	5	3.00	0.71
22	5.5	3.00	0.71
23	6	3.00	0.67
24	6.5	3.00	0.67
25	7	3.00	0.64
26	7.5	3.00	0.63
27	8	3.00	0.62
28	8.5	3.00	0.61
29	9	3.00	0.61
30	9.5	3.00	0.60
31	10	3.00	0.59
32	10.5	3.00	0.59
33	11	3.00	0.57
34	11.5	3.00	0.56
35	12	3.00	0.56

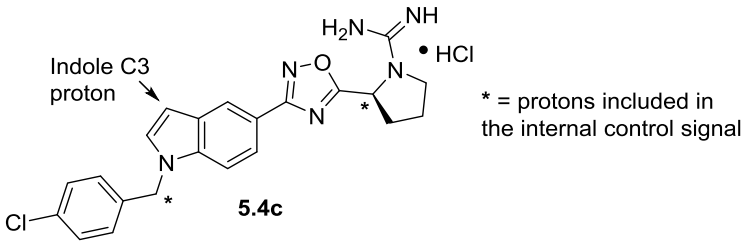

5.4c

entry	Time (hours) after sample preparation	Integration of Control Peak (δ 5.44)	Integration of C3 proton (δ 6.64)
36	12.5	3.00	0.55
37	13	3.00	0.55
38	13.5	3.00	0.53
39	14	3.00	0.50
40	14.5	3.00	0.50
41	15	3.00	0.48
42	15.5	3.00	0.49
43	16	3.00	0.46
44	16.5	3.00	0.45
45	17	3.00	0.45
46	17.5	3.00	0.45
47	18	3.00	0.44
48	18.5	3.00	0.43
49	19	3.00	0.42
50	19.5	3.00	0.41

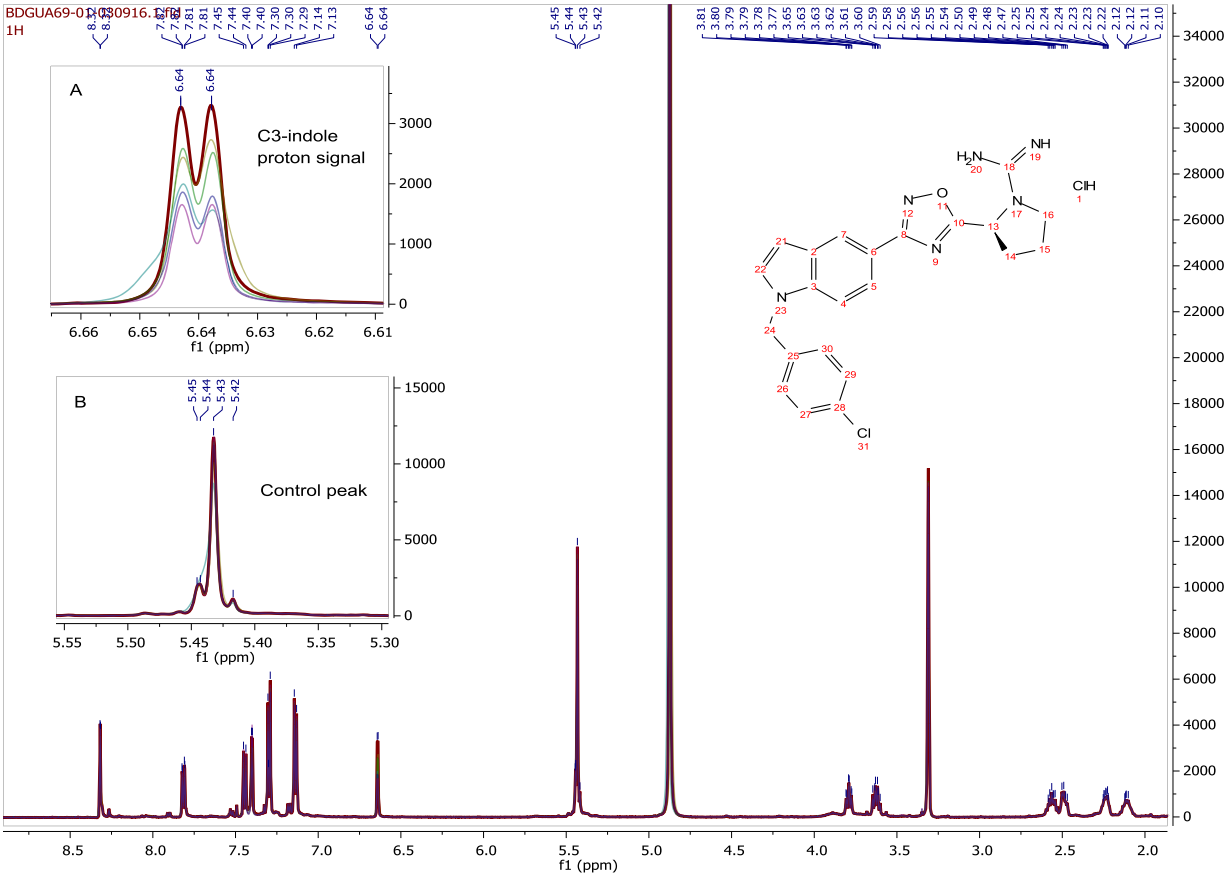

Figure 7.2. Overlay of Spectra Highlighting the Deuterium-Hydrogen Exchange at the Indole C3 Position. Overlay includes entries 1, 10, 20, 30, 40 and 50 of Table 7.1 (colored red, through purple respectively). Insert A shows the decreasing intensity of the indole C3 proton signal. Insert B shows that no substantial variation occurred in the peak which was used as the internal control.

7.1.6 General Synthetic Procedures for Chapter 2

General Procedure 2.1 – Sonogashira Cross-coupling

Alkyne (2 equiv.) and TEA (5 equiv.) were added to a round bottom flask containing **2.1a**, **2.3a** or **2.8** (1 equiv.) in DMF (20 vol/wt) under N_2. The reaction mixture was degassed for 30 minutes by passing N_2 to remove oxygen. To the above solution were added CuI (0.03 equiv.) and $PdCl_2(PPh_3)_2$ (0.05 equiv.) and the reaction mixture was stirred at 80 °C for 18 hours. The reaction mixture was poured into a solution of LiBr and extracted with EtOAc. The combined organic solution was washed with NH_4Cl, brine, dried over Na_2SO_4, filtered and concentrated under reduced pressure. The resulting residue was purified by flash chromatography over silica gel to yield the corresponding product **2.1b,c, 2.7**, **2.9a,b**.

General Procedure 2.2 - Hydroboration and Suzuki Cross-coupling

Alkene (1.4 equiv.) was placed into a N_2 flushed round bottom flask along with 0.5M 9-BBN-H in THF (1.4 equiv.). The mixture was stirred at room temperature overnight. **2.1a** (1 equiv.) was dissolved in DMF with Cs_2CO_3 (2 equiv.) and the solution was degassed for 15 minutes. The THF reaction mixture was transferred via cannula into the DMF containing flask and the solution was degassed for an additional 15 minutes. $Pd(dppf)Cl_2$ (0.3 equiv.) was added to the reaction mixture and followed by a final 5 minute period of degassing. The reaction mixture was heated to 70 °C for 8–12 hours. The reaction mixture was poured into a solution of LiBr and extracted with EtOAc. The combined organic solution was washed with NH_4Cl, brine, dried over Na_2SO_4, filtered and concentrated under reduced pressure. The resulting residue was purified by flash chromatography over silica gel to yield the corresponding product **2.1d,e.**

General Procedure 2.3 – Amidoxime Formation

Nitrile **2.1a–e, 2.20, 2.27,** or **2.34a–c** (1 equiv.), $HONH_2$•HCl (3 equiv.), TEA (3 equiv.) were added to a round bottom flask containing 190 proof ethanol. The reaction mixture was heated to 80 °C for 6–18 hours and monitored via TLC. Once TLC indicated that the starting material was consumed, the solution was cooled to room temperature, concentrated under reduced pressure, loaded onto Celite and purified on a silica column with hexanes and EtOAc to yield pure product **2.2a–e, 2.21, 2.28,** or **2.35a–c.**

General Procedure 2.4 – 1,2,4-Oxadiazole Formation with HCTU

Amidoxime (**2.2a–e, 2.21, 2.28,** or **2.35a**) (1 equiv.), Boc-*L*-proline (1.4 equiv.) or Boc-*L*-azetidine (1.4 equiv.), and DIEA (1.4 equiv.) were added to a round bottom flask containing DMF. HCTU (1.8 equiv.) was added to the reaction solution, the flask was connected to a reflux condenser and heated to 120 °C for 12–16 hours. Once the reaction cooled to room temperature, the solution was extracted with EtOAc and saturated LiBr solution. The combined organic layers were washed with brine and dried over Na_2SO_4. After filtration to remove the Na_2SO_4 and concentration via reduced pressure, the resulting brown oil was purified on a silica column with hexanes and EtOAc to yield pure product **2.3a–e, 2.8, 2.22, 2.29** or **2.36a**.

General Procedure 2.5 – Boc-Deprotection

Boc-amine **2.3a–f, 2.9c–g, 2.22, 2.29, 2.36a–c** or **Di-Boc-guanidine 2.5a,d–h, 2.11c–g, 2.16a–d, 2.24, 2.31, 2.39a–c** was dissolved in MeOH. HCl gas was bubbled into the solution for 1 minute. The solution was stirred until TLC indicated that all of the Boc-protected amine had been consumed. The solvent was removed under reduced pressure. The resulting white to light yellow solid was washed with Et_2O to yield pure product. In instances where the neutral amine

was isolated, the acidic MeOH was neutralized to pH 10. The product was extracted with Et_2O which was removed under reduced pressure. This procedure produced products **2.4a–f, 2.6a,d–h, 2.10c–g, 2.12c–g, 2.17a–d, 2.23, 2.25, 2.30, 2.32, 2.38a–c, 2.40a–c.**

General Procedure 2.6 – Guanylation of Secondary Amines

Hydrogen chloride salt **2.10c–g, 2.15a–d, 2.23, 2.30, 2.38a–c** or amine **2.4a,d–h,** (1 equiv.) was added to a round bottom flask with CH_3CN and DIEA (3 equiv.). The solution was allowed to stir for 10 minutes before the addition of *N*,*N*′-di-Boc-1*H*-pyrazole-1-carboxamidine (1.05 equiv.). The solution was stirred at room temperature, under N_2 for three days. The solvent was removed under reduced pressure. The resulting residue was purified on a silica column with hexanes and EtOAc as the eluent to yield pure product **2.5a,d–h, 2.11c–g, 2.16a–d, 2.24, 2.31, 2.39a–c**.

General Procedure 2.7 – Reduction of Alkynes with 4-toluenesulfonyl hydrazide

To a solution of the alkyne (**2.4a,c, 2.7,** or **2.9a,b**) (1 equiv) in DME (20 vol/wt) were added 4-methylbenzenesulfonohydrazide (10 equiv) and TEA (5 equiv). The resulting reaction mixture was refluxed overnight, until complete consumption of starting alkyne was observed. The reaction was quenched by addition of water. The product was extracted using Et_2O, the organics were combined, dried over anhydrous Na_2SO_4 and concentrated under reduced pressure to yield a pale yellow oil which was purified by flash chromatography over silica gel to yield corresponding product **2.3f, 2.4g,h,** or **2.9f,g.**

General Procedure 2.8 – Buchwald-Hartwig coupling

Amine (4.5 equiv.) was added to a round bottom containing **2.3a** or **2.8** (1 equiv.) in toluene. The reaction mixture was degassed for 10 min by bubbling N_2 through the solution. Cs_2CO_3 (1.1 equiv.), $P(^tBu)_3$ (0.4 equiv.), and $Pd_2(dba)_3$ (0.08 equiv.) were added together. The resulting reaction mixture was then stirred at 100 ^oC for 24 h, after which it was poured into water and extracted three times with EtOAc. The combined organic extracts were washed with brine, dried over Na_2SO_4 and concentrated under reduced pressure. The resulting brown residue was purified by flash chromatography over silica gel, with 5–20% MeOH in DCM as the eluent, to give the desired compounds **2.9d,e**, and **2.13a,b.**

General Procedure 2.9 – Amide coupling

BnBr (7 equiv.) or acid chloride (18 equiv.) was added to a round bottom containing **2.13a** or **2.13b** (1 equiv.) and TEA (1.6 equiv.) in DCM which had been cooled to 0 ºC. The reaction mixture was then warmed to room temperature and stirred for 17 h. The organic solvent was removed under reduced pressure and the residue was purified by silica gel column chromatography with 30–50% EtOAc in hexanes as the eluent to yield pure product **2.14a–d.**

General Procedure 2.10 – Boc-Deprotection with TFA

Boc-amine **2.14a–d** was dissolved in DCM and TFA (4 equiv.) was added to the solution. The solution was stirred until TLC indicated that all of the Boc-protected amine had been consumed. The solvent was removed under reduced pressure. The resulting white to light yellow solid was washed with Et_2O to yield pure product **2.15a–d**.

General Procedure 2.11 – S_N2 reaction to Install Nitrile

Alkyl halide (**2.33a–c**) (1 equiv.) and 9:1 ethanol:water were added to a round bottom flask. KCN (3 equiv.) was added to the solution. The reaction was refluxed at 80°C for 18 hours and cooled to room temperature. After removing the EtOH under reduced pressure, the aqueous layer was extracted with EtOAc. The combined organic layers were washed with brine and dried over Na_2SO_4. The crude product was purified on a silica column using 0–10% EtOAc in hexanes to yield pure product **2.34a–c**.

General Procedure 2.12 – HCTU Coupling

Compound **2.35b** or **2.35c** (1 equiv.), Boc-*L*-proline (1 equiv.), and HCTU (1 equiv.) were suspended in DCM (15 mL). DIEA (4 equiv.) was added dropwise to the reaction mixture. The reaction mixture was stirred for 4 hours at room temperature. The solvent was removed under reduced pressure and the resulting residue was purified on a silica column in 40–80% EtOAc in hexanes to yield pure product **2.37b** or **2.37c.**

General Procedure 2.13 – Cyclization and Dehydration with TBAF

To a solution of **2.37b** or **2.37c** (1 equiv.) in THF (10 mL) was added a 0.1 M solution of TBAF in THF (1 equiv.). The solution was stirred at room temperature for 1 hour. The solvent was removed under reduced pressure. The resulting residue was purified on a silica column using 10–40% EtOAc in hexanes to yield pure product, **2.36b** or **2.36c**.

7.1.7 General Synthetic Procedures for Chapter 3

General Procedure 3.1 – Williamson Ether Synthesis

6-Hydroxy-2-napthalnitrile **3.1** (1 equiv.), K_2CO_3 (4 equiv.) and alkyl halide or TsCl (1.2 equiv.) were added to a round bottom flask containing CH_3CN. The reaction mixture was heated to 80 °C for 4–12 hours until TLC indicated the starting material had been fully consumed. The reaction mixture was extracted with EtOAc and D.I. water. The combined organic layers were washed with brine and dried over Na_2SO_4. After filtration and concentration via reduced pressure, the resulting brown oil was purified on a silica column with hexanes and EtOAc as the eluent to yield pure product **3.2a**–**h**.

General Procedure 3.2 – Amidoxime Formation

Nitrile **3.2a**–**h** (1 equiv.), hydroxylamine hydrochloride (3 equiv.), and TEA (3 equiv.) were added to a round bottom flask containing EtOH. The reaction mixture was heated to 80 °C for 6–12 hours and monitored via TLC. Once the starting material was consumed, the solution was cooled to room temperature, concentrated under reduced pressure, loaded onto Celite, and purified on a silica column with hexanes and EtOAc as the eluent to yield pure product **3.3a**–**h**.

General Procedure 3.3 – 1,2,4-Oxadiazole Formation with HCTU

Amidoxime (**3.3a**–**h**) (1 equiv.), Boc-*L*-proline (1.4 equiv.) or (3*S*)-hydroxy-Boc-*L*-proline (1.4 equiv.), and DIEA (1.4 equiv.) were added to a round bottom flask containing DMF. HCTU (1.8 equiv.) was added to the reaction mixture, the flask was connected to a reflux condenser and heated to 120 °C for 12–16 hours. Once the reaction cooled to room temperature, the solution was extracted with EtOAc and saturated LiBr solution. The combined organic layers were washed with brine and dried over Na_2SO_4. After filtration to remove the Na_2SO_4 and

concentration via reduced pressure, the resulting brown oil was purified on a silica column with hexanes and EtOAc as the eluent to yield pure product **3.4a**–**j**.

General Procedure 3.4 – Boc-Deprotection

Boc-amine **3.4a**–**j** or di-Boc-guanidine **3.6a**–**j** was dissolved in MeOH. HCl gas was bubbled into the solution for 1 minute. The solution was stirred until TLC indicated that the starting material had been consumed. The solvent was removed under reduced pressure. The resulting white to light yellow solid was washed with Et_2O to yield pure product **3.5a**–**j** or **3.7a**–**j**.

General Procedure 3.5 – Guanylation of Secondary Amines

Compound **3.5a**–**j** (1 equiv.) was added to a round bottom flask containing CH_3CN and DIEA (3 equiv.). The solution was allowed to stir for 10 minutes before the addition of *N*,*N*′-di-Boc-1*H*-pyrazole-1-carboxamidine (1.05 equiv.). The solution was stirred at room temperature under N_2 until TLC indicated that the starting material had been consumed. The solvent was removed under reduced pressure and the resulting residue was purified on a silica column with hexanes and EtOAc as the eluent to yield pure product **3.6a**–**j.**

General Procedure 3.6 – Boc-Deprotection in Microwave

Boc-protected **3.9** or di-Boc-guanidine **3.6n–q** was dissolved in a 4N HCl in dioxane solution (3 equiv.). The solution was heated to 100 °C for 1 minute in the microwave. The solvent was removed under reduced pressure. The resulting white to light yellow solid was washed with Et_2O to yield pure product **3.10** or **3.7n–q**.

General Procedure 3.7 – Williamson Ether Synthesis in Microwave

Di-Boc-guanidine **3.11** or Boc-pyrrolidine **3.9** (1 equiv.), K_2CO_3 (2 equiv.) alkyl halide (1.2 equiv.), and NaI (0.1 equiv.) were added to a microwave vial containing EtOH. The reaction mixture was heated to 100 °C for 15 minutes. The solvent was removed under reduced pressure and the resulting residue was extracted with EtOAC and D.I. water. The combined organic layers were washed with brine and dried over Na_2SO_4. After filtration and concentration via reduced pressure, the resulting residue was purified on a silica column with hexanes and EtOAc as the eluent to yield pure product **3.6k–ab** and **3.12**.

General Procedure 3.8 – Trifluoroacetic Acid Boc-Deprotection

Di-Boc-guanidine **3.11** or **3.6k–m, r–ab** was dissolved in DCM. TFA (3 equiv.) was added to a round bottom flask and stirred at room temperature for 2 hours. The solvent was removed under reduced pressure. The resulting white to light yellow solid was washed with Et_2O to yield pure product **3.7k–m, r–ac**.

7.1.8 General Synthetic Procedures for Chapter 4

General Procedure 4.1: Amidoxime Formation

Cyanoindole **4.1**, **4.8**, **4.15**, **4.22** or **4.29** (1 equiv.) and $HONH_2$•HCl (3 equiv.), and TEA (3 equiv.) were added to a round bottom flask containing EtOH. The reaction mixture was heated to 80 °C for 12 hours or until the reaction appeared to have gone to completion via monitoring by TLC. The solution was cooled to room temperature and the solvent was removed under reduced pressure. The resulting solid was loaded onto Celite and purified on a silica gel column with 0–10% MeOH in EtOAc as the eluent to produce product **4.2**, **4.9**, **4.16**, **4.23**, or **4.30**.

General Procedure 4.2: 1,2,4-Oxadiazole Formation

Amidoxime **4.2**, **4.9**, **4.16**, **4.23**, or **4.30**. (1 equiv.), Boc-*L*-Proline or (3*S*)-hydroxy-Boc-*L*-Proline (1.4 equiv.), and DIEA (1.4 equiv.) were added to a round bottom flask containing DMF. After adding HCTU (1.8 equiv.) to the reaction, the solution was heated to 120 °C for 12–16 hours. Once the reaction cooled to room temperature, the solution was extracted with EtOAc and saturated LiBr solution. The combined organic layers were washed with brine and dried over Na_2SO_4. After filtration to remove the Na_2SO_4 and concentration via reduced pressure, the resulting brown oil was purified on a silica column with hexanes and EtOAc as the eluent to produce **4.3**, **4.10**, **4.17**, **4.24**, or **4.31**.

General Procedure 4.3: *N*-alkylation of Indole

Indole **4.3**, **4.10**, **4.15**, **4.17**, or **4.24** was added to a round bottom flask which was subsequently purged with N_2 and sealed with a rubber septum. The flask was placed in an ice bath and DMF (1 mL) was added. NaH (1.5 equiv.) was added to the flask in one addition and the septum was replaced on the vessel. The reaction mixture was stirred for 30 minutes at 0 °C and the ice bath was replenished. Alkyl halide (3 equiv.) was added to the cooled solution drop-wise. Liquid alkyl halides were added neat while solid alkyl halides were dissolved in 0.5 mL of DMF. The reaction solution was stirred for an additional 2 hours while the solution warmed to room temperature. The reaction was quenched with the slow addition of D.I. water. The product was extracted with EtOAc and saturated LiBr. The combined organic layers were washed with brine, dried over Na_2SO_4, filtered and concentration via reduced pressure. The resulting oil was purified on a silica column with hexanes and EtOAc as the eluent to yield pure product **4.4a–f**, **4.11a–d**, **4.18a–e**, **4.25a–d**, or **4.29**.

General Procedure 4.4: Boc-deprotection with HCl

Boc-amine **4.4a–f**, **4.11a–d**, **4.18a–e**, **4.25a–d**, or **4.31** or di-Boc-guanidine **4.6a–f**, **4.13a–d**, **4.20a–e**, **4.27a–d**, or **4.33** was dissolved in MeOH. HCl gas was bubbled into the solution for 1 minute. The solution was stirred until TLC indicated that the starting material had been consumed. The solvent was removed under reduced pressure. The resulting white to light yellow solid was washed with Et_2O to yield pure product **4.5a–f**, **4.12a–d**, **4.19a–e**, **4.26a–d**, **4.32**, **4.7a–f**, **4.14a–d**, **4.21a–e**, **4.28a–d**, or **4.34**.

General Procedure 4.5: Guanylation of Secondary Amines

Salt **4.5a–f**, **4.12a–d**, **4.19a–e**, **4.26a–d**, or **4.32** (1 equiv.) was added to a round bottom flask with CH_3CN and DIEA (3 equiv.). The solution was allowed to stir for 10 minutes before being transferred to a microwave vial containing *N*,*N*′-di-Boc-1*H*-pyrazole-1-carboxamidine, (1.05 equiv.). The vessel was capped and placed in a CEM microwave where it was heated to 50 °C for 2 hours. The solvent was removed under reduced pressure and the resulting yellow oil was purified on silica gel with hexanes and EtOAc as the eluent to yield pure product **4.6a–f**, **4.13a–d**, **4.20a–e**, **4.27a–d**, or **4.33**.

7.1.9 General Procedures for Chapter 5

General Procedure 5.1 – *N*-Alkylation of Indole

Indole **4.3e** was added to a round bottom flask which was subsequently purged with N_2 and sealed with a rubber septum. The flask was placed in an ice bath and DMF (1 mL) was added. NaH (1.5 equiv.) was added to the flask in one addition and the septum was replaced on the vessel. The reaction mixture was stirred for 30 minutes at 0 °C and the ice bath was replenished. Alkyl halide (3 equiv.) was added to the cooled solution drop-wise. Liquid alkyl

halides were added neat while solid alkyl halides were dissolved in 0.5 mL of DMF. The reaction solution was stirred for an additional 2 hours. During this time, the solution warmed to room temperature. The reaction was quenched with the slow addition of D.I. water. The product was extracted with EtOAc and saturated LiBr. The combined organic layers were washed with brine, dried over Na_2SO_4, filtered and concentration via reduced pressure. The resulting oil was purified on a silica column with hexanes and EtOAc as the eluent to yield pure product **5.1a–k**.

General Procedure 5.2- Boc-Deprotection with HCl

Boc-amine **5.1a–k** or di-Boc-guanidine **5.3a–k** was dissolved in MeOH. HCl gas was bubbled into the solution for 1 minute. The solution was stirred until TLC indicated that the starting material had been consumed. The solvent was removed under reduced pressure. The resulting white to light yellow solid was washed with Et_2O to yield pure product **5.2a**–**k** or **5.4a**–**k**.

General Procedure 5.3 – Guanylation of Secondary Amines

Salt **5.2a–k** (1 equiv.) was added to a round bottom flask with CH_3CN and DIEA (3 equiv.). The solution was allowed to stir for 10 minutes before being transferred to a microwave vial containing *N,N′*-di-Boc-1H-pyrazole-1-carboxamidine, (1.05 equiv). The vessel was capped and placed in a CEM microwave where it was heated to 50 °C for 2 hours. The solvent was removed under reduced pressure and the resulting yellow oil was purified on silica gel with hexanes and EtOAc as the eluent to yield pure product **5.3a–k**.

7.1.10 Characterization for Chapter 2

4-(dec-1-yn-1-yl)benzonitrile (2.1b):

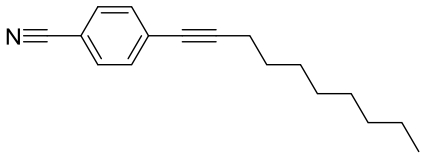

Using **2.1a** and dec-1-yne as starting material, **2.1b** was synthesized and isolated in 93% yield. ^{1}H NMR (500 MHz, $CDCl_3$) δ 7.56 (d, *J* = 8.5 Hz, 2H), 7.45 (d, *J* = 8.5 Hz, 2H), 2.42 (t, *J* = 7.1 Hz, 2H), 1.67–1.56 (m, 2H), 1.44 (dt, *J* = 8.6, 3.5 Hz, 2H), 1.37–1.24 (m, 9H), 0.89 (t, *J* = 6.9, 3H).

4-(dodec-1-yn-1-yl)benzonitrile (2.1c):

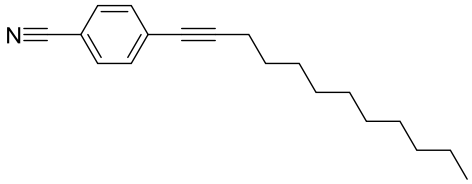

Using **2.1a** and dodec-1-yne as starting material, **2.1.c** was synthesized and isolated in 72% yield. ^{1}H NMR (400 MHz, $CDCl_3$) δ 7.56 (d, *J* = 8.3 Hz, 2H), 7.45 (d, *J* = 8.4 Hz, 2H), 2.42 (t, *J* = 7.1 Hz, 2H), 1.64–1.54 (m, 2H), 1.44 (t, *J* = 7.6 Hz, 2H), 1.39–1.16 (m, 15H), 0.88 (t, *J* = 7.1 Hz, 3H). ^{13}C NMR (101 MHz, $CDCl_3$) δ 132.2, 132.0, 129.3, 118.7, 110.9, 95.8, 79.5, 33.1, 32.0, 29.7, 29.7, 29.62, 29.56, 29.42, 29.38, 29.3, 29.2, 29.0, 28.6, 22.8, 19.6, 14.2.

4-tetradecylbenzonitrile (2.1d):

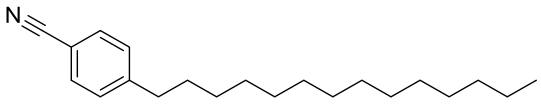

Using **2.1a** and dodec-1-yne as starting material, **2.1.d** was synthesized and isolated as an oil (242 mg, 92%). ^{1}H NMR (400 MHz, $CDCl_3$) δ 7.54 (d, J = 8.2 Hz, 2H), 7.26 (d, *J* = 8.2 Hz, 2H), 2.69–2.59 (m, 2H), 1.61 (t, *J* = 7.6 Hz, 2H), 1.32–1.18 (m, 21H), 0.87 (t, *J* = 7.0 Hz, 3H). ^{13}C NMR (101 MHz, $CDCl_3$) δ 148.5, 132.0, 129.1, 119.1, 109.5, 36.1, 31.9, 30.9, 29.70, 29.68, 29.65, 29.63, 29.60, 29.5, 29.4, 29.34, 29.34, 29.2, 22.7, 14.1.

4-phenethylbenzonitrile (2.1e):

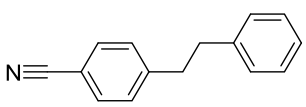

Compound **2.1e** was synthesized from **2.1a** and styrene using general procedure 2.2. Purification on a silica column with 0-5% EtOAc in hexane yielded **2.1e** (45 mg, 99%). ^{1}H NMR (400 MHz, $CDCl_3$) δ 7.57–7.54 (m, 2H), 7.31–7.19 (m, 5H), 7.16–7.12 (m, 2H), 3.03–2.90 (m, 4H). ^{13}C NMR (101 MHz, $CDCl_3$) δ 147.3, 140.4, 132.2, 129.4, 128.6, 128.5, 126.4, 119.2, 110.0, 38.0, 37.3.

***N'*-hydroxy-4-iodobenzimidamide (2.2a):**

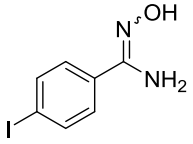

Compound **2.2a** was synthesized from **2.1a** using general procedure 2.3 and isolated as a white solid. The organic solvent was removed under reduced pressure and the residue was purified by silica gel column chromatography with 3:7 (v:v) EtOAc:hexanes to yield **2.2a** (1.0 g, 88%) as white solid. ^{1}H NMR (400 MHz, CD_3OD) δ 7.78 (dt, *J* = 7.8, 3.6 Hz, 2H), 7.44 (dt, *J* = 7.4, 0.1 Hz, 2H); ^{13}C NMR (101 MHz, CD_3OD) δ 154.5, 138.7, 133.8, 129.0, 96.2. HRMS (ESI+): Calcd for $C_7H_8N_2OI$ [M+H]: 262.9681, Found: 262.9695.

4-(dec-1-yn-1-yl)-*N'*-hydroxybenzimidamide (2.2b):

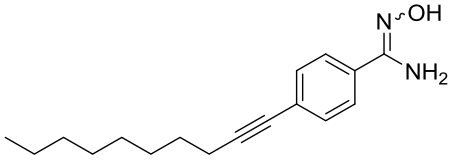

Compound **2.2b** was synthesized from **2.1c** using general procedure 2.3. Purification resulted in the isolation of **2.2b** (58%) as a white solid. ^{1}H NMR (400 MHz, $CDCl_3$) δ 7.55 (d, *J* = 6.5 Hz, 1H), 7.48–7.39 (m, 2H), 4.86 (s, 2H), 2.41 (t, *J* = 7.1 Hz, 2H), 1.64–1.56 (m, 2H), 1.44 (p, J = 6.7 Hz, 2H), 1.34–1.20 (m, 8H), 0.89 (t, *J* = 7.0 Hz, 3H).

4-(dodec-1-yn-1-yl)-*N'*-hydroxybenzimidamide (2.2c):

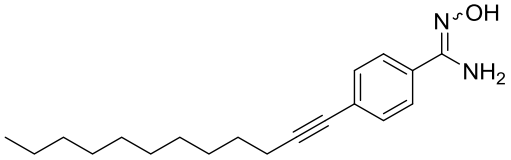

Compound **2.2c** was synthesized from **2.1c** using general procedure 2.3. Purification resulted in the isolation of **2.2c** (184 mg, 91%) as a white solid. ^{1}H NMR (400 MHz, $CDCl_3$) δ 7.60–7.52 (m, 2H), 7.49–7.40 (m, 2H), 2.42 (t, *J* = 7.1 Hz, 2H), 1.44 (p, *J* = 7.6 Hz, 2H), 1.26 (d, *J* = 7.8 Hz, 14H), 0.88 (t, *J* = 6.6 Hz, 3H).

***N'*-hydroxy-4-tetradecylbenzimidamide (2.2d):**

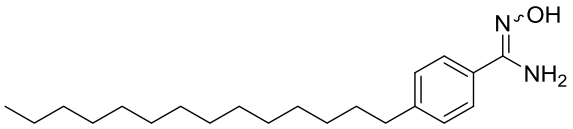

Compound **2.2d** was synthesized from **2.1d** using general procedure 2.3. Purification resulted in the isolation of **2.2d** (0.192 g, 43%) as a white solid. ^{1}H NMR (400 MHz, $CDCl_3$) δ 7.53 (d, *J* = 8.2 Hz, 2H), 7.20 (d, *J* = 8.2 Hz, 2H), 4.98 (s, 2H), 2.65–2.53 (m, 2H), 1.63–1.51 (m, 2H), 1.26 (s, 24H), 0.87 (t, *J* = 7.0 Hz, 3H). ^{13}C NMR (101 MHz, $CDCl_3$) δ 145.6, 129.4, 128.9, 128.8, 127.5, 126.0, 35.9, 32.1, 31.4, 29.9, 29.83, 29.81, 29.7, 29.6, 29.5, 29.4, 22.8, 14.3.

***N'*-hydroxy-4-phenethylbenzimidamide (2.2e):**

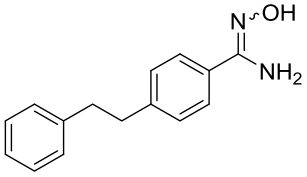

Compound **2.2e** was synthesized from **2.1e** using general procedure 2.3 and isolated as a white solid. The organic solvent was removed under reduced pressure and the residue was purified on a silica gel column in 40-80% EtOAc in hexane to yield **2.2e** (50 mg, 95%). ^{1}H NMR (400 MHz, CD_3OD) δ 7.52 (d, J = 8.1 Hz, 2H), 7.27 – 7.10 (m, 7H), 2.97 – 2.87 (m, 4H). ^{13}C NMR (101 MHz, CD_3OD) δ 155.68, 144.98, 142.74, 131.73, 129.67, 129.55, 129.28, 127.22, 126.91, 38.74. HRMS (ESI+): Calcd for $C_{15}H_{16}N_2O$ [M+H]: 241.3083, Found: 241.1335.

***tert*-butyl (*S*)-2-(3-(4-iodophenyl)-1,2,4-oxadiazol-5-yl)pyrrolidine-1-carboxylate (2.3a)**

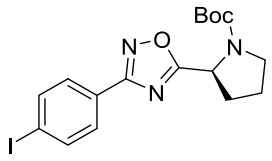

Compound **2.3a** was synthesized from **2.2a** and Boc-*L*-proline using general procedure 2.4. The residue was purified by silica gel column chromatography with 1:7 (v:v) EtOAc:hexanes to yield **2.3a** (225 mg, 53%) as an oil. ^{1}H NMR (2:1 rotamer ratio, asterisk indicates minor rotamer peak, 500 MHz, $CDCl_3$) δ 7.85–7.76 (m, 4H), 5.28–5.14* (m, 1H), 5.05 (dd, *J* = 8.3, 3.8 Hz, 1H), 3.77–3.63 (m, 1H), 3.58–3.44 (m, 1H), 2.48–2.31 (m, 1H), 2.23–1.92 (m, 3H), 1.45* (s, 3H), 1.28 (s, 6H). ^{13}C NMR (2:1 rotamer ratio, asterisk indicates minor rotamer peak, 126 MHz, $CDCl_3$) δ 181.1, 180.6*, 167.9, 154.4*, 153.6, 138.3, 138.1*, 129.2*, 129.1, 126.6*, 126.3, 98.1, 80.6, 53.9, 46.8*, 46.5, 32.5, 31.6*, 28.5*, 28.3, 24.5*, 23.8. HRMS (ESI+): Calcd for $C_{17}H_{20}N_3O_3INa$ [M+Na]: 464.0447, Found: 464.0405.

***tert*-butyl (*S*)-2-(3-(4-(dec-1-yn-1-yl)phenyl)-1,2,4-oxadiazol-5-yl)pyrrolidine-1-carboxylate (2.3b):**

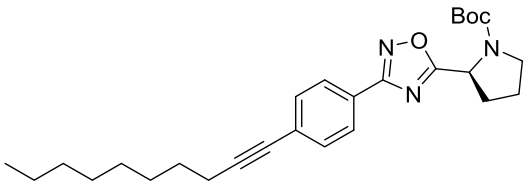

Compound **2.3b** was synthesized from **2.3a** and 1-decyne using general procedure 2.1. The resulting residue was purified on a silica column to yield **2.3b** (20%), an oil. ^{1}H NMR (2:1 rotamer ratio, asterisk denotes minor rotamer peak, 500 MHz, $CDCl_3$) δ 7.99 (d, *J* = 8.4Hz, 2H), 7.49 (d, *J* = 8.3 Hz, 2H), 5.27–5.13* (m, 1H), 5.06 (dd, *J* = 8.2, 3.7 Hz, 1H), 3.76–3.64 (m, 1H), 3.59–3.46 (m, 1H), 2.42 (t, *J* = 7.1 Hz, 2H), 2.21–2.11 (m, 2H), 2.05–1.96 (m, 1H), 1.66–.57 (m, 3H), 1.46* (s, 3H), 1.40–1.22 (m, 13H), 0.89 (t, *J* = 7.1Hz, 3H).

***tert*-butyl (*S*)-2-(3-(4-(dodec-1-yn-1-yl)phenyl)-1,2,4-oxadiazol-5-yl)pyrrolidine-1-carboxylate (2.3c):**

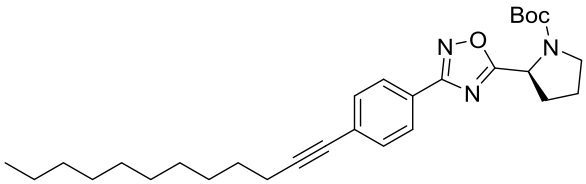

Compound **2.3c** was synthesized from **2.3a** and 1-dodecyne using general procedure 2.1. The resulting residue was purified on a silica column to yield **2.3c** (65%) an oil. ^{1}H NMR (2:1 rotamer ratio, asterisk indicates minor rotamer peak, 500 MHz, $CDCl_3$): δ 7.99 (d, *J* = 8.1 Hz, 2H), 7.48 (dd, *J* = 12.4, 6.0 Hz, 2H), 5.20* (d, *J* = 7.9 Hz, 1H), 5.06 (dd, *J* = 8.0, 3.5 Hz, 1H), 3.80–3.63 (m, 1H), 3.61–3.44 (m, 1H), 2.42 (q, *J* = 11.2, 9.1 Hz, 2H), 2.15 (dd, *J* = 12.8, 8.7 Hz, 2H), 2.00 (d, *J* = 11.8 Hz, 1H), 1.62 (p, *J* = 7.2 Hz, 2H), 1.57 (s, 6H), 1.45* (d, *J* = 11.8 Hz, 5H), 1.37–1.19 (m, 14H), 0.88 (t, *J* = 6.9 Hz, 3H).

***tert*-butyl (*S*)-2-(3-(4-tetradecylphenyl)-1,2,4-oxadiazol-5-yl)pyrrolidine-1-carboxylate (2.3d):**

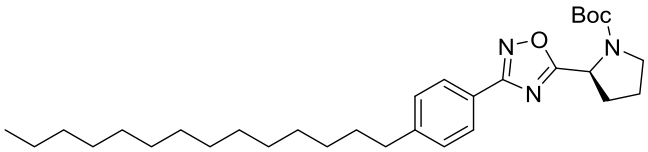

Compound **2.3d** was synthesized from **2.2d** and Boc-*L*-proline using general procedure 2.4. The residue was purified on a silica column to yield **2.3d** (82 mg, 53%). ^{1}H NMR (2:1 rotamer ratio, asterisk indicates minor rotamer peak, 400 MHz, $CDCl_3$) δ 8.00–7.94 (m, 2H), 7.28 (d, *J* = 8.3 Hz, 2H), 5.20* (d, *J* = 8.3 Hz, 1H), 5.06 (dd, *J* = 8.3, 3.6 Hz, 1H), 3.76–3.65 (m, 1H), 3.59–3.44 (m, 1H), 2.65 (t, *J* = 7.7 Hz, 2H), 2.46–2.26 (m, 1H), 2.22–2.08 (m, 2H), 2.05–1.90 (m, 1H), 1.69–1.58 (m, 2H), 1.46* (s, 3H), 1.27 (d, *J* = 17.2 Hz, 27H), 0.88 (t, *J* = 7.0 Hz, 3H). ^{13}C NMR (101 MHz, $CDCl_3$) δ 180.6, 168.5, 153.7, 146.7, 129.0, 128.9, 127.5, 124.2, 80.6, 54.0, 46.5, 36.1, 32.5, 32.1, 31.4, 29.82, 29.80, 29.78, 29.7, 29.61, 29.58, 29.5, 29.4, 28.5, 28.3, 23.8, 22.8, 14.2.

***tert*-butyl (*S*)-2-(3-(4-phenethylphenyl)-1,2,4-oxadiazol-5-yl)pyrrolidine-1-carboxylate (2.3e):**

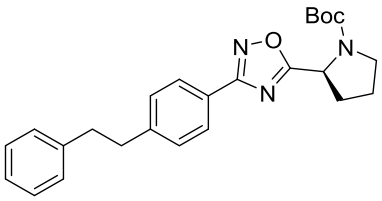

Compound **2.3e** was synthesized from **2.2e** and Boc-*L*-proline using general procedure 2.4. The residue was purified on a silica column in 10-30% EtOAc in hexane to yield **2.3e** (22 mg, 25%) as an oil. ^{1}H NMR (2:1 rotamer ratio, asterisk indicates minor rotamer peak, 500 MHz, $CDCl_3$) δ 7.98 (d, *J* = 7.7 Hz, 2H), 7.31–7.24 (m, 4H), 7.24–7.15 (m, 2H), 5.21* (d, *J* = 6.6 Hz, 1H), 5.07 (dd, *J* = 7.9, 3.4 Hz, 1H), 3.76–3.62 (m, 1H), 3.61–3.42 (m, 1H), 3.01–2.91 (m, 3H), 2.46–2.32 (m, 1H), 2.20–2.07 (m, 2H), 2.09–1.97 (m, 1H), 1.45* (s, 3H), 1.28 (d, *J* = 23.1 Hz, 6H). ^{13}C NMR (2:1 rotamer ratio, asterisk indicates minor rotamer peak, 126 MHz, $CDCl_3$) δ 180.7, 180.2*, 168.5, 154.4*, 153.7, 145.4, 145.2*, 141.4, 129.2, 129.1*, 128.6, 128.5, 127.6, 126.2, 124.8*, 124.6, 80.6, 54.0, 46.8*, 46.4, 38.0, 37.7, 32.5, 31.6*, 29.8, 28.6*, 28.3, 24.5*, 23.8. HRMS (ESI+): Calcd for $C_{25}H_{29}N_3O_3$ [M+H]: 420.5240, Found: 420.2280.

***tert*-butyl (*S*)-2-(3-(4-hexylphenyl)-1,2,4-oxadiazol-5-yl)pyrrolidine-1-carboxylate (2.3f):**

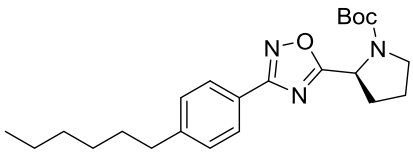

Compound **2.3f** was synthesized from **2.7** using general procedure 2.7. Purification on a silica column produced **2.3f** (45 mg, 65%). ^{1}H NMR (500 MHz, $CDCl_3$) δ 7.90 (d, *J* = 7.9 Hz, 2H), 7.27–7.13 (m, 2H), 5.12 (d, *J* = 7.6 Hz, 1H), 4.98 (dd, *J* = 8.1, 3.5 Hz, 1H), 3.71–3.54 (m, 1H), 3.44 (dq, *J* = 38.8, 9.1, 8.2 Hz, 1H), 3.12 (s, 1H), 2.58 (t, *J* = 7.6 Hz, 2H), 2.15–1.99 (m, 2H), 1.99–1.85 (m, 1H), 1.81 (s, 1H), 1.39 (s, 9H), 1.20 (d, *J* = 21.5 Hz, 9H), 0.80 (t, *J* = 6.9 Hz, 3H). ^{13}C NMR (101 MHz, $cdcl_3$) δ 180.4, 168.2, 153.4, 146.5, 128.9, 128.8, 127.4, 124.0, 80.4, 53.8, 46.6, 46.3, 35.9, 32.4, 31.9, 31.5, 31.2, 29.3, 28.4, 28.1.

(*S*)-3-(4-iodophenyl)-5-(pyrrolidin-2-yl)-1,2,4-oxadiazole (2.4a)

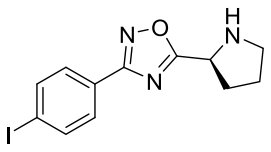

Compound **2.4a** was synthesized from **2.3a** using general procedure 2.5 to provide **2.3a** (130 mg, 79%) as an oil without further purification. ^{1}H NMR (400 MHz, $CDCl_3$) δ 7.79 (s, 4H), 4.53 (dd, *J* = 8.2, 5.5 Hz, 1H), 3.23–3.02 (m, 2H), 2.34–2.25 (m, 2H), 2.19–2.06 (m, 1H), 2.03–1.81 (m, 1H); ^{13}C NMR (101 MHz, $CDCl_3$) δ 182.3, 167.7, 138.1, 129.1, 126.4, 97.9, 54.4, 47.0, 31.2, 25.4; HRMS (ESI+): Calcd for $C_{12}H_{13}N_3OI$ [M+H]: 342.0103, Found: 342.0080.

(*S*)-2-(3-(4-phenethylphenyl)-1,2,4-oxadiazol-5-yl)pyrrolidin-1-ium chloride (2.4e):

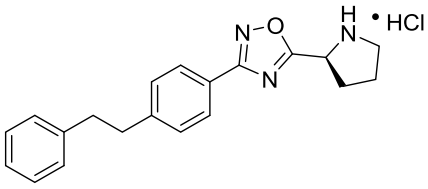

Compound **2.4e** was synthesized from **2.3e** using general procedure 2.5. The solvent was removed under reduced pressure and the resulting residue was washed with diethyl ether to yield **2.4e** (19 mg, 100%) a white solid. ^{1}H NMR (500 MHz, CD_3OD) δ 7.98 (d, *J* = 8.1 Hz, 2H), 7.33 (d, *J* = 8.1 Hz, 2H), 7.25–7.20 (m, 2H), 7.16 (d, *J* = 7.3 Hz, 3H), 5.18 (t, *J* = 7.7 Hz, 1H), 3.63–3.55 (m, 1H), 3.53 (dd, *J* = 7.2, 4.2 Hz, 1H), 3.00 (dd, *J* = 8.0, 5.8 Hz, 2H), 2.95 (dd, *J* = 7.9, 5.8 Hz, 2H), 2.67 (dd, *J* = 13.4, 5.9 Hz, 1H), 2.42 (dd, *J* = 13.4, 7.6 Hz, 1H), 2.27 (dq, *J* = 13.6, 6.4 Hz, 2H). ^{13}C NMR (126 MHz, CD_3OD) δ 175.9, 169.8, 147.6, 142.5, 130.5, 129.6, 129.3, 128.5, 127.0, 124.8, 55.7, 47.4, 38.9, 38.6, 30.2, 24.5. HRMS (ESI+): Calcd for $C_{20}H_{21}N_3O$ [M+H]: 320.4082, Found: 320.1755.

(*S*)-3-(4-decylphenyl)-5-(pyrrolidin-2-yl)-1,2,4-oxadiazole (2.4g):

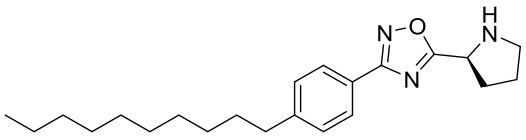

Compound **2.4b** was synthesized from **2.3b** using general procedure 2.5 and carried forward without purification. Compound **2.4g** was synthesized from **2.4b** using general procedure 2.7 and isolated

in 76% yield. ^{1}H NMR (500 MHz, $CDCl_3$) δ 7.91 (d, *J* = 8.2 Hz, 2H), 7.21 (d, *J* = 8.2 Hz, 2H), 4.48 (s, 1H), 4.05 (q, *J* = 7.1 Hz, 1H), 3.99 (t, *J* = 6.7 Hz, 1H), 3.16 (q, *J* = 8.1, 7.0 Hz, 2H), 3.09–2.96 (m, 2H), 2.65–2.54 (m, 3H), 2.30–2.20 (m, 2H), 2.07 (ddd, *J* = 18.8, 7.5, 5.2 Hz, 2H), 1.56 (dq, *J* = 12.1, 6.1, 4.8 Hz, 4H), 1.33–1.11 (m, 14H), 0.81 (t, *J* = 7.0 Hz, 3H).

(*S*)-3-(4-dodecylphenyl)-5-(pyrrolidin-2-yl)-1,2,4-oxadiazole (2.4h):

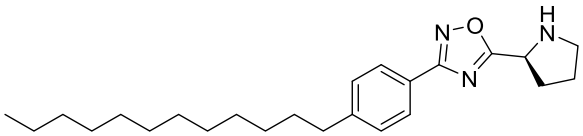

Compound **2.4c** was synthesized from **2.3c** using general procedure 2.5 and carried forward without purification. Compound **2.4h** was synthesized from **2.4c** using general procedure 2.7. ^{1}H NMR (500 MHz, $CDCl_3$) δ 7.91 (d, *J* = 8.2 Hz, 2H), 7.21 (d, *J* = 8.2 Hz, 3H), 4.48 (s, 1H), 4.05 (q, *J* = 7.1 Hz, 1H), 3.99 (t, *J* = 6.7 Hz, 1H), 3.16 (q, *J* = 8.1, 7.0 Hz, 2H), 3.09–2.96 (m, 2H), 2.65–2.54 (m, 3H), 2.30–2.20 (m, 2H), 2.07 (ddd, *J* = 18.8, 7.5, 5.2 Hz, 2H), 1.95–1.74 (m, 9H), 1.56 (dq, *J* = 12.1, 6.1, 4.8 Hz, 4H), 1.33–1.11 (m, 16H), 0.81 (t, *J* = 7.0 Hz, 3H).

***tert*-butyl (*S*,*Z*)-(((*tert*-butoxycarbonyl)imino)(2-(3-(4-iodophenyl)-1,2,4-oxadiazol-5-yl)pyrrolidin-1-yl)methyl)carbamate (2.5a)**

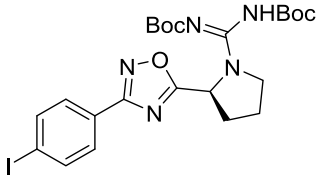

Compound **2.5a** was synthesized from **2.4a** using general procedure 2.6. The organic solvent was removed under reduced pressure and the residue was purified by silica gel column chromatography with 1:7 (v:v) EtOAc:hexanes to yield **2.5a** (29 mg, 27%). ^{1}H NMR (400 MHz, $CDCl_3$) δ 7.78 (d, *J* = 2.8 Hz, 4H), 5.58 (dd, *J* = 7.5, 4.6 Hz, 1H), 3.93–3.68 (m, 2H), 2.43 (dd, *J* = 12.8, 6.9 Hz, 1H), 2.22–2.13 (m, 2H), 2.08–1.98 (m, 1H), 1.53–1.32 (m, 18H); ^{13}C NMR (126 MHz, $CDCl_3$) δ 179.4, 167.8, 162.0, 150.4, 138.1, 129.1, 128.8, 127.6, 126.3, 98.0, 82.3, 79.7, 77.4, 77.2, 76.9,

60.4, 55.4, 49.5, 34.7, 34.6, 31.7, 29.8, 29.1, 28.2, 25.4, 24.1, 22.7, 21.1, 20.8, 18.8, 14.3, 14.2, 11.5; HRMS (ESI+): Calcd for $C_{23}H_{31}IN_5O_5$ [M+H]: 584.1370 , Found: 584.15.

tert-butyl (*S,Z*)-(((_tert_-butoxycarbonyl)imino)(2-(3-(4-tetradecylphenyl)-1,2,4-oxadiazol-5-yl)pyrrolidin-1-yl)methyl)carbamate (2.5d):

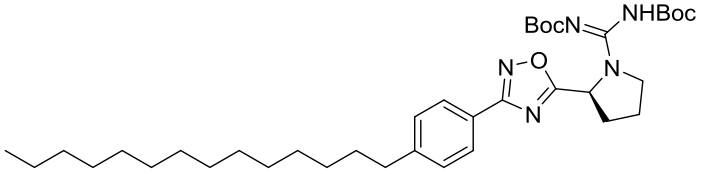

Compound **2.4d** was synthesized from **2.3d** using general procedure 2.5 and carried forward without purification. Compound **2.5d** was synthesized from **2.4d** using general procedure 2.6. The resulting residue was purified on a silica column to yield **2.5d**, an oil. ^{1}H NMR (400 MHz, $CDCl_3$) δ 7.89 (d, *J* = 8.1 Hz, 2H), 7.19 (d, *J* = 8.0 Hz, 2H), 5.52 (dd, *J* = 7.7, 4.5 Hz, 1H), 4.10–3.95 (m, 1H), 3.81 (dt, *J* = 11.4, 7.3 Hz, 1H), 3.76–3.63 (m, 1H), 2.57 (t, *J* = 7.7 Hz, 2H), 2.45–2.25 (m, 1H), 2.25–2.03 (m, 1H), 2.03–1.88 (m, 1H), 1.55 (p, *J* = 7.6 Hz, 3H), 1.38 (s, 18H), 1.30–1.06 (m, 18H), 0.80 (t, *J* = 6.6 Hz, 3H). ^{13}C NMR (101 MHz, $CDCl_3$) δ 178.7, 168.3, 162.1, 153.5, 146.5, 128.8, 127.4, 123.9, 82.2, 80.5, 55.2, 49.3, 35.9, 31.7, 31.2, 29.6, 29.5, 29.4, 29.3, 29.2, 28.1, 22.7, 14.1.

tert-butyl (*S,Z*)-(((_tert_-butoxycarbonyl)imino)(2-(3-(4-phenethylphenyl)-1,2,4-oxadiazol-5-yl)pyrrolidin-1-yl)methyl)carbamate (2.5e):

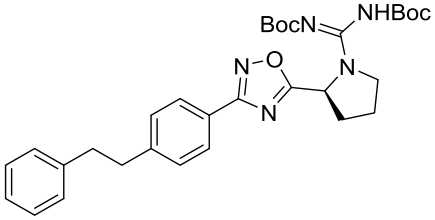

Compound **2.5e** was synthesized from **2.4e** using general procedure 2.6. The solvent was removed under reduced pressure and the resulting residue was washed with diethyl ether to yield **2.5e** (19 mg, 63%) a clear residue. ^{1}H NMR (500 MHz, $CDCl_3$) δ 7.90 (d, *J* = 8.3 Hz, 2H), 7.20 (q, *J* = 7.5 Hz, 5H), 7.16–7.07 (m, 3H), 5.53 (dd, *J* = 7.6, 4.6 Hz, 1H), 3.82 (dt, *J* = 13.7, 7.2 Hz, 1H), 3.76–3.68 (m, 1H), 2.93–2.85 (m, 4H),

2.37 (dd, *J* = 12.7, 7.4 Hz, 1H), 2.23–2.05 (m, 2H), 2.01–1.94 (m, 1H), 1.48–1.31 (m, 18H). ^{13}C NMR (126 MHz, $CDCl_3$) δ 179.0, 168.5, 162.2, 153.7, 150.6, 145.4, 141.4, 129.1, 128.6, 128.5, 127.7, 126.2, 124.5, 81.9, 79.9, 55.5, 49.6, 38.0, 37.7, 36.8, 31.4, 28.3, 28.1. HRMS (ESI+): Calcd for $C_{31}H_{39}N_5O_5$ [M+Na]: 584.6616, Found: 584.2855.

***tert*-butyl (*S,Z*)-(((*tert*-butoxycarbonyl)imino)(2-(3-(4-hexylphenyl)-1,2,4-oxadiazol-5-yl)pyrrolidin-1-yl)methyl)carbamate (2.5f):**

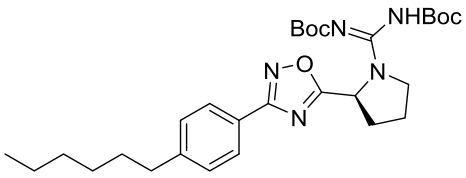

Compound **2.4f** was synthesized from **2.3f** using general procedure 2.5 and carried forward without purification. Compound **2.5f** was synthesized from **2.4f** using general procedure 2.6. The resulting residue was purified on a silica column to yield **2.5f** (48 mg, 92%), an oil. ^{1}H NMR (400 MHz, $CDCl_3$) δ 7.89 (d, *J* = 8.1 Hz, 2H), 7.19 (d, *J* = 8.0 Hz, 2H), 5.52 (dd, *J* = 7.7, 4.5 Hz, 1H), 3.81 (dt, *J* = 11.4, 7.3 Hz, 1H), 3.76–3.63 (m, 1H), 2.57 (t, *J* = 7.7 Hz, 2H), 2.03–1.88 (m, 1H), 1.55 (m, *J* = 7.6 Hz, 2H), 1.38 (s, 9H), 1.30–1.06 (m, 18H), 0.80 (t, *J* = 6.6 Hz, 3H).

***tert*-butyl (*S,Z*)-(((*tert*-butoxycarbonyl)imino)(2-(3-(4-decylphenyl)-1,2,4-oxadiazol-5-yl)pyrrolidin-1-yl)methyl)carbamate (2.5g):**

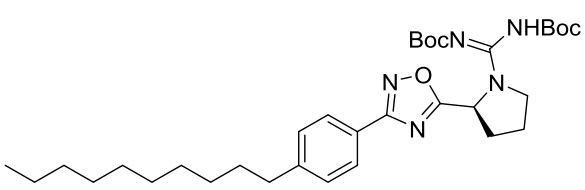

Compound **2.5g** was synthesized from **2.4g** using general procedure 2.6. The resulting residue was purified on a silica column to yield **2.5g** (35%), an oil. ^{1}H NMR (500 MHz, $CDCl_3$) δ 7.90 (d, *J* = 8.1 Hz, 2H), 7.24–7.16 (m, 3H), 5.52 (s, 1H), 3.81 (s, 1H), 3.73 (s, 1H), 2.58 (t, *J* = 7.7 Hz, 2H), 2.36 (s, 1H), 2.11 (s, 2H), 1.96 (s, 1H), 1.56 (s, 2H), 1.41 (d, *J* = 21.5 Hz, 14H), 1.21 (d, *J* = 26.9 Hz, 18H), 0.80 (t, *J* = 6.8 Hz, 3H). ^{13}C

NMR (101 MHz, $CDCl_3$) δ 178.773, 168.3, 153.5, 146.5, 128.8, 127.4, 123.9, 81.3, 80.8, 55.2, 49.4, 35.9, 31.9, 31.2, 29.6, 29.5, 29.4, 29.3, 29.2, 28.1, 23.9, 22.7, 14.1.

tert-butyl (_S,Z_)-(((_tert_-butoxycarbonyl)imino)(2-(3-(4-dodecylphenyl)-1,2,4-oxadiazol-5-yl)pyrrolidin-1-yl)methyl)carbamate (2.5h):

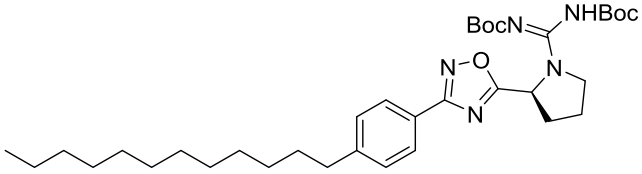

Compound **2.5h** was synthesized from **2.4h** using general procedure 2.6. The resulting residue was purified on a silica column to yield **2.5h**, (63%) an oil. ^{1}H NMR (500 MHz, $CDCl_3$): δ 7.90 (d, J = 8.1 Hz, 2H), 7.24–7.16 (m, 2H), 5.52 (s, 1H), 3.81 (s, 1H), 3.73 (s, 1H), 2.58 (t, J = 7.7 Hz, 2H), 2.36 (s, 1H), 2.11 (s, 2H), 1.96 (s, 1H), 1.56 (s, 2H), 1.41 (d, J = 21.5 Hz, 16H), 1.21 (d, J = 26.9 Hz, 18H), 0.80 (t, J = 6.8 Hz, 3H). ^{13}C NMR (101 MHz, $CDCl_3$) δ 177.7, 167.3, 152.677, 147.8, 145.5, 127.8, 126.5, 126.4, 122.9, 81.2, 54.3, 48.4, 36.1, 34.9, 30.91, 30.90, 30.2, 29.0, 28.7, 28.64, 28.63, 28.61, 28.59, 28.56, 28.51, 28.46, 28.35, 28.33, 28.2, 27.1, 27.00, 26.96, 21.7, 13.1.

(_S_)-2-(3-(4-iodophenyl)-1,2,4-oxadiazol-5-yl)pyrrolidine-1-carboximidamide hydrochloride (2.6a)

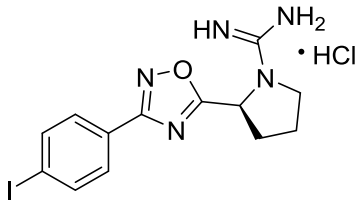

Compound **2.6a** was synthesized from **2.5a** using general procedure 2.5. The organic solvent was then removed under reduced pressure to yield **2.6a** (20 mg, 95%) as white solid. ^{1}H NMR (400 MHz, CD_3OD) δ 7.94 (d, J = 7.7 Hz, 2H), 7.84 (d, J = 7.8 Hz, 2H), 5.49 (s, 1H), 3.86-3.63 (m, 2H), 2.57 (s, 1H) 2.47 (s, 1H), 2.23 (s, 1H) 2.09 (s, 1H). ^{13}C NMR (101 MHz, CD_3OD) δ 179.2, 169.1, 157.0, 139.5, 129.9, 127.1, 99.0, 56.6, 49.3, 32.9, 24.4; HRMS (ESI+): Calcd for $C_{13}H_{15}N_5OI$ [M+H]: 384.0321, Found: 384.0313.

(*S*)-amino(2-(3-(4-tetradecylphenyl)-1,2,4-oxadiazol-5-yl)pyrrolidin-1-yl)methaniminium chloride (2.6d):

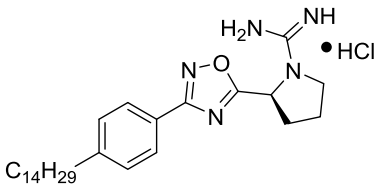

Compound **2.6d** was synthesized from **2.5d** using general procedure 2.5. The organic solvent was then removed under reduced pressure to yield **2.6d** as white solid. ^{1}H NMR (400 MHz, CD_3OD) δ 7.95 (d, *J* = 8.1 Hz, 2H), 7.33 (d, *J* = 8.0 Hz, 2H), 5.46 (d, *J* = 7.3 Hz, 1H), 3.77 (dd, *J* = 9.2, 2.3 Hz, 1H), 3.67–3.54 (m, 1H), 2.67 (dd, *J* = 8.5, 6.7 Hz, 2H), 2.64–2.51 (m, 1H), 2.46 (dd, *J* = 12.9, 6.3 Hz, 1H), 2.23 (d, *J* = 7.0 Hz, 1H), 2.08 (d, *J* = 7.8 Hz, 1H), 1.64 (t, *J* = 7.4 Hz, 2H), 1.27 (s, 20H), 0.89 (t, *J* = 7.0 Hz, 3H). ^{13}C NMR (101 MHz, CD_3OD) δ 178.8, 169.6, 157.1, 148.3, 130.1, 128.4, 124.9, 56.4, 36.8, 33.0, 32.7, 32.4, 30.8, 30.74, 30.72, 30.69, 30.65, 30.5, 30.4, 30.3, 24.3, 23.7, 14.5.

(*S*)-amino(2-(3-(4-phenethylphenyl)-1,2,4-oxadiazol-5-yl)pyrrolidin-1-yl)methaniminium (2.6e):

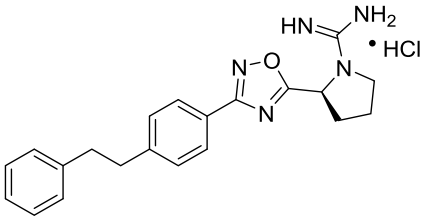

Compound **2.6e** was synthesized from **2.5e** using general procedure 2.5. The organic solvent was then removed under reduced pressure to yield **2.6e** (13 mg, 100%) as white solid. ^{1}H NMR (400 MHz, CD_3OD) δ 7.95–7.90 (m, 2H), 7.31 (d, *J* = 8.4 Hz, 2H), 7.23 (dd, *J* = 7.8, 6.8 Hz, 2H), 7.17–7.07 (m, 3H), 5.43 (dd, *J* = 7.9, 2.0 Hz, 1H), 3.80–3.74 (m, 1H), 3.62 (td, *J* = 9.7, 7.4 Hz, 1H), 3.03–2.93 (m, 4H), 2.61–2.45 (m, 2H), 2.26–2.18 (m, 1H), 2.14–2.07 (m, 1H). ^{13}C NMR (126 MHz, CD_3OD) δ 178.9, 169.7, 157.1, 147.3, 142.6, 130.5, 130.4, 129.6, 129.3, 128.5, 128.4, 127.0, 125.2, 56.5, 38.9, 38.6, 32.7, 24.3. HRMS (ESI+): Calcd for $C_{21}H_{23}N_5O$ [M+H]: 362.4482, Found: 362.1980.

(*S*)-amino(2-(3-(4-hexylphenyl)-1,2,4-oxadiazol-5-yl)pyrrolidin-1-yl)methaniminium chloride 2.6f):

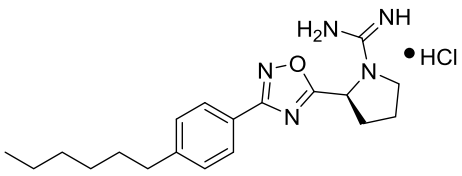

Compound **2.6f** was synthesized from **2.5f** using general procedure 2.5. The organic solvent was then removed under reduced pressure to yield **2.6f** as white solid. ^{1}H NMR (400 MHz, CD_3OD) δ 8.00–7.93 (m, 2H), 7.50 (dd, *J* = 8.4, 3.3 Hz, 1H), 7.34 (d, *J* = 8.3 Hz, 1H), 5.45 (dt, *J* = 7.9, 2.2 Hz, 1H), 3.83–3.73 (m, 1H), 3.67–3.57 (m, 1H), 2.72–2.64 (m, 1H), 2.58–2.51 (m, 1H), 2.49–2.40 (m, 2H), 2.29–2.20 (m, 2H), 2.15–2.04 (m, 1H), 1.68–1.60 (m, 1H), 1.54–1.47 (m, 2H), 1.03–0.89 (m, 3H). ^{13}C NMR (101 MHz, CD_3OD) δ 179.1, 169.3, 157.1, 148.4, 133.0, 130.2, 128.3, 56.5, 36.9, 32.7, 30.0, 24.3, 23.6, 23.0, 19.7, 14.4. HRMS (ESI+): Calcd for $C_{19}H_{27}N_5O$ [M+H]: 342.2296, Found: 342.2296.

(*S*)-amino(2-(3-(4-decylphenyl)-1,2,4-oxadiazol-5-yl)pyrrolidin-1-yl)methaniminium chloride (2.6g):

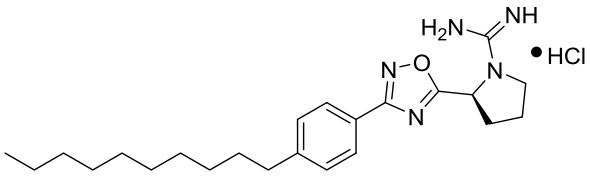

Compound **2.6g** was synthesized from **2.5g** using general procedure 2.5. The organic solvent was then removed under reduced pressure to yield **2.6g** as white solid. ^{1}H NMR (400 MHz, CD_3OD) δ 7.94 (d, *J* = 7.7 Hz, 2H), 7.32 (d, *J* = 7.7 Hz, 2H), 5.46 (d, *J* = 6.0 Hz, 1H), 3.77 (d, *J* = 8.4 Hz, 1H), 3.63 (d, *J* = 9.0 Hz, 1H), 2.67 (t, *J* = 7.5 Hz, 2H), 2.57 (s, 1H), 2.52–2.44 (m, 1H), 2.23 (s, 1H), 2.09 (s, 1H), 1.64 (t, *J* = 7.3 Hz, 2H), 1.37–1.25 (m, 15H), 0.88 (t, *J* = 6.7 Hz, 3H). ^{13}C NMR (101 MHz, CD_3OD) δ 178.8, 169.6, 157.0, 148.2, 130.1, 128.4, 124.9, 56.5, 36.8, 33.0, 32.8, 32.3, 30.6, 30.5, 30.4, 30.2, 24.4, 23.7, 14.4.

(*S*)-amino(2-(3-(4-dodecylphenyl)-1,2,4-oxadiazol-5-yl)pyrrolidin-1-yl)methaniminium chloride (2.6h):

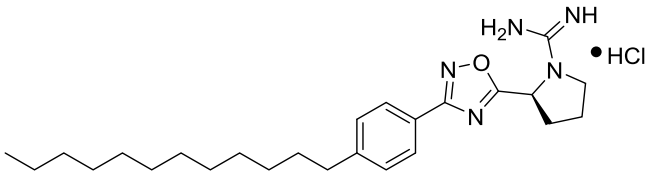

Compound **2.6h** was synthesized from **2.5h** using general procedure 2.5. The organic solvent was then removed under reduced pressure to yield **2.6h** (9 mg, 18%) as white solid. ^{1}H NMR (400 MHz, CD_3OD) δ 7.94 (d, *J* = 8.1 Hz, 2H), 7.34 (d, *J* = 8.1 Hz, 2H), 5.43 (dd, *J* = 7.8, 1.6 Hz, 1H), 3.77 (td, *J* = 9.2, 2.5 Hz, 1H), 3.66–3.56 (m, 1H), 3.30 (p, *J* = 1.6 Hz, 9H), 2.72–2.64 (m, 2H), 2.61–2.43 (m, 2H), 2.29–2.02 (m, 1H), 1.75–1.56 (m, 1H), 1.41–1.22 (m, 23H), 0.89 (t, *J* = 6.8 Hz, 3H). ^{13}C NMR (101 MHz, CD_3OD) δ 178.8, 169.7, 157.1, 148.4, 130.6, 129.7, 128.5, 128.3, 125.0, 57.1, 36.9, 33.1, 32.4, 30.7, 30.3, 24.3, 23.7.

***tert*-butyl (*S*)-2-(3-(4-(hex-1-yn-1-yl)phenyl)-1,2,4-oxadiazol-5-yl)pyrrolidine-1-carboxylate (2.7):**

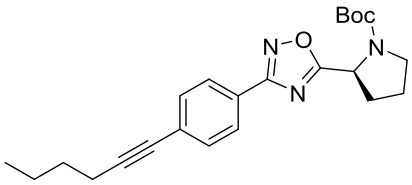

Compound **2.7** was synthesized from **2.3a** and 1-hexyne using general procedure 2.1. The resulting residue was purified on a silica column to yield **2.7** (69 mg, 72%), an oil.

(*S*)-*tert*-butyl 2-(3-(4-iodophenyl)-1,2,4-oxadiazol-5-yl)azetidine-1-carboxylate (2.8):

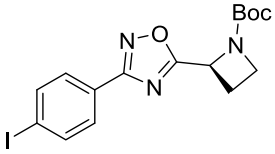

Compound **2.8** was synthesized from **2.2a** and Boc-L-azetidine using general procedure 2.4. The residue was purified by silica gel column chromatography with 3:7 (v:v) EtOAc:hexanes to yield **2.8** (63 mg, 11%) as an oil. ^{1}H NMR (400 MHz, $CDCl_3$) δ 7.83 (s, 4H), 5.41 (dd, *J* = 8, 4 Hz, 1H), 4.23–4.17 (m, 1H), 4.08–4.02 (m, 1H) 2.76–2.67 (m, 1H), 2.58–2.52 (m, 1H), 1.35 (bs, 9H); ^{13}C NMR (101

MHz, $CDCl_3$) δ 178.8, 168.1, 138.3, 129.1, 126.3, 98.1, 80.8, 55.3, 47.7, 28.3, 22.0; HRMS (ESI+): Calcd for $C_{16}H_{18}IN_3NaO_3$ $[M+Na]^+$: 450.0291, Found: 450.0314.

***tert*-butyl (*S*)-2-(3-(4-(hex-1-yn-1-yl)phenyl)-1,2,4-oxadiazol-5-yl)azetidine-1-carboxylate (2.9a):**

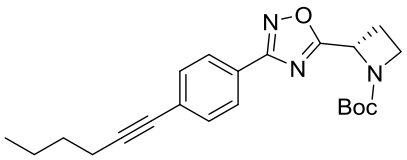

Compound **2.9a** was synthesized from **2.8** and 1-hexyne using general procedure 2.1. The resulting brown oil was purified on a silica column with 0–20% EtOAc in hexanes to yield **2.9a** (92 mg, 100%). ^{1}H NMR (400 MHz, $CDCl_3$) δ 8.02 (d, *J* = 8.1 Hz, 2H), 7.48 (d, *J* = 8.1 Hz, 2H), 5.41 (dd, *J* = 8.8, 5.7 Hz, 1H), 4.19 (ddd, *J* = 9.1, 8.1, 5.8 Hz, 1H), 4.08–4.00 (m, 1H), 2.75–2.66 (m, 1H), 2.59–2.51 (m, 1H), 2.43 (t, *J* = 7.0 Hz, 2H), 1.65–1.55 (m, 2H), 1.54–1.46 (m, 2H), 1.34 (s, 9H), 0.95 (t, *J* = 7.3 Hz, 3H). ^{13}C NMR (101 MHz, $CDCl_3$) δ 178.5, 168.3, 132.1, 127.38, 127.35, 125.5, 93.2, 80.8, 80.3, 30.8, 28.3, 22.2, 22.0, 19.3, 13.8.

***tert*-butyl (*S*)-2-(3-(4-(dec-1-yn-1-yl)phenyl)-1,2,4-oxadiazol-5-yl)azetidine-1-carboxylate (2.9b):**

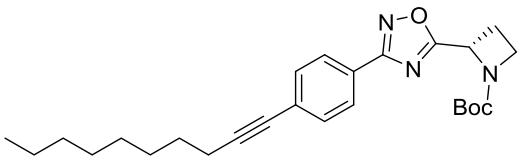

Compound **2.9b** was synthesized from **2.8** and 1-decyne using general procedure 2.1. The resulting brown oil was purified on a silica column with 0–20% EtOAc in hexanes to yield **2.9b** (92 mg, 100%). ^{1}H NMR (500 MHz, $CDCl_3$) δ 8.02 (d, *J* = 8.1 Hz, 2H), 7.36–7.30 (m, 2H), 5.35 (s, 1H), 3.87 (d, *J* = 18.7 Hz, 1H), 2.83–2.64 (m, 1H), 2.59–2.50 (m, 2H), 1.63 (h, *J* = 7.1, 6.6 Hz, 2H), 1.52 (s, 9H), 1.29 (d, *J* = 27.6 Hz, 15H), 0.88 (t, *J* = 7.0 Hz, 3H). ^{13}C NMR (126 MHz, $CDCl_3$) δ 180.7, 179.5, 168.4, 146.5, 128.9, 128.8, 128.7, 127.4, 124.0, 117.0, 110.2 55.3, 36.0, 31.9, 31.2, 29.6, 29.6, 29.49, 29.47, 29.31, 29.26, 14.1, 11.9.

***tert*-butyl (*S*)-2-(3-([1,1'-biphenyl]-4-yl)-1,2,4-oxadiazol-5-yl)azetidine-1-carboxylate (2.9c):**

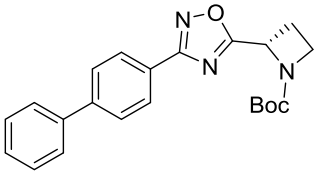

Phenyl boronic acid (0.034 g, 0.3 mmol) and Cs_2CO_3 (0.084 g, 0.26 mmol) were added to a round bottom flask containing **2.8** (0.100 g, 0.234 mmol) in DMF (3 mL) under N_2. The reaction mixture was degassed for 30 minutes by passing N_2 to remove oxygen. To the above solution was added Pd(dppf)Cl_2 (0.034 g, 0.047 mmol) and the brown reaction mixture was stirred at 80 °C for 18 hours. The reaction mixture was poured into a solution of LiBr and extracted with EtOAc (3 × 20 mL). The combined organic solution was washed with NH_4Cl, brine, dried over Na_2SO_4, filtered and concentrated under reduced pressure. The resulting residue was purified by flash chromatography over silica gel to yield **2.9c** (0.08g, 91% yield), a colorless oil. ^{1}H NMR (400 MHz, $CDCl_3$) δ 8.18 (d, *J* = 8.1 Hz, 2H), 7.72 (d, *J* = 8.1 Hz, 2H), 7.65 (dd, *J* = 7.6 Hz, 2H), 7.47 (t, *J* = 7.7 Hz, 2H), 7.42–7.34 (m, 1H), 5.45 (dd, *J* = 8.8, 5.7 Hz, 1H), 4.28–4.17 (m, 1H), , 4.12–4.01 (m, 1H), 2.79–2.68 (m, 1H), 2.62–2.52 (m, 1H), 1.37 (s, 9H). ^{13}C NMR (101 MHz, $CDCl_3$) δ 178.5, 168.5, 140.3, 129.0, 128.1, 127.7, 127.3, 105.1, 80.8, 28.3, 22.0.

***tert*-butyl (*S*)-2-(3-(4-morpholinophenyl)-1,2,4-oxadiazol-5-yl)azetidine-1-carboxylate (2.9d):**

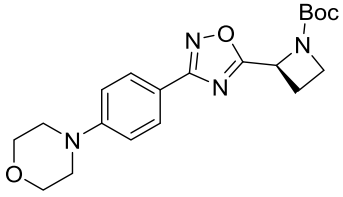

Compound **2.9d** was synthesized from **2.8** and morpholine using general procedure 2.8**.** The resulting brown residue was purified by flash chromatography over silica gel 1:4 (v:v) EtOAc:hexanes to give **2.9d** (146.5 mg, 81%) as a white-yellow solid. ^{1}H NMR (500 MHz, $CDCl_3$) δ 7.99 (dt, *J* = 9, 2.5 Hz, 2H), 6.95 (dt, *J* = 9, 2.5 Hz, 2H), 5.40 (dd, *J* = 9, 5.5 Hz, 1H), 4.23–4.16 (m, 1H), 4.07–4.01 (m, 1H), 3.87 (approx. dd, *J* = 5 Hz, 4H), 3.27 (approx. dd *J* = 5, 1H), 2.74–.66 (m, 1H), 2.58–2.51 (m, 1H), 1.34 (bs, 9H); ^{13}C NMR (101 MHz, $CDCl_3$) δ 178.0, 168.4, 153.3,

128.9, 117.4, 114.8, 80.7, 66.8, 48.3, 28.3, 22.0; HRMS (ESI+): Calcd for $C_{20}H_{27}N_4O_4$ [M+H]: 387.2032, Found: 387.2022.

(*S*)-*tert*-butyl 2-(3-(4-(4-methylpiperazin-1-yl)phenyl)-1,2,4-oxadiazol-5-yl)azetidine-1-carboxylate (2.9e):

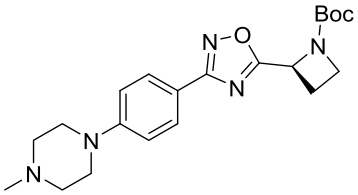

Compound **2.9e** was synthesized from **2.8** and 1-methylpiperazine using general procedure 2.8. The resulting brown residue was purified by flash chromatography over silica gel with 5:95 (v:v) MeOH:DCM to give **2.9e** (88 mg, 47%) as a white-yellow solid. ^{1}H NMR (400 MHz, $CDCl_3$) δ 7.94 (d, *J* = 8.4 Hz, 2H), 6.93 (d, *J* = 8.5 Hz, 2H), 5.37 (dd, *J* = 8.6, 5.5 Hz, 1H), 4.17 (dd, *J* = 8.6, 5.5 Hz, 1H), 4.05–3.96 (m, 1H), 3.37–3.24 (m, 4H), 2.66 (m, 1H), 2.60–2.44 (m, 5H), 2.33 (s, 3H), 1.34 (br s, 9 H); ^{13}C NMR (101 MHz, $CDCl_3$) δ 177.9, 168.4, 153.1, 128.7, 116.7, 114.9, 80.6, 77.5, 77.2, 76.8, 54.9, 47.9, 46.2, 29.1, 28.2, 21.9; HRMS (ESI+): Calcd for $C_{21}H_{30}N_5O_3$ [M+H]: 400.2349, Found: 400.2376.

***tert*-butyl (*S*)-2-(3-(4-hexylphenyl)-1,2,4-oxadiazol-5-yl)azetidine-1-carboxylate (2.9f):**

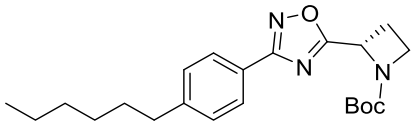

Compound **2.9f** was synthesized from **2.9a** general procedure 2.7. The resulting brown oil was purified on a silica column with 0–20% EtOAc in hexane to yield **2.9a** (83 mg, 89%). ^{1}H NMR (400 MHz, $CDCl_3$) δ 8.06–7.93 (m, 2H), 7.26 (dd, *J* = 8.2, 1.8 Hz, 2H), 5.38 (dd, *J* = 8.8, 5.7 Hz, 1H), 4.17 (ddd, *J* = 9.1, 8.1, 5.8 Hz, 1H), 4.10–3.98 (m, 1H), 2.74–2.58 (m, 3H), 2.56–2.46 (m, 1H), 1.67–1.53 (m, 2H), 1.45–1.17 (m, 14H), 0.89 (t, *J* = 7.1 Hz, 3H). ^{13}C NMR (101 MHz, $CDCl_3$) δ 178.3, 168.7, 146.7, 129.0, 127.5, 124.1, 80.6, 36.1, 31.8, 31.3, 29.0, 28.3, 22.7, 22.0, 14.2.

***tert*-butyl (*S*)-2-(3-(4-decylphenyl)-1,2,4-oxadiazol-5-yl)azetidine-1-carboxylate (2.9g):**

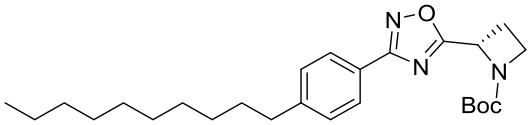

Compound **2.9g** was synthesized from **2.9b** general procedure 2.7. The resulting brown oil was purified on a silica column with 0–20% EtOAc in hexanes to yield **2.9g** (174 mg, 95%). ^{1}H NMR (500 MHz, $CDCl_3$) δ 8.01 (d, *J* = 8.2 Hz, 2H), 7.31–7.26 (m, 2H), 5.15 (s, 1H), 3.77 (d, *J* = 18.7 Hz, 1H), 2.87–2.69 (m, 1H), 2.69–2.60 (m, 2H), 2.48–2.33 (m, 2H), 1.63 (h, *J* = 7.1, 6.6 Hz, 2H), 1.52 (s, 9H), 1.39–1.21 (m, 17H), 0.88 (t, *J* = 7.0 Hz, 3H). ^{13}C NMR (126 MHz, $CDCl_3$) δ 180.7, 179.5, 168.4, 146.5, 128.9, 128.8, 128.7, 127.4, 124.0, 55.3, 36.0, 31.9, 31.2, 29.59, 29.56, 29.49, 29.47, 29.31, 29.26, 26.74, 22.67, 14.1, 11.9.

(*S*)-2-(3-(4-morpholinophenyl)-1,2,4-oxadiazol-5-yl)azetidin-1-ium chloride (2.10d):

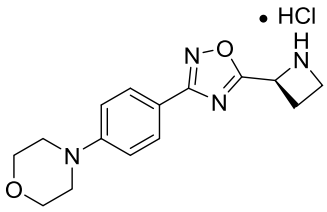

Compound **2.10d** was synthesized from **2.9d** using general procedure 2.5. The organic solvent was then removed under reduced pressure to yield **2.10d** (106.4 mg, 91%) as a yellow solid. ^{1}H NMR (400 MHz, CD_3OD) δ 8.13 (t, *J* = 8.9 Hz, 2H), 7.46 (d, *J* = 8.5 Hz, 2H), 5.94 (t, *J* = 8.5 Hz, 1H), 4.33 (q, *J* = 9.3 Hz, 1H), 4.19 (td, *J* = 9.9, 6.0 Hz, 1H), 4.02–3.93 (m, 5H), 3.54–3.45 (m, 5H), 3.18–3.01 (m, 2H). ^{13}C NMR (101 MHz, CD_3OD) δ 175.3, 169.5, 130.1, 118.9, 66.8, 54.3, 52.1, 46.1, 25.4; HRMS (ESI+): Calcd for $C_{15}H_{19}N_4O_2$ [M+]: 287.1508, Found: 287.1492.

(*S*)-4-(4-(5-(azetidin-1-ium-2-yl)-1,2,4-oxadiazol-3-yl)phenyl)-1-methylpiperazin-1-ium chloride (2.10e):

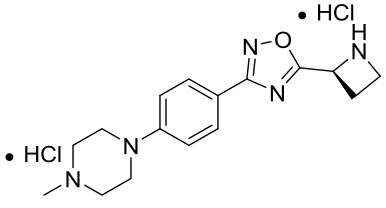

Compound **2.10e** was synthesized from **2.9e** using general procedure 2.5.The organic solvent was then removed under reduced pressure to yield **2.10e** (17 mg, 96%) as an off-white solid. ^{1}H NMR (400 MHz, CD_3OD) δ 8.03 (d, *J* = 7.4 Hz, 2H),

7.18 (d, *J* = 7.9 Hz, 2H), 5.93 (dd, *J* = 7.9 Hz, 1H), 4.32 (dd, *J* = 8.8 Hz, 1H), 4.24–4.14 (m, 1H), 4.06 (d, *J* = 10.9 Hz, 2H), 3.71–3.57 (m, 2H), 3.28 (s, 5H), 3.09 (t, *J* = 8.9 Hz, 1H), 2.98 (s, 3H). ^{13}C NMR (101 MHz, CD_3OD) δ 175.0, 169.7, 153.4, 130.0, 118.7, 117.13, 117.11, 54.5, 54.3, 46.8, 46.2, 43.9, 25.4; HRMS (ESI+): Calcd for $C_{16}H_{23}N_5O$ [M+]: 301.1827, Found: 301.1903

tert-butyl (_S_,_E_)-((2-(3-([1,1'-biphenyl]-4-yl)-1,2,4-oxadiazol-5-yl)azetidin-1-yl)((_tert_-butoxycarbonyl)imino)methyl)carbamate (2.11c):

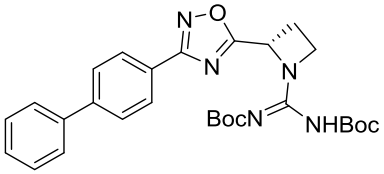

Compound **2.10c** was synthesized from **2.9c** using general procedure 2.5 and carried forward without purification. Compound **2.11c** was synthesized from **2.10c** using general procedure 2.6. The organic solvent was removed under reduced pressure and the residue was purified on a silica gel column to yield **2.11c** (82 mg, 91%). ^{1}H NMR (400 MHz, $CDCl_3$) δ 8.18–8.14 (m, 2H), 7.73–7.69 (m, 2H), 7.66–7.63 (m, 2H), 7.50–7.44 (m, 2H), 7.41–7.36 (m, 1H), 4.65 (d, *J* = 8.5 Hz, 1H), 4.26–4.19 (m, 1H), 4.15–3.94 (m, 1H), 2.92–2.81 (m, 1H), 2.63–2.51 (m, 1H), 1.54–1.20 (m, 18H). ^{13}C NMR (101 MHz, $CDCl_3$) δ 177.4, 168.4, 144.2, 140.2, 129.1, 129.0, 128.12, 128.08, 127.8, 127.7, 127.3, 125.4, 31.7, 28.3, 28.2, 22.8, 22.6, 14.3.

(_S_)-_tert_-butyl (((_tert_-butoxycarbonyl)imino)(2-(3-(4-morpholinophenyl)-1,2,4-oxadiazol-5-yl)azetidin-1-yl)methyl)carbamate (2.11d):

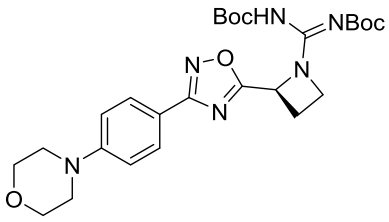

Compound **2.11d** was synthesized from **2.10d** using general procedure 2.6. The organic solvent was removed under reduced pressure and the residue was purified by silica gel column chromatography with 1:2 (v:v) EtOAc:hexanes to yield **2.11d** (45 mg, 66%). ^{1}H NMR (400 MHz, $CDCl_3$) δ 7.98 (d, *J* = 8.4 Hz, 2H), 6.95 (d, *J* = 8.5 Hz, 2H), 6.01 (s, 1H), 4.63 (dd, *J* = 8.7, 8.2 Hz, 1H), 4.19 (td, *J* = 9.4, 5.5 Hz, 1H), 3.87 (dd, *J* = 4.8 Hz,

4H), 3.27 (dd, *J* = 4.8 Hz, 4H), 2.90–2.76 (m, 1H), 2.56 (m, 1H), 1.45 (br s, 18H). ^{13}C NMR (101 MHz, $CDCl_3$) δ 176.9, 168.4, 159.9, 153.3, 128.9, 117.2, 114.7, 80.1, 66.9, 48.3, 28.2, 22.5; HRMS: Calcd for $C_{26}H_{37}N_6O_6$ [M+H]: 529.2775, Found: 529.2795.

(*S*)-*tert*-butyl (((tert-butoxycarbonyl)imino)(2-(3-(4-(4-methylpiperazin-1-yl)phenyl)-1,2,4-oxadiazol-5-yl)azetidin-1-yl)methyl)carbamate (2.11e):

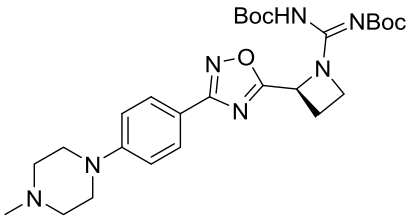

Compound **2.11e** was synthesized from **2.10e** using general procedure 2.6. The organic solvent was removed under reduced pressure and the residue was purified by silica gel column chromatography 1:7 (v:v) EtOAc:hexanes to yield **2.11e** (9 mg, 43%). ^{1}H NMR (400 MHz, $CDCl_3$) δ 10.84 (s, 1H), 7.99–7.92 (m, 2H), 6.99–6.93 (m, 2H), 6.02 (s, 1H), 4.67–4.56 (m, 1H), 4.18 (td, *J* = 9.4, 5.6 Hz, 1H), 3.36–3.30 (m, 4H), 2.90–2.77 (m, 1H), 2.61–2.51 (m, 5H), 2.36 (s, 3H), 1.54–1.37 (m, 18H); ^{13}C NMR (101 MHz, $CDCl_3$) δ 191.2, 176.6, 162.7, 153.4, 128.9, 128.8, 125.5, 115.0, 114.9, 81.8, 78.9, 58.2, 55.0, 48.0, 46.3, 41.1, 31.4, 29.9, 29.2, 28.2, 22.5, 20.9, 20.5; HRMS (ESI+): Calcd for $C_{27}H_{40}N_7O_5$ [M+H]: 542.3091 , Found: 542.3108.

***tert*-butyl (*S,E*)-(((*tert*-butoxycarbonyl)imino)(2-(3-(4-hexylphenyl)-1,2,4-oxadiazol-5-yl)azetidin-1-yl)methyl)carbamate (2.11f):**

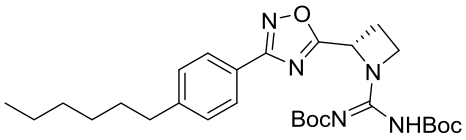

Compound **2.10f** was synthesized from **2.9f** using general procedure 2.5 and carried forward without purification. Compound **2.11f** was synthesized from **2.10f** using general procedure 2.6. The organic solvent was removed under reduced pressure and the residue was purified on a silica column to yield **2.11f** (66 mg, 58%). ^{1}H NMR (400 MHz, $CDCl_3$) δ 7.99 (d, *J* = 8.2 Hz, 2H), 7.25 (d, *J* = 4.8 Hz, 2H), 6.02 (s, 1H), 4.66–4.53 (m, 1H), 4.18 (td, *J* = 9.4,

5.6 Hz, 1H), 2.90–2.75 (m, 1H), 2.64 (t, *J* = 7.9 Hz, 2H), 2.59–2.49 (m, 1H) 1.86–1.57 (m, 3H), 1.45 (s, 18H), 1.36–1.19 (m, 7H), 0.88 (t, *J* = 6.9 Hz, 3H). ^{13}C NMR (101 MHz, $CDCl_3$) δ 177.2, 168.68, 162.8, 155.3, 146.8, 129.0, 127.6, 123.9, 82.4, 80.1, 36.1, 31.8, 31.3, 29.1, 28.2, 22.7, 22.5, 14.2.

tert-butyl (_S_,_E_)-(((_tert_-butoxycarbonyl)imino)(2-(3-(4-decylphenyl)-1,2,4-oxadiazol-5-yl)azetidin-1-yl)methyl)carbamate (2.11g):

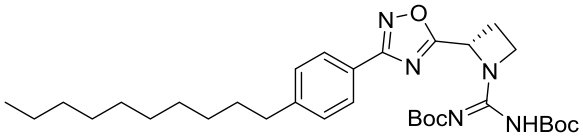

Compound **2.10g** was synthesized from **2.9g** using general procedure 2.5 and carried forward without purification. Compound **2.11g** was synthesized from **2.10g** using general procedure 2.6. The organic solvent was removed under reduced pressure and the residue was purified on a silica column to yield **2.11g** (160 mg, 81%). ^{1}H NMR (400 MHz, $CDCl_3$) δ 7.99 (d, *J* = 8.2 Hz, 3H), 7.29 (d, *J* = 8.2 Hz, 3H), 4.64 (s, 1H), 4.27–4.11 (m, 1H), 2.85 (t, *J* = 9.4 Hz, 1H), 2.69–2.64 (m, 3H), 2.61–2.53 (m, 1H), 1.64 (t, *J* = 7.5 Hz, 2H), 1.55–1.38 (m, 33H), 1.38–1.20 (m, 21H), 0.89 (t, *J* = 6.5 Hz, 3H). ^{13}C NMR (101 MHz, $CDCl_3$) δ 168.56, 162.68, 157.36, 146.70, 142.77, 139.15, 128.94, 127.52, 123.84, 109.84, 83.31, 82.46, 81.34, 79.77, 36.00, 31.93, 31.25, 29.63, 29.61, 29.51, 29.36, 29.28, 28.23, 28.13, 28.03, 27.94, 22.72, 22.43, 14.16.

(_S_)-(2-(3-([1,1'-biphenyl]-4-yl)-1,2,4-oxadiazol-5-yl)azetidin-1-yl)(amino)methaniminium chloride (2.12c):

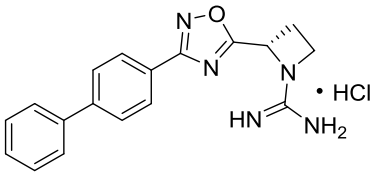

Compound **2.12c** was synthesized from **2.11c** using general procedure 2.5. The organic solvent was then removed under reduced pressure to yield **2.12c** (17 mg, 78%). ^{1}H NMR (400 MHz, CD_3OD) δ 8.21 (d, *J* = 8.4 Hz, 2H), 7.85 (d, *J* = 8.3 Hz, 2H), 7.73 (d, *J* = 7.3 Hz, 2H), 7.52 (t, *J* = 7.5 Hz, 3H), 7.43 (t, *J* = 7.3 Hz, 1H), 5.91 (dd, *J* = 9.4, 5.3 Hz, 1H), 4.47–4.40 (m, 1H),

4.36–4.28 (m, 1H), 3.20–3.07 (m, 1H), 2.79–2.65 (m, 1H). ^{13}C NMR (101 MHz, CD_3OD) δ 176.9, 168.2, 157.2, 144.3, 139.8, 129.3, 128.5, 128.0, 127.7, 127.4, 127.1, 126.8, 126.1, 124.9, 85.0, 57.1, 26.6, 21.5. HRMS (ESI+): Calcd for $C_{18}H_{17}N_5O$ [M+H]: 320.1506, Found: 320.1497.

(*S*)-amino(2-(3-(4-morpholinophenyl)-1,2,4-oxadiazol-5-yl)azetidin-1-yl)methaniminium chloride (2.12d):

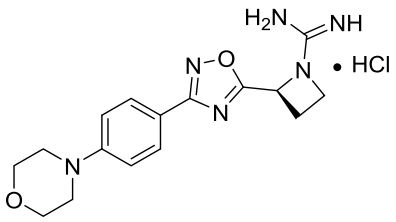

Compound **2.12d** was synthesized from **2.11d** using general procedure 2.5. The organic solvent was then removed under reduced pressure to yield **2.12d** (17 mg, 78%) as a white solid. ^{1}H NMR (400 MHz, CD_3OD) δ 7.95 (d, *J* = 8.9 Hz, 2H), 7.06 (d, *J* = 8.9 Hz, 2H), 5.80 (dd, *J* = 9.4, 5.2 Hz, 1H), 4.37 (m, 1H), 4.26 (m, 1H), 3.86–3.82 (m, 4H), 3.30–3.26 (m, 4H), 3.10–3.00 (m, 1H), 2.62 (m, 1H).; ^{13}C NMR (101 MHz, CD_3OD) δ 177.8, 169.7, 158.6, 155.1, 129.6, 117.6, 115.8, 67.8, 58.4, 50.8, 22.9. HRMS (ESI+): Calcd for $C_{16}H_{21}N_6O_2$ [M+H]: 329.1729, Found: 329.1719.

(*S*)-4-(4-(5-(1-(amino(iminio)methyl)azetidin-2-yl)-1,2,4-oxadiazol-3-yl)phenyl)-1-methylpiperazin-1-ium chloride (2.12e):

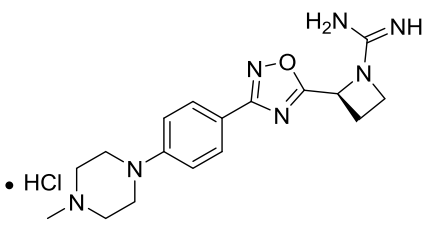

Compound **2.12e** was synthesized from **2.11e** using general procedure 2.5. The organic solvent was then removed under reduced pressure to yield **2.12e** (7 mg, 83%) as a white solid. ^{1}H NMR (400 MHz, CD_3OD) δ 7.94 (d, *J* = 8.9 Hz, 2H), 7.07 (d, *J* = 8.9 Hz, 2H), 5.80 (m, 1H), 4.37 (m, 1H), 4.26 (m, 1H), 3.38–3.34 (m, 9H), 3.05 (dtd, *J* = 11.6, 9.4, 6.2 Hz, 1H), 2.67–2.61 (m, 5H), 2.38 (s, 3H); ^{13}C NMR (126 MHz, CD_3OD) δ 177.3, 167.5, 157.2, 146.5, 129.0, 125.0, 120.0, 64.6, 57.1, 53.1, 49.6, 21.6; HRMS (ESI+): Calcd for $C_{17}H_{25}N_7O$ [M+H]: 343.2121, Found: 343.2027.

(*S*)-amino(2-(3-(4-hexylphenyl)-1,2,4-oxadiazol-5-yl)azetidin-1-yl)methaniminium chloride (2.12f):

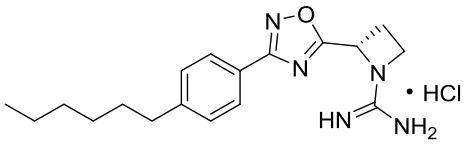

Compound **2.12f** was synthesized from **2.11f** using general procedure 2.5. The organic solvent was removed under reduced pressure to yield **2.12f** (33 mg, 73%). ^{1}H NMR (400 MHz, CD_3OD) δ 7.98 (d, *J* = 8.1 Hz, 2H), 7.35 (d, *J* = 8.1 Hz, 2H), 5.85 (dd, *J* = 9.4, 5.2 Hz, 1H), 4.38 (q, *J* = 8.5 Hz, 1H), 4.32–4.23 (m, 1H), 3.12–3.01 (m, 1H), 2.72–2.58 (m, 3H), 1.70–1.60 (m, 2H), 0.89 (t, *J* = 6.8 Hz, 3H). ^{13}C NMR (101 MHz, CD_3OD) δ 178.2, 169.8, 158.6, 148.4, 130.2, 128.4, 124.9, 58.4, 50.9, 36.9, 32.8, 32.4, 30.0, 28.1, 23.7, 23.6, 23.0, 14.4. HRMS (ESI+): Calcd for $C_{18}H_{25}N_5O$ [M+H]: 328.2132, Found: 328.2743.

(*S*)-amino(2-(3-(4-decylphenyl)-1,2,4-oxadiazol-5-yl)azetidin-1-yl)methaniminium chloride (2.12g):

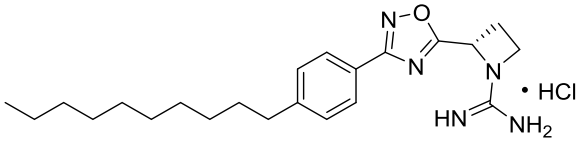

Compound **2.12g** was synthesized from **2.11g** using general procedure 2.5. The organic solvent was removed under reduced pressure to yield **2.12g** (90 mg, 80%). ^{1}H NMR (400 MHz, CD_3OD) δ 7.95 (d, *J* = 8.0 Hz, 2H), 7.31 (d, *J* = 7.9 Hz, 2H), 5.85 (dd, *J* = 8.8, 5.2 Hz, 1H), 4.36 (q, *J* = 7.9 Hz, 1H), 4.31–4.22 (m, 1H), 3.05 (dt, *J* = 17.5, 9.4 Hz, 1H), 2.68–2.57 (m, 3H), 1.62 (s, 2H), 1.38–1.20 (m, 14H), 0.86 (t, *J* = 6.7 Hz, 3H). ^{13}C NMR (101 MHz, CD_3OD) δ 178.2, 169.8, 158.5, 148.3, 130.1, 128.2, 124.9, 58.4, 51.0, 36.8, 33.0, 32.4, 30.7, 30.5, 30.4, 30.3, 23.7, 23.0, 14.5. HRMS (ESI+): Calcd for $C_{22}H_{33}N_5O$ [M+H]: 384.2758, Found: 384.2764.

***tert*-butyl (*S*)-2-(3-(4-(piperazin-1-yl)phenyl)-1,2,4-oxadiazol-5-yl)azetidine-1-carboxylate (2.13a):**

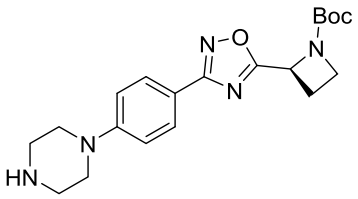

Compound **2.13a** was synthesized from **2.8** with piperazine using general procedure 2.8. The resulting brown residue was purified by flash chromatography over silica gel with 5–20% MeOH in DCM to give the desired compound **2.13a** (32 mg, 40%) as a beige solid. ^{1}H NMR (400 MHz, $CDCl_3$) δ 7.97 (d, *J* = 8.8 Hz, 2H), 6.96 (d, *J* = 8.8 Hz, 2H), 5.40 (dd, *J* = 8.8, 5.7 Hz, 1H), 4.25–4.15 (m, 1H), 4.08–3.99 (m, 1H), 3.27 (dd, 4H), 3.04 (dd, 4H), 2.75–2.65 (m, 1H), 2.59–2.47 (m, 1H), 1.35 (s, 9H); ^{13}C NMR (101 MHz, $CDCl_3$) δ 177.8, 168.3, 153.2, 128.7, 117.1, 115.1, 80.5, 55.3, 48.5, 45.5, 29.7, 28.2, 21.9; HRMS (ESI+): Calcd for $C_{20}H_{28}N_5O_3$ [M+H]: 386.2192, Found: 386.2202.

***tert*-butyl (*S*)-2-(3-(4-(piperazin-1-yl)phenyl)-1,2,4-oxadiazol-5-yl)pyrrolidine-1-carboxylate (2.13b)**

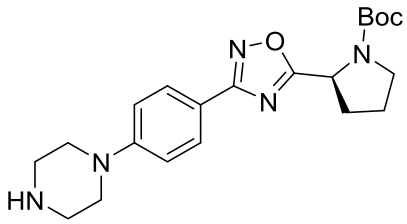

Compound **2.13b** was synthesized from **2.3a** with piperazine using general procedure 2.8. The resulting brown residue was purified by flash chromatography over silica gel with 5–20% MeOH in DCM to give the desired compound **2.13b** (36 mg, 50%) as an off-white solid. ^{1}H NMR (400 MHz, $CDCl_3$) δ 7.93 (d, 2H), 6.94 (d, *J* = 8.5 Hz, 2H), 5.19 – 4.96 (m, 1H), 4.59 (s, 1H), 3.79–3.59 (m, 1H), 3.56–3.40 (m, 1H), 3.33 (dd, 4H), 3.11 (dd, *J* = 5.0 Hz, 4H), 2.45–2.28 (m, 1H), 2.20–2.05 (m, 2H), 2.02–1.90 (m, 1H), 1.43 (s, 3H), 1.27 (s, 6H); ^{13}C NMR (101 MHz, $CDCl_3$) δ 180.2, 168.1, 153.1, 128.7, 117.4, 115.2, 80.5, 53.9, 48.3, 46.4, 45.3, 32.4, 29.8, 28.5, 28.3, 23.8; HRMS (ESI+): Calcd for $C_{21}H_{30}N_5O_3$ [M+H]: 400.2349, Found: 400.2352.

***tert*-butyl (*S*)-2-(3-(4-(4-(3-methylbutanoyl)piperazin-1-yl)phenyl)-1,2,4-oxadiazol-5-yl)pyrrolidine-1-carboxylate (2.14a):**

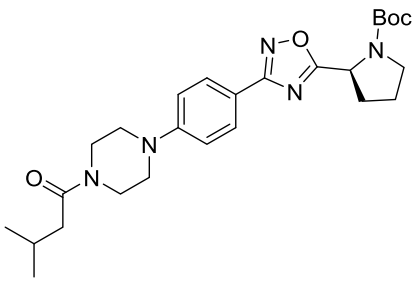

Compound **2.14a** was synthesized using general procedure 2.10 and isovaleryl chloride as starting material. The residue was purified by silica gel column chromatography with 30–50% EtOAc in hexane to yield **2.14a** (19 mg, 86%) as a beige oily solid. ^{1}H NMR (2:1 rotamer ration, asterisk indicates minor rotamer peak, 400 MHz, $CDCl_3$) δ 7.97 (d, *J* = 8.5 Hz, 2H), 6.95 (d, *J* = 8.3 Hz, 2H), 5.18* (d, J = 8.2 Hz, 1H), 5.05–5.00 (m, 1H), 3.85–3.75 (m, 2H), 3.77–3.61 (m, 2H), 3.60–3.43 (m, 1H), 3.34–3.24 (m, 4H), 2.47–2.30 (m, 1H), 2.26 (d, *J* = 7.0 Hz, 2H), 2.22–2.06 (m, 2H), 2.05–1.92 (m, 1H), 1.46* (s, 3H), 1.29 (s, 6H), 0.99 (d, *J* = 6.5 Hz, 6H); ^{13}C NMR (2:1 rotamer ration, asterisk indicates minor rotamer peak, 101 MHz, $CDCl_3$) δ 180.3, 171.3, 168.2, 152.8, 128.9, 117.8, 115.5, 80.5, 54.0, 48.6*, 48.4, 46.5, 45.6, 42.2, 41.3, 32.5, 28.6*, 28.3, 26.0, 24.5*, 23.8, 22.9; HRMS (ESI+): Calcd for $C_{26}H_{38}N_5O_4$ [M+H]: 484.2924, Found: 484.2887.

***tert*-butyl (*S*)-2-(3-(4-(4-((3*r*,5*r*,7*r*)-adamantane-1-carbonyl)piperazin-1-yl)phenyl)-1,2,4-oxadiazol-5-yl)pyrrolidine-1-carboxylate (2.14b):**

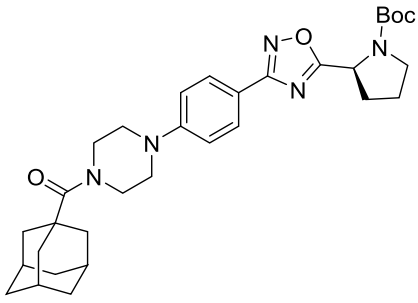

Compound **2.14b** was synthesized using general procedure 2.10 and adamantanecarbonyl chloride as starting material. The residue was purified by silica gel column chromatography with 33% EtOAc in hexanes to yield **2.14b** (17 mg, 68%) as a yellow oily solid. ^{1}H NMR (2:1 rotamer ration, asterisk indicates minor rotamer peak, 400 MHz, $CDCl_3$) δ 7.96 (d, 2H), 6.95 (d, *J* = 8.2 Hz, 2H), 5.18* (d, *J* = 8.2 Hz, 1H), 5.04 (dd, *J* = 8.1, 3.7 Hz,, 1H), 3.86 (dd, 4H), 3.70 (tt, *J* = 17.9, 8.8 Hz, 1H),

3.60–3.42 (m, 1H), 3.28 (dd, *J* = 5.0 Hz, 4H), 2.45–2.28 (m, 1H), 2.21–2.11 (m, 2H), 2.07–1.95 (m, 9H), 1.80–1.68 (m, 7H), 1.46* (s, 3H), 1.29 (s, 6H); ^{13}C NMR (101 MHz, $CDCl_3$) δ 191.6, 180.3, 176.0, 168.2, 152.9, 128.8, 117.6, 115.2, 80.5, 54.0, 48.6, 46.5, 45.1, 41.9, 39.3, 36.8, 36.7, 32.5, 28.6, 28.3, 28.1, 23.8; HRMS (ESI+): Calcd for $C_{32}H_{44}N_5O_4$ [M+H]: 562.3393, Found: 562.3384.

***tert*-butyl (*S*)-2-(3-(4-(4-(2-phenylacetyl)piperazin-1-yl)phenyl)-1,2,4-oxadiazol-5-yl)pyrrolidine-1-carboxylate (2.14c):**

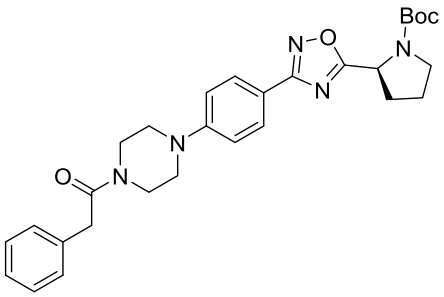

Compound **2.14c** was synthesized using general procedure 2.10 and phenylacetal chloride as the starting material. The residue was purified by silica gel column chromatography with 30–50% EtOAc in hexanes to yield **2.14c** (18 mg, 67 %) as a beige oily solid. ^{1}H NMR (2:1 rotamer ration, asterisk indicates minor rotamer peak, 400 MHz, $CDCl_3$) δ 7.92 (d, 2H), 7.34–7.27 (m, 2H), 7.27–7.20 (m, 3H), 6.88 (d, *J* = 8.3 Hz, 2H), 5.29–5.13* (m, 1H), 5.02 (dd, *J* = 8.0, 3.3 Hz, 1H), 3.85–3.75 (m, 3H), 3.73–3.40 (m, 4H), 3.29–3.19 (m, 2H), 3.12–3.02 (m, 2H), 2.44–2.24 (m, 1H), 2.20–2.04 (m, 2H), 2.02–1.91 (m, 1H), 1.44* (s, 3H), 1.27 (s, 6H); ^{13}C NMR (2:1 rotamer ration, asterisk indicates minor rotamer peak, 101 MHz, $CDCl_3$) δ 180.3, 169.8, 168.1, 153.7, 152.7, 134.9, 129.5, 129.0, 128.8, 128.69, 128.65, 128.5, 127.3, 127.1, 117.8, 115.4, 80.6, 54.0, 48.3, 48.1, 46.5, 45.9, 41.6, 41.2, 32.5, 28.5*, 28.3, 24.5*, 23.8; HRMS (ESI+): Calcd for $C_{29}H_{36}N_5O_4$ [M+H]: 518.2767, Found: 518.2812.

***tert*-butyl (*S*)-2-(3-(4-(4-benzylpiperazin-1-yl)phenyl)-1,2,4-oxadiazol-5-yl)azetidine-1-carboxylate (2.14d):**

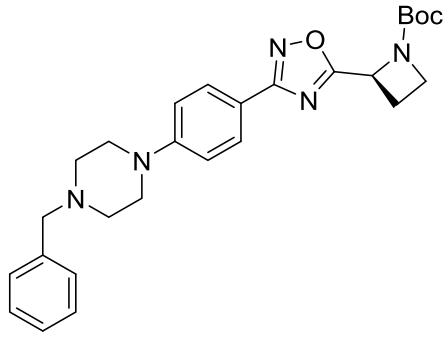

Compound **2.14d** was synthesized from **2.8** and benzylbromide using general procedure 2.9. The resulting brown residue was purified by flash chromatography over silica gel with 50–70% EtOAc in hexanes to yield **2.14d** (20 mg, 49%) as an off-white solid. ^{1}H NMR (400 MHz, $CDCl_3$) δ 7.96 (d, *J* = 8.4 Hz, 2H), 7.38–7.31 (m, 4H), 7.30–7.27 (m, 1H), 6.94 (d, *J* = 8.5 Hz, 2H), 5.39 (dd, *J* = 8.8, 5.6 Hz, 1H), 4.25–4.15 (m, 1H), 4.08–3.98 (m, 1H), 3.58 (s, 2H), 3.36–3.29 (m, 4H), 2.75–2.47 (m, 6H), 1.35 (s, 9H); ^{13}C NMR (101 MHz, $CDCl_3$) δ 177.9, 168.5, 153.3, 129.3, 128.8, 128.5, 127.4, 114.9, 80.7, 63.2, 53.0, 48.1, 28.3, 22.0; HRMS (ESI+): Calcd for $C_{27}H_{34}N_5O_3$ [M+H]: 476.2662, Found: 476.2644.

***tert*-butyl (*S,E*)-(((*tert*-butoxycarbonyl)imino)(2-(3-(4-(4-(3-methylbutanoyl)piperazin-1-yl)phenyl)-1,2,4-oxadiazol-5-yl)pyrrolidin-1-yl)methyl)carbamate (2.16a):**

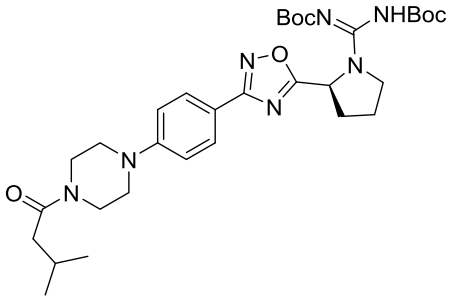

Compound **2.15a** was synthesized from **2.14a** using general procedure 2.10 and carried forward without purification. Compound **2.16a** was synthesized from **2.15a** using general procedure 2.7. The residue was purified by silica gel column chromatography with 50% EtOAc in hexanes to yield **2.16a** (10 mg, 43%) as an off-white oily solid. ^{1}H NMR (500 MHz, $CDCl_3$) δ 7.96 (d, *J* = 8.4 Hz, 2H), 6.94 (dd, 2H), 5.57 (dd, *J* = 7.6, 4.5 Hz, 1H), 3.90–3.84 (m, 1H), 3.83–3.75 (m, 3H), 3.66 (dd, 2H), 3.33–3.25 (m, 4H), 2.47–2.37 (m, 1H), 2.26 (d, *J* = 7.0 Hz, 2H), 2.19–2.10 (m, 2H), 2.07–1.98 (m, 1H), 1.45 (s, 18H), 0.99 (d, *J* = 6.6 Hz, 6H); ^{13}C NMR (101 MHz,

$CDCl_3$) δ 178.4, 171.4, 168.2, 153.5, 152.8, 132.0, 129.0, 128.8, 128.4, 125.4, 117.6, 115.4, 81.4, 55.6, 49.8, 48.6, 48.3, 45.6, 42.2, 41.4, 35.1, 31.5, 28.3, 28.1, 26.0, 24.1, 22.9; MS: Calcd for $C_{32}H_{48}N_7O_6$ [M+H]: 626.3666, Found: 626.3685.

***tert*-butyl ((*E*)-((*S*)-2-(3-(4-(4-((3*r*,5*r*,7*r*)-adamantane-1-carbonyl)piperazin-1-yl)phenyl)-1,2,4-oxadiazol-5-yl)pyrrolidin-1-yl)((*tert*-butoxycarbonyl)imino)methyl)carbamate (2.16b):**

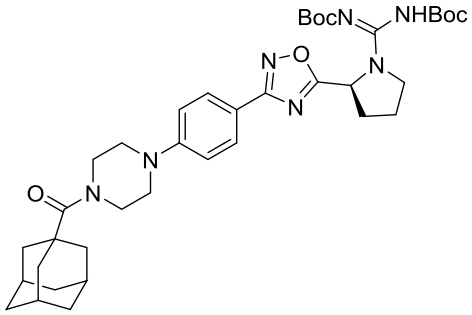

Compound **2.15b** was synthesized from **2.14b** using general procedure 2.10 and carried forward without purification. Compound **2.16b** was synthesized from **2.15b** using general procedure 2.6. The residue was purified by silica gel column chromatography with 50% EtOAc in hexanes to yield **2.16b** (10 mg, 26%) as a yellow oily solid. ^{1}H NMR (500 MHz, $CDCl_3$) δ 7.96 (d, *J* = 8.4 Hz, 2H), 6.94 (d, *J* = 8.4 Hz, 2H), 5.58 (dd, *J* = 7.5, 4.4 Hz, 1H), 3.87 (dd, 5H), 3.81 (q, *J* = 6.4, 5.7 Hz, 1H), 3.29 (dd, *J* = 5.0 Hz, 4H), 2.47–2.38 (m, 1H), 2.29–2.22 (m, 1H), 2.21–2.12 (m, 1H), 2.09–2.00 (m, 10H), 1.78–1.68 (m, 6H), 1.46 (s, 18H); ^{13}C NMR (101 MHz, $CDCl_3$) δ 178.6, 176.0, 175.7, 168.5, 168.2, 152.9, 128.9, 117.6, 115.2, 114.8, 103.7, 80.9, 55.4, 49.6, 48.5, 45.1, 44.8, 41.9, 39.3, 38.8, 36.8, 36.6, 31.6, 31.5, 31.2, 29.8, 29.4, 29.1, 28.6, 28.3, 27.8, 27.2, 24.1; HRMS: Calcd for $C_{38}H_{54}N_7O_6$ [M+H]: 704.4136, Found: 704.4191.

***tert*-butyl (*S*,*E*)-(((*tert*-butoxycarbonyl)imino)(2-(3-(4-(4-(2-phenylacetyl)piperazin-1-yl)phenyl)-1,2,4-oxadiazol-5-yl)pyrrolidin-1-yl)methyl)carbamate (2.16c):**

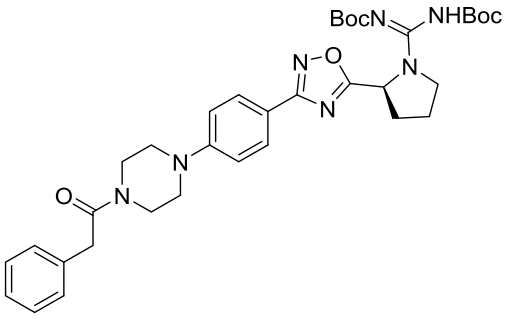

Compound **2.15c** was synthesized from **2.14c** using general procedure 2.10 and carried forward without purification. Compound **2.16c** was synthesized from **2.15c** using general procedure 2.6. The residue was purified by silica gel column chromatography (50% EtOAc in hexane) to yield the **2.16c** (12 mg, 74%) as an off-white oily solid. ^{1}H NMR (500 MHz, $CDCl_3$) δ 10.22–10.05 (m, 1H), 7.97–7.89 (m, 2H), 7.33 (dd, *J* = 8.3, 6.9 Hz, 2H), 7.27 (d, *J* = 6.6 Hz, 3H), 6.93–6.81 (m, 2H), 5.56 (dd, *J* = 6.1 Hz, 1H), 3.91–3.73 (m, 6H), 3.61 (dd, 2H), 3.27 (dd, *J* = 5.3 Hz, 2H), 3.10 (dd, *J* = 5.1 Hz, 2H), 2.47–2.38 (m, 1H), 2.29–2.11 (m, 2H), 2.07–1.98 (m, 1H), 1.46 (s, 18H); ^{13}C NMR (126 MHz, $CDCl_3$) δ 178.6, 169.7, 168.2, 153.8, 152.7, 135.0, 129.0, 128.7, 128.5, 127.8, 127.1, 117.73, 115.65, 115.4, 115.0, 114.8, 100.4, 100.1, 82.3, 79.8, 63.2, 55.4, 49.6, 48.3, 48.1, 45.9, 41.9, 41.6, 41.3, 31.7, 31.45, 28.3, 28.0; MS: Calcd for $C_{35}H_{46}N_7O_6$ [M+H]: 660.3510, Found: 660.3520.

***tert*-butyl (*S*,*Z*)-((2-(3-(4-(4-benzylpiperazin-1-yl)phenyl)-1,2,4-oxadiazol-5-yl)azetidin-1-yl)((*tert*-butoxycarbonyl)imino)methyl)carbamate: (2.16d)**

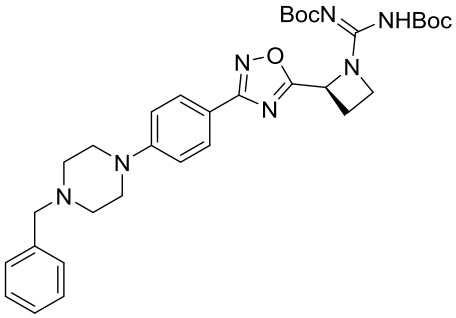

Compound **2.15d** was synthesized from **2.14d** using general procedure 2.10 and carried forward without purification. Compound **2.16d** was synthesized from **2.15d** using general procedure 2.6. The residue was purified by silica gel column chromatography with 33% EtOAc in hexanes to yield **2.16d** (13 mg, 44%) as a yellow oily solid.^{1}H NMR (400 MHz, $CDCl_3$) δ

10.91–10.74 (m, 1H), 7.94 (d, *J* = 8.4 Hz, 2H), 7.39–7.31 (m, 4H), 7.30–7.27 (m, 1H), 6.94 (d, *J* = 8.5 Hz, 2H), 6.07–5.92 (m, 1H), 4.68–4.56 (m, 1H), 4.23–4.10 (m, 1H), 3.58 (s, 2H), 3.32 (dd, *J* = 5.0 Hz, 4H), 2.89–2.74 (m, 1H), 2.66–2.49 (m, 5H), 1.45 (s, 18H); ^{13}C NMR (101 MHz, $CDCl_3$) δ 176.7, 168.5, 162.8, 153.3, 138.0, 129.3, 129.5, 128.9, 128.7, 128.5, 127.4, 116.6, 114.9, 82.5, 79.9, 63.2, 53.0, 48.1, 28.2, 28.1, 22.5; MS: Calcd for $C_{33}H_{44}N_7O_5$ [M+H]: 618.3404, Found: 618.3431.

(*S*)-amino(2-(3-(4-(4-(3-methylbutanoyl)piperazin-1-yl)phenyl)-1,2,4-oxadiazol-5-yl)pyrrolidin-1-yl)methaniminium chloride (2.17a):

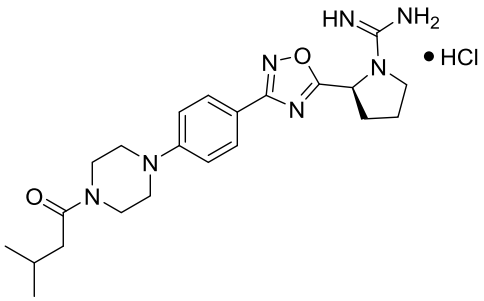

Compound **2.17a** was synthesized from **2.16a** using general procedure 2.5. The organic solvent was then removed under reduced pressure to yield **2.17a** (7 mg, 88%) as a white solid. ^{1}H NMR (400 MHz, CD_3OD) δ 8.03 (d, *J* = 8.0 Hz, 2H), 7.31 (d, *J* = 8.4 Hz, 2H), 5.47 (d, *J* = 7.4 Hz, 1H), 3.91–3.77 (m, 6H), 3.65 (q, *J* = 9.3 Hz, 1H), 3.48 (dt, *J* = 18.2, 4.2 Hz, 4H), 3.34 (dt, *J* = 3.3, 1.7 Hz, 4H), 2.66–2.45 (m, 2H), 2.39 (d, *J* = 7.0 Hz, 2H), 2.26 (q, *J* = 6.3 Hz, 1H), 2.19–2.06 (m, 1H), 1.03 (d, *J* = 6.5 Hz, 6H).; ^{13}C NMR (101 MHz, CD_3OD) δ 175.8, 173.4, 169.4, 152.2, 130.0, 120.5, 118.6, 55.7, 51.2, 50.8, 47.4, 46.1, 42.7, 41.9, 30.2, 27.0, 24.5, 22.9; HRMS (ESI+): Calcd for $C_{22}H_{32}N_7O_2^+$ [M+H]: 426.2617, Found: 426.2617.

((*S*)-2-(3-(4-(4-((3*r*,5*r*,7*r*)-adamantane-1-carbonyl)piperazin-1-yl)phenyl)-1,2,4-oxadiazol-5-yl)pyrrolidin-1-yl)(amino)methaniminium chloride (2.17b):

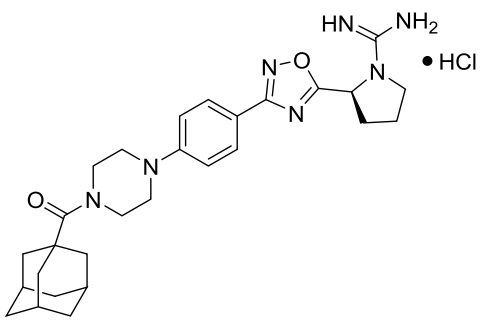

Compound **2.17b** was synthesized from **2.16b** using general procedure 2.5 under reduced pressure to yield **2.17b** (7 mg, 91%) as an off-white solid. ^{1}H NMR (500 MHz, CD_3OD) δ 7.94–7.89 (m, 2H), 7.09–7.04 (m, 2H), 5.40 (dd, *J* = 8.0, 1.9 Hz, 1H), 3.88 (t, *J* = 5.1 Hz, 4H), 3.80–3.73 (m, 1H), 3.60 (td, *J* = 9.7, 7.2 Hz, 1H), 3.34–3.31 (m, 4H), 2.59–2.43 (m, 2H), 2.26–2.17 (m, 1H), 2.05 (s, 10H), 1.80 (s, 6H).; ^{13}C NMR (126 MHz, CD_3OD) δ 178.4, 178.0, 169.6, 157.1, 154.6, 129.6, 117.7, 116.1, 56.4, 46.3, 43.0, 40.1, 37.6, 32.7, 30.0, 24.3.; HRMS (ESI+): Calcd for $C_{28}H_{38}N_7O_2^+$ [M+H]: 504.3087, Found: 504.3059.

(*S*)-amino(2-(3-(4-(4-(2-phenylacetyl)piperazin-1-yl)phenyl)-1,2,4-oxadiazol-5-yl)pyrrolidin-1-yl)methaniminium chloride (2.17c):

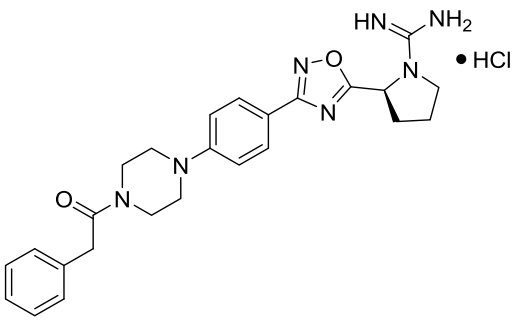

Compound **2.17c** was synthesized from **2.16c** using general procedure 2.5 under reduced pressure to yield **2.17b** (9 mg, 92%) as a white solid. ^{1}H NMR (500 MHz, CD_3OD) δ 7.94 (d, *J* = 8.6 Hz, 2H), 7.36–7.21 (m, 5H), 7.12 (d, *J* = 8.6 Hz, 2H), 5.40 (d, *J* = 7.4 Hz, 1H), 3.84 (s, 2H), 3.81 (t, *J* = 5.2 Hz, 2H), 3.75 (d, *J* = 6.7 Hz, 3H), 3.52–5.68 (m, 2H), 3.35 (q, *J* = 6.0, 5.2 Hz, 3H), 3.22 (d, *J* = 4.9 Hz, 2H), 2.53 (dd, *J* = 12.8, 6.6 Hz, 1H), 2.44 (dd, *J* = 13.2, 6.4 Hz, 1H), 2.25–2.16 (m, 1H), 2.11–2.02 (m, 1H).; ^{13}C NMR (126 MHz, CD_3OD) δ 178.6, 172.3, 169.4, 157.0, 153.7, 153.3, 136.3, 129.9, 129.83, 129.76, 128.0, 119.3, 119.1, 117.2,

117.0, 56.5, 50.0, 49.6, 46.7, 46.6, 44.6, 42.5, 41.3, 32.7, 24.3.HRMS (ESI+): Calcd for $C_{25}H_{30}N_7O_2^+$ [M+H]: 460.2461, Found: 460.2477.

(*S*)-4-(4-(5-(1-(amino(iminio)methyl)azetidin-2-yl)-1,2,4-oxadiazol-3-yl)phenyl)-1-benzylpiperazin-1-ium chloride (2.17d):

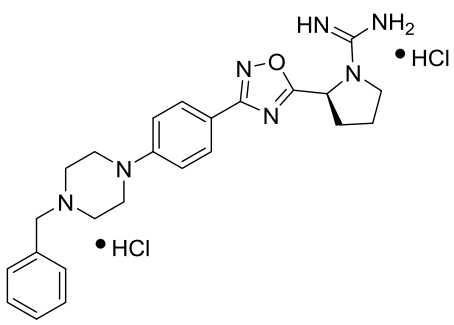

Compound **2.17d** was synthesized from **2.16d** using general procedure 2.5. The organic solvent was then removed under reduced pressure to yield **2.17d** (8 mg, 97 %) as an off-white solid. ^{1}H NMR (400 MHz, CD_3OD) δ 8.05–7.99 (m, 2H), 7.65 (dd, *J* = 6.5, 3.0 Hz, 2H), 7.58–7.52 (m, 3H), 7.18 (d, *J* = 8.7 Hz, 2H), 5.85 (dd, *J* = 9.4, 5.2 Hz, 1H), 4.48 (s, 2H), 4.40 (td, *J* = 8.9, 6.1 Hz, 1H), 4.30 (ddd, *J* = 9.4, 8.2, 5.8 Hz, 1H), 4.08 (d, *J* = 13.2 Hz, 2H), 3.68–3.58 (m, 2H), 3.31–3.22 (m, 2H), 3.18–3.04 (m, 1H), 2.76–2.60 (m, 1H); ^{13}C NMR (101 MHz, CD_3OD) δ 178.0, 169.5, 158.6, 153.3, 132.6, 131.4, 130.4, 130.0, 129.7, 119.1, 117.0, 61.6, 58.5, 52.6, 50.9, 46.6, 23.0. HRMS (ESI+): Calcd for $C_{23}H_{29}N_7O^{2+}$ [M+2H]: 209.62115, Found: 209.6207

1-(bromomethyl)-3-(ethoxymethyl)-5-methylbenzene (2.19):

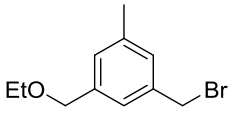

EtOH was added to a suspension of hexane washed NaI at 0 °C. the resulting mixture progressed from a cloudy white suspension to clear. Once the solution was clear, **2.18** was added and the reaction was allowed to warm to room temperature. After stirring for 18 h an aqueous workup was performed and the resulting oil was purified on a silica column in 0–10% EtOAc in hexanes to yield **2.19** (400 mg, 91%). ^{1}H NMR (400 MHz, $CDCl_3$) δ 7.16 (s, 1H), 7.11 (s, 1H), 7.09 (s, 1H), 4.45 (s, 4H), 3.54 (q, *J* = 7.0 Hz, 2H), 2.33 (s, 3H), 1.25 (t, *J* = 7.0, Hz, 3H). ^{13}C NMR (101 MHz, $CDCl_3$) δ 139.2, 138.6, 137.7, 129.8, 128.9, 128.5, 125.3, 72.3, 65.9, 33.6, 33.0, 21.2, 15.2.

4-(3-(ethoxymethyl)-5-methylbenzyl)benzonitrile (2.20):

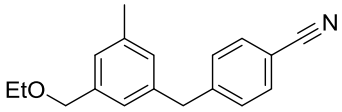

Compound **2.19** (0.2 g, 0.823 mmol) as a solution in 3 mL THF was added to a solution of (4-cyanophenyl)boronic acid (0.133 g, 0.905 mmol) and Na_2CO_3 (0.349 g, 3.29 mmol), in 5 mL water and 2 mL THF. This mixture was degassed with Ar for 15 min. and $Pd(PPh_3)_4$ (0.048 g, 0.041 mmol) was added in a single portion. The resulting orange solution was degassed with Ar for an additional 5 min., after which it was refluxed overnight. The following morning, the black colored solution was partitioned between water and EtOAc. The organic layer was washed with water, brine, dried over Na_2SO_4 and concentrated. Purification on a silica column with 0–20% EtOAc in hexanes yielded **2.20** (206 mg, 94%). ^{1}H NMR (500 MHz, $CDCl_3$) δ 7.57–7.54 (m, 2H), 7.31–7.27 (m, 2H), 7.06 (td, *J* = 1.6, 0.9 Hz, 1H), 6.98–6.95 (m, 1H), 6.91–6.88 (m, 1H), 4.44 (s, 2H), 3.99 (s, 2H), 3.55 (q, *J* = 7.0 Hz, 2H), 2.32 (d, *J* = 0.8 Hz, 3H), 1.25 (t, *J* = 7.0 Hz, 3H). ^{13}C NMR (126 MHz, $CDCl_3$) δ 146.8, 139.4, 139.1, 138.5, 132.3, 129.7, 128.9, 126.8, 125.4, 119.0, 110.0, 72.6, 65.9, 41.9, 21.3, 15.3.

4-(3-(ethoxymethyl)-5-methylbenzyl)-*N'*-hydroxybenzimidamide (2.21):

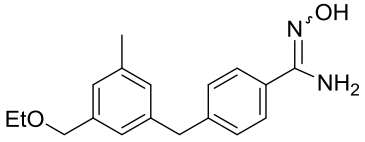

Compound **2.21** was synthesized from **2.20** using general procedure 2.3. Purification on a silica column yielded **2.21** (210 mg, 93%). ^{1}H NMR (500 MHz, $CDCl_3$) δ 7.58–7.53 (m, 2H), 7.24–7.19 (m, 2H), 7.04 (s, 1H), 6.99 (d, *J* = 1.9 Hz, 1H), 6.92 (d, *J* = 1.7 Hz, 1H), 4.93 (s, 2H), 4.45 (s, 2H), 3.96 (s, 2H), 3.55 (q, *J* = 7.0 Hz, 2H), 2.32 (s, 3H), 1.26 (t, *J* = 7.0 Hz, 3H). ^{13}C NMR (126 MHz, $CDCl_3$) δ 152.6, 143.2, 140.6, 138.7, 138.3, 130.3, 129.2, 129.0, 126.6, 126.0, 125.5, 72.7, 65.9, 41.6, 21.4, 15.3.

***tert*-butyl (*S*)-2-(3-(4-(3-(ethoxymethyl)-5-methylbenzyl)phenyl)-1,2,4-oxadiazol-5-yl)pyrrolidine-1-carboxylate (2.22):**

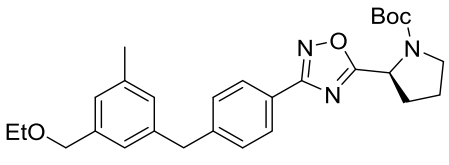

Compound **2.22** was synthesized from **2.21** and Boc-*L*-proline using general procedure 2.4. Purification on a silica column yielded **2.22** (175 mg, 82%). ^{1}H NMR (2:1 rotamer ratio, asterisk indicates minor rotamer peak, 400 MHz, $CDCl_3$) δ 7.98 (d, *J* = 8.2 Hz, 2H), 7.30 (d, *J* = 8.1 Hz, 2H), 7.02 (s, 1H), 6.98 (s, 1H), 6.92 (s, 1H), 5.19* (d, *J* = 8.3 Hz, 1H), 5.06 (dd, *J* = 8.2, 3.6 Hz, 1H), 4.43 (s, 2H), 3.99 (s, 2H), 3.76–3.63 (m, 1H), 3.59–3.47 (m, 3H), 2.44–2.34 (m, 1H), 2.31 (s, 3H), 2.18–2.08 (m, 2H), 2.06–1.96 (m, 1H), 1.46* (s, 3H), 1.30 (s, 6H), 1.22 (t, *J* = 7.0 Hz, 3H). ^{13}C NMR (2:1 rotamer ratio, asterisk indicates minor rotamer peak, 101 MHz, $CDCl_3$) δ 180.6, 168.4, 153.6, 144.8, 140.5, 138.9, 138.4, 129.5, 129.1, 127.7, 126.7, 125.5, 124.7, 80.5, 72.8, 65.9, 53.9, 46.7*, 46.5, 41.9, 32.5, 31.6*, 28.5*, 28.3, 24.4*, 23.8, 21.4, 15.3.

***tert*-butyl (*S,Z*)-(((*tert*-butoxycarbonyl)imino)(2-(3-(4-(3-(ethoxymethyl)-5-methylbenzyl)phenyl)-1,2,4-oxadiazol-5-yl)pyrrolidin-1-yl)methyl)carbamate (2.24):**

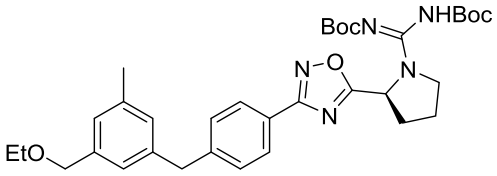

Compound **2.23** was synthesized from **2.22** using general procedure 2.5 and carried forward without purification. Compound **2.24** was synthesized from **2.23** using general procedure 2.6. Purification on a silica column yielded **2.24** (130 mg, 83%). ^{1}H NMR (400 MHz, $CDCl_3$) δ 8.03–7.94 (m, 2H), 7.28 (d, *J* = 8.5 Hz, 2H), 7.02 (s, 1H), 6.99–6.94 (m, 1H), 6.90 (s, 1H), 5.59 (dd, *J* = 7.8, 4.5 Hz, 1H), 4.42 (s, 2H), 3.98 (s, 2H), 3.89 (dt, *J* = 11.5, 7.3 Hz, 1H), 4.02–3.75 (m, 1H), 3.61–3.49 (m, 2H), 2.49–2.36 (m, 1H), 2.30 (s, 3H), 2.28–2.13 (m, 2H), 2.08–1.96 (m, 1H), 1.57–1.32 (m, 18H), 1.23 (t, *J* = 7.0 Hz, 3H). ^{13}C NMR (101 MHz,

$CDCl_3$) δ 178.8, 168.2, 161.9, 153.5, 150.3, 144.6, 140.4, 138.8, 138.3, 129.4, 128.9, 127.6, 126.5, 125.4, 124.5, 82.2, 79.5, 72.6, 65.8, 55.2, 49.4, 41.7, 31.4, 28.1, 28.0, 23.9, 21.3, 15.2.

(*S*)-amino(2-(3-(4-(3-(ethoxymethyl)-5-methylbenzyl)phenyl)-1,2,4-oxadiazol-5-yl)pyrrolidin-1-yl)methaniminium chloride (2.25):

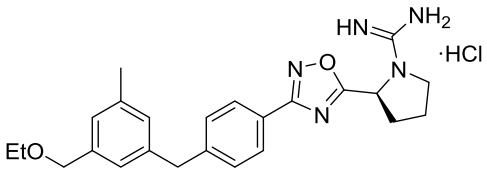

Compound **2.25** was synthesized from **2.24** using general procedure 2.5. The solvent was removed under reduced pressure to yield **2.25** (6 mg, 91%) as a white solid. ^{1}H NMR (500 MHz, CD_3OD) δ 7.94 (d, *J* = 8.2 Hz, 2H), 7.34 (d, *J* = 8.1 Hz, 2H), 7.01–6.94 (m, 3H), 5.44 (d, *J* = 7.3 Hz, 1H), 4.41 (s, 2H), 3.98 (s, 2H), 3.79–3.73 (m, 1H), 3.61 (q, *J* = 9.6 Hz, 1H), 3.51 (q, *J* = 7.0 Hz, 2H), 2.59–2.50 (m, 1H), 2.49–2.40 (m, 1H), 2.29 (s, 3H), 2.25–2.17 (m, 1H), 2.11–2.01 (m, 1H), 1.18 (t, *J* = 7.0 Hz, 3H). ^{13}C NMR (126 MHz, CD_3OD) δ 178.9, 169.6, 157.0, 146.9, 141.9, 140.0, 139.4, 130.6, 130.0, 128.5, 127.6, 126.6, 125.3, 73.6, 66.8, 56.4, 42.5, 32.7, 24.3, 21.4, 15.4.

4-((phenylsulfonyl)methyl)benzonitrile (2.27)

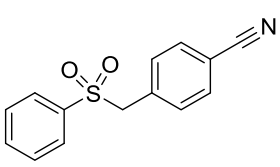

Sodium benzenesulfinate (523 mg, 3.19 mmol) was slurred in DMF (10 mL) and heated to 60 °C. 4-(bromomethyl)nitrile (500 mg, 2.55 mmol) was added slowly. The reaction solution was heated for 2 hours before being allowed to cool to room temperature. Deionized water was added to produce a white precipitate. The solid was filtered and dried under vacuum overnight to produce **2.27** (586 mg, 89%) as a white solid. ^{1}H NMR (400 MHz, $(CD_3)_2SO$) δ 7.79–7.66 (m, 5H), 7.59 (t, *J* = 7.7 Hz, 2H), 7.33 (d, *J* = 8.5 Hz, 2H), 4.84 (s, 2H); ^{13}C NMR (101 MHz, $CDCl_3$) δ 138.5, 134.9, 134.5, 132.6, 132.3, 129.7, 128.5, 119.0, 111.6, 60.6, 40.0. HRMS (ESI-): Calcd for $C_{14}H_{10}NO_2S$ [M-H]: 256.2997, Found: 256.0444.

***N'*-hydroxy-4-((phenylsulfonyl)methyl)benzimidamide (2.28)**

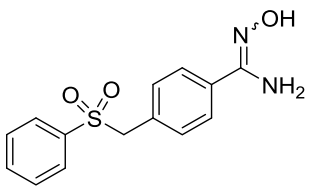

Compound **2.28** was synthesized from **2.27** using general procedure 2.3. The reaction mixture was cooled to room temperature and filtered to produce **2.28** (160 mg, 71%), a white solid. ^{1}H NMR (400 MHz, CD_3OD) δ 7.68–7.63 (m, 3H), 7.54–7.49 (m, 4H), 7.16–7.12 (m, 2H), 4.51 (s, 2H); ^{13}C NMR (101 MHz, CD_3OD) δ154.8, 139.4, 135.1, 132.2, 130.2, 129.7, 127.2, 62.7; HRMS (ESI+): Calcd for $C_{14}H_{14}N_2O_3S$ [M+H]: 291.0175, Found: 291.0788.

(*S*)-*tert*-butyl 2-(3-(4-((phenylsulfonyhl)methyl)phenyl)-1,2,4-oxadiazol-5-l)pyrrolidine-1-carboxylate (2.29)

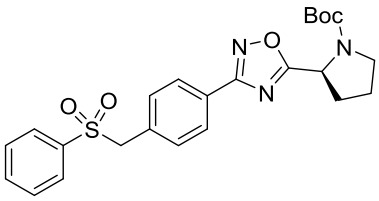

Compound **2.29** was synthesized from **2.28** and Boc-L-proline using general procedure 2.4. The resulting residue was purified on a silica column with 33% EtOAc in hexanes to yield **2.29** (57 mg, 46%), a white solid; ^{1}HNMR (2:1 rotamer ratio, asterisk denotes minor rotamer peak, 400 MHz, $CDCl_3$) δ 7.96 (d, *J* = 7.9 Hz, 2H), 7.66 (d, *J* = 7.7 Hz, 1H), 7.64–7.57 (m, 2H), 7.46 (d, *J* = 7.2 Hz, 2H), 7.20 (d, *J* = 7.9 Hz, 1H), 7.15 (d, *J* = 7.9 Hz, 1H), 5.18* (d, *J* = 8.0 Hz, 1H), 5.05 (dd, J = 8.2, 3.6 Hz, 1H), 4.35 (s, 2H), 3.73–3.62 (m, 1H), 3.59–3.42 (m, 1H), 2.45–2.31 (m, 1H), 2.19–2.07 (m, 2H), 2.04–1.95 (m, 1H), 1.45* (s, 3H), 1.28 (s, 6H) 0.89 –0.74 (m, 2H); ^{13}C NMR (2:1 rotamer ratio, asterisk denotes minor rotamer peak, 101 MHz, $CDCl_3$) δ 181.01, 167.89, 153.60, 137.91, 134.02, 131.25, 129.14, 128.72, 127.70, 127.29, 80.57, 65.94, 62.78, 53.90, 46.77*, 46.46, 32.48, 31.61*, 28.50*, 28.26, 24.48*, 23.81, 15.38. HRMS (ESI+): Calcd for $C_{24}H_{27}N_3O_5S$ [M+Na]: 492.5430, Found: 492.1559.

(*S*)-*tert*-butyl (((*tert*-butylcaronyl)imino)(2-(3-(4-((phenylsulfonyl)methyl)phenyl)-1,2,4-oxadiazol-5-yl)pyrrolidin-1-yl)methyl)carbamate (2.31)

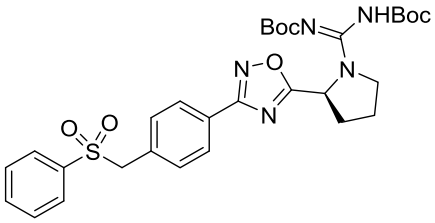

Compound **2.30** was synthesized from **2.29** using general procedure 2.5 and carried forward without purification. Compound **2.31** was synthesized from **2.30** using general procedure 2.4. The residue was purified on a silica column with 5–40% EtOAc in hexanes to yield **2.31** (16 mg, 53%), a white solid; ^{1}HNMR (400 MHz, $CDCl_3$) δ 7.96 (d, *J* = 8.4 Hz, 2H), 7.70–7.55 (m, 3H), 7.46 (t, *J* = 7.8 Hz, 2H), 7.18 (d, *J* = 8.3 Hz, 2H), 5.60 (dd, *J* = 7.9, 4.5 Hz, 1H), 4.36 (s, 2H), 3.94–3.84 (m, 1H), 3.84–3.73 (m, 1H), 2.49–2.40 (m, 2H), 2.29–2.12 (m, 3H), 2.08–1.97 (m, 2H), 1.55–1.38 (m, 18H); ^{13}C NMR (101 MHz, $CDCl_3$) δ167.9, 137.8, 134.1, 131.4, 129.2, 128.8, 127.8, 103.5, 62.9, 49.6, 29.9, 29.6, 28.3. HRMS (ESI+): Calcd for $C_{30}H_{37}N_5O_7S$ [M-H]: 610.7011, Found: 610.2343.

(*S*)-amino(2-(3-(4-((phenylsulfonyl)methyl)phenyl)-1,2,4-oxadiazol-5-yl)pyrrolidin-1-yl)methaniminium chloride (2.32):

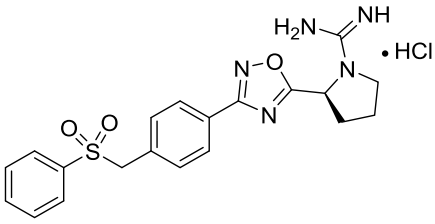

Compound **2.32** was synthesized from **2.31** using general procedure 2.5. The solvent was removed under reduces pressure and the resulting white solid was washed with diethyl ether to yield **2.32** (4 mg, 33%). ^{1}H NMR (400 MHz, CD_3OD) δ 7.93 (d, *J* = 6.5 Hz, 1H), 7.72–7.65 (m, 3H), 7.56–7.48 (m, 2H), 7.37 (s, 1H), 7.32–7.28 (m, 2H), 5.41 (dd, *J* = 7.9, 1.9 Hz, 1H), 4.58 (s, 2H), 3.79–3.69 (m, 1H), 3.64–3.56 (m, 1H), 2.61–2.52 (m, 1H), 2.50–2.41 (m, 1H), 2.24–2.18 (m, 1H), 2.12–2.02 (m, 1H). ^{13}C NMR (101 MHz, CD_3OD) δ 179.2, 169.2, 157.1, 139.4, 135.2, 133.7, 132.9, 130.3, 129.7, 128.3, 127.8,

62.6, 56.8, 32.7, 24.3. HRMS (ESI+): Calcd for $C_{20}H_{21}N_5O_3S$ [M+H]: 412.4854, Found: 412.1444.

Nonanenitrile (2.34a):

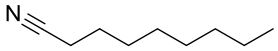

Compound **2.34a** was synthesized from **2.33a** using general procedure 2.11. Purification on a silica column in 0–10% EtOAc in hexane yielded **2.34a** (0.323 g, 20%) a clear yellow liquid. ^{1}H NMR (400 MHz, $CDCl_3$), δ 2.32 (t, *J* = 7.1, 2H), 1.64 (p, *J* = 7.2 Hz, 2H), 1.43 (p, *J* = 7.2 Hz, 2H), 1.36–1.21 (m, 8H), 0.87 (t, *J* = 6.9 Hz, 3H); ^{13}C NMR (101 MHz, $CDCl_3$) δ 119.9, 31.8, 29.0, 28.8, 28.7, 25.5, 22.7, 17.2, 14.1.

Tridecanenitrile (2.34b):

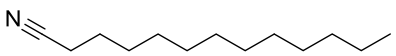

Compound **2.34b** was synthesized from **2.33b** using general procedure 2.11. Purification on a silica column in 0–10% EtOAc in hexane yielded **2.34b** (0.38 g, 93%) a white solid; ^{1}H NMR (400 MHz, $CDCl_3$) δ 2.32 (dd, *J* = 8.5, 5.8 Hz, 2H), 1.64 (dt, *J* = 14.9, 7.2 Hz, 2H), 1.47–1.39 (m, 2H), 1.33–1.17 (m, 16H), 0.87 (t, *J* = 6.9 Hz, 3H); ^{13}C NMR (101 MHz, $CDCl_3$) δ 120.0, 32.0, 29.7, 29.6, 29.43, 29.40, 28.9, 28.8, 25.5, 22.8, 17.2, 14.2.

Heptadecanenitrile (2.34c):

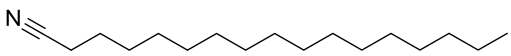

Compound **2.34c** was synthesized from **2.33c** using general procedure 2.11. Purification on a silica column in 0-10% EtOAc in hexane yielded **2.34c** (1.513 g, 92%) a white solid. ^{1}H NMR (400 MHz, $CDCl_3$) δ 2.32 (t, *J* = 7.1 Hz, 2H), 1.65 (p, *J* = 7.2 Hz, 2H), 1.43 (p, *J* = 7.0 Hz, 2H), 1.33–1.21 (m, 24H), 0.87 (t, *J* = 6.8 Hz, 3H); ^{13}C NMR (101 MHz, $CDCl_3$) δ 120.0, 32.1, 29.8, 29.82, 29.80, 29.79, 29.77, 29.7, 29.6, 29.5, 29.4, 28.9, 28.8, 25.5, 22.8, 17.3, 14.3..

***N'*-hydroxylnonanimidamide (2.35a):**

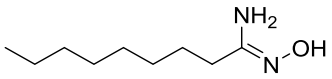

Compound **2.35a** was synthesized from **2.34a** using general procedure 2.3. Purification on a silica column using 50–80% EtOAc in hexane yielded **2.35a** (0.831 g, 67%) a white solid; ^{1}H NMR (2:1 mixture of diastereomers, asterisk denote minor diastereomer peak, 400 MHz, $CDCl_3$) δ 4.58 (s, 2H), 2.21* (t, *J* = 7.6 Hz, 2H), 2.12 (t, *J* = 7.4 Hz, 2H), 1.68–1.58* (m, 2H), 1.53 (p, *J* = 7.4 Hz, 2H), 1.36–1.16 (m, 26H), 0.86 (t, *J* = 6.7 Hz, 6H). ^{13}C NMR (101 MHz, $CDCl_3$) δ 154.3, 36.1, 31.9, 31.4, 29.8, 29.42, 29.40, 29.35, 29.3, 29.2, 26.8, 25.7, 22.8, 22.7, 14.2. HRMS (ESI+): Calcd for $C_9H_{20}N_2O$ [M+H]: 173.1648, Found: 173.1659.

***N'*-hydroxyltridecanimidamide (2.35b):**

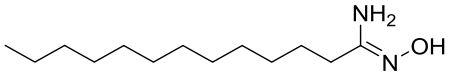

Compound **2.35b** was synthesized from **2.34b** using general procedure 2.3. Purification on a silica column using 50–80% EtOAc in hexanes yielded **2.35b** (186 mg, 53%), white solid. ^{1}H NMR (500 MHz, CD_3OD) δ 2.11–2.03 (m, 2H), 1.57 (t, *J* = 7.5 Hz, 2H), 1.36–1.29 (m, 21H), 0.90 (t, *J* = 6.9 Hz, 3H). ^{13}C NMR (101 MHz, $CDCl_3$) δ 157.6, 33.1, 31.8, 30.79, 30.76, 30.75, 30.7, 30.6, 30.5, 30.2, 28.3, 23.7, 14.5. HRMS (ESI+): Calcd for $C_{13}H_{28}N_2O$ [M+H]: 228.37, Found: 229.2271.

***N'*-hydroxylheptadecanimidamide (2.35c):**

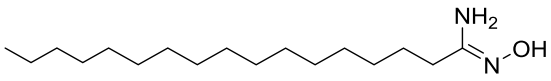

Compound **2.35c** was synthesized from **2.34c** using general procedure 2.3. Purification on a silica column using 50–80% EtOAc in hexane yielded **2.35c** (310 mg, 69%), a white solid; ^{1}H NMR (400 MHz, CD_3OD) δ 2.24–2.10 (m, 2H), 1.59 (q, *J* = 7.4 Hz, 2H), 1.36–1.25 (m, 30H), 0.90 (t, *J* = 6.9 Hz, 3H). ^{13}C NMR (101 MHz, CD_3OD) δ 106.4, 36.5, 33.1, 31.5, 30.79, 30.77, 30.74,

30.67, 30.65, 30.49, 30.47, 30.3, 30.1, 28.3, 26.9, 23.8, 14.5. HRMS (ESI+): Calcd for $C_{17}H_{36}N_2O$ [M+H]: 285.2823, Found: 285.2896.

(*S*)-*tert*-butyl 2-(3-octyl-1,2,4-oxadiazol-5-yl)pyrrolidine-1-carboxylate (2.36a):

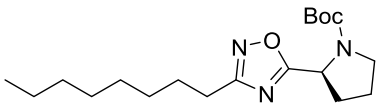

Compound **2.36a** was synthesized from **2.35a** and Boc-L-proline using general procedure 2.4. Purification on a silica column with 10–30% EtOAc in hexane yielded **2.36a** (512 mg, 50%), a white solid; ^{1}H NMR (2:1 rotamer ration, asterisk denotes minor rotamer peak, 400 MHz, $CDCl_3$) δ 5.11* (d, *J* = 8.0 Hz, 1H), 5.02–4.92 (m, 1H), 3.72–3.60 (m, 1H), 3.57–3.43 (m, 1H), 2.70 (t, *J* = 7.6 Hz, 2H), 2.40–2.26 (m, 1H), 2.14–2.02 (m, 2H), 2.01–1.91 (m, 1H), 1.71 (p, *J* = 7.4 Hz, 2H), 1.45* (s, 3H), 1.38–1.19 (m, 21H), 0.87 (t, *J* = 6.9 Hz, 3H). ^{13}C NMR (2:1 rotamer ration, asterisk denotes minor rotamer peak, 101 MHz, $CDCl_3$) δ 180.4, 170.8, 153.6, 80.4, 53.8, 46.7*, 46.4, 32.5, 31.9, 31.6*, 29.3, 29.2, 28.5*, 28.2, 27.2, 27.0*, 26.2*, 26.1, 24.4*, 23.8, 22.7, 14.2. HRMS (ESI+): Calcd for $C_{19}H_{33}N_3O_3$ [M+Na]: 374.48, Found: 374.2429.

(*S*)-*tert*-butyl 2-(3-dodecyl-1,2,4-oxadiazol-5-yl)pyrrolidine-1-carboxylate (2.36b):

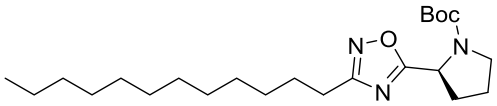

Compound **2.36b** was synthesized from **2.37b** using general procedure 2.13. Purification on a silica column with 10–30% EtOAc in hexanes yielded **2.36b** (107 mg, 93%), a yellow oil. ^{1}H NMR (2:1 rotamer ration, asterisk denotes minor rotamer peak, 500 MHz, $CDCl_3$) δ 5.11* (d, *J* = 7.2 Hz, 1H), 4.97 (d, *J* = 4.6 Hz, 1H), 3.71–3.61 (m, 1H), 3.55–3.47 (m, 1H), 2.70 (t, *J* = 7.5 Hz, 2H), 2.38–2.27 (m, 1H), 2.13–2.03 (m, 2H), 2.00–1.93 (m, 1H), 1.71 (p, *J* = 7.5 Hz, 2H), 1.63–1.55 (m, 2H), 1.45* (s, 3H), 1.30 (s, 9H), 1.25 (s, 20H), 0.88 (t, *J* = 6.8 Hz, 6H). ^{13}C NMR (2:1 rotamer ration, asterisk denotes minor rotamer peak, 126 MHz, $CDCl_3$) δ 180.4, 170.9, 153.6, 80.5, 53.9, 46.5,

32.7*, 32.1, 29.9, 29.79, 29.77, 29.75, 29.6, 29.5, 29.4, 29.3*, 29.1, 28.5*, 28.3, 27.2, 27.0*, 26.1, 24.5*, 23.8, 22.8, 14.3. HRMS (ESI+): Calcd for $C_{23}H_{41}N_3O_3$ [M+Na]: 430.3148, Found: 430.3002.

(*S*)-*tert*-butyl 2-(3-hexadecyl-1,2,4-oxadiazol-5-yl)pyrrolidine-1-carboxylate (2.36c):

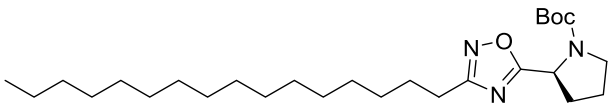

Compound **2.36c** was synthesized from **2.37c** using general procedure 2.13. Purification on a silica column with 10–30% EtOAc in hexane yielded **2.36c** (91 mg, 95%), a yellow oil; ^{1}H NMR (2:1 rotamer ration, asterisk denotes minor rotamer peak, 400 MHz, $CDCl_3$) δ 5.11* (d, *J* = 7.2 Hz, 1H), 4.97 (dd, *J* = 8.1, 3.5 Hz, 1H), 3.69–3.58 (m, 1H), 3.57–3.43 (m, 1H), 2.70 (t, *J* = 7.6 Hz, 2H), 2.39–2.24 (m, 1H), 2.12–2.02 (m, 2H), 1.99–1.92 (m, 1H), 1.72 (p, *J* = 7.5 Hz, 2H), 1.44* (s, 3H), 1.40–1.15 (m, 41H), 0.87 (t, *J* = 7.0 Hz, 3H). ^{13}C NMR (2:1 rotamer ration, asterisk denotes minor rotamer peak, 101 MHz, $CDCl_3$) δ 180.4, 170.8, 153.6, 80.4, 53.9, 46.7*, 46.5, 32.6*, 32.1, 31.6, 29.84, 29.80*, 29.75*, 29.6, 29.5, 29.4, 29.3*, 28.5*, 28.3, 27.2, 27.0*, 26.3*, 26.1, 24.5*, 23.8, 22.8, 14.3. HRMS (ESI+): Calcd for $C_{27}H_{49}N_3O_3$ [M+Na]: 486.377, Found: 486.3686.

(*S*)-*tert*-butyl 2-((((1-aminotridecylidene)amino)oxy)carbonyl)pyrrilidine-1-carboxylate (2.37b):

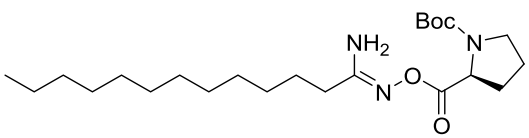

Compound **2.37b** was synthesized from **2.35b** and Boc-*L*-proline using general procedure 2.12. Purification on a silica column with 40–80% EtOAc in hexanes yielded **2.37b** (188 mg, 80%), a yellow oil; ^{1}H NMR (400 MHz, $CDCl_3$) δ 4.41–4.32 (m, 1H), 3.57–3.46 (m, 1H), 3.42–3.33 (m, 1H), 2.24 (q, *J* = 8.3 Hz, 3H), 2.21–2.15 (m, 1H), 2.07–1.96 (m, 1H), 1.89–1.85(m, 1H), 1.59 (p,

J = 7.9 Hz, 3H), 1.45 (s, 6H), 1.41 (s, 3H), 1.34–1.22 (m, 24H), 0.87 (t, *J* = 6.9 Hz, 3H). ^{13}C NMR (126 MHz, $CDCl_3$) δ 170.7, 170.3, 161.6, 158.9, 155.3, 154.2, 80.5, 80.3, 77.7, 59.1, 58.6, 47.0, 32.1, 31.6, 31.2, 31.2, 29.84, 29.78, 29.76, 29.7, 29.6, 29.5, 29.4, 29.23, 29.20, 28.6, 28.4, 27.2, 27.0, 24.6, 23.8, 22.8, 14... HRMS (ESI+): Calcd for $C_{23}H_{43}N_3O_4$ [M+H]: 426.6123, Found: 426.3344.

(*S*)-*tert*-butyl 2-((((1-aminoheptadecylidene)amino)oxy)carbonyl)pyrrilidine-1-carboxylate (2.37c):

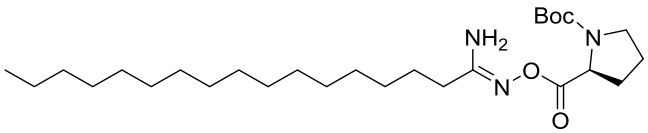

Compound **2.37c** was synthesized from **2.35c** and Boc-*L*-proline using general procedure 2.12. Purification on a silica column with 40–80% EtOAc in hexanes yielded **2.37c** (48 mg, 57%), a yellow oil; ^{1}H NMR (400 MHz, $CDCl_3$) δ 4.76 (s, 1H), 4.39–4.30 (m, 1H), 3.59–3.45 (m, 1H), 3.42–3.32 (m, 1H), 2.29–2.13 (m, 4H), 2.04–1.93 (m, 1H), 1.91–1.82 (m, 1H), 1.63–1.52 (m, 2H), 1.43 (s, 6H), 1.39 (s, 3H), 1.23 (s, 30H), 0.86 (t, *J* = 6.8 Hz, 3H). ^{13}C NMR (101 MHz, $CDCl_3$) δ 170.6, 170.3, 161.5, 158.9, 155.2, 154.1, 80.4, 80.2, 59.0, 58.6, 46.9, 46.5, 32.0, 31.5, 29.79, 29.77, 29.76, 29.75, 29.7, 29.6, 29.5, 29.4, 29.2, 28.6, 28.3, 27.2, 27.0, 24.5, 23.8, 22.8, 14.2. HRMS (ESI+): Calcd for $C_{27}H_{51}N_3O_4$ [M+H]: 482.39, Found: 482.3984.

(*S*)-*tert*-butyl (((*tert*-butylcarbonyl)imino)(2-(3-octyl-1,2,4-oxadiazol-5-yl)pyrrolidin-1-yl)methyl)carbamate (2.39a):

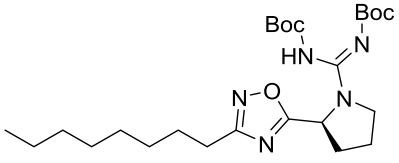

Compound **2.38a** was synthesized from **2.37a** using general procedure 2.5 and carried forward without purification. Compound **2.39a** was synthesized from **2.38a** using general procedure 2.6. Purification on a silica column with 5–30% EtOAc in hexane yielded **2.39a** (18 mg, 66%), an oil; ^{1}H NMR (400 MHz, $CDCl_3$) δ 10.09 (s, 1H), 5.48 (dd, *J* = 7.4, 4.5 Hz, 1H), 3.88–3.70 (m, 2H), 2.69 (t, *J* = 7.8 Hz, 2H), 2.44–2.31 (m, 1H), 2.18–2.07 (m, 2H), 2.04-1.93 (m, 1H), 1.71 (p, *J* = 7.0 Hz, 3H), 1.49–1.38 (m, 19H), 1.37–1.21 (m, 12H), 0.86 (dd, *J* = 7.3, 6.2 Hz, 3H). ^{13}C NMR (101 MHz, $CDCl_3$) δ 178.7, 170.9, 82.3, 79.7, 55.4, 49.6, 31.9, 29.3, 29.23, 29.21, 28.2, 27.1, 26.1, 22.8, 14.2. HRMS (ESI+): Calcd for $C_{25}H_{43}N_5O_5$ [M+H]: 494.33, Found: 494.3358.

(*S*)-*tert*-butyl (((*tert*-butylcarbonyl)imino)(2-(3-dodecyl-1,2,4-oxadiazol-5-yl)pyrrolidin-1-yl)methyl)carbamate (2.39b):

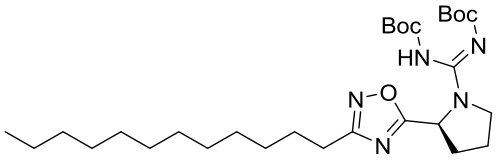

Compound **2.38b** was synthesized from **2.37b** using general procedure 2.5 and carried forward without purification Compound **2.39b** was synthesized from **2.38b** using general procedure 2.6. Purification on a silica column with 5–30% EtOAc in hexane yielded **2.39b** (38 mg, 71%), an oil; ^{1}H NMR (400 MHz, $CDCl_3$) δ 5.49 (dd, *J* = 7.7, 4.5 Hz, 1H), 3.87–3.79 (m, 1H), 3.79–3.70 (m, 1H), 2.72–2.66 (m, 2H), 2.44–2.33 (m, 1H), 2.19–2.06 (m, 2H), 2.06–1.93 (m, 1H), 1.72 (p, *J* = 8.3 Hz, 2H), 1.52–1.40 (m, 18H), 1.38–1.19 (m, 21H), 0.87 (t, *J* = 6.8 Hz, 3H). ^{13}C NMR (101 MHz, $CDCl_3$) δ 178.5, 162.0, 153.6, 150.3, 82.2, 79.4,

55.2, 49.4, 31.9, 29.7, 29.62, 29.61, 29.59, 29.4, 29.3, 29.2, 29.1, 28.1, 28.0, 26.9, 26.0, 22.7, 14.1. HRMS (ESI+): Calcd for $C_{29}H_{51}N_5O_5$ [M+H]: 550.3895, Found: 550.3968.

(*S*)-*tert*-butyl (((*tert*-butylcarbonyl)imino)(2-(3-hexadecyl-1,2,4-oxadiazol-5-yl)pyrrolidin-1-yl)methyl)carbamate (2.39c):

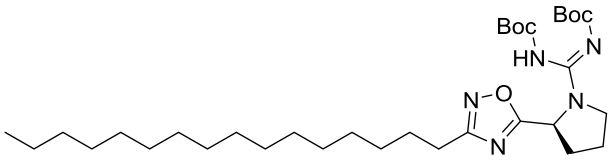

Compound **2.38c** was synthesized from **2.37c** using general procedure 2.5 and carried forward without purification. Compound **2.39c** was synthesized from **2.38c** using general procedure 2.6. Purification on a silica column with 5–30% EtOAc in hexane yielded **2.39c** (12 mg, 51%), an oil; ^{1}H NMR (400 MHz, $CDCl_3$) δ 5.49 (dd, *J* = 7.9, 4.5 Hz, 1H), 3.85–3.80 (m, 1H), 3.80–3.69 (m, 1H), 2.69 (t, *J* = 7.7 Hz, 2H), 2.42–2.34 (m, 1H), 2.14–2.07 (m, 2H), 2.02–1.95 (m, 1H), 1.71 (p, *J* = 7.9 Hz, 2H), 1.45 (s, 18H), 1.24 (s, 32H), 0.87 (t, *J* = 6.8 Hz, 3H). ^{13}C NMR (400 MHz, $CDCl_3$) δ 178.6, 170.8, 162.2, 153.5, 150.2, 82.2, 79.6, 55.4, 49.6, 32.1, 29.8, 29.5, 29.3, 28.2, 27.1, 26.1, 22.8, 14.2. HRMS (ESI+): Calcd for $C_{33}H_{59}N_5O_5$ [M+H]: 606.4516, Found: 606.4581.

(*S*)-amino(2-(3-octyl-1,2,4-oxadiazol-5-yl)pyrrolidin-1-yl)methaniminium chloride (2.40a):

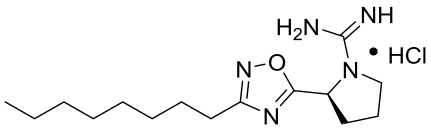

Compound **2.40a** was synthesized from **2.39a** using general procedure 2.5. The solvent was removed under reduced pressure and the residue was washed with diethyl ether to yield **2.40a** (10 mg, 86%), a white solid; ^{1}H NMR (500 MHz, CD_3OD) δ 5.36 (dd, *J* = 8.0, 1.5 Hz, 1H), 3.71 (td, *J* = 9.3, 2.5 Hz, 1H), 3.62–3.54 (m, 1H), 2.72 (t, *J* = 7.5 Hz, 2H), 2.55–2.46 (m, 1H), 2.38 (dd, *J* = 13.0, 6.5 Hz, 1H), 2.26–2.15 (m, 1H), 2.06–1.96 (m, 1H), 1.73 (p, *J* = 7.5 Hz, 2H), 1.41–1.25 (m, 11H), 0.90 (t, *J* = 6.9 Hz, 3H). ^{13}C NMR (126 MHz, CD_3OD) δ 178.5, 172.1, 157.0, 56.3, 48.9, 33.0, 32.6,

30.2, 30.0, 27.9, 26.6, 24.3, 23.7, 14.4; HRMS (ESI+): Calcd for $C_{15}H_{28}N_5O$ [M+H]: 294.42, Found 294.2292

(*S*)-amino(2-(3-dodecyl-1,2,4-oxadiazol-5-yl)pyrrolidin-1-yl)methaniminium chloride (2.40b):

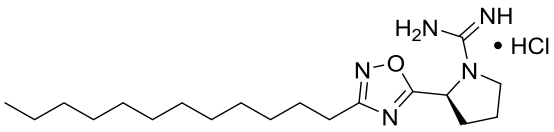

Compound **2.40b** was synthesized from **2.39b** using general procedure 2.5. The solvent was removed under reduced pressure and the residue was washed with diethyl ether to yield **2.40b** (22 mg, 92%), a white solid; ^{1}HNMR (500 MHz, CD_3OD) δ 5.36 (d, *J* = 7.5 Hz, 1H), 3.71 (t, *J* = 8.3 Hz, 1H), 3.58 (dd, *J* = 16.8, 9.3 Hz, 1H), 2.72 (t, *J* = 7.5 Hz, 2H), 2.56–2.46 (m, 1H), 2.38 (dd, *J* = 12.4, 6.2 Hz, 1H), 2.23–2.17 (m, 1H), 2.06–1.96 (m, 1H), 1.73 (p, *J* = 7.4 Hz, 2H), 1.45–1.22 (m, 20H), 0.90 (t, *J* = 6.9 Hz, 3H), ^{13}C NMR (126 MHz, CD_3OD) δ 178.5, 172.1, 157.0, 56.4, 33.1, 32.6, 30.8, 30.74, 30.70, 30.6, 30.5, 30.3, 30.1, 27.9, 26.6, 24.3, 23.7, 14.4; HRMS (ESI+): Calcd for $C_{19}H_{36}N_5O$ [M+H]: 350.2915, Found: 350.2909.

(*S*)-amino(2-(3-hexadecyl-1,2,4-oxadiazol-5-yl)pyrrolidin-1-yl)methaniminium chloride (2.40c):

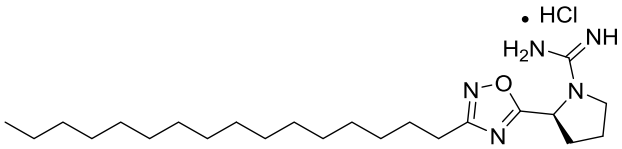

Compound **2.40c** was synthesized from **2.39c** using general procedure 2.5. The solvent was removed under reduced pressure and the residue was washed with diethyl ether to yield **2.40c** (11 mg, 66%), a white solid.^{1}H NMR (400 MHz, CD_3OD) δ 5.35 (d, *J* = 6.7 Hz, 1H), 3.73–3.66 (m, 1H), 3.63–3.51 (m, 1H), 2.72 (t, *J* = 7.5 Hz, 2H), 2.55–2.43 (m, 1H), 2.42–2.34 (m, 1H), 2.24–2.15 (m, 1H), 2.05–1.97 (m, 1H), 1.77–1.68 (m, 2H),). 1.43–1.22 (m, 28H), 0.90 (t, *J* = 6.8 Hz, 3H). ^{13}C NMR (101 MHz, CD_3OD) δ

178.5, 172.0, 157.0, 56.3, 33.1, 32.7, 30.78, 30.75, 30.7, 30.6, 30.5, 30.3, 30.1, 27.9, 26.6, 24.3, 23.7, 14.4. HRMS (ESI+): Calcd for $C_{23}H_{44}N_5O$ [M+H]: 406.3546, Found: 406.3571.

7.1.11 Characterization for Chapter 3

6-(butyloxy)-2-naphthonitrile (3.2a):

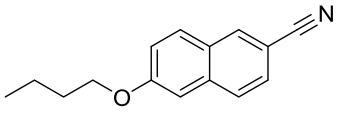

Compound **3.2a** was synthesized via general procedure 3.1with butyl bromide as starting material. Purification on a silica gel column with 0–20% EtOAc in hexanes produced **2a** (498 mg, 93%), a white solid. ^{1}H NMR (500 MHz, $CDCl_3$) δ 8.05 (d, *J* = 1.7 Hz, 1H), 7.71 (dd, *J* = 8.7, 2.6 Hz, 2H), 7.50 (dd, *J* = 8.5, 1.7 Hz, 1H), 7.21 (dd, *J* = 9.0, 2.5 Hz, 1H), 7.09 (d, *J* = 2.5 Hz, 1H), 4.06 (t, *J* = 6.5 Hz, 2H), 1.87–1.78 (m, 2H), 1.53 (m, *J* = 7.5 Hz, 2H), 1.00 (t, *J* = 7.4 Hz, 3H). ^{13}C NMR (126 MHz, $CDCl_3$) δ 159.6, 136.4, 133.7, 129.8, 127.7, 127.5, 126.9, 120.9, 119.6, 106.51, 106.45, 67.9, 31.1, 19.3, 13.9. HRMS (ESI+): Calcd for $C_{15}H_{15}NO$ $[M+H]^+$: 226.2936, Found: 226.1230.

6-(pentyloxy)-2-naphthonitrile (3.2b):

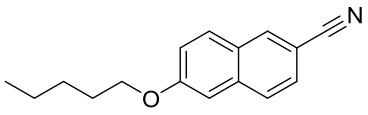

Compound **3.2b** was synthesized via general procedure 3.1 with pentyl bromide as starting material. Purification on a silica gel column with 0–20% EtOAc in hexanes produced **2b** (416 mg, 98%), a white solid. ^{1}H NMR (400 MHz, $CDCl_3$) δ 8.10 (s, 1H), 7.75 (dd, *J* = 8.7, 3.3 Hz, 2H), 7.53 (dd, *J* = 8.5, 1.6 Hz, 1H), 7.26–7.22 (m, 1H), 7.12 (d, *J* = 2.3 Hz, 1H), 4.09 (t, *J* = 6.6 Hz, 2H), 1.90–1.82 (m, 2H), 1.54–1.37 (m, 4H), 0.96 (t, *J* = 7.2 Hz, 3H). ^{13}C NMR (101 MHz, $CDCl_3$) δ 159.7, 136.6, 133.8, 130.0, 127.8, 127.7, 127.1, 121.1, 119.7, 106.7, 106.7, 77.5, 77.2, 76.8, 68.4, 28.9, 28.3, 22.6, 14.1. HRMS (ESI+): Calcd for $C_{16}H_{17}NO$ $[M+H]^+$: 240.3032, Found: 240.1381.

6-(hexyloxy)-2-naphthonitrile (3.2c):

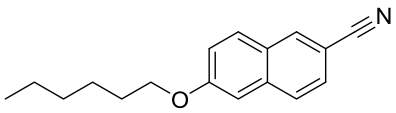

Compound **3.2c** was synthesized via general procedure 3.1 with hexyl bromide as starting material. Purification on a silica gel column with 0–20% EtOAc in hexanes produced **2c** (517 mg, 86%), a white solid. ^{1}H NMR (500 MHz, $CDCl_3$) δ 8.06 (d, *J* = 1.6 Hz, 1H), 7.72 (d, *J* = 8.7 Hz, 2H), 7.51 (dd, *J* = 8.4, 1.7 Hz, 1H), 7.22 (dd, *J* = 9.0, 2.5 Hz, 1H), 7.10 (d, *J* = 2.4 Hz, 1H), 4.06 (t, *J* = 6.6 Hz, 2H), 1.84 (p, *J* = 6.7 Hz, 2H), 1.49 (dq, *J* = 11.7, 7.4, 5.2 Hz, 2H), 1.36 (tt, *J* = 7.1, 2.9 Hz, 4H), 0.91 (t, *J* = 7.1 Hz, 3H).^{13}C NMR (126 MHz, $CDCl_3$) δ 159.6, 136.5, 133.8, 129.9, 127.7, 127.6, 126.9, 121.0, 119.7, 106.54, 106.49, 77.4, 77.2, 76.9, 68.3, 31.6, 29.1, 25.8, 22.6, 14.1. HRMS (ESI+): Calcd for $C_{17}H_{19}NO$ $[M+H]^+$: 254.3468, Found: 254.1536.

6-(heptyloxy)-2-naphthonitrile (3.2d):

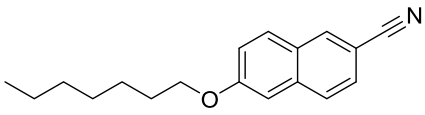

Compound **3.2d** was synthesized via general procedure 3.1 with heptyl bromide as starting material. Purification on a silica gel column with 0–20% EtOAc in hexanes produced **2d** (147 mg, 85%), a white solid. ^{1}H NMR (400 MHz, $CDCl_3$) δ 8.10 (s, 1H), 7.75 (dd, *J* = 8.8, 2.2 Hz, 2H), 7.53 (dd, *J* = 8.5, 1.6 Hz, 1H), 7.29–7.19 (m, 1H), 7.12 (d, *J* = 2.4 Hz, 1H), 4.08 (t, *J* = 6.6 Hz, 2H), 1.92–1.80 (m, 2H), 1.54–1.46 (m, 2H), 1.42–1.30 (m, 6H), 0.91 (t, *J* = 7.2 Hz, 3H).^{13}C NMR (101 MHz, CDCl3) δ 159.7, 136.6, 133.8, 130.0, 127.8, 127.7, 127.1, 121.0, 119.7, 106.7, 106.6, 68.4, 31.9, 29.21, 29.15, 26.1, 22.7, 14.2. HRMS (ESI+): Calcd for $C_{18}H_{21}NO$ $[M+H]^+$: 268.3734, Found: 268.1681.

6-isobutoxy-2-naphthonitrile (3.2e):

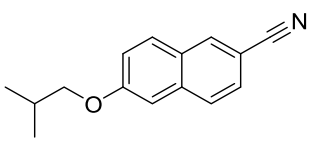

Compound **3.2e** was synthesized via general procedure 3.1 with isobutyl bromide as starting material. Purification on a silica gel column with 0–20% EtOAc in hexanes produced **2e** (223 mg, 84%), a white solid. ^{1}H NMR (400 MHz, $CDCl_3$) δ 8.09–8.05 (m, 1H), 7.73 (d, *J* = 8.7 Hz, 2H), 7.51 (dd, *J* = 8.5, 1.6 Hz, 1H), 7.27–7.20 (m, 1H), 7.11 (d, *J* = 2.4 Hz, 1H), 3.85 (d, *J* = 6.5 Hz, 2H), 2.16 (dt, *J* = 13.3, 6.7 Hz, 1H), 1.08 (d, *J* = 6.7 Hz, 6H). ^{13}C NMR (101 MHz, $CDCl_3$) δ 159.7, 136.5, 133.7, 129.9, 127.8, 127.7, 127.0, 121.0, 119.7, 106.7, 106.6, 77.5, 77.2, 76.8, 74.7, 28.3, 19.3. HRMS (ESI+): Calcd for $C_{15}H_{15}NO$ $[M+H]^+$: 226.2936, Found: 226.1234.

6-(benzyloxy)-2-naphthonitrile (3.2f):

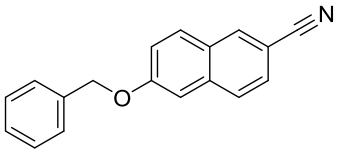

Compound **3.2f** was synthesized via general procedure 3.1 with benzyl bromide as starting material. Purification on a silica gel column with 0–20% EtOAc in hexanes produced **2f** (153 mg, 100%), a white solid. ^{1}H NMR (400 MHz, $CDCl_3$) δ 8.08 (s, 1H), 7.75 (dd, *J* = 8.7, 5.3 Hz, 2H), 7.55–.48 (m, 3H), 7.44 (t, *J* = 7.3 Hz, 2H), 7.42–7.37 (m, 1H), 7.33 (dd, *J* = 9.0, 2.4 Hz, 1H), 7.23 (d, *J* = 2.1 Hz, 1H), 5.20 (s, 2H). ^{13}C NMR (101 MHz, $CDCl_3$) δ 159.1, 136.3, 136.2, 133.7, 130.1, 128.7, 128.3, 127.9, 127.8, 127.6, 127.0, 120.9, 119.6, 107.3, 106.8, 70.2. HRMS (ESI+): Calcd for $C_{18}H_{13}NO$ $[M+H]^+$: 260.3099, Found: 260.1060.

6-((4-methylbenzyl)oxy)-2-naphthonitrile (3.2g):

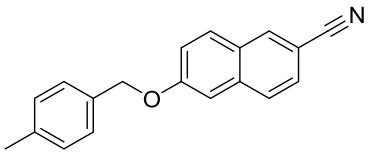

Compound **3.2g** was synthesized via general procedure 3.1 with para-methylbenzyl bromide as starting material. Purification on a silica gel column with 0–20% EtOAc in hexanes produced **2g** (237 mg, 98%), a white solid. ^{1}H NMR (400 MHz, $CDCl_3$) δ 8.08 (s, 1H), 7.74 (dd, *J* = 8.7, 4.9 Hz, 2H), 7.52 (dd, *J* = 8.5, 1.6 Hz, 1H), 7.37 (d, *J* = 8.0 Hz, 2H), 7.30 (dd, *J* = 9.0, 2.5 Hz, 1H), 7.23 (dd, *J* = 8.4, 2.3 Hz, 3H), 5.15 (s, 2H), 2.38 (s, 3H). ^{13}C NMR (101 MHz, $CDCl_3$) δ 159.2, 138.2, 136.4, 133.8, 133.2, 130.1, 129.5, 127.9, 127.82, 127.78, 127.1, 121.0, 119.6, 107.3, 106.8, 70.3, 21.3. HRMS (ESI+): Calcd for $C_{19}H_{15}NO$ $[M+H]^+$: 274.3364, Found: 274.1237.

6-cyanonaphthalen-2-yl 4-methylbenzenesulfonate (3.2h):

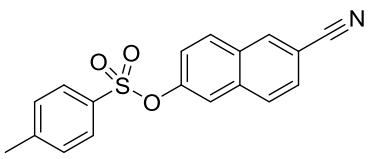

Compound **3.2h** was synthesized via general procedure 3.1 with tosyl chloride as starting material. Purification on a silica gel column with 0–20% EtOAc in hexanes produced **2h** (242 mg, 95%), a white solid. ^{1}H NMR (400 MHz, $CDCl_3$) δ 8.16 (s, 1H), 7.80 (d, *J* = 8.6 Hz, 2H), 7.71 (d, *J* = 8.0 Hz, 2H), 7.58 (d, *J* = 8.4 Hz, 1H), 7.53 (s, 1H), 7.29 (d, *J* = 7.9 Hz, 2H), 7.20 (d, *J* = 8.6 Hz, 1H), 2.42 (s, 3H). ^{13}C NMR (101 MHz, $CDCl_3$) δ 149.4, 145.9, 135.0, 133.9, 132.2, 130.7, 130.5, 130.0, 129.2, 128.5, 127.4, 123.2, 120.2, 118.8, 110.0, 21.8. HRMS (ESI+): Calcd for $C_{18}H_{13}NO_3S$ $[M+Cl]^+$: 358.8187, Found: 358.0309.

***N'*-hydroxy-6-(butyloxy)-2-naphthimidamide (3.3a):**

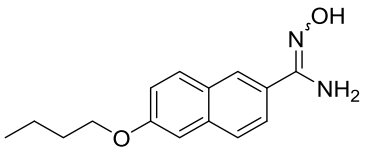

Using **3.2a** as starting material, **3.3a** was synthesized using general procedure 3.2. Purification on a silica gel column with 50–100% EtOAc in hexanes produced **3a** as a mixture of E/Z isomers (192 mg, 67%), a white solid. ^{1}H NMR (400 MHz, CD_3OD) δ 8.04–8.01 (m, 1H), 7.87–7.65 (m, 3H), 7.25–7.10 (m, 2H), 4.13–4.04 (m, 2H), 1.86–1.73 (m, 2H), 1.59–1.48 (m, 2H), 0.99 (td, *J* = 7.4, 1.2 Hz, 3H). ^{13}C NMR (101 MHz, CD_3OD) δ 171.1, 158.8, 157.9, 154.2, 136.7, 135.5, 130.1, 129.4, 128.3, 128.2, 127.9, 127.7, 127.62, 126.60, 126.5, 125.0, 124.1, 123.6, 119.5, 119.1, 106.01, 105.96, 67.5, 67.1, 31.03, 30.99, 18.93, 18.92, 12.8. HRMS (ESI+): Calcd for $C_{15}H_{18}N_2O_2$ $[M+H]^+$: 259.3236, Found: 259.1417.

***N'*-hydroxy-6-(pentyloxy)-2-naphthimidamide (3.3b):**

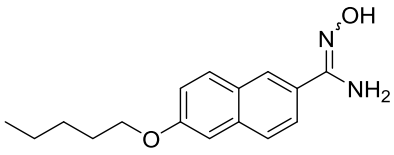

Using **3.2b** as starting material, **3.3b** was synthesized using general procedure 3.2. Purification on a silica gel column with 50–100% EtOAc in hexanes produced **3.3b** as a mixture of E/Z isomers (360 mg, 99%), a white solid. ^{1}H NMR (400 MHz, CD_3OD) δ 8.05 (d, *J* = 1.4 Hz, 1H), 7.81–7.68 (m, 3H), 7.22 (d, *J* = 2.5 Hz, 1H), 7.15 (dd, *J* = 8.9, 2.5 Hz, 1H), 4.10 (t, *J* = 6.5 Hz, 2H), 1.85 (dd, *J* = 8.2, 6.6 Hz, 2H), 1.56–1.38 (m, 4H), 0.97 (t, *J* = 7.2 Hz, 3H). ^{13}C NMR (101 MHz, CD_3OD) δ 159.4, 155.7, 136.9, 130.9, 129.7, 129.1, 127.9, 126.4, 125.1, 120.6, 107.5, 69.1, 49.6, 49.4, 49.2, 49.0, 48.8, 48.6, 48.4, 30.1, 29.5, 23.6, 14.4. HRMS (ESI+): Calcd for $C_{16}H_{20}N_2O_2$ $[M+H]^+$: 273.3501, Found: 273.1610.

6-(hexyloxy)-*N'*-hydroxy-2-naphthimidamide (3.3c):

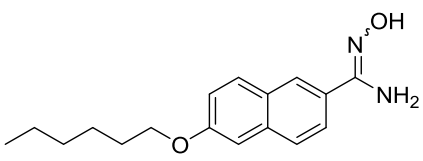

Using **3.2c** as starting material, **3.3c** was synthesized using general procedure 3.2. Purification on a silica gel column with 50–100% EtOAc in hexanes produced **3.3c** as a mixture of E/Z isomers (225 mg, 77%), a white solid. ^{1}H NMR (400 MHz, $CDCl_3$) δ 8.05 (d, *J* = 1.4 Hz, 1H), 7.91–7.65 (m, 4H), 7.28–7.10 (m, 2H), 4.10 (dt, *J* = 7.7, 6.5 Hz, 2H), 1.87–1.80 (m, 2H), 1.59–1.48 (m, 2H), 1.41–1.36 (m, 4H), 0.94 (t, *J* = 7.1 Hz, 3H). ^{13}C NMR (101 MHz, CD_3OD) δ 158.8, 157.9, 136.7, 135.5, 130.1, 129.4, 128.3, 128.2, 127.9, 127.7, 127.6, 126.6, 126.5, 125.0, 124.1, 123.6, 119.5, 119.1, 106.02, 105.97, 67.8, 67.4, 48.2, 48.0, 47.8, 47.6, 47.3, 47.1, 46.9, 31.4, 31.3, 28.90, 28.86, 25.5, 22.2, 12.92. HRMS (ESI+): Calcd for $C_{17}H_{22}N_2O_2$ $[M+H]^+$: 287.3767, Found: 287.1728.

6-(heptyloxy)-*N'*-hydroxy-2-naphthimidamide (3.3d):

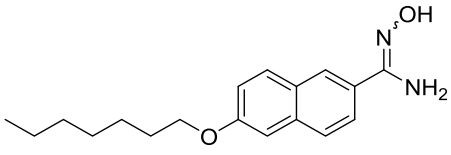

Using **3.2d** as starting material, **3.3d** was synthesized using general procedure 3.2. Purification on a silica gel column with 50–100% EtOAc in hexanes produced **3.3d** as a mixture of E/Z isomers (60 mg, 71%), a white solid. ^{1}H NMR (400 MHz, $CDCl_3$) δ 8.26 (s, 1H), 7.83–7.73 (m, 3H), 7.20 (dd, *J* = 8.9, 2.5 Hz, 1H), 7.14 (d, *J* = 2.4 Hz, 1H), 4.09 (t, *J* = 6.6 Hz, 2H), 1.90–1.82 (m, 2H), 1.54–1.46 (m, 2H), 1.43–1.28 (m, 7H), 1.26 (s, 1H), 0.90 (t, *J* = 6.9 Hz, 3H).^{13}C NMR (101 MHz, $CDCl_3$) δ 169.6, 159.0, 136.8, 130.6, 128.1, 128.0, 127.3, 124.4 120.3, 106.5, 68.4, 32.0, 29.3, 29.2, 26.2, 22.8, 14.2. HRMS (ESI+): Calcd for $C_{18}H_{24}N_2O_2$ $[M+H]^+$: 301.4033, Found: 301.1920.

***N′*-hydroxy-6-isobutoxy-2-naphthimidamide (3.3e):**

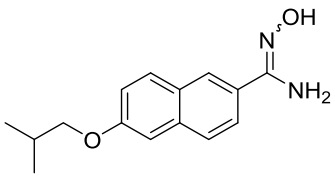

Using **3.2e** as starting material, **3.3e** was synthesized using general procedure 3.2. Purification on a silica gel column with 50–100% EtOAc in hexanes produced **3.3e** as a mixture of E/Z isomers (221 mg, 91%), a white solid. ^{1}H NMR (400 MHz, $CDCl_3$) δ 8.30–8.23 (m, 1H), 7.86–7.67 (m, 3H), 7.20 (ddd, *J* = 12.1, 8.9, 2.5 Hz, 1H), 7.13 (dd, *J* = 8.7, 2.5 Hz, 1H), 3.85 (dd, *J* = 6.5, 5.2 Hz, 2H), 2.16 (td, *J* = 6.7, 3.0 Hz, 1H), 1.08 (dd, *J* = 6.7, 1.6 Hz, 6H). ^{13}C NMR (101 MHz, $CDCl_3$) δ 169.7, 159.1, 158.3, 153.2, 136.8, 135.7, 130.6, 130.0, 128.4, 128.1, 127.32, 127.28, 125.2, 124.4, 123.8, 120.3, 120.0, 106.7, 106.6, 74.7, 74.7, 29.9, 28.4, 19.5. HRMS (ESI+): Calcd for $C_{15}H_{18}N_2O_2$ $[M+H]^+$: 259.3236, Found: 259.1465.

6-(benzyloxy)-*N′*-hydroxy-2-naphthimidamide (3.3f):

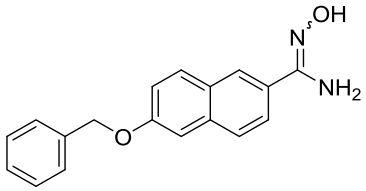

Using **3.2f** as starting material, **3.3f** was synthesized using general procedure 3.2. Purification on a silica gel column with 50–100% EtOAc in hexanes produced **3.3f** as a mixture of E/Z isomers (122 mg, 90%), a white solid. ^{1}H NMR (400 MHz, CD_3OD) δ 8.39–8.05 (m, 2H), 7.91–7.70 (m, 3H), 7.55–7.47 (m, 2H), 7.43–7.22 (m, 5H), 5.28–5.19 (m, 2H). ^{13}C NMR (101 MHz, $(CD_3)_2SO$) δ 156.8, 150.9, 136.9, 134.5, 129.9, 128.5, 128.0, 127.9, 126.4, 124.2, 123.9, 119.2, 107.3, 69.4. HRMS (ESI+): Calcd for $C_{18}H_{16}N_2O_2$ $[M+H]^+$: 293.3398, Found: 293.1627.

***N'*-hydroxy-6-((4-methylbenzyl)oxy)-2-naphthimidamide (3.3g):**

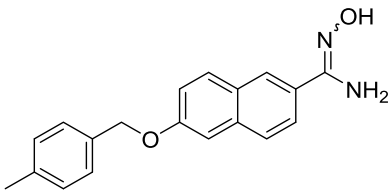

Using **3.2g** as starting material, **3.3g** was synthesized using general procedure 3.2. Purification on a silica gel column with 50–100% EtOAc in hexanes produced **3.3g** as a mixture of E/Z isomers (175 mg, 98%), a white solid. ^{1}H NMR (400 MHz, CD_3OD) δ 8.06 (d, *J* = 1.7 Hz, 1H), 7.88 (dd, *J* = 8.6, 1.6 Hz, 1H), 7.84–7.79 (m, 1H), 7.76–7.69 (m, 1H), 7.41–7.29 (m, 3H), 7.28–7.14 (m, 3H), 5.16 (d, *J* = 8.1 Hz, 2H), 2.35 (s, 3H). ^{13}C NMR (101 MHz, CD_3OD) δ 159.9, 159.0, 155.6, 138.92, 138.85, 138.0, 136.8, 135.4, 135.3, 131.7, 131.0, 130.2, 130.1, 129.9, 129.5, 129.2, 128.9, 128.8, 128.1, 128.0, 126.4, 125.6, 125.2, 121.0, 120.6, 108.2, 108.1, 71.10, 71.05, 21.2. HRMS (ESI+): Calcd for $C_{19}H_{18}N_2O_2$ $[M+H]^+$: 307.3364, Found: 307.1465.

6-(*N'*-hydroxycarbamimidoyl)naphthalen-2-yl 4-methylbenzenesulfonate (3.3h):

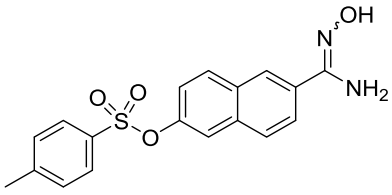

Using **3.2h** as starting material, **3.3h** was synthesized using general procedure 3.2. Purification on a silica gel column with 50–100% EtOAc in hexanes produced **3.3h** as a mixture of E/Z isomers (122 mg, 92%), a white solid. ^{1}H NMR (400 MHz, $CDCl_3$) δ 8.06–8.02 (m, 1H), 7.81–7.76 (m, 3H), 7.73 (dd, *J* = 8.4, 1.9 Hz, 2H), 7.48 (d, *J* = 2.4 Hz, 1H), 7.33–7.28 (m, 2H), 7.14 (dd, *J* = 8.9, 2.4 Hz, 1H), 4.97 (s, 2H), 2.45 (s, 3H). ^{13}C NMR (101 MHz, $CDCl_3$) δ 152.5, 148.1, 145.7, 134.6, 132.5, 131.6, 130.5, 130.4, 130.0, 128.7, 128.6, 125.1, 124.5, 122.1, 120.0, 21.9. HRMS (ESI+): Calcd for $C_{18}H_{16}N_2O_4S$ $[M+H]^+$: 357.4036, Found: 357.0922.

***tert*-butyl (*S*)-2-(3-(6-(butyloxy)naphthalen-2-yl)-1,2,4-oxadiazol-5-yl)pyrrolidine-1-carboxylate (3.4a):**

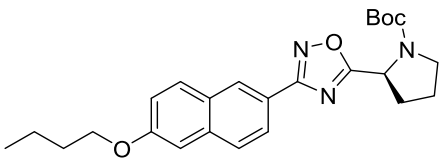

Using **3.3a** and Boc-*L*-proline as starting material, **3.4a** was synthesized using general procedure 3.3. Purification on a silica gel column with 15–30% EtOAc in hexanes produced **3.4a** (63 mg, 39%), a yellow oil. ^{1}H NMR (2:1 rotamer ratio, asterisk denote minor rotamer peak, 400 MHz, $CDCl_3$) δ 8.51 (d, *J* = 1.9 Hz, 1H), 8.08 (d, *J* = 8.5 Hz, 1H), 7.86–7.74 (m, 2H), 7.24–7.11 (m, 2H), 5.24* (d, *J* = 7.3 Hz, 1H), 5.09 (dd, *J* = 8.1, 3.7 Hz, 1H), 4.10 (t, *J* = 6.4 Hz, 2H), 3.82–3.66 (m, 1H), 3.63–3.47 (m, 1H), 2.49–2.34 (m, 1H), 2.29–2.12 (m, 2H), 2.09–1.95 (m, 1H), 1.84 (p, *J* = 6.4 Hz, 2H), 1.60–1.47 (m, 2H), 1.50–1.38* (m, 3H), 1.31 (s, 5H),), 1.01 (t, *J* = 7.4 Hz, 3H). ^{13}C NMR (2:1 rotamer ratio, asterisk denote minor rotamer peak, 101 MHz, $CDCl_3$) δ 180.7, 168.7, 158.7, 153.7, 136.3, 130.4, 128.5, 127.9, 127.6, 124.5, 121.8, 120.1, 106.8, 80.6, 68.0, 54.0, 46.8*, 46.5, 32.6, 31.4, 28.6, 28.3, 24.5*, 23.9, 19.4, 14.0. HRMS (ESI+): Calcd for $C_{25}H_{31}N_3O_4$ $[M+Na]^+$: 460.5211, Found: 460.2208.

***tert*-butyl (*S*)-2-(3-(6-(pentyloxy)naphthalen-2-yl)-1,2,4-oxadiazol-5-yl)pyrrolidine-1-carboxylate (3.4b):**

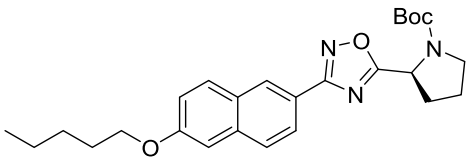

Using **3.3b** and Boc-*L*-proline as starting material, **3.4b** was synthesized using general procedure 3.3. Purification on a silica gel column with 15–30% EtOAc in hexanes produced **3.4b** (65 mg, 49%), a yellow oil. ^{1}H NMR (2:1 rotamer ratio, asterisk denote minor rotamer peak, 400 MHz, $CDCl_3$) δ 8.51 (s, 1H), 8.08 (d, *J* = 8.5 Hz, 1H), 7.81 (dd, *J* = 15.8, 8.8 Hz, 2H), 7.22–7.13 (m, 2H), 5.24* (d, *J* = 7.0 Hz, 1H), 5.09 (dd, *J* = 7.9, 3.3 Hz, 1H), 4.08 (t, *J* = 6.6 Hz, 2H), 3.79–3.66 (m, 1H), 3.62–3.47 (m, 1H), 2.47–2.32 (m, 1H), 2.22–2.13 (m, 2H),

2.07–1.97 (m, 1H), 1.86 (p, *J* = 6.6 Hz, 2H), 1.54–1.35 (m, 7H), 1.31 (s, 6H), 0.95 (t, *J* = 7.2 Hz, 3H). ^{13}C NMR (2:1 rotamer ratio, asterisk denote minor rotamer peak, 101 MHz, $CDCl_3$) δ 180.5, 168.5, 158.5, 153.6, 136.2, 130.2, 128.3, 127.7, 127.4, 127.2, 124.4, 124.3, 121.6, 119.9, 106.6, 80.4, 77.3, 77.0, 76.7, 68.1, 53.9, 46.6*, 46.4, 32.4, 31.5, 28.9, 28.4, 28.2, 28.1, 24.4*, 23.7, 22.4, 14.0. HRMS (ESI+): Calcd for $C_{26}H_{33}N_3O_4$ $[M+H]^+$: 452.5659, Found: 452.2535.

***tert*-butyl (*S*)-2-(3-(6-(hexyloxy)naphthalen-2-yl)-1,2,4-oxadiazol-5-yl)pyrrolidine-1-carboxylate (3.4c):**

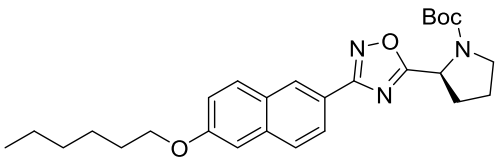

Using **3.3c** and Boc-*L*-proline as starting material, **3.4c** was synthesized using general procedure 3.3. Purification on a silica gel column with 15–30% EtOAc in hexanes produced **3.4c** (67 mg, 37%), a yellow oil. ^{1}H NMR (2:1 rotamer ratio, asterisk denote minor rotamer peak, 500 MHz, $CDCl_3$) δ 8.58–8.49 (m, 1H), 8.08 (dd, *J* = 8.2, 1.8 Hz, 1H), 7.87–7.72 (m, 2H), 7.23–7.10 (m, 2H), 5.26–5.22* (m, 1H), 5.09 (dd, *J* = 8.2, 3.8 Hz, 1H), 4.09 (t, *J* = 6.6 Hz, 2H), 3.78–3.70 (m, 1H), 3.65–3.48 (m, 1H), 2.50–2.33 (m, 1H), 2.21–2.16 (m, 2H), 2.03–2.01 (m, 1H), 1.85 (p, *J* = 6.8 Hz, 2H), 1.54–1.44 (m, 5H), 1.40–1.33 (m,, 4H), 1.30 (s, 6H), 0.91 (t, *J* = 6.8 Hz, 3H). ^{13}C NMR (2:1 rotamer ratio, asterisk denote minor rotamer peak, 126 MHz, $CDCl_3$) δ 180.7, 168.7, 158.6, 153.7, 136.3, 130.4, 128.5, 127.9, 127.6, 127.4, 124.6, 124.4, 121.8, 120.1, 119.9, 106.7, 80.6, 68.3, 54.0, 46.8*, 46.5, 32.6, 31.7, 29.3, 28.5, 28.3, 25.9, 24.5*, 23.*, 22.8, 14.2. HRMS (ESI+): Calcd for $C_{27}H_{35}N_3O_4$ $[M+Na]^+$: 488.5743, Found: 488.2527.

***tert*-butyl (*S*)-2-(3-(6-(heptyloxy)naphthalen-2-yl)-1,2,4-oxadiazol-5-yl)pyrrolidine-1-carboxylate (3.4d):**

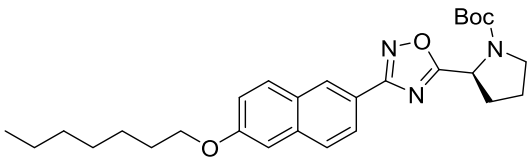

Using **3.3d** and Boc-*L*-proline as starting material, **3.4d** was synthesized using general procedure 3.3. Purification on a silica gel column with 15–30% EtOAc in hexanes produced **3.4d** (30 mg, 63%), a yellow oil. ^{1}H NMR (2:1 rotamer ratio, asterisk denote minor rotamer peak, 400 MHz, $CDCl_3$) δ 8.51 (s, 1H), 8.08 (d, *J* = 8.5 Hz, 1H), 7.81 (dd, *J* = 15.8, 8.8 Hz, 1H), 7.25–7.06 (m, 2H), 5.24* (d, *J* = 7.2 Hz, 1H), 5.10 (dd, *J* = 7.8, 3.3 Hz, 1H), 4.09 (t, *J* = 6.6 Hz, 2H), 3.78–3.65 (m, 1H), 3.63–3.44 (m, 1H), 2.49–2.28 (m, 1H), 2.19 (td, *J* = 12.7, 11.7, 7.1 Hz, 2H), 2.07–1.96 (m, 1H), 1.86 (dt, *J* = 14.5, 6.6 Hz, 2H), 1.56–1.44 (m, 4H), 1.43–1.21 (m, 11H), 0.90 (t, *J* = 6.9 Hz, 3H). ^{13}C NMR (2:1 rotamer ratio, asterisk denote minor rotamer peak, 101 MHz, $CDCl_3$) δ 180.7, 168.7, 158.7, 153.8, 136.3, 130.4, 128.5, 127.9, 127.6, 124.5, 121.8, 120.1, 106.8, 80.6, 68.3, 54.0, 46.8*, 46.5, 32.6, 31.9, 29.4, 29.2, 28.6*, 28.3, 26.2, 24.5*, 23.9, 22.8, 14.2. HRMS (ESI+): Calcd for $C_{28}H_{37}N_3O_4$ $[M+Na]^+$: 502.6008, Found: 502.2706.

***tert*-butyl (*S*)-2-(3-(6-isobutoxynaphthalen-2-yl)-1,2,4-oxadiazol-5-yl)pyrrolidine-1-carboxylate (3.4e):**

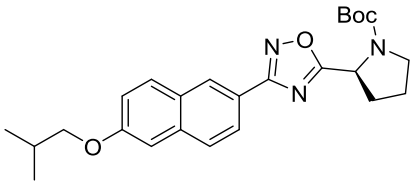

Using **3.3e** and Boc-*L*-proline as starting material, **3.4e** was synthesized using general procedure 3.3. Purification on a silica gel column with 15–30% EtOAc in hexanes produced **3.4e** (176 mg, 87%), a yellow oil. ^{1}H NMR (2:1 rotamer ratio, asterisk denote minor rotamer peak, 400 MHz, $CDCl_3$) δ 8.51 (s, 1H), 8.08 (d, *J* = 8.5 Hz, 1H), 7.81 (dd, *J* = 17.0, 8.8 Hz, 2H), 7.21 (dd, *J* = 8.8, 2.2 Hz, 1H), 7.15 (s, 1H), 5.24* (d, *J* = 8.2 Hz, 1H), 5.09 (dd, *J* = 8.1, 3.6 Hz,

1H), 3.86 (d, *J* = 6.5 Hz, 2H), 3.80–3.66 (m, 1H), 3.58 (d, *J* = 10.5 Hz, 1H), 2.42 (s, 1H), 2.23–2.11 (m, 3H), 2.02 (d, *J* = 4.9 Hz, 1H), 1.47* (d, *J* = 6.3 Hz, 3H), 1.31 (s, 6H), 1.08 (d, *J* = 6.7 Hz, 6H). ^{13}C NMR (2:1 rotamer ratio, asterisk denote minor rotamer peak , 101 MHz, $CDCl_3$) δ 180.5, 168.5, 158.6, 136.2, 130.2, 128.3, 127.7, 127.4, 124.3, 121.6, 119.9, 106.6, 80.4, 74.5, 53.9, 46.6*, 46.3, 32.4, 31.5*, 28.4*, 28.2, 28.1, 24.4*, 23.7, 19.3. HRMS (ESI+): Calcd for $C_{25}H_{31}N_3O_4$ $[M+H]^+$: 438.5393, Found: 438.2412.

***tert*-butyl (*S*)-2-(3-(6-(benzyloxy)naphthalen-2-yl)-1,2,4-oxadiazol-5-yl)pyrrolidine-1-carboxylate (3.4f):**

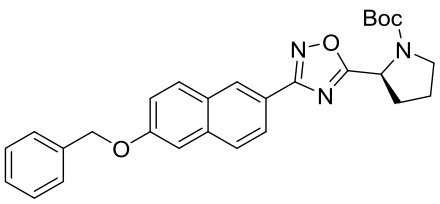

Using **3.3f** and Boc-*L*-proline as starting material, **3.4f** was synthesized using general procedure 3.3. Purification on a silica gel column with 15–30% EtOAc in hexanes produced **3.4f** (59 mg, 39%), a yellow oil. ^{1}H NMR (2:1 rotamer ratio, asterisk denote minor rotamer peak, 400 MHz, $CDCl_3$) δ 8.51 (s, 1H), 8.08 (d, *J* = 8.2 Hz, 1H), 7.82 (dd, *J* = 23.5, 8.7 Hz, 2H), 7.50–7.45 (m, 2H), 7.43–7.37 (m, 2H), 7.36–7.31 (m, 1H), 7.29–7.21 (m, 2H), 5.23* (d, *J* = 8.1 Hz, 1H), 5.19 (s, 2H), 5.09 (dd, *J* = 8.0, 3.5 Hz, 1H), 3.78–3.63 (m, 1H), 3.62–3.46 (m, 1H), 2.46–2.28 (m, 1H), 2.22–2.12 (m, 2H), 2.06–1.95 (m, 1H), 1.51–1.40* (m, 3H), 1.30 (s, 6H). ^{13}C NMR (2:1 rotamer ratio, asterisk denote minor rotamer peak, 101 MHz, $CDCl_3$) δ 180.5, 168.4, 158.1, 153.6, 136.5, 136.0, 130.4, 128.63, 128.55, 128.1, 127.7, 127.5, 124.4, 121.9, 119.9, 107.2, 80.5, 70.1, 53.8, 46.7*, 46.3, 32.4, 31.5, 28.5*, 28.4, 28.1, 24.4*, 23.7. HRMS (ESI+): Calcd for $C_{28}H_{29}N_3O_4$ $[M+Na]^+$: 494.5373, Found: 494.2094.

***tert*-butyl (*S*)-2-(3-(6-((4-methylbenzyl)oxy)naphthalen-2-yl)-1,2,4-oxadiazol-5-yl)pyrrolidine-1-carboxylate (3.4g):**

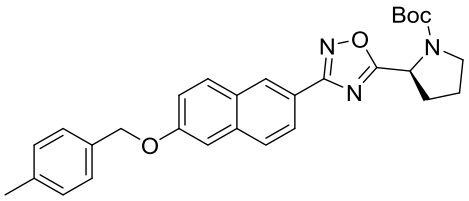

Using **3.3g** and Boc-*L*-proline as starting material, **3.4g** was synthesized using general procedure 3.3. Purification on a silica gel column with 15–30% EtOAc in hexanes produced **3.4g** (30 mg, 13%), a yellow oil. ^{1}H NMR (2:1 rotamer ratio, asterisk denote minor rotamer peak, 400 MHz, $CDCl_3$) δ 8.51 (s, 1H), 8.07 (d, *J* = 8.6 Hz, 1H), 7.88–7.74 (m, 2H), 7.36 (d, *J* = 8.0 Hz, 2H), 7.27–7.17 (m, 4H), 5.23* (d, *J* = 7.7 Hz, 1H), 5.14 (s, 2H), 5.08 (dd, *J* = 8.1, 3.7 Hz, 1H), 3.81–3.63 (m, 1H), 3.60–3.43 (m, 1H), 2.36 (s, 4H), 2.21–2.10 (m, 2H), 2.05–1.94 (m, 1H), 1.64 (s, 1H), 1.46* (s, 3H), 1.29 (s, 6H). ^{13}C NMR (2:1 rotamer ratio, asterisk denote minor rotamer peak, 101 MHz, $CDCl_3$) δ 180.5, 168.5, 158.1, 153.6, 137.7, 136.0, 133.4, 130.4, 129.3, 128.5, 127.7, 127.5, 126.7, 124.3, 121.8, 121.4, 120.0, 109.0, 107.1, 80.5, 76.6, 70.0, 53.9, 46.7*, 46.4, 32.4, 31.5*, 29.7, 28.4*, 28.1, 24.4*, 23.7, 21.2. HRMS (ESI+): Calcd for $C_{29}H_{31}N_3O_4$ $[M+H]^+$: 508.5639, Found: 508.2244.

***tert*-butyl (*S*)-2-(3-(6-(tosyloxy)naphthalen-2-yl)-1,2,4-oxadiazol-5-yl)pyrrolidine-1-carboxylate (3.4h):**

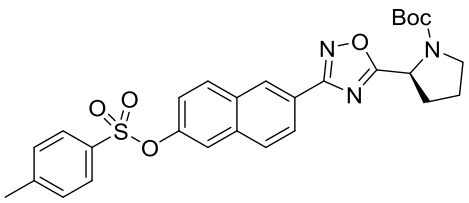

Using **3.3h** and Boc-*L*-proline as starting material, **3.4h** was synthesized using general procedure 3.3. Purification on a silica gel column with 15–30% EtOAc in hexanes produced **3.4h** (15 mg, 13%), a yellow oil. ^{1}H NMR (2:1 rotamer ratio, asterisk denote minor rotamer peak, 400 MHz, $CDCl_3$) δ 8.56 (d, *J* = 6.4 Hz, 1H), 8.14 (t, *J* = 8.5 Hz, 1H), 7.88–7.79 (m, 2H), 7.74 (d, *J* = 8.0 Hz, 2H), 7.55–7.48 (m, 1H), 7.35–7.29 (m, 2H), 7.19–7.11 (m, 1H), 5.24* (d, *J* = 8.3 Hz, 1H), 5.10 (dd, *J* = 8.2, 3.7 Hz, 1H), 3.78-

3.66 (m, 1H), 3.62–3.48 (m, 1H), 2.45 (s, 3H), 2.23–2.12 (m, 2H), 2.07–1.98 (m, 1H), 1.47* (s, 3H), 1.29 (s, 6H). ^{13}C NMR (2:1 rotamer ratio, asterisk denote minor rotamer peak, 101 MHz, $CDCl_3$) δ 181.1, 168.2, 153.7, 148.5, 145.7, 134.9, 132.4, 131.6, 130.9, 130.0, 128.9, 128.7, 127.8, 125.1, 124.5, 124.8, 122.3, 122.2, 120.2, 80.7, 54.0, 46.8*, 46.5, 36.8, 32.6, 31.7, 31.1, 28.5*, 28.3, 24.8, 24.6, 24.0*, 23.9, 23.5, 21.9. HRMS (ESI+): Calcd for $C_{28}H_{29}N_3O_6S$ $[M+Na]^+$: 558.6011, Found: 558.1710.

***tert*-butyl (2*S*,3*S*)-3-hydroxy-2-(3-(6-(pentyloxy)naphthalen-2-yl)-1,2,4-oxadiazol-5-yl)pyrrolidine-1-carboxylate (3.4i):**

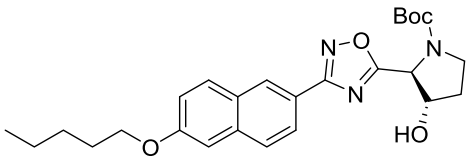

Using **3.3** and (3*S*)-hydroxy-Boc-*L*-proline as starting material, **3.4i** was synthesized using general procedure 3.3. Purification on a silica gel column with 15–30% EtOAc in hexanes produced **3.4i** (232 mg, 90%), a yellow oil. ^{1}H NMR (2:1 rotamer ratio, asterisk denote minor rotamer peak, 400 MHz, $CDCl_3$) δ 8.51–8.43 (m, 1H), 8.10–7.98 (m, 1H), 7.84–7.68 (m, 2H), 7.22–7.06 (m, 2H), 5.18* (s, 1H), 5.01 (d, J = 2.0 Hz, 1H), 4.65–4.58 (m, 1H), 4.07 (t, J = 6.5 Hz, 2H), 3.85–3.71 (m, 2H), 2.41–2.29 (m, 1H), 2.12–2.02 (m, 1H), 1.85 (p, J = 6.8 Hz, 2H), 1.51–1.37 (m, 6H), 1.30 (s, 6H), 0.95 (t, J = 7.1 Hz, 3H). ^{13}C NMR (2:1 rotamer ratio, asterisk denote minor rotamer peak, 101 MHz, $CDCl_3$) δ 178.1, 168.6, 158.6, 153.7, 136.2, 130.3, 128.3, 127.8, 127.4, 124.3, 121.3, 120.0, 106.6, 80.8, 76.1, 75.1*, 68.12, 62.6*, 62.3, 44.8*, 44.3, 32.5*, 32.2, 28.9, 28.3, 28.2, 28.1, 22.4, 14.0. HRMS (ESI+): Calcd for $C_{26}H_{33}N_3O_5$ $[M+Na]^+$: 490.5471, Found: 490.2309.

***tert*-butyl (2*S*,3*S*)-3-hydroxy-2-(3-(6-isobutoxynaphthalen-2-yl)-1,2,4-oxadiazol-5-yl)pyrrolidine-1-carboxylate (3.4j):**

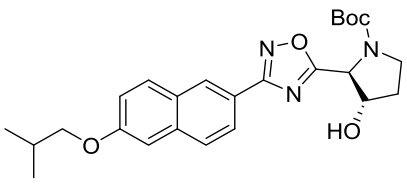

Using **3.3e** and (3*S*)-hydroxy-Boc-*L*-proline as starting material, **3.4j** was synthesized using general procedure 3.3. Purification on a silica gel column with 40–70% EtOAc in hexanes produced **3.4j** (52 mg, 49%), a yellow oil. ^{1}H NMR (2:1 rotamer ratio, asterisk denote minor rotamer peak, 400 MHz, $CDCl_3$) δ 8.46 (d, *J* = 22.8 Hz, 1H), 8.07–7.97 (m, 1H), 7.87–7.68 (m, 2H), 7.23–7.06 (m, 2H), 5.19* (s, 1H), 5.01 (d, *J* = 2.0 Hz, 1H), 4.62 (d, *J* = 6.9 Hz, 1H), 3.90–3.70 (m, 5H), 2.77–2.27 (m, 1H), 2.23–2.01 (m, 2H), 1.48* (s, 3H), 1.31 (s, 6H), 1.07 (d, *J* = 6.7 Hz, 6H). ^{13}C NMR (101 MHz, $CDCl_3$) δ 178.2, 168.6, 158.7, 153.9, 136.2, 130.3, 128.3, 127.8, 127.5, 124.2, 121.3, 120.0, 106.6, 80.9, 76.0, 74.5, 62.4, 44.4, 32.1, 28.4, 28.2, 28.1, 19.3. HRMS (ESI+): Calcd for $C_{25}H_{31}N_3O_5$ $[M+Na]^+$: 476.5205, Found: 476.2168.

***tert*-butyl (*S*,*Z*)-(((*tert*-butoxycarbonyl)amino)(2-(3-(6-(butyloxy)naphthalen-2-yl)-1,2,4-oxadiazol-5-yl)pyrrolidin-1-yl)methylene)carbamate (3.6a):**

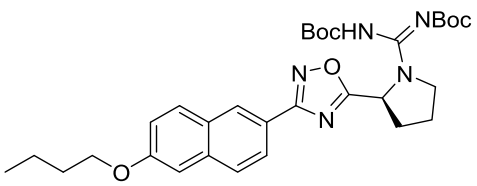

Compound **3.5a** was prepared from **3.4a** using general procedure 3.4 and carried on to the next reaction without purification. Using **3.5a** as starting material, **3.6a** was synthesized using general procedure 3.5. Purification on a silica gel column with 10–30% EtOAc in hexanes produced **3.6a** (25 mg, 67%), a clear oil. ^{1}H NMR (400 MHz, $CDCl_3$) δ 8.51 (d, *J* = 1.6 Hz, 1H), 8.07 (dd, *J* = 8.6, 1.7 Hz, 1H), 7.80 (dd, *J* = 16.6, 8.8 Hz, 2H), 7.22–7.12 (m, 2H), 5.63 (dd, *J* = 7.9, 4.6 Hz, 1H), 4.11 (t, *J* = 6.5 Hz, 2H), 3.95–3.89 (m, 1H), 3.87–3.76 (m, 1H), 2.52–2.41 (m, 1H), 2.33–2.17 (m, 2H), 2.12–2.00 (m, 1H), 1.85 (p, *J* = 6.7 Hz, 2H), 1.57–1.39 (m, 18H), 1.01 (t, *J* = 7.4 Hz, 3H). ^{13}C NMR (101 MHz, $CDCl_3$) δ 168.7, 158.7, 153.8, 150.6,

136.3, 130.4, 128.5, 128.0, 127.5, 124.6, 120.0, 106.8, 82.4, 79.7, 68.0, 49.6, 31.4, 28.3, 19.5, 14.0. HRMS (ESI+): Calcd for $C_{31}H_{41}N_5O_6$ $[M+H]^+$: 560.6951, Found: 580.3122.

tert-butyl (*S,Z*)-(((*tert*-butoxycarbonyl)amino)(2-(3-(6-(pentyloxy)naphthalen-2-yl)-1,2,4-oxadiazol-5-yl)pyrrolidin-1-yl)methylene)carbamate (3.6b):

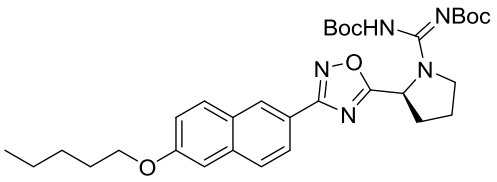

Compound **3.5b** was prepared from **3.4b** using general procedure 3.4 and carried on to the next reaction without purification. Using **3.5b** as starting material, **3.6b** was synthesized using general procedure 3.5. Purification on a silica gel column with 10–30% EtOAc in hexanes produced **3.6b** (23 mg, 63%), a clear oil. ^{1}H NMR (400 MHz, $CDCl_3$) δ 8.51 (d, *J* = 1.6 Hz, 1H), 8.07 (dd, *J* = 8.6, 1.7 Hz, 1H), 7.80 (dd, *J* = 17.4, 8.8 Hz, 2H), 7.21–7.13 (m, 2H), 5.63 (dd, *J* = 7.9, 4.5 Hz, 1H), 4.09 (t, *J* = 6.6 Hz, 2H), 3.95–3.88 (m, 1H), 3.87–3.77 (m, 1H), 2.53–2.41 (m, 1H), 2.32–2.15 (m, 2H), 2.11–2.02 (m, 1H), 1.90–1.82 (m, 2H), 1.79–1.68 (m, 1H), 1.60–1.36 (m, 24H), 0.95 (t, *J* = 7.1 Hz, 3H).^{13}C NMR (101 MHz, $CDCl_3$) δ 179.0, 168.7, 158.6, 154.1, 150.6, 136.3, 130.4, 128.5, 128.0, 127.5, 124.5, 121.7, 120.0, 106.8, 82.3, 79.8, 68.3, 55.5, 49.6, 36.8, 29.0, 28.4, 28.3, 28.1, 24.8, 23.5, 22.6, 14.2. HRMS (ESI+): Calcd for $C_{32}H_{43}N_5O_6$ $[M+H]^+$: 594.7217, Found: 594.3323.

tert-butyl (*S,Z*)-(((*tert*-butoxycarbonyl)amino)(2-(3-(6-(hexyloxy)naphthalen-2-yl)-1,2,4-oxadiazol-5-yl)pyrrolidin-1-yl)methylene)carbamate (3.6c):

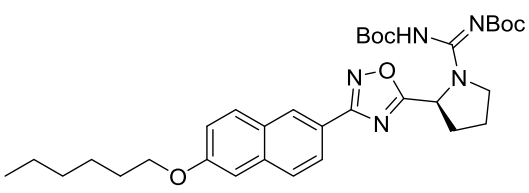

Compound **3.5c** was prepared from **3.4c** using general procedure 3.4 and carried on to the next reaction without purification. Using **3.5c** as starting material, **3.6c** was synthesized using general procedure 3.5. Purification on a silica gel column with 15–

30% EtOAc in hexanes produced **3.6c** (25 mg, 66%), a clear oil. ^{1}H NMR (500 MHz, $CDCl_3$) δ 8.51 (d, *J* = 1.6 Hz, 1H), 8.07 (dd, *J* = 8.5, 1.7 Hz, 1H), 7.80 (dd, *J* = 20.7, 8.8 Hz, 2H), 7.19 (dd, *J* = 8.9, 2.5 Hz, 1H), 7.15 (d, *J* = 2.4 Hz, 1H), 5.64 (d, *J* = 6.3 Hz, 1H), 4.09 (t, *J* = 6.6 Hz, 2H), 3.98–3.86 (m, 1H), 3.83 (s, 1H), 2.51–2.41 (m, 1H), 2.34–2.16 (m, 2H), 2.12–2.00 (m, 1H), 1.91–1.79 (m, 2H), 1.64–1.29 (m, 27H), 0.93 (t, *J* = 7.0 Hz, 3H). ^{13}C NMR (126 MHz, $CDCl_3$) δ 178.9, 168.7, 158.6, 136.3, 130.4, 128.0, 127.5, 124.5, 120.0, 106.7, 68.3, 55.5, 49.6, 31.7, 29.3, 28.3, 25.9, 22.8, 14.2.HRMS (ESI+): Calcd for $C_{33}H_{45}N_5O_6$ $[M+H]^+$: 608.7482, Found: 608.3447.

***tert*-butyl (*S*,*Z*)-(((*tert*-butoxycarbonyl)amino)(2-(3-(6-(heptyloxy)naphthalen-2-yl)-1,2,4-oxadiazol-5-yl)pyrrolidin-1-yl)methylene)carbamate (3.6d):**

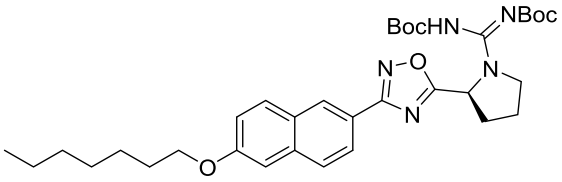

Compound **3.5d** was prepared from **3.4d** using general procedure 3.4 and carried on to the next reaction without purification. Using **3.5d** as starting material, **3.6d** was synthesized using general procedure 3.5. Purification on a silica gel column with 15–30% EtOAc in hexanes produced **3.6d** (14 mg, 59%), a clear oil. ^{1}H NMR (400 MHz, $CDCl_3$) δ 8.49 (d, *J* = 1.6 Hz, 1H), 8.05 (dd, *J* = 8.6, 1.7 Hz, 1H), 7.78 (dd, *J* = 17.1, 8.8 Hz, 2H), 7.21–7.11 (m, 2H), 5.61 (dd, *J* = 7.9, 4.5 Hz, 1H), 4.08 (t, *J* = 6.5 Hz, 2H), 3.97–3.88 (m, 1H), 3.85–3.75 (m, 1H), 2.51–2.39 (m, 1H), 2.31–2.15 (m, 2H), 2.05 (dd, *J* = 12.8, 6.3 Hz, 1H), 1.84 (p, *J* = 6.7 Hz, 2H), 1.67–1.17 (m, 26H), 0.88 (t, *J* = 7.1 Hz, 3H).^{13}C NMR (126 MHz, $CDCl_3$) δ 178.9, 168.2, 162.0, 158.5, 150.4, 136.2, 130.3, 128.3, 127.9, 127.3, 124.4, 121.6, 119.9, 106.3, 82.3, 79.6, 77.6, 77.3, 77.0, 76.8, 68.2, 55.4, 49.5, 36.6, 31.8, 29.7, 29.2, 29.1, 28.1, 26.1, 22.6, 14.1. HRMS (ESI+): Calcd for $C_{34}H_{47}N_5O_6$ $[M+H]^+$: 622.7748, Found: 622.3606.

***tert*-butyl (*S,Z*)-(((*tert*-butoxycarbonyl)amino)(2-(3-(6-isobutoxynaphthalen-2-yl)-1,2,4-oxadiazol-5-yl)pyrrolidin-1-yl)methylene)carbamate (3.6e):**

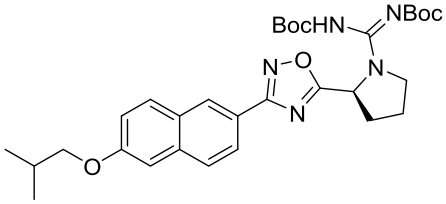

Compound **3.5e** was prepared from **3.4e** using general procedure 3.4 and carried on to the next reaction without purification. Using **3.5e** as starting material, **3.6e** was synthesized using general procedure 3.5. Purification on a silica gel column with 1530% EtOAc in hexanes produced **3.6e** (34 mg, 65%), a clear oil. ^{1}H NMR (500 MHz, $CDCl_3$) δ d) δ 8.51 (d, *J* = 1.7 Hz, 1H), 8.07 (dd, *J* = 8.5, 1.7 Hz, 1H), 7.80 (dd, *J* = 22.6, 8.8 Hz, 2H), 7.20 (dd, *J* = 9.0, 2.5 Hz, 1H), 7.14 (d, *J* = 2.5 Hz, 1H), 5.63 (dd, *J* = 8.0, 4.6 Hz, 1H), 3.97–3.88 (m, 1H), 3.95–3.82 (m, 3H), 2.50–2.42 (m, 1H), 2.29–2.14 (m, 3H), 2.12–1.97 (m, 1H), 1.55–1.38 (m, 20H), 1.08 (d, *J* = 6.7 Hz, 6H).^{13}C NMR (126 MHz, $CDCl_3$) δ 179.0, 168.7, 162.1, 158.7, 153.8, 150.5, 136.3, 130.4, 128.5, 128.0, 127.5, 124.5, 121.7, 120.0, 106.8, 82.4, 79.7, 74.6, 55.5, 49.6, 31.6, 28.4, 28.3, 24.1, 19.5. HRMS (ESI+): Calcd for $C_{31}H_{41}N_5O_6$ $[M+H]^+$: 580.6951, Found: 580.3123.

***tert*-butyl (*S,E*)-((2-(3-(6-(benzyloxy)naphthalen-2-yl)-1,2,4-oxadiazol-5-yl)pyrrolidin-1-yl)((*tert*-butoxycarbonyl)amino)methylene)carbamate (3.6f):**

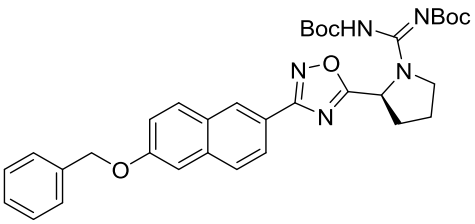

Compound **3.5f** was prepared from **3.4f** using general procedure 3.4 and carried on to the next reaction without purification. Using **3.5f** as starting material, **3.6f** was synthesized using general procedure 3.5. Purification on a silica gel column with 15–30% EtOAc in hexanes produced **3.6f** (12 mg, 40%), a clear oil. ^{1}H NMR (400 MHz, $CDCl_3$) δ 8.53 (d, *J* = 1.6 Hz, 1H), 8.09 (dd, *J* = 8.6, 1.7 Hz, 1H), 7.85 (d, *J* =

8.8 Hz, 1H), 7.79 (d, *J* = 8.6 Hz, 1H), 7.53–7.48 (m, 2H), 7.45–7.40 (m, 2H), 7.39–7.33 (m, 1H), 7.30–7.25 (m, 2H), 5.64 (dd, *J* = 7.9, 4.5 Hz, 1H), 5.21 (s, 2H), 3.97–3.88 (m, 1H), 3.86–3.75 (m, 1H), 2.55–2.40 (m, 1H), 2.31–2.16 (m, 2H), 2.10–2.00 (m, 1H), 1.57–1.33 (m, 18H). ^{13}C NMR (101 MHz, $CDCl_3$) δ 179.0, 168.6, 158.2, 153.7, 150.7, 136.7, 136.2, 130.6, 128.8, 128.7, 128.3, 128.0, 127.7, 127.6, 124.7, 122.1, 120.0, 107.4, 82.4, 79.7, 77.4, 55.5, 49.6, 32.1, 29.8, 28.3, 22.8, 14.3. HRMS (ESI+): Calcd for $C_{34}H_{39}N_5O_6$ $[M+H]^+$: 614.7113, Found: 614.2990.

tert-butyl (*S,E*)-(((_tert_-butoxycarbonyl)amino)(2-(3-(6-((4-methylbenzyl)oxy)naphthalen-2-yl)-1,2,4-oxadiazol-5-yl)pyrrolidin-1-yl)methylene)carbamate (3.6g):

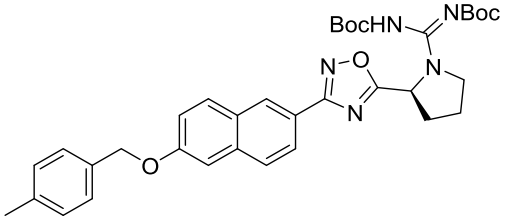

Compound **3.5g** was prepared from **3.4g** using general procedure 3.4 and carried on to the next reaction without purification. Using **3.5g** as starting material, **3.6g** was synthesized using general procedure 3.5. Purification on a silica gel column with 15–30% EtOAc in hexanes produced **3.6g** (4 mg, 27%), a clear oil. ^{1}H NMR (400 MHz, $CDCl_3$) δ 8.50 (s, 1H), 8.06 (dd, *J* = 8.6, 1.7 Hz, 1H), 7.83 (d, *J* = 8.5 Hz, 1H), 7.77 (d, *J* = 8.7 Hz, 1H), 7.36 (d, *J* = 8.0 Hz, 2H), 7.24–7.18 (m, 4H), 5.62 (dd, *J* = 7.8, 4.6 Hz, 1H), 5.15 (s, 2H), 3.95–3.86 (m, 1H), 3.85–3.77 (m, 1H), 2.50–2.38 (m, 1H), 2.36 (s, 3H), 2.33–2.14 (m, 2H), 2.10–1.99 (m, 1H), 1.49–1.38 (m, 18H). ^{13}C NMR (101 MHz, CD_3OD) δ 178.3, 168.6, 156.2, 154.2, 153.7, 152.9, 137.6, 135.4, 135.2, 129.2, 128.5, 128.4, 127.7, 124.1, 123.9, 120.1, 118.8, 118.6, 83.2, 81.4, 55.5, 49.8, 31.4, 30.3, 28.3, 28.2, 24.3, 21.1. HRMS (ESI+): Calcd for $C_{35}H_{41}N_5O_6$ $[M+H]^+$: 628.3154, Found: 628.7379.

(*S*,*E*)-6-(5-(1-(*N*,*N'*-bis(*tert*-butoxycarbonyl)carbamimidoyl)pyrrolidin-2-yl)-1,2,4-oxadiazol-3-yl)naphthalen-2-yl 4-methylbenzenesulfonate (3.6h):

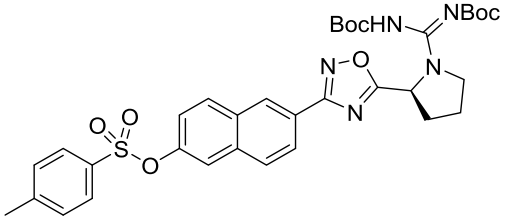

Compound **3.5h** was prepared from **3.4h** using general procedure 3.4 and carried on to the next reaction without purification. Using **3.5h** as starting material, **3.6h** was synthesized using general procedure 3.5. Purification on a silica gel column with 15–30% EtOAc in hexanes produced **3.6h** (7 mg, 61%), a clear oil. ^{1}H NMR (500 MHz, $CDCl_3$) δ 8.57 (d, *J* = 1.6 Hz, 1H), 8.14 (dd, *J* = 8.6, 1.6 Hz, 1H), 7.85 (d, *J* = 9.0 Hz, 1H), 7.82 (d, *J* = 8.7 Hz, 1H), 7.78–7.70 (m, 2H), 7.52 (d, *J* = 2.3 Hz, 1H), 7.34–7.27 (m, 2H), 7.16 (dd, *J* = 8.9, 2.4 Hz, 1H), 5.64 (dd, *J* = 7.9, 4.6 Hz, 1H), 3.97–3.89 (m, 1H), 3.86–3.77 (m, 1H), 2.54–2.46 (m, 1H), 2.45 (s, 3H), 2.33–2.14 (m, 2H), 2.10–2.01 (m, 1H), 1.46 (s, 18H).^{13}C NMR (126 MHz, $CDCl_3$) δ 179.4, 168.2, 162.1, 153.9, 150.4, 148.5, 145.7, 134.9, 132.5, 131.6, 130.9, 130.0, 128.8, 128.7, 128.0, 125.1, 124.8, 122.3, 120.2, 82.5, 79.9, 55.5, 49.6, 31.4, 29.8, 28.3, 24.2, 21.9. HRMS (ESI+): Calcd for $C_{34}H_{39}N_5O_8S$ $[M+H]^+$: 678.7751, Found: 678.2600.

***tert*-butyl ((*E*)-((*tert*-butoxycarbonyl)amino)((2*S*,3*S*)-3-hydroxy-2-(3-(6-(pentyloxy)naphthalen-2-yl)-1,2,4-oxadiazol-5-yl)pyrrolidin-1-yl)methylene)carbamate (3.6i):**

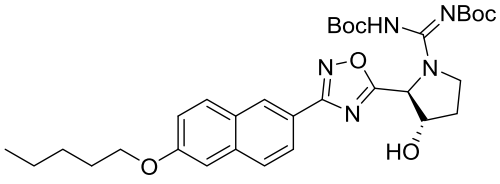

Compound **3.5i** was prepared from **3.4i** using general procedure 3.4 and carried on to the next reaction without purification. Using **3.5i** as starting material, **3.6i** was synthesized using general procedure 3.5. Purification on a silica gel column with 20–40%

EtOAc in hexanes produced **3.6i** (34 mg, 66%), a clear oil. ^{1}H NMR (400 MHz, $CDCl_3$) δ 8.45 (d, *J* = 1.6 Hz, 1H), 8.02 (dd, *J* = 8.6, 1.7 Hz, 1H), 7.78–7.70 (m, 2H), 7.20–7.08 (m, 2H), 5.62–5.56 (m, 1H), 4.69 (s, 1H), 4.05 (t, *J* = 6.5 Hz, 2H), 4.02–3.93 (m, 2H), 2.40–2.33 (m, 1H), 2.22–2.08 (m, 1H), 1.89–1.78 (m, 2H), 1.50–1.35 (m, 21H), 0.95 (t, *J* = 7.1 Hz, 3H). ^{13}C NMR (126 MHz, $CDCl_3$) δ 176.6, 168.7, 158.6, 136.2, 130.3, 128.3, 128.0, 127.4, 124.3, 121.4, 119.9, 106.6, 82.5, 79.9, 77.6, 77.3, 77.0, 76.8, 74.9, 68.1, 63.4, 46.9, 31.9, 29.7, 28.9, 28.4, 28.3, 28.1, 28.0, 22.7, 22.5, 14.1, 14.0. HRMS (ESI+): Calcd for $C_{32}H_{43}N_5O_7$ $[M+H]^+$: 610.7211, Found: 610.3248.

***tert*-butyl ((*Z*)-((*tert*-butoxycarbonyl)amino)((2*S*,3*S*)-3-hydroxy-2-(3-(6-isobutoxynaphthalen-2-yl)-1,2,4-oxadiazol-5-yl)pyrrolidin-1-yl)methylene)carbamate (3.6j):**

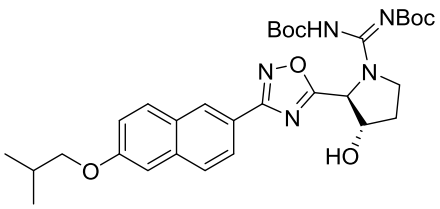

Compound **3.5j** was prepared from **3.4j** using general procedure 3.4 and carried on to the next reaction without purification. Using **3.5j** as starting material, **3.6j** was synthesized using general procedure 3.5. Purification on a silica gel column with 20–40% EtOAc in hexanes produced **3.6j** (32 mg, 70%), a clear oil. ^{1}H NMR (500 MHz, $CDCl_3$) δ 8.48 (s, 1H), 8.04 (dd, *J* = 8.6, 1.4 Hz, 1H), 7.78 (dd, *J* = 17.2, 8.8 Hz, 2H), 7.21–7.17 (m, 1H), 7.13 (s, 1H), 5.57 (s, 1H), 4.69 (s, 1H), 4.05–3.96 (m, 2H), 3.84 (d, *J* = 6.5 Hz, 2H), 2.44–2.34 (m, 1H), 2.19–2.10 (m, 2H), 1.55–1.35 (m, 22H), 1.07 (d, *J* = 6.7 Hz, 7H).^{13}C NMR (126 MHz, $CDCl_3$) δ 176.8, 168.8, 158.8, 153.9, 136.4, 130.4, 128.4, 128.1, 127.5, 124.5, 121.4, 120.1, 106.8, 77.7, 77.4, 77.2, 76.9, 75.0, 74.6, 63.6, 47.1, 32.1, 29.84, 29.80, 29.5, 28.4, 28.1, 22.8, 19.5, 14.2. HRMS (ESI+): Calcd for $C_{31}H_{41}N_5O_7$ $[M+H]^+$: 596.6945, Found: 596.3020.

(*S*)-amino(2-(3-(6-(butyloxy)naphthalen-2-yl)-1,2,4-oxadiazol-5-yl)pyrrolidin-1-yl)methaniminium chloride (3.7a):

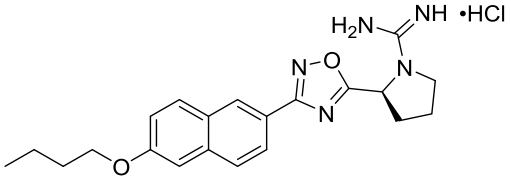

Using **3.6a** as starting material, **3.7a** was synthesized using general procedure 3.4 and isolated as a light yellow tinted solid (6 mg, 42%). Compound found to be > 99% pure by HPLC. ^{1}H NMR (400 MHz, CD_3OD) δ 8.50 (d, *J* = 1.6 Hz, 1H), 8.03 (dd, *J* = 8.6, 1.7 Hz, 1H), 7.88 (d, *J* = 8.8 Hz, 2H), 7.30 (d, *J* = 2.4 Hz, 1H), 7.21 (dd, *J* = 9.0, 2.4 Hz, 1H), 5.46 (dd, *J* = 7.7, 1.9 Hz, 1H), 4.14 (t, *J* = 6.4 Hz, 2H), 3.85–3.77 (m, 1H), 3.68–3.61 (m, 1H), 2.64–2.47 (m, 2H), 2.29–2.19 (m, 1H), 2.18–2.07 (m, 1H), 1.88–1.80 (m, 2H), 1.63–1.51 (m, 2H), 1.02 (t, *J* = 7.4 Hz, 3H). ^{13}C NMR (101 MHz, CD_3OD) δ 177.4, 168.5, 155.7, 150.4, 129.8, 127.4, 125.5, 123.5, 121.0, 119.7, 118.8, 117.2, 106.3, 104.8, 67.5, 55.1, 31.0, 22.9, 18.9, 12.7. HRMS (ESI+): Calcd for $C_{21}H_{25}N_5O_2$ $[M+H]^+$: 380.4636, Found: 380.2069.

(*S*)-amino(2-(3-(6-(pentyloxy)naphthalen-2-yl)-1,2,4-oxadiazol-5-yl)pyrrolidin-1-yl)methaniminium chloride (3.7b)[SLC5081308]:

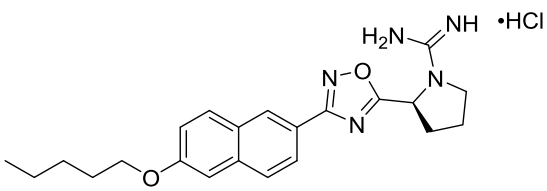

Using **3.6b** as starting material, **3.7b** was synthesized using general procedure 3.4 and isolated as a light yellow tinted solid (5 mg, 95%). Compound found to be 99% pure by HPLC. ^{1}H NMR (400 MHz, CD_3OD) δ 8.50 (d, *J* = 1.6 Hz, 1H), 8.03 (dd, *J* = 8.5, 1.7 Hz, 1H), 7.88 (d, *J* = 8.7 Hz, 2H), 7.30 (d, *J* = 2.4 Hz, 1H), 7.22 (dd, *J* = 9.0, 2.4 Hz, 1H), 5.47 (dd, *J* = 7.8, 2.0 Hz, 1H), 4.13 (t, *J* = 6.4 Hz, 2H), 3.85–3.77 (m, 1H), 3.69–3.60 (m, 2H), 2.64–2.48 (m, 2H), 2.31–2.21 (m, 1H), 2.19–2.05 (m, 1H), 1.87 (dq, *J* = 8.1, 6.5 Hz, 2H), 1.57–1.26 (m, 6H), 0.98 (t, *J* = 7.2 Hz, 3H).^{13}C NMR (126 MHz, CD_3OD) δ 178.9,

169.9, 160.2, 157.1, 137.9, 131.3, 129.7, 128.8, 125.0, 122.4, 121.2, 107.7, 69.2, 56.5, 49.5, 32.7, 30.1, 29.2, 24.4, 23.6, 14.4. HRMS (ESI+): Calcd for $C_{22}H_{27}N_5O_2$ $[M+H]^+$: 394.4900, Found: 394.2237.

(*S*)-amino(2-(3-(6-(hexyloxy)naphthalen-2-yl)-1,2,4-oxadiazol-5-yl)pyrrolidin-1-yl)methaniminium chloride (3.7c) [SLC5011416]:

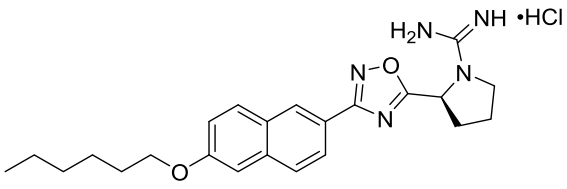

Using **3.6c** as starting material, **3.7c** was synthesized using general procedure 3.4 and isolated as a light yellow tinted solid (14 mg, 96%). Compound found to be 98% pure by HPLC. ^{1}H NMR (400 MHz, CD_3OD) δ 8.51–8.46 (m, 1H), 8.00 (dd, *J* = 8.5, 1.6 Hz, 1H), 7.85 (d, *J* = 8.7 Hz, 2H), 7.29–7.25 (m, 1H), 7.19 (dd, *J* = 9.0, 2.4 Hz, 1H), 5.44 (dd, *J* = 7.8, 2.0 Hz, 1H), 4.11 (t, *J* = 6.4 Hz, 2H), 3.81–3.73 (m, 1H), 3.66–3.55 (m, 1H), 2.61–2.46 (m, 2H), 2.26–2.19 (m, 1H), 2.14–2.06 (m, 1H), 1.88–1.80 (m, 2H), 1.56–1.47 (m, 2H), 1.40–1.32 (m, 4H), 0.90 (t, *J* = 7.3 Hz 3H).^{13}C NMR (101 MHz, CD_3OD) δ 178.8, 169.9, 160.2, 157.1, 138.0, 131.3, 129.7, 128.8, 125.0, 122.4, 121.2, 107.7, 69.3, 56.5, 49.6, 49.4, 49.2, 49.0, 48.8, 48.6, 48.4, 32.8, 32.7, 30.3, 26.3, 24.4, 23.7, 14.4. HRMS (ESI+): Calcd for $C_{23}H_{29}N_5O_2$ $[M+H]^+$: 408.5166, Found: 408.2408.

(*S*)-amino(2-(3-(6-(heptyloxy)naphthalen-2-yl)-1,2,4-oxadiazol-5-yl)pyrrolidin-1-yl)methaniminium chloride (3.7d):

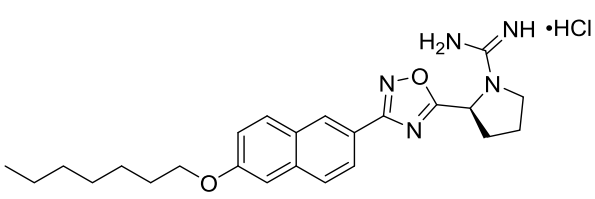

Using **3.6d** as starting material, **3.7d** was synthesized using general procedure 3.4 and isolated as a light yellow tinted solid (8 mg, 78%). Compound found to be > 99% pure by HPLC. ^{1}H NMR (500 MHz, CD_3OD) δ 8.51–8.47

(m, 1H), 8.02 (dd, *J* = 8.5, 1.5 Hz, 1H), 7.87 (d, *J* = 8.7 Hz, 2H), 7.44 (s, 1H), 7.29 (d, *J* = 2.1 Hz, 1H), 7.21 (dd, *J* = 8.9, 2.3 Hz, 1H), 5.47 (d, *J* = 7.2 Hz, 1H), 4.12 (t, *J* = 6.4 Hz, 2H), 3.80 (d, *J* = 7.6 Hz, 1H), 3.65 (t, *J* = 8.4 Hz, 1H), 2.59–2.50 (m, 2H), 2.30–2.20 (m, 1H), 2.12 (d, *J* = 7.2 Hz, 1H), 1.87–1.79 (m, 2H), 1.56–1.48 (m, 2H), 1.45–1.28 (m, 7H), 0.91 (t, *J* = 7.0 Hz, 3H). ^{13}C NMR (126 MHz, CD_3OD) δ 178.9, 169.9, 160.2, 157.1, 137.9, 131.3, 129.7, 128.8, 125.0, 122.4, 121.2, 107.7, 69.2, 56.5, 33.0, 32.8, 30.3, 30.2, 27.2, 24.4, 23.7, 14.4. HRMS (ESI+): Calcd for $C_{24}H_{31}N_5O_2$ $[M+H]^+$: 422.5432, Found: 422.2564.

(*S*)-amino(2-(3-(6-isobutoxynaphthalen-2-yl)-1,2,4-oxadiazol-5-yl)pyrrolidin-1-yl)methaniminium chloride (3.7e):

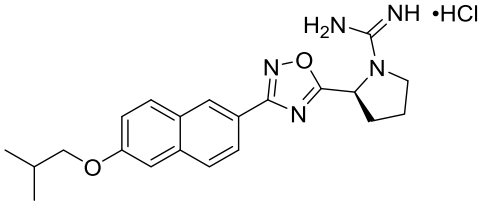

Using **3.6e** as starting material, **3.7e** was synthesized using general procedure 3.4 and isolated as a light yellow tinted solid (17 mg, 99%). Compound found to be > 99% pure by HPLC. ^{1}H NMR (500 MHz, CD_3OD δ 8.50 (s, 1H), 8.02 (dd, *J* = 8.5, 1.3 Hz, 1H), 7.87 (d, *J* = 8.7 Hz, 2H), 7.44 (s, 2H), 7.29 (d, *J* = 2.1 Hz, 1H), 7.22 (dd, *J* = 8.9, 2.2 Hz, 1H), 5.47 (d, *J* = 7.0 Hz, 1H), 3.90 (d, *J* = 6.4 Hz, 2H), 3.85–3.79 (m, 1H), 3.64 (q, *J* = 9.1 Hz, 1H), 2.63–2.54 (m, 1H), 2.54–2.47 (m, 1H), 2.24 (s, 1H), 2.21–2.07 (m, 2H), 1.09 (d, *J* = 6.7 Hz, 6H). ^{13}C NMR (126MHz, CD_3OD) δ 178.9, 169.9, 160.3, 157.1, 137.9, 131.3, 129.7, 128.8, 125.0, 122.4, 121.1, 107.7, 75.6, 56.5, 49.5, 49.3, 49.2, 49.0, 48.8, 48.6, 48.5, 32.8, 29.5, 24.4, 19.6. HRMS (ESI+): Calcd for $C_{21}H_{25}N_5O_2$ $[M+H]^+$: 380.4634, Found: 380.2109.

(*S*)-amino(2-(3-(6-(benzyloxy)naphthalen-2-yl)-1,2,4-oxadiazol-5-yl)pyrrolidin-1-yl)methaniminium chloride (3.7f):

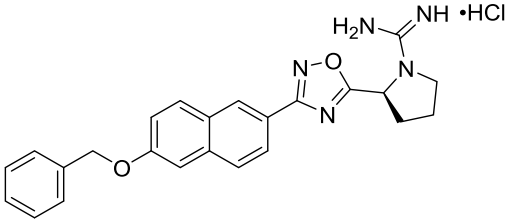

Using **3.6f** as starting material, **3.7f** was synthesized using general procedure 3.4 and isolated as a light yellow tinted solid (7 mg, 95%). Compound found to be 94% pure by HPLC. ^{1}H NMR (500 MHz, CD_3OD) δ 8.52 (d, *J* = 1.6 Hz, 1H), 8.03 (dd, *J* = 8.6, 1.7 Hz, 1H), 7.89 (dd, *J* = 14.2, 8.8 Hz, 2H), 7.53–7.49 (m, 2H), 7.43–7.37 (m, 3H), 7.36–7.28 (m, 2H), 5.49–5.45 (m, 1H), 5.24 (s, 2H), 3.84–3.79 (m, 1H), 3.68–3.60 (m, 1H), 2.64–2.54 (m, 1H), 2.53–2.47 (m, 1H), 2.28–2.20 (m, 1H), 2.16–2.06 (m, 1H). ^{13}C NMR (126 MHz, CD_3OD) δ 178.9, 169.8, 159.8, 157.1, 138.3, 137.8, 131.4, 129.9, 129.6, 129.0, 128.9, 128.8, 128.7, 125.0, 122.6, 121.2, 108.5, 71.2, 56.5, 32.8, 24.4. HRMS (ESI+): Calcd for $C_{24}H_{23}N_5O_2$ $[M+H]^+$: 414.4797, Found: 414.1926.

(*S*)-amino(2-(3-(6-((4-methylbenzyl)oxy)naphthalen-2-yl)-1,2,4-oxadiazol-5-yl)pyrrolidin-1-yl)methaniminium chloride (3.7g):

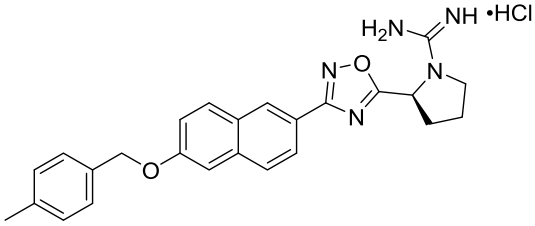

Using **3.6g** as starting material, **3.7g** was synthesized using general procedure 3.4 and isolated as a light yellow tinted solid (3 mg, 100%). Compound found to be 75% pure by HPLC due to degradation. ^{1}H NMR (400 MHz, CD_3OD) δ 8.50 (d, *J* = 15.9 Hz, 1H), 8.06–7.96 (m, 1H), 7.88 (dd, J = 21.9, 8.7 Hz, 1H), 7.76 (d, *J* = 8.9 Hz, 1H), 7.40 (d, *J* = 20.1 Hz, 4H), 7.31–7.20 (m, 1H), 7.16 (d, *J* = 8.2 Hz, 1H), 5.49 (d, *J* = 1.3 Hz, 1H), 5.46 (d, *J* = 6.9 Hz, 1H), 5.19 (s, 1H), 3.85–3.75 (m, 1H), 3.68–3.58 (m, 1H), 2.65–2.46 (m, 2H), 2.35 (s, 3H), 2.29–2.19 (m, 1H), 2.18–2.06 (m, 1H). ^{13}C

NMR (126 MHz, CD_3OD) (also contains some impurity peaks) δ 207.0, 206.9, 198.0, 185.3, 184.0, 167.5, 166.3, 165.0, 164.3, 159.7, 158.2, 158.0, 157.9, 157.8, 157.4, 157.1, 156.4, 153.7, 153.0, 152.7, 150.0, 149.4, 148.7, 148.6, 148.1, 138.3, 84.7, 60.9, 59.1, 52.5, 49.2. HRMS (ESI+): Calcd for $C_{25}H_{25}N_5O_2$ $[M+H]^+$: 428.5062, Found: 428.2083.

(*S*)-amino(2-(3-(6-(tosyloxy)naphthalen-2-yl)-1,2,4-oxadiazol-5-yl)pyrrolidin-1-yl)methaniminium chloride (3.7h):

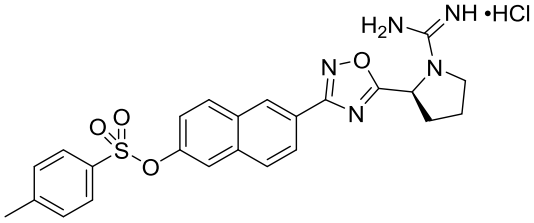

Using **3.6h** as starting material, **3.7h** was synthesized using general procedure 3.4 and isolated as a light yellow tinted solid (7 mg, 100%). Compound found to be > 99% pure by HPLC. ^{1}H NMR (400 MHz, CD_3OD) δ 8.59 (dd, *J* = 1.6, 0.8 Hz, 1H), 8.11 (dd, *J* = 8.6, 1.7 Hz, 1H), 7.99–7.89 (m, 2H), 7.75–7.70 (m, 2H), 7.56 (d, *J* = 2.4 Hz, 1H), 7.43–7.37 (m, 2H), 7.20 (dd, *J* = 8.9, 2.4 Hz, 1H), 5.46 (dd, *J* = 7.9, 2.0 Hz, 1H), 3.78 (td, *J* = 9.2, 2.6 Hz, 1H), 3.66–3.58 (m, 1H), 2.62–2.54 (m, 1H), 2.52–2.45 (m, 1H), 2.43 (s, 3H), 2.27–2.17 (m, 1H), 2.15–2.03 (m, 1H). ^{13}C NMR (126 MHz, CD_3OD) δ 179.3, 169.5, 157.1, 150.1, 147.4, 136.3, 133.6, 132.9, 131.9, 131.1, 130.0, 129.7, 128.8, 125.7, 125.6, 123.5, 121.2, 56.5, 49.6, 32.8, 24.3, 21.6. HRMS (ESI+): Calcd for $C_{24}H_{23}N_5O_4S$ $[M+H]^+$: 478.5435, Found: 478.1561.

Amino((2*S*,3*S*)-3-hydroxy-2-(3-(6-(pentyloxy)naphthalen-2-yl)-1,2,4-oxadiazol-5-yl)pyrrolidin-1-yl)methaniminium chloride (3.7i) [SLC5111312]:

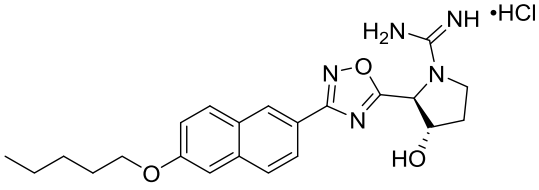

Using **3.6i** as starting material, **3.7i** was synthesized using general procedure 3.4 and isolated as a light yellow tinted solid (73 mg, 100%). Compound found

to be 93% pure by HPLC with 93% ee by SFC with a chiral column. ^{1}H NMR (500 MHz, CD_3OD) δ 8.51–8.50 (m, 1H), 8.03 (dd, *J* = 8.5, 1.6 Hz, 1H), 7.88 (d, *J* = 8.7 Hz, 2H), 7.50 (s, 1H), 7.30 (d, *J* = 2.3 Hz, 1H), 7.22 (dd, *J* = 9.0, 2.4 Hz, 1H), 5.25 (s, 1H), 4.82 (d, *J* = 3.5 Hz, 1H), 4.13 (t, *J* = 6.5 Hz, 2H), 3.88–3.80 (m, 2H), 2.29–2.16 (m, 2H), 1.88–1.84 (m, 2H), 1.57–1.49 (m, 2H), 1.47–1.42 (m, 2H), 0.98 (t, *J* = 7.2 Hz, 3H). ^{13}C NMR (126 MHz, CD_3OD) δ 176.7, 170.0, 160.3, 157.6, 138.0, 131.3, 129.7, 128.9, 128.8, 125.0, 122.3, 121.2, 107.7, 76.0, 69.2, 64.9, 49.51, 49.49, 49.45, 49.34, 49.28, 49.2, 49.1, 49.0, 48.9, 48.8, 48.7, 48.5, 47.4, 32.5, 30.0, 29.5, 23.6, 14.4. HRMS (ESI+): Calcd for $C_{22}H_{27}N_5O_3$ $[M+H]^+$: 410.4894, Found: 410.2204.

Amino((2*S*,3*S*)-3-hydroxy-2-(3-(6-isobutoxynaphthalen-2-yl)-1,2,4-oxadiazol-5-yl)pyrrolidin-1-yl)methaniminium chloride (3.7j) [SLC5121314]:

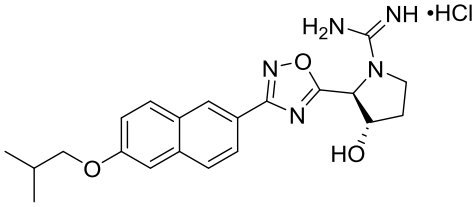

Using **3.6j** as starting material, **3.7j** was synthesized using general procedure 3.4 and isolated as a light yellow tinted solid (9 mg, 62%). Compound found to be 98% pure by HPLC with 92% ee by SFC with a chiral column. ^{1}H NMR (500 MHz, CD_3OD) δ 8.50 (s, 1H), 8.04–7.98 (m, 1H), 7.88 (d, *J* = 7.9 Hz, 2H), 7.51 (s, 1H), 7.29 (d, *J* = 1.9 Hz, 1H), 7.22 (dd, *J* = 8.9, 2.1 Hz, 1H), 5.25 (s, 1H), 4.81 (d, *J* = 2.9 Hz, 1H), 3.93–3.74 (m, 4H), 2.29–2.10 (m, 3H), 1.09 (d, *J* = 6.7 Hz, 6H).^{13}C NMR (126 MHz, CD_3OD) δ 176.7, 170.0, 160.3, 157.6, 138.0, 131.3, 129.7, 128.84, 128.83, 124.9, 122.3, 121.1, 107.8, 76.0, 75.6, 64.8, 49.5, 49.3, 49.2, 49.0, 48.8, 48.7, 48.5, 47.4, 32.5, 29.5, 19.6. HRMS (ESI+): Calcd for $C_{21}H_{25}N_5O_3$ $[M+H]^+$: 396.4628, Found: 396.2020.

***N'*,6-dihydroxy-2-naphthimidamide (3.8):**

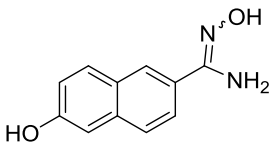

Nitrile **3.1** (3.0 mmol, 0.5g), hydroxylamine hydrochloride (5.9 mmol, 0.411 g), TEA (8.9 mmol, 1.24 mL) were added to a 20 mL microwave vial containing EtOH. The reaction mixture was heated to 150 °C for 2 minutes in the microwave. The reaction mixture was concentrated under reduced pressure, loaded onto Celite, and purified on a silica column with 80–100% EtOAc and hexanes to yield **3.8** as a mixture of E/Z isomers and a beige solid (293 mg, 49%). ^{1}H NMR (400 MHz, CD_3OD) δ 8.02 (d, *J* = 1.4 Hz, 1H), 7.85–7.80 (m, 1H), 7.66–7.61 (m, 2H), 7.15 (d, *J* = 1.7 Hz, 1H), 7.11 (s, 1H). ^{13}C NMR (101 MHz, CD_3OD) δ 188.8, 157.5, 137.1, 131.9, 131.1, 129.4, 129.1, 128.7, 128.3, 127.4, 126.6, 125.4, 124.9, 120.3, 119.9, 109.8. HRMS (ESI+): Calcd for $C_{11}H_{10}N_2O_2$ $[M+H]^+$: 203.2172, Found: 203.0821.

***tert*-butyl (*S*)-2-(3-(6-hydroxynaphthalen-2-yl)-1,2,4-oxadiazol-5-yl)pyrrolidine-1-carboxylate (3.9):**

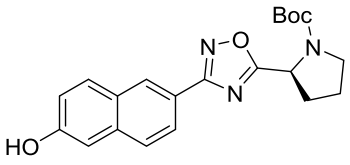

Amidoxime (**3.8**) (0.99 mmol, 0.2 g), Boc-*L*-proline (1.09 mmol, 0.23 g) and DIEA (2.97 mmol, 0.52 mL) were added to a round bottom flask containing DMF. PyBOP (1.19 mmol, 0.62 g) was added to the flask and the solution was heated to 110 °C overnight. Once the reaction cooled to room temperature, the solution was extracted with EtOAc and saturated Na_2CO_3 solution. The combined organic layers were washed with brine and dried over Na_2SO_4. After filtration to remove the $Na_2SO_4$and concentration via reduced pressure, the resulting brown oil was purified on a silica column with 20–35% EtOAc in hexane to yield **3.9** as a light yellow solid (218 mg, 58%). ^{1}H NMR (1:1 rotamer ratio, 400 MHz, $CDCl_3$) δ 1H NMR (400 MHz, $CDCl_3$) δ 8.50 (s,

1H), 8.06 (d, *J* = 8.6 Hz, 1H), 7.93 (s, 1H), 7.82 (d, *J* = 8.8 Hz, 1H), 7.78–7.71 (m, 1H), 7.70 (s, 1H), 7.50 (d, *J* = 8.7 Hz, 1H), 7.43 (d, *J* = 8.7 Hz, 1H), 7.20 (s, 1H), 7.16 (d, *J* = 8.9 Hz, 1H), 7.00 (d, *J* = 7.3 Hz, 1H), 6.91 (s, 1H), 5.30–5.07 (m, 1H), 3.76 (d, *J* = 7.9 Hz, 1H), 3.69–3.50 (m, 1H), 2.43 (d, *J* = 12.3 Hz, 1H), 2.26–2.09 (m, 2H), 2.07–1.97 (m, 1H), 1.54 (s, 4.5H), 1.32 (s, 4.5H). ^{13}C NMR (101 MHz, $CDCl_3$) δ 180.6, 179.2, 168.5, 156.2, 156.0, 155.1, 154.2, 136.5, 136.1, 130.8, 130.6, 128.2, 128.1, 127.5, 127.3, 126.5, 124.3, 123.7, 121.4, 120.4, 119.2, 118.8, 109.8, 109.4, 81.6, 81.3, 54.3, 54.1, 47.2, 46.6, 32.5, 31.9, 28.6, 28.3, 24.4, 23.9. HRMS (ESI+): Calcd for $C_{21}H_{23}N_3O_4$ $[M+Na]^+$: 404.4148, Found: 404.1569.

(*S*)-2-(3-(6-hydroxynaphthalen-2-yl)-1,2,4-oxadiazol-5-yl)pyrrolidin-1-ium chloride (3.10):

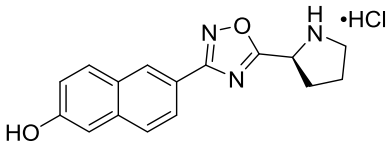

Using **3.9** as starting material, **3.10** was synthesized using general procedure 3.6 and isolated as a light yellow solid (160 mg, 96%). ^{1}H NMR (400 MHz, CD_3OD) δ 8.55–8.52 (m, 1H), 8.02 (dd, *J* = 8.6, 1.7 Hz, 1H), 7.88–7.83 (m, 1H), 7.78 (dt, *J* = 8.7, 0.7 Hz, 1H), 7.17 (d, *J* = 8.2 Hz, 2H), 5.21 (t, *J* = 7.8 Hz, 1H), 3.68–3.51 (m, 2H), 2.75–2.67 (m, 1H), 2.53–2.42 (m, 1H), 2.35–2.24 (m, 2H). ^{13}C NMR (101 MHz, CD_3OD) δ 175.8, 170.1, 158.7, 138.2, 131.6, 129.2, 129.1, 128.3, 124.8, 121.4, 120.6, 110.2, 55.7, 49.7, 49.5, 49.4, 49.3, 49.2, 49.0, 48.8, 48.6, 48.4, 47.4, 30.2, 24.5. HRMS (ESI+): Calcd for C16H15N3O2 [M+H] +: 282.3171, Found: 282.1243.

***tert*-butyl (*S,Z*)-(((*tert*-butoxycarbonyl)amino)(2-(3-(6-hydroxynaphthalen-2-yl)-1,2,4-oxadiazol-5-yl)pyrrolidin-1-yl)methylene)carbamate (3.11):**

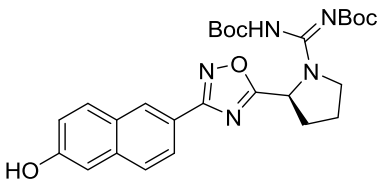

Compound **3.10** (0.49, 0.15 g) was added to microwave vial with acetonitrile and DIEA (1.46 mmol, 0.27 mL). The solution was allowed to stir for 30 seconds before the addition of *N,N′*-DiBoc-1*H*-pyrazole-1-carboxamidine (0.39 mmol, 0.12 g). The solution was heated to 85 °C in the microwave for 30 minutes. The solvent was removed by reduced pressure and the resulting residue was purified on a silica column with hexane and EtOAc to yield **3.11** as a light yellow solid (90 mg, 35%). ^{1}H NMR (400 MHz, $CDCl_3$) δ 7.79 (s, 1H), 7.65 (d, *J* = 8.0 Hz, 2H), 7.39 (t, *J* = 9.8 Hz, 2H), 7.02 (d, *J* = 2.4 Hz, 1H), 6.88 (d, *J* = 2.3 Hz, 1H), 5.65 (dd, *J* = 8.0, 4.5 Hz, 1H), 3.97–3.86 (m, 1H), 3.86–3.76 (m, 1H), 2.54–2.44(m, 1H), 2.31–2.2. (m, 1H), 2.17–1.99 (m, 2H), 1.56–1.34 (d, *J* = 4.7 Hz, 20H). ^{13}C NMR (101 MHz, $CDCl_3$) δ 177.9, 168.6, 156.4, 154.2, 136.2, 130.4, 127.9, 127.6, 127.4, 126.6, 123.7, 120.2, 119.0, 109.5, 81.7, 77.5, 77.4, 77.2, 76.8, 55.7, 49.9, 31.5, 29.8, 28.2, 24.3. HRMS (ESI+): Calcd for $C_{27}H_{33}N_5O_6$ $[M+H]^+$: 524.5888, Found: 524.2532.

***tert*-butyl (*S,Z*)-(((*tert*-butoxycarbonyl)amino)(2-(3-(6-(cyclopentylmethoxy)naphthalen-2-yl)-1,2,4-oxadiazol-5-yl)pyrrolidin-1-yl)methylene)carbamate (3.6k):**

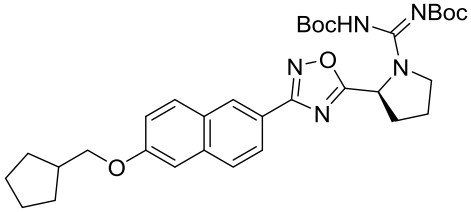

Using **3.11** and cyclopentylmethyl bromide as starting material, **3.6k** was synthesized using general procedure 3.7 and isolated in as a clear film (2 mg, 6%). ^{1}H NMR (400 MHz, $CDCl_3$) δ 8.51 (d, *J* = 1.6 Hz, 1H), 8.07 (dd, *J* = 8.6, 1.7 Hz, 1H), 7.80 (dd, *J* = 17.6, 8.8 Hz, 2H), 7.22–7.10 (m, 2H), 5.63 (dd, *J* = 7.8, 4.5 Hz, 1H), 3.97 (d, *J* = 7.0 Hz, 2H), 3.91 (dt,

J = 7.5, 5.0 Hz, 1H), 3.81 (s, 1H), 2.44 (dt, *J* = 15.0, 7.4 Hz, 2H), 2.21 (dd, *J* = 12.6, 6.5 Hz, 2H), 2.06 (q, *J* = 6.6 Hz, 2H), 1.94–1.84 (m, 2H), 1.71–1.59 (m, 4H), 1.55–1.32 (m, 19H). ^{13}C NMR (101 MHz, $CDCl_3$) δ 178.8, 168.5, 158.6, 153.6, 150.4, 136.2, 130.2, 128.3, 127.9, 127.3, 124.4, 121.5, 119.9, 106.6, 82.1, 79.5, 72.3, 55.4, 49.5, 39.0, 31.4, 29.7, 29.8, 28.1, 25.4, 24.1, 24.0. HRMS (ESI+): Calcd for $C_{33}H_{43}N_5O_6$ $[M+H]^+$: 606.7324, Found: 606.3291.

tert-butyl (*S*,*E*)-(((*tert*-butoxycarbonyl)amino)(2-(3-(6-(3-methoxypropoxy)naphthalen-2-yl)-1,2,4-oxadiazol-5-yl)pyrrolidin-1-yl)methylene)carbamate (3.6l):

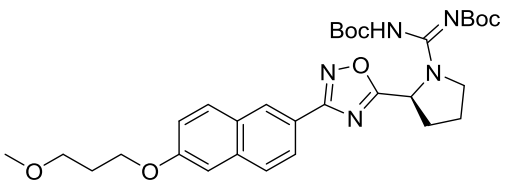

Using **3.11** and 1-bromo-3-methoxypropane as starting material, **3.6l** was synthesized using general procedure 3.7 and isolated in as a clear film (3 mg, 9%). ^{1}H NMR (500 MHz, $CDCl_3$) δ 8.51 (s, 1H), 8.07 (dd, *J* = 8.5, 1.6 Hz, 1H), 7.82 (d, *J* = 8.6 Hz, 1H), 7.78 (d, *J* = 8.6 Hz, 1H), 7.18 (d, *J* = 9.3 Hz, 2H), 5.62 (dd, *J* = 7.8, 4.6 Hz, 1H), 4.20 (t, *J* = 6.3 Hz, 2H), 3.95–3.85 (m, 1H), 3.83–3.75 (m, 1H), 3.60 (t, *J* = 6.1 Hz, 2H), 3.37 (s, 3H), 2.50–2.33 (m, 1H), 2.25–2.16 (m, 2H), 2.13 (q, *J* = 6.2 Hz, 2H), 2.09–2.01 (m, 1H), 1.57–1.25 (m, 23H). ^{13}C NMR (126 MHz, $CDCl_3$) δ 179.0, 168.6, 162.1, 158.4, 154.2, 150.5, 136.3, 133.9, 130.4, 128.5, 128.0, 127.5, 124.6, 121.8, 119.9, 106.8, 82.3, 79.7, 69.3, 65.1, 58.9, 55.5, 49.6, 31.6, 29.8, 29.7, 28.24, 28.16, 28.1, 24.1. HRMS (ESI+): Calcd for $C_{31}H_{41}N_5O_7$ $[M+H]^+$: 596.6945, Found: 596.3101.

***tert*-butyl (*S,Z*)-(((*tert*-butoxycarbonyl)amino)(2-(3-(6-(4-methoxybutoxy)naphthalen-2-yl)-1,2,4-oxadiazol-5-yl)pyrrolidin-1-yl)methylene)carbamate(3.6m):**

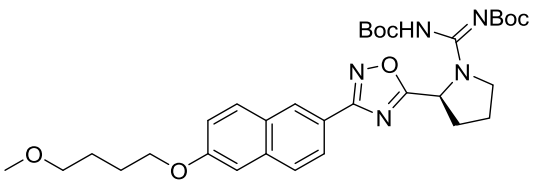

Using **3.11** and 1-bromo-4-methoxypropane as starting material, **3.6m** was synthesized using general procedure 3.7 and isolated in as a clear film (5 mg, 14%). ^{1}H NMR (400 MHz, $CDCl_3$) δ 8.51 (d, *J* = 1.6 Hz, 1H), 8.07 (dd, *J* = 8.5, 1.7 Hz, 1H), 7.82 (d, *J* = 8.8 Hz, 2H), 7.78 (d, *J* = 8.8 Hz, 2H), 7.20–7.11 (m, 2H), 5.62 (dd, *J* = 7.9, 4.5 Hz, 1H), 4.12 (t, *J* = 6.3 Hz, 2H), 3.95–3.85 (m, 1H), 3.84–3.77 (m, 1H), 3.48 (t, *J* = 6.3 Hz, 2H), 3.36 (s, 3H), 2.51–2.43 (m, 1H), 2.29–2.13 (m, 2H), 2.10–2.01 (m, 1H), 1.94–1.87 (m, 2H), 1.82–1.76 (m, 2H), 1.52–1.37 (m, 18H). ^{13}C NMR (101 MHz, $CDCl_3$) δ 179.0, 168.6, 162.0, 158.5, 153.7, 150.3, 136.3, 130.4, 128.5, 128.0, 127.5, 124.6, 121.8, 120.0, 106.7, 82.5, 79.8, 72.5, 67.9, 58.8, 55.5, 49.6, 31.6, 29.8, 28.2, 26.4, 26.2, 24.1. HRMS (ESI+): Calcd for $C_{32}H_{43}N_5O_7$ $[M+H]^+$: 610.7211, Found: 610.3275.

***tert*-butyl (*S,Z*)-(((*tert*-butoxycarbonyl)amino)(2-(3-(6-((4-(trifluoromethyl)benzyl)oxy)naphthalen-2-yl)-1,2,4-oxadiazol-5-yl)pyrrolidin-1-yl)methylene)carbamate (3.6n):**

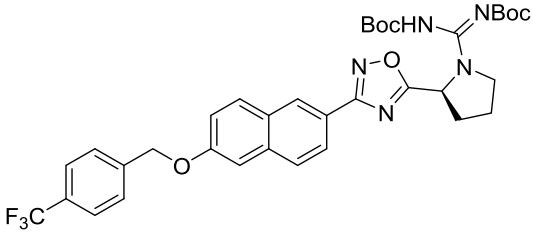

Using **3.11** and 4-(trifloromethyl)benzyl bromide as starting material, **3.6n** was synthesized using general procedure 3.7 and isolated in as a clear film (8 mg, 20%). ^{1}H NMR (400 MHz, $CDCl_3$) δ 8.54 (d, *J* = 1.6 Hz, 1H), 8.09 (dd, *J* = 8.6, 1.6 Hz, 1H), 7.87 (d, *J* = 8.9 Hz, 1H), 7.79 (d, *J* = 8.6 Hz, 1H), 7.69 (s, 1H), 7.61 (d, *J* = 8.1 Hz, 2H), 7.28 (dd, *J* = 8.9, 2.5 Hz, 1H), 7.22 (d, *J* = 2.5 Hz, 1H), 5.63

(dd, *J* = 7.9, 4.6 Hz, 1H), 5.26 (s, 2H), 3.95–3.88 (m, 1H), 3.86–3.77 (m, 1H), 2.52–2.41 (m, 1H), 2.32–2.14 (m, 2H), 2.09–2.01 (m, 1H), 1.57–1.35 (m, 18H). ^{19}F NMR (376 MHz, $CDCl_3$) δ –62.59. ^{13}C NMR (151 MHz, $CDCl_3$) δ 179.1, 168.6, 157.8, 153.8, 150.9, 140.9, 136.1, 130.8, 130.6, 130.9, 128.9, 128.0, 127.8, 127.6, 125.8, 124.8, 122.4, 119.8, 107.5, 83.5, 82.1, 79.9, 69.4, 55.5, 49.6, 31.6, 29.9, 28.3, 28.1, 24.1. HRMS (ESI+): Calcd for $C_{35}H_{38}F_3N_5O_6$ [M+H] +: 682.7093, Found: 682.2889.

tert-butyl (*S,Z*)-(((_tert_-butoxycarbonyl)amino)(2-(3-(6-((3-(trifluoromethyl)benzyl)oxy)naphthalen-2-yl)-1,2,4-oxadiazol-5-yl)pyrrolidin-1-yl)methylene)carbamate (3.6o):

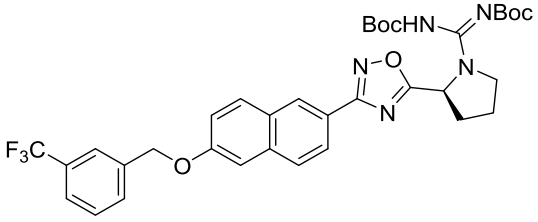

Using **3.11** and 3-(trifloromethyl)benzyl bromide as starting material, **3.6o** was synthesized using general procedure 3.7 and isolated in as a clear film (4 mg, 10%). ^{1}H NMR (500 MHz, $CDCl_3$) δ 8.55–8.52 (m, 1H), 8.10 (dd, *J* = 8.6, 1.7 Hz, 1H), 7.87 (d, *J* = 9.0 Hz, 1H), 7.80 (d, *J* = 8.6 Hz, 1H), 7.77 (d, *J* = 1.7 Hz, 1H), 7.70–7.67 (m, 1H), 7.62 (d, *J* = 8.7 Hz, 1H), 7.55 (d, *J* = 7.7 Hz, 1H), 7.29 (dd, *J* = 8.9, 2.5 Hz, 1H), 7.24 (d, *J* = 2.5 Hz, 1H), 5.63 (dd, *J* = 7.9, 4.6 Hz, 1H), 5.25 (s, 2H), 3.97–3.89 (m, 1H), 3.82 (s, 1H), 2.53–2.42 (m, 1H), 2.19–2.28 (m, 2H), 2.09–2.03 (m, 1H), 1.49–1.39 (m, 18H). ^{19}F NMR (376 MHz, $CDCl_3$) δ –62.67. ^{13}C NMR (126 MHz, $CDCl_3$) δ 179.1, 168.6, 162.2, 157.8, 153.8, 150.6, 137.7, 136.1, 131.3, 131.1, 130.82, 130.75, 129.3, 128.8, 128.0, 127.6, 125.2, 125.1, 124.8, 124.3, 123.1, 122.2, 119.8, 107.3, 82.4, 79.8, 69.1, 55.5, 49.6, 31.6, 29.8, 28.2, 28.1, 24.2. HRMS (ESI+): Calcd for $C_{35}H_{38}F_3N_5O_6$ [M+H] $^+$: 682.7093, Found: 682.2889.

***tert*-butyl (*S*,*Z*)-((2-(3-(6-((4-bromobenzyl)oxy)naphthalen-2-yl)-1,2,4-oxadiazol-5-yl)pyrrolidin-1-yl)((*tert*-butoxycarbonyl)amino)methylene)carbamate (3.6p):**

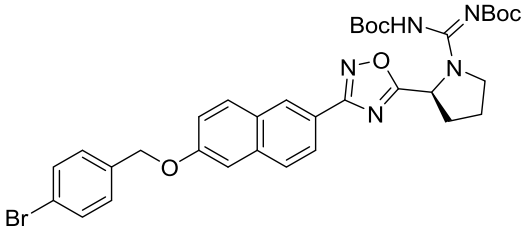

Using **3.11** and 4-(bromo)benzyl bromide as starting material, **3.6p** was synthesized using general procedure 3.7 and isolated in as a clear film (3 mg, 8%). ^{1}H NMR (400 MHz, $CDCl_3$) δ 8.52 (d, *J* = 1.6 Hz, 1H), 8.08 (dd, *J* = 8.6, 1.7 Hz, 1H), 7.85 (d, *J* = 8.9 Hz, 1H), 7.78 (d, *J* = 8.7 Hz, 1H), 7.60–7.50 (m, 2H), 7.40–7.34 (m, 2H), 7.28–7.19 (m, 2H), 5.63 (dd, *J* = 7.8, 4.5 Hz, 1H), 5.15 (s, 2H), 3.98–3.88 (m, 1H), 3.88–3.77 (m, 1H), 2.55–2.40 (m, 1H), 2.33–2.16 (m, 2H), 2.11–2.00 (m, 1H), 1.54–1.38 (m, 18H). ^{13}C NMR (101 MHz, $CDCl_3$) δ 179.0, 168.6, 162.1, 157.9, 153.7, 150.5, 136.1, 135.7, 131.9, 130.7, 129.3, 128.7, 128.0, 127.6, 124.7, 122.2, 119.9, 107.4, 82.2, 79.8, 69.5, 55.5, 49.6, 31.6, 28.2, 28.1, 24.1. HRMS (ESI+): Calcd for $C_{34}H_{38}BrN_5O_6$ $[M+H]^+$: 693.6074, Found: 693.2114.

***tert*-butyl (*S*,*Z*)-((2-(3-(6-((3-bromobenzyl)oxy)naphthalen-2-yl)-1,2,4-oxadiazol-5-yl)pyrrolidin-1-yl)((*tert*-butoxycarbonyl)amino)methylene)carbamate (3.6q):**

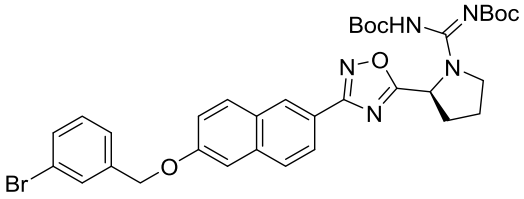

Using **3.11** and 3-(bromo)benzyl bromide as starting material, **3.6q** was synthesized using general procedure 3.7 and isolated in as a clear film (2 mg, 5%). ^{1}H NMR (500 MHz, $CDCl_3$) δ 8.53 (d, *J* = 1.6 Hz, 1H), 8.09 (dd, *J* = 8.6, 1.7 Hz, 1H), 7.86 (d, *J* = 9.0 Hz, 1H), 7.79 (d, *J* = 8.6 Hz, 1H), 7.65 (d, *J* = 1.8 Hz, 1H), 7.48 (dd, *J* = 7.9, 1.9 Hz, 1H), 7.40 (d, *J* = 7.6 Hz, 1H), 7.30–7.25 (m, 3H), 7.21 (d, *J* = 2.4 Hz, 1H), 5.63 (dd, *J* = 7.9, 4.6 Hz, 1H), 5.16 (s, 2H), 3.96–3.87 (m, 1H), 3.85–3.78 (m, 1H), 2.51–2.44 (m, 1H), 2.35–2.17 (m,

2H), 2.09–1.98 (m, 1H), 1.53–1.24 (m, 18H). ^{13}C NMR (126 MHz, $CDCl_3$) δ 179.0, 168.5, 162.1, 157.8, 150.5, 139.0, 136.1, 131.3, 130.7, 130.5, 130.4, 128.7, 128.0, 127.6, 126.0, 124.7, 122.9, 122.1, 119.8, 107.3, 82.3, 79.7, 69.3, 55.5, 49.6, 31.6, 28.2, 28.1, 24.2. HRMS (ESI+): Calcd for $C_{34}H_{38}BrN_5O_6$ $[M+H]^+$: 693.6074, Found: 694.2055.

***tert*-butyl (*S,Z*)-(((*tert*-butoxycarbonyl)amino)(2-(3-(6-((4-chlorobenzyl)oxy)naphthalen-2-yl)-1,2,4-oxadiazol-5-yl)pyrrolidin-1-yl)methylene)carbamate (3.6r):**

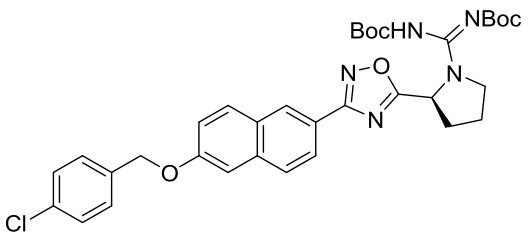

Using **3.11** and 4-(chloro)benzyl bromide as starting material, **3.6r** was synthesized using general procedure 3.7 and isolated in as a clear film (4 mg, 10%).^{1}H NMR (500 MHz, $CDCl_3$) δ 8.53 (d, *J* = 1.6 Hz, 1H), 8.09 (dd, *J* = 8.6, 1.7 Hz, 1H), 7.86 (d, *J* = 9.0 Hz, 1H), 7.79 (d, *J* = 8.6 Hz, 1H), 7.45–7.37 (m, 5H), 7.22 (d, *J* = 2.5 Hz, 1H), 5.63 (dd, *J* = 7.9, 4.6 Hz, 1H), 5.17 (s, 2H), 3.98–3.89 (m, 1H), 3.82 (s, 1H), 2.51–2.44 (m, 1H), 2.29–2.14 (m, 2H), 2.08–1.96 (m, 2H), 1.53–1.38 (m, 18H). ^{13}C NMR (126 MHz, $CDCl_3$) δ 179.1, 168.6, 162.2, 157.9, 153.7, 150.9, 148.8, 136.1, 135.2, 134.1, 130.7, 129.0, 128.8, 128.0, 127.6, 124.7, 122.2, 119.9, 107.4, 83.6, 82.4, 69.5, 55.5, 49.6, 31.6, 29.8, 28.3, 28.2, 28.1, 24.8, 24.1. HRMS (ESI+): Calcd for $C_{34}H_{38}ClN_5O_6$ $[M+H]^+$: 649.1564, Found: 648.2587.

***tert*-butyl (*S,Z*)-(((*tert*-butoxycarbonyl)amino)(2-(3-(6-((3-chlorobenzyl)oxy)naphthalen-2-yl)-1,2,4-oxadiazol-5-yl)pyrrolidin-1-yl)methylene)carbamate (3.6s):**

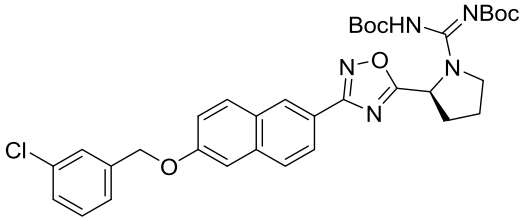

Using **3.11** and 3-(chloro)benzyl bromide as starting material, **3.6s** was synthesized using general procedure 3.7 and isolated in as a clear film (7 mg, 19%).[1]H NMR (500 MHz, $CDCl_3$) δ 8.53 (s, 1H), 8.09 (dd, *J* = 8.6, 1.6 Hz, 1H), 7.86 (d, *J* = 8.9 Hz, 1H), 7.79 (d, *J* = 8.6 Hz, 1H), 7.50 (s, 1H), 7.38–7.32 (m, 3H), 7.28 (d, *J* = 2.5 Hz, 1H), 7.22 (d, *J* = 2.4 Hz, 1H), 5.63 (dd, *J* = 7.9, 4.7 Hz, 1H), 5.17 (s, 2H), 3.97–3.87 (m, 1H), 3.84–3.76 (m, 1H), 2.51–2.43 (m, 1H), 2.29–2.09 (m, 2H), 2.04 (s, 2H), 1.54–1.36 (m, 26H). ^{13}C NMR (126 MHz, $CDCl_3$) δ 179.0, 168.6, 157.9, 153.7, 138.8, 136.1, 134.7, 130.7, 130.1, 128.8, 128.4, 128.0, 127.6, 125.6, 124.7, 122.2, 119.9, 107.3, 81.1, 69.4, 55.5, 49.6, 31.6, 28.2, 28.1, 24.1, 21.2. HRMS (ESI+): Calcd for $C_{34}H_{38}ClN_5O_6$ $[M+H]^+$: 649.1564, Found: 648.2587.

***tert*-butyl (*S,Z*)-(((*tert*-butoxycarbonyl)amino)(2-(3-(6-((4-cyanobenzyl)oxy)naphthalen-2-yl)-1,2,4-oxadiazol-5-yl)pyrrolidin-1-yl)methylene)carbamate (3.6t):**

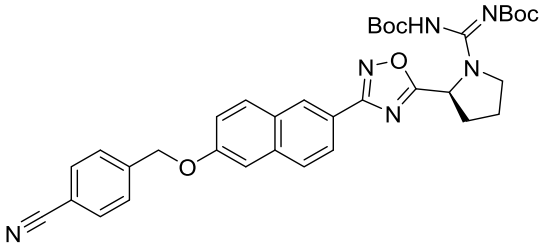

Using **3.11** and 4-(bromomethyl)benzonitrile as starting material, **3.6t** was synthesized using general procedure 3.7 and isolated in as a clear film (4 mg, 11%). [1]H NMR (400 MHz, $CDCl_3$) δ 8.56–8.52 (m, 1H), 8.09 (dd, *J* = 8.6, 1.7 Hz, 1H), 7.89–7.85 (m, 1H), 7.78 (dt, *J* = 9.0, 0.7 Hz, 1H), 7.73–7.68 (m, 2H), 7.63–7.59 (m, 3H), 7.29–7.26 (m, 2H), 7.20 (d, *J* = 2.5 Hz, 1H), 5.63 (dd, *J* = 7.9, 4.6 Hz, 1H), 5.26 (s, 2H), 3.96–3.88 (m, 1H), 3.86–3.78 (m, 1H), 2.47 (m, 1H), 2.32–2.18 (m, 2H),

2.12–2.04 (m, 1H), 1.51–1.39 (m, 18H). ^{13}C NMR (101 MHz, $CDCl_3$) δ 179.1, 168.5, 157.6, 153.7, 142.2, 136.0, 134.0, 132.6, 132.4, 130.8, 128.9, 128.0, 127.8, 127.6, 127.1, 124.8, 122.4, 121.8, 119.7, 119.0, 118.8, 112.0, 107.4, 105.3, 83.1, 81.2, 77.5, 77.2, 76.8, 69.1, 64.3, 55.5, 49.6, 31.6, 29.8, 28.2, 24.2. HRMS (ESI+): Calcd for $C_{35}H_{38}N_6O_6$ $[M+H]^+$: 639.7208, Found: 639.2948.

***tert*-butyl (*S*,*Z*)-((2-(3-(6-([1,1'-biphenyl]-4-ylmethoxy)naphthalen-2-yl)-1,2,4-oxadiazol-5-yl)pyrrolidin-1-yl)((*tert*-butoxycarbonyl)amino)methylene)carbamate (3.6u):**

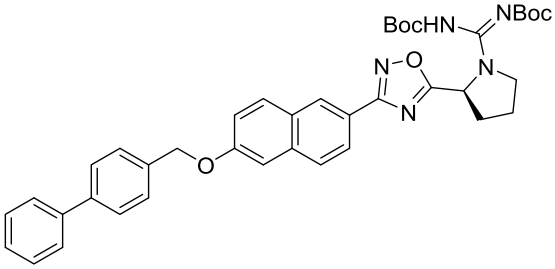

Using **3.11** and 4-(bromomethyl)-1,1'-biphenyl as starting material, **3.6u** was synthesized using general procedure 3.7 and isolated in as a clear film (3 mg, 8%). ^{1}H NMR (400 MHz, $CDCl_3$) δ 8.53 (s, 1H), 8.09 (dd, *J* = 8.5, 1.7 Hz, 1H), 7.86 (d, *J* = 8.6 Hz, 1H), 7.82 (s, 1H), 7.67–7.55 (m, 5H), 7.48–7.43 (m, 2H), 7.42–7.34 (m, 2H), 7.32–7.27 (m, 2H), 5.63 (dd, *J* = 7.8, 4.6 Hz, 1H), 5.25 (s, 2H), 3.99–3.89 (m, 1H), 3.87–3.81 (s, 1H), 2.50–2.40 (m, 2H), 2.31–2.19 (m, 2H), 2.11–2.02 (m, 1H), 1.56–1.38 (m, 18H). ^{13}C NMR (101 MHz, $cdcl_3$) δ 158.2, 148.8, 135.7, 130.6, 129.0, 128.3, 128.0, 127.6, 127.3, 124.7, 120.0, 107.4, 83.6, 70.0, 55.5, 49.6, 29.9, 28.3, 28.1. HRMS (ESI+): Calcd for $C_{40}H_{43}N_5O_6$ $[M+H]^+$: 690.8073, Found: 690.3286.

***tert*-butyl (*S*,*Z*)-(((*tert*-butoxycarbonyl)amino)(2-(3-(6-((5,5,8,8-tetramethyl-5,6,7,8-tetrahydronaphthalen-2-yl)methoxy)naphthalen-2-yl)-1,2,4-oxadiazol-5-yl)pyrrolidin-1-yl)methylene)carbamate (3.6v):**

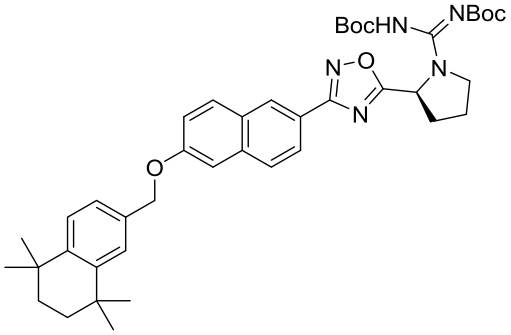

Using **3.11** and 6-(bromomethyl)-1,1,4,4-tetramethyl-1,2,3,4-tetrahydronaphthalene as starting material, **3.6v** was synthesized using general procedure 3.7 and isolated in as a clear film (10 mg, 24%). ^{1}H NMR (400 MHz, $CDCl_3$) δ 8.14–8.06 (m, 1H), 7.87 (d, *J* = 1.2 Hz, 2H), 7.65 (s, 1H), 7.43 (d, *J* = 8.5 Hz, 1H), 7.24 (d, *J* = 2.0 Hz, 1H), 7.12 (d, *J* = 8.2 Hz, 1H), 7.07 (d, *J* = 8.8 Hz, 1H), 6.92 (dd, *J* = 8.2, 1.9 Hz, 1H), 5.61 (dd, *J* = 7.9, 4.6 Hz, 1H), 4.30 (d, *J* = 3.2 Hz, 2H), 3.97–3.86 (m, 1H), 3.85–3.78 (m, 1H), 2.51–2.42 (m, 1H), 2.36–2.27 (m, 1H), 2.19–2.13 (m, 1H), 2.13–2.02 (m, 1H), 1.63 (s, 4H), 1.55–1.34 (m, 18H), 1.23–1.16 (m, 9H). ^{13}C NMR (101 MHz, $CDCl_3$) δ 178.4, 168.6, 156.4, 153.7, 153.6, 144.85, 142.5, 137.2, 135.3, 133.7, 129.2, 128.6, 128.4, 126.7, 126.6, 125.7, 124.2, 124.0, 120.3, 118.9, 118.8, 83.2, 81.4, 77.4, 55.5, 49.7, 35.3, 35.3, 34.3, 34.0, 32.03, 32.00, 31.4, 30.5, 28.3, 28.23, 28.17, 28.15, 28.1, 24.2. HRMS (ESI+): Calcd for $C_{42}H_{53}N_5O_6$ $[M+H]^+$: 742.9081, Found: 724.4136.

***tert*-butyl (*S*,*Z*)-(((*tert*-butoxycarbonyl)amino)(2-(3-(6-(4-(trifluoromethyl)phenethoxy)naphthalen-2-yl)-1,2,4-oxadiazol-5-yl)pyrrolidin-1-yl)methylene)carbamate (3.6w):**

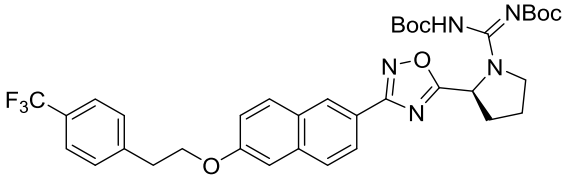

Using **3.11** and 4-(trifluoromethyl)phenethyl bromide as starting material, **3.6w** was synthesized using general procedure 3.7 and isolated in as a

clear film (4 mg, 10%). ^{1}H NMR (500 MHz, $CCDl_3$) δ 8.51 (s, 1H), 8.12–8.02 (m, 1H), 7.82 (d, *J* = 8.9 Hz, 1H), 7.76 (d, *J* = 8.7 Hz, 1H), 7.64–7.57 (m, 3H), 7.44 (d, *J* = 7.9 Hz, 2H), 7.20–7.13 (m, 2H), 5.63 (dd, *J* = 7.9, 4.6 Hz, 1H), 4.33 (t, *J* = 6.6 Hz, 2H), 3.98–3.88 (m, 1H), 3.84–3.76 (m, 1H), 3.23 (t, *J* = 6.6 Hz, 2H), 2.54–2.39 (m, 1H), 2.29–2.10 (m, 2H), 2.07–2.00 (m, 1H), 1.53–1.30 (m, 25H). ^{19}F NMR (376 MHz, $CDCl_3$) δ –62.43. ^{13}C NMR (126 MHz, $CDCl_3$) δ 179.0, 168.6, 162.1, 158.0, 153.7, 150.8, 142.5, 136.1, 134.0, 130.8, 130.6, 129.5, 129.2, 128.9, 128.8, 128.6, 128.0, 127.6, 127.5, 125.8, 125.6, 124.7, 123.3, 122.0, 119.8, 106.8, 105.3, 81.7, 80.4, 68.2, 55.5, 49.6, 35.6, 31.6, 28.2, 28.1, 24.1.HRMS (ESI+): Calcd for $C_{36}H_{40}F_3N_5O_6$ $[M+H]^+$: 696.7358, Found: 696.3011.

tert-butyl (*S,Z*)-(((_tert_-butoxycarbonyl)amino)(2-(3-(6-(3-(trifluoromethyl)phenethoxy)naphthalen-2-yl)-1,2,4-oxadiazol-5-yl)pyrrolidin-1-yl)methylene)(3.6x):

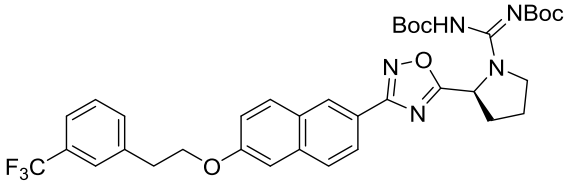

Using **3.11** and 3-(trifluoromethyl)phenethyl bromide as starting material, **3.6x** was synthesized using general procedure 3.7 and isolated in as a clear film (3 mg, 8%). ^{1}H NMR (400 MHz, $CDCl_3$) δ 8.51 (d, *J* = 1.6 Hz, 1H), 8.07 (dd, *J* = 8.6, 1.7 Hz, 1H), 7.82 (d, *J* = 9.0 Hz, 1H), 7.77 (d, *J* = 8.6 Hz, 1H), 7.61–7.56 (m, 1H), 7.56–7.48 (m, 2H), 7.44 (ddt, *J* = 8.3, 6.8, 0.8 Hz, 1H), 7.20–7.13 (m, 2H), 5.63 (dd, *J* = 7.9, 4.6 Hz, 1H), 4.33 (t, *J* = 6.7 Hz, 2H), 3.97–3.89 (m, 1H), 3.88–3.76 (m, 1H), 3.23 (t, *J* = 6.6 Hz, 2H), 2.52–2.43 (m, 1H), 2.32–2.16 (m, 2H), 2.09–2.02 (m, 1H), 1.52–1.33 (m, 18H). ^{19}F NMR (376 MHz, $CDCl_3$) δ –62.59. ^{13}C NMR (101 MHz, $CDCl_3$) δ 179.0, 168.6, 158.0, 153.7, 139.3, 136.2, 132.6, 130.6, 129.1, 128.6, 128.0, 127.5, 126.0, 125.9, 124.6, 123.6, 122.0, 119.8, 106.9, 81.1, 77.4,

68.3, 55.5, 49.6, 35.6, 31.6, 28.2, 28.1, 24.1. HRMS (ESI+): Calcd for $C_{36}H_{40}F_3N_5O_6$ $[M+H]^+$: 696.7358, Found: 696.3006.

***tert*-butyl (*S,Z*)-(((*tert*-butoxycarbonyl)amino)(2-(3-(6-(2-(trifluoromethyl)phenethoxy)naphthalen-2-yl)-1,2,4-oxadiazol-5-yl)pyrrolidin-1-yl)methylene)carbamate (3.6y):**

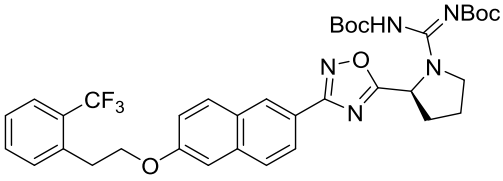

Using **3.11** and 2-(trifluoromethyl)phenethyl bromide as starting material, **3.6y** was synthesized using general procedure 3.7 and isolated in as a clear film (2 mg, 5%). ^{1}H NMR (500 MHz, $CDCl_3$) δ 8.51 (d, *J* = 1.6 Hz, 1H), 8.07 (dd, *J* = 8.6, 1.6 Hz, 1H), 7.83 (d, *J* = 9.0 Hz, 1H), 7.77 (d, *J* = 8.6 Hz, 2H), 7.68 (d, *J* = 7.8 Hz, 1H), 7.52 (d, *J* = 4.3 Hz, 2H), 7.39–7.32 (m, 1H), 7.20 (dd, *J* = 9.0, 2.4 Hz, 1H), 5.63 (dd, *J* = 7.9, 4.6 Hz, 1H), 4.33 (t, *J* = 6.9 Hz, 2H), 3.95–3.88 (m, 1H), 3.86–3.76 (m, 1H), 3.38 (t, *J* = 6.9 Hz, 2H), 2.53 –2.43 (m, 1H), 2.31–2.15 (m, 2H), 2.10–2.01 (m, 2H), 1.51–1.39 (m, 28H). ^{19}F NMR (376 MHz, $CDCl_3$) δ –59.47. ^{13}C NMR (126 MHz, $CDCl_3$) δ 179.0, 168.6, 158.1, 153.7, 150.9, 148.85, 136.7, 136.2, 132.2, 131.9, 130.5, 128.6, 128.0, 127.5, 126.9, 126.3, 124.6, 122.0, 119.8, 106.8, 83.6, 81.8, 80.1, 68.2, 55.5, 49.6, 32.6, 31.6, 28.3, 28.1, 24.1. HRMS (ESI+): Calcd for $C_{36}H_{40}F_3N_5O_6$ $[M+H]^+$: 696.7358, Found: 696.3016.

***tert*-butyl (*S,Z*)-(((*tert*-butoxycarbonyl)amino)(2-(3-(6-(2-oxo-2-phenylethoxy)naphthalen-2-yl)-1,2,4-oxadiazol-5-yl)pyrrolidin-1-yl)methylene)carbamate6p (3.6z):**

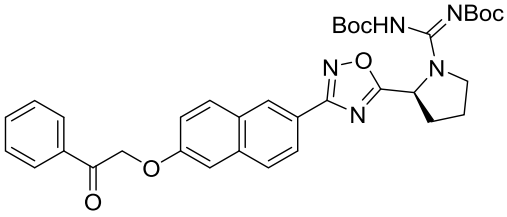

Using **3.11** and 2-bromoacetophenone as starting material, **3.6z** was synthesized using general procedure 3.7 and isolated in as a clear film (3 mg, 8%). ^{1}H NMR (500 MHz, $CDCl_3$) δ 8.52 (d, *J* = 1.6 Hz, 1H), 8.10–8.01 (m, 3H), 7.87 (d, *J* = 9.0 Hz, 1H), 7.77 (d, *J* = 8.6 Hz, 1H), 7.69–7.61 (m, 2H), 7.53 (t, *J* = 7.7 Hz, 2H), 7.32 (dd, *J* = 9.0, 2.5 Hz, 1H), 7.14 (d, *J* = 2.5 Hz, 1H), 5.63 (dd, *J* = 7.9, 4.6 Hz, 1H), 5.43 (s, 2H), 3.98–3.84 (m, 1H), 3.81 (s, 1H), 2.52–2.36 (m, 1H), 2.27–2.13 (m, 2H), 2.10–2.03 (m, 1H), 1.53–1.30 (m, 25H). ^{13}C NMR (126 MHz, $CDCl_3$) δ 194.2, 179.1, 168.5, 162.1, 157.4, 154.1, 152.9, 150.6, 135.9, 134.6, 134.2, 133.9, 130.9, 129.1, 128.3, 128.0, 127.7, 124.8, 122.4, 119.7, 107.5, 105.3, 83.1, 82.4, 79.8, 70.9, 55.5, 49.6, 31.6, 29.9, 28.2, 24.2. HRMS (ESI+): Calcd for $C_{35}H_{39}N_5O_7$ $[M+H]^+$: 642.7214, Found: 642.2962.

***tert*-butyl (*S,Z*)-(((*tert*-butoxycarbonyl)amino)(2-(3-(6-(2-oxo-2-(4-(trifluoromethyl)phenyl)ethoxy)naphthalen-2-yl)-1,2,4-oxadiazol-5-yl)pyrrolidin-1-yl)methylene)carbamate (3.6aa):**

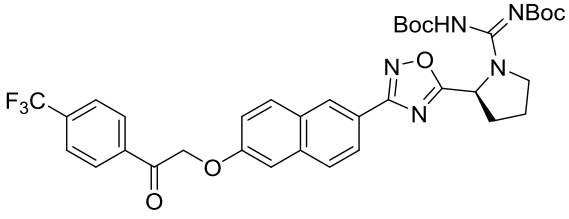

Using **3.11** and 2-bromo-4'-(trifluoromethyl)acetophenone as starting material, **3.6aa** was synthesized using general procedure 3.7 and isolated in as a clear film (4 mg, 10%). ^{1}H NMR (400 MHz, $CDCl_3$) δ 8.53 (d, *J* = 1.6 Hz, 1H), 8.18–8.14 (m, 2H), 8.09 (dd, *J* = 8.6, 1.7 Hz, 1H), 7.87 (d, *J* = 9.0 Hz, 1H), 7.78 (dd, *J* = 8.4, 5.0 Hz, 3H), 7.32–7.28 (m, 1H), 7.15 (d, *J* = 2.6 Hz, 1H), 5.63 (dd, *J* = 7.9, 4.5 Hz,

1H), 5.40 (s, 2H), 3.96–3.89 (m, 1H), 3.82 (s, 1H), 2.50–2.52 (m, 1H), 2.24–2.16 (m, 3H), 2.11–2.00 (m, 2H), 1.51–1.39 (m, 18H). ^{19}F NMR (376 MHz, $CDCl_3$) δ –63.28. ^{13}C NMR (101 MHz, $CDCl_3$) δ 193.8, 179.1, 168.5, 162.2, 157.1, 153.7, 137.3, 135.9, 135.5, 135.2, 131.0, 129.1, 128.9, 128.0, 127.7, 126.1, 125.5, 124.9, 122.6, 122.2, 119.5, 107.5, 82.4, 77.4, 71.1, 55.5, 49.6, 31.6, 29.8, 28.3, 28.1, 24.1. HRMS (ESI+): Calcd for $C_{36}H_{38}F_3N_5O_7$ $[M+H]^+$: 710.7194, Found: 710.2802.

tert-butyl (_S,Z_)-((2-(3-(6-(2-([1,1'-biphenyl]-4-yl)-2-oxoethoxy)naphthalen-2-yl)-1,2,4-oxadiazol-5-yl)pyrrolidin-1-yl)((_tert_-butoxycarbonyl)amino)methylene)carbamate(3.6ab):

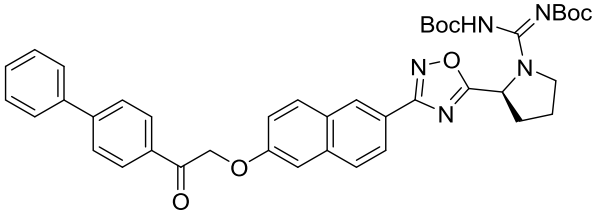

Using **3.11** and 2-bromo-4'-phenylacetophenone as starting material, **3.6ab** was synthesized using general procedure 3.7 and isolated in as a clear film (6 mg, 15%). ^{1}H NMR (400 MHz, $CDCl_3$) δ 8.53 (d, J = 1.6 Hz, 1H), 8.15–8.11 (m, 1H), 8.08 (dd, J = 8.6, 1.7 Hz, 1H), 7.87 (d, J = 9.0 Hz, 1H), 7.78 (d, J = 8.6 Hz, 1H), 7.76–7.73 (m, 1H), 7.66–7.62 (m, 2H), 7.52–7.46 (m, 2H), 7.45–7.40 (m, 1H), 7.33 (dd, J = 9.0, 2.5 Hz, 1H), 7.17 (d, J = 2.5 Hz, 1H), 5.63 (dd, J = 7.9, 4.7 Hz, 1H), 5.44 (s, 2H), 3.97–3.88 (m, 1H), 3.86–3.79 (m, 1H), 2.53–2.40 (m, 1H), 2.32–2.11 (m, 2H), 2.11–2.03 (m, 2H), 1.51–1.40 (m, 18H). ^{13}C NMR (126 MHz, $CDCl_3$) δ 193.8, 179.1, 168.5, 162.1, 157.4, 154.1, 152.9, 150.5, 146.9, 139.8, 135.9, 134.0, 133.3, 130.9, 129.2, 129.0, 128.6, 128.0, 127.7, 127.4, 124.8, 122.4, 119.7, 107.5, 82.4, 79.8, 70.9, 55.5, 49.6, 31.5, 29.8, 28.24, 28.16, 24.1. HRMS (ESI+): Calcd for $C_{41}H_{43}N_5O_7$ $[M+H]^+$: 718.8174, Found: 718.3275.

(*S*)-amino(2-(3-(6-(cyclopentylmethoxy)naphthalen-2-yl)-1,2,4-oxadiazol-5-yl)pyrrolidin-1-yl)methaniminium trifluoroacetate (3.7k):

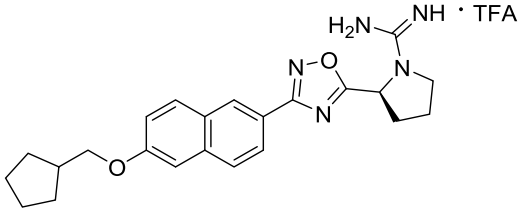

Using **3.6k** as starting material, **3.7k** was synthesized using general procedure 3.8. The final product was isolated as a white solid (1 mg, 69%) and found to be > 99% pure by HPLC. ^{1}H NMR (400 MHz, CD_3OD) δ 8.48 (d, *J* = 1.8 Hz, 1H), 8.00 (dd, *J* = 8.6, 1.7 Hz, 1H), 7.85 (dd, *J* = 8.7, 0.6 Hz, 2H), 7.27 (d, *J* = 2.5 Hz, 1H), 7.20 (d, *J* = 2.4 Hz, 1H), 5.44 (dd, *J* = 7.8, 2.0 Hz, 1H), 3.99 (d, *J* = 6.9 Hz, 2H), 3.85–74 (m, 1H), 3.66–3.58 (m, 1H), 2.63–2.49 (m, 2H), 2.49–2.35 (m, 2H), 2.27–2.16 (m, 1H), 2.16–2.05 (m, 1H), 1.94–1.83 (m, 2H), 1.73–1.55 (m, 5H), 1.47–1.40 (m, 2H). ^{13}C NMR (101 MHz, CD_3OD) δ 178.9, 169.9, 160.3, 157.1, 137.9, 131.3, 129.7, 128.8, 125.0, 122.4, 121.2, 107.8, 73.5, 56.5, 40.4, 32.7, 30.5, 26.5, 24.4. HRMS (ESI+): Calcd for $C_{23}H_{27}N_5O_2$ $[M+H]^+$: 406.5007, Found: 406.2223.

(*S*)-amino(2-(3-(6-(3-methoxypropoxy)naphthalen-2-yl)-1,2,4-oxadiazol-5-yl)pyrrolidin-1-yl)methaniminium trifluoroacetate (3.7l):

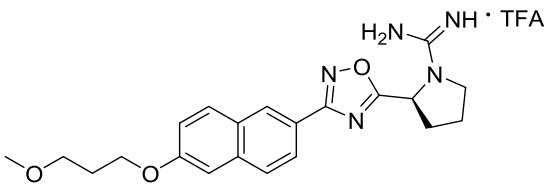

Using **3.6l** as starting material, **3.7l** was synthesized using general procedure 3.8. The final product was isolated as a white solid (1 mg, 47%) and found to be > 99% pure by HPLC. ^{1}H NMR (400 MHz, CD_3OD) δ 8.51 (d, *J* = 1.9 Hz, 1H), 8.03 (dd, *J* = 8.6, 1.7 Hz, 1H), 7.88 (d, *J* = 8.7 Hz, 2H), 7.35–7.28 (m, 1H), 7.22 (dd, *J* = 8.9, 2.5 Hz, 1H), 5.47 (dd, *J* = 7.8, 2.0 Hz, 1H), 4.21 (t, *J* = 6.3 Hz, 2H), 3.80 (dd, *J* = 9.0, 2.6 Hz, 1H), 3.62 (t, *J* = 6.2 Hz, 3H), 2.63–2.46 (m, 2H), 2.23 (s, 1H), 2.11 (p, *J* = 6.2 Hz, 3H). ^{13}C NMR (101 MHz, CD_3OD) δ 178.9, 169.9, 160.1, 157.1, 137.9, 131.3, 129.8, 128.8, 128.8, 125.0, 122.5, 121.1,

107.8, 70.3, 66.1, 58.9, 56.5, 32.7, 30.5, 24.4. HRMS (ESI+): Calcd for $C_{21}H_{25}N_5O_3$ $[M+H]^+$: 396.4628, Found: 396.2031.

(*S*)-amino(2-(3-(6-(4-methoxybutoxy)naphthalen-2-yl)-1,2,4-oxadiazol-5-yl)pyrrolidin-1-yl)methaniminium trifluoroacetate (3.7m):

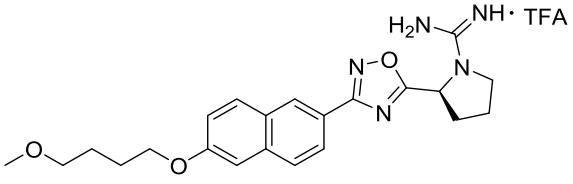

Using **3.6m** as starting material, **3.7m** was synthesized using general procedure 3.8. The final product was isolated as a white solid (2 mg, 91%) and found to be > 99% pure by HPLC. ^{1}H NMR (400 MHz, CD_3OD) δ 8.51–8.48 (m, 1H), 8.03 (dd, *J* = 8.6, 1.6 Hz, 1H), 7.88 (dd, *J* = 8.7, 0.6 Hz, 2H), 7.30 (d, *J* = 2.5 Hz, 1H), 7.21 (dd, *J* = 8.9, 2.5 Hz, 1H), 5.47 (dd, *J* = 7.8, 2.0 Hz, 1H), 4.15 (t, *J* = 6.3 Hz, 2H), 3.86–3.76 (m, 1H), 3.64 (td, *J* = 9.7, 7.2 Hz, 1H), 3.53–3.46 (m, 2H), 3.36 (d, *J* = 0.5 Hz, 3H), 2.60–2.50 (m, 2H), 2.27–2.21 (m, 1H), 2.13 (s, 1H), 1.97–1.89 (m, 2H), 1.84–1.76 (m, 2H). ^{13}C NMR (101 MHz, CD_3OD) δ 178.9, 169.9, 160.1, 157.1, 137.9, 131.3, 129.8, 128.8, 125.0, 122.4, 121.1, 107.7, 73.5, 69.0, 58.8, 56.5, 32.7, 27.3, 27.1, 24.3, 24.2. HRMS (ESI+): Calcd for $C_{22}H_{27}N_5O_3$ $[M+H]^+$: 410.4894, Found: 410.2200.

(*S*)-amino(2-(3-(6-((4-(trifluoromethyl)benzyl)oxy)naphthalen-2-yl)-1,2,4-oxadiazol-5-yl)pyrrolidin-1-yl)methaniminium chloride (3.7n):

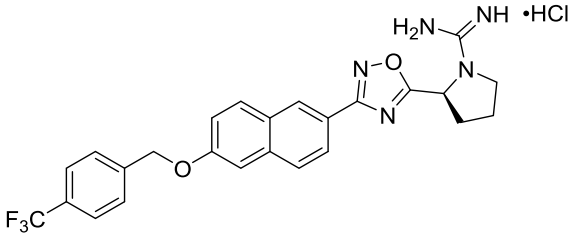

Using **3.6n** as starting material, **3.7n** was synthesized using general procedure 3.6. The compound was isolated as a white solid (2 mg, 66%) and found to be 96% pure by HPLC. ^{1}H NMR (400 MHz, CD_3OD) δ 8.53 (d, J = 1.6 Hz, 1H), 8.05 (dd, J = 8.6, 1.7 Hz, 1H), 7.91 (dd, J =

16.7, 8.8 Hz, 2H), 7.71 (s, 4H), 7.41 (d, J = 2.5 Hz, 1H), 7.33 (dd, J = 8.9, 2.5 Hz, 1H), 5.48 (dd, J = 7.8, 1.9 Hz, 1H), 5.34 (s, 2H), 3.84–3.78 (m, 1H), 3.68–3.60 (m, 1H), 2.64–2.56 (m, 1H), 2.55–2.47 (m, 1H), 2.30–2.21 (m, 1H), 2.18–2.07 (m, 1H). ^{19}F NMR (376 MHz, CD_3OD) δ –64.04. ^{13}C NMR (101 MHz, CD_3OD) δ 178.9, 169.8, 159.4, 157.1, 143.0, 142.9, 137.7, 131.6, 130.0, 128.9, 128.9, 128.9, 128.8, 126.5, 126.4, 126.4, 125.1, 122.8, 121.0, 108.6, 70.2, 56.5, 32.8, 24.4. HRMS (ESI+): Calcd for $C_{25}H_{22}F_3N_5O_2$ [M+H] +: 482.4776, Found: 482.1772.

(*S*)-amino(2-(3-(6-((3-(trifluoromethyl)benzyl)oxy)naphthalen-2-yl)-1,2,4-oxadiazol-5-yl)pyrrolidin-1-yl)methaniminium chloride (3.7o):

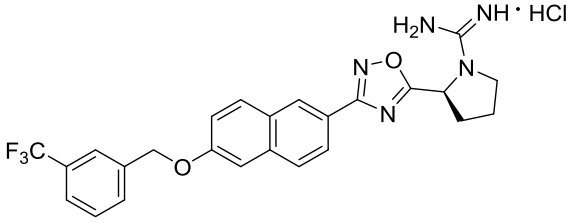

Using **3.6o** as starting material, **3.7o** was synthesized using general procedure 3.6. The final product was isolated as a white solid (2 mg, 66%) and found to be 95% pure by HPLC. ^{1}H NMR (500 MHz, CD_3OD) δ 8.53 (d, *J* = 1.6 Hz, 1H), 8.05 (dd, *J* = 8.6, 1.6 Hz, 1H), 7.92 (dd, *J* = 17.2, 8.8 Hz, 2H), 7.83 (s, 1H), 7.79 (d, *J* = 7.5 Hz, 1H), 7.63 (dt, *J* = 15.3, 7.8 Hz, 2H), 7.44 (d, *J* = 2.4 Hz, 2H), 7.34 (dd, *J* = 8.9, 2.4 Hz, 1H), 5.50–5.46 (m, 1H), 5.33 (s, 2H), 3.83–3.77 (m, 1H), 3.72–3.64 (m, 1H), 2.64–2.55 (m, 1H), 2.54–2.47 (m, 1H), 2.29–2.15 (m, 1H), 2.16–2.07 (m, 1H). ^{19}F NMR (376 MHz, CD_3OD) δ –64.15. ^{13}C NMR (126 MHz, CD_3OD) δ 178.9, 169.8, 159.5, 157.1, 139.8, 137.7, 132.3, 132.0, 131.8, 131.6, 130.5, 130.0, 128.9, 128.8, 126.7, 125.73, 125.70, 125.2, 125.14, 125.11, 124.6, 122.8, 121.1, 108.5, 70.2, 56.5, 32.8, 24.4. HRMS (ESI+): Calcd for $C_{25}H_{22}F_3N_5O_2$ $[M+H]^+$: 482.4776, Found: 482.1806.

(*S*)-amino(2-(3-(6-((4-bromobenzyl)oxy)naphthalen-2-yl)-1,2,4-oxadiazol-5-yl)pyrrolidin-1-yl)methaniminium chloride (3.7p):

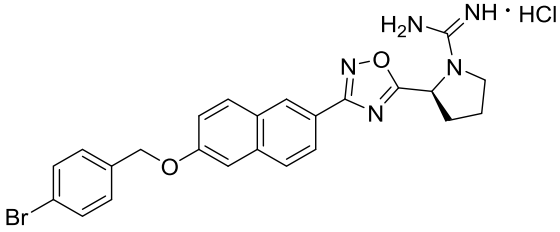

Using **3.6p** as starting material, **3.7p** was synthesized using general procedure 3.6. The final product was isolated as a white solid (2 mg, 87%) and found to be 89% pure by HPLC. ^{1}H NMR (400 MHz, CD_3OD) δ 8.49 (d, *J* = 1.6 Hz, 1H), 8.02 (dd, *J* = 8.6, 1.7 Hz, 1H), 7.87 (dd, *J* = 12.1, 8.9 Hz, 2H), 7.56–7.48 (m, 2H), 7.45–7.34 (m, 3H), 7.27 (dd, *J* = 9.0, 2.4 Hz, 1H), 5.45 (d, *J* = 7.7 Hz, 1H), 5.18 (s, 2H), 3.81–3.73 (m, 1H), 3.65–3.58 (m, 1H), 2.60–2.46 (m, 2H), 2.23 (d, *J* = 9.6 Hz, 1H), 2.16–2.05 (m, 1H). ^{13}C NMR (101 MHz, CD_3OD) δ 178.9, 169.8, 159.6, 157.1, 137.8, 137.6, 132.7, 131.5, 130.5, 130.0, 128.9, 128.8, 125.1, 122.8, 122.7, 121.1, 108.5, 70.3, 56.5, 32.8, 24.4. HRMS (ESI+): Calcd for $C_{24}H_{22}BrN_5O_2$ $[M+H]^+$: 493.3757, Found: 494.1020.

(*S*)-amino(2-(3-(6-((3-bromobenzyl)oxy)naphthalen-2-yl)-1,2,4-oxadiazol-5-yl)pyrrolidin-1-yl)methaniminium chloride (3.7q):

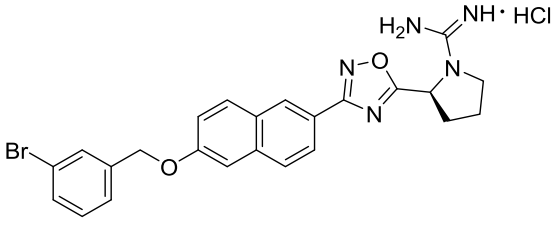

Using **3.6q** as starting material, **3.7q** was synthesized using general procedure 3.6. The final product was isolated as a white solid (1 mg, 66%) and found to be > 99% pure by HPLC. ^{1}H NMR (500 MHz, CD_3OD) δ 8.52 (d, *J* = 1.6 Hz, 1H), 8.04 (dd, *J* = 8.6, 1.7 Hz, 1H), 7.96–7.88 (m, 2H), 7.69 (t, *J* = 1.8 Hz, 1H), 7.49 (ddt, *J* = 8.8, 5.8, 1.1 Hz, 2H), 7.39 (d, *J* = 2.4 Hz, 1H), 7.37–7.27 (m, 2H), 5.47 (dd, *J* = 8.0, 1.9 Hz, 1H), 5.23 (s, 2H), 3.84–3.77 (m, 1H), 3.69–3.59 (m, 1H), 2.62–2.53 (m, 1H), 2.53–2.45 (m, 1H), 2.29–2.20 (m, 1H), 2.19–2.07 (m, 1H). ^{13}C NMR (126

MHz, CD_3OD) δ 178.9, 169.8, 159.5, 157.1, 141.0, 137.7, 132.0, 131.5, 131.4, 131.4, 130.0, 128.9, 128.8, 127.3, 125.1, 123.5, 122.8, 121.1, 108.5, 70.1, 56.5, 32.8, 24.4. HRMS (ESI+): Calcd for $C_{24}H_{22}BrN_5O_2$ $[M+H]^+$: 493.3757, Found: 492.1036.

(*S*)-amino(2-(3-(6-((4-chlorobenzyl)oxy)naphthalen-2-yl)-1,2,4-oxadiazol-5-yl)pyrrolidin-1-yl)methaniminium trifluoroacetate (3.7r):

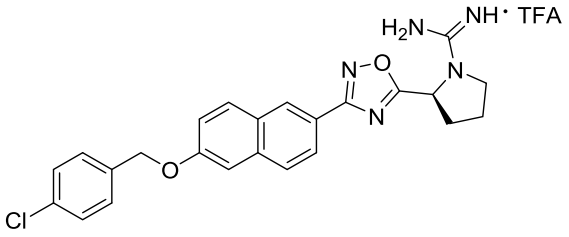

Using **3.6r** as starting material, **3.7r** was synthesized using general procedure 3.8. The final product was isolated as a white solid (2 mg, 67%) and found to be > 99% pure by HPLC. ^1H NMR (400 MHz, CD_3OD) δ 8.53 (dd, *J* = 1.8, 0.7 Hz, 1H), 8.05 (dd, *J* = 8.6, 1.7 Hz, 1H), 7.94–7.86 (m, 2H), 7.54–7.46 (m, 2H), 7.44–7.38 (m, 3H), 7.31 (dd, *J* = 8.9, 2.5 Hz, 1H), 5.49–5.45 (m, 1H), 5.24 (s, 2H), 3.85–3.78 (m, 1H), 3.68–3.61 (m, 1H), 2.63–2.46 (m, 3H), 2.30–2.20 (m, 2H), 2.19–2.10 (m, 1H). ^{13}C NMR (101 MHz, CD_3OD) δ 178.9, 169.8, 159.6, 157.1, 137.8, 137.2, 134.8, 131.5, 130.3, 130.0, 129.7, 128.9, 128.8, 125.1, 122.7, 121.1, 108.5, 70.3, 56.5, 32.8, 24.4. HRMS (ESI+): Calcd for $C_{24}H_{22}ClN_5O_2$ $[M+H]^+$: 448.9247, Found: 448.1572.

(*S*)-amino(2-(3-(6-((3-chlorobenzyl)oxy)naphthalen-2-yl)-1,2,4-oxadiazol-5-yl)pyrrolidin-1-yl)methaniminium trifluoroacetate (3.7s):

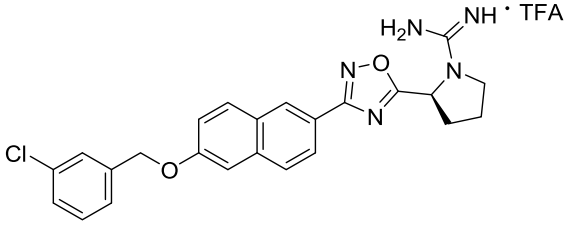

Using **3.6s** as starting material, **3.7s** was synthesized using general procedure 3.8. The final product was isolated as a white solid (2 mg, 89%) and found to be > 99% pure by HPLC. ^1H NMR (500 MHz, CD_3OD) δ 8.53 (d, *J* = 1.7 Hz, 1H), 8.04 (dd, *J* = 8.6, 1.7 Hz, 1H), 7.90 (dd, *J* = 17.8,

8.8 Hz, 2H), 7.54 (t, *J* = 1.8 Hz, 1H), 7.44 (d, *J* = 7.8 Hz, 2H), 7.41–7.29 (m, 4H), 5.47 (dd, *J* = 7.9, 1.9 Hz, 1H), 5.24 (s, 2H), 3.86–3.77 (m, 1H), 3.69–3.58 (m, 1H), 2.68–2.46 (m, 2H), 2.28–2.21 (m, 1H), 2.18–2.07 (m, 1H). ^{13}C NMR (126 MHz, CD_3OD) δ 178.9, 169.8, 159.5, 157.1, 140.7, 137.8, 135.5, 131.5, 131.2, 130.0, 129.0, 128.9, 128.8, 128.5, 126.8, 125.1, 122.8, 121.1, 108.5, 70.2, 56.5, 32.7, 24.3. HRMS (ESI+): Calcd for $C_{24}H_{22}ClN_5O_2$ $[M+H]^+$: 448.9247, Found: 448.1533.

(*S*)-amino(2-(3-(6-((4-cyanobenzyl)oxy)naphthalen-2-yl)-1,2,4-oxadiazol-5-yl)pyrrolidin-1-yl)methaniminium trifluoroacetate (3.7t):

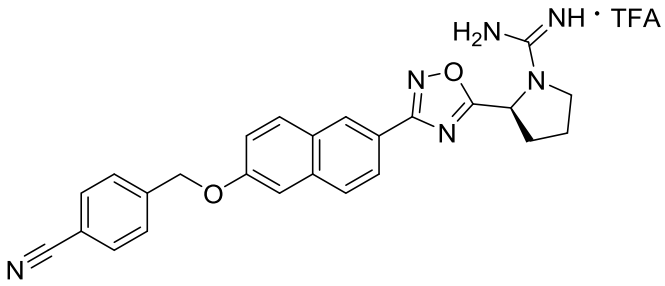

Using **3.6t** as starting material, **3.7t** was synthesized using general procedure 3.8. The final product was isolated as a white solid (2 mg, 67%) and found to be > 99% pure by HPLC. ^{1}H NMR (500 MHz, $(CD_3)_2CO$) δ 8.57 (d, *J* = 1.5 Hz, 1H), 8.09–8.03 (m, 2H), 7.95 (d, *J* = 8.6 Hz, 1H), 7.85 (d, *J* = 8.1 Hz, 2H), 7.79 (d, *J* = 8.1 Hz, 2H), 7.52 (d, *J* = 2.4 Hz, 1H), 7.39 (dd, *J* = 9.0, 2.5 Hz, 1H), 5.64 (dd, *J* = 8.2, 1.5 Hz, 1H), 5.45 (s, 2H), 3.97–3.89 (m, 1H), 3.84–3.76 (m, 1H), 2.75–2.62 (m, 1H), 2.62–2.56 (m, 1H), 2.37–2.30 (m, 1H), 2.30–2.16 (m, 1H). ^{13}C NMR (126 MHz, $(CD_3)_2CO$) δ 178.7, 169.2, 158.9, 143.6, 137.2, 133.3, 132.8, 131.5, 129.6, 129.0, 128.8, 128.4, 127.8, 125.0, 122.6, 120.8, 119.2, 112.4, 108.6, 69.7, 56.0, 48.5, 32.4, 24.2. HRMS (ESI+): Calcd for $C_{32}H_{37}N_6O_2$ $[M+H]^+$: 439.4891, Found: 439.1877.

(*S*)-(2-(3-(6-([1,1'-biphenyl]-4-ylmethoxy)naphthalen-2-yl)-1,2,4-oxadiazol-5-yl)pyrrolidin-1-yl)(amino)methaniminium trifluoroacetate (3.7u):

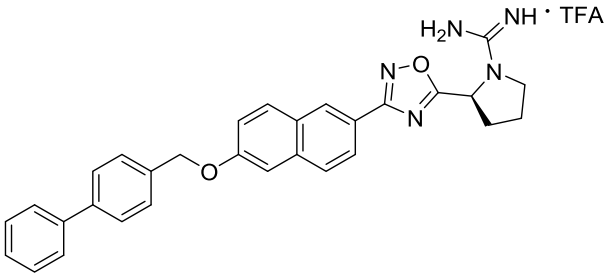

Using **3.6u** as starting material, **3.7u** was synthesized using general procedure 3.8. The final product was isolated as a white solid (2 mg, 87%) and found to be 45% pure by HPLC due to degradation . ^{1}H NMR (500 MHz, CD_3OD) δ 8.53 (dd, *J* = 19.5, 1.6 Hz, 1H), 8.09–7.77 (m, 4H), 7.69 (dd, *J* = 8.3, 1.9 Hz, 1H), 7.67–7.64 (m, 1H), 7.61 (d, *J* = 8.0 Hz, 1H), 7.58–7.54 (m, 1H), 7.47 (dt, *J* = 11.0, 7.2 Hz, 3H), 7.41–7.28 (m, 3H), 5.47 (d, *J* = 2.7 Hz, 1H), 5.32 (s, 1H), 4.52 (s, 1H), 3.86–3.79 (b, 1H), 3.71–3.59 (m, 1H), 2.67–2.51 (m, 2H), 2.27–2.19 (m, 1H), 2.17–2.09 (m, 1H). ^{13}C NMR (126 MHz, CD_3OD) δ 178.9, 169.9, 163.6, 159.6, 157.1, 155.9, 142.4, 142.3, 142.0, 141.7, 137.8, 137.4, 136.8, 131.6, 131.5, 130.5, 130.2, 129.9, 129.9, 129.8, 129.7, 129.7, 129.2, 129.0, 128.9, 128.8, 128.5, 128.4, 128.2, 128.0, 127.83, 127.80, 125.5, 125.1, 124.7, 122.7, 121.2, 120.2, 120.0, 108.5, 70.9, 57.5, 56.5, 32.8, 24.4. HRMS (ESI+): Calcd for $C_{30}H_{27}N_5O_2$ $[M+H]^+$: 490.5756, Found: 490.2249.

(*S*)-amino(2-(3-(6-((5,5,8,8-tetramethyl-5,6,7,8-tetrahydronaphthalen-2-yl)methoxy)naphthalen-2-yl)-1,2,4-oxadiazol-5-yl)pyrrolidin-1-yl)methaniminium trifluoroacetate (3.7v):

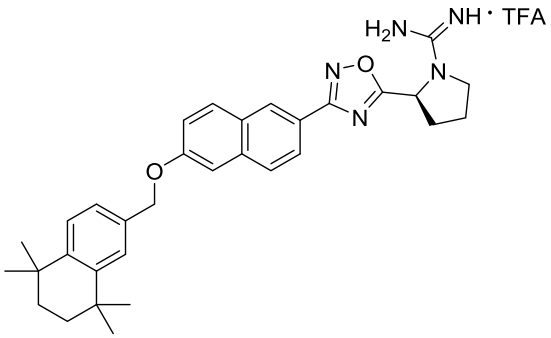

Using **3.6v** as starting material, **3.7v** was synthesized using general procedure 3.8. The final product was isolated as a white solid (3 mg, 93%) and found to be 75% pure by HPLC. ^{1}H NMR (500 MHz, CD_3OD) δ 8.48 (d, *J* = 1.6 Hz, 1H), 8.02–7.90 (m, 2H), 7.78 (d, *J* = 8.9 Hz, 1H), 7.70 (d, *J* = 2.2 Hz, 1H), 7.27 (d, *J* = 8.8 Hz, 1H), 7.21 (d, *J* = 1.9 Hz, 1H), 7.12 (d, *J* = 8.2 Hz, 1H), 6.93 (dd, *J* = 8.2, 1.9 Hz, 1H), 5.45 (dd, *J* = 8.0, 1.9 Hz, 1H), 4.38 (s, 2H), 3.82–3.69 (m, 1H), 3.68–3.59 (m, 1H), 2.60–2.53 (m, 1H), 2.53–2.44 (m, 1H), 2.27–2.19 (m, 1H), 2.15–2.06 (m, 1H), 1.63 (s, 4H), 1.20 (s, 6H), 1.16 (s, 7H). ^{13}C NMR (126 MHz, CD_3OD) δ 178.8, 169.9, 157.1, 155.8, 145.4, 143.0, 139.2, 136.8, 130.0, 129.7, 129.6, 127.5, 127.3, 126.7, 125.6, 124.5, 121.2, 120.6, 120.0, 56.5, 36.3, 36.3, 35.0, 34.8, 32.7, 32.27, 32.25, 31.0, 24.3. HRMS (ESI+): Calcd for $C_{32}H_{37}N_5O_2$ $[M+H]^+$: 524.6764, Found: 524.3019.

(*S*)-amino(2-(3-(6-(4-(trifluoromethyl)phenethoxy)naphthalen-2-yl)-1,2,4-oxadiazol-5-yl)pyrrolidin-1-yl)methaniminium trifluoroacetate (3.7w):

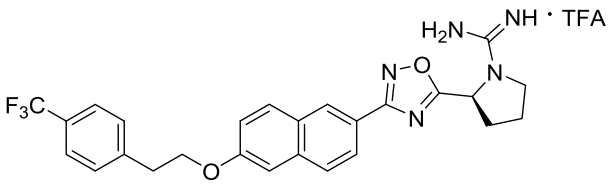

Using **3.6w** as starting material, **3.7w** was synthesized using general procedure 3.8. The final product was isolated as a white solid (3 mg, 98%) and found to be 90% pure by HPLC. ^{1}H NMR (500 MHz, CD_3OD) δ 8.50 (d, *J* = 1.6

Hz, 1H), 8.03 (dd, *J* = 8.5, 1.7 Hz, 1H), 7.88 (d, *J* = 8.8 Hz, 2H), 7.63 (s, 1H), 7.56 (d, *J* = 8.1 Hz, 2H), 7.33 (d, *J* = 2.3 Hz, 1H), 7.25–7.19 (m, 1H), 5.46 (dd, *J* = 7.9, 1.9 Hz, 1H), 4.40 (t, *J* = 6.5 Hz, 2H), 3.80 (td, *J* = 9.2, 2.5 Hz, 1H), 3.63 (td, *J* = 9.7, 7.2 Hz, 1H), 3.25 (t, *J* = 6.5 Hz, 2H), 2.61–2.54 (m, 1H), 2.54–2.48 (m, 1H), 2.29–2.21 (m, 1H), 2.17–2.06 (m, 1H). ^{19}F NMR (376 MHz, CD_3OD) δ -63.92, –77.04. ^{13}C NMR (126 MHz, CD_3OD) δ 178.9, 169.8, 159.8, 157.1, 144.71, 144.70, 137.8, 131.4, 130.8, 129.9, 128.88, 128.86, 128.8, 126.31, 126.28, 126.25, 125.0, 122.6, 121.0, 107.9, 69.3, 56.5, 36.4, 32.7, 24.3. HRMS (ESI+): Calcd for $C_{26}H_{24}F_3N_5O_2$ [M+H]$^+$: 496.5042, Found: 496.1965.

(*S*)-amino(2-(3-(6-(3-(trifluoromethyl)phenethoxy)naphthalen-2-yl)-1,2,4-oxadiazol-5-yl)pyrrolidin-1-yl)methaniminium trifluoroacetate (3.7x):

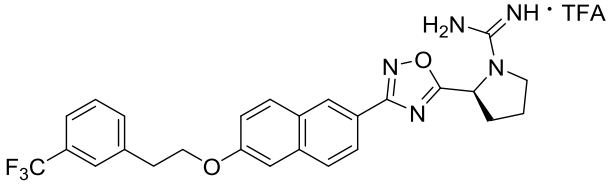

Using **3.6x** as starting material, **3.7x** was synthesized using general procedure 3.8. The final product was isolated as a white solid (2 mg, 87%) and found to be > 99% pure by HPLC. ^{1}H NMR (500 MHz, CD_3OD) δ 8.50 (d, *J* = 1.6 Hz, 1H), 8.03 (dd, *J* = 8.6, 1.6 Hz, 1H), 7.87 (d, *J* = 8.8 Hz, 2H), 7.71–7.60 (m, 2H), 7.54–7.47 (m, 2H), 7.33 (d, *J* = 2.4 Hz, 1H), 7.19 (dd, *J* = 8.9, 2.4 Hz, 1H), 5.46 (dd, *J* = 8.0, 1.8 Hz, 1H), 4.39 (t, *J* = 6.4 Hz, 2H), 3.83–3.77 (m, 1H), 3.69–3.58 (m, 1H), 3.25 (t, *J* = 6.4 Hz, 2H), 2.62–2.49 (m, 2H), 2.27–2.21 (m, 1H), 2.17–2.08 (m, 1H). ^{19}F NMR (376 MHz, CD_3OD) δ –64.08, –77.04. ^{13}C NMR (126 MHz, CD_3OD) δ 178.9, 169.8, 159.4, 157.1, 141.4, 137.8, 133.97, 133.96, 131.4, 130.2, 129.9, 128.8, 126.9, 126.8, 125.0, 124.28, 124.25, 122.6, 121.0, 108.0, 69.5, 56.5, 36.3, 32.7, 24.3. HRMS (ESI+): Calcd for $C_{26}H_{24}F_3N_5O_2$ [M+H]$^+$: 496.5042, Found: 496.1969.

(*S*)-amino(2-(3-(6-(2-(trifluoromethyl)phenethoxy)naphthalen-2-yl)-1,2,4-oxadiazol-5-yl)pyrrolidin-1-yl)methaniminium trifluoroacetate (3.7y):

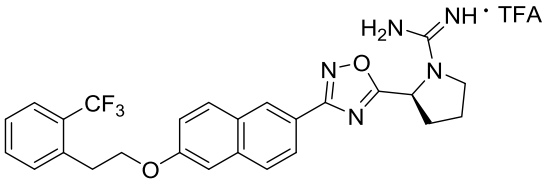

Using **3.6y** as starting material, **3.7y** was synthesized using general procedure 3.8. The final product was isolated as a white solid (1 mg, 65%) and found to be 91% pure by HPLC. ^{1}H NMR (400 MHz, CD_3OD) δ 8.51 (t, *J* = 1.1 Hz, 1H), 8.03 (dd, *J* = 8.6, 1.7 Hz, 1H), 7.92–7.85 (m, 2H), 7.74–7.67 (m, 1H), 7.66–7.55 (m, 2H), 7.43 (t, *J* = 7.3 Hz, 1H), 7.32 (d, *J* = 2.5 Hz, 1H), 7.22 (dd, *J* = 9.0, 2.5 Hz, 1H), 5.46 (dd, *J* = 7.8, 2.1 Hz, 1H), 4.38 (t, *J* = 6.9 Hz, 2H), 3.85–3.74 (m, 1H), 3.69–3.57 (m, 1H), 3.41–3.36 (m, 2H), 2.62–2.50 (m, 2H), 2.29–2.21 (m, 1H), 2.19–2.11 (m, 1H). ^{19}F NMR (376 MHz, CD_3OD) δ –60.73, –77.32. ^{13}C NMR (101 MHz, CD_3OD) δ 178.9, 169.9, 159.7, 157.1, 137.8, 133.3, 131.4, 129.9, 128.9, 128.8, 128.1, 127.04, 126.99, 125.0, 122.6, 121.0, 107.9, 69.5, 56.5, 33.3, 32.7, 24.4. HRMS (ESI+): Calcd for $C_{26}H_{24}F_3N_5O_2$ $[M+H]^+$: 496.5042, Found: 496.1978.

(*S*)-amino(2-(3-(6-(2-oxo-2-phenylethoxy)naphthalen-2-yl)-1,2,4-oxadiazol-5-yl)pyrrolidin-1-yl)methaniminium trifluoroacetate (3.7z):

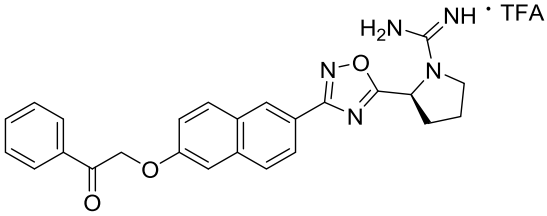

Using **3.6z** as starting material, **3.7z** was synthesized using general procedure 3.8. The final product was isolated as a white solid (2 mg, 90%) and found to be > 99% pure by HPLC. ^{1}H NMR (400 MHz, CD_3OD) δ 8.53 (dd, *J* = 1.7, 0.7 Hz, 1H), 8.13–8.09 (m, 2H), 8.04 (dd, *J* = 8.6, 1.7 Hz, 1H), 7.97–7.91 (m, 1H), 7.87 (d, *J* = 8.7 Hz, 1H), 7.74–7.65 (m, 1H), 7.60–7.53 (m, 2H), 7.40–7.32 (m, 2H), 5.64 (s, 2H), 5.47 (dd, *J* = 7.8, 2.0 Hz, 1H), 3.86–3.79 (m, 1H), 3.66–3.59

(m, 1H), 2.63–2.48 (m, 2H), 2.29–2.21 (m, 1H), 2.21–2.07 (m, 1H). ^{13}C NMR (101 MHz, CD_3OD) δ 196.3, 178.9, 169.8, 159.1, 157.1, 137.6, 135.9, 135.2, 131.6, 130.1, 130.0, 129.2, 129.0, 128.8, 125.1, 122.9, 120.9, 108.6, 71.7, 56.5, 32.7, 24.3. HRMS (ESI+): Calcd for $C_{25}H_{23}N_5O_3$ $[M+H]^+$: 442.4898, Found: 442.1870.

(*S*)-amino(2-(3-(6-(2-oxo-2-(4-(trifluoromethyl)phenyl)ethoxy)naphthalen-2-yl)-1,2,4-oxadiazol-5-yl)pyrrolidin-1-yl)methaniminium trifluoroacetate (3.7aa):

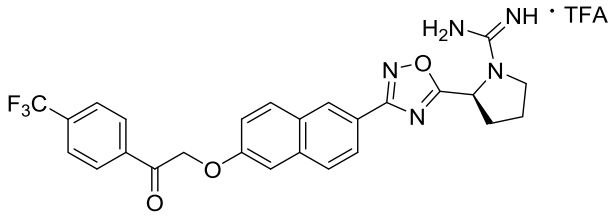

Using **3.6aa** as starting material, **3.7aa** was synthesized using general procedure 3.8. The final product was isolated as a white solid (2 mg, 65%) and found to be > 99% pure by HPLC. ^{1}H NMR (400 MHz, CD_3OD) δ 8.54 (dd, *J* = 1.7, 0.7 Hz, 1H), 8.29–8.24 (m, 2H), 8.05 (dd, *J* = 8.6, 1.7 Hz, 1H), 7.97–7.84 (m, 4H), 7.39–7.33 (m, 2H), 5.67 (s, 2H), 5.47 (dd, *J* = 7.8, 2.0 Hz, 1H), 3.86–3.79 (m, 1H), 3.68–3.61 (m, 1H), 2.62–2.47 (m, 2H), 2.28–2.21 (m, 1H), 2.17–2.08 (m, 1H). ^{19}F NMR (376 MHz, CD_3OD) δ –64.75, –77.17. ^{13}C NMR (101 MHz, $CD3_3OD$) δ 195.5, 178.9, 169.8, 159.0, 157.1, 137.6, 131.6, 130.2, 129.9, 129.2, 128.96, 128.8, 127.0, 126.9, 125.2, 123.0, 120.8, 108.6, 71.9, 56.5, 32.8, 24.3. HRMS (ESI+): Calcd for $C_{26}H_{22}F_3N_5O_3$ $[M+H]^+$: 510.4877, Found: 510.1747.

(*S*)-(2-(3-(6-(2-([1,1'-biphenyl]-4-yl)-2-oxoethoxy)naphthalen-2-yl)-1,2,4-oxadiazol-5-yl)pyrrolidin-1-yl)(amino)methaniminium trifluoroacetate (3.7ab):

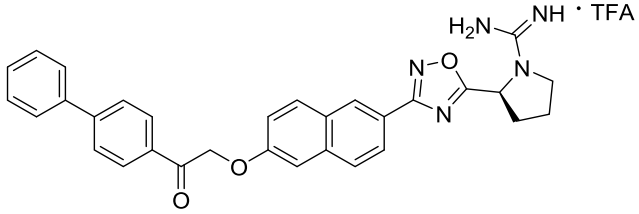

Using **3.6ab** as starting material, **3.7ab** was synthesized using general procedures 3.8. The final product was isolated as a white solid (6 mg, 66 %) and found to be > 99% pure by HPLC. ^{1}H NMR (500 MHz, CD_3OD) δ 8.54 (d, *J* = 1.7 Hz, 1H), 8.20 (d, *J* = 8.4 Hz, 2H), 8.04 (dd, *J* = 8.6, 1.7 Hz, 1H), 7.97–7.92 (m, 1H), 7.88 (d, *J* = 8.7 Hz, 1H), 7.84 (d, *J* = 8.3 Hz, 2H), 7.74–7.70 (m, 2H), 7.50 (dd, *J* = 8.5, 6.9 Hz, 2H), 7.45–7.41 (m, 2H), 7.38 (d, *J* = 7.6 Hz, 2H), 5.66 (s, 2H), 5.47 (dd, *J* = 7.9, 1.9 Hz, 1H), 3.85–3.77 (m, 1H), 3.69–3.58 (m, 1H), 2.65–2.43 (m, 2H), 2.33–2.23 (m, 1H), 2.18–2.07 (m, 1H). ^{13}C NMR (126 MHz, CD_3OD) δ 195.9, 178.9, 169.8, 159.2, 157.1, 148.0, 140.9, 137.6, 134.6, 131.6, 130.1, 129.9, 129.6, 129.0, 128.8, 128.4, 128.3, 125.1, 122.9, 120.9, 108.6, 71.7, 56.5, 32.8, 24.3. HRMS (ESI+): Calcd for $C_{31}H_{27}F_3N_5O_3$ $[M+H]^+$: 518.5857, Found: 518.2206.

(*S*)-amino(2-(3-(6-hydroxynaphthalen-2-yl)-1,2,4-oxadiazol-5-yl)pyrrolidin-1-yl)methaniminium trifluoroacetate (3.7ac):

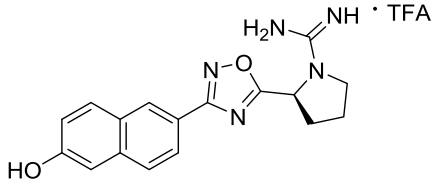

Using **3.11** as starting material, **3.7ac** was synthesized using general procedure 3.8 and isolated as a white solid (7 mg, 93%) and found to be > 99% pure by HPLC. ^{1}H NMR (400 MHz, CD_3OD) δ 8.48 (dd, *J* = 1.7, 0.7 Hz, 1H), 7.98 (dd, *J* = 8.6, 1.7 Hz, 1H), 7.89–7.84 (m, 1H), 7.76 (d, *J* = 8.6 Hz, 1H), 7.69 (s, 1H), 7.16 (d, *J* = 8.3 Hz, 1H), 5.46 (dd, *J* = 7.9, 2.1 Hz, 1H), 3.84–3.76 (m, 1H), 3.68–3.59 (m, 1H), 2.64–2.48 (m, 2H), 2.29–2.20 (m, 1H), 2.17–2.09 (m, 1 Hz, 1H). ^{13}C NMR (101 MHz, CD_3OD) δ 178.8, 169.9, 158.6, 157.1, 138.1, 131.6, 129.1,

129.0, 128.2, 124.8, 121.8, 120.5, 110.1, 56.5, 32.7, 24.4. HRMS (ESI+): Calcd for $C_{17}H_{17}N_5O_2$ $[M+H]^+$: 324.3571, Found: 324.1452.

***tert*-butyl (*S*)-2-(3-(6-(4-methoxybutoxy)naphthalen-2-yl)-1,2,4-oxadiazol-5-yl)pyrrolidine-1-carboxylate (3.12):**

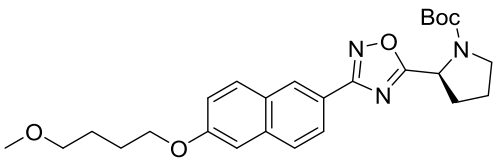

Using **3.11** and 1-bromo-4-methoxypropane as starting material, **3.12** was synthesized using general procedure 3.7 and isolated as a clear film (3 mg, 14%). ^{1}H NMR (2:1 rotamer ratio, asterisk denote minor rotamer peak, 400 MHz, $CDCl_3$) δ 8.53–8.50 (m, 1H), 8.08 (dd, *J* = 8.7, 1.7 Hz, 1H), 7.81 (dd, *J* = 15.5, 8.8 Hz, 2H), 7.22–7.12 (m, 2H), 5.23* (d, *J* = 8.3 Hz, 1 H), 5.09 (dd, *J* = 8.1, 3.7 Hz, 1H), 4.12 (t, *J* = 6.3 Hz, 2H), 3.79–3.67 (m, 1H), 3.62–3.52 (m, 1H), 3.47 (t, *J* = 6.3 Hz, 2H), 3.36 (s, 3H), 2.48–2.36 (m, 1H), 2.24–2.12 (m, 2H), 2.06–1.97 (m, 1H), 1.95–1.90 (m, 2H), 1.84–1.76 (m, 2H), 1.47* (s, 3H), 1.30 (s, 6H). ^{13}C NMR (101 MHz, $CDCl_3$) δ 180.7, 168.6, 158.5, 153.7, 136.3, 130.4, 128.5, 127.9, 127.6, 127.4, 124.6, 124.5, 121.8, 120.0, 119.9, 106.7, 80.6, 72.5, 67.9, 58.7, 54.0, 46.8, 46.5, 32.6, 31.7, 28.5, 28.3, 26.4, 26.2, 24.5, 23.9. HRMS (ESI+): Calcd for $C_{26}H_{33}N_3O_5$ $[M+H]^+$: 468.5653, Found: 468.2494.

7.1.12 Characterization for Chapter 4

N'-hydroxy-1*H*-indole-3-carboximidamide (4.2):

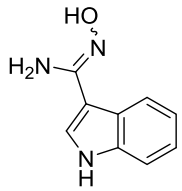

Using **4.1** as starting material, **4.2** was prepared using general procedure 4.1. Purification on a silica gel column with 0–10% MeOH in EtOAc produced **4.2** as a mixture of enantiomers (0.61 g, 99%), a tan solid. ^{1}H NMR (400 MHz, CD_3OD) δ 7.94 (ddd, *J* = 8.0, 1.3, 0.8 Hz, 1H), 7.59 (s, 1H), 7.39–7.36 (m, 1H), 7.14 (ddd, *J* = 8.1, 7.0, 1.2 Hz, 1H), 7.07 (ddd, *J* = 8.1, 7.0, 1.1 Hz, 1H). ^{13}C NMR (101 MHz, CD_3OD) δ 153.6, 138.2, 126.3, 125.8, 123.2, 121.9, 121.1, 112.5, 109.2. HRMS (ESI+): Calcd for $C_9H_9N_3O$ $[M+H]^+$: 176.1592, Found: 176.0813.

tert-butyl (*S*)-2-(3-(1*H*-indol-3-yl)-1,2,4-oxadiazol-5-yl)pyrrolidine-1-carboxylate (4.3):

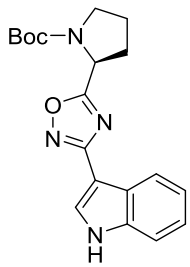

Using **4.2** and Boc-*L*-proline as starting material, **4.3** was prepared using general procedure 4.2. Purification on a silica gel column with 10–30% EtOAc in hexanes produced **4.3** (100 mg, 5%), a light yellow solid. ^{1}H NMR (2:1 rotamer ratio, asterisk denote minor rotamer peak, 500 MHz, $CDCl_3$) δ 9.62* (s, 1H), 9.10 (s, 1H), 8.25 (dd, *J* = 6.2, 3.2 Hz, 1H), 8.19–8.16* (m, 1H), 8.13* (d, *J* = 2.8 Hz, 1H), 7.92 (d, *J* = 2.8 Hz, 1H), 7.45 (dd, *J* = 6.3, 3.2 Hz, 1H), 7.42–7.37* (m, 1H), 7.32–7.26 (m, 2H), 7.26–7.21* (m, 1H), 5.29–5.24* (m, 1H), 5.08 (dd, *J* = 8.2, 3.8 Hz, 1H), 3.78–3.69 (m, 1H), 3.62–3.48 (m, 1H), 2.43–2.32 (m, 1H), 2.26–2.10 (m, 2H), 2.05–1.93 (m, 1H), 1.51* (s, 3H), 1.31 (s, 6H). ^{13}C NMR (2:1 rotamer ratio, asterisk denote minor rotamer peak, 126 MHz, $CDCl_3$) δ 179.3, 178.4*, 165.4, 154.7*, 154.0, 136.7, 128.4*, 127.4, 124.9, 123.4, 123.1*, 121.9, 121.7*, 121.6, 121.4*, 111.7, 104.3, 80.7, 60.6, 54.0, 47.0 *, 46.5, 32.5, 31.6*, 28.6*, 28.3, 24.5*, 23.8. HRMS (ESI+): Calcd for $C_{19}H_{22}N_4O_3$ [M+Na]: 377.3927, Found: 377.1582.

***tert*-butyl (*S*)-2-(3-(1-heptyl-1*H*-indol-3-yl)-1,2,4-oxadiazol-5-yl)pyrrolidine-1-carboxylate (4.4a):**

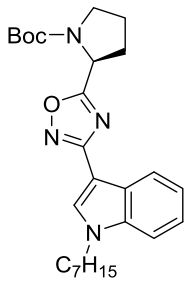

Using **4.3** and 1-bromoheptane as starting material, **4.4a** was prepared using general procedure 4.3. Purification on a silica gel column with 0–20% EtOAc in hexanes produced **4.4a** (34 mg, 89%), a yellow oil. ^{1}H NMR (2:1 rotamer ratio, asterisk denote minor rotamer peak, 400 MHz, $CDCl_3$) δ 8.30–8.21 (m, 1H), 7.83 (s, 1H), 7.42–7.36 (m, 1H), 7.35–7.26 (m, 2H), 5.23* (d, *J* = 7.2 Hz, 1H), 5.07 (dd, *J* = 8.2, 3.7 Hz, 1H), 4.16 (t, *J* = 7.0 Hz, 2H), 3.82–3.66 (m, 1H), 3.62–3.44 (m, 1H), 2.44–2.30 (m, 1H), 2.23–2.11 (m, 2H), 2.04–1.93 (m, 1H), 1.88 (p, *J* = 7.0 Hz, 2H), 1.47* (s, 3H), 1.39–1.16 (m, 13H), 0.87 (t, *J* = 7.0 Hz, 3H).^{13}C NMR (101 MHz, $CDCl_3$) δ 179.2, 165.3, 153.8, 136.9, 130.6, 125.6, 122.9, 122.7, 122.1, 121.3, 121.2, 110.0, 102.9, 80.5, 53.9, 47.0, 46.8, 46.5, 32.5, 31.8, 31.6, 30.1, 29.0, 28.6, 28.3, 27.0, 24.5, 23.8, 22.7, 14.2. HRMS (ESI+): Calcd for $C_{26}H_{36}N_4O_3$ $[M+K]^+$: 491.6873, Found: 491.2428.

***tert*-butyl (*S*)-2-(3-(1-octyl-1*H*-indol-3-yl)-1,2,4-oxadiazol-5-yl)pyrrolidine-1-carboxylate (4.4b):**

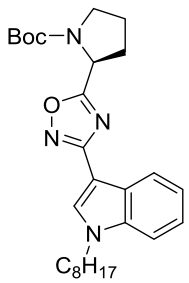

Using 4.3 and 1-bromooctane as starting material, **4.4b** was prepared using general procedure 4.3. Purification on a silica gel column with 0–20% EtOAc in hexanes produced **4.4b** (15 mg, 9%), a yellow oil. ^{1}H NMR (2:1 rotamer ratio, asterisk denote minor rotamer peak, 400 MHz, $CDCl_3$) δ 8.24 (dd, *J* = 7.0, 2.0 Hz, 1H), 7.83 (s, 1H), 7.42–7.36 (m, 1H), 7.34–7.27 (m, 2H), 5.22* (d, *J* = 8.2 Hz, 1H), 5.07 (dd, *J* = 8.1, 3.6 Hz, 1H), 4.17 (t, *J* = 7.1 Hz, 2H), 3.80–3.67 (m, 1H), 3.61–3.49 (m, 1H), 2.47–2.30 (m, 1H), 2.21–2.12 (m, 2H), 2.07–1.97 (m, 1H), 1.94–1.82 (m, 2H), 1.47* (s, 3H), 1.37–1.20 (m,

18H), 0.86 (t, J = 7.0 Hz, 3H).^{13}C NMR (101 MHz, $CDCl_3$) δ 179.2, 165.3, 153.8, 136.9, 130.6, 125.7, 122.9, 122.2, 121.4, 110.0, 102.9, 80.5, 53.9, 47.1, 46.5, 32.6, 31.9, 30.1, 29.3, 29.3, 28.6, 28.3, 27.1, 23.9, 22.8, 14.2. HRMS (ESI+): Calcd for $C_{27}H_{38}N_4O_3$ [M+K]: 505.7139, Found: 505.2567.

***tert*-butyl (*S*)-2-(3-(1-nontyl-1*H*-indol-3-yl)-1,2,4-oxadiazol-5-yl)pyrrolidine-1-carboxylate (4.4c):**

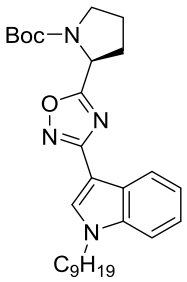

Using **4.3** and 1–bromononane as starting material, **4.4c** was prepared using general procedure 4.3. Purification on a silica gel column with 0–20% EtOAc in hexanes produced **4.4c** (40 mg, 74%), a yellow oil. ^{1}H NMR (2:1 rotamer ratio, asterisk denote minor rotamer peak, 400 MHz, $CDCl_3$) δ 8.31–8.20 (m, 1H), 7.83 (s, 1H), 7.44–7.35 (m, 1H), 7.35–7.21 (m, 2H), 5.29–5.20* (m, 1H), 5.07 (dd, J = 8.2, 3.6 Hz, 1H), 4.16 (t, J = 7.1 Hz, 2H), 3.81–3.63 (m, 1H), 3.61–3.50 (m, 1H), 2.45–2.31 (m, 1H), 2.26–2.09 (m, 2H), 2.05–1.95 (m, 1H), 1.89 (p, J = 7.0 Hz, 2H), 1.47* (s, 3H), 1.38–1.19 (m, 16H), 0.87 (t, J = 7.0 Hz, 3H). ^{13}C NMR (101 MHz, $CDCl_3$) δ 179.2, 165.3, 153.8, 136.9, 130.6, 125.6, 122.9, 122.7, 122.1, 121.3, 110.0, 102.9, 80.5, 77.5, 77.2, 76.8, 53.9, 47.0, 46.5, 32.5, 31.9, 31.6, 30.1, 29.5, 29.3, 28.5, 28.3, 27.0, 24.5, 23.8, 22.8, 22.7, 14.2. HRMS (ESI+): Calcd for $C_{28}H_{40}N_4O_3$ $[M+K]^+$: 519.7405, Found: 519.2736.

***tert*-butyl (*S*)-2-(3-(1-decyl-1*H*-indol-3-yl)-1,2,4-oxadiazol-5-yl)pyrrolidine-1-carboxylate (4.4d):**

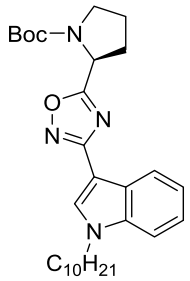

Using **4.3** and 1-bromodecane as starting material, **4.4d** was prepared using general procedure 3. Purification on a silica gel column with 0–20% EtOAc in hexanes produced **4.4d** (42 mg, 100%), a yellow oil. ^{1}H NMR (2:1 rotamer ratio, asterisk denote minor rotamer peak, 400 MHz, $CDCl_3$) δ 8.26–8.20 (m, 1H), 7.84 (s, 1H), 7.44–7.35 (m, 1H), 7.35–7.24 (m, 2H), 5.27–5.19* (m, 1H), 5.07 (dd, *J* = 8.2, 3.7 Hz, 1H), 4.16 (t, *J* = 7.0 Hz, 2H), 3.80–3.66 (m, 1H), 3.61–3.52 (m, 1H), 2.46–2.31 (m, 1H), 2.26–2.12 (m, 2H), 2.07–1.94 (m, 1H), 1.93–1.83 (m, 2H), 1.47* (s, 3H), 1.39–1.20 (m, 19H), 0.87 (t, *J* = 7.0 Hz, 3H). ^{13}C NMR (101 MHz, $CDCl_3$) δ 179.2, 165.3, 153.8, 136.9, 130.6, 125.6, 122.9, 122.7, 122.1, 121.3, 121.2, 110.0, 102.9, 80.5, 53.9, 47.0, 46.8, 46.5, 32.5, 32.0, 31.6, 30.1, 29.61, 29.56, 29.4, 29.3, 28.5, 28.3, 27.0, 24.5, 23.8, 22.8, 14.2. HRMS (ESI+): Calcd for $C_{29}H_{42}N_4O_3$ $[M+K]^+$: 533.7616, Found: 533.2902.

***tert*-butyl (*S*)-2-(3-(1-undecyl-1*H*-indol-3-yl)-1,2,4-oxadiazol-5-yl)pyrrolidine-1-carboxylate (4.4e):**

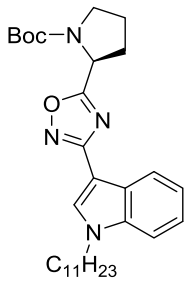

Using **4.3** and 1-bromoundecane as starting material, **4.4e** was prepared using general procedure 4.3. Purification on a silica gel column with 0–20% EtOAc in hexanes produced **4.4e** (22 mg, 77%), a yellow oil. ^{1}H NMR (2:1 rotamer ratio, asterisk denote minor rotamer peak, 400 MHz, $CDCl_3$) δ 8.24 (dd, *J* = 6.9, 2.0 Hz, 1H), 7.83 (s, 1H), 7.40 (d, *J* = 7.8 Hz, 1H), 7.28 (d, *J* = 14.4 Hz, 2H), 5.27–5.17* (m, 1H), 5.07 (dd, *J* = 8.3, 3.6 Hz, 1H), 4.16 (t, *J* = 7.1 Hz, 2H), 3.80–3.70 (m, 1H), 3.62–3.51 (m, 1H), 2.45–2.29 (m, 1H), 2.24–2.10 (m, 2H), 2.06–1.98 (m, 1H), 1.89 (p, *J* = 6.6 Hz, 2H), 1.47* (s,

3H), 1.38–1.14 (m, 21H), 0.88 (t, J = 7.0 Hz, 3H). ^{13}C NMR (101 MHz, $CDCl_3$) δ 179.2, 165.3, 153.8, 137.0, 130.6, 125.7, 122.9, 122.2, 121.3, 110.0, 103.0, 80.5, 54.0, 47.1, 46.5, 32.6, 32.0, 30.2, 29.7, 29.6, 29.43, 29.36, 28.6, 28.3, 27.1, 23.9, 22.8, 14.3. HRMS (ESI+): Calcd for $C_{30}H_{44}N_4O_3$ $[M+Na]^+$: 531.6851, Found: 531.3354.

tert-butyl (_S_)-2-(3-(1-dodecyl-1_H_-indol-3-yl)-1,2,4-oxadiazol-5-yl)pyrrolidine-1-carboxylate (4.4f):

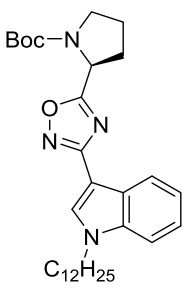

Using **4.3** and 1-bromododecane as starting material, **4.4f** was prepared using general procedure 4.3. Purification on a silica gel column with 0–20% EtOAc in hexanes produced **4.4f** (26 mg, 59%), a yellow oil. ^{1}H NMR (2:1 rotamer ratio, asterisk denote minor rotamer peak, 400 MHz, $CDCl_3$) δ 8.24 (d, J = 6.8, 1H), 7.83 (s, 1H), 7.40 (d, J = 7.7 Hz, 1H), 7.3–7.25 (m, 2H), 5.22* (d, J = 8.3 Hz, 1H), 5.07 (dd, J = 8.2, 3.6 Hz, 1H), 4.16 (t, J = 7.1 Hz, 2H), 3.80–3.65 (m, 1H), 3.61–3.50 (m, 1H), 2.46–2.31 (m, 1H), 2.22–2.12 (m, 2H), 2.04–1.95 (m, 1H), 1.88 (p, J = 6.9 Hz, 2H), 1.47* (s, 3H), 1.39–1.14 (m, 30H), 0.89 (t, J = 7.0 Hz, 3H). ^{13}C NMR (101 MHz, $CDCl_3$) δ 179.2, 165.3, 153.8, 136.9, 130.6, 125.6, 122.9, 122.2, 121.3, 110.0, 102.9, 80.5, 54.0, 47.1, 46.5, 32.6, 32.1, 30.2, 29.74, 29.69, 29.6, 29.5, 29.4, 28.6, 28.3, 27.1, 23.9, 22.8, 14.3. HRMS (ESI+): Calcd for $C_{31}H_{46}N_4O_3$ $[M+Na]^+$: 545.7117, Found: 545.3447.

***tert*-butyl (*S,Z*)-(((*tert*-butoxycarbonyl)imino)(2-(3-(1-hexyl-1*H*-indol-3-yl)-1,2,4-oxadiazol-5-yl)pyrrolidin-1-yl)methyl)carbamate (4.6a):**

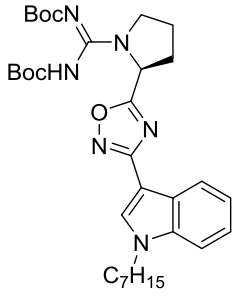

Compound **4.5a** was prepared from **4.4a** using general procedure 4.4 and carried on to the next reaction without purification Using **4.5a** as starting material, **4.6a** was prepared using general procedure 4.5. Purification on a silica gel column with 10–40% EtOAc in hexanes produced **4.6a** (21 mg, 53%), a clear oil. ^{1}H NMR (500 MHz, $CDCl_3$) δ 8.27–8.12 (m, 1H), 7.84 (s, 1H), 7.41–7.36 (m, 1H), 7.32–7.24 (m, 3H), 5.59 (s, 1H), 4.16 (t, *J* = 7.2 Hz, 2H), 3.93–3.86 (m, 1H), 3.84–3.76 (m, 1H), 2.49–2.40 (m, 1H), 2.34–2.24 (m, 1H), 2.22–2.12 (m, 1H), 2.08–1.99 (m, 1H), 1.88 (p, *J* = 7.3 Hz, 2H), 1.50–1.45 (m, 19H), 1.35–1.31 (m, 4H), 1.28–1.22 (m, 4H), 0.86 (t, *J* = 6.9 Hz, 3H).^{13}C NMR (126 MHz, $CDCl_3$) δ 177.5, 165.3, 161.9, 153.5, 151.1, 136.9, 130.8, 125.6, 122.9, 122.1, 121.4, 110.0, 102.8, 81.8, 79.8, 55.4, 49.5, 47.1, 36.8, 31.8, 31.5, 30.2, 29.0, 28.3, 28.1, 27.0, 22.7, 14.2. HRMS (ESI+): Calcd for $C_{32}H_{46}N_6O_5$ $[M+H]^+$: 595.7528, Found: 595.3608.

***tert*-butyl (*S,Z*)-(((*tert*-butoxycarbonyl)imino)(2-(3-(1-octcyl-1*H*-indol-3-yl)-1,2,4-oxadiazol-5-yl)pyrrolidin-1-yl)methyl)carbamate (4.6b):**

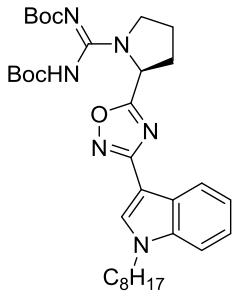

Compound **4.5b** was prepared from **4.4b** using general procedure 4.4 and carried on to the next reaction without purification Using **4.5b** as starting material, **4.6b** was prepared using general procedure 4.5. Purification on a silica gel column with 10–40% EtOAc in hexanes produced **4.6b** (15 mg, 76%), a clear oil. ^{1}H NMR (500 MHz, $CDCl_3$) δ 8.24–8.18 (m, 1H), 7.83 (s, 1H), 7.42–7.36 (m, 1H), 7.32–7.25 (m, 2H), 5.60 (s, 1H), 4.16 (t, *J* = 7.2 Hz, 2H), 3.93–3.88 (m,

1H), 3.85–3.77 (m, 1H), 2.51–2.41 (m, 1H), 2.33–2.23 (m, 1H), 2.21–2.13 (m, 1H), 2.09–2.01 (m, 1H), 1.89 (p, *J* = 7.1 Hz, 2H), 1.53–1.41 (m, 23H), 1.38–1.31 (m, 4H), 1.31–1.21 (M, 6H), 0.86 (t, *J* = 7.1 Hz, 3H). ^{13}C NMR (126 MHz, $CDCl_3$) δ 177.5, 165.4, 162.0, 153.5, 150.7, 137.0, 130.8, 125.7, 122.9, 122.2, 121.4, 110.0, 102.9, 81.7, 79.8, 55.5, 49.6, 47.1, 31.9, 31.5, 30.2, 29.3, 29.2, 28.3, 28.1, 27.7, 27.1, 24.0, 22.7, 14.2. HRMS (ESI+): Calcd for $C_{33}H_{48}N_6O_5$ $[M+H]^+$: 609.7794, Found: 609.3371.

tert-butyl (_S,Z_)-(((_tert_-butoxycarbonyl)imino)(2-(3-(1-nonyl-1_H_-indol-3-yl)-1,2,4-oxadiazol-5-yl)pyrrolidin-1-yl)methyl)carbamate (4.6c):

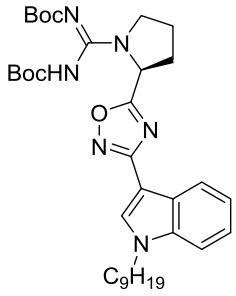

Compound **4.5c** was prepared from **4.4c** using general procedure 4.4 and carried on to the next reaction without purification Using **4.5c** as starting material, **4.6c** was prepared using general procedure 4.5. Purification on a silica gel column with 10–40% EtOAc in hexanes produced **4.6c** (25 mg, 64%), a clear oil. ^{1}H NMR (500 MHz, $CDCl_3$) δ 8.31–8.19 (m, 1H), 7.86 (s, 1H), 7.46–7.41 (m, 1H), 7.37–7.28 (m, 2H), 5.61 (s, 1H), 4.18 (t, *J* = 7.2 Hz, 2H), 3.94–3.88 (m, 1H), 3.85–3.79 (m, 1H), 2.51–2.45 (m, 1H), 2.36–2.26 (m, 1H), 2.24–2.15 (m, 1H), 2.08–1.98 (m, 1H), 1.90 (p, *J* = 7.4 Hz, 3H), 1.64–1.43 (m, 18H), 1.40–1.32 (m, 4H) 1.32–1.21 (m, 8H), 0.89 (t, *J* = 6.9 Hz, 3H). ^{13}C NMR (126 MHz, $CDCl_3$) δ 177.5, 165.3, 162.1, 153.6, 150.6, 136.9, 130.8, 125.6, 122.8, 122.1, 121.4, 110.0, 102.8, 82.2, 79.7, 55.4, 49.5, 47.1, 31.9, 31.5, 31.4, 30.2, 29.5, 29.4, 28.3, 28.1, 27.1, 22.8, 14.2. HRMS (ESI+): Calcd for $C_{34}H_{50}N_6O_5$ $[M+H]^+$: 623.8059, Found: 623.3915.

***tert*-butyl (*S,Z*)-(((*tert*-butoxycarbonyl)imino)(2-(3-(1-decyl-1*H*-indol-3-yl)-1,2,4-oxadiazol-5-yl)pyrrolidin-1-yl)methyl)carbamate (4.6d):**

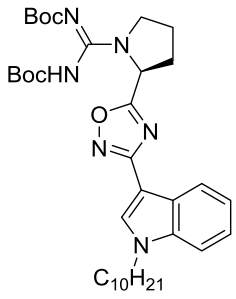

Compound **4.5d** was prepared from **4.4d** using general procedure 4.4 and carried on to the next reaction without purification Using **4.5d** as starting material, **4.6d** was prepared using general procedure 4.5. Purification on a silica gel column with 10–40% EtOAc in hexanes produced **4.6d** (23 mg, 52%), a clear oil. ^{1}H NMR (500 MHz, $CDCl_3$) δ 8.17 – 8.12 (m, 1H), 7.77 (s, 1H), 7.34–7.28 (m, 1H), 7.26–7.20 (m, 2H), 5.52 (s, 1H), 4.09 (t, *J* = 7.2 Hz, 2H), 3.86–3.79 (m, 1H), 3.76–3.68 (m, 1H), 2.39–2.34 (m, 1H), 2.29–2.17 (m, 1H), 2.16–2.06 (m, 1H), 2.01–1.92 (m, 1H), 1.81 (p, *J* = 7.4 Hz, 2H), 1.48–1.32 (m, 22H), 1.27–1.23 (m, 4H), 1.23–1.08 (m, 10H), 0.80 (t, *J* = 7.0 Hz, 3H). ^{13}C NMR (126 MHz, $CDCl_3$) δ 177.46, 165.30, 162.12, 153.53, 150.94, 136.94, 130.79, 125.64, 122.84, 122.13, 121.35, 109.98, 102.78, 82.17, 79.82, 55.42, 49.53, 47.07, 31.97, 31.53, 31.37, 30.21, 29.64, 29.57, 29.37, 28.27, 28.12, 27.98, 27.07, 22.79, 14.23. HRMS (ESI+): Calcd for $C_{35}H_{52}N_6O_5$ $[M+H]^+$: 637.8325, Found: 637.4073.

***tert*-butyl (*S,Z*)-(((*tert*-butoxycarbonyl)imino)(2-(3-(1-undecyl-1*H*-indol-3-yl)-1,2,4-oxadiazol-5-yl)pyrrolidin-1-yl)methyl)carbamate (4.6e):**

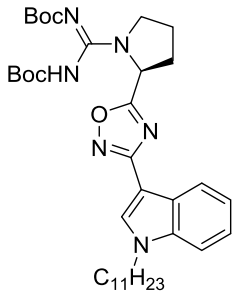

Compound **4.5e** was prepared from **4.4e** using general procedure 4.4 and carried on to the next reaction without purification Using **4.5e** as starting material, **4.6e** was prepared using general procedure 4.5. Purification on a silica gel column with 10–40% EtOAc in hexanes produced **4.6e** (21 mg, 100%), a clear oil. ^{1}H NMR (500 MHz, $CDCl_3$) δ 8.26–8.19 (m, 1H), 7.83 (s, 1H), 7.44–7.36 (m, 1H), 7.33–7.26 (m, 2H), 5.59 (s, 1H), 4.16 (t, *J* = 7.2 Hz, 2H), 3.97–3.88

(m, 1H), 3.85–3.77 (m, 1H), 2.51–2.42 (m, 1H), 2.35–2.24 (m, 1H), 2.22–2.14 (m, 1H), 2.09–1.99 (m, 1H), 1.89 (t, *J* = 7.2 Hz, 2H), 1.58–1.41 (m, 18H), 1.37–1.30 (m, 4H), 1.29–1.21 (m, 12H), 0.87 (t, *J* = 7.0 Hz, 3H). ^{13}C NMR (126 MHz, $CDCl_3$) δ 177.4, 165.3, 161.8, 153.3, 150.3, 137.0, 130.8, 125.7, 122.9, 122.2, 121.4, 110.0, 102.8, 82.2, 79.7, 55.5, 49.6, 47.1, 32.0, 31.5, 30.2, 29.7, 29.6, 29.4, 28.3, 27.1, 24.1, 22.8, 14.3. HRMS (ESI+): Calcd for $C_{36}H_{54}N_6O_5$ $[M+H]^+$: 651.8591, Found: 651.4249.

tert-butyl (_S,Z_)-(((_tert_-butoxycarbonyl)imino)(2-(3-(1-dodecyl-1_H_-indol-3-yl)-1,2,4-oxadiazol-5-yl)pyrrolidin-1-yl)methyl)carbamate (4.6f):

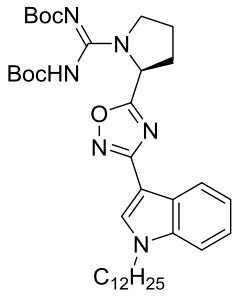

Compound **4.5f** was prepared from **4.4f** using general procedure 4.4 and carried on to the next reaction without purification Using **4.5f** as starting material, **4.6f** was prepared using general procedure 4.5. Purification on a silica gel column with 10–40% EtOAc in hexanes produced **4.6f** (21 mg, 99%), a clear oil. ^{1}H NMR (500 MHz, $CDCl_3$) δ 8.26–.18 (m, 1H), 7.83 (s, 1H), 7.45–7.35 (m, 1H), 7.32–7.26 (m, 2H), 5.58 (s, 1H), 4.16 (t, *J* = 7.2 Hz, 2H), 3.93–3.86 (m, 1H), 3.84–3.76 (m, 1H), 2.50–2.38 (m, 1H), 2.22–2.18 (m, 1H), 2.09–1.99 (m, 1H), 1.88 (p, *J* = 7.5 Hz, 2H), 1.54–1.34 (m, 18H), 1.36–1.30 (m, 4H), 1.28–1.20 (m, 14H), 0.87 (t, *J* = 7.0 Hz, 3H). ^{13}C NMR (126 MHz, $CDCl_3$) δ 177.5, 165.3, 162.1, 152.9, 150.6, 148.7, 136.9, 130.8, 125.6, 122.8, 122.1, 121.4, 110.0, 102.8, 82.2, 79.7, 55.4, 49.5, 47.1, 32.0, 31.5, 30.2, 29.8, 29.73, 29.70, 29.62, 29.58, 29.5, 29.4, 28.3, 28.1, 27.1, 22.8, 14.3. HRMS (ESI+): Calcd for $C_{37}H_{56}N_6O_5$ $[M+H]^+$: 665.8857, Found: 665.4401.

(*S*)-amino(2-(3-(1-heptyl-1*H*-indol-3-yl)-1,2,4-oxadiazol-5-yl)pyrrolidin-1-yl)methaniminium chloride (4.7a):

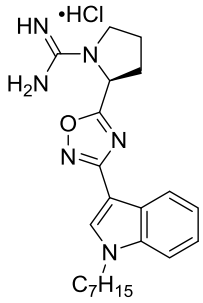

Using **4.6a** as starting material, **4.7a** was prepared using general procedure 4.4, isolated as a light yellow tinted solid (11 mg, 100%) and found to be 92% pure by HPLC. ^{1}H NMR (400 MHz, CD_3OD) δ 8.10 (ddd, *J* = 7.9, 1.3, 0.8 Hz, 1H), 7.98 (s, 1H), 7.51 (dt, *J* = 8.3, 0.9 Hz, 1H), 7.29 (ddd, *J* = 8.3, 7.1, 1.3 Hz, 1H), 7.22 (ddd, *J* = 8.0, 7.1, 1.0 Hz, 1H), 5.44 (dd, *J* = 7.8, 2.0 Hz, 1H), 4.26 (t, *J* = 7.0 Hz, 2H), 3.82–3.74 (m, 1H), 3.67–3.56 (m, 1H), 2.61–2.45 (m, 2H), 2.31–2.21 (m, 1H), 2.17–2.06 (m, 1H), 1.88 (p, *J* = 7.1 Hz, 2H), 1.40–1.18 (m, 9H), 0.87 (t, *J* = 7.0 Hz, 3H). ^{13}C NMR (101 MHz, CD_3OD) δ 177.3, 166.7, 157.1, 138.4, 132.3, 126.7, 123.9, 122.5, 122.2, 111.4, 103.1, 56.4, 47.7, 32.8, 32.7, 31.2, 30.0, 27.8, 24.4, 23.6, 14.3. HRMS (ESI+): Calcd for $C_{22}H_{30}N_6O$ $[M+H]^+$: 395.5211, Found: 395.2543.

(*S*)-amino(2-(3-(1-octyl-1*H*-indol-3-yl)-1,2,4-oxadiazol-5-yl)pyrrolidin-1-yl)methaniminium chloride (4.7b):

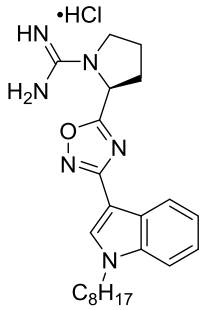

Using **4.6b** as starting material, **4.7b** was prepared using general procedure 4.4, isolated as a light yellow tinted solid (10 mg, 91%) and found to be 90% pure by HPLC. ^{1}H NMR (500 MHz, CD_3OD) δ 8.12 (dt, *J* = 8.0, 1.0 Hz, 1H), 8.00 (s, 1H), 7.53 (dt, *J* = 8.3, 0.9 Hz, 1H), 7.31 (ddd, *J* = 8.3, 7.1, 1.2 Hz, 1H), 7.26–7.21 (m, 1H), 5.45 (dd, *J* = 7.9, 1.9 Hz, 1H), 4.29 (t, *J* = 7.0 Hz, 2H), 3.84–3.77 (m, 1H), 3.67–3.58 (m, 1H), 2.63–2.48 (m, 2H), 2.29–2.22 (m, 1H), 2.18–2.07 (m, 1H), 1.92–1.85 (m, 2H), 1.38–1.19 (m, 12H), 0.88 (t, *J* = 7.2 Hz, 3H).^{13}C NMR (126 MHz, CD_3OD) δ 177.3, 166.7, 157.1, 138.4, 132.3, 126.7, 123.9, 122.5, 122.2, 111.4, 103.1, 56.5, 47.7,

32.9, 32.7, 31.2, 30.3, 30.2, 27.8, 24.4, 23.6, 14.4. HRMS (ESI+): Calcd for $C_{23}H_{32}N_6O$ $[M+H]^+$: 409.5477, Found: 409.2728.

(*S*)-amino(2-(3-(1-nonyl-1*H*-indol-3-yl)-1,2,4-oxadiazol-5-yl)pyrrolidin-1-yl)methaniminium chloride (4.7c):

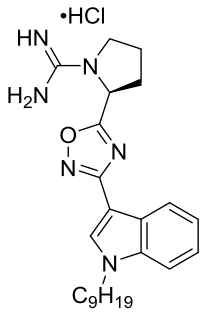

Using **4.6c** as starting material, **4.7c** was prepared using general procedure 4.4, isolated as a light yellow tinted solid (15 mg, 100%) and found to be 89% pure by HPLC. ^{1}H NMR (400 MHz, CD_3OD) δ 8.10 (ddd, *J* = 7.9, 1.3, 0.7 Hz, 1H), 7.98 (s, 1H), 7.51 (dt, *J* = 8.3, 0.9 Hz, 1H), 7.32–7.26 (m, 1H), 7.22 (ddd, *J* = 8.0, 7.1, 1.0 Hz, 1H), 5.45–5.41 (m, 1H), 4.27 (t, *J* = 7.0 Hz, 2H), 3.83–3.76 (m, 1H), 3.66–3.59 (m, 1H), 2.60–2.48 (m, 2H), 2.30–2.20 (m, 1H), 2.17–2.08 (m, 1H), 1.92–1.83 (p, *J* = 7.1 Hz, 2H), 1.35–1.21 (m, 14H), 0.86 (t, *J* = 6.8 Hz, 3H).^{13}C NMR (101 MHz, CD_3OD) δ 177.3, 166.7, 157.1, 138.4, 132.3, 126.7, 123.9, 122.5, 122.2, 111.4, 103.1, 56.4, 47.7, 32.9, 32.7, 31.2, 30.5, 30.3, 27.8, 24.4, 23.7, 14.4. HRMS (ESI+): Calcd for $C_{24}H_{34}N_6O$ $[M+H]^+$: 423.5743, Found: 423.2890.

(*S*)-amino(2-(3-(1-decyl-1*H*-indol-3-yl)-1,2,4-oxadiazol-5-yl)pyrrolidin-1-yl)methaniminium chloride (4.7d):

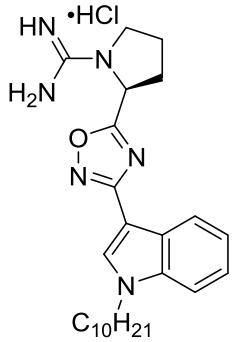

Using **4.6d** as starting material, **4.7d** was prepared using general procedure 4.4, isolated as a light yellow tinted solid (13 mg, 100%) and found to be 84% pure by HPLC.. ^{1}H NMR (500 MHz, CD_3OD) δ 8.14–8.09 (m, 1H), 7.98 (s, 1H), 7.55–7.50 (m, 1H), 7.29 (ddd, *J* = 8.3, 7.0, 1.2 Hz, 1H), 7.22 (ddd, *J* = 8.0, 7.0, 1.0 Hz, 1H), 5.43 (dd, *J* = 7.9, 1.9 Hz, 1H), 4.27 (t, *J* = 7.0 Hz, 2H), 3.81–3.76 (m, 1H), 3.65–3.57 (m, 1H), 2.60–2.47 (m, 2H), 2.28–2.21 (m, 1H), 1.89 (p,

J = 6.9 Hz, 1H), 1.40–1.24 (m, 14H), 0.87 (t, J = 7.0 Hz, 3H).^{13}C NMR (126 MHz, CD_3OD) δ 177.3, 166.7, 157.1, 138.4, 132.3, 126.7, 123.9, 122.5, 122.2, 111.4, 103.1, 56.4, 47.7, 33.0, 32.7, 31.2, 30.6, 30.4, 30.3, 27.8, 24.4, 23.7, 14.4. HRMS (ESI+): Calcd for $C_{25}H_{36}N_6O$ $[M+H]^+$: 437.6009, Found: 437.3010.

(*S*)-amino(2-(3-(1-undecyl-1*H*-indol-3-yl)-1,2,4-oxadiazol-5-yl)pyrrolidin-1-yl)methaniminium chloride (4.7e):

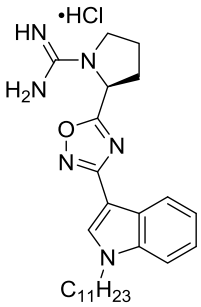

Using 4**.6e** as starting material, **4.7e** was prepared using general procedure 4.4, isolated as a light yellow tinted solid (6 mg, 80%) and found to be > 99% pure by HPLC. ^{1}H NMR (500 MHz, CD_3OD) δ 8.10 (d, J = 7.8 Hz, 1H), 7.98 (s, 1H), 7.51 (d, J = 8.2 Hz, 1H), 7.29 (ddd, J = 8.3, 7.0, 1.2 Hz, 1H), 7.22 (t, J = 7.5 Hz, 1H), 5.43 (dd, J = 7.9, 1.8 Hz, 1H), 4.27 (t, J = 7.0 Hz, 2H), 3.82–3.75 (m, 1H), 3.66–3.59 (m, 1H), 2.60–2.52 (m, 1H), 2.52–2.46 (m, 1H), 2.28–2.19 (m, 1H), 2.17–2.08 (m, 1H), 1.88 (p, J = 7.1 Hz, 2H), 1.39–1.20 (m, 18H), 0.88 (t, J = 7.0 Hz, 3H). ^{13}C NMR (126 MHz, CD_3OD) δ 177.3, 166.7, 157.1, 138.4, 132.3, 126.7, 123.9, 122.5, 122.2, 111.4, 103.1, 56.5, 47.7, 33.0, 32.7, 31.2, 30.7, 30.60, 30.56, 30.4, 30.3, 27.8, 24.4, 23.7, 14.4. HRMS (ESI+): Calcd for $C_{26}H_{38}N_6O$ $[M+H]^+$: 451.6275, Found: 451.3192.

(*S*)-amino(2-(3-(1-dodecyl-1*H*-indol-3-yl)-1,2,4-oxadiazol-5-yl)pyrrolidin-1-yl)methaniminium chloride (4.7f):

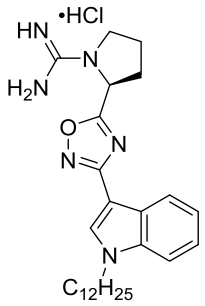

Using **4.6f** as starting material, **4.7f** was prepared using general procedure 4.4, isolated as a light yellow tinted solid (10 mg, 88%) and found to be 86% pure by HPLC. ^{1}H NMR (400 MHz, CD_3OD) δ 8.10 (ddd, *J* = 7.9, 1.3, 0.8 Hz, 1H), 7.98 (s, 1H), 7.51 (dt, *J* = 8.3, 0.9 Hz, 1H), 7.29 (ddd, *J* = 8.3, 7.1, 1.3 Hz, 1H), 7.22 (ddd, *J* = 8.0, 7.1, 1.0 Hz, 1H), 5.44 (dd, *J* = 7.8, 2.0 Hz, 1H), 4.27 (t, *J* = 7.0 Hz, 2H), 3.85–3.75 (m, 1H), 3.66–3.58 (m, 1H), 2.63–2.46 (m, 2H), 2.31–2.20 (m, 1H), 2.21–2.07 (m, 1H), 1.88 (p, *J* = 7.1 Hz, 2H), 1.25 (s, 18H), 0.89 (t, *J* = 7.1 Hz, 3H). ^{13}C NMR (101 MHz, CD_3OD) δ 177.3, 166.7, 157.1, 138.4, 132.3, 126.7, 123.9, 122.5, 122.2, 111.4, 103.1, 56.4, 47.7, 33.0, 32.7, 31.2, 30.70, 30.69, 30.58, 30.55, 30.4, 30.3, 27.8, 24.4, 23.7, 14.4. HRMS (ESI+): Calcd for $C_{27}H_{40}N_6O$ $[M+H]^+$: 465.6540, Found: 465.3352.

***N'*-hydroxy-1*H*-indole-4-carboximidamide (4.9):**

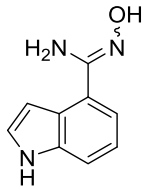

Using **4.8** as starting material, **4.9** was prepared using general procedure 4.1. Purification on a silica gel column with 70–100% EtOAc in hexanes produced **4.9** as a mixture of enantiomers (1.12 g, 91%), a tan solid. ^{1}H NMR (500 MHz, CD_3OD) δ 7.45 (dd, *J* = 8.1, 1.6 Hz, 1H), 7.28 (dd, *J* = 3.4, 1.8 Hz, 1H), 7.24 (dd, *J* = 7.2, 1.6 Hz, 1H), 7.13 (td, *J* = 7.8, 1.8 Hz, 1H), 6.78 (dd, *J* = 3.0, 1.8 Hz, 1H). ^{13}C NMR (126 MHz, CD_3OD) δ 156.6, 138.1, 127.1, 126.3, 125.7, 121.8, 119.3, 113.8, 102.5. HRMS (ESI+): Calcd for $C_9H_9N_3O$ $[M+H]^+$: 176.1592, Found: 176.0825.

***tert*-butyl (*S*)-2-(3-(1*H*-indol-4-yl)-1,2,4-oxadiazol-5-yl)pyrrolidine-1-carboxylate (4.10):**

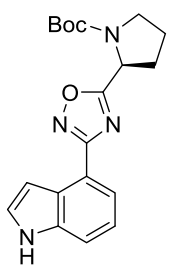

Using **4.9** and Boc-*L*-proline as starting material, **4.10** was prepared using general procedure 4.2. Purification on a silica gel column with 10–40% EtOAc in hexanes produced **4.10** (0.65 g, 32%), a tan solid. ^{1}H NMR (2:1 rotamer ratio, asterisk denote minor rotamer peak, 400 MHz, $CDCl_3$) δ 8.71 (s, 1H), 7.96 (d, *J* = 7.4 Hz, 1H), 7.92* (d, *J* = 7.4 Hz, 1H), 7.56 (d, *J* = 8.1 Hz, 1H), 7.52* (d, *J* = 8.1 Hz, 1H), 7.36 (t, *J* = 2.6 Hz, 1H), 7.31* (s, 1H), 7.30–7.26 (m, 1H), 7.25–7.20* (m, 1H), 5.33–5.23* (m, 1H), 5.13 (dd, *J* = 8.2, 3.7 Hz, 1H), 3.81–3.67 (m, 1H), 3.62–3.48 (m, 1H), 2.49–2.35 (m, 1H), 2.24–2.12 (m, 2H), 2.06–1.97 (m, 1H), 1.49* (s, 3H), 1.31 (s, 6H). ^{13}C NMR (2:1 rotamer ratio, asterisk denote minor rotamer peak, 101 MHz, $CDCl_3$) δ 179.7, 169.0, 153.9, 136.5, 126.0, 125.8, 125.7, 125.6, 121.8, 121.7, 121.3, 121.2, 118.3, 114.42, 114.37, 114.3, 104.0, 103.9, 80.7, 80.5, 54.0, 46.8*, 46.5, 32.6, 31.7*, 28.6*, 28.3, 24.4*, 23.8. HRMS (ESI+): Calcd for $C_{19}H_{22}N_4O_3$ [M+Na]: 377.3927, Found: 377.1587.

***tert*-butyl (*S*)-2-(3-(1-heptyl-1*H*-indol-4-yl)-1,2,4-oxadiazol-5-yl)pyrrolidine-1-carboxylate (4.11a):**

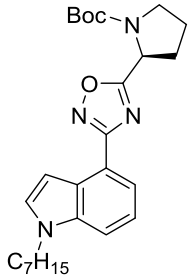

Using **4.10** and 1-bromoheptane as starting material, **4.11a** was prepared using general procedure 4.3. Purification on a silica gel column with 0–20% EtOAc in hexanes produced **4.11a** (22 mg, 57%), a yellow oil. ^{1}H NMR (2:1 rotamer ratio, asterisk denote minor rotamer peak, 500 MHz, $CDCl_3$) δ 7.97–7.91 (m, 1H), 7.50 (d, *J* = 8.2 Hz, 1H), 7.30 (t, *J* = 7.8 Hz, 1H), 7.26–7.22 (m, 1H), 7.20 (d, *J* = 3.1 Hz, 1H), 5.30–5.20* (m, 1H), 5.12 (dd, *J* = 8.2, 3.6 Hz, 1H), 4.17 (t, *J* = 7.0 Hz, 2H), 3.77–3.61 (m, 1H), 3.61–3.48 (m, 1H), 2.44–2.35 (m, 1H), 2.24–2.13 (m, 2H), 2.05–1.95 (m, 1H), 1.85 (p, *J* =

8.0, 7.4 Hz, 2H), 1.47* (s, 3H), 1.37–1.20 (m, 16H), 0.86 (t, *J* = 6.9 Hz, 3H). ^{13}C NMR (126 MHz, $CDCl_3$) δ 179.7, 169.0, 153.8, 136.7, 129.5, 126.3, 121.2, 120.8, 118.5, 112.6, 102.5, 80.6, 54.0, 46.8, 46.5, 32.6, 31.8, 30.5, 29.0, 28.6, 28.3, 27.1, 23.9, 22.7, 14.2. HRMS (ESI+): Calcd for $C_{26}H_{36}N_4O_3$ $[M+Na]^+$: 475.5788, Found: 475.2673.

***tert*-butyl (*S*)-2-(3-(1-octyl-1*H*-indol-4-yl)-1,2,4-oxadiazol-5-yl)pyrrolidine-1-carboxylate (4.11b):**

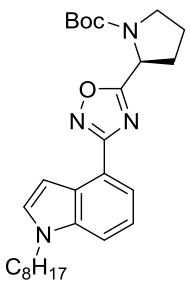

Using **4.10** and 1-bromooctane as starting material, **4.11b** was prepared using general procedure 4.3. Purification on a silica gel column with 0–20% EtOAc in hexanes produced **4.11b** (30 mg, 76%), a yellow oil. ^{1}H NMR (2:1 rotamer ratio, asterisk denote minor rotamer peak, 500 MHz, $CDCl_3$) δ 7.93 (d, *J* = 7.3 Hz, 1H), 7.51 (d, *J* = 8.2 Hz, 1H), 7.30 (t, *J* = 7.8 Hz, 1H), 7.25 (d, *J* = 3.2 Hz, 1H), 7.20 (d, *J* = 3.2 Hz, 1H), 5.36–5.20* (m, 1H), 5.12 (dd, *J* = 8.2, 3.6 Hz, 1H), 4.17 (t, *J* = 7.0 Hz, 2H), 3.80–3.66 (m, 1H), 3.54–3.45 (m, 1H), 2.40–2.30 (m, 1H), 2.24–2.14 (m, 2H), 2.07–1.95 (m, 1H), 1.85 (p, *J* = 7.0 Hz, 2H), 1.47* (s, 3H), 1.34–1.21 (m, 18H), 0.87 (t, *J* = 6.9 Hz, 3H). ^{13}C NMR (126 MHz, $CDCl_3$) δ 179.7, 169.0, 153.8, 136.6, 129.5, 126.3, 121.2, 120.8, 118.5, 112.6, 102.5, 80.6, 54.0, 46.8, 46.5, 32.6, 31.9, 30.5, 29.33, 29.28, 28.6, 28.3, 27.1, 23.9, 22.7, 14.3, 14.2. HRMS (ESI+): Calcd for $C_{27}H_{38}N_4O_3$ $[M+Na]^+$: 489.6054, Found: 489.2820

***tert*-butyl (*S*)-2-(3-(1-nonyl-1*H*-indol-4-yl)-1,2,4-oxadiazol-5-yl)pyrrolidine-1-carboxylate (4.11c):**

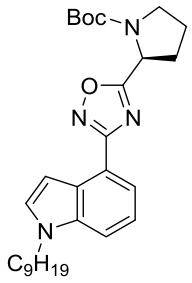

Using **4.10** and 1-bromononane as starting material, **4.11c** was prepared using general procedure 4.3. Purification on a silica gel column with 0–20% EtOAc in hexanes produced **4.11c** (29 mg, 71%), a yellow oil. ^{1}H NMR (2:1 rotamer ratio, asterisk denote minor rotamer peak, 400 MHz, $CDCl_3$) δ 7.93 (dd, *J* = 7.4, 0.9 Hz, 1H), 7.50 (d, *J* = 8.3 Hz, 1H), 7.30 (t, *J* = 7.9 Hz, 1H), 7.26–7.23 (m, 1H), 7.20 (d, *J* = 3.0 Hz, 1H), 5.37–5.20* (m, 1H), 5.12 (dd, *J* = 8.2, 3.6 Hz, 1H), 4.16 (t, *J* = 7.1 Hz, 2H), 3.81–3.68 (m, 1H), 3.62–3.49 (m, 1H), 2.47–2.34 (m, 1H), 2.26–2.13 (m, 2H), 2.06–1.96 (m, 1H), 1.86 (p, *J* = 7.2 Hz, 2H), 1.47* (m, 3H), 1.35–1.19 (m, 19H), 0.87 (t, *J* = 7.0 Hz, 3H). ^{13}C NMR (101 MHz, $CDCl_3$) δ 179.7, 169.0, 153.8, 136.6, 129.5, 126.3, 121.1, 120.7, 118.4, 112.6, 102.4, 80.5, 54.0, 46.7, 46.5, 32.6, 31.9, 30.5, 29.5, 29.33, 29.31, 28.5, 28.3, 27.1, 23.8, 22.7, 14.2. HRMS (ESI+): Calcd for $C_{28}H_{40}N_4O_3$ $[M+Na]^+$: 503.6320, Found: 503.2987.

***tert*-butyl (*S*)-2-(3-(1-decyl-1*H*-indol-4-yl)-1,2,4-oxadiazol-5-yl)pyrrolidine-1-carboxylate (4.11d):**

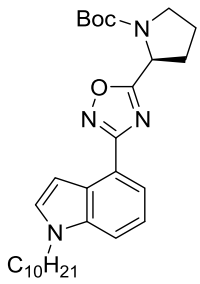

Using **4.10** and 1-bromodecane as starting material, **4.1d** was prepared using general procedure 4.3. Purification on a silica gel column with 0–20% EtOAc in hexanes produced **4.11d** (30 mg, 72%), a yellow oil. ^{1}H NMR (2:1 rotamer ratio, asterisk denote minor rotamer peak, 400 MHz, $CDCl_3$) δ 7.93 (dd, *J* = 7.4, 0.9 Hz, 1H), 7.50 (d, *J* = 8.3 Hz, 1H), 7.30 (t, *J* = 7.9 Hz, 1H), 7.22 (dd, *J* = 19.7, 3.1 Hz, 2H), 5.37–5.22* (m, 1H), 5.12 (dd, *J* = 8.2, 3.6 Hz, 1H), 4.16 (t, *J* = 7.1 Hz, 2H), 3.78–3.62 (m, 1H), 3.60–3.52 (m, 1H), 2.44–2.31 (m, 1H), 2.24–2.11 (m, 2H), 2.05–1.94 (m, 1H), 1.85 (p, *J* =

7.0 Hz, 2H), 1.47* (s, 3H), 1.31–1.20 (m, 21H), 0.87 (t, *J* = 7.0 Hz, 3H). ^{13}C NMR (101 MHz, $CDCl_3$) δ 179.7, 169.0, 153.8, 136.6, 129.5, 126.3, 121.2, 121.1, 120.8, 118.4, 112.6, 102.4, 80.5, 54.0, 46.7, 46.5, 32.6, 32.0, 30.5, 29.62, 29.60, 29.38, 29.35, 28.6, 28.3, 27.1, 23.8, 22.8, 14.2. HRMS (ESI+): Calcd for $C_{29}H_{42}N_4O_3$ [M+Na]$^+$: 517.6585, Found: 517.3177.

tert-butyl (_S,Z_)-(((_tert_-butoxycarbonyl)amino)(2-(3-(1-heptyl-1_H_-indol-4-yl)-1,2,4-oxadiazol-5-yl)pyrrolidin-1-yl)methylene)carbamate (4.13a):

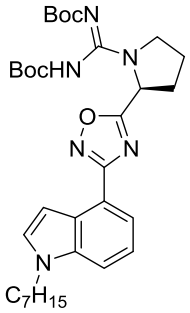

Compound **4.12a** was prepared from **4.11a** using general procedure 4.4 and carried on to the next reaction without purification. Using **4.12a** as starting material, **4.13a** was prepared using general procedure 4.5. Purification on a silica gel column with 10–40% EtOAc in hexanes produced **4.13a** (13 mg, 43%), a clear oil. ^{1}H NMR (400 MHz, $CDCl_3$) δ 7.93 (dd, *J* = 7.4, 0.9 Hz, 1H), 7.54–7.47 (m, 1H), 7.32–7.27 (m, 1H), 7.23 (t, *J* = 1.6 Hz, 1H), 7.18 (dd, *J* = 3.1, 0.8 Hz, 1H), 5.64 (t, *J* = 6.2 Hz, 1H), 4.17 (t, *J* = 7.1 Hz, 2H), 3.95–3.87 (m, 1H), 3.86–3.76 (m, 1H), 2.52–2.41 (m, 1H), 2.37–2.26 (m, 1H), 2.25–2.13 (m, 2H), 2.10–1.99 (m, 1H), 1.86 (p, *J* = 7.1 Hz, 2H), 1.53–1.39 (m, 17H), 1.35–1.29 (m, 4H), 1.29–1.20 (m, 6H), 0.86 (t, *J* = 6.9 Hz, 3H). ^{13}C NMR (126 MHz, $CDCl_3$) δ 178.0, 169.0, 162.2, 153.8, 150.7, 136.6, 129.5, 129.4, 126.3, 121.1, 121.0, 118.3, 112.7, 102.5, 81.9, 79.8, 55.5, 49.6, 46.8, 31.8, 31.6, 30.5, 29.8, 29.0, 28.3, 27.1, 24.1, 22.7, 14.2. HRMS (ESI+): Calcd for $C_{32}H_{46}N_6O_5$ [M+Na]$^+$: 617.7346, Found: 617.3426.

***tert*-butyl (*S,Z*)-(((*tert*-butoxycarbonyl)amino)(2-(3-(1-heptyl-1*H*-indol-4-yl)-1,2,4-oxadiazol-5-yl)pyrrolidin-1-yl)methylene)carbamate (4.13b):**

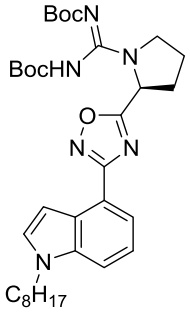

Compound **4.12b** was prepared from **4.11b** using general procedure 4.4 and carried on to the next reaction without purification. Using **4.12b** as starting material, **4.13b** was prepared using general procedure 4.5. Purification on a silica gel column with 10–40% EtOAc in hexanes produced **4.13b** (7 mg, 15%), a clear oil. ^{1}H NMR (500 MHz, $CDCl_3$) δ 7.93 (dd, *J* = 7.5, 0.9 Hz, 1H), 7.49 (d, *J* = 8.2 Hz, 1H), 7.28 (dd, *J* = 8.2, 7.4 Hz, 1H), 7.24–7.22 (m, 1H), 7.18 (dd, *J* = 3.1, 0.9 Hz, 1H), 5.65 (s, 1H), 4.17 (t, *J* = 7.1 Hz, 2H), 3.94–3.87 (m, 1H), 3.87–3.77 (m, 1H), 2.50–2.42 (m, 1H), 2.35–2.26 (m, 1H), 2.25–2.3 (m, 1H), 2.10–2.01 (m, 1H), 1.85 (p, *J* = 7.5 Hz, 2H), 1.51–1.38 (m, 20H), 1.33–1.29 (m, 4H), 1.28–1.20 (m, 8H), 0.86 (t, *J* = 7.0 Hz, 3H). ^{13}C NMR (126 MHz, $CDCl_3$) δ 178.0, 169.0, 162.1, 153.6, 150.6, 136.7, 129.5, 126.3, 121.1, 121.0, 118.4, 112.7, 102.5, 82.2, 79.8, 55.5, 49.6, 46.8, 31.9, 31.5, 30.5, 29.8, 29.32, 28.28, 27.1, 24.0, 22.8, 14.2. HRMS (ESI+): Calcd for $C_{33}H_{48}N_6O_5$ $[M+H]^+$: 609.7794, Found: 609.3785.

***tert*-butyl (*S,Z*)-(((*tert*-butoxycarbonyl)amino)(2-(3-(1-heptyl-1*H*-indol-4-yl)-1,2,4-oxadiazol-5-yl)pyrrolidin-1-yl)methylene)carbamate (4.13c):**

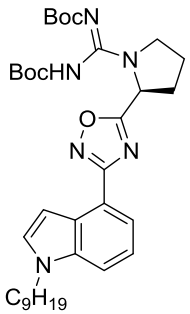

Compound **4.12c** was prepared from **4.11c** using general procedure 4.4 and carried on to the next reaction without purification. Using **4.12c** as starting material, **4.13c** was prepared using general procedure 4.5. Purification on a silica gel column with 10–40% EtOAc in hexanes produced **4.13c** (20 mg, 45%), a clear oil. ^{1}H NMR (500 MHz, $CDCl_3$) δ 7.93 (d, *J* = 7.3 Hz, 1H), 7.49 (d, *J* = 8.2 Hz, 1H), 7.33–7.26 (m, 2H), 7.24–7.22 (m, 1H), 7.18 (d, *J* = 3.1 Hz, 1H), 5.65 (s, 1H),

4.16 (t, *J* = 7.1 Hz, 2H), 3.95–3.90 (m, 1H), 3.84–3.78 (m, 1H), 2.52–2.46 (m, 1H), 2.22–2.18 (m, 1H), 2.11–2.03 (m, 1H), 1.85 (p, *J* = 7.2 Hz, 2H), 1.56–1.34 (m, 21H), 1.33–1.28 (m, 4H), 1.27–1.18 (m, 10H), 0.86 (t, *J* = 6.9 Hz, 3H). ^{13}C NMR (126 MHz, $CDCl_3$) δ 178.0, 169.0, 162.1, 153.6, 150.6, 136.6, 129.5, 126.3, 121.1, 121.0, 118.3, 112.7, 102.5, 82.3, 79.8, 55.5, 49.5, 46.8, 32.0, 31.6, 30.5, 29.9, 29.6, 29.38, 29.35, 28.3, 28.1, 27.1, 24.1, 22.8, 14.2. HRMS (ESI+): Calcd for $C_{34}H_{50}N_6O_5$ $[M+H]^+$: 623.8059, Found: 623.3915.

tert-butyl (*S*,*Z*)-(((_tert_-butoxycarbonyl)amino)(2-(3-(1-heptyl-1*H*-indol-4-yl)-1,2,4-oxadiazol-5-yl)pyrrolidin-1-yl)methylene)carbamate (4.13d):

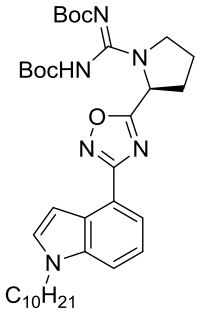

Using **4.12d** as starting material, **4.13d** was prepared using general procedure 4.5. Purification on a silica gel column with 10–40% EtOAc in hexanes produced **4.13d** (10 mg, 34%), a clear oil. ^{1}H NMR (400 MHz, $CDCl_3$) δ 7.93 (dd, *J* = 7.4, 0.9 Hz, 1H), 7.49 (d, *J* = 8.2 Hz, 1H), 7.28 (dd, *J* = 8.2, 7.4 Hz, 1H), 7.24–7.22 (m, 1H), 7.18 (dd, *J* = 3.1, 0.8 Hz, 1H), 5.64 (s, 1H), 4.16 (t, *J* = 7.1 Hz, 2H), 3.96–3.87 (m, 1H), 3.86–3.76 (m, 1H), 2.51–2.41 (m, 1H), 2.30 (s, 1H), 2.24–2.13 (m, 1H), 2.10–2.00 (m, 1H), 1.85 (p, *J* = 7.0 Hz, 2H), 1.53–1.38 (m, 21H), 1.35–1.28 (m, 6H), 1.28–1.19 (m, 12H), 0.86 (t, *J* = 7.1 Hz, 3H). ^{13}C NMR (126 MHz, $CDCl_3$) δ 178.0, 169.0, 162.1, 153.5, 150.6, 136.6, 129.5, 129.4, 126.3, 121.1, 121.0, 118.3, 112.7, 102.5, 82.3, 79.7, 55.5, 49.5, 46.8, 32.0, 31.6, 30.5, 29.9, 29.6, 29.4, 28.3, 27.1, 24.0, 22.8, 14.2. HRMS (ESI+): Calcd for $C_{35}H_{52}N_6O_5$ $[M+H]^+$: 637.8325, Found: 637.4083.

(*S*)-amino(2-(3-(1-heptyl-1*H*-indol-4-yl)-1,2,4-oxadiazol-5-yl)pyrrolidin-1-yl)methaniminium chloride (4.14a):

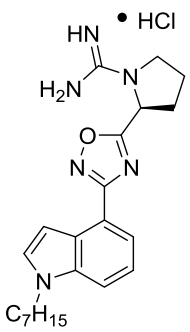

Using **4.13a** as starting material, **4.14a** was prepared using general procedure 4.4, isolated as a light yellow tinted solid (9 mg, 100%) and found to be 78% pure by HPLC. ^{1}H NMR (500 MHz, CD_3OD) δ 7.86 (dd, *J* = 7.5, 0.9 Hz, 1H), 7.64 (dd, *J* = 8.3, 0.9 Hz, 1H), 7.45–7.38 (m, 2H), 7.29 (dd, *J* = 8.3, 7.4 Hz, 1H), 7.09 (dd, *J* = 3.2, 0.8 Hz, 1H), 5.47 (dd, *J* = 7.7, 2.1 Hz, 1H), 4.25 (t, *J* = 7.0 Hz, 1H), 3.84–3.78 (m, 1H), 3.67–3.61 (m, 1H), 2.64–2.50 (m, 2H), 2.31–2.22 (m, 1H), 2.18–2.09 (m, 1H), 1.86 (p, *J* = 7.1 Hz, 2H), 1.32–1.24 (m, 10H), 0.87 (t, *J* = 7.0 Hz, 3H). ^{13}C NMR (126 MHz, CD_3OD) δ 177.8, 170.3, 157.1, 138.1, 131.0, 130.9, 127.4, 121.8, 121.6, 118.6, 114.3, 56.5, 47.3, 32.9, 32.7, 31.5, 30.0, 28.1, 27.9, 24.4, 23.6, 14.3. HRMS (ESI+): Calcd for $C_{22}H_{30}N_6O$ [M+H]: 395.5211, Found: 395.2577.

(*S*)-amino(2-(3-(1-octyl-1*H*-indol-4-yl)-1,2,4-oxadiazol-5-yl)pyrrolidin-1-yl)methaniminium chloride (4.14b):

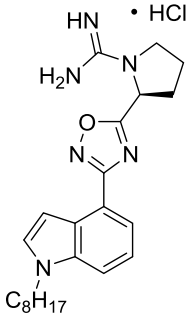

Using **4.13b** as starting material, **4.14b** was prepared using general procedure 4.4, isolated as a light yellow tinted solid (6 mg, 100%) and found to be 53% pure by HPLC. ^{1}H NMR (500 MHz, CD_3OD) δ 7.86 (dd, *J* = 7.5, 0.9 Hz, 1H), 7.64 (dd, *J* = 8.3, 0.9 Hz, 1H), 7.39 (s, 1H), 7.29 (dd, *J* = 8.2, 7.4 Hz, 1H), 5.48 (dd, *J* = 7.8, 2.0 Hz, 1H), 4.25 (t, *J* = 7.0 Hz, 2H), 3.83–3.78 (m, 1H), 3.66–3.61 (m, 1H), 2.62–2.50 (m, 2H), 2.29–2.22 (m, 1H), 2.18–2.07 (m, 1H), 1.85 (p, *J* = 6.9 Hz, 2H), 1.36–1.22 (m, 14H), 0.87 (t, *J* = 6.9 Hz, 3H).^{13}C NMR (126 MHz, CD_3OD) δ 177.8, 170.3, 157.1, 138.1, 131.0, 130.9, 127.4, 121.8, 121.6, 118.6, 114.3, 103.0, 61.5, 56.5, 47.3, 32.9, 32.7,

31.5, 30.28, 30.26, 27.9, 24.4, 23.6, 20.9, 14.5, 14.4. HRMS (ESI+): Calcd for $C_{23}H_{32}N_6O$ [M+H]: 409.5477, Found: 409.2731.

(*S*)-amino(2-(3-(1-nonyl-1*H*-indol-4-yl)-1,2,4-oxadiazol-5-yl)pyrrolidin-1-yl)methaniminium chloride (4.14c):

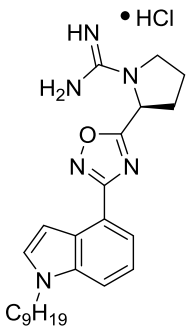

Using **4.13c** as starting material, **4.14c** was prepared using general procedure 4.4, isolated as a light yellow tinted solid (7 mg, 95%) and found to be 36% pure by HPLC. ^{1}H NMR (500 MHz, CD_3OD) δ 7.72 (dd, *J* = 7.3, 2.0 Hz, 1H), 7.45 (s, 1H), 7.42–7.38 (m, 1H), 7.36–7.33 (m, 1H), 7.11 (d, *J* = 3.1 Hz, 1H), 5.56–5.46 (m, 1H), 4.26 (t, *J* = 6.4 Hz, 2H), 3.86–3.79 (m, 1H), 3.70–3.58 (m, 1H), 2.65–2.55 (m, 1H), 2.54–2.47 (m, 1H), 2.29–2.21 (m, 1H), 2.18–2.09 (m, 1H), 1.87 (p, *J* = 7.0 Hz, 2H), 1.42–1.20 (m, 14H), 0.87 (t, *J* = 6.9 Hz, 3H). ^{13}C NMR (126 MHz, CD_3OD) δ 178.0, 157.1, 137.3, 128.7, 123.7, 122.8, 121.8, 118.9, 114.3, 104.2, 103.0, 56.5, 56.3, 47.5, 47.3, 33.0, 32.8, 32.7, 31.5, 31.3, 30.6, 30.3, 27.9, 27.8, 24.3, 23.7, 14.4. HRMS (ESI+): Calcd for $C_{24}H_{34}N_6O$ [M+H]: 423.5743, Found: 424.2938.

(*S*)-amino(2-(3-(1-decyl-1*H*-indol-4-yl)-1,2,4-oxadiazol-5-yl)pyrrolidin-1-yl)methaniminium chloride (4.14d):

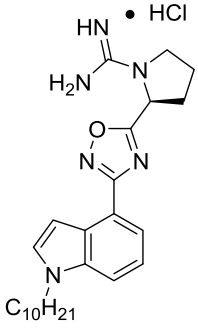

Using **4.13d** as starting material, **4.14d** was prepared using general procedure 4.4, isolated as a light yellow tinted solid (6 mg, 81%) and found to be 70% pure by HPLC. ^{1}H NMR (500 MHz, CD_3OD) δ 7.88 (d, *J* = 7.3 Hz, 1H), 7.66 (dd, *J* = 8.3, 5.0 Hz, 1H), 7.40 (d, *J* = 3.1 Hz, 1H), 7.35–7.29 (m, 1H), 7.10 (dd, *J* = 6.0, 3.1 Hz, 1H), 5.50 (dd, *J* = 7.8, 2.0 Hz, 1H), 4.27 (t, *J* = 6.7 Hz, 2H), 3.85–3.79 (m, 1H), 3.70–3.63 (m, 1H), 2.65–2.52 (m, 2H), 2.30–2.20 (m, 1H), 2.19–2.07 (m,

1H), 1.86 (q, *J* = 6.9 Hz, 2H), 1.35–1.22 (m, 20H), 0.89 (t, *J* = 6.9 Hz,, 3H).^{13}C NMR (126 MHz, CD_3OD) δ 177.8, 170.3, 157.1, 138.1, 131.0, 130.9, 128.7, 127.5, 123.8, 122.9, 121.8, 121.6, 114.3, 103.0, 56.5, 56.3, 47.3, 33.03, 33.01, 32.7, 31.4, 31.3, 30.7, 30.6, 30.5, 30.39, 30.36, 30.3, 28.1, 27.9, 24.4, 24.3, 23.72, 23.68, 14.4. HRMS (ESI+): Calcd for $C_{25}H_{36}N_6O$ [M+H]: 437.6009, Found: 437.3033.

***N′*-hydroxy-1*H*-indole-5-carboximidamide (4.16):**

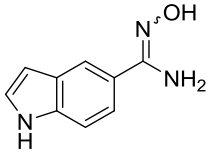

Using **4.15** as starting material, **4.16** was prepared using general procedure 4.1. Purification on a silica gel column with 70–100% EtOAc in hexanes produced **4.16** as a mixture of enantiomers (1.78 g, 96%), a tan solid. ^{1}H NMR (400 MHz, CD_3OD) δ 7.88 (dd, *J* = 1.6, 0.8 Hz, 1H), 7.43–7.37 (m, 2H), 7.25 (d, *J* = 3.2 Hz, 1H), 6.49 (dd, *J* = 3.2, 0.8 Hz, 1H). ^{13}C NMR (101 MHz, CD_3OD) δ 157.6, 148.2, 138.5, 129.1, 128.8, 127.3, 126.9, 126.8, 124.3, 121.9, 121.8, 120.7, 119.7, 112.21, 112.16, 111.9, 103.6, 103.06, 103.01. HRMS (ESI+): Calcd for $C_9H_9N_3O$ [M+H]: 176.1592, Found: 176.0812.

***tert*-butyl (*S*)-2-(3-(1*H*-indol-5-yl)-1,2,4-oxadiazol-5-yl)pyrrolidine-1-carboxylate (4.17):**

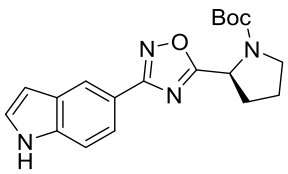

Using **4.16** and Boc-L-proline as starting material, **4.17** was prepared using general procedure 4.2. Purification on a silica gel column with 10-40% EtOAc in hexanes produced **4.17** (3.59 g, 45%), a tan solid. ^{1}H NMR (2:1 rotamer ratio, asterisk denote minor rotamer peak, 400 MHz, $CDCl_3$) δ 9.52 (s, 1H), 9.40* (s, 1H), 8.43 (d, *J* = 1.6 Hz, 1H), 8.31* (s, 1H), 7.93 (dd, *J* = 8.5, 1.6 Hz, 1H), 7.86* (dd, *J* = 6.3, 3.1 Hz, 1H), 7.81* (d, *J* = 8.6 Hz, 1H), 7.48 (d, *J* = 8.6 Hz, 1H), 7.40–7.35 (m, 1H), 7.27–7.23 (m, 1H), 7.22–7.19* (m, 1H), 6.60 (s, 1H), 6.55* (s, 1H), 5.26–5.21* (m, 1H), 5.09 (dd, *J* = 8.2, 3.9 Hz, 1H), 3.80–3.65 (m, 1H), 3.60–3.45 (m, 1H), 2.42–2.27 (m, 1H), 2.19–2.07 (m, 2H),

2.01–1.90 (m, 1H), 1.48* (s, 3H), 1.32 (s, 6H). ^{13}C NMR (2:1 rotamer ratio, asterisk denote minor rotamer peak, 101 MHz, $CDCl_3$) δ 180.0, 179.5*, 171.4*, 169.5, 154.5*, 154.0, 137.6, 137.5*, 128.0, 127.8*, 125.9, 125.8, 125.7*, 120.8, 120.7*, 117.8, 114.9, 111.8, 111.6*, 103.0, 80.8, 60.5, 53.9, 46.7*, 46.4, 32.3, 31.5*, 28.4*, 28.2, 24.3*, 23.7, 21.0, 14.1. HRMS (ESI+): Calcd for $C_{19}H_{22}N_4O_3$ [M+Na]: 377.3927, Found: 377.1589.

tert-butyl (_S_)-2-(3-(1-hexyl-1_H_-indol-5-yl)-1,2,4-oxadiazol-5-yl)pyrrolidine-1-carboxylate (4.18a):

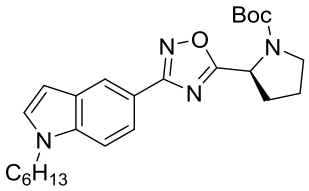

Using **4.17** and 1-bromohexane as starting material, **4.18a** was prepared using general procedure 4.3. Purification on a silica gel column with 0–20% EtOAc in hexanes produced **4.18a** (72 mg, 97%), a yellow oil. ^{1}H NMR (2:1 rotamer ratio, asterisk denote minor rotamer peak, 400 MHz, $CDCl_3$) δ 8.38 (d, *J* = 1.6 Hz, 1H), 7.92 (dd, *J* = 8.6, 1.7 Hz, 1H), 7.40 (d, *J* = 8.7 Hz, 1H), 7.14 (dt, *J* = 3.6 Hz, 1H), 6.57 (d, *J* = 3.8 Hz, 1H), 5.23* (d, *J* = 6.7 Hz, 1H), 5.07 (dd, *J* = 8.1, 3.8 Hz, 1H), 4.13 (t, *J* = 7.1 Hz, 2H), 3.78–3.65 (m, 1H), 3.60–3.45 (m, 1H), 2.48–2.34 (m, 1H), 2.22–2.08 (m, 2H), 2.06–1.94 (m, 1H), 1.84 (p, *J* = 7.2 Hz, 2H), 1.47* (s, 3H), 1.30 (s, 14H), 0.87 (t, *J* = 6.9 Hz, 3H). ^{13}C NMR (2:1 rotamer ratio, asterisk denote minor rotamer peak, 101 MHz, $CDCl_3$) δ 180.2, 169.5, 153.8, 137.6, 129.1, 129.0*, 128.6, 121.3, 120.8*, 120.6, 117.8, 109.9, 109.8*, 102.2, 80.5, 54.0, 46.7, 46.5*, 32.5*, 31.5, 30.4, 28.5*, 28.3, 26.7, 24.5*, 23.8, 22.6, 14.1. HRMS (ESI+): Calcd for $C_{25}H_{34}N_4O_3$ $[M+Na]^+$: 461.5522, Found: 461.2525.

***tert*-butyl (*S*)-2-(3-(1-heptyl-1*H*-indol-5-yl)-1,2,4-oxadiazol-5-yl)pyrrolidine-1-carboxylate (4.18b):**

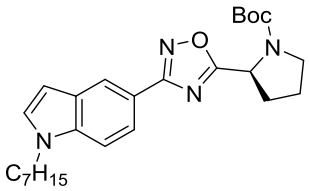

Using **4.17** and 1-bromoheptane as starting material, **4.18b** was prepared using general procedure 4.3. Purification on a silica gel column with 0–20% EtOAc in hexanes produced **4.18b** (52 mg, 82%), a yellow oil. ^{1}H NMR (2:1 rotamer ratio, asterisk denote minor rotamer peak, 400 MHz, $CDCl_3$) δ 8.38 (d, *J* = 1.6 Hz, 1H), 7.92 (dd, *J* = 8.6, 1.7 Hz, 1H), 7.40 (d, *J* = 8.8 Hz, 1H), 7.14 (d, *J* = 3.5 Hz, 1H), 6.57 (d, *J* = 3.2 Hz, 1H), 5.22* (d, *J* = 8.1 Hz, 1H), 5.07 (dd, *J* = 8.1, 3.7 Hz, 1H), 4.13 (t, *J* = 7.1, 2H), 3.78–3.65 (m, 1H), 3.61–3.51 (m, 1H), 2.46–2.32 (m, 1H), 2.25–2.13 (m, 2H), 2.06–1.95 (m, 2H), 1.84 (p, *J* = 7.0 Hz, 2H), 1.47* (s, 3H), 1.36–1.23 (m, 14H), 0.86 (t, *J* = 6.9 Hz, 3H). ^{13}C NMR (2:1 rotamer ratio, asterisk denote minor rotamer peak, 101 MHz, $CDCl_3$) δ 180.2, 169.5, 153.8, 137.6, 129.1, 129.0*, 128.6, 121.3, 120.8*, 120.6, 118.1*, 117.8, 109.9, 109.8*, 102.2, 80.5, 54.0, 46.7, 46.5*, 32.5, 31.8, 31.7*, 30.4, 29.0, 28.5*, 28.3, 27.0, 24.5*, 23.8, 22.7, 14.2. HRMS (ESI+): Calcd for $C_{26}H_{36}N_4O_3$ $[M+Na]^+$: 475.5788, Found: 475.2681.

***tert*-butyl (*S*)-2-(3-(1-octyl-1*H*-indol-5-yl)-1,2,4-oxadiazol-5-yl)pyrrolidine-1-carboxylate (4.18c):**

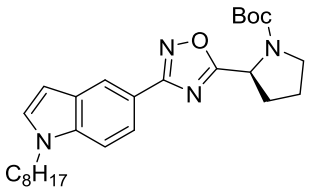

Using **4.17** and 1-bromooctane as starting material, **4.18c** was prepared using general procedure 4.3. Purification on a silica gel column with 0–20% EtOAc in hexanes produced **4.18c** (76 mg, 97%), a yellow oil. ^{1}H NMR (2:1 rotamer ratio, asterisk denote minor rotamer peak, 400 MHz, $CDCl_3$) δ 8.38 (d, *J* = 1.6 Hz, 1H), 7.92 (dd, *J* = 8.6, 1.6 Hz, 1H), 7.41 (d, *J* = 8.7 Hz, 1H), 7.15 (d, *J* = 3.2 Hz, 1H), 6.58 (d, *J* = 3.2 Hz, 1H), 5.31–5.18* (m, 1H), 5.07 (dd, *J* = 8.2, 3.7 Hz, 1H), 4.13 (t, *J* = 7.1 Hz,

2H), 3.78–3.64 (m, 1H), 3.62–3.48 (m, 1H), 2.42–2.32 (m, 1H), 2.24–2.12 (m, 2H), 2.07–1.94 (m, 1H), 1.83 (p, *J* = 6.8 Hz, 2H), 1.47* (s, 3H), 1.36–1.21 (m, 18H), 0.86 (t, *J* = 6.5 Hz, 3H). ^{13}C NMR (2:1 rotamer ratio, asterisk denote minor rotamer peak, 101 MHz, $CDCl_3$) δ 180.2, 169.5, 153.8, 137.6, 129.1, 129.0*, 128.6, 121.3, 120.8*, 120.6, 117.8, 110.1, 109.9, 109.8*, 102.2, 80.5, 77.5, 77.4, 77.2, 76.8, 54.0, 46.7, 46.5*, 32.5, 31.9, 31.7*, 30.4, 29.3, 29.3, 28.5*, 28.3, 27.1, 24.5*, 23.9, 22.7, 14.2. HRMS (ESI+): Calcd for $C_{27}H_{38}N_4O_3$ $[M+Na]^+$: 489.6054, Found: 489.2839.

tert-butyl (_S_)-2-(3-(1-nonyl-1_H_-indol-5-yl)-1,2,4-oxadiazol-5-yl)pyrrolidine-1-carboxylate (4.18d):

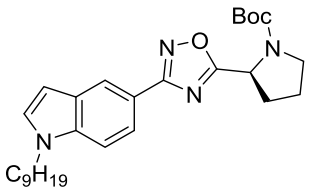

Using **4.17** and 1-bromoheptane as starting material, **4.18d** was prepared using general procedure 4.3. Purification on a silica gel column with 0–20% EtOAc in hexanes produced **4.18d** (28 mg, 52%), a yellow oil. ^{1}H NMR (2:1 rotamer ratio, asterisk denote minor rotamer peak, 400 MHz, $CDCl_3$) δ 8.38 (d, *J* = 1.6 Hz, 1H), 7.92 (dd, *J* = 8.6, 1.6 Hz, 1H), 7.40 (d, *J* = 8.6 Hz, 1H), 7.15 (d, *J* = 3.1 Hz, 1H), 6.57 (d, *J* = 3.2 Hz, 1H), 5.22* (d, *J* = 8.2 Hz, 1H), 5.07 (dd, *J* = 8.1, 3.7 Hz, 1H), 4.13 (t, *J* = 7.2 Hz, 3H), 3.79–3.66 (m, 1H), 3.63–3.51 (m, 1H), 2.45–2.33 (m, 1H), 2.22–2.10 (m, 2H), 2.06–1.96 (m, 1H), 1.85 (p, *J* = 7.4 Hz, 2H), 1.47* (s, 3H), 1.37–1.21 (m, 21H), 0.87 (t, *J* = 7.1 Hz, 3H). ^{13}C NMR (2:1 rotamer ratio, asterisk denote minor rotamer peak, 101 MHz, $CDCl_3$) δ 169.5, 153.8, 137.6, 129.1, 129.0*, 128.7, 121.3, 120.8*, 120.7, 117.9, 109.9, 109.8*, 102.3, 80.5, 54.0, 46.7, 46.5*, 32.6*, 31.9, 30.4, 29.6, 29.4, 29.3, 28.6*, 28.3, 27.1, 23.9*, 22.8, 14.2. HRMS (ESI+): Calcd for $C_{28}H_{40}N_4O_3$ $[M+Na]^+$: 503.6320, Found: 503.2966.

***tert*-butyl (*S*)-2-(3-(1-decyl-1*H*-indol-5-yl)-1,2,4-oxadiazol-5-yl)pyrrolidine-1-carboxylate (4.18e):**

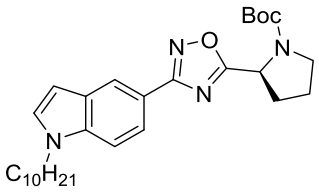

Using **4.17** and 1-bromoheptane as starting material, **4.18e** was prepared using general procedure 4.3. Purification on a silica gel column with 0–20% EtOAc in hexanes produced **4.18e** (56 mg, 80%), a yellow oil. ^{1}H NMR (2:1 rotamer ratio, asterisk denote minor rotamer peak, 400 MHz, $CDCl_3$) δ 8.39 (d, *J* = 1.6 Hz, 1H), 7.92 (dd, *J* = 8.6, 1.6 Hz, 1H), 7.40 (d, *J* = 8.7 Hz, 1H), 7.14 (d, *J* = 3.3 Hz, 1H), 6.57 (d, *J* = 3.2 Hz, 1H), 5.22* (d, *J* = 8.1 Hz, 1H), 5.07 (dd, *J* = 8.0, 3.5 Hz, 1H), 4.13 (t, *J* = 7.1 Hz, 2H), 3.78–3.67 (m, 1H), 3.62–3.49 (m, 1H), 2.45–2.33 (m, 1H), 2.23–2.11 (m, 2H), 2.09–1.97 (m, 1H), 1.84 (p, *J* = 7.5 Hz, 2H), 1.47* (s, 3H), 1.3–1.19 (m, 20H), 0.87 (t, *J* = 7.0 Hz, 3H). ^{13}C NMR (2:1 rotamer ratio, asterisk denote minor rotamer peak, 101 MHz, $CDCl_3$) δ 180.2, 169.5, 153.8, 137.6, 129.1, 128.9*, 128.7, 121.3, 120.8*, 120.7, 118.1*, 117.9, 109.9*, 109.8, 102.2, 80.5, 54.0, 46.7, 46.5*, 32.5*, 32.0, 30.4, 29.60, 29.58, 29.5, 29.4, 29.3, 28.5*, 28.3, 27.1, 23.8*, 22.8, 14.2. HRMS (ESI+): Calcd for $C_{29}H_{42}N_4O_3$ $[M+Na]^+$: 517.6585, Found: 517.3111.

***tert*-butyl (*S,Z*)-(((*tert*-butoxycarbonyl)imino)(2-(3-(1-hexyl-1*H*-indol-5-yl)-1,2,4-oxadiazol-5-yl)pyrrolidin-1-yl)methyl)carbamate (4.20a):**

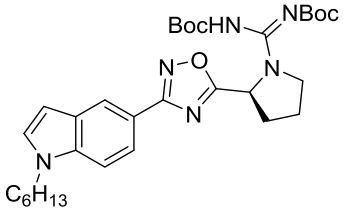

Compound **4.19a** was prepared from **4.18a** using general procedure 4.4 and carried on to the next reaction without purification. Using **4.19a** as starting material, **4.20a** was prepared using general procedure 4.5. Purification on a silica gel column with 10–40% EtOAc in hexanes produced **4.20a** (30 mg, 48%), a clear oil. ^{1}H NMR (500 MHz, $CDCl_3$) δ 8.37 (d, *J* = 1.6 Hz, 1H), 7.90 (d,

J = 1.6 Hz, 1H), 7.39 (d, *J* = 8.6 Hz, 1H), 7.14 (d, *J* = 3.2 Hz, 1H), 6.56 (dd, *J* = 3.1, 0.8 Hz, 1H), 5.59 (s, 1H), 4.13 (t, *J* = 7.2 Hz, 2H), 3.92–3.86 (m, 1H), 3.84–3.75 (m, 1H), 2.49–2.39 (m, 1H), 2.34–2.24 (m, 1H), 2.22–2.15 (m, 1H), 2.09–1.99 (m, 1H), 1.85 (p, *J* = 7.2 Hz, 2H), 1.54–1.35 (m, 22H), 1.34–1.22 (m, 9H), 0.87 (t, *J* = 7.1 Hz, 3H). ^{13}C NMR (126 MHz, $CDCl_3$) δ 178.4, 169.5, 162.1, 153.5, 150.6, 137.7, 129.1, 128.7, 121.5, 120.8, 117.7, 109.9, 102.3, 82.3, 79.7, 55.5, 49.6, 46.7, 31.5, 30.4, 28.3, 28.1, 26.8, 24.1, 22.7, 14.1. HRMS (ESI+): Calcd for $C_{31}H_{44}N_6O_5$ $[M+H]^+$: 581.7262, Found: 581.3475.

tert-butyl (*S*,*Z*)-(((_tert_-butoxycarbonyl)imino)(2-(3-(1-heptyl-1*H*-indol-5-yl)-1,2,4-oxadiazol-5-yl)pyrrolidin-1-yl)methyl)carbamate (4.20b):

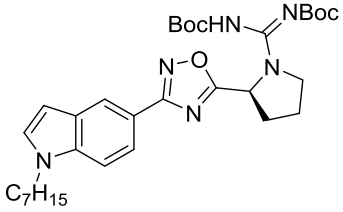

Compound **4.19b** was prepared from **4.18b** using general procedure 4.4 and carried on to the next reaction without purification. Using **4.19b** as starting material, **4.20b** was prepared using general procedure 4.5. Purification on a silica gel column with 10–40% EtOAc in hexanes produced **4.20b** (25 mg, 52%), a clear oil. ^{1}H NMR (500 MHz, $CDCl_3$) δ 8.37 (d, *J* = 1.7 Hz, 1H), 7.91 (dd, *J* = 8.7, 1.7 Hz, 1H), 7.39 (d, *J* = 8.7 Hz, 1H), 7.14 (d, *J* = 3.2 Hz, 1H), 6.56 (dd, *J* = 3.1, 0.8 Hz, 1H), 5.59 (s, 1H), 4.13 (t, *J* = 7.2 Hz, 2H), 3.93–3.85 (m, 1H), 3.83–3.77 (m, 1H), 2.49–2.40 (m, 1H), 2.34–2.25 (m, 1H), 2.22–2.14 (m, 1H), 2.09–2.02 (m, 1H), 1.85 (p, *J* = 7.0 Hz, 2H), 1.52–1.39 (m, 17H), 1.34–1.21 (m, 9H), 0.86 (t, *J* = 7.0 Hz, 3H). ^{13}C NMR (126 MHz, $CDCl_3$) δ 178.4, 169.5, 162.0, 153.7, 150.7, 137.7, 129.1, 128.7, 121.5, 120.8, 117.7, 109.9, 102.3, 82.3, 79.7, 55.5, 49.6, 46.8, 31.8, 31.5, 30.4, 29.0, 28.5, 28.3, 28.1, 27.1, 24.0, 22.7, 14.4, 14.2. HRMS (ESI+): Calcd for $C_{32}H_{46}N_6O_5$ $[M+H]^+$: 595.7528, Found: 595.3620.

***tert*-butyl (*S,Z*)-(((*tert*-butoxycarbonyl)imino)(2-(3-(1-octyl-1*H*-indol-5-yl)-1,2,4-oxadiazol-5-yl)pyrrolidin-1-yl)methyl)carbamate (4.20c):**

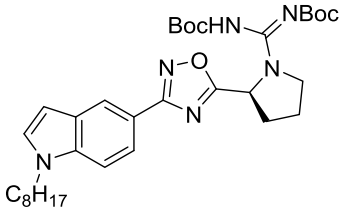

Compound **4.19c** was prepared from **4.18c** using general procedure 4.4 and carried on to the next reaction without purification. Using **4.19c** as starting material, **4.20c** was prepared using general procedure 4.5. Purification on a silica gel column with 10–40% EtOAc in hexanes produced **4.20c** (32 mg, 50%), a clear oil. ^{1}H NMR (400 MHz, $CDCl_3$) δ 8.37 (dd, *J* = 1.6, 0.7 Hz, 1H), 7.91 (dd, *J* = 8.6, 1.6 Hz, 1H), 7.39 (dt, *J* = 8.7, 0.8 Hz, 1H), 7.14 (d, *J* = 3.1 Hz, 1H), 6.56 (dd, *J* = 3.2, 0.8 Hz, 1H), 5.59 (s, 1H), 4.13 (t, *J* = 7.2 Hz, 2H), 3.93–3.87 (m, 1H), 3.85–3.76 (m, 1H), 2.48–2.40 (m, 1H), 2.35–2.26 (m, 1H), 2.23–2.15 (m, 1H), 2.05 (p, *J* = 6.4 Hz, 1H), 1.85 (p, *J* = 7.2 Hz, 2H), 1.51–1.37 (m, 19H), 1.34–1.21 (m, 11H), 0.86 (t, *J* = 6.9 Hz, 3H). ^{13}C NMR (101 MHz, $CDCl_3$) δ 178.4, 169.5, 162.0, 153.5, 150.6, 137.6, 129.1, 128.6, 121.5, 120.7, 117.7, 109.9, 102.3, 82.3, 79.7, 55.4, 49.6, 46.7, 31.9, 31.5, 30.4, 29.3, 28.3, 28.1, 27.1, 22.7, 14.2. HRMS (ESI+): Calcd for $C_{33}H_{48}N_6O_5$ $[M+H]^+$: 609.7794, Found: 609.3793.

***tert*-butyl (*S,Z*)-(((*tert*-butoxycarbonyl)imino)(2-(3-(1-nonyl-1*H*-indol-5-yl)-1,2,4-oxadiazol-5-yl)pyrrolidin-1-yl)methyl)carbamate (4.20d):**

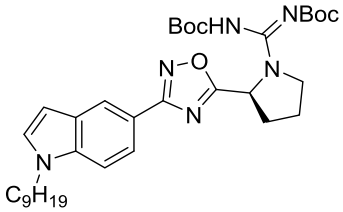

Compound **4.19d** was prepared from **4.18d** using general procedure 4.4 and carried on to the next reaction without purification. Using **4.19d** as starting material, **4.20d** was prepared using general procedure 4.5. Purification on a silica gel column with 1040% EtOAc in hexanes produced **4.20d** (11 mg, 41%), a clear oil. ^{1}H NMR (500 MHz, $CDCl_3$) δ 8.37 (d, *J* = 1.5 Hz, 1H), 7.91 (dd, *J* = 8.6, 1.6 Hz, 1H), 7.39 (d, *J* = 8.7 Hz, 1H), 7.14 (t, *J* = 1.6 Hz,

1H), 6.56 (dd, *J* = 3.1, 0.8 Hz, 1H), 5.59 (dd, *J* = 7.9, 4.6 Hz, 1H), 4.13 (t, *J* = 7.2 Hz, 2H), 3.94–3.89 (m, 1H), 3.84–3.78 (m, 1H), 2.50–2.42 (m, 1H), 2.34–2.26 (m, 1H), 2.23–2.15 (m, 1H), 2.09–2.01 (m, 1H), 1.86–1.79 (m, 2H), 1.55–1.38 (m, 20H), 1.37–1.17 (m, 14H), 0.86 (t, *J* = 6.9 Hz, 3H). ^{13}C NMR (126 MHz, $CDCl_3$) δ 178.4, 169.5, 153.5, 137.7, 129.1, 128.6, 121.5, 120.8, 117.7, 109.9, 102.3, 81.1, 55.5, 49.6, 46.8, 32.0, 31.5, 30.4, 29.9, 29.6, 29.4, 28.3, 28.0, 27.1, 24.1, 22.8, 14.2. HRMS (ESI+): Calcd for $C_{34}H_{50}N_6O_5$ [M+Na]: 645.7878, Found: 645.3714.

tert-butyl (*S*,*Z*)-(((_tert_-butoxycarbonyl)imino)(2-(3-(1-decyl-1*H*-indol-5-yl)-1,2,4-oxadiazol-5-yl)pyrrolidin-1-yl)methyl)carbamate (4.20e):

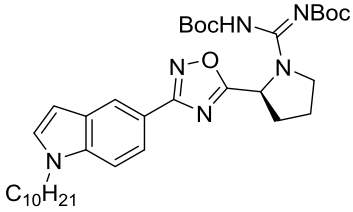

Compound **4.19e** was prepared from **4.18e** using general procedure 4.4 and carried on to the next reaction without purification. Using **4.19e** as starting material, **4.20e** was prepared using general procedure 4.5. Purification on a silica gel column with 10–30% EtOAc in hexanes produced **4.20e** (36 mg, 61%), a clear oil. ^{1}H NMR (500 MHz, $CDCl_3$) δ 8.37 (d, *J* = 1.5 Hz, 1H), 7.91 (dd, *J* = 8.7, 1.6 Hz, 1H), 7.39 (d, *J* = 8.7 Hz, 1H), 7.14 (d, *J* = 1.7 Hz, 1H), 6.56 (d, *J* = 3.1 Hz, 1H), 5.59 (t, *J* = 6.0 Hz, 1H), 4.13 (t, *J* = 7.2 Hz, 2H), 3.94–3.86 (m, 1H), 3.85–3.77 (m, 1H), 2.47–2.41 (m, 1H), 2.35–2.25 (m, 1H), 2.26–2.16 (m, 1H), 2.11–1.98 (m, 1H), 1.84 (p, *J* = 7.9, 7.0 Hz, 2H), 1.54–1.41 (m, 18H), 1.35–120 (m, 16H), 0.87 (t, *J* = 7.0 Hz, 3H). ^{13}C NMR (126 MHz, $CDCl_3$) δ 178.4, 169.5, 161.8, 153.4, 150.6, 137.6, 129.1, 129.0, 128.6, 128.5, 121.5, 120.7, 117.7, 109.9, 102.3, 82.1, 79.8, 55.5, 49.6, 46.7, 32.0, 31.5, 30.4, 29.8, 29.6, 29.4, 28.6, 28.3, 28.1, 27.6, 27.1, 24.8, 24.0, 22.8, 14.2. HRMS (ESI+): Calcd for $C_{35}H_{52}N_6O_5$ [M+Na]: 659.8143, Found: 659.3884.

(*S*)-amino(2-(3-(1-hexyl-1*H*-indol-5-yl)-1,2,4-oxadiazol-5-yl)pyrrolidin-1-yl)methaniminium chloride (4.21a):

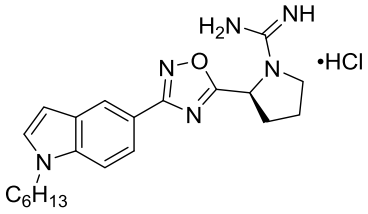

Using **4.20a** as starting material, **4.21a** was prepared using general procedure 4.4 and isolated as a light yellow tinted solid (9 mg, 82%). ^{1}H NMR (500 MHz, CD_3OD) δ 8.34–8.00 (m, 1H), 7.79 (ddd, *J* = 67.4, 8.7, 1.6 Hz, 1H), 7.49 (dd, *J* = 46.9, 8.8 Hz, 1H), 7.36–7.27 (m, 1H), 7.10–6.99 (m, 1H), 6.73–6.60 (m, 1H), 5.43 (ddd, *J* = 31.8, 7.9, 1.9 Hz, 1H), 4.23 (q, *J* = 7.5 Hz, 2H), 3.88–3.75 (m, 1H), 3.68–3.57(m, 1H), 2.58–2.40 (m, 2H), 2.32–2.20 (m, 1H), 2.17–2.03 (m, 1H), 1.92–1.82 (m, 2H), 1.43–1.21 (m, 8H), 0.87 (t, *J* = 7.0 Hz, 3H). ^{13}C NMR (126 MHz, CD_3OD) δ 178.2, 170.9, 157.1, 156.0, 143.5, 140.4, 130.9, 130.1, 128.7, 128.1, 127.3, 126.2, 122.0, 121.9, 121.24, 121.19, 117.0, 115.5, 111.1, 111.0, 102.9, 56.4, 47.3, 47.1, 42.5, 35.9, 32.7, 32.6, 32.5, 31.7, 31.4, 31.0, 27.6, 27.5, 24.4, 23.59, 23.55, 14.34, 14.27. HRMS (ESI+): Calcd for $C_{21}H_{28}N_6O$ [M+H]: 381.4946, Found: 381.2419.

(*S*)-amino(2-(3-(1-heptyl-1*H*-indol-5-yl)-1,2,4-oxadiazol-5-yl)pyrrolidin-1-yl)methaniminium chloride (4.21b):

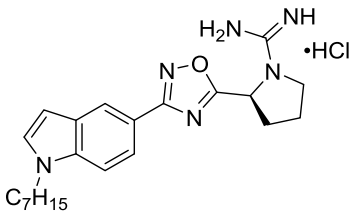

Using **4.20b** as starting material, **4.21b** was prepared using general procedure 4 and isolated as a light yellow tinted solid (8 mg, 80%). ^{1}H NMR (500 MHz, CD_3OD) δ 8.29 (d, *J* = 1.5 Hz, 1H), 7.84 (dd, *J* = 8.6, 1.6 Hz, 1H), 7.51 (d, *J* = 8.6 Hz, 1H), 7.32 (d, *J* = 3.0 Hz, 1H), 6.83 (dd, *J* = 180.1, 8.7 Hz, 1H), 6.56 (d, *J* = 3.1 Hz, 1H), 5.44 (d, *J* = 7.5 Hz, 1H), 4.22 (t, *J* = 7.0 Hz, 2H), 3.83–3.71 (m, 1H), 3.66–3.60 (m, 1H), 2.61–2.44 (m, 2H), 2.28–2.18 (m, 1H), 2.17–2.03 (m, 1H), 1.84 (p, *J* = 7.0 Hz, 2H), 1.35–1.16 (m, 10H), 0.87 (t, *J* = 6.9 Hz, 3H). ^{13}C

NMR (126 MHz, CD_3OD) δ 178.3, 170.8, 157.1, 139.1, 130.8, 130.0, 128.7, 121.9, 121.2, 118.1, 115.5, 111.1, 56.5, 47.3, 32.9, 32.7, 31.4, 30.0, 27.9, 24.4, 23.6, 14.3. HRMS (ESI+): Calcd for $C_{22}H_{30}N_6O$ [M+H]: 395.5211, Found: 395.2573.

(*S*)-amino(2-(3-(1-octyl-1*H*-indol-5-yl)-1,2,4-oxadiazol-5-yl)pyrrolidin-1-yl)methaniminium chloride (4.21c):

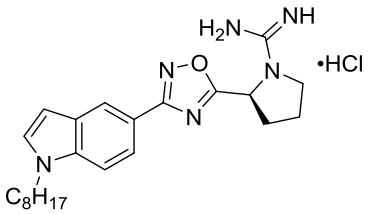

Using **4.20c** as starting material, **4.21c** was prepared using general procedure 4.4 and isolated as a light yellow tinted solid (13 mg, 87%). ^{1}H NMR (1:1 rotomer ratio, 500 MHz, CD_3OD) δ 8.29 (dd, *J* = 1.7, 0.6 Hz, 1H), 7.84 (dd, *J* = 8.6, 1.6 Hz, 1H), 7.52* (dd, *J* = 8.7, 0.8 Hz, 1H), 7.32 (d, *J* = 3.2 Hz, 1H), 7.02* (d, *J* = 8.7 Hz, 1H), 6.66 (s, 1H), 6.56 (dd, *J* = 3.2, 0.8 Hz, 1H), 5.44 (dd, *J* = 7.9, 2.0 Hz, 1H), 4.22 (t, *J* = 7.0 Hz, 2H), 3.85–3.76 (m, 1H), 3.62 (t, *J* = 7.2 Hz, 1H), 2.60–2.54 (m, 1H), 2.53–2.47 (m, 1H), 2.27–2.22 (m, 1H), 2.17–2.08 (m, 1H), 1.84 (p, *J* = 7.0 Hz, 2H), 1.32–1.19 (m, 14H), 0.87 (t, *J* = 7.0 Hz, 3H). ^{13}C NMR (126 MHz, CD_3OD) δ 178.3, 170.8, 157.1, 156.0, 143.5, 139.2, 130.9, 130.8, 130.1, 130.0, 128.7, 121.97, 121.95, 121.2, 118.2, 115.5, 111.1, 102.9, 56.5, 47.3, 42.5, 32.9, 32.7, 31.7, 31.4, 30.3, 30.3, 27.9, 24.4, 23.6, 14.4. HRMS (ESI+): Calcd for $C_{23}H_{32}N_6O$ [M+H]: 409.5477, Found: 409.2717.

(*S*)-amino(2-(3-(1-nonyl-1*H*-indol-5-yl)-1,2,4-oxadiazol-5-yl)pyrrolidin-1-yl)methaniminium chloride (4.21d):

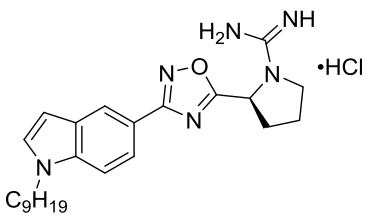

Using **4.20d** as starting material, **4.21d** was prepared using general procedure 4.4, and isolated as a light yellow solid (7 mg, 95%) and found to be 71% pure by HPLC. ^{1}H NMR (500 MHz, CD_3OD) δ 8.29 (d, *J* = 1.6 Hz, 1H), 7.84 (dd, *J* = 8.7, 1.6 Hz, 1H),

7.52 (d, *J* = 8.7 Hz, 1H), 7.32 (d, *J* = 3.2 Hz, 1H), 6.56 (dd, *J* = 3.2, 0.8 Hz, 1H), 5.44 (dd, *J* = 7.9, 1.9 Hz, 1H), 4.22 (t, *J* = 7.0 Hz, 2H), 3.87–3.72 (m, 1H), 3.67–3.58 (m, 1H), 2.63–2.51 (m, 1H), 2.25–2.19 (m, 1H), 2.16–2.07 (m, 1H), 1.84 (p, *J* = 7.0 Hz, 2H), 1.34–1.07 (m, 14H), 0.86 (t, *J* = 7.1 Hz, 3H). ^{13}C NMR (126 MHz, CD_3OD) δ 178.4, 170.8, 157.1, 139.2, 130.9, 130.1, 122.3, 122.0, 121.2, 118.2, 112.0, 111.2, 102.9, 56.5, 47.3, 33.0, 32.7, 31.4, 30.6, 30.30, 30.29, 27.9, 24.4, 23.7, 14.4. HRMS (ESI+): Calcd for $C_{24}H_{34}N_6O$ [M+H]: 423.5743, Found: 423.2858.

(*S*)-amino(2-(3-(1-decyl-1*H*-indol-5-yl)-1,2,4-oxadiazol-5-yl)pyrrolidin-1-yl)methaniminium chloride (4.21e):

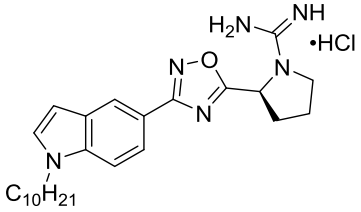

Using **4.20e** as starting material, **4.21e** was prepared using general procedure 4.4, isolated as a light yellow tinted solid (17 mg, 92%) and found to be 57% pure by HPLC. ^{1}H NMR (1:1 rotamer ratio, 500 MHz, CD_3OD) δ 8.29 (dd, *J* = 1.7, 0.6 Hz, 1H), 8.04* (d, *J* = 1.7 Hz, 1H), 7.84 (dd, *J* = 8.7, 1.6 Hz, 1H), 7.70* (s, 1H), 7.52 (dd, *J* = 8.7, 0.8 Hz, 1H), 7.43* (d, *J* = 8.9 Hz, 1H), 7.34–7.31 (m, 1H), 7.27* (s, 1H), 5.41 (ddd, *J* = 29.5, 8.0, 1.9 Hz, 1H), 4.21 (t, *J* = 7.2 Hz, 2H), 3.81–3.71 (m, 1H), 3.67–3.56 (m, 1H), 2.59–2.39 (m, 2H), 2.28–2.18 (m, 1H), 2.16–2.05 (m, 1H), 1.85 (t, *J* = 7.1 Hz, 2H), 1.32–1.19 (m, 14H), 0.87 (t, *J* = 7.0 Hz, 3H). ^{13}C NMR (126 MHz, CD_3OD) δ 178.3, 170.9, 170.8, 157.1, 139.2, 130.9, 130.1, 122.0, 121.2, 118.2, 111.2, 102.9, 56.5, 56.4, 47.3, 33.0, 32.72, 32.69, 31.4, 31.3, 30.6, 30.54, 30.50, 30.49, 30.38, 30.37, 30.3, 30.1, 27.9, 27.8, 24.4, 23.7, 14.44, 14.41. HRMS (ESI+): Calcd for $C_{25}H_{36}N_6O$ [M+H]: 437.6009, Found: 437.3018.

***N'*-hydroxy-1*H*-indole-6-carboximidamide (4.23):**

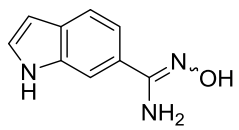

Using **4.22** as starting material, **4.23** was prepared using general procedure 4.1. Purification on a silica gel column with 70–100% EtOAc in hexanes produced **4.23** as a mixture of enantiomers (1.12 g, 91%), a tan solid. ^{1}H NMR (400 MHz, CD_3OD) δ 7.72 (dt, *J* = 1.7, 0.8 Hz, 1H), 7.61–7.54 (m, 1H), 7.34 (dd, *J* = 8.3, 1.6 Hz, 1H), 7.27 (d, *J* = 3.2 Hz, 1H), 6.46 (dd, *J* = 3.1, 1.0 Hz, 1H). ^{13}C NMR (101 MHz, CD_3OD) δ 157.2, 137.0, 130.7, 128.9, 127.6, 127.4, 126.6, 121.1, 120.9, 119.2, 118.4, 112.6, 110.5, 102.6, 102.4. HRMS (ESI+): Calcd for $C_9H_9N_3O$ [M+H]: 176.1592, Found: 176.0812.

***tert*-butyl (*S*)-2-(3-(1*H*-indol-6-yl)-1,2,4-oxadiazol-5-yl)pyrrolidine-1-carboxylate (4.24):**

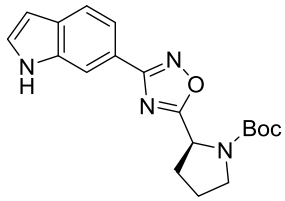

Using **4.23** and Boc-*L*-proline as starting material, **4.24** was prepared using general procedure 4.2. Purification on a silica gel column with 15–40% EtOAc in hexanes produced **4.24** (0.57 g, 28%), a tan solid. ^{1}H NMR (2:1 rotamer ratio, asterisk denote minor rotamer peak, 500 MHz, $CDCl_3$) δ 8.85 (s, 1H), 8.18 (s, 1H), 8.08* (s, 1H), 7.85 (dd, *J* = 8.2, 1.5 Hz, 1H), 7.81–7.77* (m, 1H), 7.72 (d, *J* = 8.3 Hz, 1H), 7.66* (d, *J* = 8.2 Hz, 1H), 7.34–7.31 (m, 1H), 7.31–7.28* (m, 1H), 6.59 (t, *J* = 2.5 Hz, 1H), 6.56* (s, 1H), 5.24* (dd, *J* = 8.4, 2.6 Hz, 1H), 5.09 (dd, *J* = 8.2, 3.8 Hz, 1H), 3.80–3.72 (m, 1H), 3.71–3.66* (d, *J* = 7.4 Hz, 1H), 3.63–3.55 (m, 1H), 3.54–3.47* (m, 1H), 2.48–2.31 (m, 1H), 2.22–2.10 (m, 2H), 2.07–1.93 (m, 1H), 1.48* (s, 3H), 1.31 (s, 6H). ^{13}C NMR (2:1 rotamer ratio, asterisk denote minor rotamer peak, 126 MHz, $CDCl_3$) δ 180.2, 169.3, 153.9, 135.6, 130.3, 126.7, 121.1, 120.1, 118.8, 111.0, 102.9, 80.7, 53.9, 46.8*, 46.4, 32.4, 31.5*, 28.4*, 28.2, 24.4*, 23.7. HRMS (ESI+): Calcd for $C_{19}H_{22}N_4O_3$ $[M+H]^+$: 377.3927, Found: 377.1600.

***tert*-butyl (*S*)-2-(3-(1-heptyl-1*H*-indol-6-yl)-1,2,4-oxadiazol-5-yl)pyrrolidine-1-carboxylate (4.25a):**

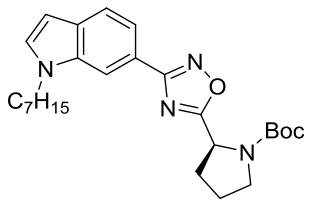

Using **4.24** as starting material, **4.25a** was prepared using general procedure 4.3. Purification on a silica gel column with 0–20% EtOAc in hexanes produced **4.25a** (55 mg, 86%), a yellow oil. ^{1}H NMR (2:1 rotamer ratio, asterisk denote minor rotamer peak, 400 MHz, $CDCl_3$) δ 8.09 (d, *J* = 1.3 Hz, 1H), 7.83 (dd, *J* = 8.2, 1.5 Hz, 1H), 7.69 (d, *J* = 8.4 Hz, 1H), 7.20 (t, *J* = 3.6 Hz, 1H), 6.53 (d, *J* = 3.2 Hz, 1H), 5.31–5.19* (m, 1H), 5.09 (dd, *J* = 8.2, 3.9 Hz, 1H), 4.18 (t, *J* = 7.0 Hz, 2H), 3.80–3.67 (m, 1H), 3.62–3.42 (m, 1H), 2.48–2.33 (m, 1H), 2.26–2.09 (m, 2H), 2.06–1.96 (m, 1H), 1.86 (p, *J* = 7.1 Hz, 2H), 1.47* (s, 3H), 1.37–1.20 (m, 14H), 0.86 (t, *J* = 7.0 Hz, 3H). ^{13}C NMR (2:1 rotamer ratio, asterisk denote minor rotamer peak, 101 MHz, $CDCl_3$) δ 180.3, 169.5, 153.8, 135.9, 131.0, 130.2, 130.0*, 121.4, 121.3*, 119.7, 118.6*, 118.5, 109.4*, 109.2, 101.5, 80.5, 54.0, 46.8*, 46.7, 46.5*, 32.5, 31.8, 31.7*, 30.5, 29.0, 28.5*, 28.3, 27.0, 24.5*, 23.8, 22.7, 14.2. HRMS (ESI+): Calcd for $C_{26}H_{36}N_4O_3$ $[M+Na]^+$: 475.5788, Found 475.2677.

***tert*-butyl (*S*)-2-(3-(1-octyl-1*H*-indol-6-yl)-1,2,4-oxadiazol-5-yl)pyrrolidine-1-carboxylate (4.25b):**

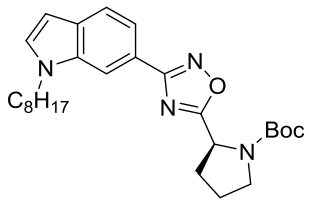

Using **4.24** as starting material, **4.25b** was prepared using general procedure 4.3. Purification on a silica gel column with 020% EtOAc in hexanes produced **4.25b** (51 mg, 97%), a yellow oil. ^{1}H NMR (2:1 rotamer ratio, asterisk denote minor rotamer peak, 400 MHz, $CDCl_3$) δ 8.09 (s, 1H), 7.83 (d, *J* = 8.1 Hz, 1H), 7.69 (d, *J* = 8.4 Hz, 1H), 7.21 (d, *J* = 3.2 Hz, 1H), 6.53 (d, *J* = 3.2 Hz, 1H), 5.28–5.18* (m, 1Hz), 5.09 (dd, *J* = 8.1, 3.9 Hz, 1H), 4.18 (t, *J* = 7.1 Hz, 2H), 3.81–3.69 (m, 1H), 3.64–

3.46 (m, 1H), 2.48–2.32 (m, 1H), 2.28–2.13 (m, 2H), 2.07–1.96 (m, 1H), 1.86 (p, J = 7.2 Hz, 2H), 1.47* (s, 3H), 1.37–1.19 (m, 15H), 0.86 (t, J = 7.1 Hz, 3H). ^{13}C NMR (2:1 rotamer ratio, asterisk denote minor rotamer peak, 101 MHz, $CDCl_3$) δ 180.3, 169.6, 153.8, 135.9, 131.0, 130.2, 130.0*, 121.4, 121.3*, 119.7, 118.6*, 118.5, 109.4*, 109.2, 101.5, 80.6, 54.0, 46.7, 46.5, 32.6, 31.9, 31.7*, 30.5, 29.33, 29.28, 28.5*, 28.3, 27.1, 24.5*, 23.9, 22.7, 14.2. HRMS (ESI+): Calcd for $C_{27}H_{38}N_4O_3$ $[M+Na]^+$: 489.6054, Found: 489.2836.

tert-butyl (_S_)-2-(3-(1-nontyl-1_H_-indol-6-yl)-1,2,4-oxadiazol-5-yl)pyrrolidine-1-carboxylate (4.25c):

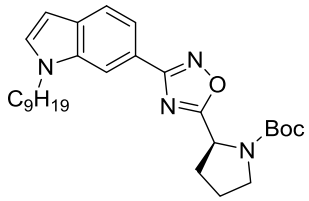

Using **4.24** as starting material, **4.25c** was prepared using general procedure 4.3. Purification on a silica gel column with 0–20% EtOAc in hexanes produced **4.25c** (62 mg, 65%), a yellow oil. ^{1}H NMR (2:1 rotamer ratio, asterisk denote minor rotamer peak, 400 MHz, $CDCl_3$) δ 8.09 (p, J = 0.9 Hz, 1H), 7.83 (d, J = 8.2 Hz, 1H), 7.69 (d, J = 8.4 Hz, 1H), 7.21 (d, J = 3.1 Hz, 1H), 6.53 (d, J = 3.1 Hz, 1H), 5.37–5.16* (m, 1H), 5.09 (dd, J = 8.2, 3.9 Hz, 1H), 4.18 (t, J = 7.0 Hz, 2H), 3.80–3.69 (m, 1H), 3.63–3.49 (m, 1H), 2.48–2.34 (m, 1H), 2.26–2.10 (m, 2H), 2.05–1.98 (m, 1H), 1.86 (p, J = 7.2 Hz, 2H), 1.47* (s, 3H), 1.36–1.19 (m, 17H), 0.86 (t, J = 7.1 Hz, 3H). ^{13}C NMR (2:1 rotamer ratio, asterisk denote minor rotamer peak, 101 MHz, $CDCl_3$) δ 180.3, 169.5, 153.8, 135.9, 131.0, 130.2, 130.0*, 121.4, 121.3*, 119.7, 118.6*, 118.5, 109.4*, 109.2, 101.5, 80.6, 54.0, 46.7*, 46.5, 32.6, 31.9, 31.7*, 30.5, 29.6, 29.4, 29.3, 28.5*, 28.3, 27.1, 24.5*, 23.9, 22.8, 14.2. HRMS (ESI+): Calcd for $C_{28}H_{40}N_4O_3$ $[M+Na]^+$: 503.6320, Found: 503.2975.

***tert*-butyl (*S*)-2-(3-(1-decyl-1*H*-indol-6-yl)-1,2,4-oxadiazol-5-yl)pyrrolidine-1-carboxylate (4.25d):**

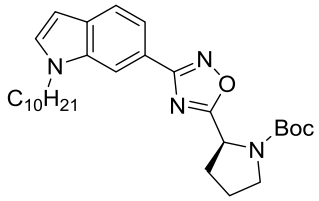

Using **4.24** as starting material, **4.25d** was prepared using general procedure 4.3. Purification on a silica gel column with 0–20% EtOAc in hexanes produced **4.25d** (92 mg, 94%), a yellow oil. ^{1}H NMR (2:1 rotamer ratio, asterisk denote minor rotamer peak, 400 MHz, $CDCl_3$) δ 8.09 (s, 1H), 7.83 (d, *J* = 8.1 Hz, 1H), 7.69 (d, *J* = 8.4 Hz, 1H), 7.21 (d, *J* = 3.1 Hz, 1H), 6.53 (d, *J* = 3.1 Hz, 1H), 5.23* (t, *J* = 4.3 Hz, 1H), 5.09 (dd, *J* = 8.2, 3.9 Hz, 1H), 4.18 (t, *J* = 7.1 Hz, 2H), 3.82–3.68 (m, 1H), 3.63–3.50 (m, 1H), 2.48–2.32 (m, 1H), 2.25–2.13 (m, 2H), 2.07–1.97 (m, 1H), 1.85 (p, *J* = 7.1 Hz, 2H), 1.47* (s, 3H), 1.37–1.19 (m, 19H), 0.87 (t, *J* = 7.1 Hz, 3H). ^{13}C NMR (2:1 rotamer ratio, asterisk denote minor rotamer peak, 101 MHz, $CDCl_3$) δ 180.3, 169.5, 153.8, 135.8, 131.0, 130.2, 130.1*, 121.4, 121.3*, 119.7, 118.6*, 118.5, 109.4*, 109.2, 101.5, 101.4* 80.5, 54.0, 46.8*, 46.7, 46.5*, 32.5, 32.0, 31.7*, 30.5, 29.61, 29.60, 29.55, 29.37, 29.36, 28.5*, 28.3, 27.1, 24.5*, 23.9, 22.8, 14.2. HRMS (ESI+): Calcd for $C_{29}H_{42}N_4O_3$ $[M+Na]^+$: 517.6585, Found: 517.3124.

***tert*-butyl (*S,Z*)-(((*tert*-butoxycarbonyl)imino)(2-(3-(1-heptyl-1*H*-indol-6-yl)-1,2,4-oxadiazol-5-yl)pyrrolidin-1-yl)methyl)carbamate (4.27a):**

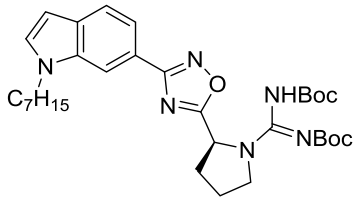

Compound **4.26a** was prepared from **4.25a** using general procedure 4.4 and carried on to the next reaction without purification. Using **4.26a** as starting material, **4.27a** was prepared using general procedure 4.5. Purification on a silica gel column with 10–40% EtOAc in hexanes produced **4.27a** (31 mg, 41%), a clear oil. ^{1}H NMR (500 MHz, $CDCl_3$) δ 8.08 (s, 1H), 7.81 (d, *J* = 8.2 Hz,

1H), 7.68 (d, *J* = 8.3 Hz, 1H), 7.21 (d, *J* = 3.0 Hz, 1H), 6.52 (d, *J* = 3.0 Hz, 1H), 5.62 (dd, *J* = 7.8, 4.8 Hz, 1H), 4.17 (t, *J* = 7.2 Hz, 2H), 3.96–3.88 (m, 1H), 3.85–3.78 (m, 1H), 2.52–2.42 (m, 1H), 2.34–2.16 (m, 2H), 2.09–2.00 (m, 1H), 1.86 (p, *J* = 7.3 Hz, 2H), 1.53–1.37 (m, 20H), 1.32 (p, *J* = 3.2 Hz, 4H) 1.29–1.21 (m, 6H), 0.85 (t, *J* = 7.0 Hz, 3H).^{13}C NMR (151 MHz, $CDCl_3$) δ 178.6, 169.6, 162.1, 153.7, 150.9, 135.9, 131.0, 130.2, 121.3, 119.7, 118.7, 109.3, 101.5, 82.0, 79.9, 55.5, 49.6, 46.7, 31.8, 30.5, 29.8, 29.1, 28.3, 28.1, 27.1, 27.0, 24.1, 22.7, 14.2. HRMS (ESI+): Calcd for $C_{32}H_{46}N_6O_5$ [M+H]: 595.7528, Found: 595.3616.

tert-butyl (_S,Z_)-(((_tert_-butoxycarbonyl)imino)(2-(3-(1-octyl-1_H_-indol-6-yl)-1,2,4-oxadiazol-5-yl)pyrrolidin-1-yl)methyl)carbamate (4.27b):

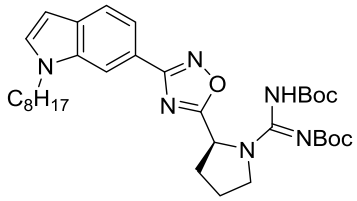

Compound **4.26b** was prepared from **4.25b** using general procedure 4.4 and carried on to the next reaction without purification. Using **4.26b** as starting material, **4.27b** was prepared using general procedure 4.5. Purification on a silica gel column with 10–40% EtOAc in hexanes produced **4.27b** (33 mg, 55%), a clear oil. ^{1}H NMR (500 MHz, $CDCl_3$) δ 8.08 (s, 1H), 7.81 (dd, *J* = 8.3, 1.4 Hz, 1H), 7.68 (d, *J* = 8.2 Hz, 1H), 7.20 (d, *J* = 3.1 Hz, 1H), 6.52 (d, *J* = 3.0 Hz, 1H), 5.62 (dd, *J* = 7.8, 4.7 Hz, 1H), 4.17 (t, *J* = 7.2 Hz, 2H), 3.95–3.89 (m, 1H), 3.86–3.77 (m, 1H), 2.51–2.41 (m, 1H), 2.34–2.12 (m, 2H), 2.09–1.99 (m, 1H), 1.85 (p, *J* = 7.0 Hz, 2H), 1.56–1.37 (m, 18H), 1.35–1.29 (m. 4H), 1.29–1.18 (m, 6H), 0.86 (t, *J* = 6.8 Hz, 3H). ^{13}C NMR (126 MHz, $CDCl_3$) δ 178.6, 169.6, 162.1, 153.7, 150.5, 135.9, 131.0, 130.2, 130.1, 121.3, 121.3, 119.6, 118.7, 109.3, 101.5, 82.3, 79.7, 49.6, 46.7, 31.9, 30.5, 29.33, 29.28, 28.3, 28.1, 27.1, 22.7, 14.2. HRMS (ESI+): Calcd for $C_{33}H_{48}N_6O_5$ [M+H]: 609.7794, Found: 609.3791.

***tert*-butyl (*S,Z*)-(((*tert*-butoxycarbonyl)imino)(2-(3-(1-nonyl-1*H*-indol-6-yl)-1,2,4-oxadiazol-5-yl)pyrrolidin-1-yl)methyl)carbamate (4.27c):**

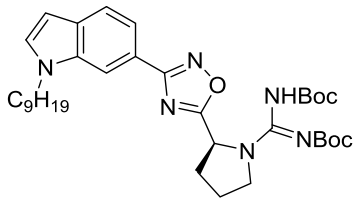

Compound **4.26c** was prepared from **4.25c** using general procedure 4.4 and carried on to the next reaction without purification. Using **4.26c** as starting material, **4.27c** was prepared using general procedure 4.5. Purification on a silica gel column with 10–40% EtOAc in hexanes produced **4.27c** (30 mg, 67%), a clear oil. ^{1}H NMR (500 MHz, $CDCl_3$) δ 8.08 (s, 1H), 7.81 (dd, *J* = 8.3, 1.4 Hz, 1H), 7.68 (d, *J* = 8.3 Hz, 1H), 7.21 (d, *J* = 3.1 Hz, 1H), 6.52 (d, *J* = 3.0 Hz, 1H), 5.62 (dd, *J* = 7.9, 4.7 Hz, 1H), 4.17 (t, *J* = 7.2 Hz, 2H), 3.96–3.89 (m, 1H), 3.87–3.76 (m, 1H), 2.52–2.42 (m, 1H), 2.32–2.15 (m, 2H), 2.08–2.01 (m, 1H), 1.85 (p, *J* = 7.1 Hz, 2H), 1.54–1.37 (m, 20H), 1.34–1.18 (m, 15H), 0.86 (t, *J* = 7.0 Hz, 3H). ^{13}C NMR (126 MHz, $CDCl_3$) δ 178.6, 169.6, 162.1, 153.7, 150.4, 135.9, 131.0, 130.8, 121.3, 119.7, 118.7, 109.3, 101.5, 82.2, 79.7, 55.5, 49.6, 46.7, 36.8, 31.9, 30.5, 29.6, 29.4, 29.3, 28.6, 27.1, 22.8, 14.2. HRMS (ESI+): Calcd for $C_{34}H_{50}N_6O_5$ [M+H]: 623.8059, Found: 623.3909.

***tert*-butyl (*S,Z*)-(((*tert*-butoxycarbonyl)imino)(2-(3-(1-decyl-1*H*-indol-6-yl)-1,2,4-oxadiazol-5-yl)pyrrolidin-1-yl)methyl)carbamate (4.27d):**

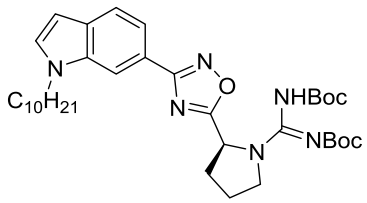

Compound **4.26d** was prepared from **4.25d** using general procedure 4.4 and carried on to the next reaction without purification. Using **4.26d** as starting material, **4.27d** was prepared using general procedure 4.5. Purification on a silica gel column with 10–40% EtOAc in hexanes produced **4.27d** (19 mg, 43%), a clear oil. ^{1}H NMR (500 MHz, $CDCl_3$) δ 8.08 (s, 1H), 7.81 (dd, *J* = 8.3, 1.4 Hz, 1H), 7.68 (d, *J* = 8.3 Hz, 1H), 7.21 (d, *J* = 3.1 Hz, 1H), 6.52 (d, *J* = 3.1 Hz, 1H),

5.63 (dd, *J* = 7.9, 4.7 Hz, 1H), 4.17 (t, *J* = 7.2 Hz, 2H), 3.96–3.88 (m, 1H), 3.86–3.78 (m, 1H), 2.51–2.42 (m, 1H), 2.32–2.16 (m, 2H), 2.09–1.99 (m, 1H), 1.85 (p, *J* = 7.2 Hz, 2H), 1.46 (s, 19H), 1.34–1.20 (m, 18H), 0.87 (t, *J* = 6.9 Hz, 3H).^{13}C NMR (126 MHz, $CDCl_3$) δ 178.6, 169.6, 162.2, 153.8, 150.5, 135.9, 131.1, 130.2, 121.3, 119.7, 118.7, 109.3, 101.5, 82.1, 80.0, 55.5, 49.6, 46.7, 36.8, 32.0, 30.5, 29.9, 29.7, 29.4, 28.6, 28.3, 28.1, 27.2, 24.8, 24.1, 22.8, 14.2. HRMS (ESI+): Calcd for $C_{35}H_{52}N_6O_5$ [M+Na]: 659.8143, Found: 659.3884.

(*S*)-amino(2-(3-(1-heptyl-1*H*-indol-6-yl)-1,2,4-oxadiazol-5-yl)pyrrolidin-1-yl)methaniminium chloride (4.28a):

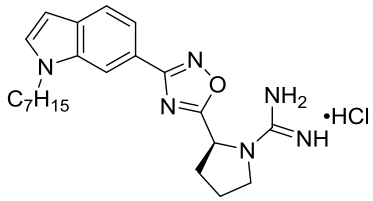

Using **4.27a** as starting material, **4.28a** was prepared using general procedure 4.4, isolated as a light yellow tinted solid (6 mg, 83%) and found to be 72% pure by HPLC. ^{1}H NMR (500 MHz, CD_3OD) δ 8.12 (dd, *J* = 21.5, 1.2 Hz, 1H), 7.73 (dd, *J* = 8.3, 1.4 Hz, 1H), 7.66 (d, *J* = 8.2 Hz, 1H), 7.39 (t, *J* = 1.5 Hz, 1H), 6.54–6.49 (m, 1H), 5.45 (dd, *J* = 7.9, 2.0 Hz, 1H), 4.25 (t, *J* = 7.1 Hz, 2H), 3.81 (td, *J* = 9.1, 2.6 Hz, 1H), 3.66–3.60 (m, 1H), 2.63–2.55 (m, 1H), 2.54–2.47 (m, 1H), 2.30–2.29 (m, 1H), 2.17–2.06 (m, 1H), 1.90–1.82 (m, 2H), 1.42–1.18 (m, 14H), 0.87 (t, *J* = 6.8 Hz, 3H). ^{13}C NMR (126 MHz, CD_3OD) δ 177.1, 169.5, 155.7, 135.7, 131.3, 130.5, 120.8, 118.6, 117.6, 108.7, 100.9, 55.1, 45.8, 31.5, 31.42, 31.39, 30.03, 29.99, 28.62, 28.57, 28.53, 26.46, 26.4, 22.3, 22.20, 22.16, 13.03, 12.98, 12.9. HRMS (ESI+): Calcd for $C_{22}H_{30}N_6O$ [M+H]: 395.5211, Found: 395.2573.

(*S*)-amino(2-(3-(1-octyl-1*H*-indol-6-yl)-1,2,4-oxadiazol-5-yl)pyrrolidin-1-yl)methaniminium chloride (4.28b):

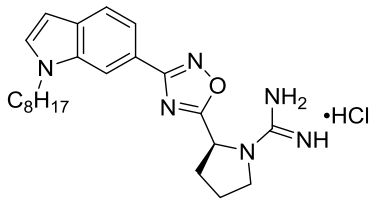

Using **4.27b** as starting material, **4.28b** was prepared using general procedure 4.4 and isolated as a light yellow tinted solid (6 mg, 82%) . ^{1}H NMR (500MHz, CD_3OD) δ 8.15 (dd, *J* = 1.3, 0.7 Hz, 1H), 7.75 (dd, *J* = 8.3, 1.4 Hz, 1H), 7.68 (dd, *J* = 7.1, 0.7 Hz, 1H), 7.44–7.38 (m, 1H), 6.54 (dd, *J* = 3.1, 0.9 Hz, 1H), 5.50–5.46 (m, 1H), 4.27 (t, *J* = 7.0, 2H), 3.82 (td, *J* = 8.2, 7.2, 5.3 Hz, 1H), 3.67–3.62 (m, 1H), 2.65–2.58 (m, 1H), 2.56–2.51 (m, 1H), 2.33–2.27 (m, 1H), 2.17–2.08 (m, 1H), 1.92–1.83 (m, 2H), 1.38–1.20 (m, 16H), 0.89 (t, *J* = 6.8 Hz, 3H).^{13}C NMR (126 MHz, CD_3OD) δ 178.5, 170.9, 157.1, 137.2, 132.0, 128.8, 122.3, 120.0, 119.9, 119.6, 119.1, 110.7, 110.1, 102.4, 56.5, 47.3, 32.9, 32.8, 31.43, 31.38, 30.29, 30.26, 30.2, 28.0, 27.8, 24.4, 23.6, 14.4. HRMS (ESI+): Calcd for $C_{23}H_{32}N_6O$ [M+H]: 409.5477, Found: 409.2732.

(*S*)-amino(2-(3-(1-nonyl-1*H*-indol-6-yl)-1,2,4-oxadiazol-5-yl)pyrrolidin-1-yl)methaniminium chloride (4.28c):

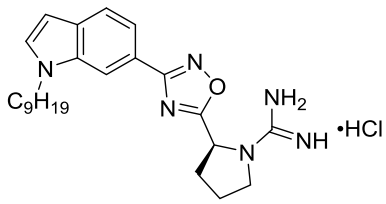

Using **4.27c** as starting material, **4.28c** was prepared using general procedure 4.4, isolated as a light yellow tinted solid (7 mg, 95%) and found to be 40% pure by HPLC. ^{1}H NMR (500 MHz, CD_3OD) δ 8.11–8.08 (m, 1H), 7.73 (dd, *J* = 8.3, 1.4 Hz, 1H), 7.66 (d, *J* = 8.3 Hz, 1H), 7.38 (d, *J* = 3.1 Hz, 1H), 6.52 (d, *J* = 3.0 Hz, 1H), 5.46 (dd, *J* = 7.8, 1.9 Hz, 1H), 4.24 (t, *J* = 6.9 Hz, 2H), 3.81 (td, *J* = 9.1, 2.5 Hz, 1H), 3.66–3.62 (m, 1H), 2.59–2.55 (m, 1H), 2.53–2.47 (m, 1H), 2.28–2.22 (m, 1H), 2.16–2.09 (m, 1H), 1.86 (p, *J* = 7.2 Hz, 2H), 1.33–1.19 (m, 16H), 0.86 (t, *J* = 7.0 Hz, 3H). ^{13}C NMR (126 MHz, CD_3OD) δ 178.5, 170.9, 157.1, 137.1, 132.8, 132.7,

132.1, 132.0, 122.3, 122.2, 120.0, 119.1, 110.1, 102.4, 56.5, 47.3, 32.99, 32.95, 32.8, 31.4, 30.58, 30.55, 30.28, 30.26, 28.1, 27.9, 24.4, 23.69, 23.67, 14.5, 14.4. HRMS (ESI+): Calcd for $C_{24}H_{34}N_6O$ [M+H]: 423.5743, Found: 423.2868.

(*S*)-amino(2-(3-(1-decyl-1*H*-indol-6-yl)-1,2,4-oxadiazol-5-yl)pyrrolidin-1-yl)methaniminium chloride (4.28d):

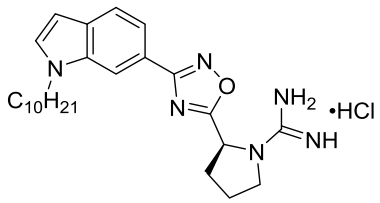

Using **4.28d** as starting material, **4.28d** was prepared using general procedure 4.4, isolated as a light yellow tinted solid (7 mg, 94%) and found to be 22% pure by HPLC. ^{1}H NMR (500 MHz, CD_3OD) δ 8.11 (d, *J* = 1.2 Hz, 1H), 7.73 (dd, *J* = 8.3, 1.4 Hz, 1H), 7.66 (d, *J* = 8.2 Hz, 1H), 7.39 (d, *J* = 3.1 Hz, 1H), 6.52 (dd, *J* = 3.1, 0.9 Hz, 1H), 5.46 (dd, *J* = 7.9, 2.0 Hz, 1H), 4.25 (t, *J* = 7.0 Hz, 2H), 3.84–3.77 (m, 1H), 3.67–3.60 (m, 1H), 2.62–2.54 (m, 1H), 2.53–2.48 (m, 1H), 2.28–2.21 (m, 1H), 2.17–2.08 (m, 1H), 1.85 (p, *J* = 7.0 Hz, 2H), 1.34–1.17 (m, 18H), 0.88 (t, *J* = 6.8 Hz, 3H). ^{13}C NMR (126 MHz, CD_3OD) δ 178.5, 170.9, 157.14, 137.2, 132.8, 132.1, 122.3, 120.0, 119.1, 110.1, 102.4, 56.5, 47.3, 33.0, 32.8, 31.4, 30.6, 30.5, 30.4, 30.3, 27.9, 24.4, 23.7, 14.4. HRMS (ESI+): Calcd for $C_{25}H_{36}N_6O$ [M+H]: 437.6009, Found: 437.3017.

1-Nonyl-1*H*-indole-3-carbonitrile (4.29):

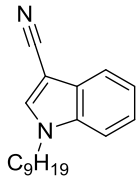

Using **4.1** and 1-bromononane as starting materials, **4.29** was synthesized using general procedure 4.3. Purification on a silica gel column with 0–10% EtOAc in hexanes produced **4.29** (360 mg, 95%), a light yellow oil. ^{1}H NMR (400 MHz, $CDCl_3$) δ 7.76–7.68 (m, 1H), 7.53 (s, 1H), 7.40–7.37 (m, 1H), 7.31 (ddd, *J* = 8.3, 7.0, 1.3 Hz, 1H), 7.25 (ddd, *J* = 8.1, 7.0, 1.1 Hz, 1H), 4.08 (t, *J* = 7.2 Hz, 2H), 1.80 (p, *J* = 7.2 Hz, 2H), 1.37–1.15 (m, 12H), 0.89 (t, *J* = 6.9 Hz, 3H). ^{13}C NMR (101 MHz, $CDCl_3$) δ 135.1, 134.2, 127.7,

123.4, 121.7, 119.4, 115.9, 110.5, 85.0, 47.0, 31.6, 29.6, 29.2, 29.0, 28.9, 26.5, 22.5, 13.9. HRMS (ESI+): Calcd for $C_{18}H_{24}N_2$ [M+H]: 269.4045, Found: 269.2025.

_N'_-hydroxy-1-nonyl-1_H_-indole-3-carboximidamide (4.30):

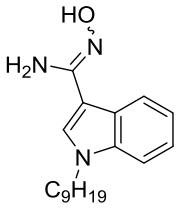

Using **4.29** as starting materials, **4.30** was synthesized using general procedure 4.2. Purification on a silica gel column with 20–40% EtOAc in hexanes produced **4.29** (240 mg, 97%), a white solid. ^{1}H NMR (400 MHz, $CDCl_3$) δ 8.05–8.01 (m, 1H), 7.43 (s, 1H), 7.36–7.31 (m, 1H), 7.25 (ddd, *J* = 8.2, 6.9, 1.3 Hz, 1H), 7.19 (ddd, *J* = 8.0, 6.9, 1.2 Hz, 1H), 4.95 (s, 2H), 4.07 (t, *J* = 7.2 Hz, 2H), 1.86–1.78 (m, 2H), 1.32–1.21 (m, 16H), 0.88 (t, *J* = 6.9 Hz, 3H). ^{13}C NMR (101 MHz, $CDCl_3$) δ 150.1, 136.6, 127.2, 125.6, 122.3, 121.2, 120.6, 109.8, 107.8, 46.7, 34.2, 31.9, 30.2, 29.5, 29.3, 27.0, 22.7, 14.2.HRMS (ESI+): Calcd for $C_{18}H_{27}N_3O$ [M+H]: 302.4344, Found: 302.2235.

***tert*-butyl (*S*)-2-((3-(1-nonyl-1*H*-indol-3-yl)-1,2,4-oxadiazol-5-yl)methyl)pyrrolidine-1-carboxylate (4.31):**

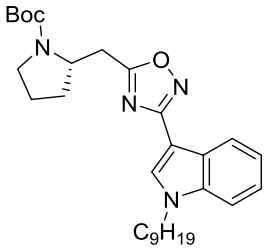

Using **4.30** and homo-Boc-*L*-Proline as starting materials, **4.31** was synthesized using general procedure 4.2. Purification on a silica gel column with 0–20% EtOAc in hexanes produced **4.31** (65 mg, 40%), a clear oil. ^{1}H NMR (400 MHz, $CDCl_3$) δ 8.24 (dd, *J* = 6.8, 1.9 Hz, 1H), 7.82 (s, 1H), 7.41–7.35 (m, 1H), 7.33–7.24 (m, 2H), 4.38–4.26 (m, 1H), 4.15 (t, *J* = 7.1 Hz, 2H), 3.50–3.40 (m, 1H), 3.39–3.31 (m, 1H), 3.16–3.08 (m, 1H), 3.04–2.96 (m, 1H), 2.12–2.03 (m, 2H), 1.87 (p, *J* = 7.0 Hz, 5H), 1.48 (s, 8H), 1.36–1.18 (m, 12H), 0.87 (t, *J* = 7.1 Hz, 3H). ^{13}C NMR (101 MHz, $CDCl_3$) δ 175.8, 165.2, 154.3, 136.9, 130.4, 125.6, 122.8, 122.1, 121.3, 110.0,

103.0, 80.1, 79.6, 55.3, 47.0, 46.4, 34.2, 31.9, 31.1, 30.8, 30.1, 29.6, 29.5, 29.3, 28.6, 27.0, 23.7, 22.9, 22.7, 14.19.HRMS (ESI+): Calcd for $C_{29}H_{42}N_4O_3$ [M+H]: 495.6767, Found: 495.3340.

tert-butyl _(S,Z)_-(((_tert_-butoxycarbonyl)amino)(2-((3-(1-nonyl-1_H_-indol-3-yl)-1,2,4-oxadiazol-5-yl)methyl)pyrrolidin-1-yl)methylene)carbamate (4.33):

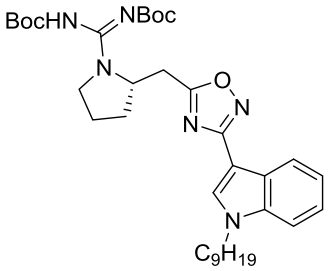

Compound **4.32** was prepared from **4.31** using general procedure 4.4 and carried on to the next reaction without purification. Using **4.32** as starting material, **4.33** was synthesized using general procedure 4.5. Purification on a silica gel column with 0–10% EtOAc in hexanes produced **4.33** (30 mg, 64%), a clear oil. ^{1}H NMR (400 MHz, $CDCl_3$) δ 8.26–8.22 (m, 1H), 7.86 (s, 1H), 7.40–7.37 (m, 1H), 7.32–7.24 (m, 2H), 4.83–4.75 (m, 1H), 4.16 (t, J = 7.2 Hz, 2H), 3.73–3.63 (m, 2H), 3.56–3.46 (m, 1H), 3.12 (dd, J = 15.1, 8.7 Hz, 1H), 2.29–2.22 (m, 1H), 1.94–1.79 (m, 5H), 1.48 (s, 18H), 1.37–1.19 (m, 14H), 0.87 (t, J = 7.1 Hz, 3H). ^{13}C NMR (101 MHz, $CDCl_3$) δ 175.7, 165.2, 162.6, 154.0, 150.5, 136.9, 130.6, 125.7, 122.8, 122.2, 122.1, 121.3, 110.0, 109.9, 103.0, 81.7, 79.6, 56.7, 47.0, 31.9, 30.6, 30.3, 30.2, 29.5, 29.3, 28.3, 27.1, 22.8, 14.2. HRMS (ESI+): Calcd for $C_{35}H_{52}N_6O_5$ [M+H]: 637.8325, Found: 637.4090.

(_S_)-amino(2-((3-(1-nonyl-1_H_-indol-3-yl)-1,2,4-oxadiazol-5-yl)methyl)pyrrolidin-1-yl)methaniminium chloride (4.34):

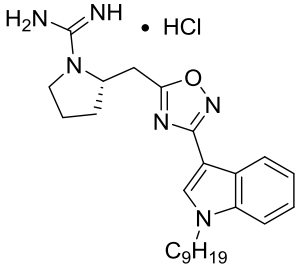

Using **4.33** as starting materials, **4.34** was synthesized using general procedure 4.4, isolated as a white solid (10 mg, 100%) and found to be > 99% pure by HPLC. ^{1}H NMR (400 MHz, CD_3OD) δ 8.10 (dd, J = 7.9, 1.1 Hz, 1H), 7.95 (s, 1H), 7.50 (d, J = 8.2 Hz, 1H), 7.29 (t, J = 7.0 Hz, 1H), 7.21 (t, J = 7.4 Hz, 1H), 4.55 (d, J = 6.3 Hz, 1H), 4.26 (t, J = 6.8 Hz, 2H), 3.58–3.53

(m, 1H), 3.50–3.41 (m, 1H), 2.33–2.24 (m, 1H), 2.18–2.10 (m, 1H), 2.08–2.01 (m, 2H), 1.87 (t, *J* = 6.7 Hz, 2H), 1.37–1.15 (m, 14H), 0.86 (t, *J* = 7.0 Hz, 3H). ^{13}C NMR (101 MHz, CD_3OD) δ 176.4, 166.5, 156.4, 138.4, 132.1, 126.6, 123.9, 122.5, 122.1, 111.4, 103.3, 57.3, 47.6, 33.0, 31.6, 31.2, 30.5, 30.3, 30.0, 27.8, 23.68, 23.67, 23.6, 14.4. HRMS (ESI+): Calcd for $C_{25}H_{36}N_6O$ [M+H]: 437.6009, Found: 437.3046.

7.1.13 Characterization for Chapter 5

***tert*-butyl (*S*)-2-(3-(1-(4-methylbenzyl)-1*H*-indol-5-yl)-1,2,4-oxadiazol-5-yl)pyrrolidine-1-carboxylate (5.1a):**

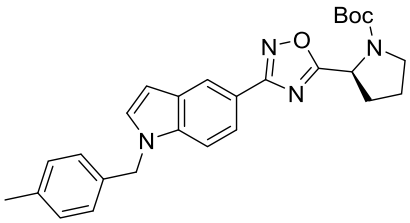

Compound **5.1a** was synthesized via general procedure 5.1 with 4-(methyl)benzyl bromide as starting material. Purification on a silica gel column with 0–20% EtOAc in hexanes produced **5.1a** (25 mg, 48%), a yellow oil. ^{1}H NMR (2:1 rotamer ratio, asterisk denote minor rotamer peak, 400 MHz, $CDCl_3$) δ 8.40 (d, *J* = 1.6 Hz, 1H), 7.89 (dd, *J* = 8.7, 1.6 Hz, 1H), 7.36 (d, *J* = 8.7 Hz, 1H), 7.19–7.14 (m, 1H), 7.11 (d, *J* = 7.9 Hz, 2H), 7.02 (d, *J* = 7.8 Hz, 2H), 6.63 (d, *J* = 3.1 Hz, 1H), 5.30 (s, 2H), 5.27–5.19* (m. 1H), 5.07 (dd, *J* = 8.2, 3.7 Hz, 1H), 3.78–3.65 (m, 1H), 3.62–3.48 (m, 1H), 2.49–2.36 (m, 1H), 2.32 (s, 3H), 2.24–2.12 (m, 2H), 2.06–1.94 (m, 1H), 1.47* (s, 3H), 1.31 (s, 6H). ^{13}C NMR (2:1 rotamer ratio, asterisk denote minor rotamer peak, 101 MHz, $CDCl_3$) δ 180.2, 169.4, 153.8, 137.9, 137.7, 134.06, 129.8, 129.6, 129. 6, 129.4, 129.3, 128.9, 127.2, 127.2, 126.94, 126.92, 121.3, 121.0, 118.2, 110.3, 110.1, 102.9, 80.5, 54.00, 50.2, 46.8*, 46.5, 32.5, 28.5*, 28.3, 24.5*, 23.8, 21.2. HRMS (ESI+): Calcd for $C_{27}H_{30}N_4O_3$ $[M+H]^+$: 459.5600, Found: 459.2397.

***tert*-butyl (*S*)-2-(3-(1-(4-(*tert*-butyl)benzyl)-1*H*-indol-5-yl)-1,2,4-oxadiazol-5-yl)pyrrolidine-1-carboxylate (5.1b):**

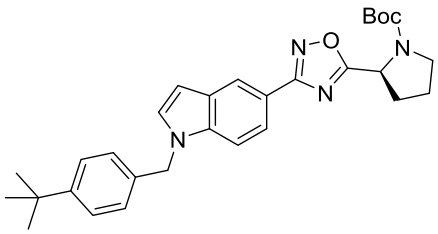

Compound **5.1b** was synthesized via general procedure 5.1 with 4-(*tert*-butyl)benzyl bromide as starting material. Purification on a silica gel column with 0–20% EtOAc in hexanes produced **5.1b** (28 mg, 50%), a yellow oil. ^{1}H NMR

(2:1 rotamer ratio, asterisk denote minor rotamer peak, 400 MHz, $CDCl_3$) δ 8.41 (d, *J* = 1.7 Hz, 1H), 7.91 (dd, *J* = 8.5, 1.7 Hz, 1H), 7.42–7.37 (m, 1H), 7.35–7.31 (m, 2H), 7.19 (d, *J* = 3.2 Hz, 1H), 7.06 (d, *J* = 8.0 Hz, 2H), 6.64 (d, *J* = 3.3 Hz, 1H), 5.32 (s, 2H), 5.23* (d, *J* = 8.2 Hz, 1H), 5.08 (dd, *J* = 8.1, 3.7 Hz, 1H), 3.79–3.70 (m, 1H), 3.61–3.49 (m, 1H), 2.47–2.34 (m, 1H), 2.23–2.10 (m, 2H), 2.06–1.96 (m, 1H), 1.48* (s, 3H), 1.33–1.26 (m, 16H). ^{13}C NMR (2:1 rotamer ratio, asterisk denote minor rotamer peak, 101 MHz, $CDCl_3$) δ 180.2, 169.4, 153.8, 150.9, 137.9, 134.1, 129.6, 129.4*, 128.8, 127.0, 126.9, 126.8, 126.7, 126.0*, 125.9, 125.6, 121.3, 121.1*, 121.0, 118.2, 110.3, 110.1, 102.9, 80.5, 80.3*, 54.0, 50.0, 46.7*, 46.5, 34.6, 32.5, 31.5*, 31.4, 28.6*, 28.3, 23.8. HRMS (ESI+): Calcd for $C_{30}H_{36}N_4O_3$ $[M+H]^+$: 501.6398, Found: 501.2835.

tert-butyl (*S*)-2-(3-(1-(4-chlorobenzyl)-1*H*-indol-5-yl)-1,2,4-oxadiazol-5-yl)pyrrolidine-1-carboxylate (5.1c):

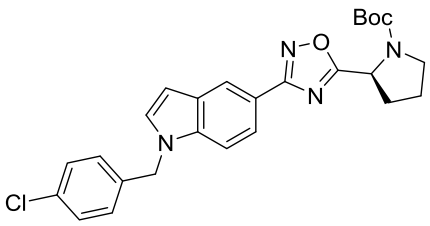

5.1c was synthesized via general procedure 5.1 with 4-(chloro)benzyl bromide as starting material. Purification on a silica gel column with 0–20% EtOAc in hexanes produced **5.1c** (20 mg, 46%), a yellow oil. ^1H NMR (2:1 rotamer ratio, asterisk denote minor rotamer peak, 400 MHz, Chloroform-d) δ 8.41 (d, *J* = 1.6 Hz, 1H), 7.90 (dd, *J* = 8.6, 1.7 Hz, 1H), 7.33–7.26 (m, 3H), 7.18–7.13 (m, 1H), 7.05–7.00 (m, 2H), 6.65 (d, *J* = 3.2 Hz, 1H), 5.32 (s, 2H), 5.22* (d, *J* = 8.1 Hz, 1H), 5.07 (dd, *J* = 8.2, 3.7 Hz, 1H), 3.78–3.67 (m, 1H), 3.62–3.52 (m, 1H), 2.45–2.35 (m, 1H), 2.22–2.12 (m, 2H), 2.04–1.95 (m, 1H), 1.47* (s, 3H), 1.30 (s, 6H). ^{13}C NMR (2:1 rotamer ratio, asterisk denote minor rotamer peak, 101 MHz, $CDCl_3$) δ δ 180.3, 169.4, 153.8, 137.8, 135.7, 133.8, 129.5, 129.2, 128.9, 128.2, 121.5, 121.4, 121.2, 118.5, 110.1, 103.3, 80.6, 54.0, 49.8, 46.8*, 46.5, 32.6, 28.6*, 28.3, 24.5*, 23.9. HRMS (ESI+): Calcd for $C_{26}H_{27}ClN_4O_3$ $[M+H]^+$: 479.9785, Found: 479.1821.

***tert*-butyl (*S*)-2-(3-(1-(3-chlorobenzyl)-1*H*-indol-5-yl)-1,2,4-oxadiazol-5-yl)pyrrolidine-1-carboxylate (5.1d):**

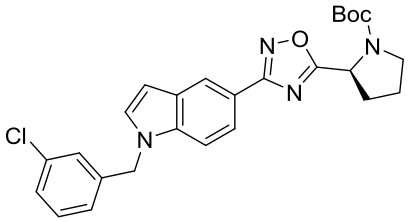

5.1d was synthesized via general procedure 5.1 with 3-(chloro)benzyl bromide as starting material. Purification on a silica gel column with 0–20% EtOAc in hexanes produced **5.1d** (23 mg, 43%), a yellow oil. ^{1}H NMR (2:1 rotamer ratio, asterisk denote minor rotamer peak, 400 MHz, $CDCl_3$) δ 8.42 (d, *J* = 1.6 Hz, 1H), 7.91 (dd, *J* = 8.6, 1.6 Hz, 1H), 7.32 (d, *J* = 8.7 Hz, 1H), 7.24–7.21 (m, 2H), 7.17 (d, *J* = 3.2 Hz, 1H), 7.10 (t, *J* = 1.9 Hz, 1H), 6.96 (d, *J* = 7.1 Hz, 1H), 6.66 (d, *J* = 3.2 Hz, 1H), 5.31 (s, 2H), 5.24–5.19* (m, 1H), 5.07 (dd, *J* = 8.2, 3.7 Hz, 1H), 3.78–3.68 (m, 1H), 3.61–3.52 (m, 1H), 2.44–2.34 (m, 1H), 2.21–2.12 (m, 2H), 2.03–1.96 (m, 1H), 1.47* (s, 3H), 1.30 (s, 6H). ^{13}C NMR (2:1 rotamer ratio, asterisk denote minor rotamer peak, 101 MHz, $CDCl_3$) δ 180.3, 179.8*, 169.3, 154.4*, 153.7, 139.2, 137.7, 134.9, 130.3, 129.5, 129.3, 128.9, 128.1, 126.9, 125.0, 124.9, 121.5, 121.41, 121.2, 118.7*, 118.5, 110.0, 110.0*, 103.4, 80.5, 80.4*, 54.0, 49.8, 46.7*, 46.5, 32.5, 31.6*, 28.5, 28.3, 24.4*, 23.8. HRMS (ESI+): Calcd for $C_{26}H_{27}ClN_4O_3$ $[M+H]^+$: 479.9785, Found: 479.1826.

***tert*-butyl (*S*)-2-(3-(1-(4-bromobenzyl)-1*H*-indol-5-yl)-1,2,4-oxadiazol-5-yl)pyrrolidine-1-carboxylate (5.1e):**

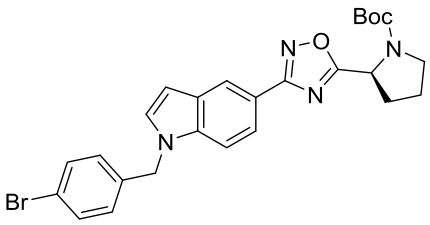

Compound **5.1e** was synthesized via general procedure 5.1 with 4-(bromo)benzyl bromide as starting material. Purification on a silica gel column with 0–20% EtOAc in hexanes produced **5.1e** (22 mg, 34%), a yellow oil. ^{1}H NMR (2:1 rotamer ratio, asterisk denote minor rotamer peak,400 MHz, $CDCl_3$) δ 8.41 (d, *J* = 1.6 Hz,

1H), 7.90 (dd, *J* = 8.6, 1.7 Hz, 1H), 7.46* (d, *J* = 8.4 Hz, 1H), 7.42 (d, *J* = 8.4 Hz, 2H), 7.30 (d, *J* = 8.7 Hz, 1H), 7.23* (d, *J* = 8.3 Hz, 1H), 7.18–7.12 (m, 1H), 6.99–6.94 (m, 2H), 6.65 (d, *J* = 3.2 Hz, 1H), 5.29 (s, 2H), 5.22* (d, *J* = 8.2 Hz, 1H), 5.07 (dd, *J* = 8.2, 3.7 Hz, 1H), 3.78–3.67 (m, 1H), 3.62–3.51 (m, 1H), 2.44–2.34 (m, 1H), 2.21–2.12 (m, 2H), 2.06–1.95 (m, 1H), 1.47* (s, 3H), 1.30 (s, 6H). ^{13}C NMR (2:1 rotamer ratio, asterisk denote minor rotamer peak,101 MHz, $CDCl_3$) δ 180.3, 179.8*, 169.3, 154.4*, 153.7, 137.7, 136.2, 132.1, 131.7*, 129.5, 129.3*, 128.9, 128.67*, 128.5, 121.8, 121.4, 121.2, 118. 7*, 118.5, 110.1, 110.0*, 103.3, 80.5, 54.0, 49.8, 46.7*, 46.5, 32.5, 31.7*, 28.5*, 28.3, 24.5*, 23.8. HRMS (ESI+): Calcd for $C_{26}H_{27}BrN_4O_3$ $[M+H]^+$: 524.4295, Found: 525.1308.

tert-butyl (_S_)-2-(3-(1-(3-bromobenzyl)-1_H_-indol-5-yl)-1,2,4-oxadiazol-5-yl)pyrrolidine-1-carboxylate (5.1f):

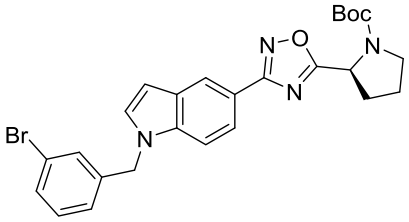

Compound **5.1f** was synthesized via general procedure 5.1 with 3-(bromo)benzyl bromide as starting material. Purification on a silica gel column with 0–20% EtOAc in hexanes produced **5.1f** (22 mg, 37%), a yellow oil. ^{1}H NMR (2:1 rotamer ratio, asterisk denote minor rotamer peak,400 MHz, $CDCl_3$) δ 8.41 (d, *J* = 1.6 Hz, 1H), 7.94–7.87 (m, 1H), 7.43–7.37 (m, 1H), 7.32 (d, *J* = 8.7 Hz, 1H), 7.28 (t, *J* = 1.9 Hz, 1H), 7.18–7.13 (m, 2H), 6.99 (d, *J* = 7.8 Hz, 1H), 6.66 (d, *J* = 3.3 Hz, 1H), 5.31 (s, 2H), 5.22* (d, *J* = 8.0 Hz, 1H), 5.07 (dd, *J* = 8.4, 3.5 Hz, 1H), 3.79–3.68 (m, 1H), 3.63–3.51 (m, 1H), 2.44–2.35 (m, 1H), 2.21–2.10 (m, 2H), 2.04–1.95 (m, 1H), 1.47* (s, 3H), 1.30 (s, 6H). ^{13}C NMR (2:1 rotamer ratio, asterisk denote minor rotamer peak,101 MHz, $CDCl_3$) δ 180.3, 179.8*, 169.3, 154.4*, 153.7, 139.5, 137.7, 131.1, 130.6, 129.8, 129.5, 129.3, 128.9, 125.4, 123.1, 121.4, 121.3, 118.5, 110.1, 110.0,

103.4, 80.5, 80.4*, 54.0, 49.7*, 46.7, 46.5, 32.5, 31.6*, 29.8*, 28.5*, 28.3, 24.5*, 23.8. HRMS (ESI+): Calcd for $C_{26}H_{27}BrN_4O_3$ $[M+H]^+$: 524.4295, Found: 525.1304.

***tert*-butyl (*S*)-2-(3-(1-(4-(trifluoromethyl)benzyl)-1*H*-indol-5-yl)-1,2,4-oxadiazol-5-yl)pyrrolidine-1-carboxylate (5.1g):**

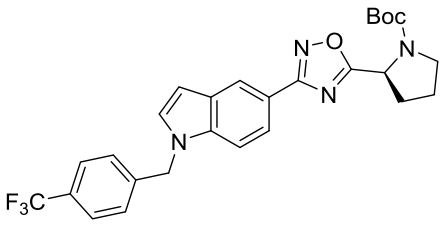

5.1g was synthesized via general procedure 5.1 with 4-(trifluoromethyl)benzyl bromide as starting material. Purification on a silica gel column with 0–20% EtOAc in hexanes produced **5.1g** (37 mg, 64%), a yellow oil. ^{1}H NMR (2:1 rotamer ratio, asterisk denote minor rotamer peak, 400 MHz, $CDCl_3$) δ 8.43 (d, *J* = 1.6 Hz, 1H), 7.92–7.86 (m, 1H), 7.56 (d, *J* = 8.1 Hz, 2H), 7.30 (d, *J* = 8.7 Hz, 1H), 7.22–7.16 (m, 3H), 6.68 (d, *J* = 3.2 Hz, 1H), 5.41 (s, 2H), 5.28–5.19* (m, 1H), 5.07 (dd, *J* = 8.1, 3.7 Hz, 1H), 3.78–3.64 (m, 1H), 3.60–3.51 (m, 1H), 2.47–2.38 (m, 1H), 2.22–2.08 (m, 2H), 2.03–1.94 (m, 1H), 1.47* (s, 3H), 1.30 (s, 6H). ^{19}F NMR (376 MHz, $CDCl_3$) δ –62.63. ^{13}C NMR (2:1 rotamer ratio, asterisk denote minor rotamer peak, 101 MHz, $CDCl_3$) δ 180.3, 169.3, 153.8, 141.2, 137.8, 129.5, 128.9, 127.1, 127.0, 126.9, 126.03, 126.00, 125.96, 125.92, 125.4, 122.7, 121.5, 121.4, 118.6, 110.1, 109.9*, 103.5, 80.5, 80.4*, 54.0, 49.9, 46.8*, 46.5, 32.5, 31.7*, 28.5*, 28.3, 24.5*, 23.8. HRMS (ESI+): Calcd for $C_{27}H_{27}F_3N_4O_3$ $[M+H]^+$: 513.5314, Found: 513.1446.

***tert*-butyl (*S*)-2-(3-(1-(3-(trifluoromethyl)benzyl)-1*H*-indol-5-yl)-1,2,4-oxadiazol-5-yl)pyrrolidine-1-carboxylate (5.1h):**

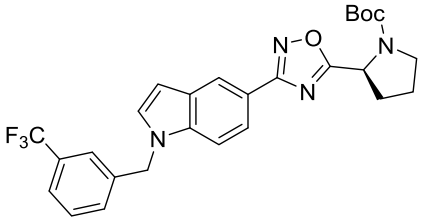

Compound **5.1h** was synthesized via general procedure 5.1 with 3-(trifluoromethyl)benzyl bromide as starting material. Purification on a silica gel column with 0–20% EtOAc in hexanes produced **5.1h** (34 mg, 58%), a yellow oil. ^{1}H NMR (2:1 rotamer ratio, asterisk denote minor rotamer peak, 400 MHz, $CDCl_3$) δ 8.42 (d, *J* = 1.6 Hz, 1H), 7.91 (dd, *J* = 8.6, 1.6 Hz, 1H), 7.54 (d, *J* = 7.9 Hz, 1H), 7.44 (s, 1H), 7.41 (t, *J* = 7.8 Hz, 1H), 7.32 (d, *J* = 8.8 Hz, 1H), 7.23–7.14 (m, 2H), 6.68 (d, *J* = 3.3 Hz, 1H), 5.40 (s, 2H), 5.22* (d, *J* = 8.1 Hz, 1H), 5.07 (dd, *J* = 8.1, 3.7 Hz, 1H), 3.76–3.67 (m, 1H), 3.60–3.49 (m, 1H), 2.46–2.32 (m, 1H), 2.25–2.12 (m, 2H), 2.05–1.95 (m, 1H), 1.47* (s, 3H), 1.30 (s, 6H). ^{19}F NMR (376 MHz, $CDCl_3$) δ –62.70. ^{13}C NMR (2:1 rotamer ratio, asterisk denote minor rotamer peak, 101 MHz, $CDCl_3$) δ 180.3, 179.9*, 169.3, 154.4*, 153.8, 138.3, 137.8, 131.5, 131.2, 130.1, 129.6, 129.4, 129.3, 128.9, 125.3, 124.9, 123.6, 123.6, 122.6, 121.5, 121.4, 118.6, 110.0, 103.6, 80.5, 54.0, 49.9, 46.6*, 46.5, 32.6, 31.7,* 29.8*, 28.5*, 28.3, 24.5*, 23.8. HRMS (ESI+): Calcd for $C_{27}H_{27}F_3N_4O_3$ $[M+H]^+$: 513.5314, Found: 513.1391.

***tert*-butyl (*S*)-2-(3-(1-(2-(trifluoromethyl)benzyl)-1*H*-indol-5-yl)-1,2,4-oxadiazol-5-yl)pyrrolidine-1-carboxylate (5.1i):**

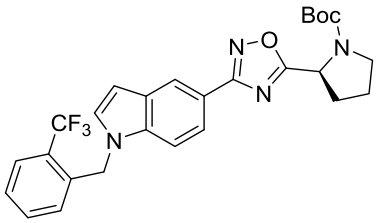

Compound **5.1i** was synthesized via general procedure 5.1 with 2-(trifluoromethyl)benzyl bromide as starting material. Purification on a silica gel column with 0–20% EtOAc in hexanes produced **5.1i** (28 mg, 48%), a yellow oil. ^{1}H NMR (2:1

rotamer ratio, asterisk denote minor rotamer peak, 400 MHz, $CDCl_3$) δ 8.44 (d, *J* = 1.6 Hz, 1H), 7.89 (dd, *J* = 8.6, 1.6 Hz, 1H), 7.76–7.68 (m, 1H), 7.40–7.29 (m, 2H), 7.27–7.22 (m, 1H), 7.20–7.16 (m, 1H), 6.72–6.66 (m, 1H), 6.59–6.53 (m, 1H), 5.58 (s, 2H), 5.25–5.17* (m, 1H), 5.08 (dd, *J* = 8.1, 3.6 Hz, 1H), 3.80–3.65 (m, 1H), 3.59–3.44 (m, 1H), 2.46–2.30 (m, 1H), 2.22–2.10 (m, 2H), 2.04–1.91 (m, 1H), 1.47* (s, 3H), 1.31 (s, 6H). ^{19}F NMR (376 MHz, $CDCl_3$) δ –60.35. ^{13}C NMR (2:1 rotamer ratio, asterisk denote minor rotamer peak, 101 MHz, $CDCl_3$) δ 180.3, 179.9*, 169.3, 154.4*, 153.8, 137.9, 136.0, 132.6, 129.9, 129.8*, 128.9, 128.6, 127.8, 127.4, 127.1, 126.8, 126.2, 126.2, 125.9, 123.2, 121.5, 121.4, 120.5, 118.9*, 118.7, 110.1, 110.0*, 103.6, 80.5, 80.4*, 54.0, 46.70, 46.66*, 46.5, 32.5, 31.7*, 28.5*, 28.3, 24.5*, 23.8. HRMS (ESI+): Calcd for $C_{27}H_{27}F_3N_4O_3$ $[M+H]^+$: 513.5314, Found: 513.2107.

***tert*-butyl (*S*)-2-(3-(1-([1,1'-biphenyl]-4-ylmethyl)-1*H*-indol-5-yl)-1,2,4-oxadiazol-5-yl)pyrrolidine-1-carboxylate (5.1j):**

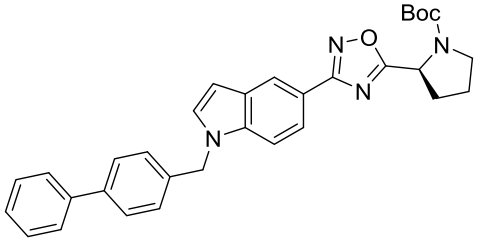

Compound **5.1j** was synthesized via general procedure 5.1 with 4-(bromomethyl)-1,1'-biphenyl as starting material. Purification on a silica gel column with 0–20% EtOAc in hexanes produced **5.1i** (32 mg, 55%), a yellow oil. ^1H NMR (2:1 rotamer ratio, asterisk denote minor rotamer peak, 400 MHz, $CDCl_3$) δ 8.44 (d, *J* = 1.7 Hz, 1H), 7.93 (dd, *J* = 8.7, 1.6 Hz, 1H), 7.57–7.50 (m, 4H), 7.45–7.38 (m, 3H), 7.37–7.31 (m, 1H), 7.24–7.16 (m, 3H), 6.68 (d, *J* = 3.2 Hz, 1H), 5.39 (s, 2H), 5.25–5.20* (m, 1H), 5.08 (dd, *J* = 8.1, 3.7 Hz, 1H), 3.82–3.70 (m, 1H), 3.60–3.45 (m, 1H), 2.46–2.32 (m, 1H), 2.23–2.18 (m, 2H), 2.05–1.95 (m, 1H), 1.48* (s, 3H), 1.32 (s, 6H). ^{13}C NMR (2:1 rotamer ratio, asterisk denote minor rotamer peak, 101 MHz, $CDCl_3$) δ 180.2, 169.4, 153.7, 140.9, 140.6, 137.9, 136.1, 129.6, 129.4, 128.9, 127.8, 127.7, 127.5, 127.3, 127.1, 121.4, 121.2*, 121.1, 118.3, 110.3, 103.1, 80.5,

80.3*, 54.0, 53.6*, 50.1, 46.7*, 46.5, 32.5, 31.6*, 28.5*, 28.3, 24.4*, 23.8. HRMS (ESI+): Calcd for $C_{32}H_{32}N_4O_3$ $[M+H]^+$: 521.6294, Found: 521.2546.

***tert*-butyl (*S*)-2-(3-(1-([1,1'-biphenyl]-3-ylmethyl)-1*H*-indol-5-yl)-1,2,4-oxadiazol-5-yl)pyrrolidine-1-carboxylate (5.1k):**

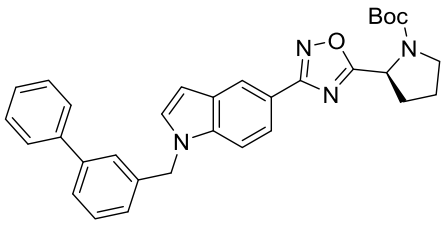

Compound **5.1k** was synthesized via general procedure 5.1 with 3-(bromomethyl)-1,1'-biphenyl as starting material. Purification on a silica gel column with 0–20% EtOAc in hexanes produced **5.1k** (31 mg, 53%), a yellow oil. ^{1}H NMR (2:1 rotamer ratio, asterisk denote minor rotamer peak, 400 MHz, $CDCl_3$) δ 8.44 (d, *J* = 1.7 Hz, 1H), 7.93 (dd, *J* = 8.6, 1.7 Hz, 1H), 7.55–7.49 (m, 3H), 7.48–7.30 (m, 7H), 7.22 (s, 1H), 7.08 (d, *J* = 7.6 Hz, 1H), 6.67 (d, *J* = 3.2 Hz, 1H), 5.41 (s, 2H), 5.23* (d, *J* = 7.8 Hz, 1H), 5.08 (dd, *J* = 8.1, 3.7 Hz, 1H), 3.79–3.68 (m, 1H), 3.61–3.49 (m, 1H), 2.45–2.31 (m, 1H), 2.21–2.11 (m, 2H), 2.02–1.93 (m, 1H), 1.48* (s, 3H), 1.32 (s, 6H). ^{13}C NMR (2:1 rotamer ratio, asterisk denote minor rotamer peak, 101 MHz, $CDCl_3$) δ 180.2, 169.4, 153.7, 142.0, 140.7, 137.9, 137.7, 129.6, 129.4, 128.9, 128.8, 127.6, 127.2, 126.8, 125.8, 125.7, 121.4, 121.2, 121.1, 118.3, 110.2, 103.1, 80.5, 80.3*, 54.0, 50.4, 46.7*, 46.5, 32.5, 31.6*, 28.5*, 28.3, 24.4*, 23.8. HRMS (ESI+): Calcd for $C_{32}H_{32}N_4O_3$ $[M+H]^+$: 521.6294, Found: 521.2551.

***tert*-butyl (S,Z)-(((tert-butoxycarbonyl)amino)(2-(3-(1-(4-methylbenzyl)-1H-indol-5-yl)-1,2,4-oxadiazol-5-yl)pyrrolidin-1-yl)methylene)carbamate (5.3a):**

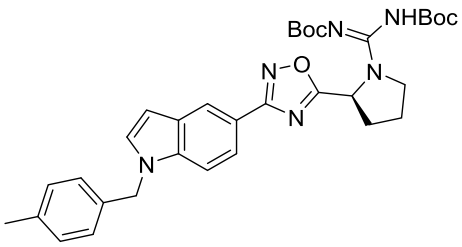

Compound **5.2a** was synthesized from **5.1a** using general procedure 5.2 and carried forward without purification. Using **5.2a** as starting material **5.3a** was synthesized using general procedure 5.3. Purification on a silica gel column with 10–30% EtOAc in hexanes produced **5.3a** (23 mg, 50%), a clear oil. ^{1}H NMR (600 MHz, $CDCl_3$) δ 8.39 (s, 1H), 7.88–7.86 (m, 1H), 7.34 (d, *J* = 8.6 Hz, 1H), 7.16 (d, *J* = 3.2 Hz, 1H), 7.11 (d, *J* = 7.8 Hz, 2H), 7.01 (d, *J* = 7.8 Hz, 2H), 6.61 (d, *J* = 3.1 Hz, 1H), 5.62 (s, 1H), 5.31 (s, 2H), 3.94–3.88 (m, 1H), 3.87–3.81 (m, 1H), 2.49–2.42 (m, 1H), 2.31 (s, 4H), 2.23–2.14 (m, 1H), 2.10–2.04 (m, 1H), 1.52–1.42 (m, 18H). ^{13}C NMR (151 MHz, CDCl3) δ 178.4, 169.4, 153.4, 151.0, 148.8, 138.0, 137.7, 134.1, 129.8, 129.7, 129.5, 128.8, 127.2, 127.0, 122.2, 121.5, 121.3, 121.1, 118.1, 110.6, 110.2, 102.9, 83.5, 81.2, 55.5, 50.2, 49.6, 36.8, 31.4, 29.8, 28.3, 28.1, 27.7, 24.8, 24.0, 21.2, 20.7. HRMS (ESI+): Calcd for $C_{33}H_{40}N_6O_6$ $[M+H]^+$: 601.7158, Found: 601.3129.

***tert*-butyl (*S,Z*)-(((*tert*-butoxycarbonyl)amino)(2-(3-(1-(4-(*tert*-butyl)benzyl)-1*H*-indol-5-yl)-1,2,4-oxadiazol-5-yl)pyrrolidin-1-yl)methylene)carbamate (5.3b):**

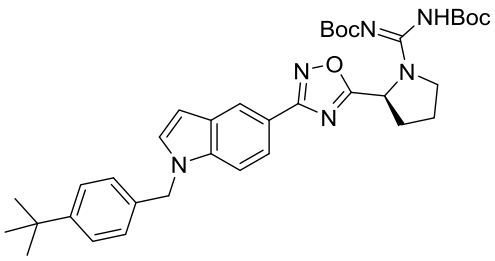

Compound **5.2b** was synthesized from **5.1b** using general procedure 5.2 and carried forward without purification. Using **5.2b** as starting material, **5.3b** was synthesized using general procedure 5.3. Purification on a silica gel column with 10–30% EtOAc in hexanes produced **5.3b** (16 mg, 36%), a clear oil. ^{1}H

NMR (400 MHz, $CDCl_3$) δ 8.40 (dd, *J* = 1.6, 0.7 Hz, 1H), 7.93–7.87 (m, 1H), 7.36 (dt, *J* = 8.7, 0.8 Hz, 1H), 7.34–7.30 (m, 2H), 7.17 (d, *J* = 3.2 Hz, 1H), 7.06–7.03 (m, 2H), 6.62 (dd, *J* = 3.2, 0.8 Hz, 1H), 5.59 (dd, *J* = 7.7, 4.5 Hz, 1H), 5.32 (s, 2H), 3.93–3.86 (m, 1H), 3.85–3.76 (m, 1H), 2.48–2.39 (m, 1H), 2.33–2.24 (m, 1H), 2.22–2.13 (m, 1H), 2.09–2.00 (m, 1H), 1.51–1.41 (m, 18H), 1.28 (s, 9H). ^{13}C NMR (101 MHz, $CDCl_3$) δ 178.4, 169.4, 153.4, 150.9, 138.0, 134.1, 129.5, 128.787, 126.7, 125.9, 121.5, 121.1, 118.1, 110.2, 102.9, 83.7, 80.7, 55.4, 50.0, 49.5, 34.7, 31.4, 28.3, 28.1. HRMS (ESI+): Calcd for $C_{36}H_{46}N_6O_5$ $[M+H]^+$: 643.7956, Found: 643.3577.

***tert*-butyl (*S,Z*)-(((*tert*-butoxycarbonyl)amino)(2-(3-(1-(4-chlorobenzyl)-1*H*-indol-5-yl)-1,2,4-oxadiazol-5-yl)pyrrolidin-1-yl)methylene)carbamate (5.3c):**

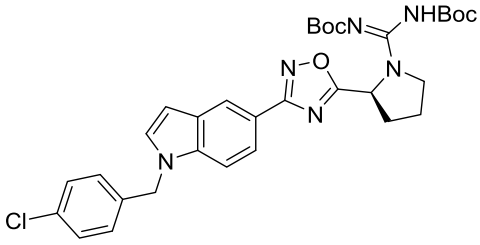

Compound **5.2c** was synthesized from **5.1c** using general procedure 5.2 and carried forward without purification. Using **5.2c** as starting material, **5.3c** was synthesized using general procedure 5.3. Purification on a silica gel column with 10–30% EtOAc in hexanes produced **5.3c** (25mg, 76%), a clear oil. ^1H NMR (500 MHz, $CDCl_3$) δ 8.36 (d, *J* = 1.6 Hz, 1H), 7.85 (dd, *J* = 8.6, 1.7 Hz, 1H), 7.23 (d, *J* = 9.1 Hz, 4H), 7.11 (d, *J* = 3.3 Hz, 1H), 6.98 (d, *J* = 8.1 Hz, 3H), 6.60 (d, *J* = 3.3 Hz, 1H), 5.55 (t, *J* = 6.1 Hz, 1H), 5.28 (s, 2H), 3.90–3.81 (m, 1H), 3.80–3.72 (m, 1H), 2.46–2.35 (m, 1H), 2.31–2.19 (m, 1H), 2.18–2.09 (m, 1H), 2.06–1.96 (m, 1H), 1.49–1.39(m, 18H). ^{13}C NMR (126 MHz, $CDCl_3$) δ 178.5, 171.3, 169.3, 161.9, 153.5, 150.9, 148.8, 137.8, 135.7, 133.8, 129.6, 129.4, 129.2, 128.9, 128.3, 128.2, 121.6, 121.3, 118.3, 110.1, 103.3, 82.4, 79.8, 55.4, 49.8, 49.5, 31.5, 29.8, 28.3, 28.1, 27.6. HRMS (ESI+): Calcd for $C_{32}H_{37}ClN_6O_5$ $[M+H]^+$: 622.1343, Found: 622.0283.

***tert*-butyl (*S*,*Z*)-(((*tert*-butoxycarbonyl)amino)(2-(3-(1-(3-chlorobenzyl)-1*H*-indol-5-yl)-1,2,4-oxadiazol-5-yl)pyrrolidin-1-yl)methylene)carbamate (5.3d):**

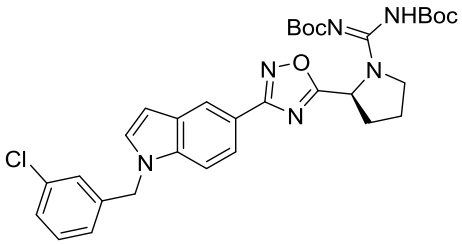

Compound **5.2d** was synthesized from **5.1d** using general procedure 5.2 and carried forward without purification. Using **5.2d** as starting material, **5.3d** was synthesized using general procedure 5.3. Purification on a silica gel column with 10–30% EtOAc in hexanes produced **5.3d** (21 mg, 64%), a clear oil. ^{1}H NMR (500 MHz, $CDCl_3$) δ 8.43 (s, 1H), 7.92 (d, *J* = 8.6 Hz, 1H), 7.32 (d, *J* = 8.5 Hz, 1H), 7.29–7.22 (m, 2H), 7.19 (d, *J* = 3.3 Hz, 1H), 7.13 (s, 1H), 6.97 (d, *J* = 7.0 Hz, 1H), 6.67 (d, *J* = 3.3 Hz, 1H), 5.67–5.58 (m, 1H), 5.34 (s, 2H), 3.98–3.88 (m, 1H), 3.87–3.78 (m, 1H), 2.52–2.41 (m, 1H), 2.36–2.28 (m, 1H), 2.24–2.15 (m, 1H), 2.12–2.03 (m, 1H), 1.58–1.43 (m, 18H). ^{13}C NMR (126 MHz, $CDCl_3$) δ 178.5, 169.3, 153.5, 150.8, 148.9, 139.2, 137.8, 135.0, 130.3, 129.4, 128.9, 128.2, 126.9, 124.9, 121.6, 121.4, 118.4, 110.0, 103.4, 83.5, 81.4, 77.4, 55.4, 49.8, 49.5, 31.5, 31.4, 29.8, 28.3, 28.1, 27.6, 24.0. HRMS (ESI+): Calcd for $C_{32}H_{37}ClN_6O_5$ $[M+H]^+$: 622.1343, Found: 622.0236.

***tert*-butyl (*S*,*Z*)-(((*tert*-butoxycarbonyl)amino)(2-(3-(1-(4-bromobenzyl)-1*H*-indol-5-yl)-1,2,4-oxadiazol-5-yl)pyrrolidin-1-yl)methylene)carbamate (5.3e):**

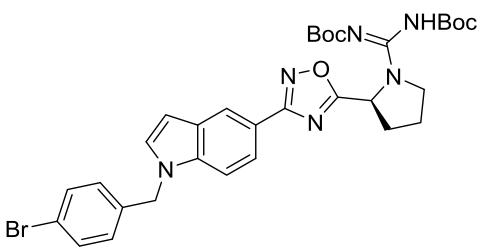

Compound **5.2e** was synthesized from **5.1e** using general procedure 5.2 and carried forward without purification. Using **5.2e** as starting material, **5.3e** was synthesized using general procedure 5.3. Purification on a silica gel column with 10–30% EtOAc in hexanes produced **5.3e** (22 mg, 70%), a clear oil. ^{1}H NMR (500

MHz, $CDCl_3$) δ 8.40 (d, *J* = 1.5 Hz, 1H), 7.89 (dd, *J* = 8.6, 1.5 Hz, 1H), 7.45–7.40 (m, 2H), 7.29 (d, *J* = 8.6 Hz, 1H), 7.15 (d, *J* = 3.2 Hz, 1H), 6.96 (d, *J* = 8.1 Hz, 2H), 6.64 (d, *J* = 3.2 Hz, 1H), 5.59 (dd, *J* = 7.9, 4.5 Hz, 1H), 5.30 (s, 2H), 3.93–3.85 (m, 1H), 3.84–3.76 (m, 1H), 2.49–2.39 (m, 1H), 2.33–2.23 (m, 1H), 2.22–2.13 (m, 1H), 2.09–2.00 (m, 1H), 1.53–1.41 (m, 18H). ^{13}C NMR (126 MHz, $CDCl_3$) δ 178.5, 169.3, 162.1, 153.6, 150.7, 148.8, 137.8, 136.2, 132.2, 132.1, 129.6, 129.4, 129.1, 128.9, 128.7, 128.5, 122.4, 121.8, 121.6, 121.3, 118.3, 110.4, 110.1, 103.3, 83.5, 82.2, 79.8, 55.4, 49.8, 49.5, 31.5, 31.4, 29.8, 28.3, 28.1, 27.6, 24.0, 23.5. HRMS (ESI+): Calcd for $C_{32}H_{37}BrN_6O_5$ $[M+H]^+$: 666.5853, Found: 666.9992.

***tert*-butyl (*S*,*Z*)-(((*tert*-butoxycarbonyl)amino)(2-(3-(1-(3-bromobenzyl)-1*H*-indol-5-yl)-1,2,4-oxadiazol-5-yl)pyrrolidin-1-yl)methylene)carbamate (5.3f):**

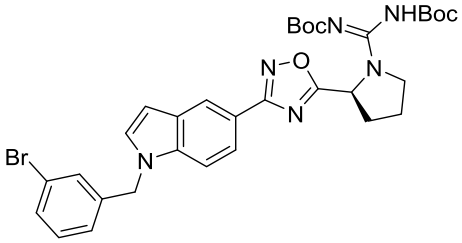

Compound **5.2f** was synthesized from **5.1f** using general procedure 5.2 and carried forward without purification. Using **5.2f** as starting material, **5.3f** was synthesized using general procedure 5.3. Purification on a silica gel column with 10–30% EtOAc in hexanes produced **5.3f** (20 mg, 64%), a clear oil. ^1H NMR (400 MHz, $CDCl_3$) δ 8.44–8.37 (m, 1H), 7.89 (dd, *J* = 8.6, 1.6 Hz, 1H), 7.40 (ddd, *J* = 8.0, 2.0, 1.0 Hz, 1H), 7.32–7.30 (m, 1H), 7.29–7.27 (m, 1H), 7.20–7.12 (m, 2H), 6.98 (ddd, *J* = 7.7, 1.8, 1.0 Hz, 1H), 6.65 (dd, *J* = 3.2, 0.8 Hz, 1H), 5.59 (dd, *J* = 7.9, 4.6 Hz, 1H), 5.31 (s, 2H), 3.94–3.84 (m, 1H), 3.84–3.76 (m, 1H), 2.50–2.42 (m, 1H), 2.31–2.22 (m, 1H), 2.22–2.13 (m, 1H), 2.09–2.00 (m, 1H), 1.52–1.42 (m, 18H). ^{13}C NMR (101 MHz, $CDCl_3$) δ 178.5, 169.3, 153.5, 139.5, 137.8, 131.1, 130.6, 129.9, 129.4, 129.2, 128.9, 125.4, 123.1, 121.6, 121.4, 118.4, 110.0, 103.4, 81.0, 55.4, 49.7, 49.5, 31.5, 29.8, 28.3, 28.1, 24.0. HRMS (ESI+): Calcd for $C_{32}H_{37}BrN_6O_5$ $[M+H]^+$: 666.5853, Found: 667.2031.

***tert*-butyl (*S*,*Z*)-(((*tert*-butoxycarbonyl)amino)(2-(3-(1-(4-(trifluoromethyl)benzyl)-1*H*-indol-5-yl)-1,2,4-oxadiazol-5-yl)pyrrolidin-1-yl)methylene)carbamate (5.3g):**

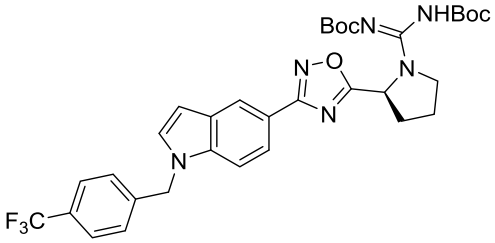

Compound **5.2g** was synthesized from **5.1g** using general procedure 5.2 and carried forward without purification. Using **5.2g** as starting material, **5.3g** was synthesized using general procedure 5.3. Purification on a silica gel column with 10–30% EtOAc in hexanes produced **5.3g** (29 mg, 65%), a clear oil. ^{1}H NMR (500 MHz, $CDCl_3$) δ 8.41 (d, *J* = 1.6 Hz, 1H), 7.89 (dd, *J* = 8.6, 1.6 Hz, 1H), 7.56 (d, *J* = 8.2 Hz, 2H), 7.32–7.24 (m, 2H), 7.18 (dd, *J* = 5.8, 2.5 Hz, 2H), 6.67 (d, *J* = 3.1 Hz, 1H), 5.60 (dd, *J* = 7.9, 4.6 Hz, 1H), 5.42 (s, 2H), 3.93–3.87 (m, 1H), 3.84–3.76 (m, 1H), 2.50–2.39 (m, 1H), 2.34–2.24 (m, 1H), 2.22–2.13 (m, 1H), 2.09–2.01 (m, 1H), 1.46 (s, 18H). ^{19}F NMR (376 MHz, $CDCl_3$) δ –62.64. ^{13}C NMR (126 MHz, $CDCl_3$) δ 178.6, 169.3, 153.5, 151.0, 148.9, 141.3, 137.8, 130.4, 130.1, 129.5, 128.9, 127.1, 127.0, 136.0, 121.7, 121.4, 118.5, 110.0, 103.6, 83.5, 81.6, 81.1, 55.4, 49.9, 49.6, 31.5, 29.8, 28.3, 28.1, 24.0, 20.7. HRMS (ESI+): Calcd for $C_{32}H_{37}F_3N_6O_5$ $[M+H]^+$: 655.6872, Found: 655.1013.

***tert*-butyl (S,Z)-(((tert-butoxycarbonyl)amino)(2-(3-(1-(3-(trifluoromethyl)benzyl)-1H-indol-5-yl)-1,2,4-oxadiazol-5-yl)pyrrolidin-1-yl)methylene)carbamate (5.3h):**

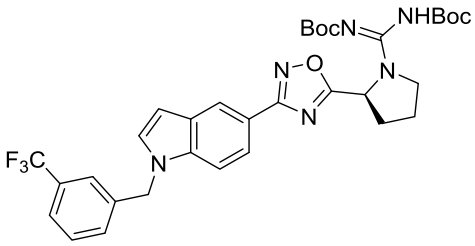

Compound **5.2h** was synthesized from **5.1h** using general procedure 5.2 and carried forward without purification. Using **5.2h** as starting material, **5.3h** was synthesized using general procedure 5.3. Purification on a silica gel column with 10–30% EtOAc in hexanes produced **5.3h** (33 mg, 74%), a clear oil. ^{1}H NMR (500

MHz, $CDCl_3$) δ 8.42 (d, *J* = 7.3 Hz, 1H), 7.90 (dd, *J* = 8.5, 1.9 Hz, 1H), 7.54 (d, *J* = 7.7 Hz, 1H), 7.46–7.39 (m, 3H), 7.31 (t, *J* = 7.8 Hz, 2H), 7.24–7.17 (m, 3H), 6.67 (d, *J* = 3.1 Hz, 1H), 5.66–5.55 (m, 1H), 5.41 (s, 2H), 3.97–3.88 (m, 1H), 3.85–3.77 (m, 1H), 2.51–2.40 (m, 1H), 2.34–2.25 (m, 1H), 2.24–2.15 (m, 1H), 2.11–2.00 (m, 1H), 1.56–1.41 (m, 18H). ^{19}F NMR (376 MHz, $CDCl_3$) δ –62.72. ^{13}C NMR (126 MHz, $CDCl_3$) δ 178.6, 169.3, 161.9, 153.6, 151.0, 138.3, 137.8, 131.5, 131.3, 130.1, 129.6, 129.4, 128.9, 125.1, 124.9, 123.6, 121.7, 121.5, 118.5, 110.0, 103.6, 83.6, 81.6, 79.9, 77.4, 55.5, 49.9, 49.6, 31.5, 31.4, 28.3, 28.1, 27.6, 24.0, 20.7. HRMS (ESI+): Calcd for $C_{32}H_{37}F_3N_6O_5$ $[M+H]^+$: 655.6872, Found: 655.2713.

tert-butyl (*S*,*Z*)-(((_tert_-butoxycarbonyl)amino)(2-(3-(1-(2-(trifluoromethyl)benzyl)-1*H*-indol-5-yl)-1,2,4-oxadiazol-5-yl)pyrrolidin-1-yl)methylene)carbamate (5.3i):

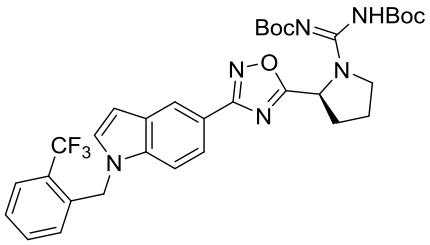

Compound **5.2i** was synthesized from **5.1i** using general procedure 5.2 and carried forward without purification. Using **5.2i** as starting material, **5.3i** was synthesized using general procedure 5.3. Purification on a silica gel column with 10–30% EtOAc in hexanes produced **5.3i** (23 mg, 79%), a clear oil. ^1H NMR (600 MHz, $CDCl_3$) δ 8.43 (d, *J* = 1.5 Hz, 1H), 7.88 (dd, *J* = 8.6, 1.6 Hz, 1H), 7.72 (dd, *J* = 7.6, 1.6 Hz, 1H), 7.38–7.30 (m, 2H), 7.24 (d, *J* = 8.6 Hz, 1H), 7.18 (d, *J* = 3.2 Hz, 1H), 6.69 (d, *J* = 3.2 Hz, 1H), 6.55 (d, *J* = 7.6 Hz, 1H), 5.58 (s, 3H), 3. 3–3.87 (m, 1H), 3.84–3.78 (m, 1H), 2.49–2.41 (m, 1H), 2.32–2.23 (m, 1H), 2.22–2.16 (m, 1H), 2.10–2.01 (m, 1H), 1.52–1.41 (m, 18H). ^{19}F NMR (376 MHz, $CDCl_3$) δ –60.39. ^{13}C NMR (151 MHz, $CDCl_3$) δ 178.6, 169.3, 162.0, 153.5, 150.8, 148.8, 138.0, 136.0, 132.6, 129.9, 128.8, 127.8, 127.4, 127.2, 126.2, 121.7, 121.5, 118.6, 110.1, 103.6, 83.5, 82.2, 79.8, 60.5, 55.4, 49.5, 46.7, 31.5, 28.3, 28.1, 24.0. HRMS (ESI+): Calcd for $C_{32}H_{37}F_3N_6O_5$ $[M+H]^+$: 655.6872, Found: 655.2797.

***tert*-butyl (*S*,*Z*)-((2-(3-(1-([1,1'-biphenyl]-4-ylmethyl)-1*H*-indol-5-yl)-1,2,4-oxadiazol-5-yl)pyrrolidin-1-yl)((*tert*-butoxycarbonyl)amino)methylene)carbamate (5.3j):**

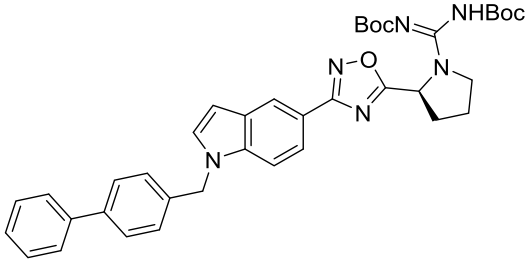

Compound **5.2j** was synthesized from **5.1j** using general procedure 5.2 and carried forward without purification. Using **5.2j** as starting material, **5.3j** was synthesized using general procedure 5.3. Purification on a silica gel column with 10–30% EtOAc in hexanes produced **5.3j** (27 mg, 75%), a clear oil. ^{1}H NMR (600 MHz, $CDCl_3$) δ 8.42 (d, *J* = 1.6 Hz, 1H), 7.91 (dd, *J* = 8.6, 1.6 Hz, 1H), 7.56–7.51 (m, 5H), 7.42 (t, *J* = 7.7 Hz, 2H), 7.38 (d, *J* = 8.6 Hz, 1H), 7.35–7.32 (m, 1H), 7.21 (d, *J* = 3.2 Hz, 1H), 7.18 (d, *J* = 8.1 Hz, 2H), 6.65 (d, *J* = 3.1 Hz, 1H), 5.61 (dd, *J* = 7.9, 4.6 Hz, 1H), 5.39 (s, 2H), 3.93–3.86 (m, 1H), 3.85–3.79 (m, 1H), 2.49–2.42 (m, 1H), 2.33–2.25 (m, 1H), 2.23–2.15 (m, 1H), 2.08–2.00 (m, 1H), 1.51–1.47 (m, 18H). ^{13}C NMR (151 MHz, $CDCl_3$) δ 178.5, 171.3, 148.8, 141.3, 140.9, 140.6, 138.0, 137.9, 136.1, 135.3, 129.54, 129.45, 129.0, 128.91, 128.90, 128.8, 128.4, 127.8, 127.7, 127.64, 127.55, 127.38, 127.37, 127.3, 127.16, 127.15, 122.3, 121.6, 121.4, 121.2, 120.0, 118.2, 110.5, 110.2, 110.1, 103.11, 103.10, 103.07, 83.5, 83.1, 81.5, 60.5, 53.6, 50.1, 49.5, 31.5, 28.29, 28.26, 28.23, 28.16, 28.1, 22.8. HRMS (ESI+): Calcd for $C_{38}H_{42}N_6O_5$ $[M+H]^+$: 663.7852, Found: 663.3279.

***tert*-butyl (*S*,*Z*)-((2-(3-(1-([1,1'-biphenyl]-3-ylmethyl)-1*H*-indol-5-yl)-1,2,4-oxadiazol-5-yl)pyrrolidin-1-yl)((*tert*-butoxycarbonyl)amino)methylene)carbamate (5.3k):**

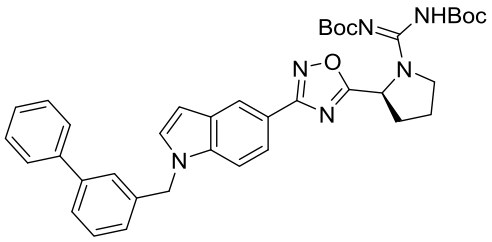

Compound **5.2k** was synthesized from **5.1k** using general procedure 5.2 and carried forward without purification. Using **5.2k** as starting material, **5.3k** was synthesized using general procedure 4. Purification on a silica gel column with 10–30% EtOAc in hexanes produced **5.3k** (22 mg, 61%), a clear oil. ^{1}H NMR (600 MHz, $CDCl_3$) δ 8.41 (d, *J* = 1.6 Hz, 1H), 7.90 (dd, *J* = 8.6, 1.7 Hz, 1H), 7.52–7.50 (m, 1H), 7.50–7.48 (m, 2H), 7.42–7.35 (m, 6H), 7.35–7.31 (m, 1H), 7.21 (d, *J* = 3.2 Hz, 1H), 7.06 (dt, *J* = 7.7, 1.4 Hz, 1H), 6.64 (d, *J* = 3.1 Hz, 1H), 5.59 (t, *J* = 6.3 Hz, 1H), 5.41 (s, 2H), 3.92–3.86 (m, 1H), 3.83–3.76 (m, 1H), 2.48–2.39 (m, 1H), 2.32–2.24 (m, 1H), 2.22–2.14 (m, 1H), 2.06–2.01 (m, 1H), 1.46 (s, 18H). ^{13}C NMR (151 MHz, $CDCl_3$) δ 178.5, 169.1, 154.3, 152.9, 149.0, 142.0, 140.7, 138.0, 137.7, 129.52, 129.45, 128.9, 128.8, 127.6, 127.3, 127.1, 126.8, 126.0, 125.8, 125.7, 121.6, 121.4, 121.2, 118.2, 110.2, 103.1, 83.5, 83.1, 55.4, 50.4, 49.5, 31.5, 31.4, 29.8, 28.3, 28.2, 28.1, 24.0. HRMS (ESI+): Calcd for $C_{38}H_{42}N_6O_5$ $[M+H]^+$: 663.7852, Found: 663.3292.

(*S*)-2-(3-(1-(4-methylbenzyl)-1*H*-indol-5-yl)-1,2,4-oxadiazol-5-yl)pyrrolidine-1-carboximidamide hydrochloride (5.4a):

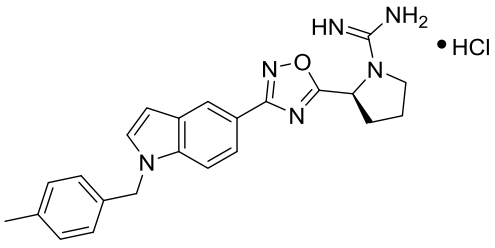

Using **5.3a** as starting material, **5.4a** was synthesized using general procedure 5.2. The final product was isolated as a white solid (7 mg, 88%) and found to be 66% pure by HPLC. ^{1}H NMR (600 MHz, CD_3OD) δ

8.30 (d, *J* = 1.5 Hz, 1H), 7.80 (dd, *J* = 8.7, 1.6 Hz, 1H), 7.45 (d, *J* = 8.6 Hz, 1H), 7.36 (d, *J* = 3.2 Hz, 1H), 7.13–7.09 (m, 2H), 7.08–7.02 (m, 3H), 6.61 (d, *J* = 3.1 Hz, 1H), 5.44 (dd, *J* = 8.0, 1.9 Hz, 1H), 5.37 (s, 2H), 3.79 (td, *J* = 9.3, 2.6 Hz, 1H), 3.67–3.59 (m, 1H), 2.58–2.54 (m, 1H), 2.51–2.46 (m, 1H), 2.28 (s, 3H), 2.25–2.21 (m, 1H), 2.17–2.08 (m, 1H). ^{13}C NMR (151 MHz, CD_3OD) δ 178.4, 170.8, 157.1, 139.3, 138.5, 136.0, 131.3, 131.2, 130.5, 130.3, 128.2, 128.0, 127.9, 122.0, 121.9, 121.4, 118.5, 111.6, 103.4, 56.5, 50.9, 32.7, 24.4, 21.1. HRMS (ESI+): Calcd for $C_{25}H_{24}N_6O$ $[M+H]^+$: 401.4842, Found: 401.2088.

(*S*)-2-(3-(1-(4-(*tert*-butyl)benzyl)-1*H*-indol-5-yl)-1,2,4-oxadiazol-5-yl)pyrrolidine-1-carboximidamide hydrochloride (5.4b):

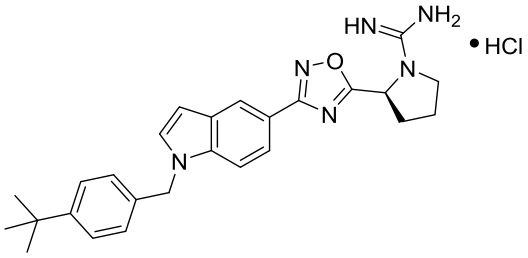

Using **5.3b** as starting material, **5.4b** was synthesized using general procedure 5.2. The final product was isolated as a white solid (11 mg, 92%) and found to be 61% pure by HPLC. ^{1}H NMR (1:1 rotamer ratio, asterisk denote minor rotamer peak, 500 MHz, $(CD_3)_2CO$) δ 8.33 (s, 1H), 7.83–7.76 (m, 1H), 7.58 (t, *J* = 9.6 Hz, 1H), 7.49 (dd, *J* = 14.6, 3.2 Hz, 1H), 7.41–7.31 (m, 2H), 7.20–7.12 (m, 2H), 6.65 (t, *J* = 2.8 Hz, 1H), 5.81 (d, *J* = 7.9 Hz, 1H), 5.45 (d, *J* = 9.0 Hz, 2H), 4.18–4.08* (m, 1H), 4.03–3.91 (m, 1H), 3.88* (t, *J* = 9.2 Hz, 1H), 3.74 (t, *J* = 8.9 Hz, 1H), 2.63–2.52 (m, 1H), 2.50–2.40* (m, 1H), 2.32–2.22 *(m, 1H), 2.22–2.15 (m, 1H), 1.47* (s, 6H), 1.25 (s, 12H). ^{13}C NMR (1:1 rotamer ratio, asterisk denote minor rotamer peak, 126 MHz, $(CD_3)_2CO$) δ 178.2, 170.0*, 169.9, 157.4, 151.17*, 151.15, 138.72*, 138.67, 135.8, 131.1*, 131.0, 129.7, 127.7, 126.3, 121.6, 121.1, 118.4, 111.6*, 111.5, 56.0, 50.2*, 50.2, 48.7, 35.0, 32.1, 31.6, 28.1, 24.0. HRMS (ESI+): Calcd for $C_{26}H_{30}N_6O$ $[M+H]^+$: 443.5639, Found: 443.1464.

(*S*)-2-(3-(1-(4-chlorobenzyl)-1*H*-indol-5-yl)-1,2,4-oxadiazol-5-yl)pyrrolidine-1-carboximidamide hydrochloride (5.4c):

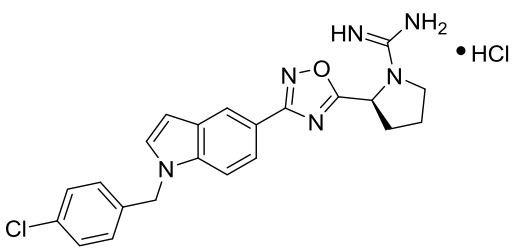

Using **5.3c** as starting material, **5.4c** was synthesized using general procedure 5.2. The final product was isolated as a white solid (8 mg, 73%) and found to be 73% pure by HPLC. ^{1}H NMR (600 MHz, CD_3OD) δ 8.32 (d, *J* = 1.5 Hz, 1H), 7.82 (dd, *J* = 8.7, 1.6 Hz, 1H), 7.44 (d, *J* = 8.6 Hz, 1H), 7.40 (d, *J* = 3.1 Hz, 1H), 7.30 (d, *J* = 8.4 Hz, 2H), 7.14 (d, *J* = 8.3 Hz, 2H), 6.64 (d, *J* = 3.1 Hz, 1H), 5.48–5.39 (m, 3H), 3.79 (td, *J* = 9.2, 2.5 Hz, 1H), 3.66–3.58 (m, 1H), 2.61–2.52 (m, 1H), 2.51–2.46 (m, 1H), 2.28–2.20 (m, 1H), 2.18–2.08 (m, 1H). ^{13}C NMR (151 MHz, CD_3OD) δ 178.4, 170.7, 138.0, 134.4, 129.8, 129.6, 122.04, 122.01, 121.6, 111.5, 103.7, 56.5, 50.2, 32.7, 24.4. HRMS (ESI+): Calcd for $C_{22}H_{21}ClN_6O$ $[M+H]^+$: 421.9027, Found: 421.1542.

(*S*)-2-(3-(1-(3-chlorobenzyl)-1*H*-indol-5-yl)-1,2,4-oxadiazol-5-yl)pyrrolidine-1-carboximidamide hydrochloride (5.4d):

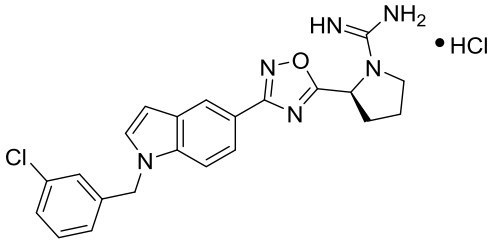

Using **5.3d** as starting material, **5.4d** was synthesized using general procedure 5.2. The final product was isolated as a white solid (8 mg, 73%) and found to be 78% pure by HPLC. ^{1}H NMR (600 MHz, CD_3OD) δ 8.33 (d, *J* = 1.5 Hz, 1H), 7.82 (dd, *J* = 8.6, 1.6 Hz, 1H), 7.44 (d, *J* = 8.6 Hz, 1H), 7.41 (dd, *J* = 3.0, 1.7 Hz, 1H), 7.28–7.23 (m, 2H), 7.13 (s, 1H), 7.09–7.05 (m, 1H), 6.65 (d, *J* = 3.1 Hz, 1H), 5.45 (dd, *J* = 6.1, 2.1 Hz, 3H), 3.79 (td, *J* = 9.2, 2.6 Hz, 1H), 3.62 (td, *J* = 9.7, 7.2 Hz, 1H), 2.62–2.52 (m, 1H), 2.51–2.45 (m, 1H), 2.27–2.21 (m, 1H), 2.15–2.06 (m, 1H). ^{13}C NMR (151 MHz,

CD_3OD) δ 178.4, 170.7, 157.1, 141.6, 139.2, 135.7, 131.34, 131.29, 131.25, 130.33, 130.25, 128.7, 127.9, 126.3, 122.07, 122.05, 121.7, 118.8, 111.5, 103.8, 56.5, 50.3, 32.7, 24.4. HRMS (ESI+): Calcd for $C_{22}H_{21}ClN_6O$ $[M+H]^+$: 421.9027, Found: 421.1543.

(*S*)-2-(3-(1-(4-bromobenzyl)-1*H*-indol-5-yl)-1,2,4-oxadiazol-5-yl)pyrrolidine-1-carboximidamide hydrochloride (5.4e):

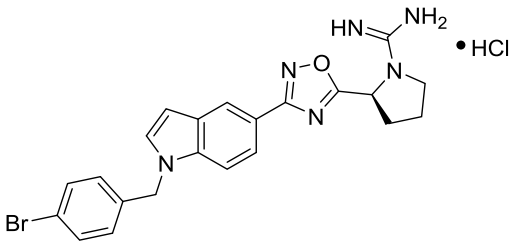

Using **5.3e** as starting material, **5.4e** was synthesized using general procedure 5.2. The final product was isolated as a white solid (9 mg, 82%). ^{1}H NMR (600 MHz, CD_3OD) δ 8.06 (s, 1H), 7.65 (d, *J* = 8.5 Hz, 1H), 7.52 (s, 1H), 7.39 (d, *J* = 8.0 Hz, 2H), 7.25 (d, *J* = 8.6 Hz, 1H), 7.10 (d, *J* = 8.0 Hz, 2H), 6.38–6.31 (m, 1H), 5.45 (s, 2H), 5.41–5.34 (m, 1H), 3.72–3.64 (m, 1H), 3.60–3.52(m, 1H), 2.55–2.46 (m, 1H), 2.45–2.38 (m, 1H), 2.28–2.21 (m, 1H), 2.20–2.13 (m, 1H). ^{13}C NMR (151 MHz, CD_3OD) δ 178.3, 170.7, 157.1, 140.4, 138.7, 132.94, 132.92, 132.86, 130.0, 129.7, 128.5, 127.8, 126.7, 122.1, 121.8, 121.6, 117.5, 111.5, 56.5, 50.3, 35.8, 32.7, 30.8, 24.4. HRMS (ESI+): Calcd for $C_{22}H_{21}BrN_6O$ $[M+H]^+$: 466.3537, Found: 466.1033.

(*S*)-2-(3-(1-(3-bromobenzyl)-1*H*-indol-5-yl)-1,2,4-oxadiazol-5-yl)pyrrolidine-1-carboximidamide hydrochloride (5.1f):

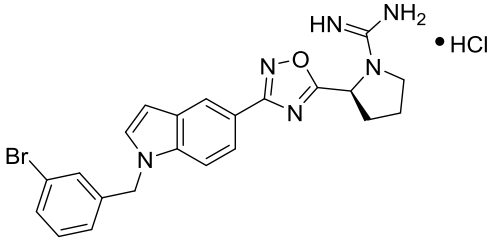

Using **5.3f** as starting material, **5.4f** was synthesized using general procedure 5.2. The final product was isolated as a white solid (14 mg, 93%) and found to be 83% pure by HPLC. ^{1}H NMR (600 MHz, CD_3OD) δ 8.32 (s, 1H), 7.82 (d, *J* = 8.5 Hz, 1H), 7.43 (d, *J* = 8.7 Hz, 1H), 7.41–7.38 (m, 2H), 7.20 (t, *J* =

7.8 Hz, 1H), 7.10 (d, *J* = 7.7 Hz, 1H), 6.65 (d, *J* = 2.9 Hz, 1H), 5.46–5.40 (m, 3H), 3.79 (t, *J* = 9.1 Hz, 1H), 3.65–3.60 (m, 1H), 2.60–2.52 (m, 1H), 2.51–2.45 (m, 1H), 2.27–2.19 (m, 1H), 2.15–2.06 (m, 1H). ^{13}C NMR (151 MHz, CD_3OD) δ 178.4, 170.7, 157.1, 141.7, 139.2, 131.71, 131.5, 131.3, 130.8, 130.3, 126.7, 123.7, 122.1, 121.7, 118.7, 111.5, 103.8, 56.5, 50.2, 32.7, 28.2, 24.4. HRMS (ESI+): Calcd for $C_{22}H_{21}BrN_6O$ $[M+H]^+$: 466.3537, Found: 466.1060.

(*S*)-2-(3-(1-(4-(trifluoromethyl)benzyl)-1*H*-indol-5-yl)-1,2,4-oxadiazol-5-yl)pyrrolidine-1-carboximidamide hydrochloride (5.4g):

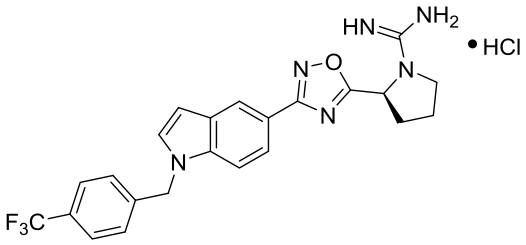

Using **5.3g** as starting material, **5.4g** was synthesized using general procedure 5.2. The final product was isolated as a white solid (8 mg, 73%) and found to be 81% pure by HPLC. ^{1}H NMR (600 MHz, CD_3OD) δ 8.33 (d, *J* = 1.5 Hz, 1H), 7.82 (dd, *J* = 8.6, 1.6 Hz, 1H), 7.60 (d, *J* = 8.1 Hz, 2H), 7.47–7.42 (m, 2H), 7.30 (d, *J* = 8.1 Hz, 2H), 6.67 (d, *J* = 3.2 Hz, 1H), 5.55 (s, 2H), 5.44 (dd, *J* = 7.9, 1.8 Hz, 1H), 3.79 (td, *J* = 9.2, 2.5 Hz, 1H), 3.68–3.59 (m, 1H), 2.59–2.52 (m, 1H), 2.52–2.47 (m, 1H), 2.28–2.20 (m, 1H), 2.16–2.07 (m, 1H). ^{19}F NMR (376 MHz, CD_3OD) δ –64.07. ^{13}C NMR (151 MHz, CD_3OD) δ 178.4, 170.7, 157.1, 143.7, 139.3, 131.4, 130.9, 130.4, 128.4, 126.7, 122.1, 121.7, 118.8, 111.5, 103.9, 56.5, 50.4, 32.7, 24.4. HRMS (ESI+): Calcd for $C_{23}H_{21}F_3N_6O$ $[M+H]^+$: 455.4556, Found: 455.1805.

(*S*)-2-(3-(1-(3-(trifluoromethyl)benzyl)-1*H*-indol-5-yl)-1,2,4-oxadiazol-5-yl)pyrrolidine-1-carboximidamide hydrochloride (5.4h):

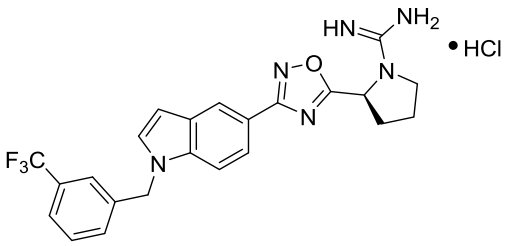

Using **5.3h** as starting material, **5.4h** was synthesized using general procedure 5.2. The final product was isolated as a white solid (10 mg, 91%) and found to be 81% pure by HPLC. ^{1}H NMR (600 MHz, CD_3OD) δ 8.34 (d, *J* = 1.5 Hz, 1H), 7.83 (dd, *J* = 8.6, 1.6 Hz, 1H), 7.56 (d, *J* = 7.9 Hz, 1H), 7.49 (t, *J* = 7.8 Hz, 1H), 7.47–7.43 (m, 3H), 7.38 (d, *J* = 7.9 Hz, 1H), 6.68 (d, *J* = 3.2 Hz, 1H), 5.55 (s, 2H), 5.44 (dd, *J* = 8.0, 1.8 Hz, 1H), 3.79 (td, *J* = 9.2, 2.6 Hz, 1H), 3.63 (td, *J* = 9.6, 7.1 Hz, 1H), 2.61–2.53 (m, 1H), 2.54–2.46 (m, 1H), 2.27–2.20 (m, 1H), 2.15–2.07 (m, 1H). ^{19}F NMR (376 MHz, CD_3OD) δ –64.26. ^{13}C NMR (151 MHz, CD_3OD) δ 178.4, 170.7, 157.1, 140.7, 139.3, 131.6, 131.3, 130.6, 130.4, 125.4, 124.548, 122.1, 121.7, 118.8, 111.4, 104.0, 56.5, 50.3, 32.7, 24.4. HRMS (ESI+): Calcd for $C_{23}H_{21}F_3N_6O$ $[M+H]^+$: 455.4556, Found: 455.1805.

(*S*)-2-(3-(1-(2-(trifluoromethyl)benzyl)-1*H*-indol-5-yl)-1,2,4-oxadiazol-5-yl)pyrrolidine-1-carboximidamide hydrochloride (5.4i):

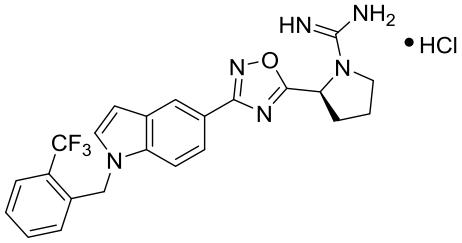

Using **5.3i** as starting material, **5.4i** was synthesized using general procedure 5.2. The final product was isolated as a white solid (9 mg, 82%) and found to be 87% pure by HPLC. ^{1}H NMR (600 MHz, CD_3OD) δ 8.36 (d, *J* = 1.5 Hz, 1H), 7.82 (dd, *J* = 1.6 Hz, 1H), 7.80–7.77 (m, 1H), 7.49–7.37 (m, 3H), 7.30 (d, *J* = 8.6 Hz, 1H), 6.71 (d, *J* = 3.2 Hz, 1H), 6.62 (d, *J* = 7.5 Hz, 1H), 5.67 (s, 2H), 5.44 (dd, *J* = 8.0, 1.8 Hz, 1H), 3.79 (td, *J* = 9.3, 2.6 Hz, 1H), 3.63 (td, *J* = 9.6, 7.2 Hz, 1H), 2.63–2.54 (m, 1H), 2.52–2.46 (m,

1H), 2.28–2.20 (m, 1H), 2.18–2.06 (m, 1H). ^{19}F NMR (376 MHz, CD_3OD) δ –61.53. ^{13}C NMR (151 MHz, CD_3OD) δ 178.5, 170.7, 157.1, 139.4, 137.6, 133.8, 131.7, 130.4, 129.0, 128.8, 127.2, 122.2, 121.9, 119.0, 111.3, 104.1, 56.5, 47.5, 32.7, 24.4. HRMS (ESI+): Calcd for $C_{23}H_{21}F_3N_6O$ $[M+H]^+$: 455.4556, Found: 455.1804.

(*S*)-2-(3-(1-([1,1'-biphenyl]-4-ylmethyl)-1*H*-indol-5-yl)-1,2,4-oxadiazol-5-yl)pyrrolidine-1-carboximidamide hydrochloride (5.4j):

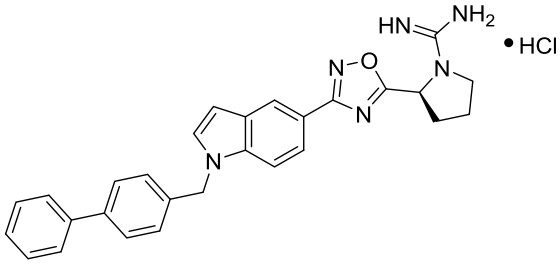

Using **5.3j** as starting material, **5.4j** was synthesized using general procedure 5.2. The final product was isolated as a white solid (8 mg, 89%) and found to be 76% pure by HPLC. ^{1}H NMR (600 MHz, CD_3OD) δ 8.33 (d, *J* = 1.5 Hz, 1H), 7.82 (dd, *J* = 8.6, 1.6 Hz, 1H), 7.56–7.52 (m, 5H), 7.49 (d, *J* = 8.6 Hz, 1H), 7.43–7.37 (m, 4H), 7.32–7.28 (m, 1H), 7.23 (d, *J* = 8.0 Hz, 2H), 6.64 (d, *J* = 3.1 Hz, 1H), 5.47 (s, 2H), 5.44 (dd, *J* = 8.1, 1.9 Hz, 1H), 3.79 (td, *J* = 9.3, 2.6 Hz, 1H), 3.62 (td, *J* = 9.7, 7.2 Hz, 1H), 2.59–2.51 (m, 1H), 2.51–2.43 (m, 1H), 2.25–2.19 (m, 1H), 2.14–2.07 (m, 1H). ^{13}C NMR (151 MHz, CD_3OD) δ 178.4, 170.7, 157.1, 141.9, 139.3, 138.1, 131.3, 130.3, 129.8, 128.6, 128.5, 128.4, 128.3, 127.9, 122.0, 121.5, 118.6, 111.6, 103.6, 56.5, 50.7, 32.7, 24.4. HRMS (ESI+): Calcd for $C_{28}H_{26}N_6O$ $[M+H]^+$: 463.5536, Found: 463.2266.

(*S*)-2-(3-(1-([1,1'-biphenyl]-3-ylmethyl)-1*H*-indol-5-yl)-1,2,4-oxadiazol-5-yl)pyrrolidine-1-carboximidamide hydrochloride (5.4k):

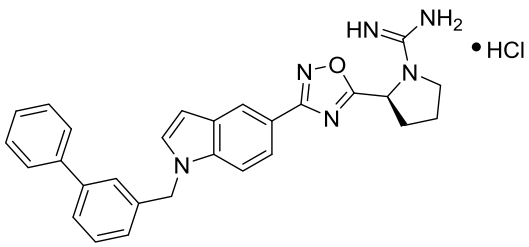

Using **5.3k** as starting material, **5.4k** was synthesized using general procedure 5.2. The final product was isolated as a white solid (7 mg, 88%) and found to be 85% pure by HPLC. ^{1}H NMR (600 MHz, CD_3OD) δ 8.33 (s, 1H), 7.82 (d, *J* = 8.7 Hz, 1H), 7.50 (d, *J* = 8.1 Hz, 3H), 7.44 (d, *J* = 2.9 Hz, 1H), 7.42–7.34 (m, 4H), 7.30 (t, *J* = 7.5 Hz, 1H), 7.11 (d, *J* = 7.9 Hz, 1H), 6.65 (d, *J* = 3.1 Hz, 1H), 5.50 (s, 2H), 5.44 (d, *J* = 8.1 Hz, 1H), 3.83–3.75 (m, 1H), 3.65–3.59 (m, 1H), 2.59–2.51 (m, 1H), 2.50–2.45 (m, 1H), 2.26–2.16 (m, 1H), 2.16–2.04 (m, 1H). ^{13}C NMR (151 MHz, CD_3OD) δ 178.4, 170.7, 157.1, 143.0, 142.0, 139.7, 139.4, 131.2, 130.3, 129.8, 128.5, 128.0, 127.3, 126.8, 126.6, 122.0, 121.5, 118.6, 111.6, 103.6, 56.5, 51.0, 32.7, 24.4. HRMS (ESI+): Calcd for $C_{23}H_{21}N_6O$ $[M+H]^+$: 463.5536, Found: 463.2243.

7.2 Biology

7.2.1 Materials

Sphk1-/- and Sphk2-/- mice were gifts from Dr. Richard Proia (National Institutes of Health/National Institute of Diabetes and Digestive and Kidney Diseases). Male C57BL/6j mice were from the Jackson Laboratories (Bar Harbor, ME), and male Sprague-Dawley rats were from Taconic (Hudson, NY). Deuterated S1P (d7-S1P), S1P, sphingosine, C17-S1P, and C17 sphingosine were purchased from Avanti Polar Lipids (Alabaster, AL). FTY720 and *S*-phosho-FTY720 were gifts from Dr. Volker Brinkmann (Novartis, Basel, Switzerland).

7.2.2 Procedures for Biological Assays

Sphingosine Kinase Inhibition Assay

The activity of SphK inhibitors was measured using recombinant SphK1 and SphK2.[1] Tests were carried out by mixing cleared cell lysates from baculovirus-infected Sf9 insect cells (0.02–0.03 mg protein) with 200 ml of a reaction mixture consisting of 20 mM Tris-Cl (pH 7.4), 1 mM 2-mercaptoethanol, 1 mM EDTA, 5 mM sodium orthovanadate, 40 mM *b*-glycerophosphate, 15 mM NaF, 1 mM phenylmethylsulfonyl fluoride, 10 mM $MgCl_2$, 0.5 mM 4-deoxypyridoxine, 10% glycerol, and 0.1 mg/mL each of leupeptin, aprotinin, and soybean trypsin inhibitor. For measuring SphK2 activity, the buffer was supplemented with KCl to 100 mM. Other additions included substrates (*D*-erythro-sphingosine, 5–10 mM, or FTY720, 1 mM, with or without inhibitors for up to 10 mM) and [γ-^{32}P]ATP (10 mM; specific activity 5 8.3 Ci/mmol). After 30 minutes at 37 °C, the reaction was stopped by placing the reaction tubes on ice. An aliquot of the reaction mixture was spotted onto 2 x 2 cm squares of P81 phosphocellulose cation exchange paper, which was washed three times with 75 mM

orthophosphoric acid, followed by soaking in acetone for 2 minutes. The amount of radionuclide bound to the dried P81 paper was measured by liquid scintillation counting. For determination of K_m and V_{max}, SphK activity was measured with or without a fixed concentration of the inhibitor, and the effect on K_m and V_{max} was determined as previously described.[1,2]

Sphingosine Kinase Inhibition in Cultured Cells

The *in vivo* effects of SphK inhibitors were tested on U937 cells grown in RPMI 1640 media supplemented with *L*-glutamate, 10% fetal bovine serum, and 1% penicillin/streptomycin at 7 °C in the presence of 5% CO_2. Twentyfour hours before adding the inhibitors, the growth media was replaced with media containing 0.5% fetal bovine serum. Cells were then treated for 2 hours with a SphK inhibitor in the presence or absence of the SphK2 selective substrate FTY720. Finally, levels of S1P and FTY720 phosphate (FTY720-P) in cells were assayed by liquid chromatography mass spectrometry (LC/MS).

Pharmacokinetic Analysis

Groups of 6–12 week old mice, strain C57BL/6j, were injected i.p. with either 5 or 10 mg/kg **SLM6031434**, **SLM6081442**, or **SLC5111312** or an equal volume of vehicle (2% solution of hydroxypropyl-β-cyclodextrin; Cargill Cavitron 82004; Cargill Inc., Cedar Rapids, IA). After injection, animals were bled at the specified time points (as soon as possible time points were 1–2 minutes after dosing). Whole blood was processed immediately for LC/MS analysis as described below. The use of mice and rats for these studies was approved by the University of Virginia's School of Medicine Animal Care and Use Committee.

LC/MS Sample Preparation

Sample preparation protocols were as described by Shaner et al. (2009), with minor modifications. Cell pellets (2 x 10^6 to 4x10^6 cells) or whole blood (5 ml) were mixed with 2 mL of methanol/chloroform (3:1) and transferred to a capped glass vial. Suspensions were supplemented with 10 mL of an internal standard solution containing 10 pmol each of C17-S1P or d7-S1P, C17 sphingosine, or deuterated sphingosine and deuterated **SLM6031434-**d17. Mixtures were placed in a bath sonicator for 10 minutes, incubated at 48°C for 16 hours, cooled to an ambient temperature, mixed with 200 mL of 1 M KOH in methanol for saponification, sonicated, and incubated for 2 hours at 37 °C. Following saponification, mixtures were neutralized by the addition of 20 ml of glacial acetic acid, transferred to 2-mL microcentrifuge tubes, and centrifuged at 12,000 g for 12 minutes at 4 °C. The supernatant fluid was collected in a separate glass vial and evaporated under a stream of N_2 gas. Immediately prior to LC/MS analysis, the dried material was dissolved in 0.3 ml of methanol and centrifuged at 12,000 g for 12 minutes at 4 °C. Ten microliters of the resulting supernatant fluid was analyzed by LC/MS.

LC/MS Analysis

Analyses were performed by LC-ESIMS using a Waters system (Milford, MA) consisting of a triple quadrupole mass spectrometer (Xevo TQ-S) and a solvent pump (Acquity UPLC). A binary solvent gradient with a flow rate of 0.4 ml/min was used to separate sphingolipids and compounds by reverse phase chromatography using an Acquity UPLC CSH C18 column (2.1 x 100 mm, 1.7-µm bead size). Mobile phases consisted of 6:4 acetonitrile/water (mobile phase A) and 9:1 isopropanol/acetonitrile (mobile phase B). Both phases were supplemented with 0.1% formic acid. Chromatographic runs started with 100% A for 1 minute.

Solvent B was then increased linearly to 100% B in 7 minutes and held at 100% for 2 minutes. The column was finally re-equilibrated to 100% A for 2 minutes. Natural sphingolipids were detected using multiple reaction monitoring in the positive mode as previously described:[2] C17-S1P (366.4 → 250.4); S1P (380.4 → 264.4); dihydroS1P (382.4 → 266.4); deuterated C18S1P-d7 (387.4 → 271.3); C17sphingosine (286.4→250.3); sphingosine (300.5→264.4); sphinganine (302.5→ 260.0); and deuterated (d7) sphingosine (307.5→271.3). Fragmentation of compounds **SLM6031434** (as well as its enantiomer SLM6081442), its deuterated form (**SLM6031434**-d17), and **SLC5111312** were analyzed by direct infusion of a 1 mM solution in methanol supplemented with 0.1% formic acid. It was found that the following transitions and cone and collision voltages gave the most intense signals in the positive mode: **SLM6031434** and **SLM6081442**, 454.2→112.1, 66 and 28 V; SLM6031434-d17, 471.4→140.1, 54 and 24 V; and **SLC5111312**, 410.2→156.1, 54 and 18 V. Retention times for all analytes under our experimental conditions were about 2 minutes. Quantification was carried out by measuring peak areas using commercially available software (Target Lynx, Waters Corp.).

7.3 Molecular Modeling

7.3.1 SphK2 Homology Modeling Methods and Results

A search of the RCSB PDB[3] website returned two suitable structures for homology modeling, PDB ID: 3VZB and 3VZD[4]. The 3VZB structure contained sphingosine, while the 3VZD structure contained ADP and magnesium. Of the two, 3VZB was the most appropriate for predicting the shape of the binding cavity because of the co-crystallized sphingosine in the binding cavity. Therefore, 3VZB was used as the template for modeling SphK2. The ligands (ADP and Mg^{2+}) contained in the 3VZD structure were used to place and build ATP (by adding an additional phosphate group to ADP) within the ATP binding cavity of the SphK2 model. A sequence alignment between the template (3VZB) and hSphk2 is provided in Figure 7.3.

The C-isoform with an extended *N*-terminal region was used to model SphK2. This sequence contains 618 amino acids.

MAPPPPPLAASTPLLHGEFGSYPARGPRFALTLTSQALHIQRLRPKPEARP
RGGLVPLAEVSGCCTLRSRSPSDSAAYFCIYTYPRGRRGARRRATRTFRA
DGAATYEENRAEAQRWATALTCLLRGLPLPGDGEITPDLLPRPPRLLLLV
NPFGGRGLAWQWCKNHVLPMISEAGLSFNLIQTERQNHARELVQGLSLS
EWDGIVTVSGDGLLHEVLNGLLDRPDWEEAVKMPVGILPCGSGNALAGA
VNQHGGFEPALGLDLLLNCSLLLCRGGGHPLDLLSVTLASGSRCFSFLSV
AWGFVSDVDIQSERFRALGSARFTLGTVLGLATLHTYRGRLSYLPATVEP
ASPTPAHSLPRAKSELTLTPDPAPPMAHSPLHRSVSDLPLPLPQPALASPGS
PEPLPILSLNGGGPELAGDWGGAGDAPLSPDPLLSSPPGSPKAALHSPVSE
GAPVIPPSSGLPLPTPDARVGASTCGPPDHLLPPLGTPLPPDWVTLEGDFV

LMLAISPSHLGADLVAAPHARFDDGLVHLCWVRSGISRAALLRLFLAME

RGSHFSLGCPQLGYAAARAFRLEPLTPRGVLTVDGEQVEYGPLQAQMHP

GIGTLLTGPPGCPGREP

The Molecular Operating Environment (MOE)[5] software suite was used to model SphK2. This program reads in the designated template structure file and model sequence file to predict and score 10 models. The program then combines aspects of the 10 models to compose a consensus structure that represents the best-predicted tertiary orientation for the modeled protein. The Loop Modeler tool in MOE was used to sample through loop orientations for the variable loop regions of the consensus model. Energy minimization utilizing the Amber12EHT force field[6] was run on the consensus structure to relax any conflicting atom locations that would occur as a result of differences in sequence between the template and model sequence. Structural analysis and validation was performed on the energy minimized consensus structure using the SwissModel[5] suite of tools and Verify3D[8,9.] The Ramachandran plot, which conveys the most detail about residue location, is presented (Figure 7.4). A majority of the predicted angles for all of the residues were within the bounds of acceptable phi (ϕ) and psi (ψ) angles. All analysis metrics used to validate the integrity of the homology model indicated that the model was favorable and a good representation of SphK2.

Figure 7.3. Sequence Alignment of hSphK1 and hSphK2 using Clustal Omega. Reproduced with permission from reference 10. Copyright (2011) EMBO and Macmillan Publishers Limited

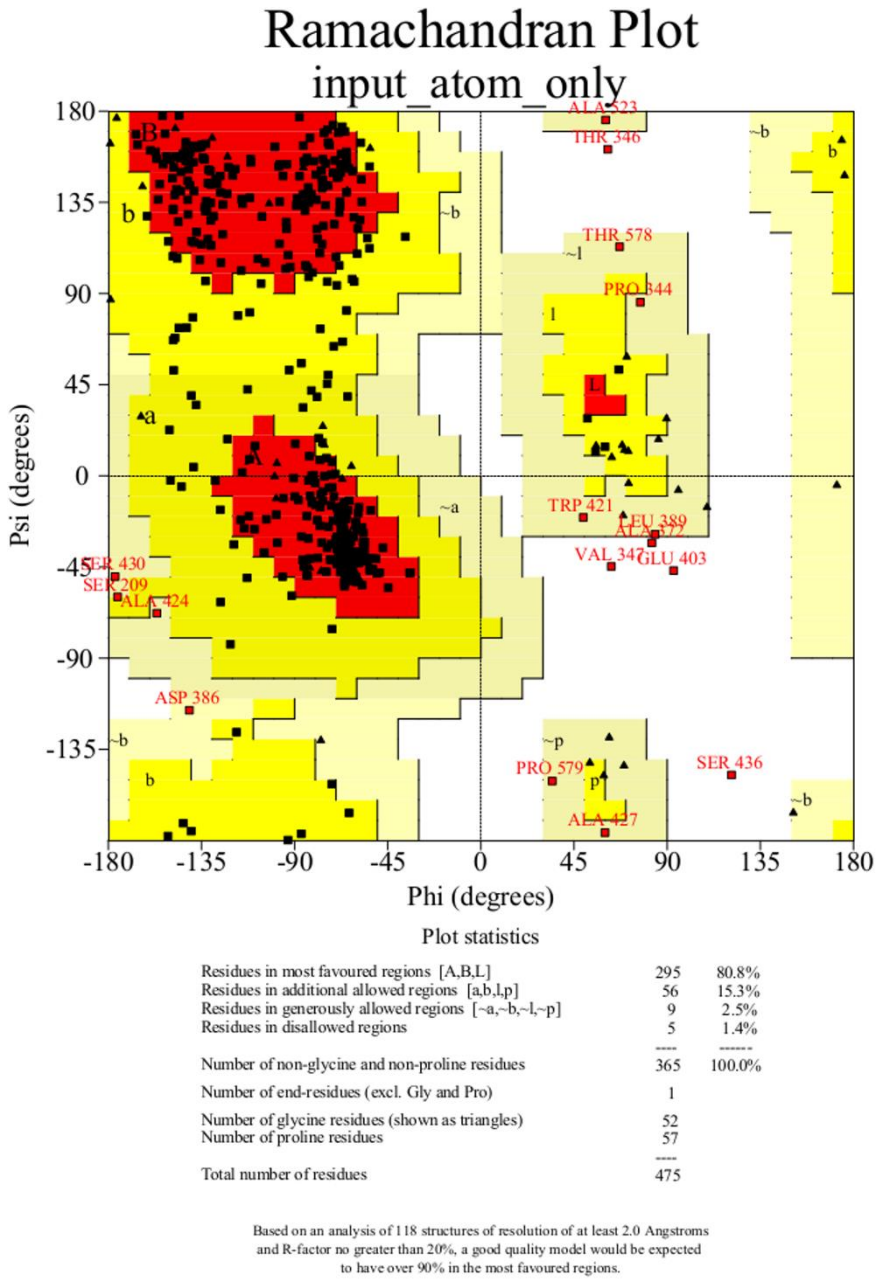

Figure 7.4. Ramachandran Plot for the SphK2 Model. Residues that did not fit the ideal phi (ϕ) and psi (ψ) angles are highlighted as a red rectangle with the three-letter residue identifier and residue number.

7.3.2 Molecular Docking

Molecular docking was performed using compounds experimentally deemed inhibitors in an attempt to elucidate protein-ligand interactions that contribute to activity. The generated SphK2 receptor model and the SphK1 template structure model (PDB ID: 3VZB) were used as the receptors for docking. Marvin was used for drawing, displaying and characterizing chemical structures, substructures and reactions, Marvin 6.2.2, 2014, ChemAxon (http://www.chemaxon.com). AutoDock Tools[11] was used to prepare the protein and ligand files, while AutoDock Vina[12] was used to perform the docking for pose prediction. The SphK1 and SphK2 structure models were overlaid in order to create a common coordinate space for docking pose comparison. This also allows for parameterization of a single grid box in which docking results would be the most comparable. The grid box was set to 20 x 20 x 28 Å, with a 1.000 Å grid spacing, which yielded 11,200 grid points for atom location sampling. The center of the box was placed at the approximate center of the ligand-binding cavity, with a portion of the ATP binding cavity included.

Up to nine docked poses were predicted for each compound. The number of predicted poses is dependent on the fitness of the sampled compound orientations. The lowest energy pose for each docked ligand was considered as the ideal binding pose for any given compound. In some instances, the orientation of the lowest energy docked pose would not be conducive to binding, but a different, less energetically favorable pose might be better positioned in the binding cavity. For such an instance, it was predicted that the compound was not as effective an inhibitor as compounds where the lowest energy pose was in the predicted orientation for binding that would lead to activity. Free energy of binding scores were cataloged for each docked compound and used as one level of comparison between compounds. The second, more

fruitful aspect of analysis was distance measurements between protein and ligand heavy atoms that would allow for prediction of interactions. Distances were assessed to predict hydrogen bonding (less than 3.5 Å), hydrophobic interactions (3.4–3.9 Å), and distal, weaker interactions (greater than 4.0 Å) that would translate to ligand binding and stability in the binding cavity.

7.4 References

1. Kharel, Y.: Mathews, T.P.; Kennedy, A.J.; Houck, J.D.; Macdonald, T.L.; Lynch, K.R.; A Rapid Assay for the Assessment of Sphingosine Kinase Inhibitors and Substrates. *Anal. Biochem*. **2011**, *411* (2), 230–235.
2. Kharel, Y.; Raje, M.; Gao, M.; Gellett, A.M.; Tomsig, J.L.; Lynch, K.R.; Santos, W.L.; Sphingosine Kinase Type 2 Inhibition Elevates Circulating Sphingosine-1-Phosphate. *Biochem. J*. **2012**, *447* (1), 149–157.
3. Bernstein, F. C.; Koetzle, T. F.; Williams, G. J.; Meyer, E. F., Jr.; Brice, M. D.; Rodgers, J. R.; Kennard, O.; Shimanouchi, T.; Tasumi, M., The Protein Data Bank: a Computer-Based Archival File for Macromolecular Structures. *J. Mol. Biol.* **1977,** *112* (3), 535–542.
4. Wang, Z.; Min, X.; Xiao, S. H.; Johnstone, S.; Romanow, W.; Meininger, D.; Xu, H.; Liu, J.; Dai, J.; An, S.; Thibault, S.; Walker, N., Molecular Basis of Sphingosine Kinase 1 Substrate Recognition and Catalysis. *Structure* **2013,** *21* (5), 798–809.
5. *Molecular Operating Enviroment (MOE), 2013.08*, 1010 Sherbooke St. West, Suite#910, Montreal, QC, Canada, H3A 2R7, 2013.
6. Case, D. A.; Darden, T. A.; Cheatham, T. E.; Simmerling, C. L.; Wang, J.; Duke, R. E.; Luo, R.; Walker, R. C.; Zhang, W.; Merz, K. M.; Roberts, B.; Hayik, S.; Roitberg, A.; Seabra, G.; Swails, J.; Goetz, A. W.; Kolossváry, I.; Wong, K. F.; Paesani, F.; Vanicek, J.; Wolf, R. M.; Liu, J.; Wu, X.; Brozell, S. R.; Steinbrecher, T.; Gohlke, H.; Cai, Q.; Ye, X.; Wang, J.; Hsieh, M. J.; Cui, G.; Roe, D. R.; Mathews, D. H.; Seetin, M. G.; Salomon-Ferrer, R.; Sagui, C.; Babin, V.; Luchko, T.; Gusarov, S.; Kovalenko, A.; Kollman, P. A., AMBER 12. University of California, San Francisco: 2012.

7. Bordoli, L.; Kiefer, F.; Arnold, K.; Benkert, P.; Battey, J.; Schwede, T., Protein Structure Homology Modeling Using SWISS-MODEL Workspace. *Nat. Protocols* **2008,** *4* (1), 1–13.

8. Bowie, J. U.; Luthy, R.; Eisenberg, D., A Method to Identify Protein Sequences that Fold Into a Known Three-Dimensional Structure. *Science* **1991,** *253* (5016), 164–170

9. Luthy, R.; Bowie, J. U.; Eisenberg, D., Assessment of Protein Models with Three-Dimensional Profiles. *Nature* **1992,** *356* (6364), 83–85.

10. Sievers, F.; Wilm, A.; Dineen, D.; Gibson, T. J.; Karplus, K.; Li, W.; Lopez, R.; McWilliam, H.; Remmert, M.; Söding, J.; Thompson, J. D.; Higgins, D. G., Fast, Scalable Generation of High-Quality Protein Multiple Sequence Alignments Using Clustal Omega. *Mol. Syst. Biol.* **2011,** *7* (1), 539.

11. Morris, G. M.; Huey, R.; Lindstrom, W.; Sanner, M. F.; Belew, R. K.; Goodsell, D. S.; Olson, A. J., AutoDock4 and AutoDockTools4: Automated Docking with Selective Receptor Flexibility. *J. Comput. Chem.* **2009,** *30* (16), 2785–2791.

12. Trott, O.; Olson, A. J., AutoDock Vina: Improving the Speed and Accuracy of Docking with a New Scoring Function, Efficient Optimization, and Multithreading. *J. Comput. Chem.* **2010,** *31* (2), 455–461.